

HEADED REINFORCING BARS:
CCT NODE TESTS, DESIGN
PROVISIONS, AND EVALUATION
OF A GRANULAR
MICROMECHANICS MODEL FOR
USE IN FINITE ELEMENT ANALYSIS
OF BOND

By
Muna M. Hano
David Darwin
Anil Misra
Matt O'Reilly

A Report on Research Sponsored by

Electric Power Research Institute
Concrete Reinforcing Steel Institute Education and Research
Foundation

BarSplice Products, Incorporated
Headed Reinforcement Corporation
LENTON® products from Pentair®

Structural Engineering and Engineering Materials
SM Report No. 135
December 2019



THE UNIVERSITY OF KANSAS CENTER FOR RESEARCH, INC.
2385 Irving Hill Road, Lawrence, Kansas 66045-7563

**HEADED REINFORCING BARS: CCT NODE TESTS, DESIGN PROVISIONS,
AND EVALUATION OF A GRANULAR MICROMECHANICS MODEL FOR
USE IN FINITE ELEMENT ANALYSIS OF BOND**

By

Muna M. Hano

David Darwin

Anil Misra

Matt O'Reilly

A Report on Research Sponsored by

Electric Power Research Institute

Concrete Reinforcing Steel Institute Education and Research Foundation

BarSplice Products, Incorporated

Headed Reinforcement Corporation

LENTON[®] products from Pentair[®]

Structural Engineering and Engineering Materials

SM Report No. 135

THE UNIVERSITY OF KANSAS CENTER FOR RESEARCH, INC.

LAWRENCE, KANSAS

December 2019

ABSTRACT

The anchorage behavior of headed bars at the end of beams within compression-compression-tension (CCT) nodes subjected to monotonic loading is assessed. The test parameters for the 10 specimens tested include the embedment length, number and spacing of the anchored bars, and the presence or absence of a head at the anchored end of the bar. The nominal compressive strength of the concrete was 5000 psi. The test results, along with that of members other than beam-column joints available in the literature, are compared with strengths based on a descriptive equation developed for headed bars anchored in beam-column joints. The test results for specimens with bars without heads are compared with anchorage strengths predicted for straight bars. More broadly, test results for headed bars anchored in beam-column joints are compared with design provisions for the development length of headed bars in ACI 318-14 and ACI 318-19 and those proposed by Shao et al. (2016) and Darwin and Dolan (2021)¹, along with the anchorage provisions in Chapter 17 of ACI 318-19. These comparisons are based on tests of 178 beam-column joint specimens containing headed bars with bearing areas between 3.8 to 9.4 times the area of the bar. In comparisons with the anchorage provisions in Chapter 17 of ACI 318-19, three modes of failure were checked—breakout, side-face blowout, and strength of the anchor reinforcement. Forty of the specimens (18 without confining reinforcement and 22 with confining reinforcement), had a ratio of effective depth of the beam to embedment length of 1.5 or more. In addition to the design provisions for development and anchorage, test results for these specimens are compared with strengths based on the strut-and-tie method in ACI 318-19. Finally, a granular micromechanics model and associated model for reinforcing steel-concrete interaction are evaluated for their general applicability for use in finite element modeling of anchorage of headed and straight reinforcing bars to concrete. A key point in the evaluation is to determine the importance of representing the local interaction between deformed bars and the surrounding concrete, which is not represented in this case, to obtain a fully objective model. Finite element results are compared with those from tests of headed bars embedded in slabs and straight bars embedded in concrete blocks.

The strength of the CCT node specimens was limited by anchorage failure, either side-face blowout for headed bars or pullout for straight bars. Anchorage type (headed bars and straight bars) had a minimal effect on initial load-deflection behavior, but did affect strength. The descriptive equation developed for the anchorage strength of headed bars in beam-column joints is very conservative (test-to-calculate ratios ranging from 1.37 to 2.68 with an average of 2.05 for the

¹ Copyright date

current study test-to-calculated ratios ranging from 1.67 to 2.21 with an average of 1.89 for a study by Thompson 2006a) for headed bars in CCT nodes that have a compressive force placed perpendicular to the bar, as is the descriptive equation developed by ACI Committee 408 (ACI 408R-03) for straight bars (test-to-calculated ratios ranging from 1.72 to 2.76 with an average of 2.25). The provisions in ACI 318-14 for the development length of headed bars do not accurately estimate the anchorage strength of headed bars with high steel strength or concrete compressive strength. The equation, however, is generally conservative. The development length design provisions proposed by Shao et al. (2016) can be safely used for the design of the development length of headed bars for steel strengths at least up to 120 ksi and concrete compressive strengths at least up to 16,000 psi, while those in ACI 318-19 for headed bars do not fully capture the effects of confining reinforcement, bar spacing, and concrete compressive strength for compressive strengths above 6000 psi. The provisions proposed by Darwin and Dolan (2021) accurately reflect the anchorage strength of headed bars and provide a similar level of accuracy as that provided by those proposed by Shao et al. (2016). The strut-and-tie method in ACI 318-19 should be used to design joints with ratios of effective depth to embedment length of 1.5 or greater. The anchorage provisions in ACI 318-19 are very conservative when compared to any of the other methods evaluated in this study and, if used, would lead to nearly unbuildable designs. The granular micromechanics model and associated model from reinforcing steel-concrete interaction provide a good representation of the anchorage strength in cases where behavior of these specimens is dominated by the compressive and tensile properties of concrete, which are well represented by the granular micromechanics model. The combined model, however, does not provide a good representation of the behavior from members with strength that depends on splitting of concrete caused by to slip of the bar. Lack of representation of the local interaction between deformed bars and the surrounding concrete prevents the model from being generally applicable for use in representing reinforced concrete members, especially in cases where strength is governed by bond between straight reinforcing steel and concrete.

Keywords: anchorage strength, beam-column joint, bond, CCT nodes, development length, finite element analysis, granular micromechanics model, headed bar, strut-and-tie method.

ACKNOWLEDGEMENTS

This report is based on a thesis presented by Muna M. Hano in partial fulfillment of the requirements for the Ph.D. degree from the University of Kansas. Support for the study was provided by the Electric Power Research Institute, Concrete Reinforcing Steel Institute Education and Research Foundation, BarSplice Products, Inc., Headed Reinforcement Corp., and LENTON[®] products from Pentair[®]. Additional materials were supplied by Commercial Metals Company, Gerdau Corporation, Nucor Corporation, MMFX Technologies Corporation, Dayton Superior, Midwest Concrete Materials, Grace Construction Products, and the Ministry of Higher Education in Iraq MOSHER. Thanks are due to Ken Barry, Mark Ruis, and David Scott who provided project oversight for the Advanced Nuclear Technology Program of the Electric Power Research Institute, and to Neal Anderson, Cary Kopczynski, Mike Mota, Javeed Munshi, and Conrad Paulson who served as industry advisors.

TABLE OF CONTENTS

ABSTRACT.....	i
ACKNOWLEDGMENTS.....	iii
TABLE OF CONTENTS.....	v
LIST OF FIGURES.....	xii
LIST OF TABLES.....	xxiii
CHAPTER 1: INTRODUCTION.....	1
1.1 GENERAL.....	1
1.2 MECHANISM OF BOND.....	2
1.2.1 Straight Reinforcing Bars.....	2
1.2.2 Hooked Reinforcing Bars.....	3
1.2.3 Headed Reinforcing Bars.....	4
1.3 HISTORICAL DEVELOPMENT OF HEADED BARS.....	5
1.4 PREVIOUS RESEARCH ON HEADED REINFORCING BAR ANCHORAGE.....	8
1.4.1 Bashandy (1996).....	8
1.4.2 Wallace, McConnell, Gupta, and Cote (1998).....	11
1.4.3 Thompson, Ziehl, Jirsa, and Breen (2005-2006); Thompson et al. (2005, 2006).....	12
1.4.4 Chun et al. (2009).....	17
1.5 STRUT-AND-TIE MODELING.....	20
1.5.1 Introduction.....	20
1.5.1.1 Strut and Node Types.....	22
1.5.2 Historical Development of Strut-and-Tie Model.....	23
1.5.3 Procedure for Strut-and-Tie Design.....	25
1.5.3.1 Dimensioning of Nodes, Struts, and Ties.....	26

1.5.3.2	Limitations of Strut-Tie Angle.....	26
1.5.3.3	Strength of Nodes.....	29
1.5.3.4	Strength of Struts.....	30
1.5.4	Experimental Studies.....	31
1.5.4.1	Ramirez and Breen (1983).....	31
1.5.4.2	Cook and Mitchell (1988).....	31
1.6	FINITE ELEMENT METHOD (FEM).....	33
1.6.1	Introduction.....	33
1.6.2	Background of Finite Element Analysis.....	34
1.6.3	Elements and Nodes.....	34
1.6.4	Degrees of Freedom (DOF).....	35
1.6.5	Modeling Material Failure-Fracture.....	35
1.6.5.1	Continuum Damage Mechanics.....	35
1.6.5.2	Fracture mechanics.....	36
1.6.6	PREVIOUS RESEARCH USING FEM FOR REINFORCED CONCRETE.....	36
1.6.6.1	Ngo and Scordelis (1967).....	37
1.6.6.2	Brown, Darwin, and McCabe (1993).....	37
1.6.6.3	Tholen and Darwin (1996).....	38
1.6.6.4	Allwood and Bajarwan (1996).....	39
1.6.6.5	Misra and Yang (2010).....	40
1.6.6.6	Misra and Poorsolhouy (2017).....	41
1.7	OBJECTIVE AND SCOPE.....	42

CHAPTER 2: EXPERIMENTAL WORK.....	44
2.1 DESCRIPTION OF SPECIMENS.....	44
2.2 TEST PARAMETERS.....	47
2.2.1 SPECIMEN DESIGNATION.....	49
2.3 MATERIAL PROPERTIES.....	50
2.3.1 Concrete properties.....	50
2.3.2 Steel properties.....	50
2.4 SPECIMEN FABRICATION.....	51
2.5 TEST PROCEDURES.....	51
2.5.1 SPECIMEN INSTRUMENTATION.....	54
2.6 SUMMARY OF TEST PROGRAM.....	59
CHAPTER 3: TEST RESULTS AND ANALYSIS OF CCT NODE SPECIMENS.....	61
3.1 CRACKING BEHAVIOR AND MODE OF FAILURE.....	61
3.1.1 Cracking Behavior.....	61
3.1.2 Modes of Failure.....	65
3.2 PEAK LOAD AND EMBEDMENT LENGTH.....	67
3.3 LOAD-DEFLECTION RESPONSE.....	70
3.4 STRAIN IN REINFORCEMENT.....	73
3.5 HEAD SLIP.....	90
3.6 ANALYSIS OF INTERNAL ACTIONS.....	92
3.6.1 Strut and Tie Forces.....	92
3.6.2 Comparison of Capacity and Demand for Struts and Nodes.....	93
3.6.3 Stresses, Forces, and Embedment Length.....	96

3.7 ANALYSIS OF TEST RESULTS USING DESCRIPTIVE EQUATION DEVELOPED BY SHAO ET. AL (2016).....	99
3.7.1 Descriptive Equation (Shao et al. 2016).....	99
3.7.2 Comparison of Descriptive Equation for the CCT Node Specimens.....	101
3.7.2.1 CCT Node Tests (Current Study).....	101
3.7.2.2 CCT Node Specimens Tested by Thompson et al. (2006a).....	101
3.8 ANALYSIS OF TEST RESULTS USING ACI 408-3 EQUATION.....	103
3.8.1 ACI 408-3 Equation.....	103
3.8.1.2 CCT Node Tests (Non-Headed End) (Current Study).....	104
3.9 SUMMARY.....	105
CHAPTER 4: COMPARISONS OF ANCHORAGE STRENGTH OF HEADED BARS WITH VALUES BASED ON DEVELOPMENT LENGTH AND ANCHORAGE DESIGN PROVISIONS.....	108
4.1 INTRODUCTION.....	108
4.2 TEST SPECIMENS.....	108
4.1.1 Beam-Column Joint Specimen (Shao et al. (2016)).....	108
4.2.2 Beam-Column Joint Specimens with $d_{eff}/\ell_{eh} \geq 1.5$	110
4.3 DESIGN APPROACHES.....	111
4.3.1 Development of Headed Bars in Tension (ACI 318-14).....	110
4.3.2 Shao et al. (2016).....	111
4.3.3 Development of Headed Bars in Tension ACI 318-19.....	113
4.3.4 Darwin and Dolan (2021).....	114
4.3.5 Anchorage Provisions ACI 318-19.....	116
4.3.5.1 Concrete Breakout Strength (N_{cb} and N_{cbg}) of Anchors in Tension.....	116
4.3.5.2 Concrete Side-Face Blowout Strength (N_{sb} and N_{sbg}) of Anchors in Tension.....	117

4.5.3.3 Strength of Anchor Reinforcement (N).....	118
4.3.6 Strut-and-Tie Approach.....	120
4.4 RESULTS AND DISCUSSION.....	121
4.4.1. Specimens with $d_{eff}/\ell_{eh} < 1.5$	121
4.4.1.1 Without Confining Reinforcement	121
4.4.1.2 With Confining Reinforcement	124
4.4.1.3 Comparison with ACI 318-14.....	126
4.4.1.4 Comparison with Shao et al. 2016.....	131
4.4.1.5 Comparison with ACI 318-19.....	135
4.4.1.6 Comparison with Darwin and Dolan 2021.....	140
4.4.1.7 Comparison with Anchorage Provisions (ACI 318-19).....	144
4.5 SPECIMENS WITH $d_{eff}/\ell_{eh} \geq 1.5$	150
4.5.1 Anchorage Strengths.....	150
4.5.2 Comparisons.....	153
4.6 SUMMARY AND CONCLUSIONS.....	160
CHAPTER 5: MODELING THE ANCHORAGE FAILURE FOR HEADED BARS AND STRAIGHT BARS USING 3D GRANULAR MICROMECHANICS BASED FINITE ELEMENT ANALYSIS.....	162
5.1 INTRODUCTION.....	162
5.2 FINITE ELEMENT ANALYSIS OF ANCHORAGE BEHAVIOR.....	163
5.2.1 Material Properties.....	163
5.2.1.1 Concrete Model.....	163
5.2.1.2 Stress-Strain Behavior of the Concrete Block under Uniaxial Tension and Compression.....	165

5.2.1.3 Stress-Strain Behavior of the Concrete Block under Different Confinement Levels.....	167
5.2.2 Steel Model.....	170
5.2.3 Concrete-Steel Interface Model.....	170
5.2.3.1 Linear Elastic Traction-Separation Behavior.....	171
5.2.3.2 Damage Modeling.....	171
5.2.3.2.1 Damage Initiation.....	172
5.2.3.2.2 Damage Evolution.....	172
5.3 ELEMENT TYPE.....	174
5.4 SHALLOW EMBEDMENT SPECIMENS.....	175
5.4.1 Specimen with one Headed Bar Embedded at the Center.....	175
5.4.2 Specimen with One Bar Embedded Close to the Edge with Unsymmetrical Supports....	177
5.4.3 Specimen with One Bar Embedded Close to the Edge with Unsymmetrical Supports.....	180
5.5 BEAM-END TEST SPECIMEN.....	183
5.6 RESULTS AND DISCUSSION.....	187
5.6.1 Simulation Designation.....	187
5.6.2 Load-Displacement Behavior for Simulation with Headed Bar Embedded at the Center and Concrete Compressive Strength of 8 ksi	187
5.6.2.1 Load-Displacement Behavior for Simulation with Headed Bar Embedded at the Center and Concrete Compressive Strength of 5 ksi.....	190
5.6.2.2 Load-Displacement Behavior for Simulation with Headed Bar Embedded Close to Edge with Unsymmetrical Supports and Concrete Compressive Strength of 8 ksi.....	191
5.6.2.3 Load-Displacement Behavior for Simulation with Headed Bar Embedded Close to Edge with Symmetrical Supports and Concrete Compressive Strength of 5 ksi.....	194
5.6.2.4 Comparison of Peak Loads.....	195
5.6.3 Reinforcement Strain.....	196

5.6.4 Summary.....	198
5.6.5 Beam-End Tests.....	198
5.6.6.1 Load-Displacement Behavior.....	198
5.6.6.2 Effect of Different Embedment Lengths and Concrete Covers.....	200
5.6.6.3 Summary.....	202
5.7 SUMMARY AND CONCLUSIONS.....	202
CHAPTER 6: SUMMARY AND CONCLUSIONS.....	204
6.1 SUMMARY.....	204
6.2 CONCLUSIONS.....	205
6.2.1 CCT Node Test.....	205
6.2.2 Anchorage Strength of Headed Bars in Tension.....	206
6.2.3 Finite Element Analysis.....	207
REFERENCE.....	208
APPENDIX A: NOTATION.....	213
APPENDIX B: DETAILED CCT NODE SPECIMEN RESULTS.....	216
APPENDIX C: TEST RESULTS AND SPECIMENS FROM OTHER STUDIES INCLUDED IN THE CURRENT STUDY.....	239
C. 1 BEAM-COLUMN JOINT WITH $d_{eff}/\ell_{eh} < 1.5$	239
C. 2 BEAM-COLUMN WITH $d_{eff}/\ell_{eh} \geq 1.5$	271

LIST OF FIGURES

Figure 1.1 Bond forces components (figure after ACI Committee 408-2003).....	2
Figure 1.2 Behavior of 90° hooked bar subjected to tensile force (deformations not shown) (figure after Minor 1971).....	3
Figure 1.3 Standard hook dimensions (figure after ACI 318-11).....	4
Figure 1.4 Headed bar (figure after Thompson 2002).....	4
Figure 1.5 Required dimensions of obstructions for headed bars (figure from ASTM A970/M970-18).....	5
Figure 1.6 Test specimen with anchorage provided by welded steel end plate (figure after CALTRANS 1974).....	6
Figure 1.7 Details of the shear studs welding (figure after Mokhtar, Ghali, and Dilger, 1985).....	7
Figure 1.8 Test configuration for an exterior beam-column joint specimen (figure after Bashandy 1996).....	9
Figure 1.9 Exterior beam-column joint and corner joint, (a) Exterior beam-column joint, (b) Corner joint (figure after Wallace, McConnell, Gupta, and Cote 1998).....	12
Figure 1.10 Details of unconfined specimen (figure after Thompson et al. 2005).....	13
Figure 1.11 Details of confined specimen (figure after Thompson et al. 2005).....	13
Figure 1.12 Pullout failure of straight bar (figure from Thompson 2002).....	14
Figure 1.13 Rupture failure in the strut and node region (figure from Thompson 2002).....	15
Figure 1.14 Dimensional variables in the bearing capacity model (figure from Thompson et al. 2006).....	16
Figure 1.15 Test configuration for beam-column joints (figure after Chun et al. 2009).....	18
Figure 1.16 Typical beam-column joint specimen. (a) Specimen with headed bar, (b) Specimen with hooked bar (figure after Chun 2009).....	19
Figure 1.17 Failure Modes: (a) Concrete Breakout; (b) and (c) Joint Shear Failure (figure after Chun et al. 2009).....	19
Figure 1.18 B-region and D-region.....	21
Figure 1.19 Examples of strut-and-tie models.....	21

Figure 1.20 Strut types (figure after Schlaich et al. 1987).....	22
Figure 1.21 Basic node types.....	23
Figure 1.22 Truss model (figure after Ritter 1899).....	24
Figure 1.23 Morsch (1902) model (figure after Morsch 1902).....	24
Figure 1.24 Truss model for torsion (figure after Thompson 2002).....	25
Figure 1.25 Extended nodal zone showing the effect of the distribution of the force (figure after ACI 318-14).....	27
Figure 1.26 Hydrostatic and non-hydrostatic nodes (figure after Thompson et al. 2002).....	29
Figure 1.27 Strut-and-tie models: (a) Double-sided corbel, (b) Rectangular dapped beam, (c) Inclined dapped beam, and (d) Beam with opening (figure after Cook and Mitchell 1988).....	33
Figure 1.28 Damage process (Continuum Damage Mechanics). (a) Localization (necking) in a bar of ductile material, (b) Stress vs. strain characteristics (figure from Runesson 2006).....	35
Figure 1.29 Fracture process (a) Preexisting edge cracks, (b) Far-field stress vs. extension characteristics. (Figure from Runesson 2006).....	36
Figure 1.30 Portion of the tested specimen represented by FEM (figure after Brown, Darwin, and McCabe 1993).....	38
Figure 1.31 Beam-end specimen, (a) Portion of the specimen with 1 in. concrete cover and 6 in. bonded length, (b) Portion of the specimen with 2 in. concrete cover and 12 in. bonded length (figure after Tholen and Darwin 1996).....	39
Figure 1.32 Analysis method (figure after Allwood and Bajarwan 1996).....	40
Figure 2.1 Strut-and-tie model.....	44
Figure 2.2 Testing configurations (a) headed end (b) non-headed end (Series 1).....	45
Figure 2.3 Testing configurations (a) headed end (b) non-headed end (Series 2).....	46
Figure 2.4 Cross-section of the specimens.....	46
Figure 2.5 Position of heads with respect to bearing plate.....	48
Figure 2.6 Position of non-headed end with respect to bearing plate.....	48
Figure 2.7 Position of bars (Strain gauges mounted on South bar).....	48

Figure 2.8 Specimen designation.....	50
Figure 2.9 Stress-Strain curve for the headed bars.....	51
Figure 2.10 Front view of the loading system.....	53
Figure 2.11 Side view of the loading system.....	54
Figure 2.12 CCT node test.....	54
Figure 2.13 Strut and Tie Model.....	55
Figure 2.14 Placement of strain gauges for series 1 specimens.....	56
Figure 2.15 Placement of strain gauges for series 2 specimens.....	57
Figure 2.16 Placement of markers for a typical specimen.....	58
Figure 2.17 Linear potentiometer.....	59
Figure 2.18 Details of load cell.....	60
Figure 3.1 Observed crack growth in specimen with longitudinal bar anchored with a headed, Specimen H-3-8-5-13-F4.1-2.....	63
Figure 3.2 Specimen H-3-8-5-13-F4.1-2 after failure.....	64
Figure 3.3 Observed crack growth in specimen with longitudinal bar anchored with straight reinforcement, Specimen NH-3-8-5-13-F4.1-2.....	65
Figure 3.4 Specimen NH-3-8-5-13-F4.1-2 after failure.....	65
Figure 3.5 Side blowout failure – Specimen H-3-8-5-13-F4.1-2.....	67
Figure 3.6 Concrete crushing failure – Specimen H-3-8-5-9-F4.1-2.....	67
Figure 3.7 Pullout failure – Specimen H-3-8-5-11-F4.1-2.....	68
Figure 3.8 Peak load recorded for headed and non-headed end-specimens identified by number of bars and embedment length (Series 1)	70
Figure 3.9 Peak load recorded for headed and non-headed end -specimens identified by number of bars and embedment length (Series 2).....	70
Figure 3.10 Load versus deflection results for the Series 1 headed-end tests	72

Figure 3.11 Load versus deflection results for the Series 2 headed-end tests.....	72
Figure 3.12 Load versus deflection results for Specimens H-2-8-5-10.4-F4.1 and NH-2-8-5-10.4-F4.1 (Series 1).....	73
Figure 3.13 Load versus deflection results for Specimens H-3-8-5-13-F4.1 and NH-3-8-5-13-F4.1 (Series 2).....	73
Figure 3.14 Position of strain gauges on longitudinal reinforcement (series 2).....	74
Figure 3.15 Strain along the longitudinal bars (a) Specimen H-2-8-5-9-F4.1-1, (b) Specimen NH-2-8-5-9-F4.1-1. Arrows correspond to location of the centroid support reaction and centroid of the applied load.....	78
Figure 3.16 Strain along the longitudinal bars (a) Specimen H-2-8-5-10.4-F4.1-1, (b) Specimen NH-2-8-5-10.4-F4.1-1. Arrows correspond to location of the centroid support reaction and centroid of the applied load.....	79
Figure 3.17 Strain along the longitudinal bars (a) Specimen H-3-8-5-11.4-F4.1-1, (b) Specimen NH-3-8-5-11.4-F4.1-1. Arrows correspond to location of the centroid support reaction and centroid of the applied load.....	80
Figure 3.18 Strain along the longitudinal bars (a) Specimen H-3-8-5-14-F4.1-1, (b) Specimen NH-3-8-5-14-F4.1-1. Arrows correspond to location of the centroid support reaction and centroid of the applied load.....	81
Figure 3.19 Strain along the longitudinal bars (a) Specimen H-2-8-5-9-F4.1-2, (b) Specimen NH-2-8-5-9-F4.1-2. Arrows correspond to location of the centroid support reaction and centroid of the applied load.....	82
Figure 3.20 Strain along the longitudinal bars (a) Specimen H-2-8-5-13-F4.1-2, (b) Specimen NH-2-8-5-13-F4.1-2. Arrows correspond to location of the centroid support reaction and centroid of the applied load.....	83
Figure 3.21 Strain along the longitudinal bars (a) Specimen H-3-8-5-9-F4.1-2, (b) Specimen NH-3-8-5-9-F4.1-2. Arrows correspond to location of the centroid support reaction and centroid of the applied load.....	84
Figure 3.22 Strain along the longitudinal bars (a) Specimen H-3-8-5-11-F4.1-2, (b) Specimen NH-3-8-5-11-F4.1-2. Arrows correspond to location of the centroid support reaction and centroid of the applied load.....	85
Figure 3.23 Strain along the longitudinal bars (a) Specimen H-3-8-5-13-F4.1-2, (b) Specimen NH-3-8-5-13-F4.1-2. Arrows correspond to location of the centroid support reaction and centroid of the applied load.....	86

Figure 3.24 Load-strain curve for specimen H-3-8-5-11-F4.1-2, (a) south bar, (b) middle bar, (c) north bar. Some data is missing because some strain gauges failed prior to failure of the specimen.....	89
Figure 3.25 Load-strain curve for specimen NH-3-8-5-11-F4.1-2, (a) south bar, (b) middle bar, (c) north bar. Some data is missing because some strain gauges failed prior to failure of the specimen.....	90
Figure 3.26 Position of bars.....	92
Figure 3.27 Load versus slip of the three headed bar ends in Specimen H-3-8-5-13-F4.1-2.....	92
Figure 3.28 Load versus average slip of headed bars for Specimens H-2-8-5-9-F4.1-2, H-2-8-5-13-F4.1-2, H-3-8-5-9-F4.1-2, and H-3-8-5-13-F4.1-2.....	93
Figure 3.29 Assumed dimensions of the strut and node.....	95
Figure 3.30 Force per bar estimated using a strut-and-tie model versus embedment length for the headed end.....	99
Figure 3.31 Force per bar estimated using a strut-and-tie model versus embedment length for the non-headed end.....	100
Figure 4.1 Typical beam-column joint specimen (a) side view (b) top view (Figure after Shao et al. 2016).....	109
Figure 4.2 Confining reinforcement for beam-column joint specimens (a) no confining reinforcement, (b) two No. 3 hoops, (c) No. 3 hoops at $3d_b$ (Figure after Shao et al. 2016).....	109
Figure 4.3 Effective depth d_{eff} (Figure after Shao et al. 2016).....	110
Figure 4.4 Concrete breakout failure (Figure after ACI 318-19).....	116
Figure 4.5 Concrete side-face blowout failure.....	118
Figure 4.6 Effective anchor reinforcement.....	119
Figure 4.7 Mechanism of load transfer through the strut-and-tie (Figure after Shao et al. 2016).....	121
Figure 4.8 Ratio of test-to-calculated failure load (T/T_{318-14}) versus measured concrete compressive strength f_{cm} for specimens with widely-spaced headed bars without confining reinforcement (ACI 318-14).....	127

Figure 4.9 Ratio of test-to-calculated failure load (T/T_{318-14}) versus measured concrete compressive strength f_{cm} for specimens with widely-spaced headed bars with confining reinforcement (ACI 318-14).....	127
Figure 4.10 Ratio of test-to-calculated failure load (T/T_{318-14}) versus center-to-center spacing for specimens with widely and closely-spaced headed bars without confining reinforcement (ACI 318-14).....	129
Figure 4.11 Ratio of test-to-calculated failure load (T/T_{318-14}) versus center-to-center spacing for specimens with widely and closely-spaced headed bars with confining reinforcement (ACI 318-14).....	130
Figure 4.12 Ratio of test-to-calculated failure load (T/T_{Shao}) versus measured concrete compressive strength f_{cm} for specimens with widely spaced headed bars without confining reinforcement (Shao et al. 2016).....	132
Figure 4.13 Ratio of test-to-calculated failure load (T/T_{Shao}) versus measured concrete compressive strength f_{cm} for specimens with widely-spaced headed bars with confining reinforcement (Shao et al. 2016).....	132
Figure 4.14 Ratio of test-to-calculated failure load (T/T_{Shao}) versus center-to-center spacing for specimens with widely and closely-spaced headed bars without confining reinforcement (Shao et al. 2016).....	133
Figure 4.15 Ratio of test-to-calculated failure load (T/T_{Shao}) versus center-to-center spacing for specimens with widely and closely-spaced headed bars with confining reinforcement (Shao et al. 2016).....	134
Figure 4.16 Ratio of test-to-calculated failure load (T/T_{318-19}) versus measured concrete compressive strength f_{cm} for specimens with widely-spaced headed bars without confining reinforcement (ACI 318-19).....	136
Figure 4.17 Ratio of test-to-calculated failure load (T/T_{318-19}) versus measured concrete compressive strength f_{cm} for specimens with widely-spaced headed bars with confining reinforcement (ACI 318-19).....	137
Figure 4.18 Ratio of test-to-calculated failure load (T/T_{318-19}) versus center-to-center spacing for specimens with widely and closely-spaced headed bars without confining reinforcement (ACI 318-19).....	138
Figure 4.19 Ratio of test-to-calculated failure load (T/T_{318-19}) versus center-to-center spacing for specimens with widely and closely-spaced headed bars with confining reinforcement (ACI 318-19).....	139

Figure 4.20 Ratio of test-to-calculated failure load (T/T_D) versus measured concrete compressive strength f_{cm} for specimens with widely-spaced headed bars without confining reinforcement (Darwin and Dolan 2021).....141

Figure 4.21 Ratio of test-to-calculated failure load (T/T_D) versus measured concrete compressive strength f_{cm} for specimens with widely-spaced headed bars with confining reinforcement (Darwin and Dolan 2021).....141

Figure 4.22 Ratio of test-to-calculated failure load (T/T_D) versus center-to-center spacing for specimens with widely and closely-spaced headed bars without confining reinforcement (Darwin and Dolan 2021).....142

Figure 4.23 Ratio of test-to-calculated failure load (T/T_D) versus center-to-center spacing for n specimens with widely and closely-spaced headed bars with confining reinforcement (Darwin and Dolan 2021).....143

Figure 4.24 Ratio of test-to-calculated failure load ($T/\phi N_{str}$) versus measured concrete compressive strength f_{cm} for specimens with widely-spaced headed bars without confining reinforcement (Anchorage provisions).....145

Figure 4.25 Ratio of test-to-calculated failure load ($T/\phi N_{str}$) versus measured concrete compressive strength f_{cm} for specimens with widely-spaced headed bars with confining reinforcement (Anchorage provisions).....146

Figure 4.26 Ratio of test-to-calculated failure load ($T/\phi N_{str}$) versus center-to-center spacing for specimens with widely and closely-spaced headed bars without confining reinforcement (Anchorage provisions).....147

Figure 4.27 Ratio of test-to-calculated failure load ($T/\phi N_{str}$) versus center-to-center spacing for specimens with widely and closely-spaced headed bars with confining reinforcement (Anchorage provisions).....148

Figure 4.28 Ratio of test-to-calculated failure load (T/T_{Shao}) versus d_{eff}/ℓ_{eh} for specimens with widely and closely-spaced headed bars without confining reinforcement (Shao et al. 2016).....154

Figure 4.29 Ratio of test-to-calculated failure load ($T/\phi N_{str}$) versus d_{eff}/h_{ef} for specimens with widely and closely-spaced headed bars without confining reinforcement (Anchorage Provisions).....155

Figure 4.30 Ratio of test-to-calculated failure load (T/T_{Shao}) versus d_{eff}/ℓ_{eh} for specimens with widely and closely-spaced headed bars with confining reinforcement (Shao et al. 2016).....157

Figure 4.31 Ratio of test-to-calculated failure load ($T/\phi N_{str}$) versus d_{eff}/h_{ef} for specimens with widely and closely-spaced headed bars with confining reinforcement (Anchorage Provisions).....158

Figure 4.32 Ratio of test-to-calculated failure load (R_1/T_{STM}) versus d_{eff}/ℓ_{eh} for specimens with widely and closely-spaced headed bars with confining reinforcement (Strut-and-tie

method).....	159
Figure 5.1 (a) Normal force-displacement relationship in compression and tension, (b) Shear force-displacement relationship in tension, (c) Shear direction damage parameter as a function of normal displacement. The local Cartesian coordinate system is shown in the inset (Misra and Poorsolhjoui 2015).....	164
Figure 5.2 Boundary condition for concrete block.....	165
Figure 5.3 Stress-Strain curve for the concrete block under uniaxial tension and compression for concrete compressive strength of 5 ksi and 8 ksi.....	166
Figure 5.4 Loading and boundary conditions for concrete block. (a) Without confinement, (b) With confining stresses.....	167
Figure 5.5 Stress-Strain curve for concrete block with confinement in compression for concrete compressive strength of 8 ksi.....	168
Figure 5.6 Stress-Strain curve for concrete block with confinement in tension	168
Figure 5.7 Volumetric strain-axial strain curve for a concrete block with confinement in compression.....	169
Figure 5.8 Stress paths plotted in the deviatoric stress–mean stress (q-p) space with confinement in compression.....	170
Figure 5.9 Typical traction-separation response.....	171
Figure 5.10 (a) Linear damage evolution (Simulia/ABAQUS V 6.11; Dassault Systèmes, RI, USA Section 35.1.10), (b) Mixed mode response in cohesive behavior (Simulia/ABAQUS V 6.11; Dassault Systèmes, RI, USA, Section 35.1.10).....	174
Figure 5.11 10-node tetrahedral element.....	174
Figure 5.12 (a) Details of the specimen with one headed bar embedded at center of slab (b) Configuration of test for specimen with one headed bar embedded at center of slab(Ghimire et al. 2018).....	176
Figure 5.13 Simulation components and meshing. (a) Concrete and (b) Headed bar	177
Figure 5.14 Boundary conditions 1 (BC1).....	177
Figure 5.15 (a) Details of the specimen with two headed bars embedded close to the edges, Configuration of test for specimen with two headed bars embedded close to the edges (Ghimire et al. 2018).....	178

Figure 5.16 Specimen meshing.....	179
Figure 5.17 Boundary conditions (a) BC1, (b) BC2, and (c) BC3.....	180
Figure 5.18 (a) Details of the specimen with three headed bars embedded in the slab, (b) Configuration of test for specimen with three headed bars embedded in the slab (Ghimire et al. 2018).....	181
Figure 5.19 Simulation components and meshing.....	182
Figure 5.20 Boundary conditions (BC2).....	182
Figure 5.21 (a) Cross section area of the modeled specimen, (b) Simulation with perpendicular reinforcement.....	183
Figure 5.22 Details of the beam-end specimen without confining reinforcement (Figure after Darwin, Graham 1993).....	184
Figure 5.23 Beam-end specimen, (a) Portion of the specimen with 1 in. concrete cover and 6 in. bonded length, (b) Portion of the specimen with 2 in. concrete cover and 12 in. bonded length (figure after Tholen and Darwin 1996).....	185
Figure 5.24 Specimen components and meshing, (a) concrete block, and (b) Steel bar.....	186
Figure 5.25 Boundary conditions.....	186
Figure 5.26 Simulations designation.....	187
Figure 5.27 Load-displacement curve for the specimen with headed bar embedded at the center with different linear-elastic coefficients.....	189
Figure 5.28 Load-displacement curve for the specimen with headed bar embedded the center with different damage (initiation and evolution) coefficients.....	189
Figure 5.29 Load-displacement curve for specimen SC; k: 0.11, 0.06, 0.06; D: 0.0039; 5.....	191
Figure 5.30 Load-displacement curve for the specimen SE; K: 0.11, 0.06, 0.06; D: 0.0039; 8, BC1.....	192
Figure 5.31 Load-displacement relationship for the simulation with headed bar close to the edge with unsymmetrical supports for the specimens SE; K: 0.11, 0.06, 0.06; D: 0.0039; 8, BC1, SE; K: 0.11, 0.06, 0.06; D: 0.0039; 8, BC2, and SE; K: 0.11, 0.06, 0.06; D: 0.0039; 8, BC3.....	193
Figure 5.32 Load-displacement curve for the simulation TE; K: 0.11, 0.06, 0.06; D: 0.0039; 5, BC2.....	194

Figure 5.33 Load-displacement curve for the simulation TE; K: 0.11, 0.06, 0.06; D: 0.0039; 5, BC2.....	195
Figure 5.34 Strain along the headed bar for the specimen (SC; K: 0.11, 0.06, 0.06; D: 0.0039; 5, BC1).....	197
Figure 5.35 (a) Load versus strain in headed bar for slab specimen SC; K: 0.11, 0.06, 0.06; D: 0.0039; 5, BC1 (b) calculated strain location.....	197
Figure 5.36 Load-displacement curve for the beam-end specimen (Darwin-Graham 1993) (12 in. embedment length and 2 in. concrete cover.....	199
Figure 5.37 (a) Load-versus displacement for 1in., 2in., and 3 in. concrete covers with 6 in. embedment length.....	201
Figure 5.38 (a) Load-versus displacement for 1in., 2in., and 3 in. concrete covers with 12 in. embedment length.....	201
Figure B1 Cross-section of the specimens with two headed bars.....	216
Figure B2 Cross-section of the specimens with three headed bars.....	216
Figure B3 Load versus deflection results for Specimens H-2-8-5-10.4-F4.1 and NH-2-8-5-10.4-F4.1 (Series 1).....	219
Figure B4 Load versus deflection results for Specimens H-2-8-5-11.4-F4.1 and NH-2-8-5-11.4-F4.1 (Series 1).....	219
Figure B5 Load versus deflection results for Specimens H-3-8-5-13-F4.1 and NH-3-8-5-13-F4.1 (Series 2).....	220
Figure B6 Load versus deflection results for Specimens H-32-8-5-11-F4.1I and NH-3-8-5-11-F4.1I (Series 2).....	220
Figure B7 Load versus deflection results for Specimens H-3-8-5-9-F4.1I and NH-3-8-5-9-F4.1I (Series 2).....	221
Figure B8 Load versus deflection results for Specimens H-2-8-5-13-F4.1I and NH-2-8-5-13-F4.1I (Series 2).....	221
Figure B9 Load-strain curve for specimen H-2-8-5-9-F4.1-1.....	222
Figure B10 Load-strain curve for specimen NH-2-8-5-9-F4.1-1.....	222
Figure B11 Load-strain curve for specimen H-2-8-5-10.4-F4.1-1.....	223

Figure B12 Load-strain curve for specimen NH-2-8-5-10.4-F4.1-1.....	223
Figure B13 Load-strain curve for specimen H-3-8-5-11.4-F4.1-1.....	224
Figure B14 Load-strain curve for specimen NH-3-8-5-11.4-F4.1-1.....	224
Figure B15 Load-strain curve for specimen H-3-8-5-14-F4.1-1.....	225
Figure B16 Load-strain curve for specimen NH-3-8-5-14-F4.1-1.....	225
Figure B17 Load-strain curve for specimen H-2-8-5-9-F4.1-2, (a) south bar, (b) north bar.....	226
Figure B18 Load-strain curve for specimen NH-2-8-5-9-F4.1-2, (a) south bar, (b) north bar.....	227
Figure B19 Load-strain curve for specimen H-2-8-5-13-F4.1-2, (a) south bar, (b) north bar.....	228
Figure B20 Load-strain curve for specimen NH-2-8-5-13-F4.1-2, (a) south bar, (b) north bar...	229
Figure B21 Load-strain curve for specimen H-3-8-5-9-F4.1-2, (a) south bar, (b) middle bar, and (c) north bar.....	231
Figure B22 Load-strain curve for specimen NH-3-8-5-9-F4.1-2, (a) south bar, (b) middle bar, and (c) north bar.....	232
Figure B23 Load-strain curve for specimen H-3-8-5-11-F4.1-2, (a) south bar, (b) middle bar, and (c) north bar.....	234
Figure B24 Load-strain curve for specimen NH-3-8-5-11-F4.1-2, (a) south bar, (b) middle bar, and (c) north bar.....	235
Figure B25 Load-strain curve for specimen H-3-8-5-13-F4.1-2, (a) south bar, (b) middle bar, and (c) north bar.....	237
Figure B26 Load-strain curve for specimen NH-3-8-5-13-F4.1-2, (a) south bar, (b) middle bar, and (c) north bar.....	238

LIST OF TABLES

Table 1.1: Nodal zone coefficient β_n	30
Table 1.2: Strut coefficient β_s	30
Table 2.1 Head dimensions	49
Table 2.2 Concrete mixture proportions.....	50
Table 2.3: Headed Bar Physical Properties.....	51
Table 2.4: Distance at center of strain gauges measured from bearing face of the head for headed end and from bar end for non-headed end (Series 1).....	57
Table 2.5: Distance at center of strain gauges measured from bearing face of the head for headed end and from bar end for non-headed end (Series 2).....	58
Table 2.6 Test Program for CCT Node Specimens.....	61
Table 3.1 Failure Modes.....	66
Table 3.2 Summary of Test Results.....	69
Table 3.3 Peak load and peak load recorded by strain gauge (kips) (Series 1).....	75
Table 3.4 Peak load and peak load recorded by strain gauge (kips) (Series 2).....	75
Table 3.5 Calculated cracking load.....	77
Table 3.6 Estimated strut and tie forces.....	94
Table 3.7 Estimated strut and node capacity and demand.....	96
Table 3.8 Estimated forces per bar using strain gauge results and strut-and-tie model.....	98
Table 3.9 Test results for headed bars in CCT node specimens in the current study and comparisons with descriptive equation [Eq. (3.2)].....	102
Table 3.10 Test results for CCT node specimens tested by Thompson et al. (2006a) and comparisons with descriptive equation [Eq. (3.2)].....	103
Table 3.11 Test results for straight bars in CCT node specimens in the current study and comparisons with ACI 408R-03 [Eq. (3.4)].....	105
Table 4.1: Modification factor ψ_{cs} for confining reinforcement and spacing.....	113

Table 4.2: Modification factors for development of headed bars in tension.....	114
Table 4.3 Confinement and spacing factor ψ_{cs}	115
Table 4.4: Test results for widely-spaced bars without confining reinforcement.....	122
Table 4.5: Test results for closely-spaced bars without confining reinforcement.....	123
Table 4.6: Comparisons for widely-spaced bars with confining reinforcement.....	125
Table 4.7: Comparisons for closely-spaced bars with confining reinforcement.....	126
Table 4.8: Max, Min, Mean, STD, and COV of T/T_{318-14} for headed bars without confining reinforcement.....	129
Table 4.9: Max, Min, Mean, STD, and COV of T/T_{318-14} for headed bars with confining reinforcement.....	130
Table 4.10: Max, Min, Mean, STD, and COV of T/T_{Shao} for headed bars without confining reinforcement.....	134
Table 4.11: Max, Min, Mean, STD, and COV of T/T_{Shao} for headed bars with confining reinforcement.....	135
Table 4.12: Max, Min, Mean, STD, and COV of T/T_{318-19} for headed bars without confining reinforcement.....	138
Table 4.13: Max, Min, Mean, STD, and COV of T/T_{318-19} for headed bars with confining reinforcement.....	139
Table 4.14: Max, Min, Mean, STD, and COV of T/T_D for headed bars without confining Reinforcement.....	142
Table 4.15: Max, Min, Mean, STD, and COV of T/T_D for headed bars with confining reinforcement.....	143
Table 4.16: Max, Min, Mean, STD, and COV of $T/\phi N_{str}$ for headed bars without confining reinforcement.....	148
Table 4.17: Max, Min, Mean, STD, and COV of $T/\phi N_{str}$ for headed bars with confining reinforcement.....	149
Table 4.18: Comparisons for widely-spaced bars without confining reinforcement ($d_{eff}/\ell_{eh} \geq 1.5$).....	151

Table 4.19: Comparisons for closely-spaced bars without confining reinforcement ($d_{eff}/\ell_{eh} \geq 1.5$).....	151
Table 4.20: Comparisons for widely-spaced bars with confining reinforcement ($d_{eff}/\ell_{eh} \geq 1.5$).....	152
Table 4.21: Comparisons for closely-spaced bars with confining reinforcement ($d_{eff}/\ell_{eh} \geq 1.5$).....	152
Table 4.22: Comparisons for widely-spaced bars with confining reinforcement (strut-and-tie).....	153
Table 4.23: Comparisons for closely-spaced bars with confining reinforcement (strut-and-tie).....	153
Table 4.24: Max, Min, Mean, STD, and COV of T/T_{Shao} for headed bar specimens with $d_{eff}/\ell_{eh} \geq 1.5$ without confining reinforcement.....	155
Table 4.25: Max, Min, Mean, STD, and COV of $T/\phi N_{str}$ for headed bar specimens with $d_{eff}/\ell_{eh} \geq 1.5$ without confining reinforcement.....	156
Table 4.26: Max, Min, Mean, STD, and COV of T/T_{Shao} for headed bar specimens with $d_{eff}/\ell_{eh} \geq 1.5$ with confining reinforcement.....	157
Table 4.27: Max, Min, Mean, STD, and COV of $T/\phi N_{str}$ for headed bar specimens with $d_{eff}/\ell_{eh} \geq 1.5$ with confining reinforcement.....	158
Table 4.28: Max, Min, Mean, STD, and COV of R_1/T_{STM} for headed bar specimens with $d_{eff}/\ell_{eh} \geq 1.5$ with confining reinforcement.....	160
Table 5.1 Model Parameters for concrete compressive strength of 5 ksi and 8 ks.....	166
Table 5.2 Values of linear-elastic and damage (initiation and evolution) coefficients.....	190
Table 5.3 Values of linear-elastic and damage (initiation and evolution) coefficients.....	193
Table 5.4 Values of linear-elastic and damage (initiation and evolution) coefficients.....	194
Table 5.5 Values of linear-elastic and damage (initiation and evolution) coefficients.....	199
Table 5.6 Values of linear-elastic and damage (initiation and evolution) coefficients.....	202
Table B.1 CCT node specimen detail.....	217
Table B.1 Cont. Details of the CCT node specimens.....	218
Table C.1 Details of the widely-spaced bars without confining reinforcement.....	239

Table C.1 Cont'd Details of the widely-spaced bars without confining reinforcement.....	240
Table C.1 Cont'd Details of the widely-spaced bars without confining reinforcement.....	241
Table C.1 Cont'd Details of the widely-spaced bars without confining reinforcement.....	242
Table C.1 Cont'd Details of the widely-spaced bars without confining reinforcement.....	243
Table C.1 Cont'd Details of the widely-spaced bars without confining reinforcement.....	244
Table C.1 Cont'd Details of the widely-spaced bars without confining reinforcement.....	245
Table C.1 Cont'd Details of the widely-spaced bars without confining reinforcement.....	246
Table C.2 Details of the closely-spaced bars without confining reinforcement.....	247
Table C.2 Cont'd Details of the closely-spaced bars without confining reinforcement.....	248
Table C.2 Cont'd Details of the closely-spaced bars without confining reinforcement.....	249
Table C.2 Cont'd Details of the closely-spaced bars without confining reinforcement.....	250
Table C.2 Cont'd Details of the closely-spaced bars without confining reinforcement.....	251
Table C.2 Cont'd Details of the closely-spaced bars without confining reinforcement.....	252
Table C.2 Cont'd Details of the closely-spaced bars without confining reinforcement.....	253
Table C.2 Cont'd Details of the closely-spaced bars without confining reinforcement.....	254
Table C.3 Details of the widely-spaced bars with confining reinforcement.....	255
Table C.3 Cont'd Details of the widely-spaced bars with confining reinforcement.....	256
Table C.3 Cont'd Details of the widely-spaced bars with confining reinforcement.....	257
Table C.3 Cont'd Details of the widely-spaced bars with confining reinforcement.....	258
Table C.3 Cont'd Details of the widely-spaced bars with confining reinforcement.....	259
Table C.3 Cont'd Details of the widely-spaced bars with confining reinforcement.....	260
Table C.3 Cont'd Details of the widely-spaced bars with confining reinforcement.....	261
Table C.3 Cont'd Details of the widely-spaced bars with confining reinforcement.....	262

Table C.4 Details of the closely-spaced bars with confining reinforcement.....	263
Table C.4 Cont'd Details of the closely-spaced bars with confining reinforcement.....	264
Table C.4 Cont'd Details of the closely-spaced bars with confining reinforcement.....	265
Table C.4 Cont'd Details of the closely-spaced bars with confining reinforcement.....	266
Table C.4 Cont'd Details of the closely-spaced bars with confining reinforcement.....	267
Table C.4 Cont'd Details of the closely-spaced bars with confining reinforcement.....	268
Table C.4 Cont'd Details of the closely-spaced bars with confining reinforcement.....	269
Table C.4 Cont'd Details of the closely-spaced bars with confining reinforcement.....	270
Table C.5 Details of the widely-spaced bars without confining reinforcement.....	271
Table C.5 Cont'd Details of the widely-spaced bars without confining reinforcement.....	271
Table C.5 Cont'd Details of the widely-spaced bars without confining reinforcement.....	272
Table C.5 Cont'd Details of the widely-spaced bars without confining reinforcement.....	272
Table C.6 Details of the closely-spaced bars without confining reinforcement.....	273
Table C.6 Cont'd Details of the closely-spaced bars without confining reinforcement.....	273
Table C.6 Cont'd Details of the closely-spaced bars without confining reinforcement.....	274
Table C.6 Cont'd Details of the closely-spaced bars without confining reinforcement.....	274
Table C.7 Details of the widely-spaced bars with confining reinforcement.....	275
Table C.7 Cont'd Details of the widely-spaced bars with confining reinforcement.....	276
Table C.7 Cont'd Details of the widely-spaced bars with confining reinforcement.....	277
Table C.7 Cont'd Details of the widely-spaced bars with confining reinforcement.....	278
Table C.8 Details of the closely-spaced bars with confining reinforcement.....	279
Table C.8 Details of the closely-spaced bars with confining reinforcement.....	280
Table C.8 Details of the closely-spaced bars with confining reinforcement.....	281

Table C.8 Details of the closely-spaced bars with confining reinforcement.....282

CHAPTER 1: INTRODUCTION

1.1 GENERAL

Reinforced concrete is a composite material consisting of reinforcing steel and concrete. Concrete is strong when loaded in compression but is very weak when loaded in tension. Reinforcing steel is very strong when loaded in compression or tension. In reinforced concrete members, sufficient bond must exist between the reinforcing bars and surrounding concrete to allow for forces to be transferred from the steel to the concrete. The ACI Building Code, ACI 318-14, does so by requiring a minimum *development length*. Development length is the length of bar in contact with concrete needed to develop its yield strength. Many factors affect the development length of reinforcing bars, including the bar diameter, spacing between bars, yield strength to be developed, amount of transverse reinforcement (confining reinforcement), and concrete compressive strength.

In practice, the dimensions of structures are not always adequate to accommodate the development length of straight bars. In such cases, hooked or headed bars can be used to shorten the required development length. Of the two, headed bars allow easier installation and result in less congestion.

In ACI 318-14, the headed bar development length provisions restrict the yield strength of the bars to 60 ksi (420 MPa). The maximum concrete compressive strength permitted in the calculation of development length is limited to 6,000 psi (42 MPa). The design equation does not consider the spacing between bars.

The experimental work in this study is a portion of a larger study performed at the University of Kansas to investigate the behavior of headed bars in tension for concrete compressive strengths up to 16,000 psi (110 MPa) and bar stresses up to 153 ksi (1055 MPa) in beam-column joints. Based on the test results, Shao et al. (2016) proposed a new code provisions for the development length of headed bars. The new provisions were developed based on tests of 202 exterior beam-column joint specimens subjected to monotonic loading. The provisions consider the effect of confining reinforcement and spacing between headed bars while permitting the use of concrete compressive strengths up to 16,000 psi (110 MPa) and steel yield strengths up to 120 ksi

(830 MPa). The experimental work in the current study focused on investigating the behavior of the headed bars anchored at the end of a beam at a compression-compression-tension (CCT) node. This study also compares the anchorage strength of headed bars in tension using design provisions for headed bars from ACI 318-14, Shao et al. (2016), ACI 318-19, and Darwin and Dolan (2021), as well as the anchorage provisions in Chapter 17 of ACI 318-19 with test results. Finally, a granular micromechanics model is evaluated for its applicability for use in finite element modeling of anchorage of headed and straight reinforcing bars to concrete.

In this chapter, the mechanism of bond for straight, hooked, and headed bars is presented with a detailed discussion of the historical background and previous research work on headed bars. A detailed discussion of the historical background of the strut-and-tie model; procedures for strut-and-tie design; dimensioning of nodes, struts, and ties; limitations on the strut-and-tie angle; strength of nodes; strength of struts; and previous research work is also covered. Finally, background of the finite element method, the concepts of elements and nodes, degrees of freedom (DOF), modeling of material failure-fracture, and previous research work are introduced.

1.2 MECHANISM OF BOND

1.2.1 Straight Reinforcing Bars

Deformed reinforcing bars are usually used in the reinforcement of concrete members rather than smooth or non-deformed bars because the deformations (ribs) on the bar provide a bearing area that allows for the force transfer from the reinforcing bar to the surrounding concrete. This is in addition to bond forces from adhesion and friction forces along the surface of the bar, as shown in Figure 1.1.

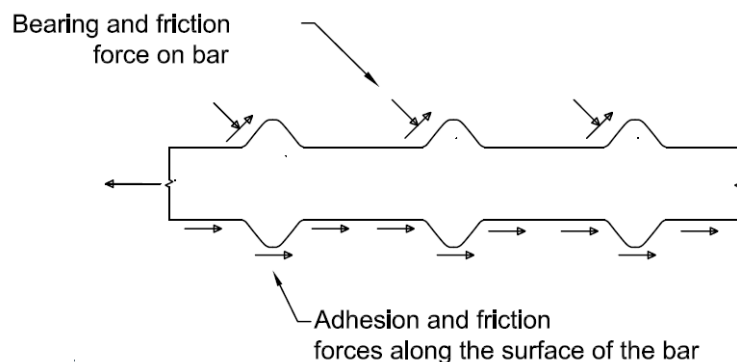


Figure 1.1 Bond forces components (figure after ACI Committee 408-2003)

1.2.2 Hooked Reinforcing Bars

The anchorage capacity of a hooked bar is the sum of the bond strength of the straight portion of the bar and the bearing of the bent portion, as shown in Figure 1.2 for a 90° hook. The hook loses bond with the neighboring concrete along the outer radius when the straight portion of the bar slips. Concrete in contact with the inside of the bend is subjected to compression. When the compressive stress increases, crushing of the concrete can occur.

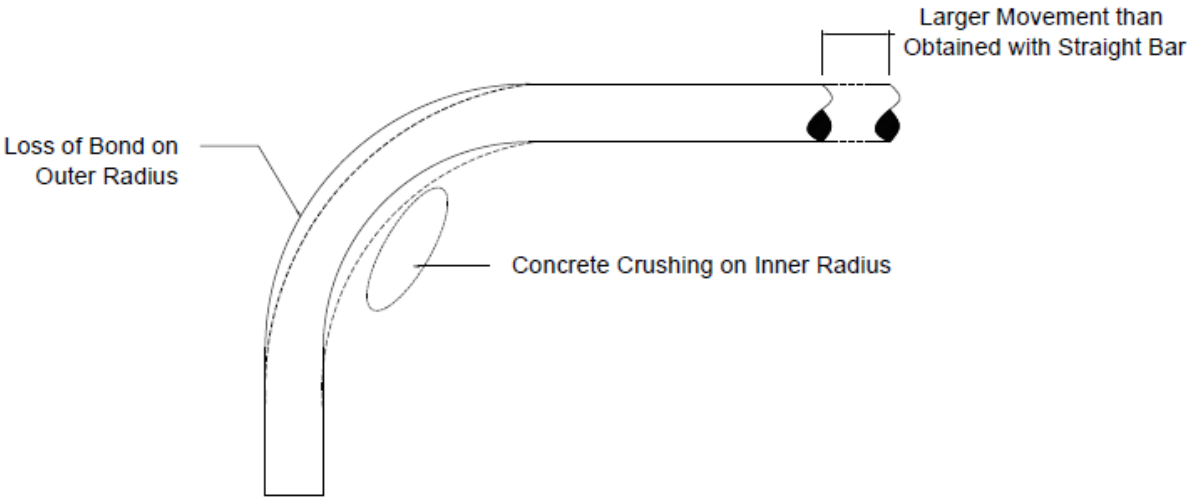


Figure 1.2 Behavior of 90° hooked bar subjected to tensile force (deformations not shown)
(figure after Minor 1971)

A standard hook is a specific type of hook, defined by ACI 318-14 in terms of radius of bend and straight tail extension after the bend, as shown in Figure 1.3, which also shows the details of 90° and 180° standard hooks.

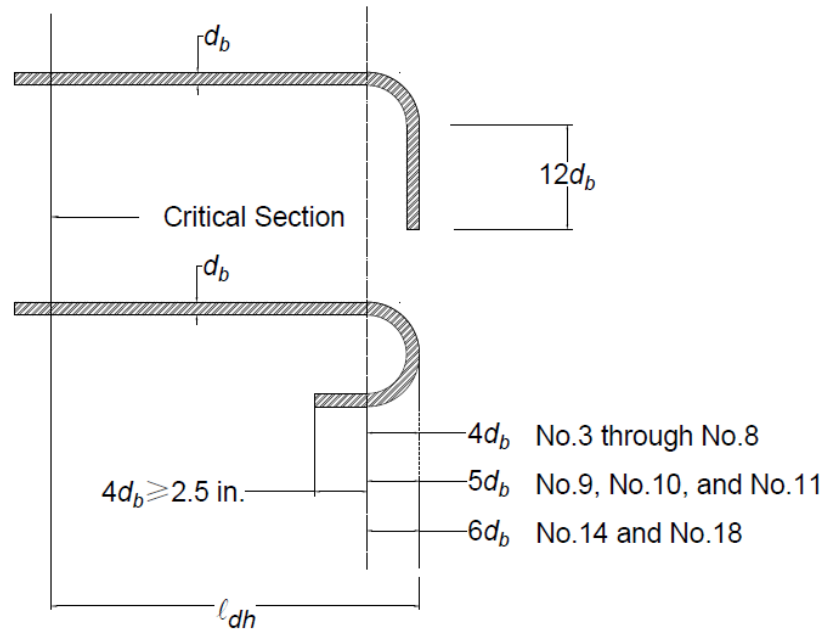


Figure 1.3 Standard hook dimensions (figure after ACI 318-11)

1.2.3 Headed Reinforcing Bars

Headed bars are made by connecting a straight reinforcing bar to a head (a plate or nut) to produce a greater bearing area which provides capacity to anchor the bar. The bond force in the bar includes a combination of the bearing of the ribs (bar deformations) and head (Thompson 2002) as shown in Figure 1.4.

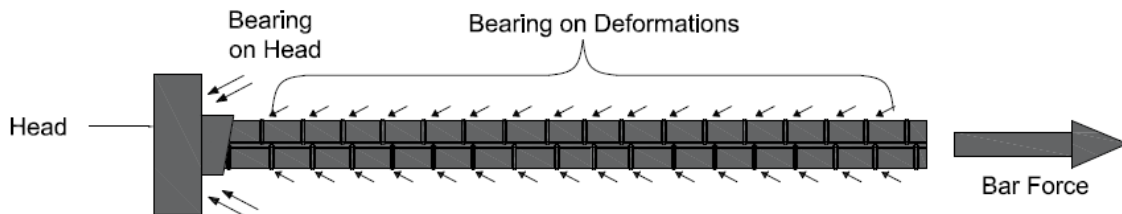


Figure 1.4 Headed bar (figure after Thompson 2002)

Heads are available in various shapes such as squares, rectangles, circles, and elliptical. According to ASTM A970, heads of Class HA must develop the specified tensile strength of the bar. ACI 318-14 permits Class HA heads to be used in reinforced concrete structures.

Heads are also available in various sizes. The head size is defined by the net bearing area (A_{brg}), equal to the gross area of the head minus the nominal area of the deformed reinforcing bar (A_b). According to Annex A1 of ASTM A970-18, the net bearing area of the head (A_{brg}) must be greater than or equal to four times the nominal cross-sectional area of the bar ($A_{brg} \geq 4A_b$).

There are also limits on obstructions on headed bars from the manufacturing process. According to ASTM A970 -18 and as shown in Figure 1.5, the obstruction length as measured from the bearing face of the head should be less than or equal to 5.25 times the nominal bar diameter. The transverse dimension should be less than or equal to 2.2 times the nominal bar diameter. The net bearing area of the bar with obstructions that meet the requirements of ASTM A970 -18 equal to the gross area of the head minus the maximum area of the obstruction and must be greater than or equal to four times the nominal cross-sectional area of the bar.

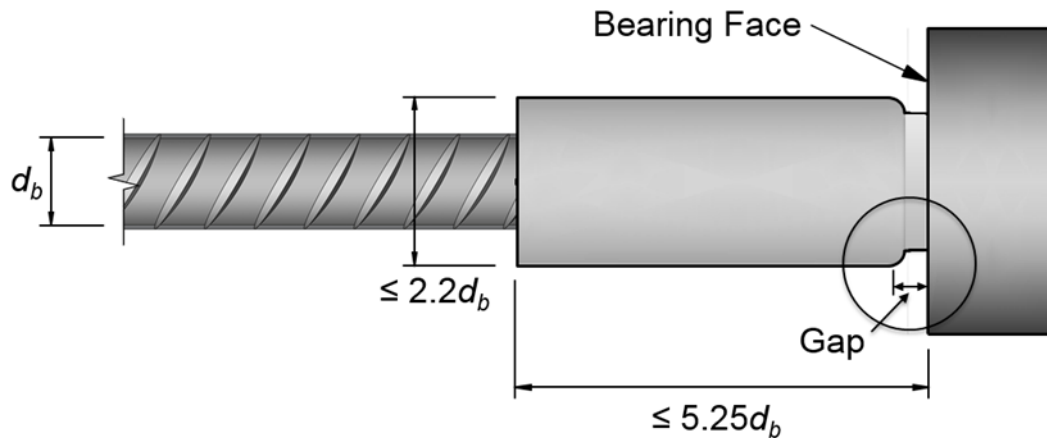


Figure 1.5 Required dimensions of obstructions for headed bars (figure from ASTM A970-18)

1.3 HISTORICAL DEVELOPMENT OF HEADED BARS

Headed reinforcing bars developed from headed steel anchor studs. Headed steel anchor studs are usually used as a link to connect steel girders and concrete deck slabs. Many studies have been performed on headed steel anchor studs. The earliest study was performed in 1973 by

McMackin, Slutter, and Fisher who tested 60 anchor studs embedded in twelve concrete blocks. Twenty-six anchor studs were subjected to combined shear and tension loading, 22 were subjected to pure tension, 12 were subjected to pure shear. The parameters under study were concrete type (normalweight and lightweight), length of the anchor studs, loading angle (for the combined shear and tension), and the distance from the free edge. The concrete compressive strength varied from 4,900 psi to 5,300 psi (34 to 37 MPa). Three modes of failure were observed from this test: severe concrete cracking; failure of the stud anchor; and concrete cone pullout. McMackin, Slutter, and Fisher suggested design requirements for headed steel anchor studs subjected to the effect of both shear and tension loading.

In a 1974 study, the California Department of Transportation (CALTRANS) performed 19 pullout tests. Figure 1.6 shows a typical test specimen. The test involved Grade 60 No. 11, No. 14, and No. 18 (No. 36, No. 44, and No. 57) bars with a welded steel end plate that provided a net bearing area of $15A_b$ for No. 11 and No. 14 bars and $13A_b$ for No. 18 bars. The concrete compressive strength was 4,600 psi (32 MPa). The objective of the study was to evaluate the end anchorage provided by a connected steel end plate. The results showed that shorter embedment lengths could be used when the steel plate was used.

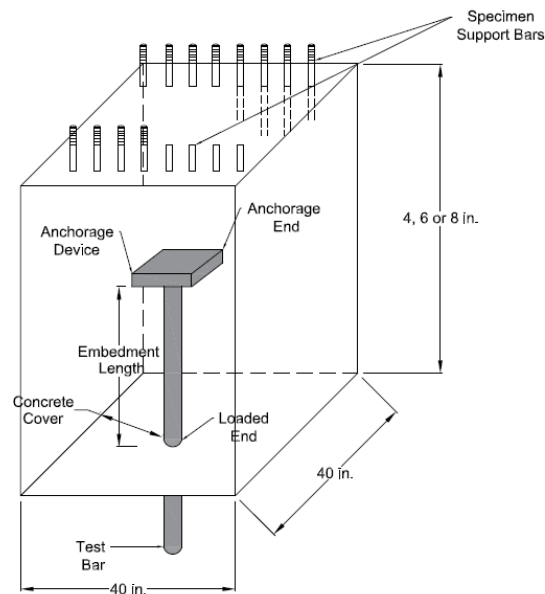


Figure 1.6 Test specimen with anchorage provided by welded steel end plate (figure after CALTRANS 1974)

Mokhtar, Ghali, and Dilger (1985) tested shear studs consisting of vertical bars with square anchor heads welded at one end and a steel strip welded at the other, as shown in Figure 1.7, used as punching shear reinforcement in flat concrete plates. Eight full-sized slab-column connections were tested under concentric load. One of the specimens was tested without reinforcement while the remaining seven specimens were reinforced against punching shear with shear studs. Concrete compressive strength ranged from 3,340 to 5,950 psi (23 to 41 MPa) and yield strength of shear studs ranged from 40.3 to 70.9 ksi (278 to 489 MPa). Mokhtar et al. (1985) found that the shear studs were effective as punching shear reinforcement.

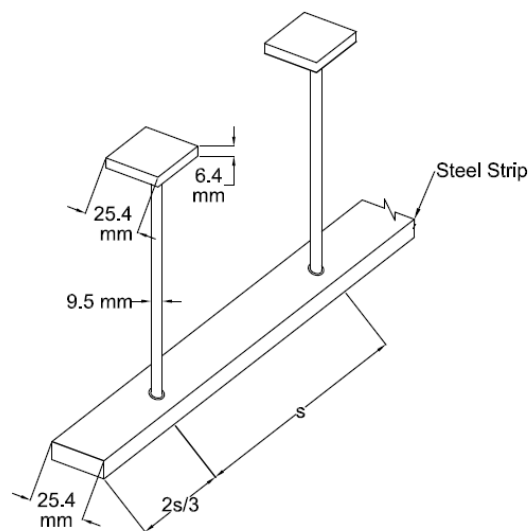


Figure 1.7 Details of the shear studs welding (figure after Mokhtar, Ghali, and Dilger, 1985)

Following the work by Mokhtar et al. (1985), the Alaska Oil and Gas Association (AOGA) studied the use of double-headed studs. Two uses were investigated: double headed-bars as shear reinforcement in heavily reinforced concrete offshore oil platforms and as an alternative to hooked bars. As a result, they recommended using headed bars as longitudinal reinforcing bars in structural members (Berner, Gerwick, and Hoff 1991). Norwegian Contractors and Metalock (a British supplier of industrial services for structural contractors) worked as a team to study and produce the headed bars. They contracted with SINTEF (an independent research organization in Norway) to design a headed bar. Based on the study, a friction-welded headed bar was designed. The friction-welded headed bars were used in many offshore and coastal structures (Berner and Hoff

1994). Metalock established Headed Reinforcement Corporation (HRC) as a North American company for producing and selling friction-welded headed bars.

1.4 PREVIOUS RESEARCH ON HEADED REINFORCING BAR ANCHORAGE

Using headed bars in structural buildings was restricted until the end of the 20th century due to limited experimental results involving headed bars. A summary of recent research on headed bars follows.

1.4.1 Bashandy (1996)

Bashandy (1996) performed 25 pullout tests on No. 11 (No. 36) headed bars with specimens divided into two groups. The first group contained 14 specimens with headed bars installed in concrete cubes. Bashandy focused on studying the impact of cyclic loading with the heads installed behind a crossing bar. The crossing bar consisted of a No. 8 (No. 25) or No. 11 (No. 36) bar installed perpendicular to the headed bar and against the bearing face of the head. The gross area of the heads ranged from $3A_b$ to $8.1A_b$. The concrete compressive strength was 3,200 psi (22 MPa), and the steel yield strength was 84 ksi (580 MPa) and 81 ksi (560 MPa) for No. 8 (No. 25) and No. 11 (No. 36) bars, respectively. The second group contained 11 specimens with No. 6 (No. 20) headed bars used as transverse reinforcement. The concrete compressive strength was 3,950 psi (72.2 MPa), and steel yield strength was 78.3 ksi (540 MPa).

Bashandy found that cyclic loading (up to 15 cycles) has no effect on the anchorage capacity, while the presence of the crossing bar enhances the capacity of the headed bars. Bashandy also found that headed bars could be used as transverse reinforcement in place of the traditional transverse reinforcement.

Bashandy (1996) also tested 32 large-scale beam-column joint specimens. The specimens were designed to represent exterior beam-column joints and were used to study the effect of bar size (No. 8 and No. 11) (No. 25 and No. 36), head size (gross area of the head) ranging from $3A_b$ to $8.1A_b$; head orientation (the long side of the rectangular head is placed horizontally or vertically); embedment length (including the thickness of the head), which ranged from 9 to 18 in. (229 to 457 mm); concrete compressive strength, which ranged from 3,200 to 5,740 psi (22 to 40 MPa); clear concrete cover, 1.5 in. (38 mm) or 3 in. (76 mm); and transverse reinforcement in the joint region,

either no hoops or No. 3 (No. 10) hoops spaced at 2 in. (51 mm) or 4 in. (102 mm). All specimens contained two headed bars. The specimen width was 12 in. (305 mm). The spacing between the headed bars varied based on the concrete cover and depth of the specimens varied based on the embedment length. For the specimens with 3 in. (76 mm) concrete cover, the outside-to-outside headed bar spacing was 6 in. (152 mm), and heads were placed inside the column core (headed bars considered to be inside column core when a side cover to the bar ≥ 2.5 in. (64 mm)). For the specimens with 1.5 in. (38 mm) concrete cover, the outside-to-outside headed bar spacing was 9 in. (229 mm) and heads were placed outside the column core. Strain gauges were placed on the bar about 1 in. (25.4 mm) from the face of the head. Figure 1.8 shows the test set up. The headed bars embedded in the column represented the longitudinal reinforcement of the assumed beam, and a 2-in. (51-mm) thick plate was placed below the headed bars to represent the compression zone of the assumed beam.

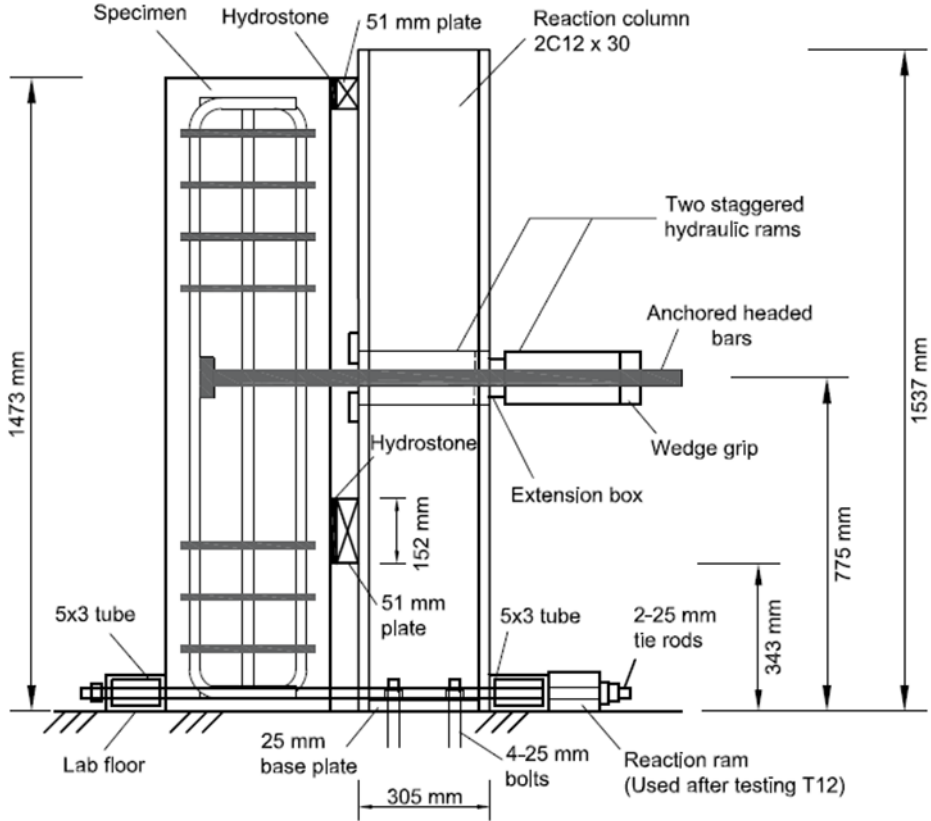


Figure 1.8 Test configuration for an exterior beam-column joint specimen (figure after Bashandy 1996)

Bashandy found that for the beam-column joint specimens, increasing the embedment length, head area, concrete cover, and confining transverse reinforcement in the joint region increased the anchorage capacity of the headed bar. The effect of the head orientation and bar diameter was insignificant. A new design equation was proposed by Bashandy to establish the development length needed for a headed bar anchored in an exterior joint, presented as Eq. (1.1).

$$l_d = \frac{A_b f_y}{14.7 \alpha \beta \gamma \sqrt[3]{A_n} \sqrt{f'_c}} + d' \quad (1.1)$$

where l_d is the embedment length, including head thickness, (mm); A_b is the area of the anchored bar (mm^2); f_y is the yield stress of the anchored bar (MPa); d' is the distance from the face of the column to the centroid of the column longitudinal reinforcement nearest to the face (mm); A_n is the head net bearing area (mm^2); f'_c is the concrete compressive strength (MPa); α is the confining reinforcement factor, taken as 1.4 for tie spacing less than 51 mm, 1.25 for spacing between 100 mm and 51 mm, and 1 for tie spacing greater than 100 mm; β is the cover size factor, taken as 0.8 for side cover less than 76 mm, and 1 for all other cases; and γ is the anchorage condition factor, taken as 1.25 for heads positively anchored behind 25 mm or larger crossing bars, and 1 for all other anchorage cases.

The embedment length of headed bars based on Eq. (1.1) for an $8A_b$ head size is about 70% of the embedment length calculated based on the ACI 318-95 provisions for standard hooks. According to ACI 318-95, the basic development length (ℓ_{hb}) for hooked bars is as shown in Eq. (1.2)

For hooked bars with f_y equal to 60,000 psi

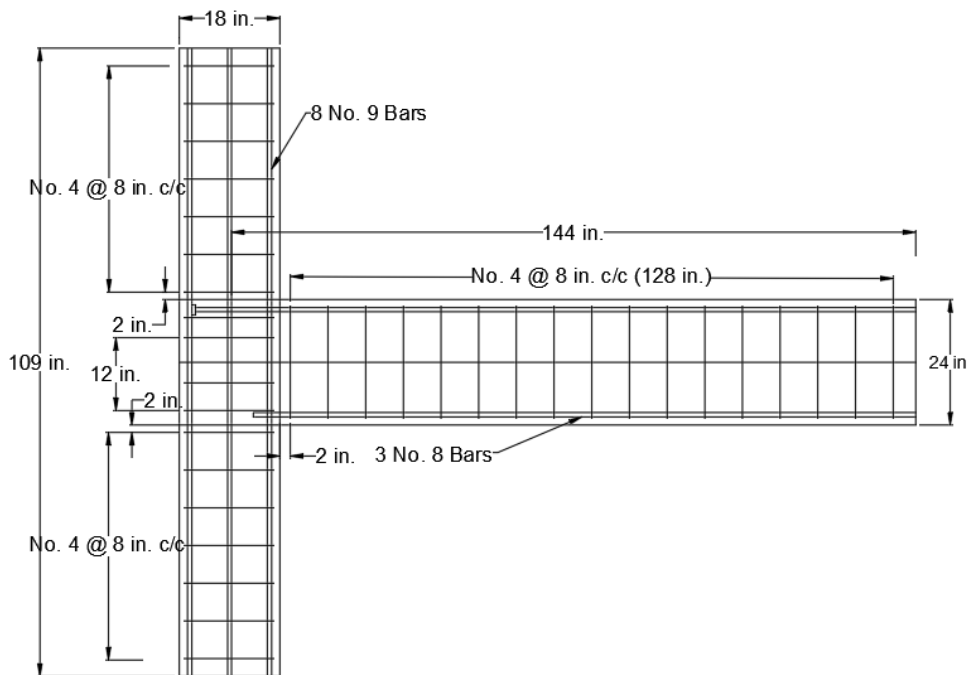
$$l_{hb} = 1200 d_b / \sqrt{f'_c} \quad (1.2)$$

For hooked bars with f_y other than 60,000 psi, basic development length (ℓ_{hb}) was multiplied by factors for bar yield strength, concrete cover, ties or stirrups, excess reinforcement, lightweight aggregate concrete, and epoxy-coated reinforcement.

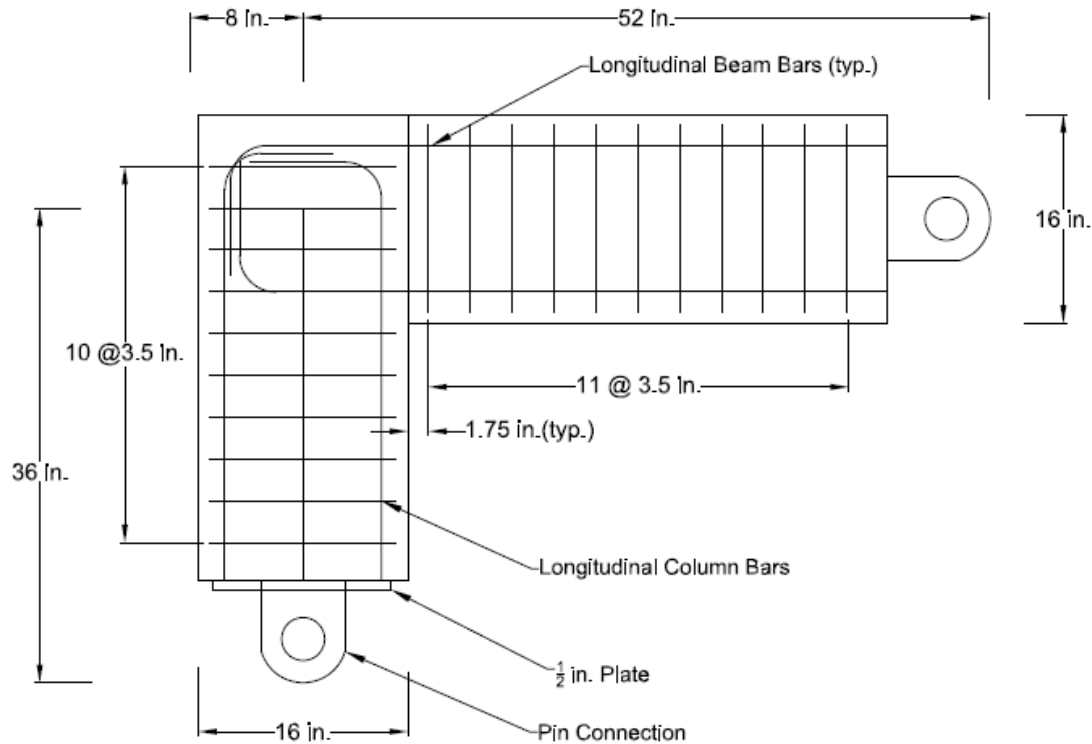
Bashandy (1996) tested one exterior beam-column subassembly under cyclic loading to study the possibility of using headed bars instead of hooked bars in seismic regions. A similar specimen anchored with a hooked bar was tested by Smith (1972). The specimen with the headed-bar exhibited little bond degradation and less capacity deterioration than the hooked-bar specimen tested by Smith (1972).

1.4.2 Wallace, McConnell, Gupta, and Cote (1998)

Wallace, McConnell, Gupta, and Cote (1998) investigated seven specimens. Two of the seven were large-scale exterior beam-column joint specimens with the beam reinforcement anchored with taper-threaded heads (Figure 1.9a), one tested under cyclic loading and the other tested under monotonic loading. The other five specimens were corner joint specimens (Figure 1.9b); three with the beam reinforcement anchored with heads and two with the beam reinforcement anchored with 90° hooks. The five corner joint specimens were tested under cyclic loading. Concrete compressive strength ranged from 5,390 to 7,480 psi (38 to 52 MPa) and the reinforcement yield stress was 60 ksi (414 MPa). The heads were circular with a diameter of 2.25 in. (57 mm) and thickness of 1.375 in. (35 mm).



(a) Exterior beam-column joint



(b) Corner joint

Figure 1.9 Exterior beam-column joint and corner joint, (a) Exterior beam-column joint, (b) Corner joint (figure after Wallace, McConnell, Gupta, and Cote 1998)

Wallace, McConnell, Gupta, and Cote (1998) concluded that for the exterior joint specimens, headed bars provided a viable option for anchoring reinforcement. For corner joint specimens, transverse reinforcement was needed to ensure that the heads were adequately restrained, not pushing off the concrete cover. Using headed bars reduced the reinforcement congestion and led to easier fabrication and concrete placement.

1.4.3 Thompson, Ziehl, Jirsa, and Breen (2005-2006); Thompson et al. (2005, 2006)

Thompson et al. (2005) tested 64 beam specimens with headed bars anchored in compression-compression-tension (CCT) nodes, with and without confining reinforcement in the nodal zone region. Fifty-nine of the specimens were tested without confining reinforcement in the nodal zone region (Figure 1.10) and reinforced with only a (tension) tie bar (bottom bar) in the

same region. Five CCT specimens were tested with confining reinforcement within the nodal zone region (Figure 1.11) in the form of stirrup perpendicular to the tie bar. The bar sizes used were No. 8 (No. 25) and No. 11 (No. 36), concrete compressive strengths ranged from 3,050 to 4,060 psi (21 to 28 MPa), yield strength of the tie bars ranged from 61-68 ksi (420-486.8 MPa). Strut angles of 30°, 45°, and 55° were used. Head size (based on net head bearing area) ranged from 1.2 to 10.44_b, rectangular heads were orientated with the long side of the head placed horizontally or vertically. For the comparison, Thompson et al. (2005) also tested specimens with hooked and straight bars.

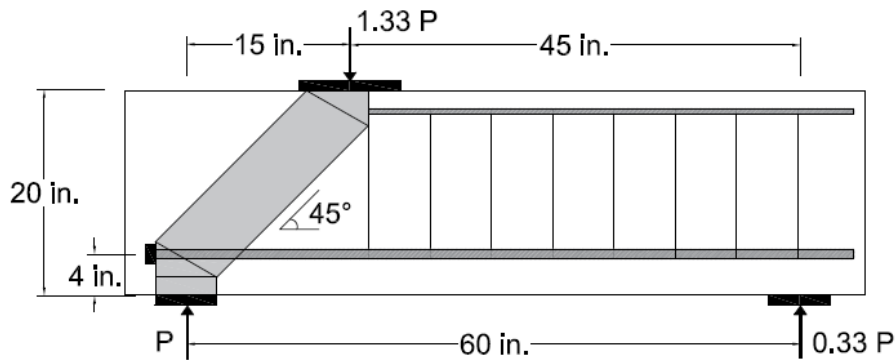


Figure 1.10 Details of unconfined specimen (figure after Thompson et al. 2005)

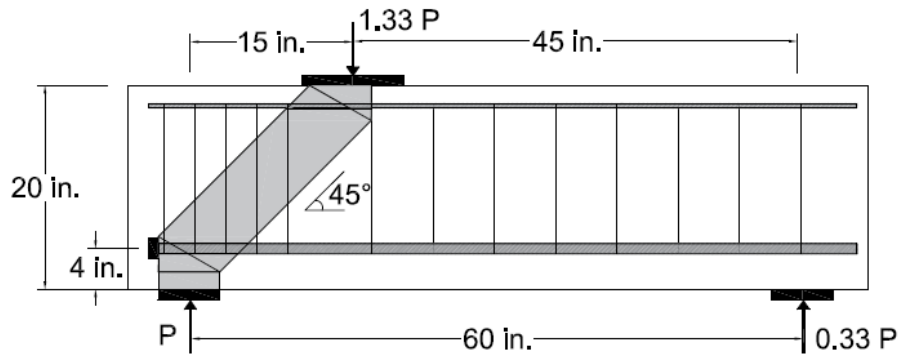


Figure 1.11 Details of confined specimen (figure after Thompson et al. 2005)

Strain gauges were installed at a number of locations on the tie reinforcing bars to measure the strain profile, which was subsequently converted to stress. Thompson et al. (2005) found that when the stress in the bar reaches the maximum value, the location of the critical anchorage point in a CCT node can be estimated as the intersection point of the tie bar with the edge of the diagonal strut. This matches the recommendation of the ACI 318-02 about the extended nodal zone.

Thompson et al. (2005) concluded that the anchorage of headed bars undergoes a transition as load is applied. Initially, load is carried by the bond force along the straight portion of the bar.

As load increases, however, bond along the straight portion of the bar decreases (due to slippage), and some of the force is transferred to the head, which bears against the concrete. The maximum bond and bearing forces do not occur at the same time, and anchorage capacity coincides with maximum bearing and a reduced contribution from the bond force along the straight portion of the bar.

During the test, three modes of failure were observed:

1. **Pullout of the tie bar from the CCT node:** This failure mode was observed in all specimens that were anchored with straight bars and is shown in Figure 1.12. Pullout failure occurred due to opening of cracks near the node. In general, the slip of the bar resulted in only one primary crack propagating at failure, with very little crack distribution.
2. **Ductile yielding of the headed tension tie bar:** Eleven headed bar specimens failed by yielding the tie bar.
3. **Rupture of the concrete strut:** Specimens in which the headed bar did not yield and all of the specimens anchored with hooked bars exhibited rupture failure in the strut and node region. For the headed bar specimens containing smaller rectangular heads oriented vertically (net bearing area $< 4.04A_b$), splitting of the diagonal compression strut along a transverse plane was observed, while for the headed bar specimens containing large rectangular heads oriented horizontally (net bearing area ranging from $4.04A_b$ to $10.4A_b$), the rupture failure was characterized by crushing of the concrete near the bottom face of the strut. Figure 1.13 shows the two rupture failure modes.

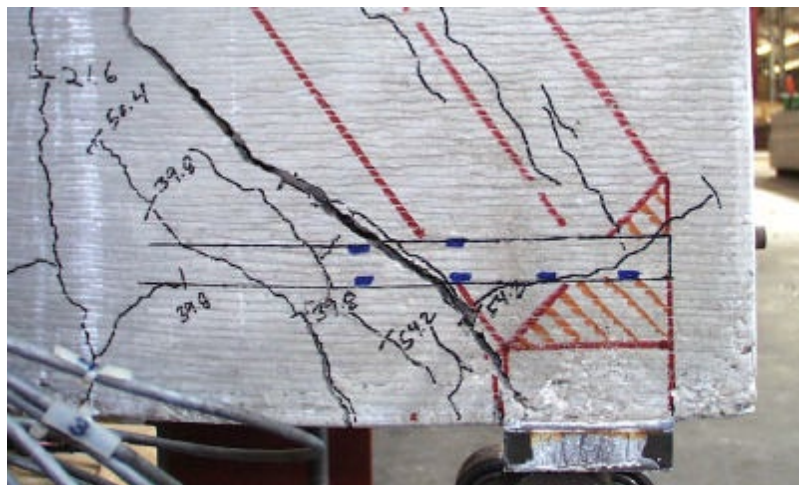


Figure 1.12 Pullout failure of straight bar (figure from Thompson 2002)

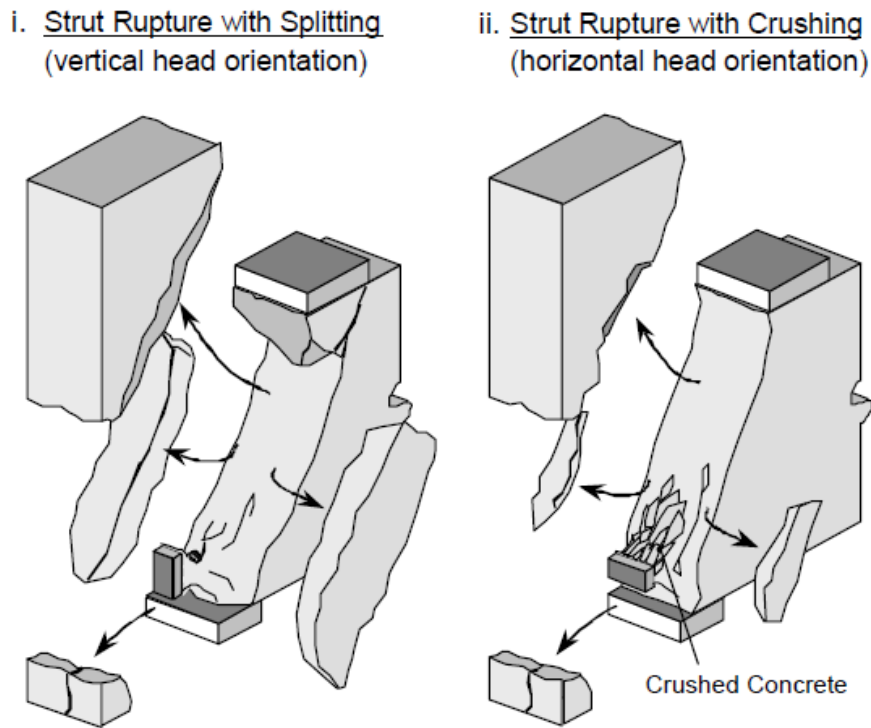


Figure 1.13 Rupture failure in the strut and node region (figure from Thompson 2002)

Thompson et al. (2005) also found that increasing the strut angle decreased the anchorage capacity of the headed bar because of the reduction in the bonded length (development length) along the tension tie bar (headed bar). The specimens in which the headed bars were confined with stirrups exhibited little change in anchorage strength compared to that measured in specimens without stirrups. Large head sizes lead to decreased slip of the head, as well as resulted in higher stress in the bar head and lower force transferred by bar over its length.

Thompson et al. (2006) used the results from the CCT node tests along with data from previous tests on deeply embedded anchor bolts, bearing strength of concrete blocks, and headed reinforcement to examine node and strut stress limits and strength models for the headed bearing. The node and strut stress limits in Appendix A of ACI 318-02 were compared with the experimental data. The values based on Appendix A of ACI 318-02 significantly underestimated of the capacity measured in the tests and comparisons exhibited significant scatter.

The failure forces at the heads from the experimental data were compared with strengths calculated in accordance with ACI 318-02, Sections D.5.4 (anchorage, side-face blowout) and

10.17 (bearing). The strut-and-tie provisions of Appendix A provided less accurate results than the results from Sections D.5.4. and 10.17. The maximum stress in the bar was calculated based on both sections, and the results were compared with 26 CCT node tests from database. The results based on side-blowout were conservative for all but four tests, with a mean ratio of test-to-calculated value of 1.25, and provided good precision, with a standard deviation of 0.23 and a coefficient of variation (COV) of 18%. The bearing model provisions were unconservative for 13 tests, with a mean of 0.93, standard deviation of 0.18, and COV of 19.3%. Thompson et al. (2006) concluded that CCT nodes in which headed bars are anchored fail when the head bearing pressure reaches its limit, which can be described by Eq. (1.3).

$$\text{Bearing pressure, } \frac{N}{A_{nh}} = 0.9 f'_c \left(\frac{2c}{\sqrt{A_{nh}}} \right) \psi \quad (1.3)$$

where N is the head capacity (kips); A_{nh} is the net head bearing area (in.²); f'_c is the concrete compressive strength (ksi); c is the minimum side cover (in.); c_2 is the secondary side cover (the smallest side cover measured perpendicular to the minimum side cover) (in.), as shown in Figure 1.14; and ψ is the radial disturbance factor, $\psi = 0.6 + 0.4(c_2/c) \leq 2.0$. The dimensional variables are shown in Figure 1.14.

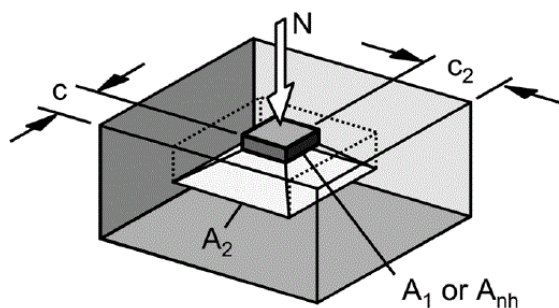


Figure 1.14 Dimensional variables in the bearing capacity model (figure from Thompson et al. 2006)

Thompson et al. (2006), found that the development length equation for deformed bars in ACI 318-02, Section 12.2.3 (see Eq. 1.4) poorly modeled the anchorage capacity of the headed bars. They suggested more research on this subject.

$$\ell_d = \left(\frac{3}{4} \frac{f_y}{\sqrt{f'_c}} \frac{\alpha\beta\gamma\lambda}{\left(\frac{c + K_{tr}}{d_b} \right)} \right) \quad (1.4)$$

where the term $(c + K_{tr})/d_b$ shall not be taken greater than 2.5.

1.4.4 Chun et al. (2009)

Chun et al. (2009) tested 30 beam-column joint specimens. Twenty-four specimens contained bars that were anchored by heads and six specimens contained bars that were anchored by 90° hooks. The specimens simulated an exterior beam-column joints but contained only one headed or hooked bar from the beam without confining reinforcement anchored in the joint region. Chun et al. (2009) did not describe the orientation of the specimen during the casting (whether the column was horizontal or vertical). The specimens were tested with the column in the horizontal position, as shown in Figure 1.15. Load was monotonically increased to failure. Figures 1.16a and b show a typical beam-column joint specimen for headed and hooked bars, respectively. Chun et al. tested No. 8 (No. 25), No. 11 (No. 36) and No. 18 (No. 57) headed and hooked bars, in specimens with concrete compressive strengths between 3,510 and 3,640 psi (24 and 25 MPa). The headed or hooked bar had a clear side cover of $2.5d_b$, embedment lengths ranged between 6.3 and 35 in. (160 and 889 mm), and a net bearing head area of $2.75A_b$, where A_b is the nominal cross-sectional area of the headed bar.

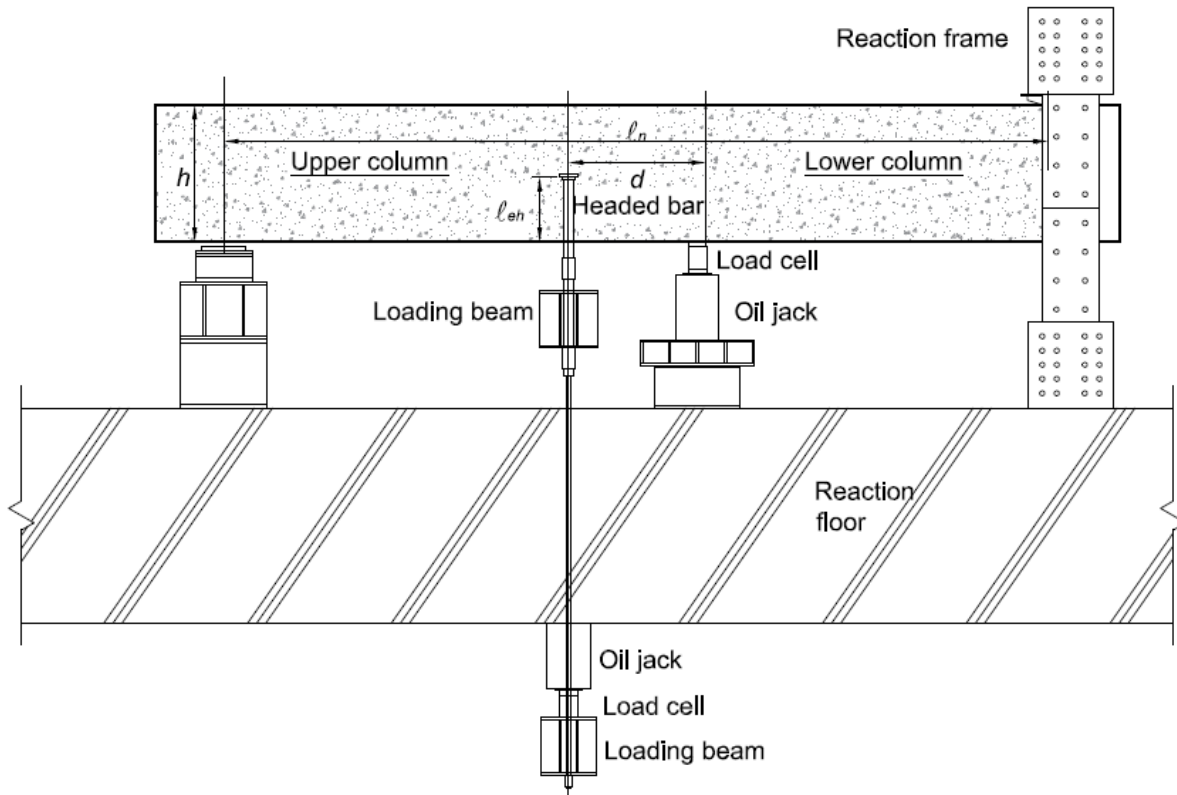
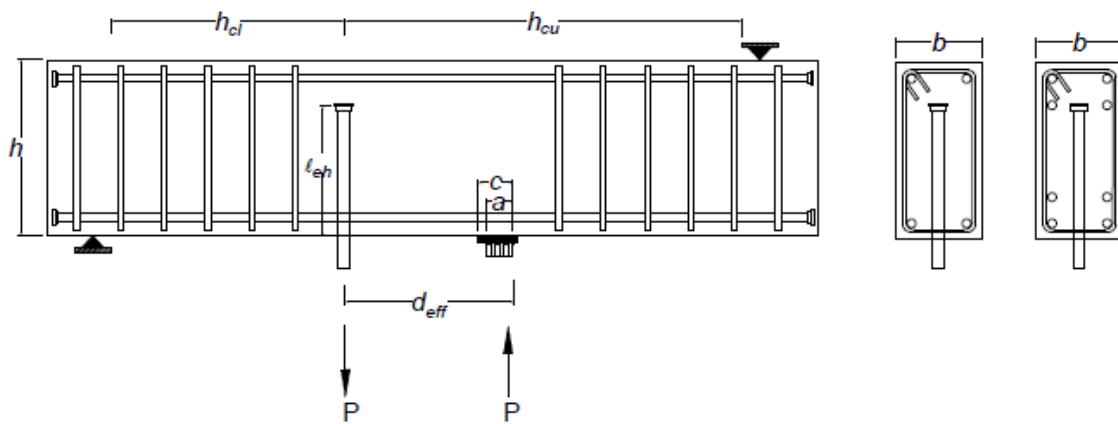


Figure 1.15 Test configuration for beam-column joints (figure after Chun et al. 2009)



(a)

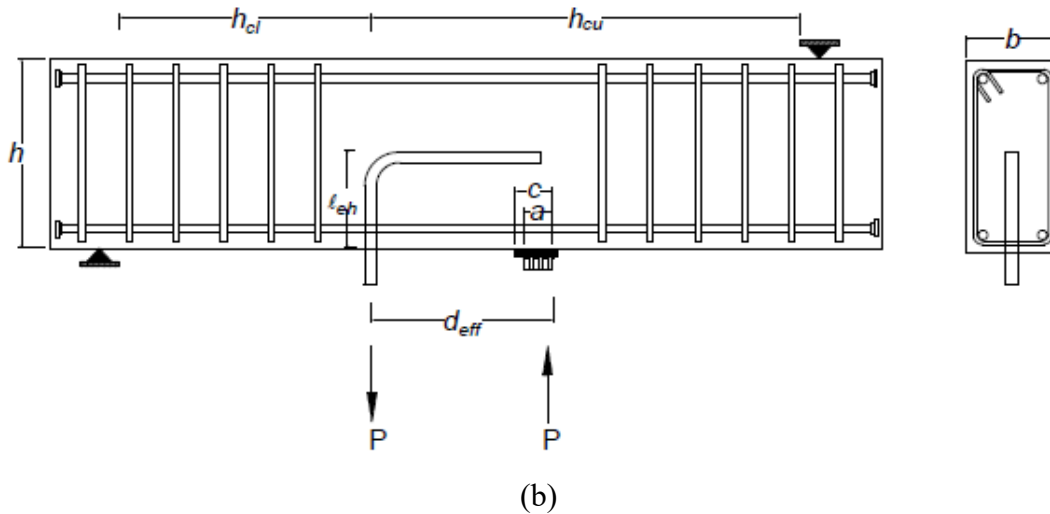


Figure 1.16 Typical beam-column joint specimen. (a) Specimen with headed bar, (b) Specimen with hooked bar (figure after Chun 2009)

Two modes of failure were observed in the tests, as shown in Figure 1.17:

Concrete breakout failure: For this mode of failure, cracks radiated diagonally from both sides of the head and a concrete cone was created.

Joint shear failure: For this mode of failure, cracks formed diagonally at the joint and extended towards the column.

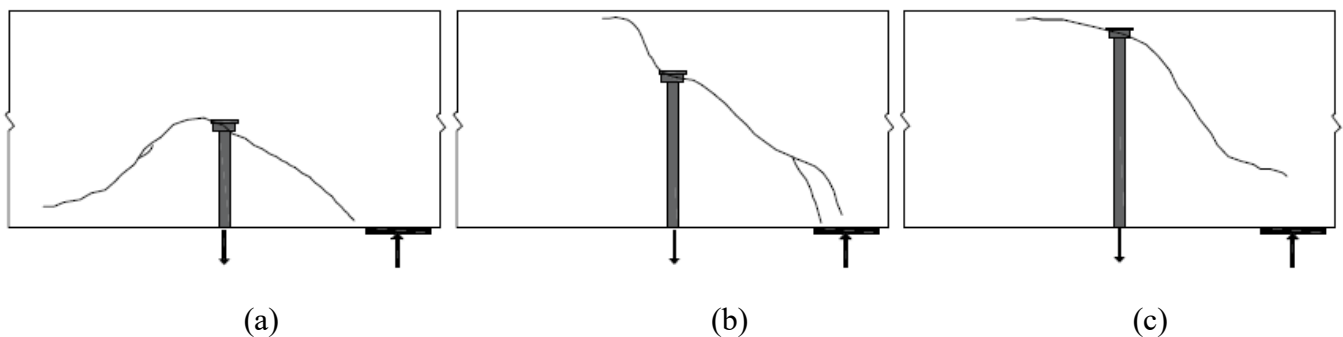


Figure 1.27 Failure Modes: (a) Concrete Breakout; (b) and (c) Joint Shear Failure (figure after Chun et al. 2009)

Chun et al. (2009) evaluated the results of the 24 specimens anchored with headed bars by comparing them to equations suggested by DeVries (1996), Bashandy (1996), and Thompson (2002), in addition to the headed bar development length equation in ACI 318-08. The

comparisons showed that these equations poorly estimated the anchorage strength of headed bars. Chun et al. (2009) proposed a new equation consisting of a combination of head bearing (P_{bearing}) and bond capacity (P_{bond}) and describing the 5% fractile (the value of a distribution for which some fraction of the sample lies below) of the anchorage capacity of headed bars in beam-column joints, as shown in Eq. (1.5).

$$\begin{aligned}
 P &= n_{5\%}(P_{\text{bearing}} + P_{\text{bond}}) \\
 &= 0.78 \left[\left(1 + 2.27 \frac{\ell_e - 0.7D_c}{D_c} \right) 0.85 f'_c A_{nh} + 6.07 \sqrt{f'_c} \phi_b (\ell_e - d_b) \right] \quad [\text{psi}]
 \end{aligned} \tag{1.5}$$

where $n_{5\%}$ is a coefficient for 5% fractile and equal to 0.78 (based on statistical analysis); ℓ_e is the embedment length; D_c is the depth of column; A_{nh} is a net head area; $\phi_b = \pi d_b$ is the bar perimeter; and d_b is the diameter of the headed bar.

1.5 STRUT-AND-TIE MODELING

1.5.1 Introduction

Reinforced concrete members are designed to resist the shear and flexural stresses at a section. Based on Bernoulli's assumptions or beam theory, the behavior of a beam is generally represented by assuming that plane sections remain plane after bending. The region of a structure where beam theory is applicable is often called the B-region. In B-regions, the internal state of stresses can be found from the equilibrium of moments, shears, and axial forces at a section using plane section theory. When concentrated loads are applied to structural members or sudden changes occur in the dimensions of a cross-section, plane section theory can no longer be used because of nonlinear strain distributions within the section. Such locations are termed discontinuity regions or D-regions. According to St. Venant's principle, D-regions are assumed to extend one member depth measured from the location of the applied load or discontinuity, as shown in Figure 1.18. Figure 1.18 illustrates a B-region and multiple D-regions for an unsymmetrically loaded, simply supported beam.

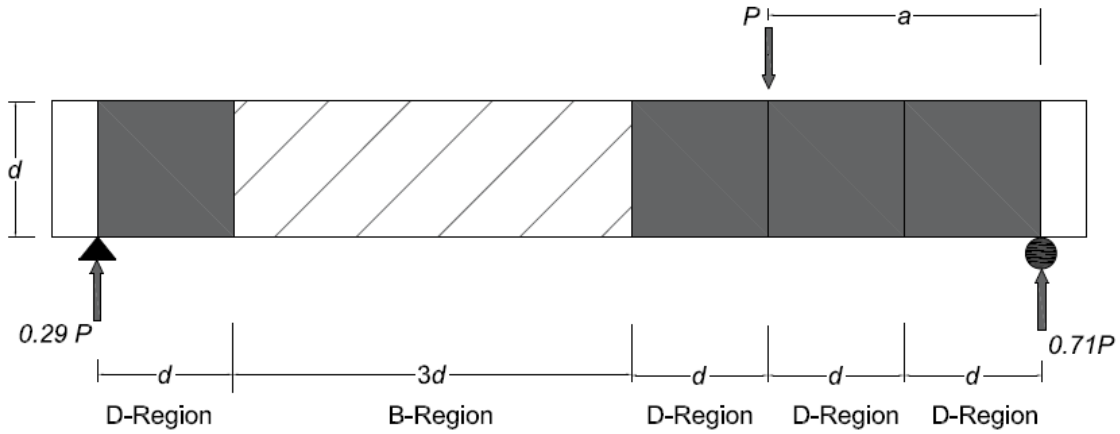
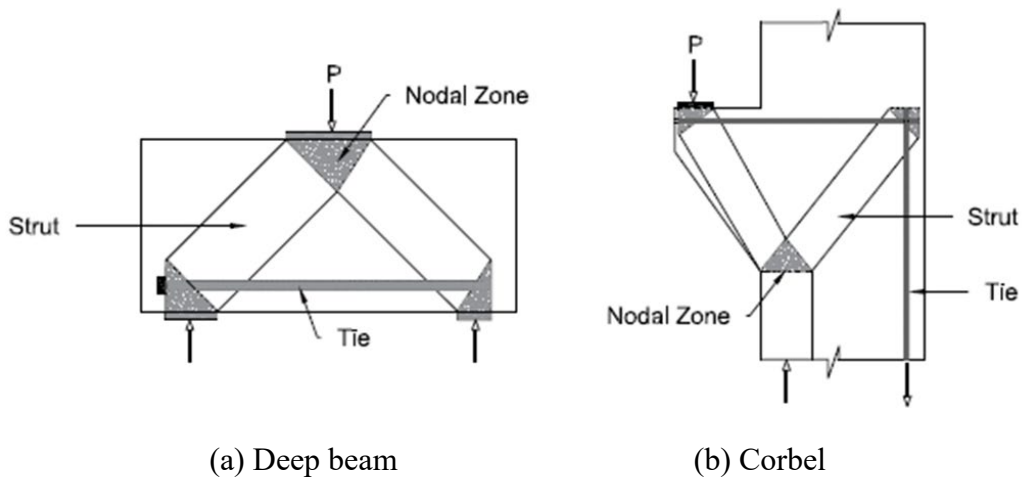


Figure 1.18 B-region and D-region

Chapter 23 of ACI 318-14 describes using the strut-and-tie method to design D-regions. Using the strut-and-tie approach simplifies the complicated state of stress in D-regions, representing them using simple, uniaxial stress paths in equivalent trusses. The uniaxial stress paths are identified as struts, ties, and nodal zones. Struts are under compressive stress while ties are subjected to tensile stresses. Nodal zones, or nodes, are formed where struts and ties intersect. Figure 1.19 illustrates strut-and-tie models for a deep beam and a corbel. The force in each member of the truss can be calculated using equilibrium if the forces acting on the boundary of the model are known.



(a) Deep beam

(b) Corbel

Figure 1.19 Examples of strut-and-tie models

1.5.1.1 Strut and Node Types

Schlaich et al. (1987) defined three strut shapes shown in Figure 1.20: **prism**, which is the simplest type with a constant width; **bottle-shape**, where the strut expands along its length resulting in tensile stresses normal to the action line of applied load (when the amount of surrounding concrete is large and the boundary conditions are well defined); and **fan**, where an array of struts with varying inclinations meet at or radiate from a single node. The fan-shaped and the bottle-shaped stress fields are usually found in D-regions while the prismatic stress field is typical for B-regions (Schlaich and Schäfer 1991).

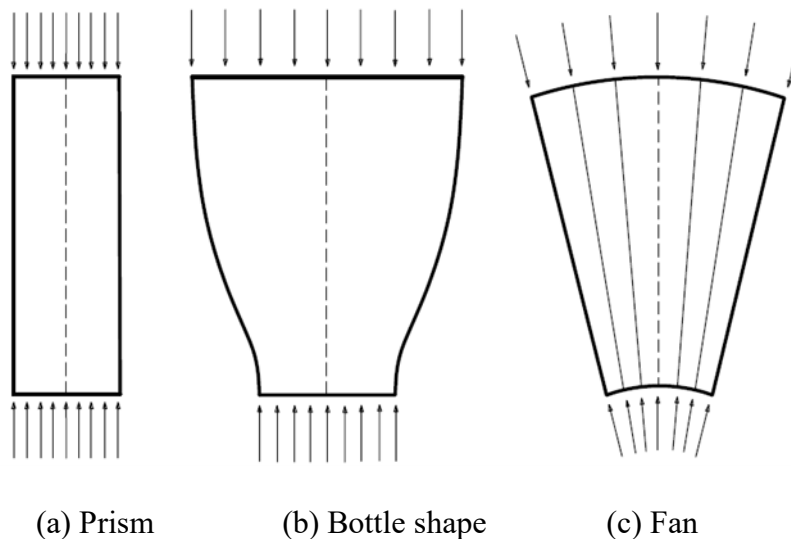


Figure 1.20 Strut types (figure after Schlaich et al. 1987)

Schlaich et al. (1987) also divided nodes into four types depending on the number of the struts and ties; when three compression struts intersect with each other they form a Compression-Compression-Compression (CCC) node, when two compression struts intersect with one tension tie they form a Compression-Compression-Tension (CCT) node, when one compression strut intersects with two tension ties they form a Compression-Tension-Tension (CTT) node, and when three tension ties intersect with each other they form a Tension-Tension-Tension (TTT) nodes. (TTT) nodes are not generally used. Figure 1.21 shows node types.

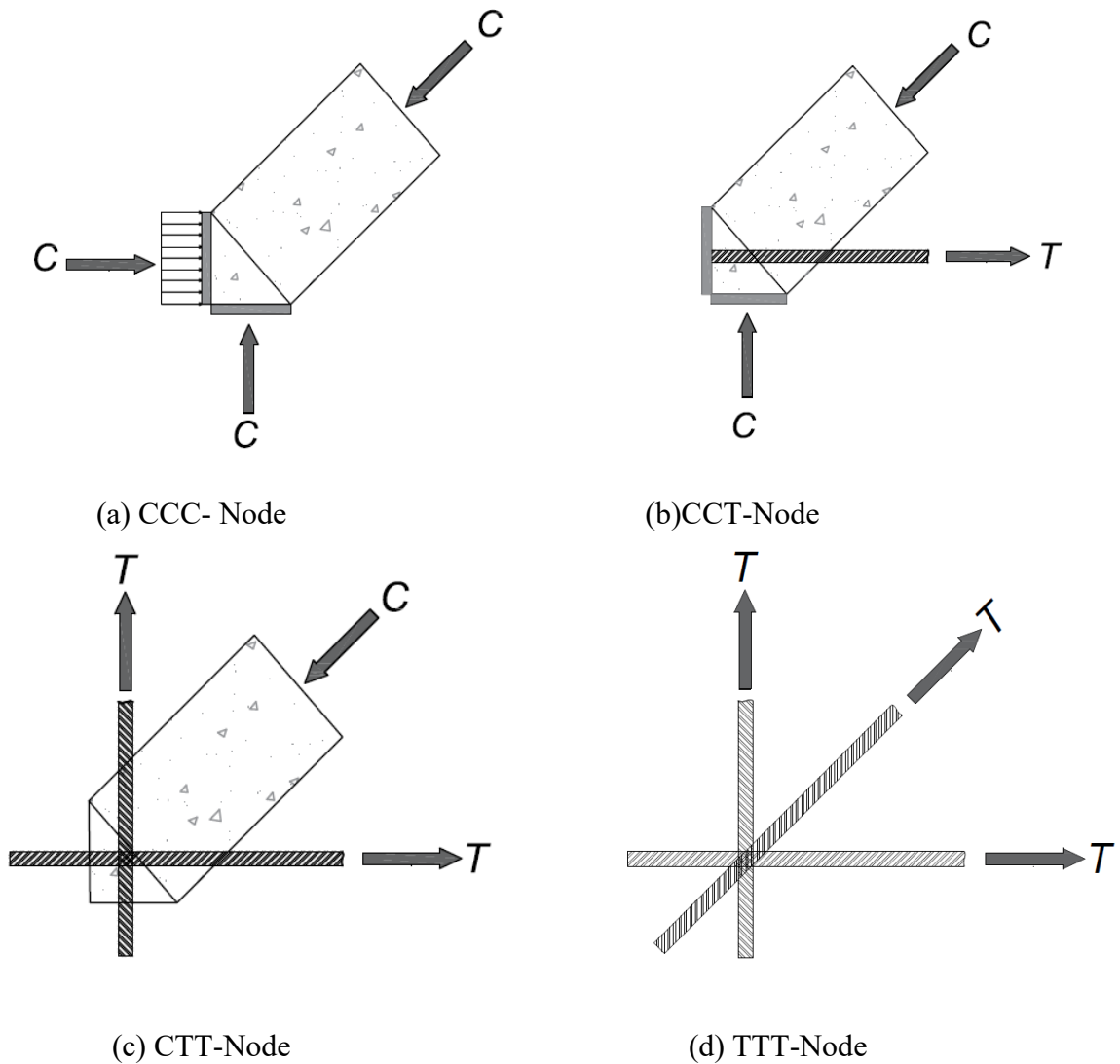


Figure 1.21 Basic node types

1.5.2 Historical Development of Strut-and-Tie Model

The use of strut-and-tie modeling dates back to more than 120 years, when Wilhelm Ritter developed a truss mechanism to study the effect of transverse reinforcement on the shear strength of a beam. The Ritter (1899) truss model is shown in Figure 1.22. Before this time, the concept was that the shear stress was resisted by dowel action. Ritter (1899) concluded that the transverse reinforcement (tie) was in tension and that dowel action was not resisting shear.

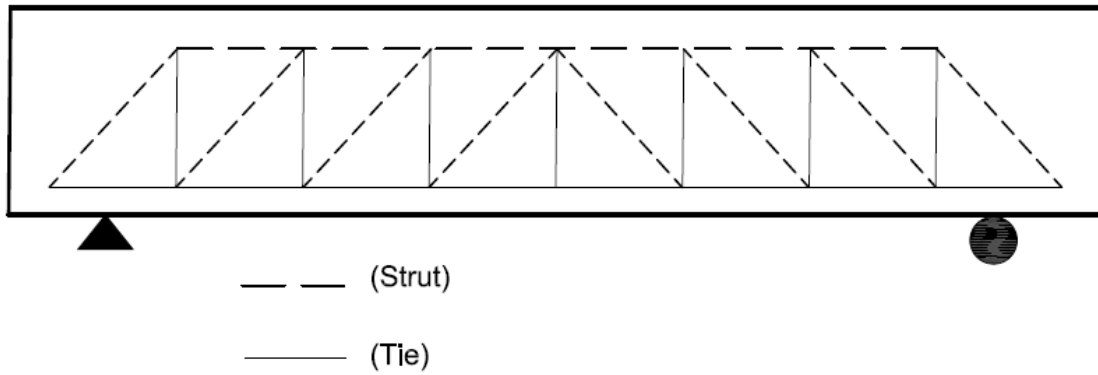


Figure 1.22 Truss model (figure after Ritter 1899)

A similar truss model was proposed by Mörsh (1902) who found that it was more beneficial to replace the diagonal forces that Ritter had used in his truss by a continuous field of diagonal compression, as shown in Figure 1.23.

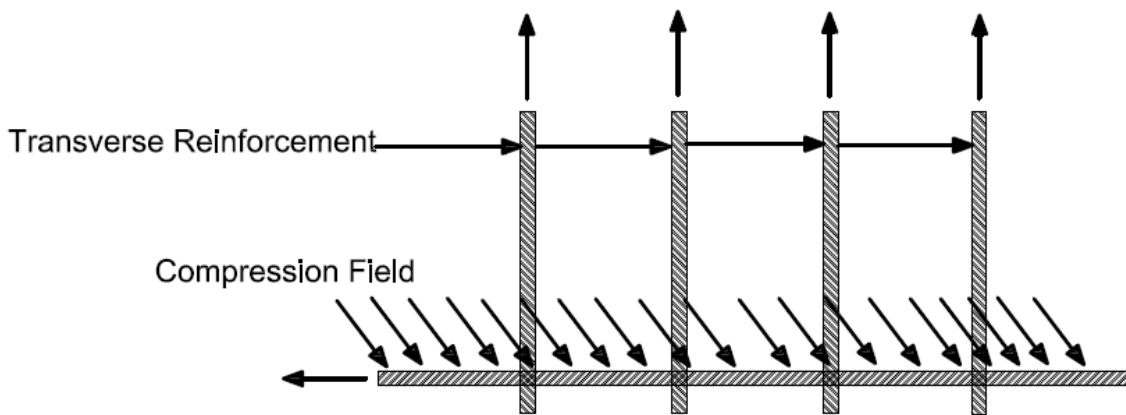


Figure 1.23 Mörsh (1902) model (figure after Mörsh 1902)

Talbot (1909) performed an experimental study in the United States and found that using truss models provided highly conservative strength estimates since the truss models did not consider the tensile strength of the concrete, which he found plays an important role in resisting shear stress.

Richart (1927) found that shear strength was affected by both concrete and steel strength and developed a new method to calculate shear strength. In the new method, the shear strength is the sum of V_c (strength of concrete) and V_s (strength of steel found from analyzing a truss model consisting of struts (concrete under compression) orientated 45° with the longitudinal reinforcement).

The truss model (strut-and-tie model) was applied again in the United States in the early 1970s. It was used to calculate the capacity of reinforced concrete subjected to both shear and torsional stress. A truss model, shown in Figure 1.24, was developed based on the plasticity theory. The model consists of tubular truss, defined as a hollow box close to the outside face of the member and was part of a new model to study the effect of axial load, shear, bending, and torsion and developed by Lüchinger (1977), Ramirez and Breen (1983), and Mitchell and Collins (1974).

In 1984, the Canadian CSA Standard added the strut-and-tie model into its code. AASHTO Bridge Design Specifications also added the strut-and-tie model. ACI introduced strut-and-tie provisions in ACI 318-02.

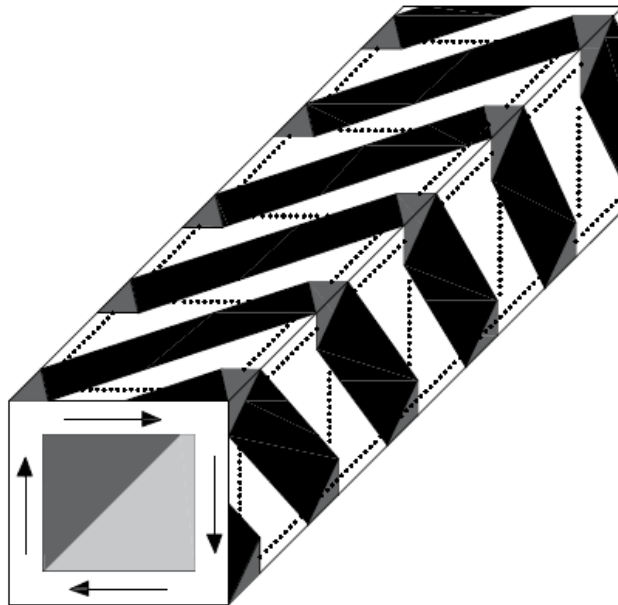


Figure 1.24 Truss model for torsion (figure after Thompson 2002)

1.5.3 Procedure for Strut-and-Tie Design

The first step in using a strut-and-tie model starts with the identification of D-regions and determining the boundary conditions surrounding this region by calculating the forces and reactions acting on it. After determining the dimensions and forces on the D-region, the next step is developing a truss model. Depending on the boundary conditions (if there is more than one applied load), more than one truss model can be used to represent a load case. For the truss model selected, the forces in the truss elements (compressive struts and tension ties) should be in equilibrium and, preferably, determinate. It is best to choose a simple truss configuration to reduce

analysis time. Concrete within the member provided the struts and reinforcing steel provides the ties. The next step is to determine the forces in the compressive struts and tension ties.

After calculating the forces in the struts and ties, the amount of steel to be supplied for the ties should be calculated. It is important to make sure that the tie bars fit within the tie region of the concrete member and satisfy required spacing and clear cover. In case the designed tie steel does not fit, a new truss model should be used and checked to ensure that the tie steel will fit.

The next step is to check the stresses at the struts and nodes. The dimensions of both the struts and nodes must be determined, and the resulting stresses compared to the allowable stress limits within the ACI Code provisions (Chapter 23-Section 4.3). The dimensions of the struts and nodes are compared with the geometry of the concrete member to help ensure that the truss model is suitable. If the strut and node dimensions are not compatible with the concrete dimensions, the truss model should be adjusted or a new truss model should be drawn to work with the geometry of the concrete member.

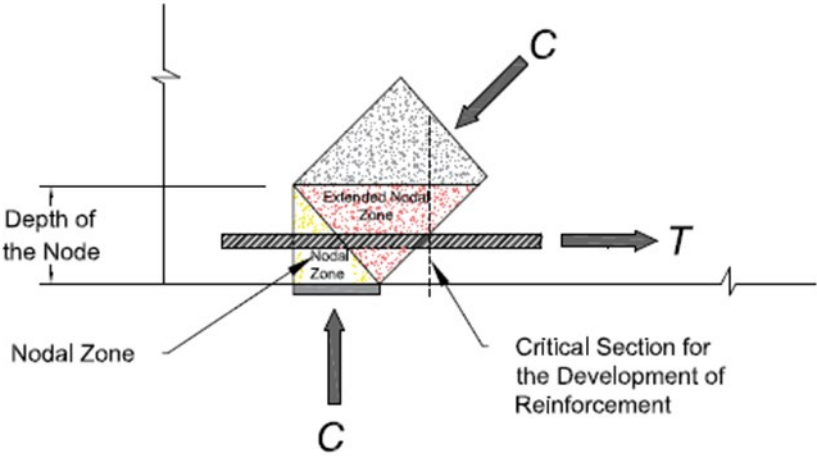
The last detail to be checked is anchorage of the steel reinforcement. The tie steel reinforcement should be designed to be fully developed in or beyond nodal zone. The development of reinforcement is required to follow the code provisions for straight, hooked, and headed bars.

1.5.3.1 Dimensioning of Nodes, Struts, and Ties

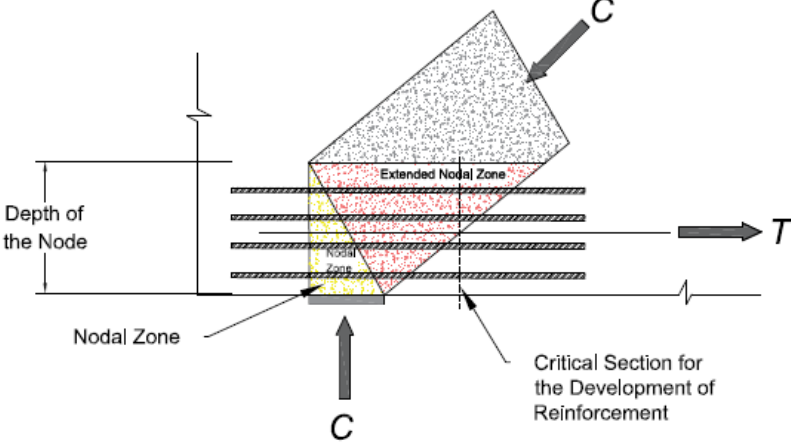
Dimensioning nodes, struts, and ties is described in ACI 318-14 (Chapter 23-Sections 2.1-2.6). The geometry of struts depends on the dimensions of the nodes at the ends of the strut (node faces). The geometry of nodes depends on several factors, such as the dimensions of the bearing surfaces at node edges, the tie bars anchored at the nodes, and consistency with struts that extend from the B-regions towards the D-regions. For the ties, dimensioning depends on the compatibility with the steel reinforcing bars that reinforce the B-regions and extend towards the D-regions. Other design requirements, such as development length, clear spacing, and ACI 318-14 recommendations, also impact the dimensioning of the ties.

Many factors impact the selection of tie reinforcement, one being the available space for the development length in the concrete member. Limited available space may lead to use many small bars which require shorter development length. Another factor that may affect the selection

of the tie reinforcement is the spacing between bars. According to ACI 318-14 (Chapter 23-Section 2.6), to get better distribution for the anchorage stresses at the nodes, wider spacing between the tie reinforcing bars may be used. Furthermore, tie reinforcement with close spacing may also be preferred. This can be accomplished by decreasing the number and increasing size of these bars as shown in Figure 1.265. Figure 1.25 shows the distribution of bars serving as tie reinforcement with different spacing.



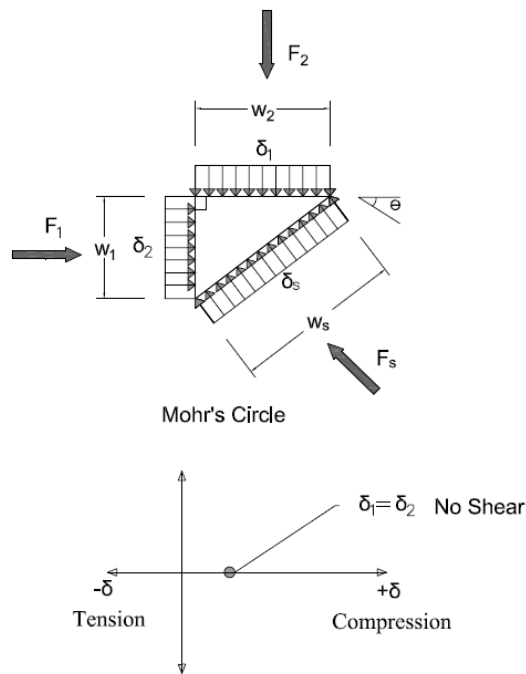
(a) One layer of reinforcement



(b) Distributed Reinforcement

Figure 1.25 Extended nodal zone showing the effect of the distribution of the force (figure after ACI 318-14)2

The dimensions of nodes are usually established after identifying the dimensions of the ties. ACI 318-14 recommends dimensioning of nodes based on hydrostatic principles. According to ACI 318-14 (Chapter 23-Section 2.6), a hydrostatic nodal zone can be defined as a nodal zone that has the same stresses on the loaded faces, that is, the in-plane stresses are equal in all directions (as shown in Figure 1.26a). However, sometimes the nodes may not be hydrostatic and the stresses are not equal in all the node faces (as shown in Figure 1.26b).



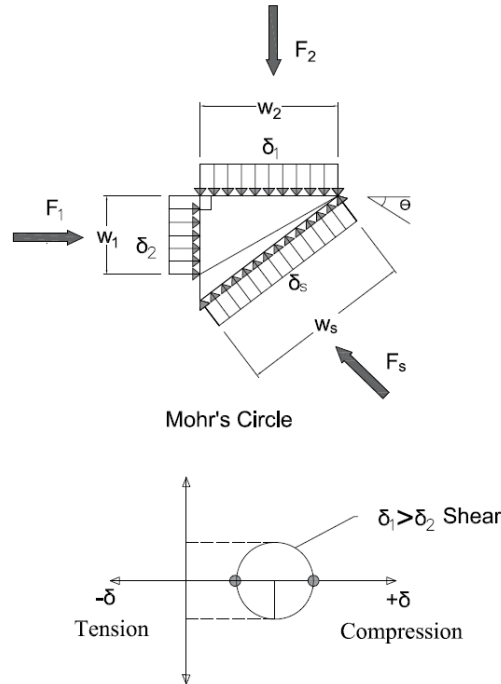
$$\sigma_1 = \sigma_2 = \sigma_s$$

$$F_s = \sqrt{(F_1)^2 + (F_2)^2}$$

$$w_s = w_1 \sin \theta + w_2 \cos \theta$$

$$w_s = \sqrt{(w_1)^2 + (w_2)^2}$$

(a) Hydrostatic Node



$$\sigma_1 > \sigma_2 > \sigma_s$$

$$F_s = \sqrt{(F_1)^2 + (F_2)^2}$$

$$w_s = w_1 \sin \theta + w_2 \cos \theta$$

$$w_s = \sqrt{(w_1)^2 + (w_2)^2}$$

(b) Non-Hydrostatic Node

Figure 1.26 Hydrostatic and non-hydrostatic nodes (figure after Thompson et al. 2002)

1.5.3.2 Limitations of Strut-Tie Angle

The strut-tie angle is defined as the angle between a tension tie and a compression strut. Several studies were performed on compression field and truss mechanisms of one-way members (beams) subjected to shear and torsion to determine the best limits for this angle. According to different researchers (Lampert and Thürlimann 1971, Mitchell and Collins 1974, and Ramirez and Breen 1983), the strut-tie angle could vary between 15° and 65° . ACI 318-14 (Chapter 23 Section 2.7) uses 25° as a lower limit of the strut-tie angle.

1.5.3.3 Strength of Nodes

The stress at a node, equal to the tie force by the node area, can be determined after identifying the force in the tie bar (from the equilibrium of the truss model) and the dimensions of the nodes, as described in Section 1.5.3.1.

Following ACI 318-14, the allowable strength (strength limits) of a node, f_{ce} , can be found using Eq. (1.6).

$$f_{ce} = 0.85\beta_n f'_c \quad (1.6)$$

where the values of β_n , in accordance with ACI 318-14, are listed in Table 1.1.

Table 1.1: Nodal zone coefficient β_n

Configuration of nodal zone	β_n	
Nodal zone bounded by struts, bearing areas, or both	1.0	(a)
Nodal zone anchoring one tie	0.80	(b)
Nodal zone anchoring two or more ties	0.6	(c)

1.5.3.4 Strength of Struts

The stress in a strut, equal to the strut force by the strut area, can be calculated after identifying the force in the struts (from the equilibrium of the truss model) and the dimensions of the struts, as described in Section 1.5.3.1.

Following ACI 318-14 (Chapter 23-Section 4.1), the allowable strength of a strut, f_{ce} , can be found from Eq. (1.7).

$$f_{ce} = 0.85\beta_s f'_c \quad (1.7)$$

where β_s is a factor that accounts for the effect of cracking and crack-control reinforcement on the effective concrete compressive strength. Table 1.2 gives values of the strut coefficient β_s based on ACI 318-14.

Table 1.2: Strut coefficient β_s

Strut geometry and location	Reinforcement crossing a strut	β_s	
Struts with uniform cross-sectional area along length	NA	1.0	(a)
Struts located in a region of a member where the width of the compressed concrete at midlength of the strut can spread laterally (bottle-shaped struts)	Satisfying 23.5	0.75	(b)
	Not Satisfying 23.5	0.60λ	(c)
Struts located in tension members or the tension zones of members	NA	0.40	(d)
All other cases	NA	0.60λ	(e)

ACI 318-14 (Chapter 23-Section 5.3) also recommend that the required reinforcement for the bottle-shaped struts (Table 1.2) must satisfy Eq. (1.8).

$$\sum \frac{A_{s_i}}{b_s s_i} \sin \alpha \geq 0.003 \quad (1.8)$$

where A_{s_i} is the area of steel that crosses the path of the strut (in.²) within spacing s_i (in.), b_s is the width of the strut perpendicular to the axis of the crossing reinforcement (in.), α_i is the angle between the axis of the strut and the axis of the crossing reinforcement; α_i must be greater than 40° if only one layer of reinforcement crosses the strut.

1.5.4 Experimental Studies

1.5.4.1 Ramirez and Breen (1983)

Ramirez and Breen (1983) studied the behavior of reinforced and prestressed beams subject to flexure, shear, and torsion with variable inclination angle truss models. Their study included several hundred experimental results for beams gathered from other researchers' work. They found that the strut angle should not be less than 26° or more than 63° to avoid the premature yielding in the longitudinal or transverse reinforcement.

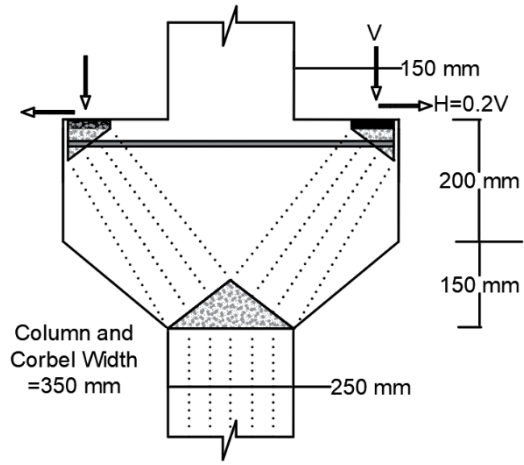
Some of the specimens failed due to web-crushing rather than yielding of the reinforcement. For those specimens, they proposed the allowable diagonal stress given Eq. (1.9).

$$f_{ce} = 30\sqrt{f'_c} \quad (1.9)$$

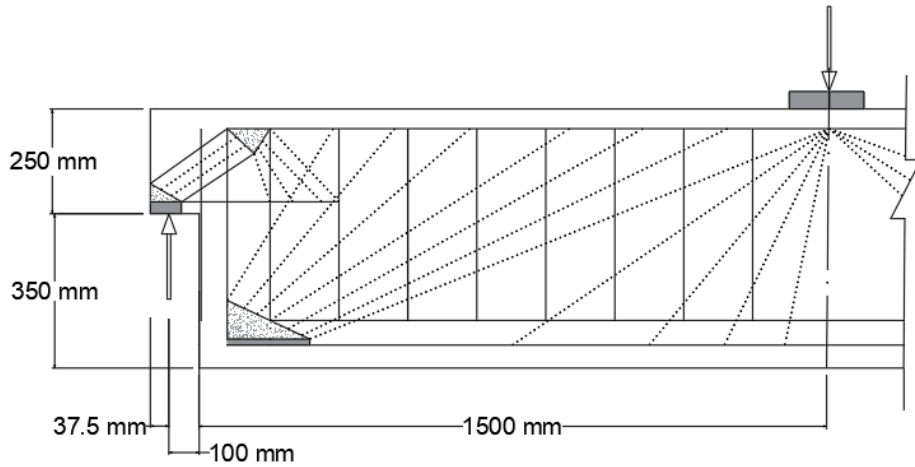
where f_{ce} is the effective stress in diagonal truss members, and f'_c is the specified concrete compressive strength (psi).

1.5.4.2 Cook and Mitchell (1988)

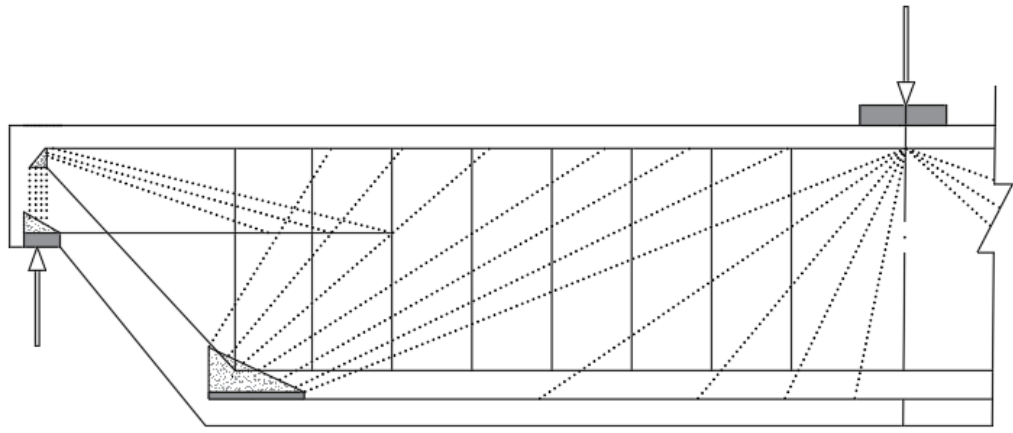
Cook and Mitchell (1988) studied the use of a simple strut-and-tie model (method in the 1984 Canadian Concrete Code) to analyze and design D-regions. Four scaled-down specimens were tested. The specimens were a double-sided corbel, a rectangular dapped beam, an inclined dapped beam, and a beam with a rectangular opening in its web. The strut-and-tie models for the tests are shown in Figure 1.27. Cook and Mitchell (1988) also developed a nonlinear finite element program to analyze the response of the four specimens. Concrete compressive strength ranged from 4,320 to 5,960 psi (30 to 41 MPa), and the steel yield strength was 64.5 ksi (320 MPa).



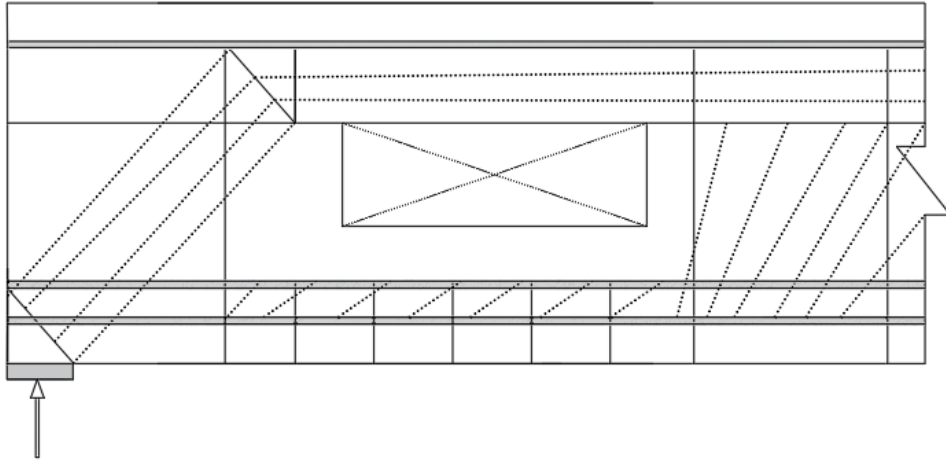
(a) Double-sided corbel



(b) Rectangular dapped beam



(c) Inclined dapped beam



(d) Beam with opening

Figure 1.27 Strut-and-tie models: (a) Double-sided corbel, (b) Rectangular dapped beam, (c) Inclined dapped beam, and (d) Beam with opening (figure after Cook and Mitchell 1988)

Cook and Mitchell (1988) found that the strut-and-tie model provided a conservative estimate of the member strength. They also found that nonlinear finite element analysis can be used to determine the behavior of D regions in reinforced concrete members, providing a prediction of response that is better than that provided by a strut-and-tie model.

1.6 FINITE ELEMENT METHOD (FEM)

1.6.1 Introduction

Finite Element Method (FEM) is a numerical technique that is used to find solutions for mathematical physics and engineering problems. FEM was created due to the need to solve the complicated problems in aerospace, automotive, mechanical, and civil engineering. The method is useful for problems that are nonlinear and members that are subject to complex loadings or have complex geometries and material properties. In these cases, analytical solutions are, typically, difficult to obtain. Using FEM to simulate the deformation behavior of a structure helps to produce visualizations that can be interpreted in terms of strength and stiffness. The results can be applied to optimize the material weight and cost. It also provides many detailed visualizations and distribution of the strains and stresses inside the simulated body.

1.6.2 Background of Finite Element Analysis

The development of the computer in the 1950s made solving a large number of simultaneous equations possible. This helped in the developing of FEM. The first paper describing Finite Element Method was published in 1960 by Ray W. Clough. In 1967, Zienkiewicz and Chung published the first book about the method. In the late 1960s and early 1970s, engineers started using FEM to solve different engineering problems and applying this method to analyze the nonlinear problems involving large deformations. Almost all the current commercial FEM software packages (ABAQUS, NASTRAN, ANSYS, etc.) were initiated in the 1970s. In the 1980s, finite element programs were used in developing algorithms dealing with electromagnetic applications, thermal analysis, and fluid flow.

It is now possible to understand structural behavior with more accuracy because of the development of Finite Element Method, accompanied by the huge increase in computing power. In structural analysis, the goal is to determine the stresses and displacements under applied loads. However, many times it is not possible to do this using conventional approaches. In these cases, the Finite Element Method can be used. In the typical approach, the displacements are considered the unknowns of the problem. The unknown displacements can be found by applying the equilibrium equations and force-displacement laws.

1.6.3 Elements and Nodes

Finite elements represent small domains that are obtained by dividing the solid (continuum) model. As a result, the original solid model is considered as a collection of a large number of small elements. These elements are connected to each other through nodes. Each element is assigned material and geometrical properties

1.6.4 Degrees of Freedom (DOF)

In general, a structure may have an infinite number of displacements. However, approximations introduced in the finite element method limit the number of displacements to be calculated to those occurring at the nodes. The displacements are described as degrees of freedom.

The number of degrees of freedom (DOF) is equal the product of the number of nodes and the number of the displacements that must be calculated at each node.

1.6.5 Modeling Material Failure-Fracture

Materials may have different behaviors, such as ductile or brittle, based on their composition, degree of aging, etc. Among other approaches, material failure can be analyzed using continuum damage mechanics and fracture mechanics.

1.6.5.1 Continuum Damage Mechanics

This approach assumes that failure begins with a gradual degradation of the deforming material. The stress will drop rapidly due to the nonlinear behavior of the material (ductile behavior) (See Figure 1.28b), resulting in a deformation that is localized within a narrow zone, as shown in Figure 1.28a. This step is known as a fracture onset. Usually, the localization of the deformation can be very intense in the sense that a single macroscopic (discrete) crack begins to develop. The transformation of the stresses through the crack leads to a fully opened crack. (Runesson 2006).

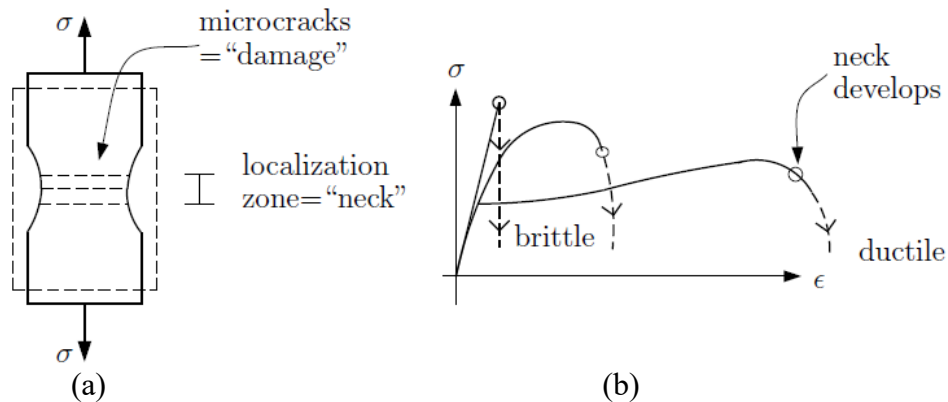


Figure 1.28 Damage process (Continuum Damage Mechanics). (a) Localization (necking) in a bar of ductile material, (b) Stress vs. strain characteristics (figure from Runesson 2006)

1.6.5.2 Fracture Mechanics

This method assumes that a microscopic flaw can form. The main idea is to determine if a crack will propagate from this flaw. Cracks that propagate only when the applied load increases are termed “stable.” The singular stress field at a crack tip can be determined based on linear elasticity (See Figure 1.29). For linear elastic fracture mechanics, the Griffith criterion (Griffith 1921) indicates that that a crack is stable if the stress intensity factor under an applied load does not exceed a critical value (Runesson 2006).

For materials like concrete, failure can be modeled also using a nonlinear fracture mechanics approach. This approach considers the behavior of the crack at the tip (also known as a fracture process zone (FPZ)) and is used when the nonlinear region at the tip of the crack is relatively large compared to the size of the structure (ACI 446 1989).

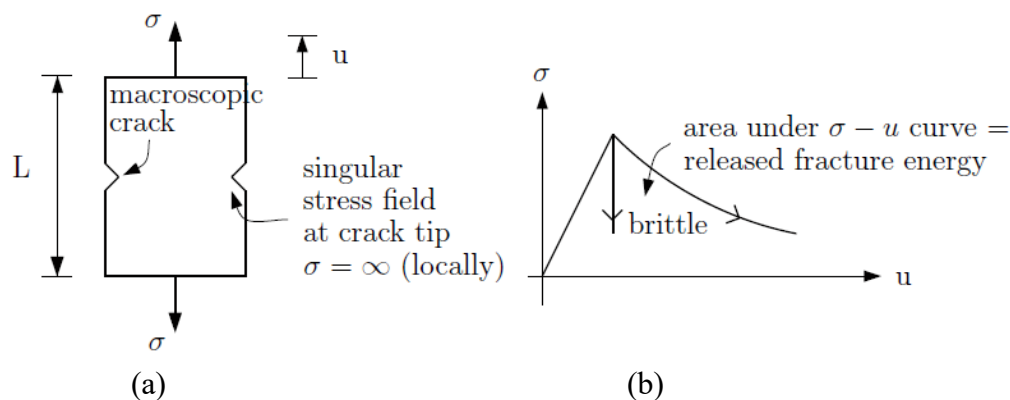


Figure 1.29 Fracture process (a) Preexisting edge cracks, (b) Far-field stress vs. extension characteristics. (Figure from Runesson 2006)

Continuum damage mechanics is used in this study to express the behavior of concrete. In this was the mechanism of concrete failure is identified by many microscopic cracks.

1.6.6 PREVIOUS RESEARCH USING FEM FOR REINFORCED CONCRETE

Many investigators have used the FEM to model reinforced concrete members after first being used by Ngo and Scordelis (1967). Here, a selected set of references that include a model

for bond between reinforcing steel and concrete are reviewed along with references that represent the constitutive behavior of cementitious materials based on continuum damage mechanics.

1.6.6.1 Ngo and Scordelis (1967)

Ngo and Scordelis (1967) developed a general analytical method to study the behavior of reinforced concrete members under an applied load. They modeled a simple beam using constant strain triangular elements for reinforcing steel and concrete. The interaction between concrete and reinforcing steel was modeled using a special bond-link element. The bond-link element represents two orthogonal springs that link the node in a steel bar to the corresponding concrete node. A linear elastic analysis was conducted to express the behavior of reinforcing steel, concrete, and the interaction between them.

1.6.6.2 Brown, Darwin, and McCabe (1993)

Brown, Darwin, and McCabe (1993) used the finite element method to study bond in beam-end specimens. Their model consisted of steel, concrete, and transverse reinforcement. The model represented a portion of the overall specimen, shown in Figure 1.30. Concrete cracking was represented using a nonlinear fracture mechanics model, known as the “fictitious crack model” (Hillerborg et al. 1976), that assumes that cracks initiate when the stress in the concrete reaches its tensile strength. The interface between concrete and steel was modeled using special link elements depending on a Mohr-Coulomb failure law. For simplicity, the steel bar was modeled with a square cross section area.

The results showed that the interface between concrete and steel can be simulated accurately by adding the special link elements only at the compression face of the ribs. Their results also showed that increasing the concrete cover and the bonded length increased the bond force and slip at peak load, as observed in practice. The amount of concrete that is split at failure and the bonded length, however, are not proportional; doubling the bonded length does not double the amount of concrete that is split. This observation explains why the bond strength does not increase linearly with bonded length and also explains why bars with short embedded lengths can have a substantial bond strength.

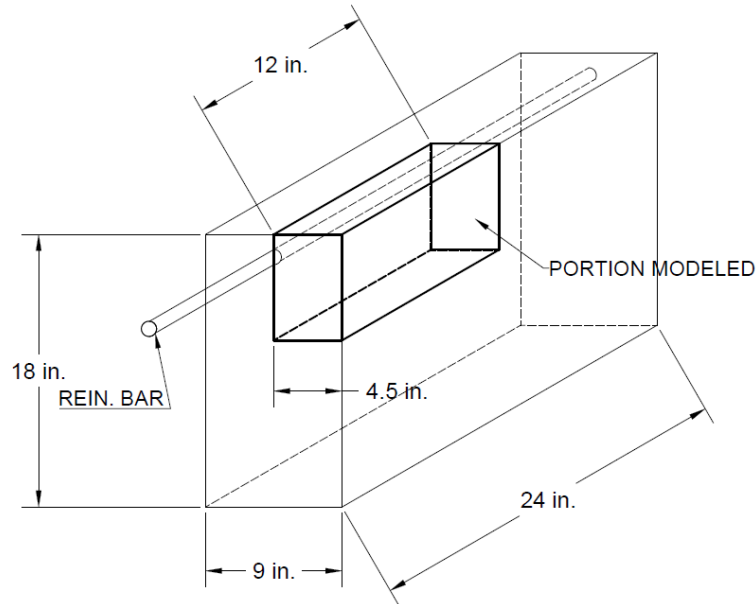


Figure 1.30 Portion of the tested specimen represented by FEM (figure after Brown, Darwin, and McCabe 1993)

1.6.6.3 Tholen and Darwin (1996)

Tholen and Darwin (1996) extended the work of Brown, Darwin, and McCabe (1993) by modeling the crack planes that radiate from the bar. In addition, a round bar was modeled instead of a square bar, and only specimens without transverse reinforcement were studied. For this study, the fictitious crack model was used to express concrete behavior. Within the model, the ability of concrete to transfer stresses decreased as the crack width increased. The interface between concrete and steel was modeled using a 3-dimensional element link.

Their study consisted of two parts. In the first, Tholen and Darwin modeled a portion of the specimen using only one rib on the steel bar to explore the influence of the number of potential concrete cracking planes and the number of sides on the cross-section of the bar. Figure 1.31a shows the portion of the specimen with a 6-in. (152-mm) bonded length and 1-in. (25-mm) concrete cover. A No. 8 (No. 25) bar was used in the simulation. Based on the results obtained with this model, a larger portion of the specimen) was modeled with multiple ribs along the bar. The bar shape and the number of crack planes were selected as well. Figure 1.31b shows the portion of the specimen with 12 in. (305 mm) bonded length and 2 in. (50.4 mm) concrete cover. A No. 8 (No. 25) bar was used in the simulation.

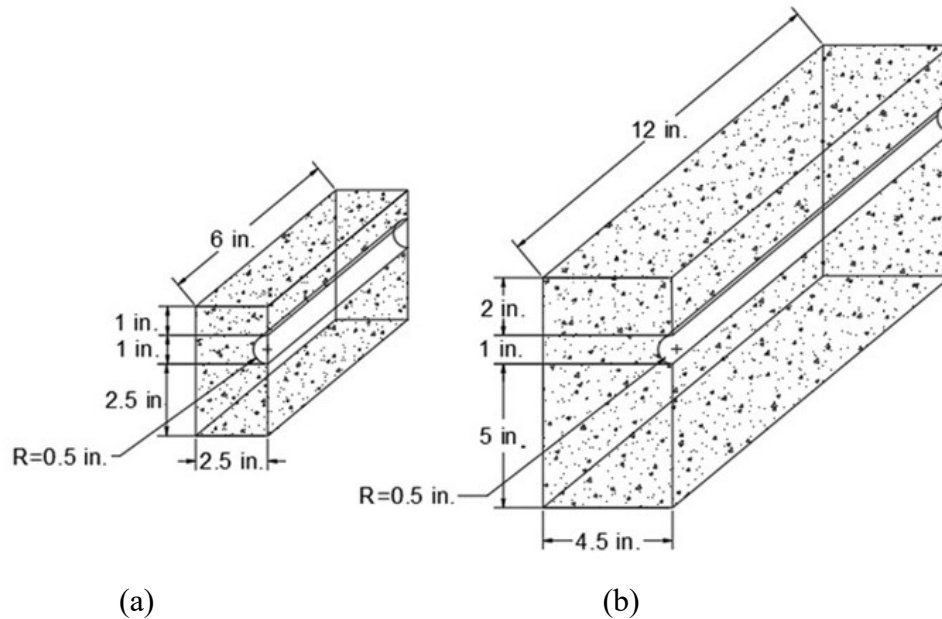


Figure 1.31 Beam-end specimen, (a) Portion of the specimen with 1 in. concrete cover and 6 in. bonded length, (b) Portion of the specimen with 2 in. concrete cover and 12 in. bonded length (figure after Tholen and Darwin 1996)

As in practice, increasing the concrete cover increased the bond force and slip at peak load. There was a nearly linear, but not proportional, relationship between bond strength and the product of bonded length and concrete cover measured to the center of the bar, also as observed in practice. Also, increasing the bonded length increased the bond force and slip at the peak load. As observed by Brown, Darwin, and McCabe (1993), the relationship between the area of cracked concrete and the bonded length was not proportional. The results of this study led to a more nuanced understanding of the mechanism of bond behavior and helped in developing a theoretical model to predict the bond strength.

1.6.6.4 Allwood and Bajarwan (1996)

Allwood and Bajarwan (1996) used the finite element method to model the nonlinear behavior of bond stress-slip. In their study, they eliminated the contribution of adhesion, and considered that the effects of friction and interlock as related to radial pressure. The radial pressure between bar and concrete results from the effect of concrete shrinkage during setting on the bar, the effect of Poisson's ratio on bar diameter, and the effect of the lateral confining stress in the neighboring concrete. Allwood and Bajarwan developed a new approach to model the nonlinear

behavior of bond stress-slip. In their approach, Allwood and Bajarwan analyzed the concrete and steel independently and then brought the solutions of the two components (steel and concrete) together using a quickly converging iterative process and modified the bond stress linking steel with concrete. Figure 1.32 illustrates the method of analyzing steel and concrete independently. The new approach provided a good match with experimental data.

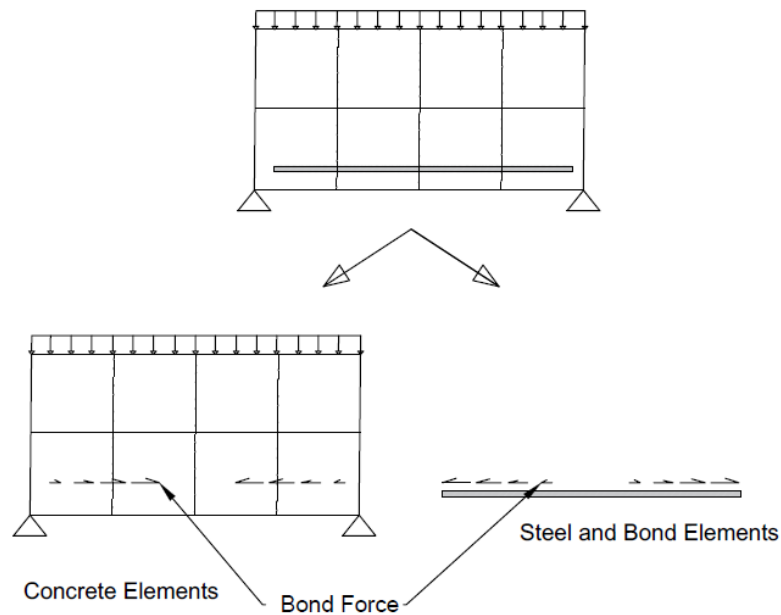


Figure 1.32 Analysis method (figure after Allwood and Bajarwan 1996)

1.6.6.5 Misra and Yang (2010)

Misra and Yang (2010) presented an approach to obtaining a constitutive relationship for cohesive materials based upon a microstructural mechanics approach used in granular mechanics. The microstructure of the cohesive materials is defined as a collection of grains, whose centroids represent material points, interacting through pseudo-bonds. The pseudo-bond or the inter-granular force-displacement relations are found based on atomistic-level particle interactions. The resulting force-displacement relationships are used to derive the incremental stiffnesses at the grain-scale. As a result, the sample-scale stress-strain relationship of a representative volume of the material is obtained.

The model is used to study the behavior of cohesive materials under multi-axial loading conditions. The calculations from the model were compared with experimental data for model validation. The comparison exhibits both quantitative and qualitative consistency with the observed behavior of a cohesive material.

1.6.6.6 Misra and Poorsolhjouy (2015-2017)

Misra and Poorsolhjouy (2015) improved on the work performed by Misra and Yang (2010). In their study, they developed a new method by including the effect of a cementitious material based upon the granular micromechanics paradigm and thermomechanics leading to macro-scale constitutive equations that represent grain-scale force-displacement relationships.

Misra and Poorsolhjouy (2015) found that the new model was able to express the microscopic behavior exhibited by these materials, such as the effects of post-peak softening, volume compression-dilatancy, and induced anisotropy. As a result, the implementation of this model into a finite element model could be considered as an efficient method to link micro-scale mechanisms to the structural scale.

Poorsolhjouy and Misra (2017) used thermo-mechanics-based granular micromechanics constitutive relationships of cementitious materials to predict failure phenomena of cemented granular materials. They also investigated the macro- and the microscale mechanisms that control behavior. For this purpose, the modeled true triaxial tests with different levels of intermediate and minor principal stress. The results show that failure depends on both the intermediate principal stress and the load path.

To demonstrate that failure depends on the load path, which is affected by the nature of the material response to loading, two different types of true triaxial loading paths were simulated. Eigenvalues of the tangent stiffness matrix were used to study macro-scale failure mechanisms. An eigenvalue analysis of the localization tensor was conducted, and the direction of the failure plane investigated. Their analysis showed that the failure plane depends on all of the components of the principal stress. In addition, the results showed that the localized macro-scale failure mechanism changed from shear at low confinement to a combination of shear and compaction at

higher confinement. This result also matched experimental results of true triaxial tests. These models have not yet been applied to reinforced concrete.

1.7 OBJECTIVE AND SCOPE

In ACI 318-14, the headed bar development length provisions have restrictions on the yield strength of the bars (up to 60 ksi) (420 MPa) and concrete compressive strength (up to 6,000 psi) (41 MPa). The provisions do not consider the effects of the spacing between the bars. New code provisions were proposed for the development length for headed bars by Shao et al. (2016). The proposed provisions were developed based on 202 exterior beam-column joint specimens subjected to monotonic loading. The proposed provisions consider the effect of confining reinforcement and spacing between the headed bars while allowing for the use of higher concrete compressive strength (up to 16,000 psi) (110 MPa) and steel yield strength (up to 120 ksi) (830 MPa).

The objective of this study is to provide better understanding for the mechanism of bond behavior of headed bars, as well as evaluate the application of the proposed code provisions to members other than beam-column joints, including bars anchored at the end of beams within compression-compression-tension (CCT) nodes. The objective of this study is also to evaluate the accuracy and conservativeness of the design provisions for headed bars from ACI 318-14, Shao et al. (2016), ACI 318-19, and Darwin and Dolan (2021), as well as the anchorage provisions in Chapter 17 of ACI 318-19. This study also includes a finite element analysis conducted to develop a model representing the anchorage behavior of headed and straight bars.

The study includes three phases. The first phase consists of tests of 10 beams to determine the anchorage capacity of headed bars anchored in compression-compression-tension (CCT) nodes. No reinforcement was located within the nodal zones with the exception of the tensile tie reinforcement, which was provided by two or three bars. The two ends of the specimen were tested separately. At one end, the bars were terminated with a head, while at the other end the bars were straight. The test results are compared with anchorage strengths based on the study by Shao et al. (2016).

The second phase of this study compares the anchorage strength of headed bars in tension using design provisions for headed bars from ACI 318-14, Shao et al. (2016), ACI 318-19, and Darwin and Dolan (2021), as well as the anchorage provisions in Chapter 17 of ACI 318-19. In addition, for beam-column joint specimens with confining reinforcement and a ratio of effective depth to embedment length of 1.5 or more, a strut-and-tie approach was used. For the ACI 318-19 anchorage provisions, three modes of failure were checked—breakout, side-face blowout, and strength of the anchor reinforcement. The analysis consisted of 178 beam-column joint specimens with head size $\leq 9.5A_b$ tested at the University of Kansas by Shao et al. (2016); 82 specimens without confining reinforcement and 96 specimens with confining reinforcement. Of those, a total of 40 specimens (18 specimens without confining reinforcement and 22 specimens with confining reinforcement) had a ratio of effective depth to embedment length of 1.5 or more.

The third phase of this research is to evaluate the ability of a granular micromechanics model for damage and plasticity of cementitious materials developed by Misra and Yang (2010), Misra and Singh (2014), Misra and Poorsolhjoui (2015), and Poorsolhjoui and Misra (2017), which has been highly successful for representing a number of nonlinear materials, but has not been used to represent reinforced concrete members, within finite element models. The models cover test specimens with strength governed by the anchorage failure of headed bars embedded in reinforced concrete slabs (shallow embedment specimens) and specimens measuring the bond performance of straight bars embedded in concrete blocks (beam-end specimens). A user material subroutine is used to implement the constitutive behavior of concrete material in tension and compression. The reinforcement (anchored bar) is represented using an elastic model. The interaction between concrete and reinforcement (anchored bar) is modeled based on cohesive behavior with damage. Three-dimensional simulations are performed for both specimens using ABAQUS linked to FORTRAN. To check the validity of the approach, the FE results are compared with those from tests by Shao et al. (2016) and Ghimire et al. (2018) for the headed bars embedded in slabs (shallow embedment specimens) and Darwin and Graham (1993) for straight bars embedded in the concrete block (beam-end specimens).

CHAPTER 2: EXPERIMENTAL WORK

This chapter describes the details of the CCT node test specimens, including beam design, test parameters, material properties, and test procedures. Section 2.1 describes the specimens, Section 2.2 describes the test parameters and specimen designation, Section 2.3 describes the material properties of the concrete and steel, Section 2.4 describes the fabrication of the specimens, Section 2.5 describes the test procedures and specimen instrumentation, and Section 2.6 provides the summary of test program.

2.1 DESCRIPTION OF SPECIMENS

The specimens were designed using the strut-and-tie method (STM) and a strut angle of 45° . Use of the STM is preferred for the analysis of discontinuity regions (D-regions) in reinforced concrete structures, such as those found near supports, openings, and connections. Using the STM models the complicated state of stress in D-regions as simple, uniaxial stress paths of a truss. The stress paths are investigated as members within the truss, identified as struts, ties, and nodal zones. Struts are members under compressive stress while ties are members subjected to tensile stress. Ties coincide with the location of reinforcement. Nodal zones, or nodes, are formed where struts and ties intersect. Figure 2.1 illustrates a strut-and-tie model. The force in each member of the truss can be determined using equilibrium if forces acting on the boundary of the strut-and-tie model are known.

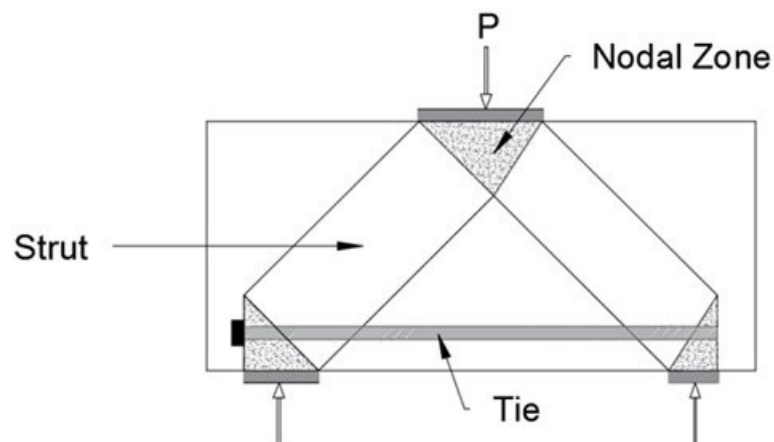


Figure 2.1 Strut-and-tie model

The CCT node specimens used in this study were 20 in. deep and 18 in. wide, with a clear span of 60 in. and total length of 104 in. Concrete with a nominal compressive strength of 5,000 psi was used for all specimens. No. 4 stirrups were used away from the strut and nodal zone to ensure that the specimens did not fail in shear. Specimens in Series 1 had stirrups spaced at 6 in., while specimens in Series 2 had stirrups spaced at 3.5 in. The tensile tie reinforcement consisted of 2 or 3 longitudinal bars. Embedment lengths were the same for both ends of a specimen. The two ends of the specimen were tested separately. At one end, the bars were terminated with a head, while at the other end, the bars were straight. Figures 2.2a and b show the test configurations for Series 1. Figures 2.3a and b show the test configurations for Series 2. Figure 2.4 shows the cross-sections of the specimens.

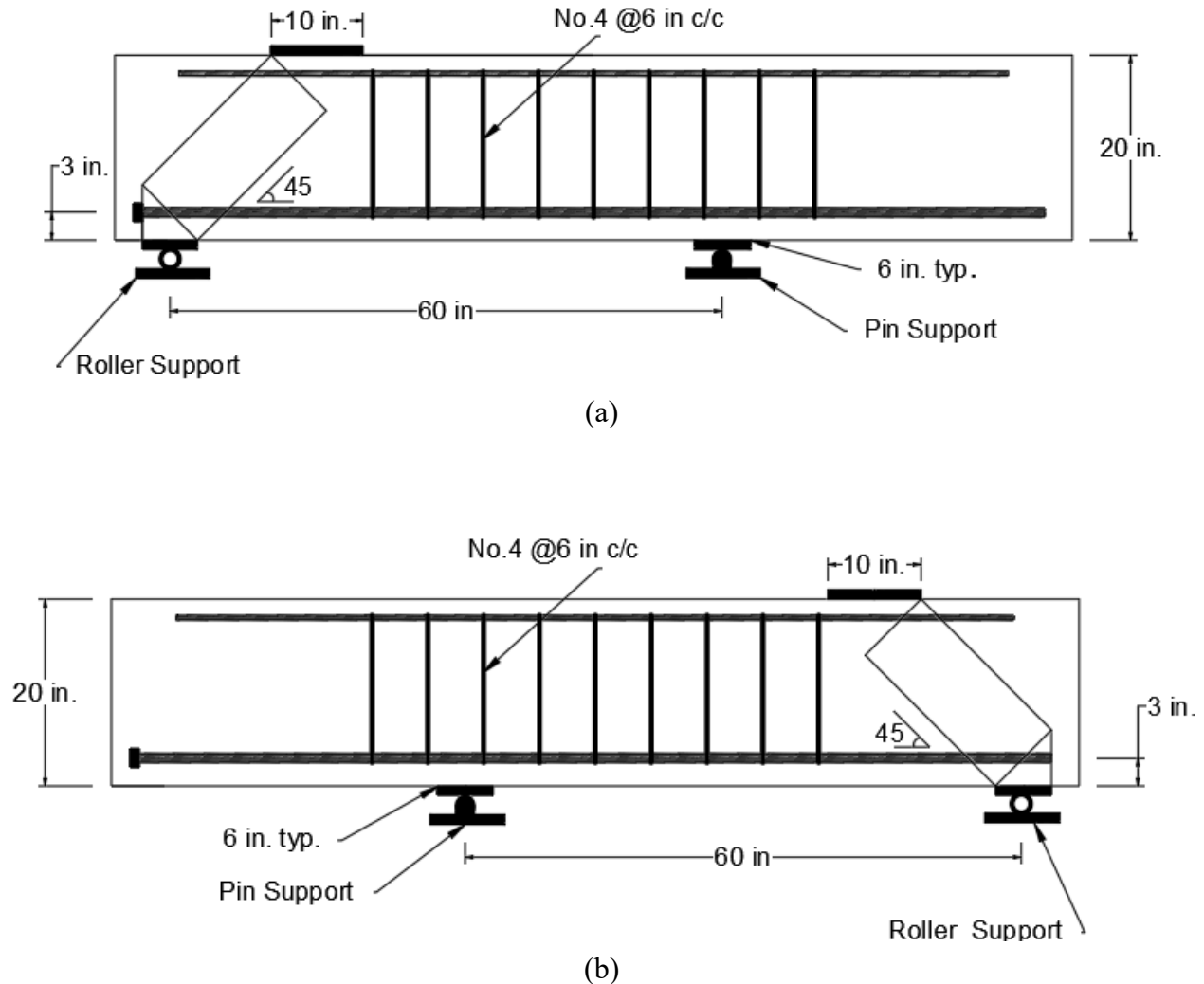
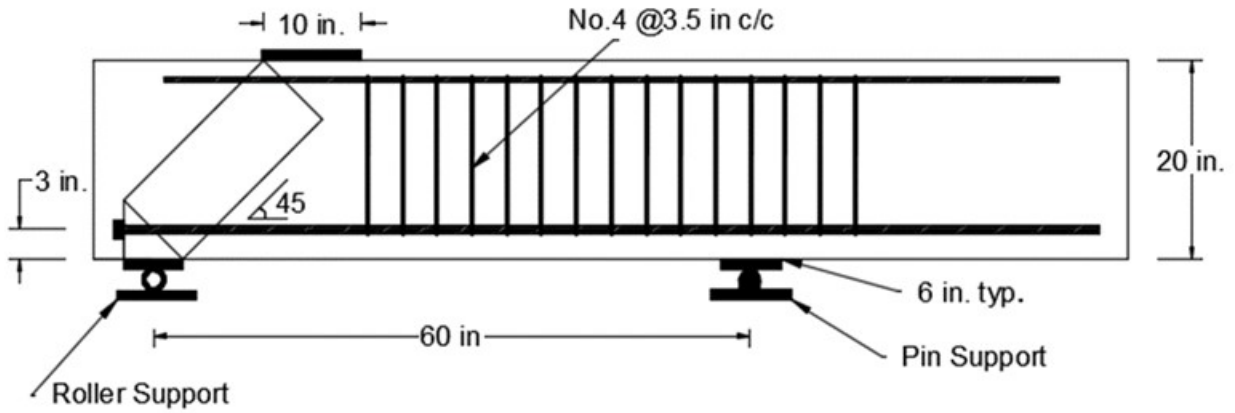
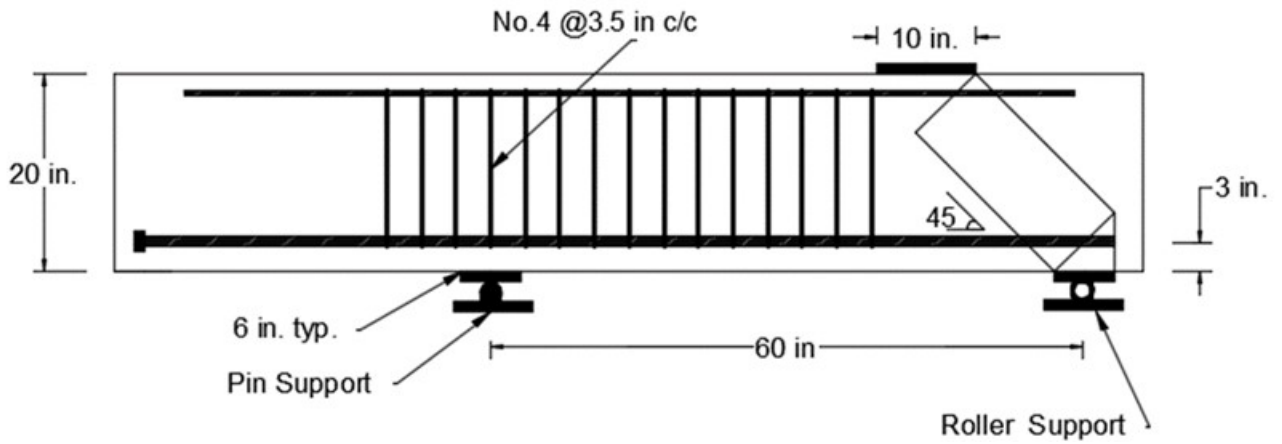


Figure 2.2 Testing configurations (a) headed end (b) non-headed end (Series 1)



(a)



(b)

Figure 2.3 Testing configurations (a) headed end (b) non-headed end (Series 2)

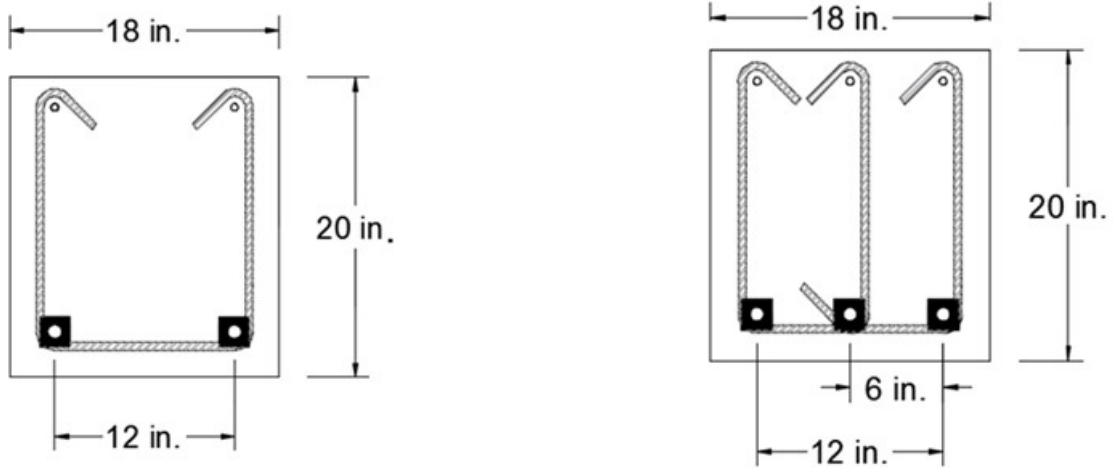


Figure 2.4 Cross-section of the specimens

2.2 TEST PARAMETERS

- 1. Bar size:** No. 8 bars were used in the study. The bars were fabricated using Grade 120 ASTM A1035 reinforcement.
- 2. Concrete compressive strength:** The target concrete compressive strength was 5,000 psi. Concrete mixture proportions are given in Section 2.3.1.
- 3. Number and spacing of headed bars:** Four specimens contained two headed bars with a center-to-center spacing of $12d_b$, while six specimens contained three headed bars with a center-to-center spacing of $6d_b$.
- 4. Embedment length:** Embedment lengths were measured from the face of the head to the intersection of the reinforcement with the extended nodal zone (ACI 318-19), as shown in Figure 2.5. For some of the specimens, the bearing face of the head aligned with the back edge of the bearing plate, providing a 9-in. embedment length. For the other specimens, the bearing face of the head was located beyond the edge of the bearing plate, providing an embedment length between 10 in. and 14 in., as shown in Figure 2.5. The same configurations were used for the non-headed end, with the embedment length measured from the end of the bar, as shown in Figure 2.6.

Two series of five specimens each were tested. Based on test results from Series 1, modifications were made to the stirrup spacing, embedment length, and strain gauge spacing (discussed later); these modifications were adapted for Series 2 specimens. In each series, two specimens contained two headed bars with a center-to-center spacing of $12d_b$, and three specimens contained three headed bars with a center-to-center spacing of $6d_b$. In Series 1, the embedment lengths varied from 9 to 14 in. Strain gauges were mounted on one bar (South bar as shown in Figure 2.7) at different locations (more details in Section 2.5.1). In Series 2, the embedment lengths varied from 9 to 13 in. Strain gauges were mounted on all bars using the same configuration (more details in Section 2.5.1)

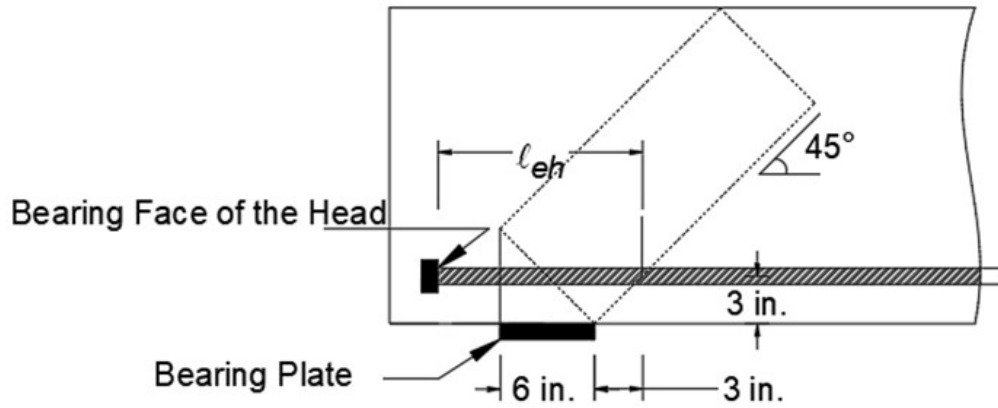


Figure 2.5 Position of heads with respect to bearing plate

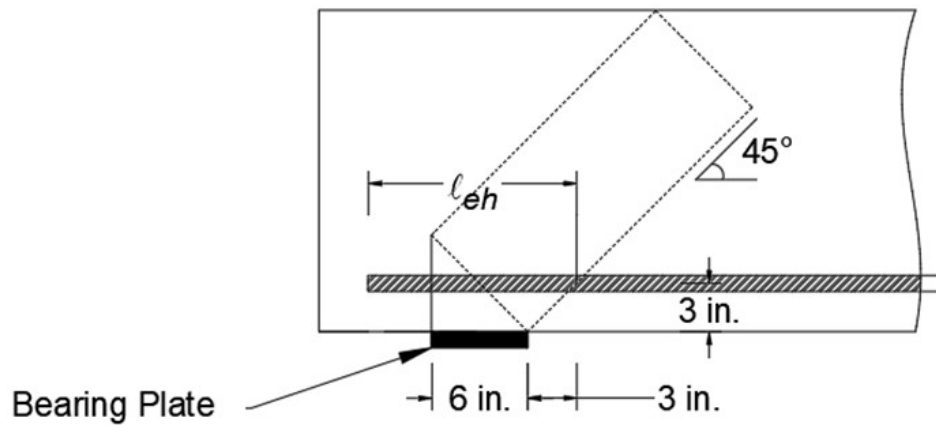


Figure 2.6 Position of non-headed end with respect to bearing plate

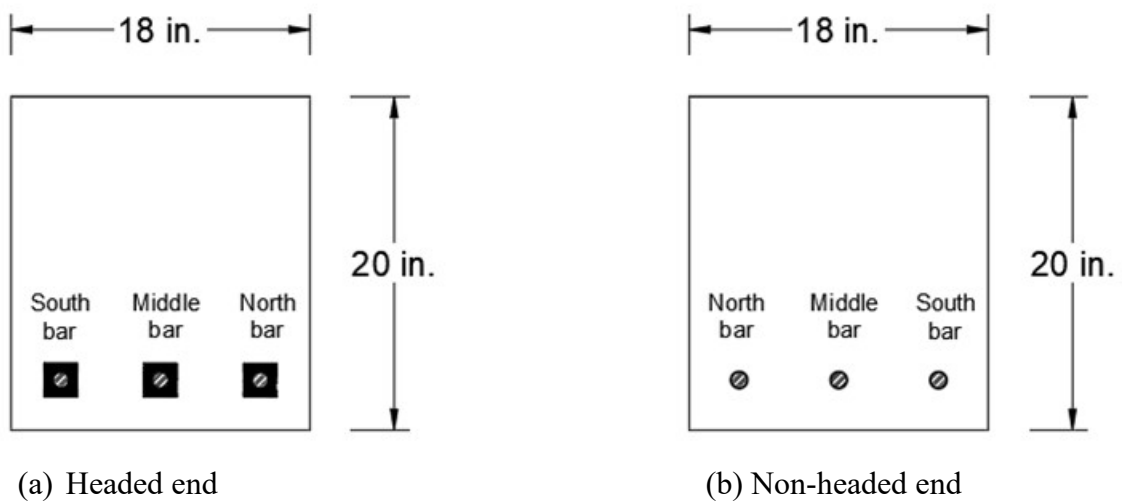



Figure 2.7 Position of bars (Strain gauges mounted on South bar)

5. Type of headed bars: Bars with F4.1 (Headed Reinforcement Corporation) heads were used in the tests. The heads had a net bearing area A_{brg} equal to 4.1 times the bar area A_b . Table 2.1 provides head dimensions and net bearing area of the headed bar.

Table 2.2 Head dimensions

Friction-Forged Headed Bars						
	Designation	Bar Size	b (in.)	h (in.)	t (in.)	Net Bearing Area
	F4.1	No. 8	2	2	1	$4.1A_b$

2.2.1 SPECIMEN DESIGNATION

The specimens are identified based on the variables used in this study, as illustrated in Figure 2.8.

The designation in Figure 2.8 indicates: 1. Type of end (H for headed end, NH for non-headed end); 2. number of headed bars in the specimen; 3. size of headed bar (ASTM designation); 4. nominal compressive strength of concrete (ksi); 5. nominal value of embedment length, ℓ_{eh} (in.); 6. type of headed bar; and 7. series designation (1 or 2). The example identifies a specimen cast with concrete with a nominal compressive strength of 5,000 psi containing three No. 8 F4.1 headed bar with a 9 in. embedment length in Series 1.

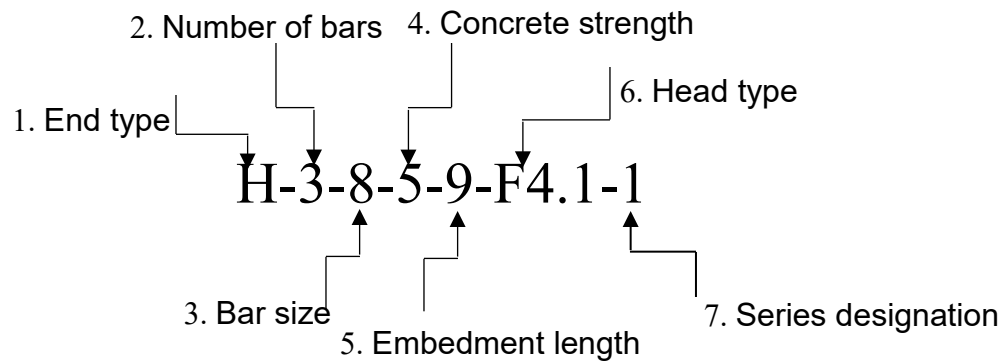


Figure 2.8 Specimen designation

2.3 MATERIAL PROPERTIES

2.3.1 Concrete properties

Concrete with a nominal compressive strength of 5,000 psi was used. The mixture proportions are given in Table 2.2.

Table 2.2 Concrete mixture proportions

Material	Quantity
Type I/II Cement, lb/yd ³	600
Water, lb/yd ³	299
Kansas River Sand, lb/yd ³ (SSD)*	1373
Crushed Limestone, lb/yd ³ (SSD)**	1721

* BSG (SSD) for Kansas River sand was 2.63

** The maximum aggregate size was ¾ in. and BSG (SSD) for limestone was 2.59

2.3.2 Steel properties

The headed bars used in this study were made of ASTM A1035 Grade 120 steel to help ensure that anchorage capacity was governed by the surrounding concrete and not the tensile strength of the headed bars. The confining reinforcement consisted of No. 4 ASTM A615 Grade 60 bars. The physical properties of the headed bars are shown in Table 2.3. The stress-strain curve for the bars is shown in Figure 2.9.

Table 2.3: Headed Bar Physical Properties

Bar Size	Heads	Yield Strength (ksi)	Tensile strength (ksi)	Nominal Diameter (in.)	Average Rib Spacing (in.)	Average Rib Height		Average Gap Width (in.)	Relative Rib Area ²
						A ¹ (in.)	B ² (in.)		
8	F4.1	129.0	169.0	1	0.633	0.065	0.060	0.347	0.084

¹ Per ASTM A615, A706. ² Per ACI 408R-03

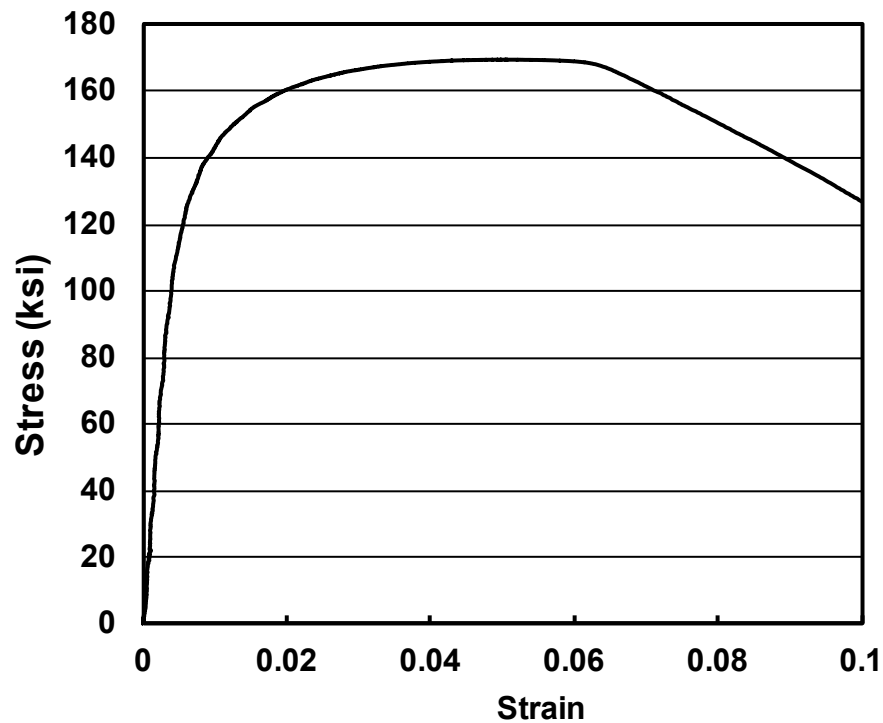


Figure 2.9 Stress-Strain curve for the headed bars

2.4 SPECIMEN FABRICATION

Forms were fabricated from plywood and 2 × 4 lumber. The reinforcing cages, consisting of the longitudinal reinforcement and stirrups, were placed in the forms, using metal chairs to provide the required cover. The specimens were cast in two layers. Each layer was consolidated using a 1¼ in. spud vibrator. The upper surface was screeded, floated, and then covered with plastic. The specimens were demolded when the concrete compressive strength reached 3,000 psi.

2.5 TEST PROCEDURES

The frame shown in Figures 2.10, 2.11, and 2.12, was used to test the specimens. Load was applied using four hydraulic jacks and transferred by threaded rods through load cells to spreader beams and a loading beam bearing on the specimen. The load cells were located so as to measure the force transmitted to the spreader beams by the threaded rod. Four load cells were used, two on the left side and two on the right side of the specimen. The headed end of the specimen was tested first, and then the specimen was turned around to test the non-headed end. The load was applied to the specimen through a 1 in. thick 10 × 18 in. steel plate. The test specimen was simply supported; the support close to the testing region was a roller, while the other support was a pin support, both of which were mounted on reinforced concrete support blocks. For the roller and pin supports, the width of the support plates was 6 in. The center to center distance between the supports plate was 60 in.

During the tests, load was applied monotonically to the specimen using hydraulic jacks in increments of 35 kips. Loading was paused at each interval to mark cracks and measure crack widths. Specimens were loaded to failure without pausing once the load approached approximately 80 % of the estimated failure load, which was estimated based on STM shown in Figure 2. 13. Tests lasted about one and a half hours.

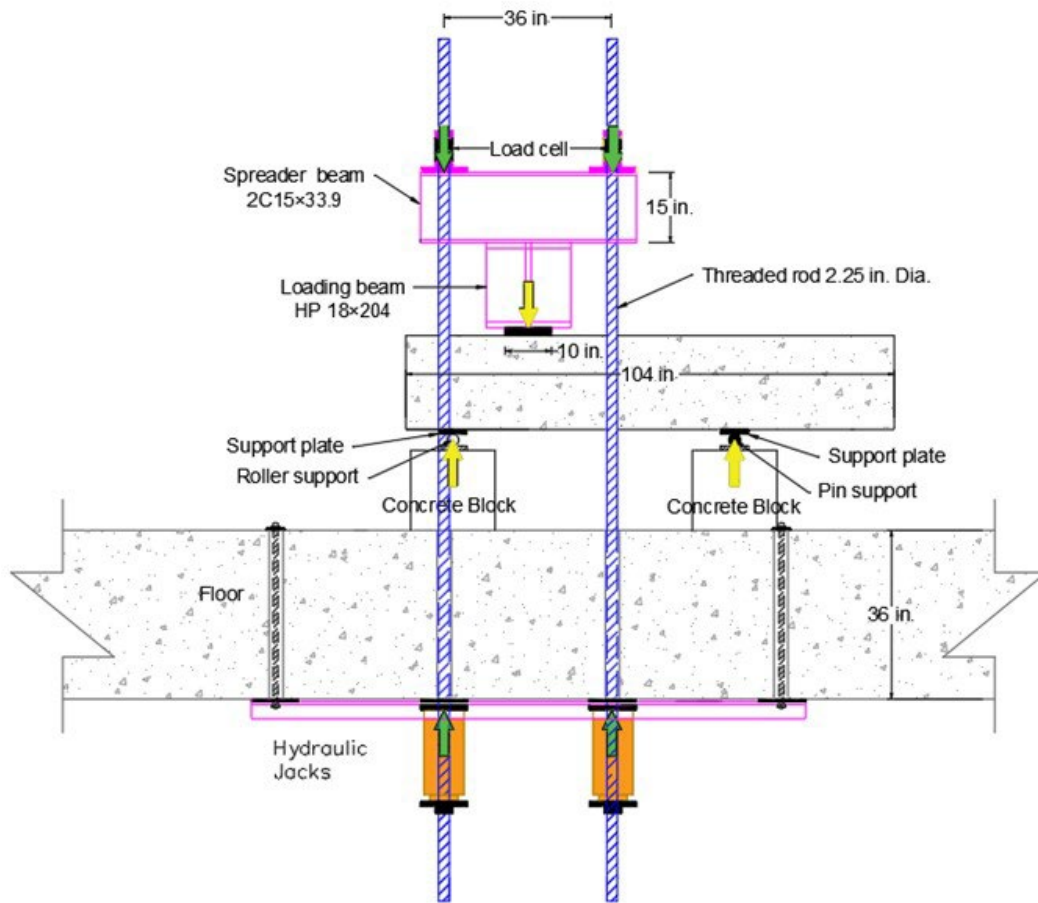


Figure 2.10 Front view of the loading system

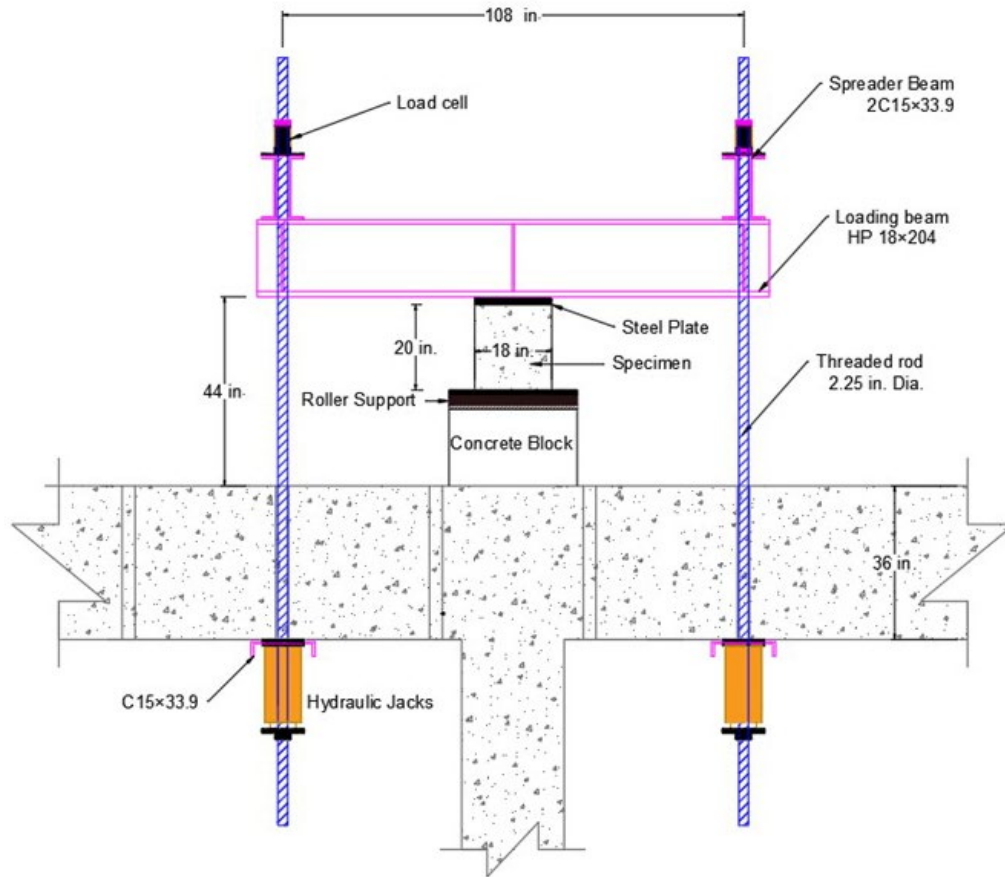


Figure 2.11 Side view of the loading system



Figure 2.12 CCT node test

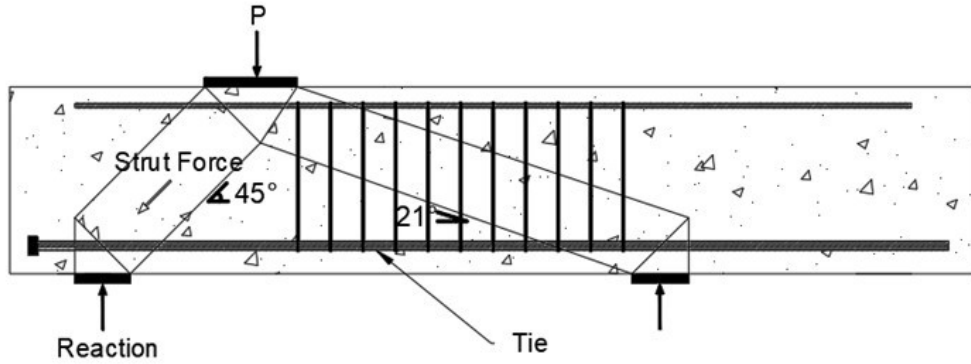
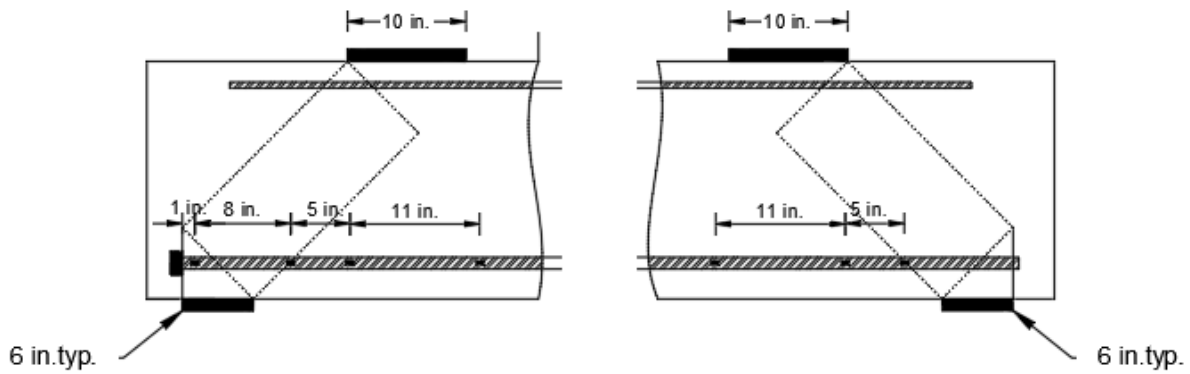


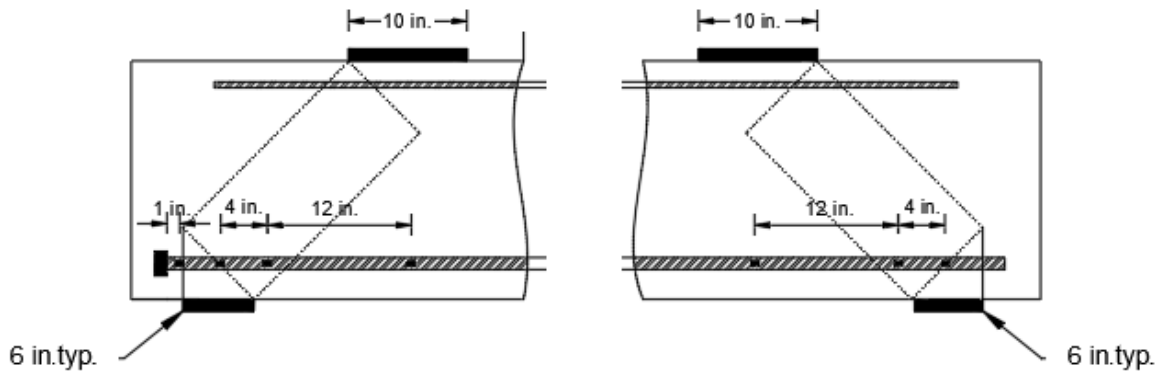
Figure 2.13 Strut and Tie Model

2.5.1 SPECIMEN INSTRUMENTATION

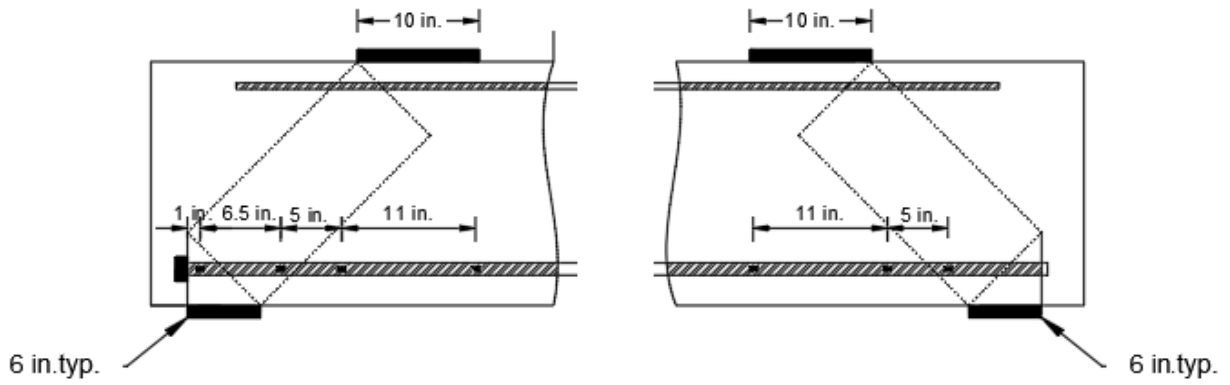
For specimens in Series 1, strain gauges were mounted on the headed bar at both the headed and non-headed ends on one bar (South bar as shown in Figure 2.7 and Figure 2.14). The position of strain gauges measured from the bearing face of the headed bar for the headed end and measured from the end of the bar for the non-headed end are listed in Table 2.4.



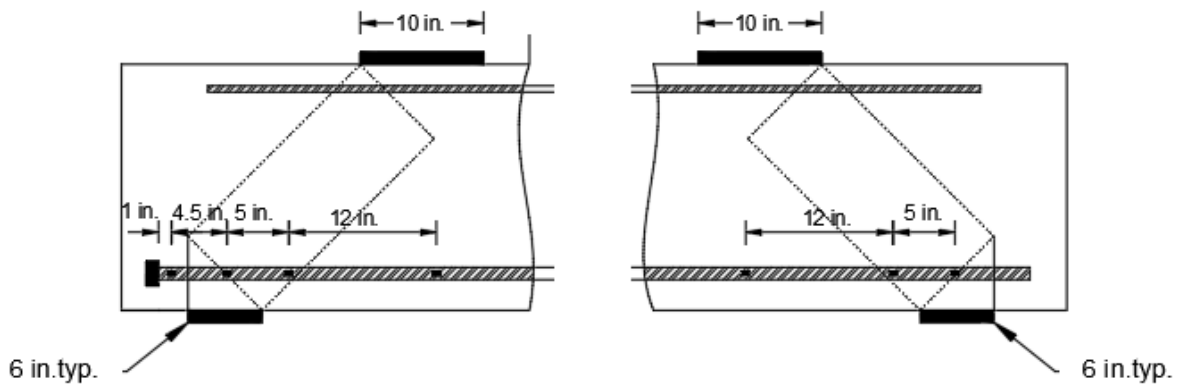
(a) Specimen H-2-8-5-9-F4.1-1 and NH-2-8-5-9-F4.1-1



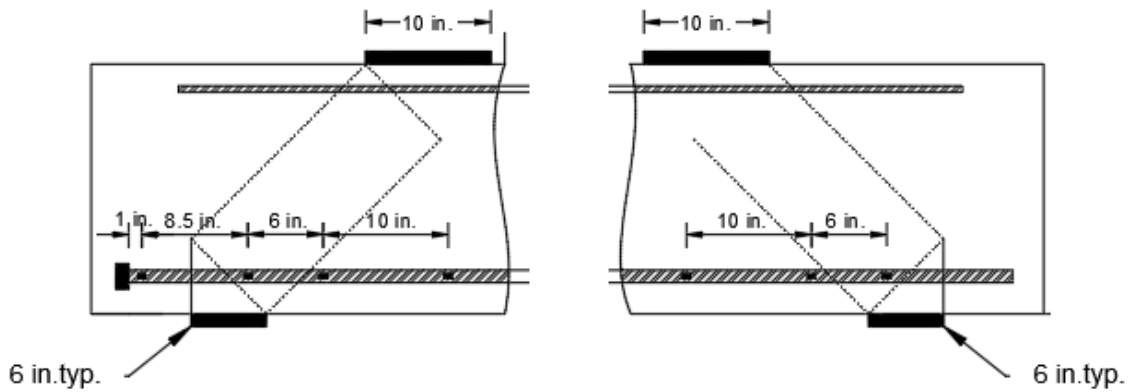
(b) Specimen H-2-8-5-10.4-F4.1-1 and NH-2-8-5-10.4-F4.1-1



(c) Specimen H-3-8-5-9-F4.1-1 and NH-3-8-5-9-F4.1-1



(d) Specimen H-3-8-5-11.4-F4.1-1 and NH-3-8-5-11.4-F4.1-1



(e) Specimen H-3-8-5-14-F4.1-1 and NH-3-8-5-14-F4.1-1

Figure 2.14 Placement of strain gauges for Series 1 specimens

Table 2.4: Distance at center of strain gauges measured from bearing face of the head for headed end and from bar end for non-headed end (Series 1)

Distance measured from bearing face of the head (in.)					Distance measured from bar end (in.)			
Beam Type	Strain gauge 1	Strain gauge 2	Strain gauge 3	Strain gauge 4	Beam Type	Strain gauge 1	Strain gauge 2	Strain gauge 3
H-2-8-5-9-F4.1-1	1.0	9.0	14.0	25.0	NH-2-8-5-9-F4.1-1	9.0	14.0	25.0
H-2-8-5-10.4-F4.1-1	1.0	4.5	8.5	20.5	NH-2-8-5-10.4-F4.1-1	4.5	8.5	20.5
H-3-8-5-9-F4.1-1	1.0	7.5	12.5	23.5	NH-3-8-5-9-F4.1-1	7.5	12.5	23.5
H-3-8-5-11.4-F4.1-1	1.0	5.5	9.5	21.5	NH-3-8-5-11.4-F4.1-1	5.5	9.5	21.5
H-3-8-5-14-F4.1-1	1.0	9.5	15.5	25.5	NH-3-8-5-14-F4.1-1	9.5	15.5	25.5

For specimens in Series 2, strain gauges were mounted on all the headed bars at both the headed and non-headed ends, as shown in Figure 2.15. At the headed end, strain gauges were placed 1 in. from the face of the head, at the center of the support, where the bar crossed the interior of the extended nodal zone, and under the center of the applied load. At the non-headed end, strain gauges were installed at the support, where the bar crossed the interior of the extended nodal zone, and under the center of the applied load point. The distance of strain gauges measured from the bearing face of the headed bar for the headed end and measured from the end of the bar for the non-headed end are listed in Table 2.5.

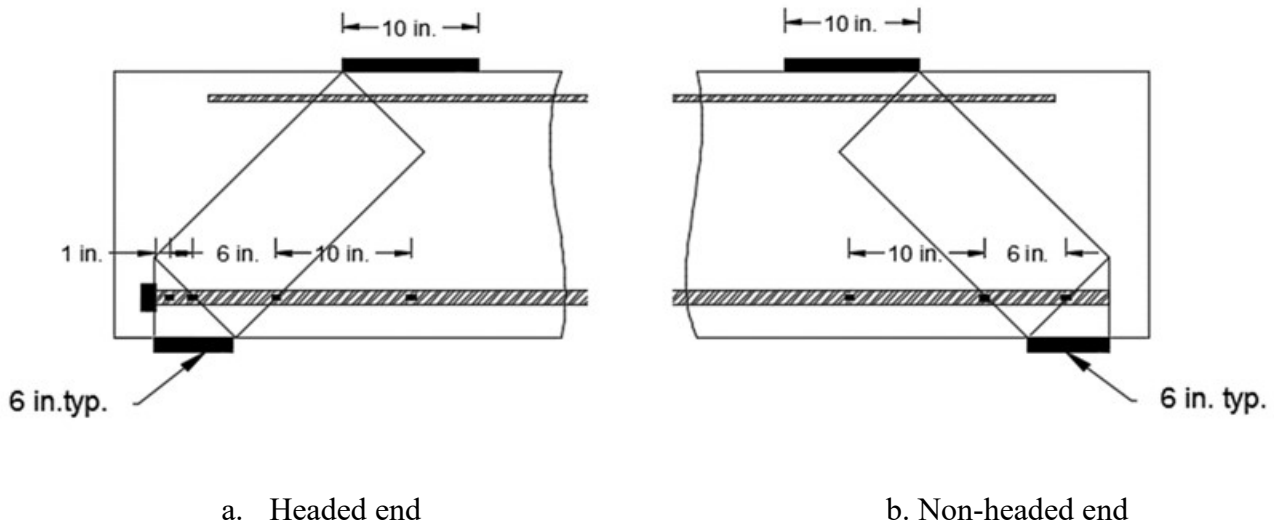


Figure 2.15 Placement of strain gauges for series 2 specimens

Table 2.5: Distance at center of strain gauges measured from bearing face of the head for headed end and from bar end for non-headed end (Series 2)

Distance from bearing face of the head (in.)					Distance from bar end (in.)			
Beam Type	Strain gauge 1	Strain gauge 2	Strain gauge 3	Strain gauge 4	Beam Type	Strain gauge 1	Strain gauge 2	Strain gauge 3
H-2-8-5-9-F4.1-2	1.0	3.0	9.0	19.0	NH-2-8-5-9-F4.1-2	3.0	9.0	19.0
H-2-8-5-13-F4.1-2	1.0	7.0	13.0	23.0	NH-2-8-5-13-F4.1-2	7.0	13.0	23.0
H-3-8-5-9-F4.1-2	1.0	3.0	9.0	19.0	NH-3-8-5-9-F4.1-2	3.0	9.0	19.0
H-3-8-5-11-F4.1-2	1.0	5.0	11.0	21.0	NH-3-8-5-11-F4.1-2	5.0	11.0	21.0
H-3-8-5-13-F4.1-2	1.0	7.0	13.0	23.0	NH-3-8-5-13-F4.1-2	7.0	13.0 </td <td>23.0</td>	23.0

A non-contact infrared-based system was used to measure displacements. Figure 2.16 shows the markers that were installed on the specimen near midspan and at the supports to provide information on the deflection, slip, and crack widths. A total of 35 markers were placed in a 5 × 7 square grid pattern on the specimen, as shown in Figures 2.16. The spacing between markers was 4 in. Five additional markers were used as stationary reference points—two on the beam, directly over the pin support (MR1 and MR2) and three on stationary support objects around the specimen (MR3, MR4, and MR5).

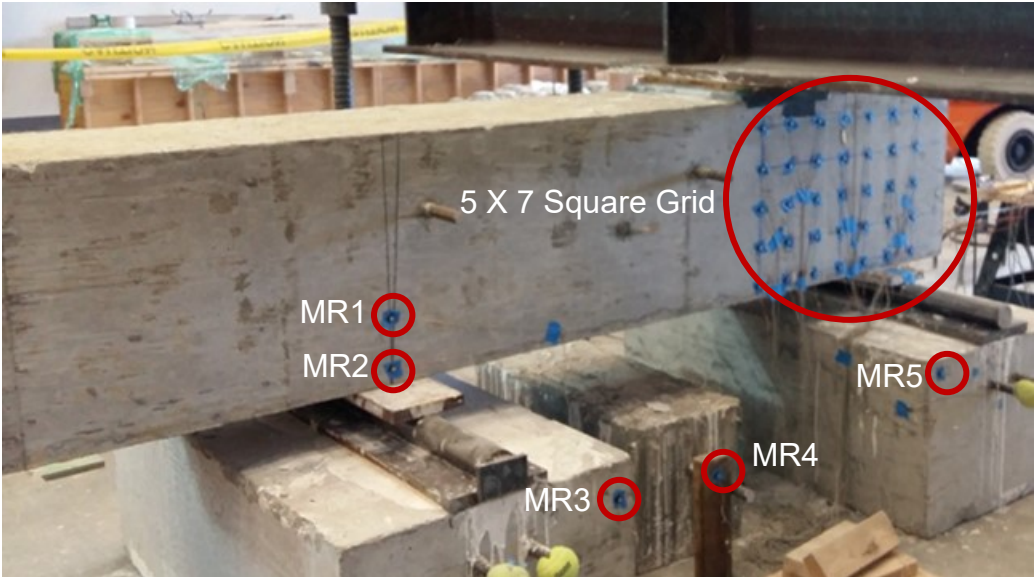


Figure 2.16 Placement of markers for a typical specimen

Linear potentiometers with displacement ranges of 2 in. and 4 in. were used to measure the horizontal slip at the ends of the bars relative to the outside face of the concrete beam, mounted as shown in Figure 2.17. The potentiometers were connected to the bar using a wire passing through a plastic tube cast into the concrete. The displacement of the linear potentiometers was subtracted from the displacement measured using the non-contact infrared based system to find the slip on the bar. Technical problems during testing prevented recording of slip at the ends of the non-headed bars.

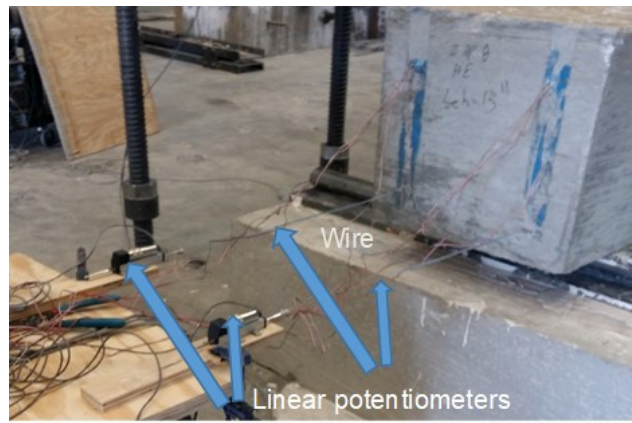


Figure 2.17 Linear potentiometer

Four load cells (Figure 2.18), each with a capacity of 200 kips, were used to measure the applied load. The load cells consisted of a hollow steel tube with an external diameter of 4 in., an internal diameter of 3 in., and a length of 6 in. Two 1-in. thick square steel plates were used on the top and bottom of the steel tube and held in place by springs at each corner, as shown in Figure 2.18. Four 350- Ω strain gauges were installed at the mid-height of the steel tube and wired as a full Wheatstone bridge; two strain gauges were oriented vertically and two were oriented horizontally.

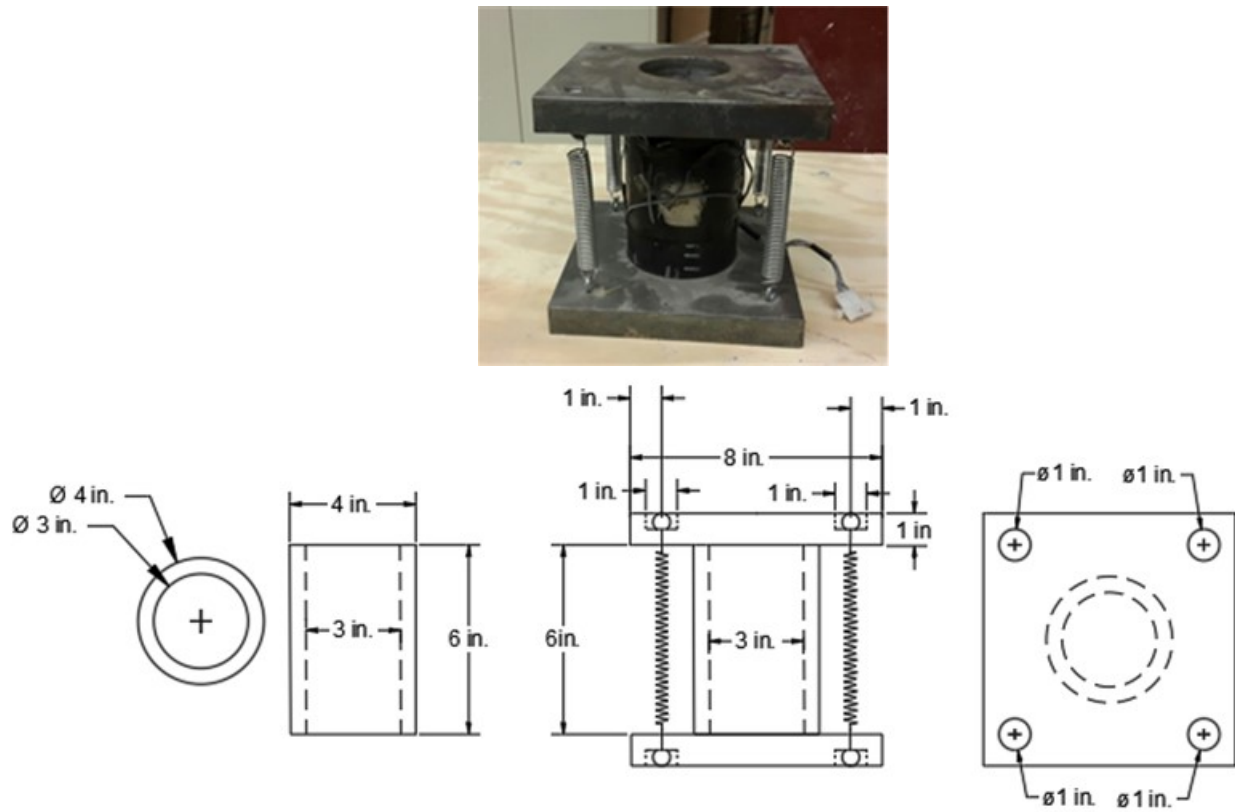


Figure 2.18 Details of load cell

2.6 SUMMARY OF TEST PROGRAM

A total of 10 CCT node specimens were tested, with embedment lengths ranging from 9.0 to 14.0 in. Concrete compressive strengths ranged from 4,630 to 5,750. Table 2.6 gives bar size, concrete compressive strength, and embedment length.

Table 2.6 Test Program for CCT Node Specimens

Beam Type	Bar Size	Concrete Compressive Strength (psi)	Embedment Length (in.)	No. of Headed Bars
Series 1 (Headed end)				
H-2-8-5-9-F4.1-1	No. 8	5740	9	2
H-2-8-5-10.4-F4.1-1		4490	10.4	2
H-3-8-5-9-F4.1-1		5800	9	3
H-3-8-5-11.4-F4.1-1		5750	11.4	3
H-3-8-5-14-F4.1-1		5750	14	3
Series 1 (Non-headed end)				
NH-2-8-5-9-F4.1-1	No. 8	5740	9	2
NH-2-8-5-10.4-F4.1-1		5330	10.4	2
NH-3-8-5-9-F4.1-1		5800	9	3
NH-3-8-5-11.4-F4.1-1		5750	11.4	3
NH-3-8-5-14-F4.1-1		5750	14	3
Series 2 (Headed end)				
H-2-8-5-9-F4.1-2	No. 8	4630	9	2
H-2-8-5-13-F4.1-2		4760	13	2
H-3-8-5-9-F4.1-2		4770	9	3
H-3-8-5-11-F4.1-2		4820	11	3
H-3-8-5-13-F4.1-2		4900	13	3
Series 2 (Non-headed end)				
NH-2-8-5-9-F4.1-2	No. 8	4630	9	2
NH-2-8-5-13-F4.1-2		4760	13	2
NH-3-8-5-9-F4.1-2		4770	9	3
NH-3-8-5-11-F4.1-2		4820	11	3
NH-3-8-5-13-F4.1-2		4900	13	3

CHAPTER 3: TEST RESULTS AND ANALYSIS OF CCT NODE SPECIMENS

This chapter describes the behavior of the CCT-node specimens during testing. Specimen behavior is reported in terms of crack development, strength, deflection, strain in the longitudinal reinforcement, and slip of the headed and non-headed ends of the reinforcing bars relative to the surrounding concrete. Analyses are presented that estimate the internal stresses acting in the anchorage region and compare them to limits prescribed by the ACI Building Code (318-19). Analyses of test results from the current and an earlier study (Thompson 2006a) are presented.

3.1 CRACKING BEHAVIOR AND MODE OF FAILURE

3.1.1 Cracking Behavior

Figure 3.1 illustrates cracking at the end of a specimen with longitudinal reinforcement terminated with a head (Specimen H-3-8-5-13-F4.1-2 is pictured). The specimens with headed reinforcement had similar cover, bar size, head size, and concrete compressive strength, and had similar cracking patterns. The first crack was observed at a load of approximately 80 kips for all specimens, and was oriented vertically under the applied load.

As the force increased, cracks propagated towards the loading point and additional vertical cracks developed. As illustrated in Figures 3.1b and 3.1c, vertical cracks that developed between the roller support and the loading point tended to become inclined as they propagated towards the region where the compressive strut was assumed to be active. Upon further loading, an inclined crack extended from the edge of the support plate up towards the load point at an angle of approximately 45 degrees from horizontal (Figure 3.1d). This inclined crack was typically first observed at about 50% of the peak load. As the load continued to increase and the specimen neared failure, existing cracks tended to widen and continue to propagate towards the load point (Figure 3.1e).

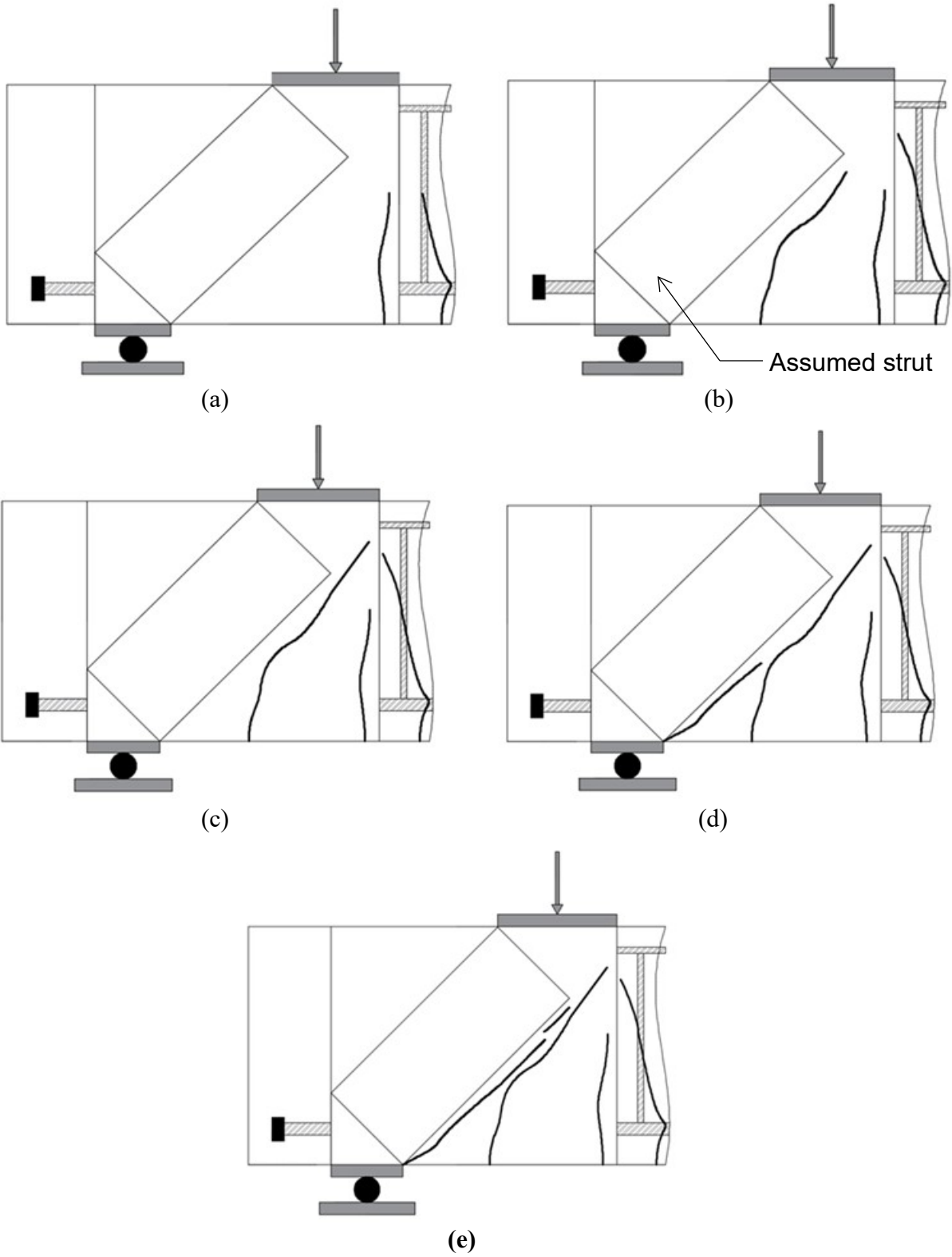


Figure 3.1 Observed crack growth in specimen with longitudinal bar anchored with a head.
Specimen H-3-8-5-13-F4.1-2

Failure modes varied slightly for the specimens, as will be described in Section 3.1.2. Failures were sudden and led to a total loss of strength. Figure 3.2 shows Specimen H-3-8-5-13-F4.1-2 after failure. The wide inclined crack extending from the edge of the support plate towards the load point and the dislodged side cover were typical for specimens with headed reinforcing bars.



Figure 3.2 Specimen H-3-8-5-13-F4.1-2 after failure

Figure 3.3 illustrates the typical pattern of cracking at the end of specimens with longitudinal reinforcement terminated without a head (specimen NH-3-8-5-13-F4.1-2, the non-headed end of specimen H-3-8-5-13-F4.1-2, is pictured). Unlike the specimens in which the longitudinal bars were anchored by a head, specimens with straight bar anchorage exhibited prominent inclined cracks near and over the support, as shown in Figure 3.3b. As the specimen neared failure, the inclined cracks widened and propagated towards the top bearing plate. The wide inclined cracks are believed to result from the longitudinal bars losing bond and pulling out of the concrete. As explained in Chapter 2, the anchorage length of the straight (non-headed) bars was the same as for the headed bars to obtain a measure of the contribution from the heads and, as such, was known to be insufficient to develop the bars.

Figure 3.4 shows a photo of Specimen NH-3-8-5-13-F4.1 after failure. The failure, which was dominated by opening of the inclined crack located near or over the support, occurred suddenly.

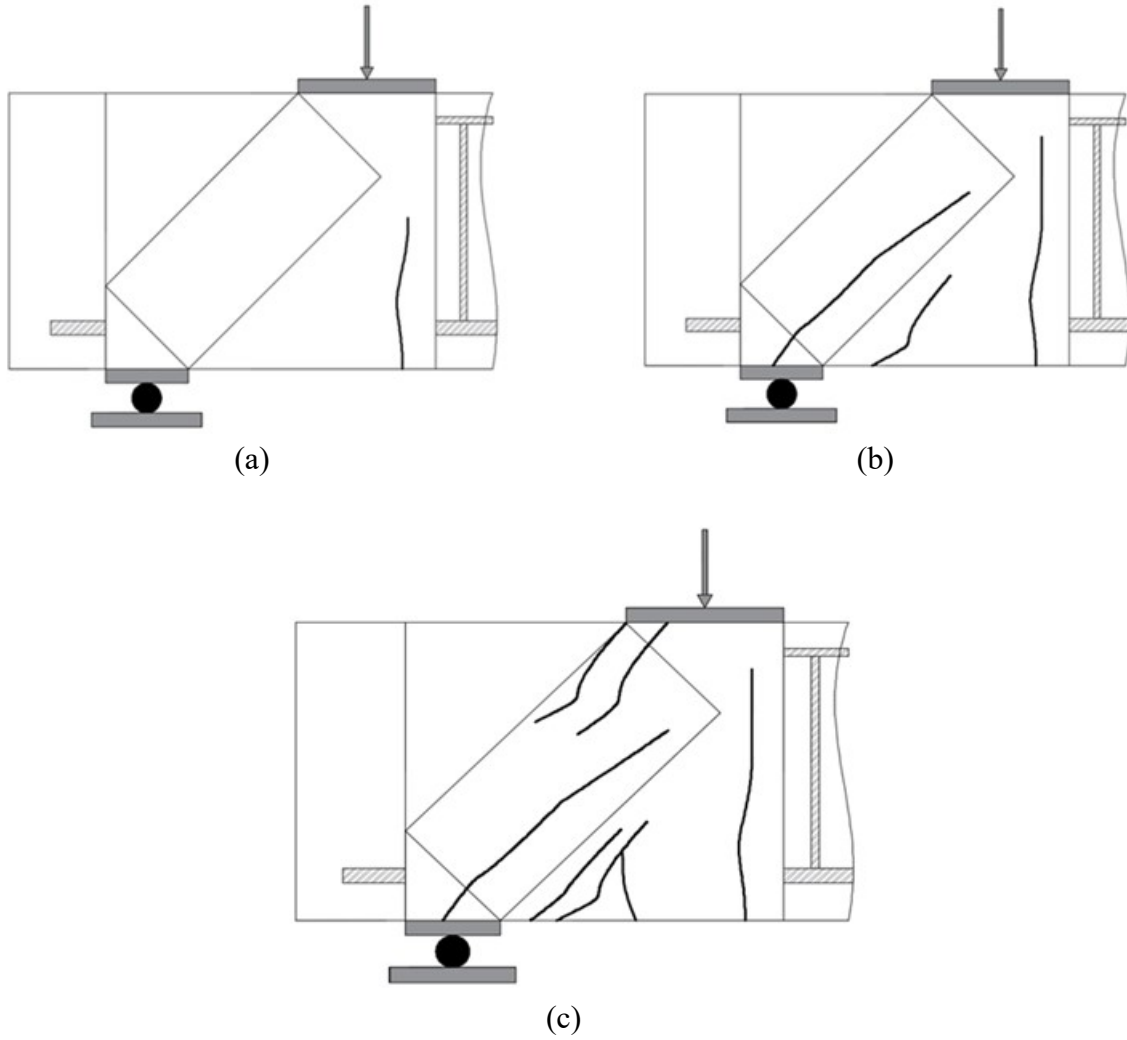


Figure 3.3 Observed crack growth in specimen with longitudinal bar anchored with straight reinforcement. Specimen NH-3-8-5-13-F4.1-2



Figure 3.4 Specimen NH-3-8-5-13-F4.1-2 after failure

3.1.2 Modes of Failure

Three failure modes were observed during the tests. Table 3.1 indicates which mode dominated in each test.

Table 3.1 Failure Modes

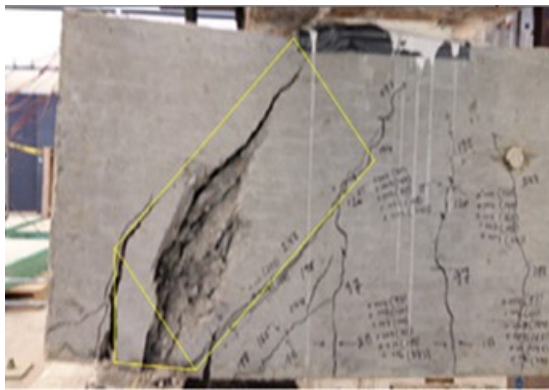
Series 1		Series 2	
Beam Type	Failure Type	Beam Type	Failure Type
H-2-8-5-9-F4.1-1	Side-face blowout	H-2-8-5-9-F4.1-2	Side-face blowout
H-2-8-5-10.4-F4.1-1	Side-face blowout	H-2-8-5-13-F4.1-2	Side-face blowout
H-3-8-5-9-F4.1-1	Side-face blowout	H-3-8-5-9-F4.1-2	Concrete crushing
H-3-8-5-11.4-F4.1-1	Side-face blowout	H-3-8-5-11-F4.1-2	Side-face blowout
H-3-8-5-14-F4.1-1	Side-face blowout	H-3-8-5-13-F4.1-2	Side-face blowout
NH-2-8-5-9-F4.1-1	Pullout	NH-2-8-5-9-F4.1-2	Pullout
NH-2-8-5-10.4-F4.1-1	Pullout	NH-2-8-5-13-F4.1-2	Pullout
NH-3-8-5-9-F4.1-1	Pullout	NH-3-8-5-9-F4.1-2	Pullout
NH-3-8-5-11.4-F4.1-1	Pullout	NH-3-8-5-11-F4.1-2	Pullout
NH-3-8-5-14-F4.1-1	Pullout	NH-3-8-5-13-F4.1-2	Pullout

Side-face blowout: The majority of the headed-end tests failed in a manner dominated by side-face blowout, which is characterized by a sudden separation of the side cover along a plane intersecting the outermost longitudinal reinforcing bar (Figure 3.5).

Concrete crushing: In one case, pronounced crushing of concrete was observed parallel to the assumed compressive strut in front of the head and within the assumed nodal zone, as shown in Figure 3.6. This occurred in Specimen H-3-8-5-9-F4.1-2, which had three No. 8 bars and an embedment length ℓ_{eh} of 9 in. measured from the boundary of the extended nodal zone (point where the bar intersects the assumed strut).



Figure 3.5 Side-face blowout failure – Specimen H-3-8-5-13-F4.1-2



a. Side view



b. Bottom of the specimen

Figure 3.6 Concrete crushing failure – Specimen H-3-8-5-9-F4.1-2

Pullout failure: All non-headed end tests failed due to pullout of the longitudinal reinforcing bar (Figure 3.7). Prior to failure, slip of the bar relative to the surrounding concrete resulted in formation of cracks at the level of the longitudinal reinforcement. This crack extended along the side and bottom of the specimen after failure.



Figure 3.7 Pullout failure – Specimen H-3-8-5-11-F4.1-2

3.2 PEAK LOAD AND EMBEDMENT LENGTH

Table 3.2 summarizes the test results, including the concrete compressive strength on the day of testing, the peak force applied to each specimen, and deflection at peak load of the specimen. Deflection, described in Section 3.3, was calculated using results from the non-contact infrared-based system described in Chapter 2. The reported deflection is the vertical displacement of the beam directly under the applied load, corrected for movement of the supports.

The peak force applied to each specimen is plotted for the beams in Series 1 and Series 2 in Figures 3.8 and 3.9, respectively. In general, the peak force increased as the embedment length increased for both the headed and non-headed bar tests. As expected, the peak load in the specimens containing three bars was greater than in those containing two bars. Deflections at failure for both headed and non-headed bar tests also increased with increases in embedment length and increases in the number of longitudinal bars.

Table 3.2 Summary of Test Results

Beam Type	Embedment Length (in.)	Concrete Compressive Strength (psi)	Peak Load (kips)	Deflection at Peak Load (in.)
Series 1 / Headed end				
H-2-8-5-9-F4.1-1	9.0	5740	278	0.20
H-2-8-5-10.4-F4.1-1	10.4	4490	346	0.30
H-3-8-5-9-F4.1-1	9.0	5800	446	*
H-3-8-5-11.4-F4.1-1	11.4	5750	386	0.33
H-3-8-5-14-F4.1-1	14.0	5750	495	*
Series 1 / Non-headed end				
NH-2-8-5-9-F4.1-1	9.0	5740	158	0.05
NH-2-8-5-10.4-F4.1-1	10.4	5330	236	0.13
NH-3-8-5-9-F4.1-1	9.0	5800	255	*
NH-3-8-5-11.4-F4.1-1	11.4	5750	245	*
NH-3-8-5-14-F4.1-1	14.0	5750	356	0.18
Series 2 / Headed end				
H-2-8-5-9-F4.1-2	9.0	4630	218	0.10
H-2-8-5-13-F4.1-2	13.0	4760	250	0.11
H-3-8-5-9-F4.1-2	9.0	4770	355	0.14
H-3-8-5-11-F4.1-2	11.0	4820	403	0.19
H-3-8-5-13-F4.1-2	13.0	4900	499	0.37
Series 2 / Non-headed end				
NH-2-8-5-9-F4.1-2	9.0	4630	218	*
NH-2-8-5-13-F4.1-2	13.0	4760	234	0.08
NH-3-8-5-9-F4.1-2	9.0	4770	205	0.08
NH-3-8-5-11-F4.1-2	11.0	4820	316	0.13
NH-3-8-5-13-F4.1-2	13.0	4900	365	0.14

*Data not available

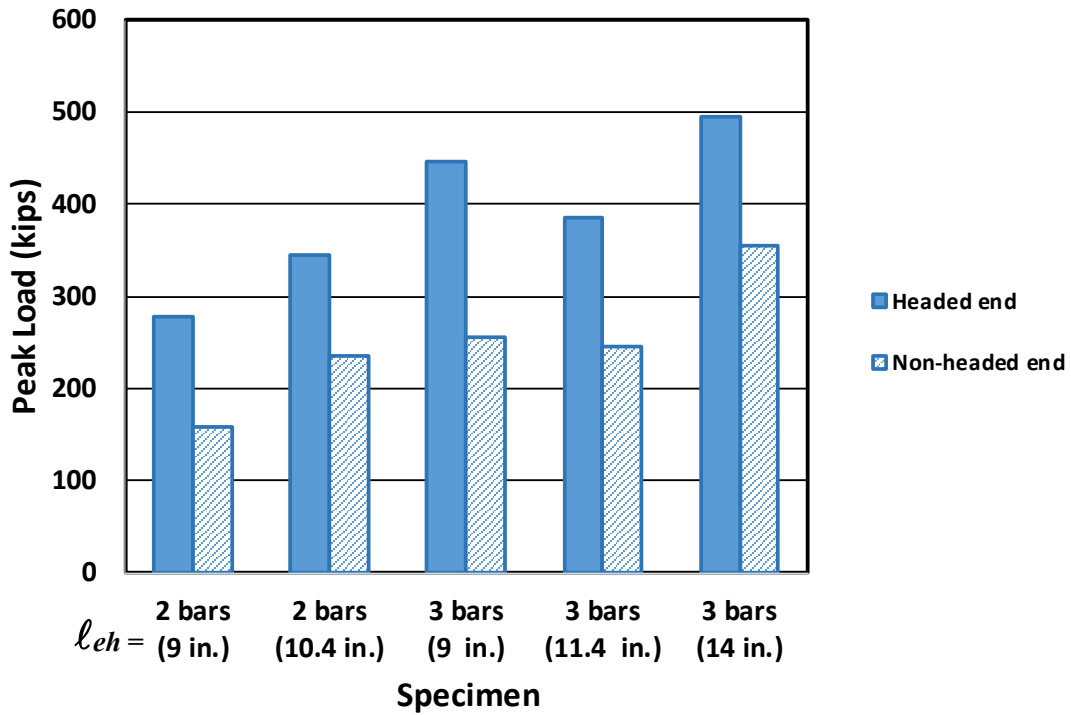


Figure 3.8 Peak load recorded for headed and non-headed end – specimens identified by number of bars and embedment length (Series 1)

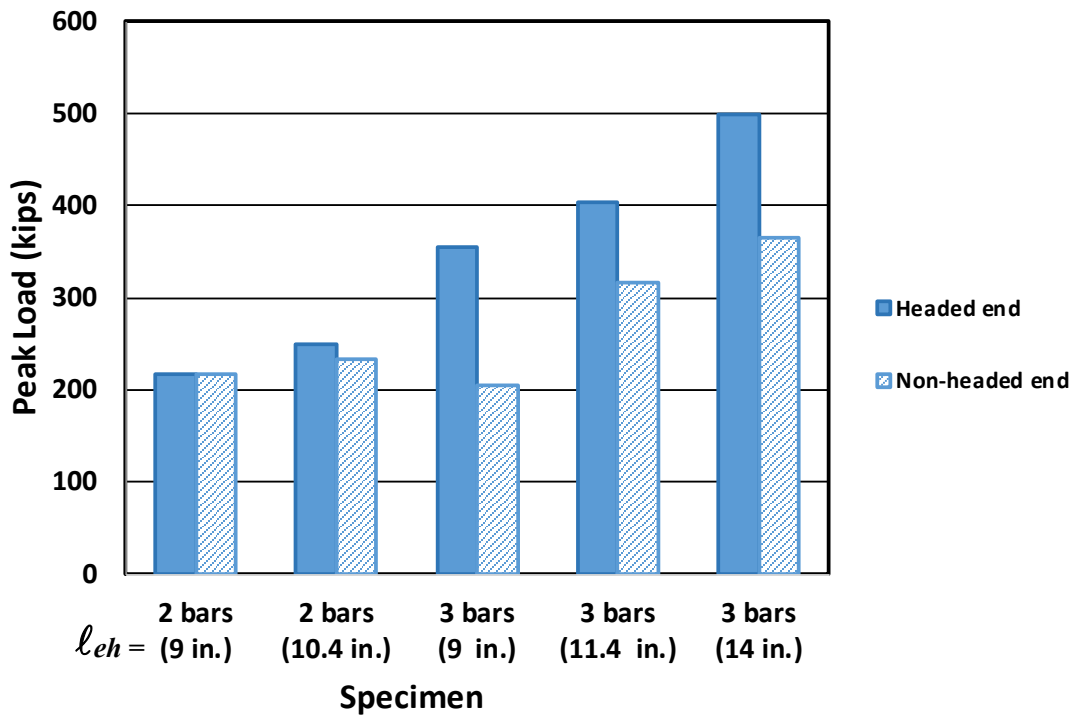


Figure 3.9 Peak load recorded for headed and non-headed end – specimens identified by number of bars and embedment length (Series 2)

3.3 LOAD-DEFLECTION RESPONSE

Figure 3.10 shows applied force versus deflection under the loading point for specimens in Series 1 with headed bar anchorages (data from specimens H-3-8-5-9-F4.1-1 and H-3-8-5-14-F4.1-1 was lost during testing). Figure 3.11 shows applied force versus deflection under the loading point for the five specimens in Series 2 with headed bar anchorages (H-2-8-5-9-F4.1-2, H-2-8-5-13-F4.1-2, H-3-8-5-9-F4.1-2, H-3-8-5-11-F4.1-2, and H-3-8-5-13-F4.1-2). The specimens in the two series exhibited similar behavior. Upon initial loading, the specimens had similar stiffness until the load reached approximately 80 kips, at which point all specimens exhibited a reduction in stiffness due to formation of the first flexural crack. After cracking, the specimens with three longitudinal bars exhibited higher stiffness than the specimens with two longitudinal bars, as expected. All the specimens with three longitudinal bars had nearly the same stiffness up to the peak load. This differs from the response of the two specimens with two longitudinal bars, in which the specimen with the longer embedment length exhibited greater post-cracking stiffness.

Figure 3.12 shows applied force versus deflection under the loading point for Specimens H-2-8-5-10.4-F4.1-1 and NH-2-8-5-10.4-F4.1-1. Figure 3.13 shows applied force versus deflection under the loading point for Specimens H-3-8-5-13-F4.1-2 and NH-3-8-5-13-F4.1-2. These two specimens, which were nominally identical except for the anchorage used for the longitudinal reinforcing bars, illustrate the effect of the headed end on beam behavior. Both specimens had similar stiffness until the specimen with the non-headed bar end failed by bar pullout due to insufficient development length. The specimen with the headed bar end continued to gain strength until it failed at a deflection that was more than double that of the beam with the non-headed reinforcement. The similarity in responses shown in Figure 3.12 and 3.13 also indicates that the test of the headed bar end of the specimen (which was tested first) did not negatively affect the non-headed end of the specimen. The load-deflection curves for all specimens are provided in Figures B.3 to B.8 in Appendix B.

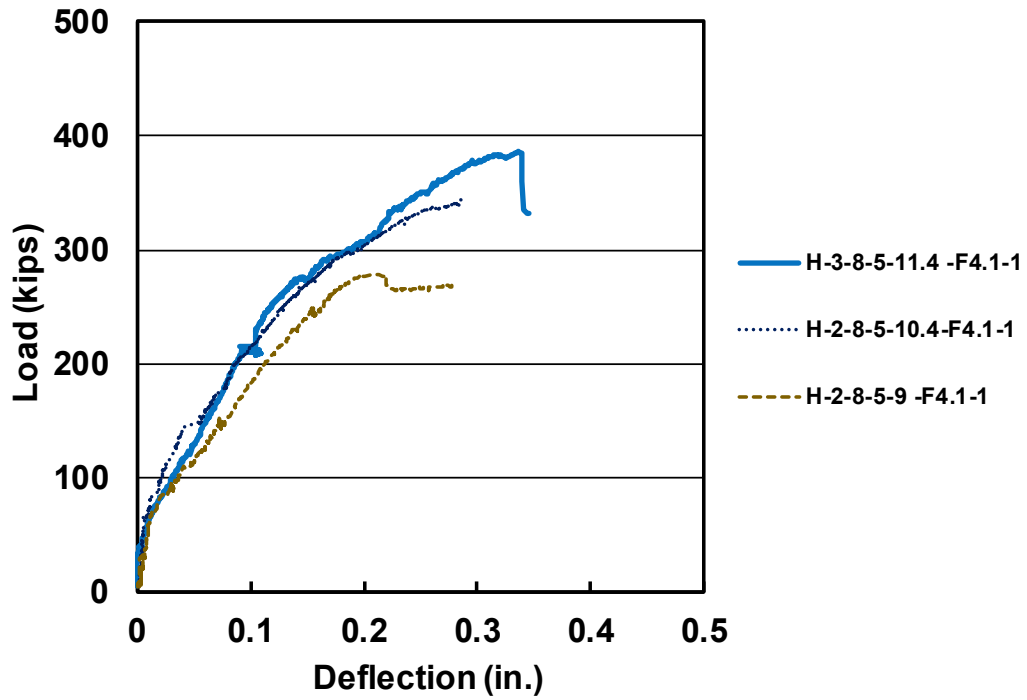


Figure 3.10 Load versus deflection results for the Series 1 headed-end tests

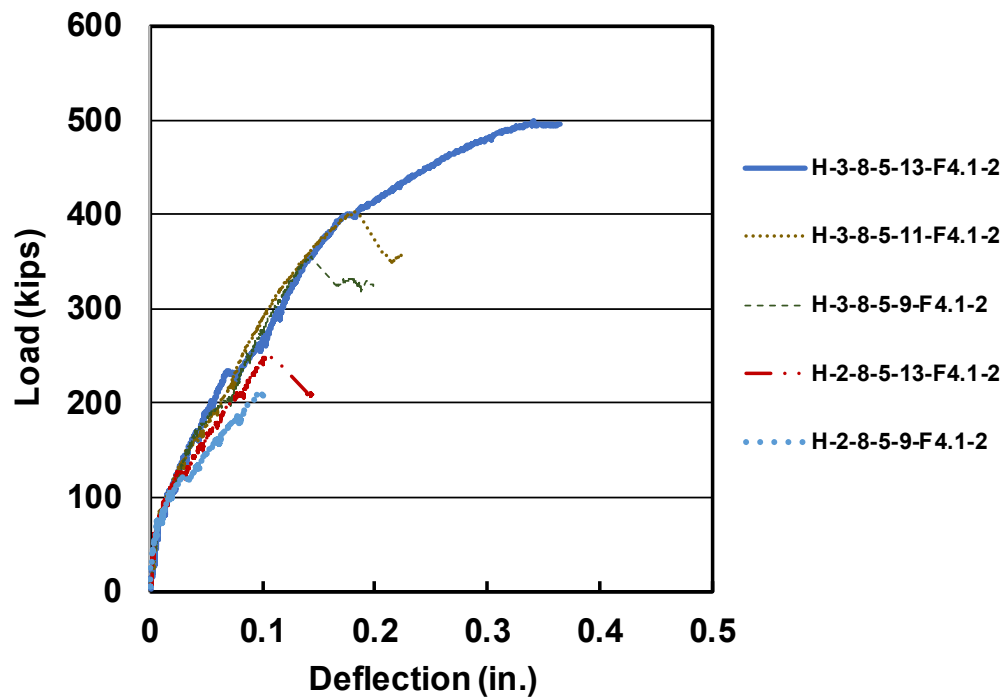


Figure 3.11 Load versus deflection results for the Series 2 headed-end tests

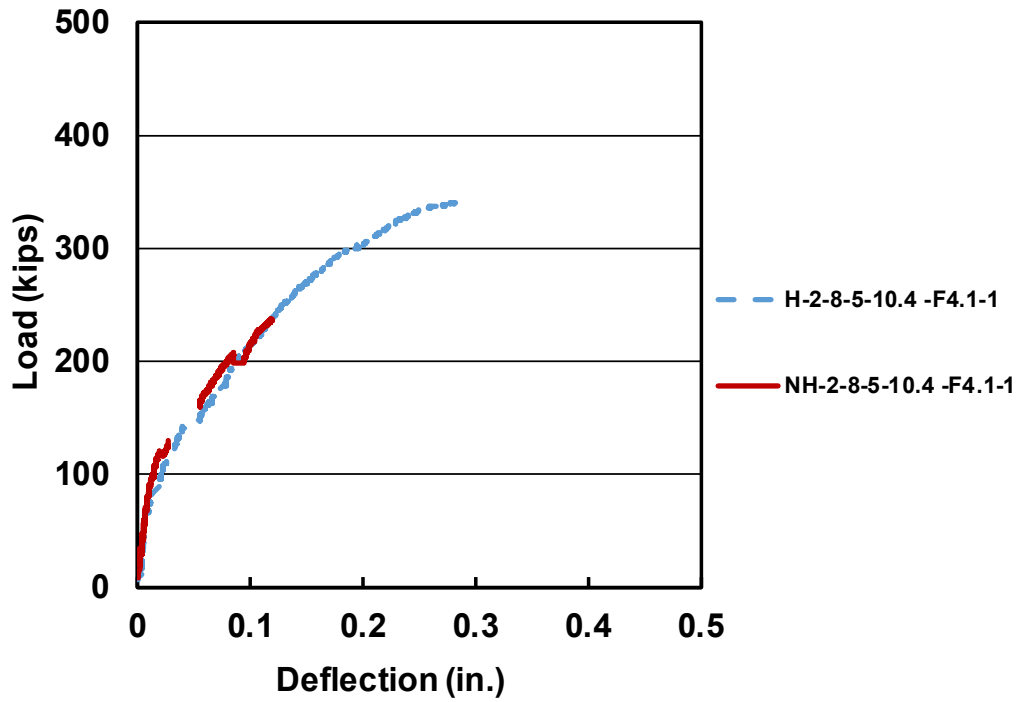


Figure 3.12 Load versus deflection results for Specimens H-2-8-5-10.4-F4.1-1 and NH-2-8-5-10.4-F4.1-1 (Series 1)

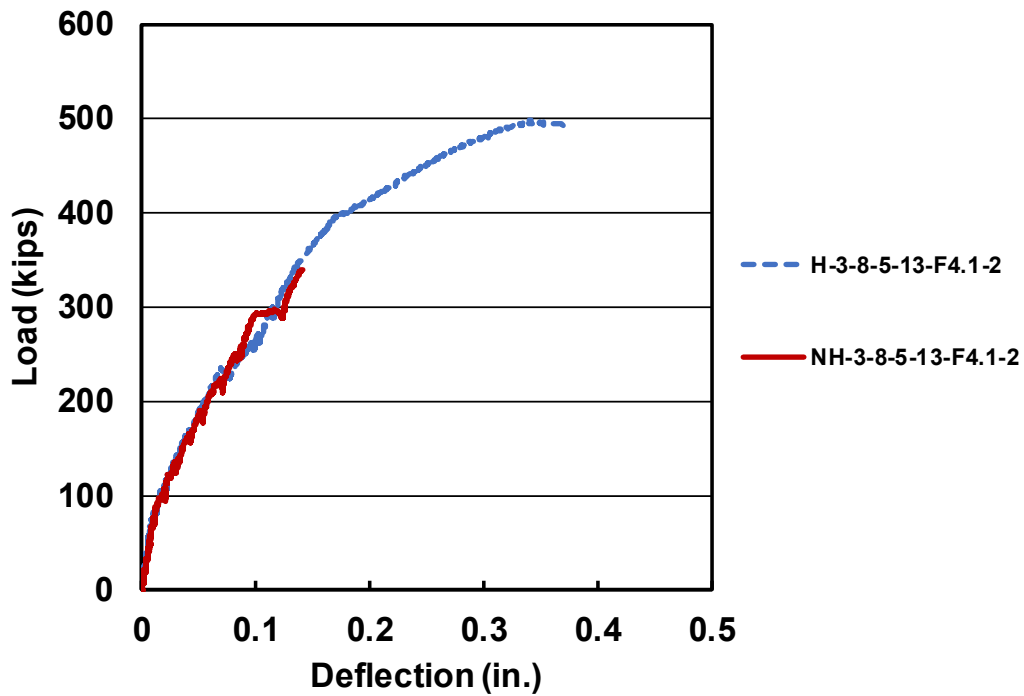


Figure 3.13 Load versus deflection results for Specimens H-3-8-5-13-F4.1-2 and NH-3-8-5-13-F4.1-2 (Series 2)

3.4 STRAIN IN REINFORCEMENT

Strain gauges were placed along the reinforcing bars to measure the strain near both the headed and non-headed end. As described in Section 2.5.1, for bars with heads, the strain gauges were centered (1) 1 in. from the face of the head, (2) at the center of the support, (3) where the bar intersected the boundary of the extended nodal zone, and (4) under the center of the applied load (Figure 3.14). For the non-headed end, the strain gauges were centered (1) at the center of the support, (2) where the bar intersected the boundary of the assumed extended nodal zone, and (3) under the center of the applied load (Figure 3.14). The strain gauges were placed on one reinforcing bar in Series 1 specimens and on all reinforcing bars in Series 2 specimens.

For the specimens in Series 1, the location of gauges varied somewhat from this layout as described in Section 2.5.1 and shown in Figure 2.13.

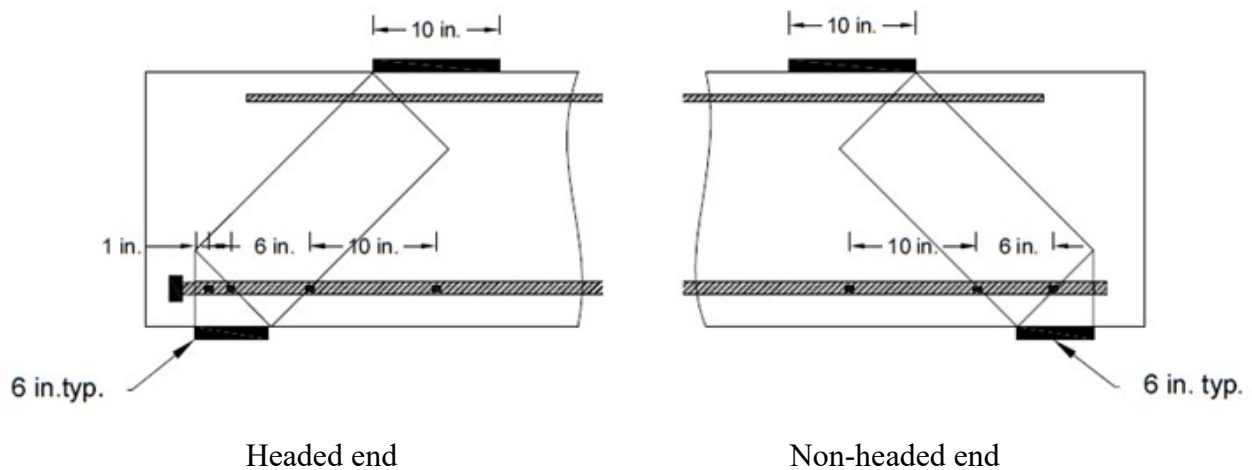


Figure 3.14 Position of strain gauges on longitudinal reinforcement (Series 2)

During the test, some strain gauges did not work and some failed prior to failure of the specimen. The peak load for each strain gauge is listed in Tables 3.3 and 3.4 for the specimens in Series 1 and 2, respectively.

Table 3.3 Peak load and peak load recorded by strain gauge (kips) (Series 1)

Beam Type	Peak Load (kips)	Strain gauge 1	Strain gauge 2	Strain gauge 3	Strain gauge 4
Series 1/Headed end					
H-2-8-5-9-F4.1-1	278	278	*	278	278
H-2-8-5-10.4-F4.1-1	346	*	346	346	346
H-3-8-5-9-F4.1-1	446	**	**	**	**
H-3-8-5-11.4-F4.1-1	386	386	386	386	386
H-3-8-5-14-F4.1-1	495	495	495	450	494
Series 1/Non-headed end					
NH-2-8-5-9-F4.1-1	158	156	*	156	Non-headed ends of specimens do not have strain gauge 4
NH-2-8-5-10.4-F4.1-1	236	236	236	236	
NH-3-8-5-9-F4.1-1	255	**	**	**	
NH-3-8-5-11.4-F4.1-1	245	214	193	211	
NH-3-8-5-14-F4.1-1	356	200	356	356	

*Strain gauge not working

**Load-strain data not available

Table 3.4 Peak load and peak load recorded by strain gauge (kips) (Series 2)

Beam Type	Peak load (kips)	Strain gauge 1			Strain gauge 2			Strain gauge 3			Strain gauge 4		
		Bar	South	Middle	North	South	Middle	North	South	Middle	North	South	Middle
Series 2/ Headed end													
H-2-8-5-9-F4.1-2	218	218	***	218	218	***	160	*	***	160	107	***	182
H-2-8-5-13-F4.1-2	250	250	***	250	250	***	228	180	***	161	198	***	250
H-3-8-5-9-F4.1-2	355	355	355	355	355	355	200	238	*	342	198	300	200
H-3-8-5-11-F4.1-2	403	403	403	403	379	362	403	240	240	264	241	331	238
H-3-8-5-13-F4.1-2	499	443	400	500	382	*	*	271	228	163	229	287	*
Series 2/ Non-headed end													
NH-2-8-5-9-F4.1-2	218	218	***	218	179	***	202	131	***	143	Non-headed ends of specimens do not have strain gauge 4		
NH-2-8-5-13-F4.1-2	234	234	***	234	*	***	165	180	***	120			
NH-3-8-5-9-F4.1-2	205	108	205	205	180	187	200	178	200	200			
NH-3-8-5-11-F4.1-2	316	286	279	*	268	237	269	221	206	247			
NH-3-8-5-13-F4.1-2	365	365	262	365	318	240	193	295	240	291			

*Strain gauge not working

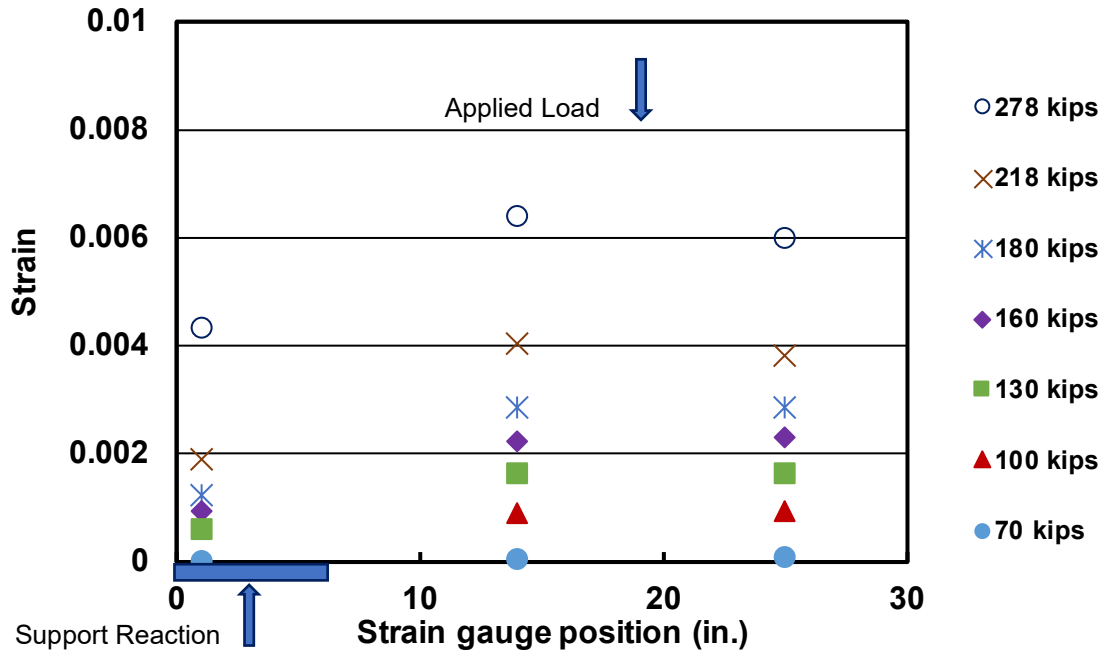
***No middle bar

Figures 3.15 through 3.23 show the strain gauge results for the specimens in this study (Data from specimen: H-3-8-5-9-F4.1-1 and NH-3-8-5-9-F4.1-1 were lost). The figures show the strain for each gauge based on location for various levels of load. The location of the center of the support plate is shown at the bottom of each figure. Plots for the nominally identical specimens with and without headed ends are placed on the same page to facilitate comparison.

Figures 3.15 through 3.23 show that, as expected, reinforcement strains were near zero until after cracking. The cracking load for each specimen, based on the concrete section and a modulus of rupture f_r of $7.5\sqrt{f_{cm}}$, where f_{cm} is the measured concrete compressive strength, is listed in Table 3.5. After the first crack formed, strains varied gradually from approximately zero at the center of the support plate to a peak under the applied load. The differences in strain observed between the end of the bar and the boundary of the extended nodal zone are consistent with the assumption that a portion of the force in the bar is transferred from the bar to the concrete via bond over this length. The strain reading in the gauge placed on the bar 1 in. from the face of the head remained less than 0.0001 until the applied force reached a value between 130 and 180 kips, at which point the strain begins to increase. The legends of Figures 3.15 through 3.23 show the loads at which the strains were measured. In addition, the strain gauge readings at maximum load are also given.

Table 3.5 Calculated cracking load

Beam Type	Concrete Compressive Strength (psi)	<i>h</i> (in.)	<i>b</i> (in.)	Cracking Moment (kip-in)	Cracking Load (kips)
Series 1/ Headed end					
H-2-8-5-9-F4.1-1	5740	20.0	18.0	682	58
H-2-8-5-10.4-F4.1-1	4490	20.3	18.1	625	53
H-3-8-5-9-F4.1-1	5800	20.1	18.3	704	60
H-3-8-5-11.4-F4.1-1	5750	20.1	18.0	689	59
H-3-8-5-14-F4.1-1	5750	20.0	18.1	686	58
Series 1/ Non-headed end					
NH-2-8-5-9-F4.1-1	5740	20.0	18.0	682	58
NH-2-8-5-10.4-F4.1-1	5330	20.0	18.3	668	57
NH-3-8-5-9-F4.1-1	5800	20.0	18.3	697	59
NH-3-8-5-11.4-F4.1-1	5750	20.3	18.3	715	61
NH-3-8-5-14-F4.1-1	5750	20.0	18.4	698	59
Series 2/ Headed end					
H-2-8-5-9-F4.1-2	4630	20.3	18.3	641	55
H-2-8-5-13-F4.1-2	4760	20.1	18.4	641	55
H-3-8-5-9-F4.1-2	4770	20.0	18.3	632	54
H-3-8-5-11-F4.1-2	4820	20.3	18.3	654	56
H-3-8-5-13-F4.1-2	4900	20.0	18.4	644	55
Series 2/ Non-headed end					
NH-2-8-5-9-F4.1-2	4630	20.3	18.4	645	55
NH-2-8-5-13-F4.1-2	4760	20.1	18.4	641	55
NH-3-8-5-9-F4.1-2	4770	20.0	18.3	632	54
NH-3-8-5-11-F4.1-2	4820	20.3	18.3	654	56
NH-3-8-5-13-F4.1-2	4900	20.0	18.4	644	55



(a)

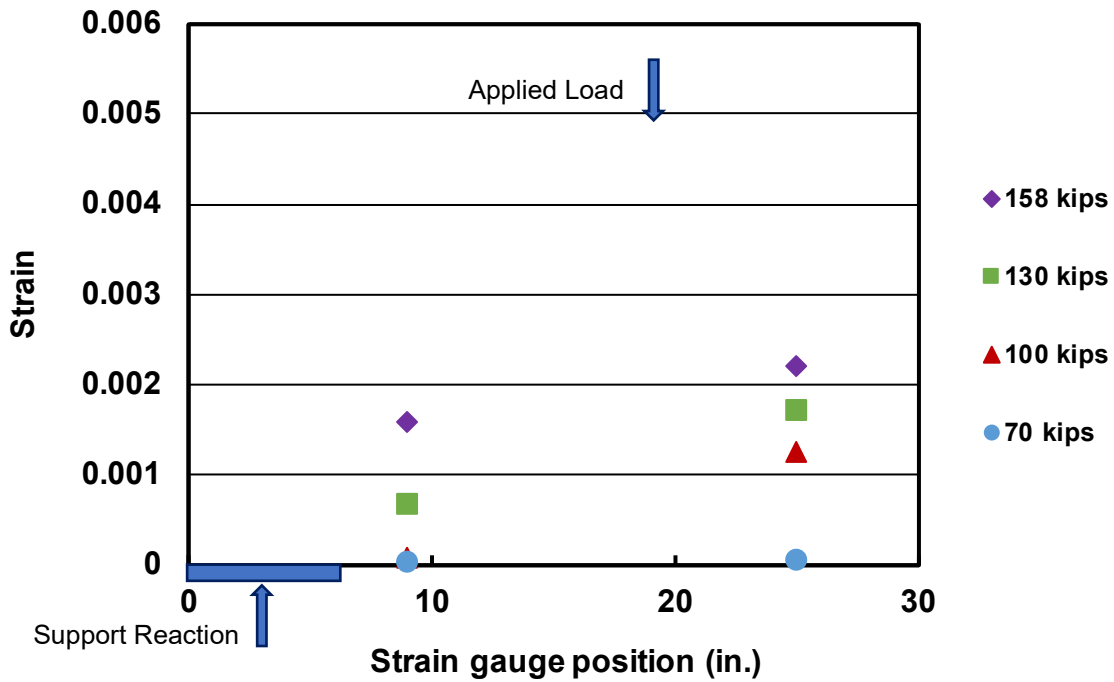
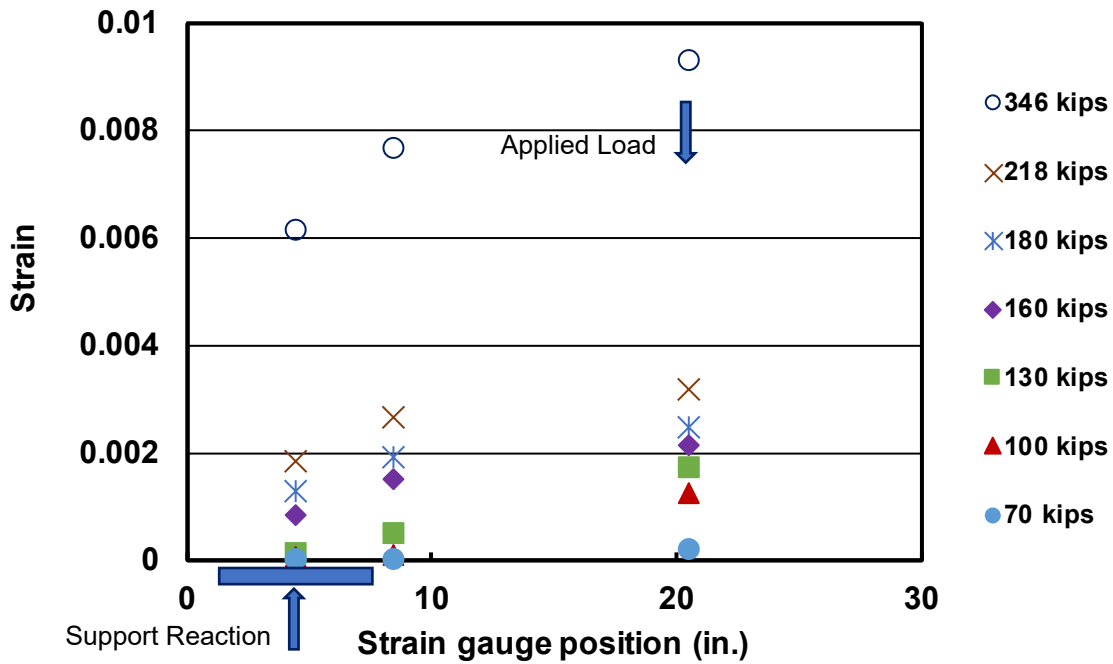


Figure 3.15 Strain along the longitudinal bars (a) Specimen H-2-8-5-9-F4.1-1, (b) Specimen NH-2-8-5-9-F4.1-1. Arrows correspond to location of the centroids of the support reaction and applied load



(a)

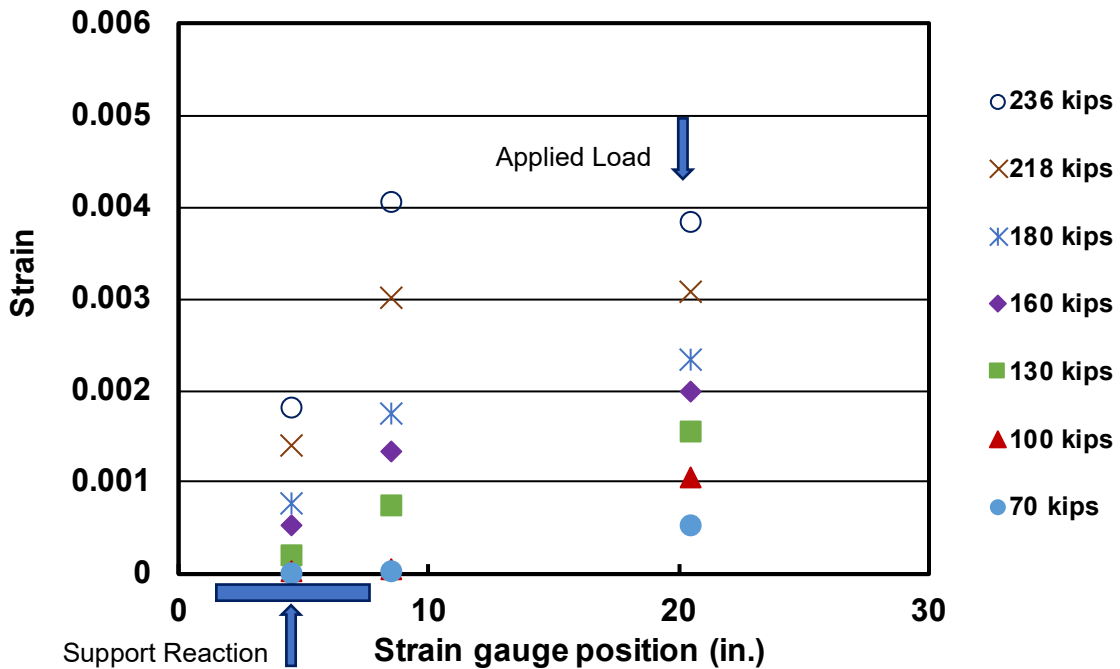
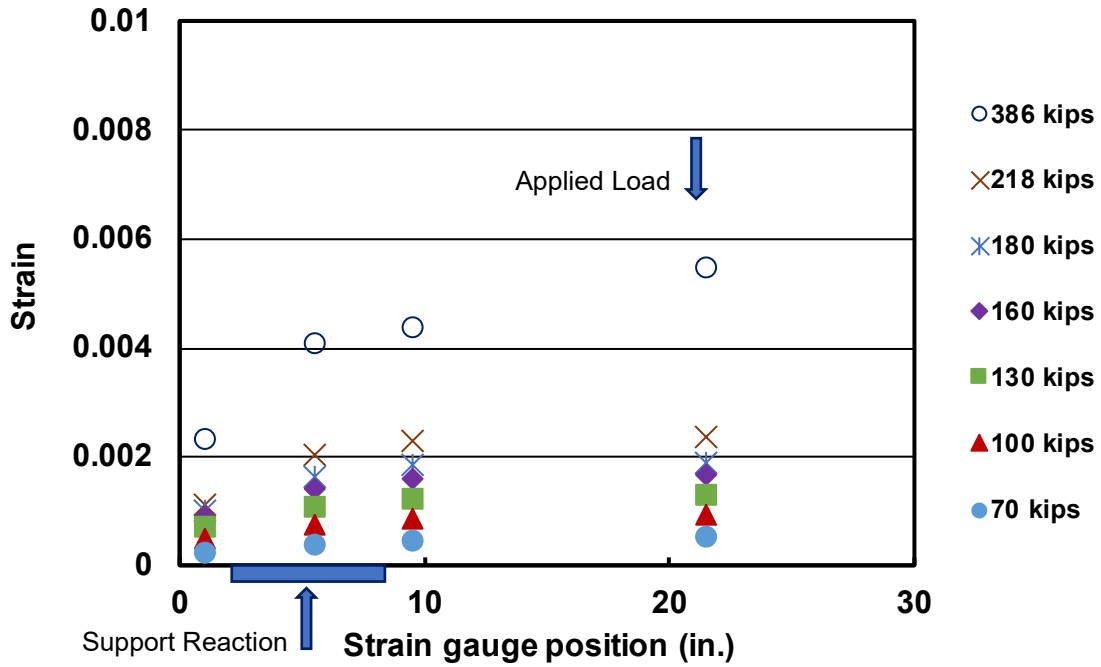
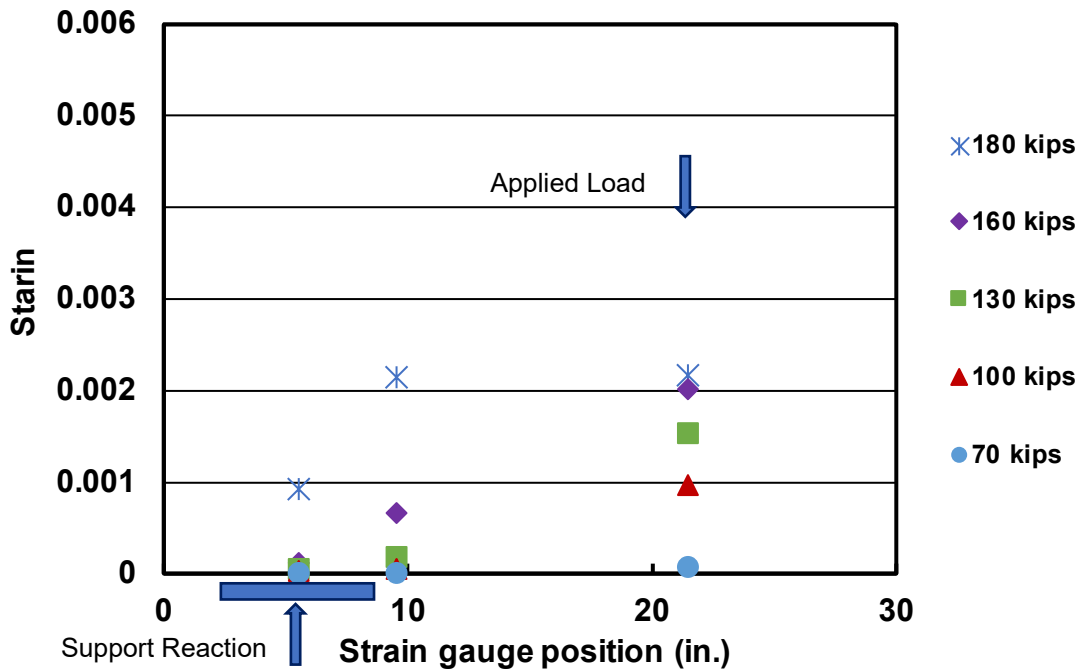


Figure 3.16 Strain along the longitudinal bars (a) Specimen H-2-8-5-10.4-F4.1-1, (b) Specimen NH-2-8-5-10.4-F4.1-1. Arrows correspond to location of the centroids of the support reaction and applied load

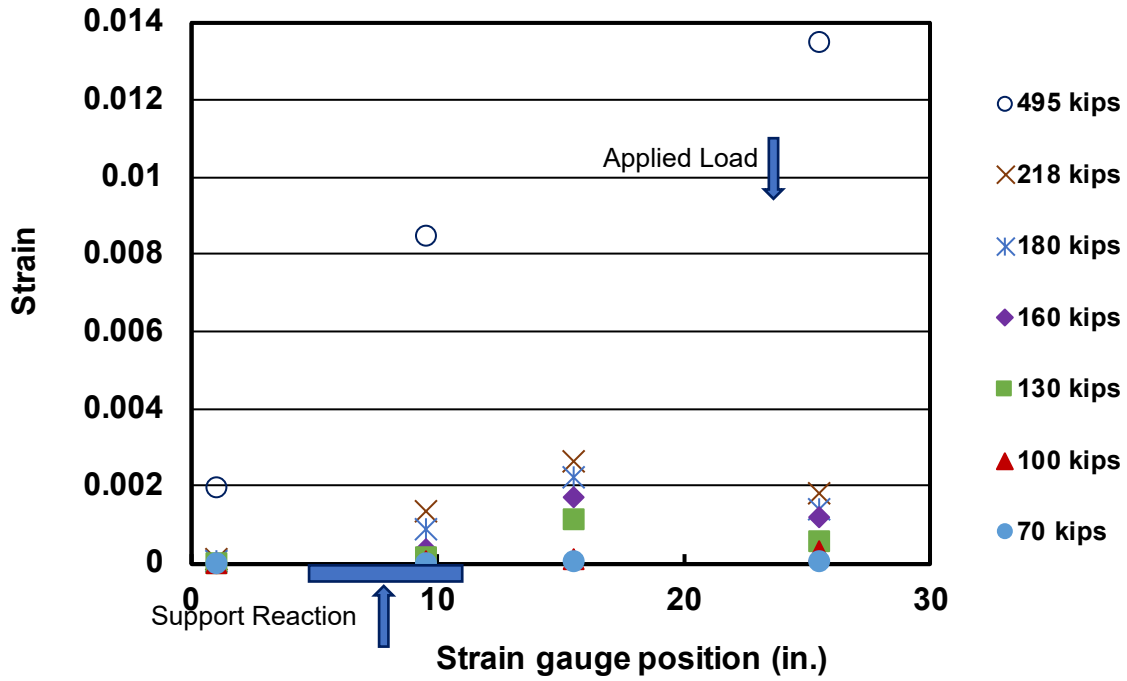


(a)

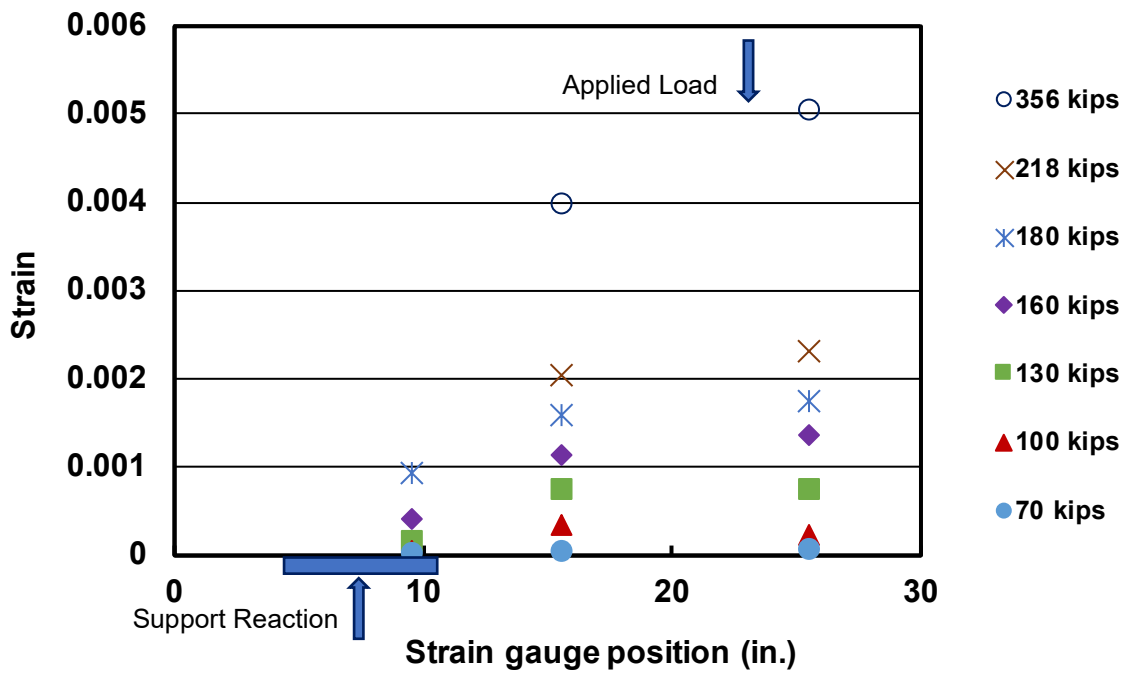


(b)

Figure 3.17 Strain along the longitudinal bars (a) Specimen H-3-8-5-11.4-F4.1-1, (b) Specimen NH-3-8-5-11.4-F4.1-1. Arrows correspond to location of the centroids of the support reaction and applied load

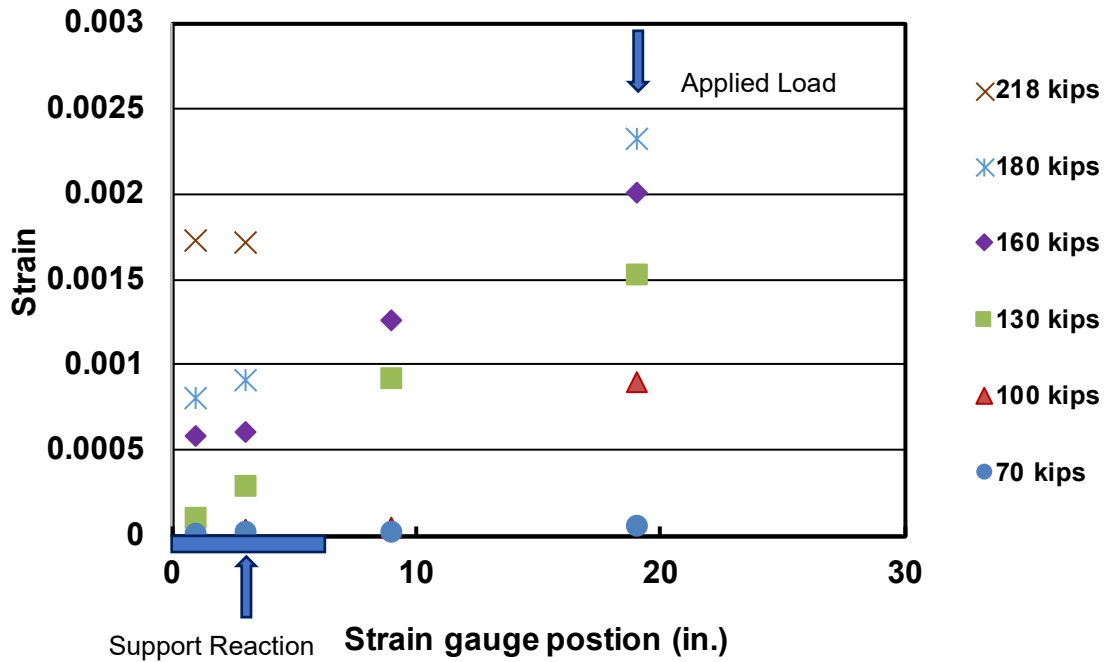


(a)

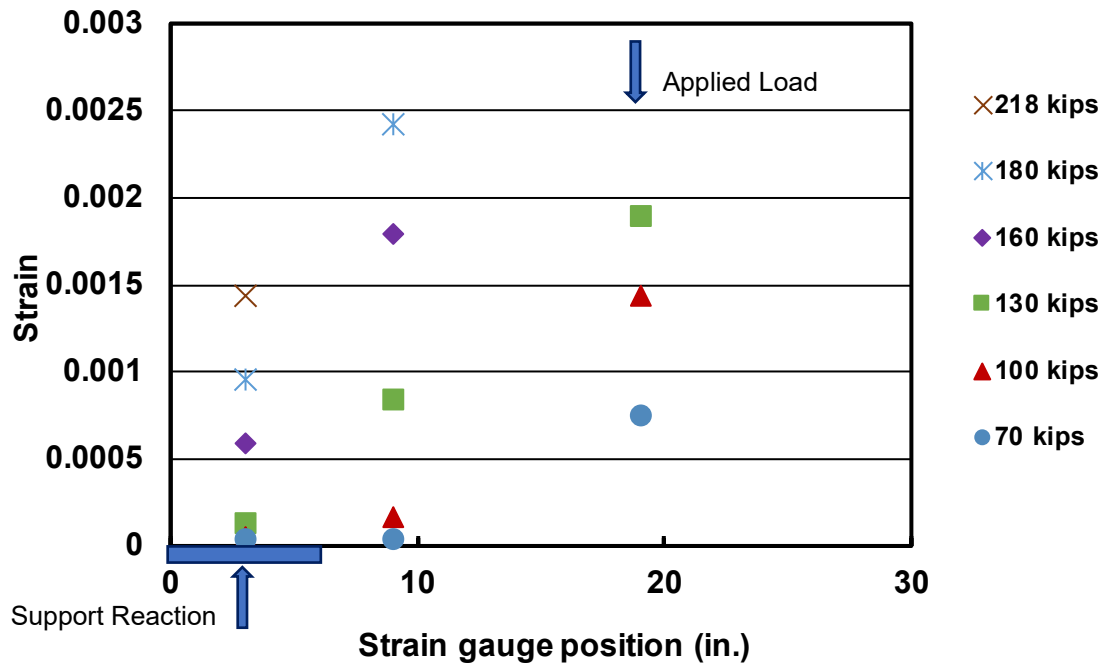


(b)

Figure 3.18 Strain along the longitudinal bars (a) Specimen H-3-8-5-14-F4.1-1, (b) Specimen NH-3-8-5-14-F4.1-1. Arrows correspond to location of the centroids of the support reaction and applied load

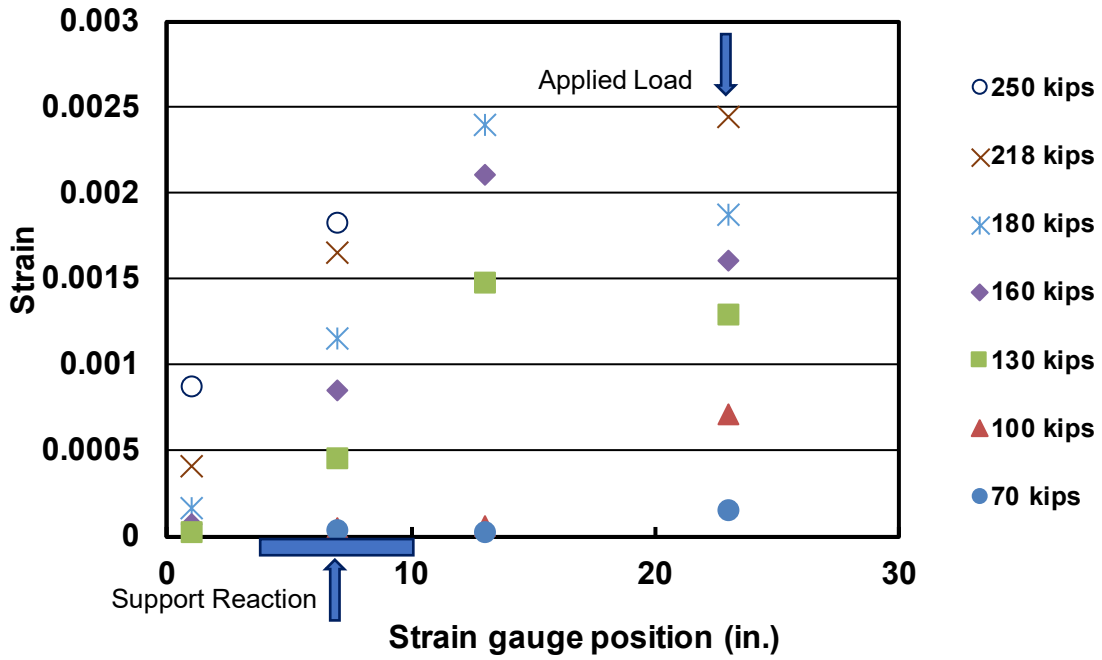


(a)

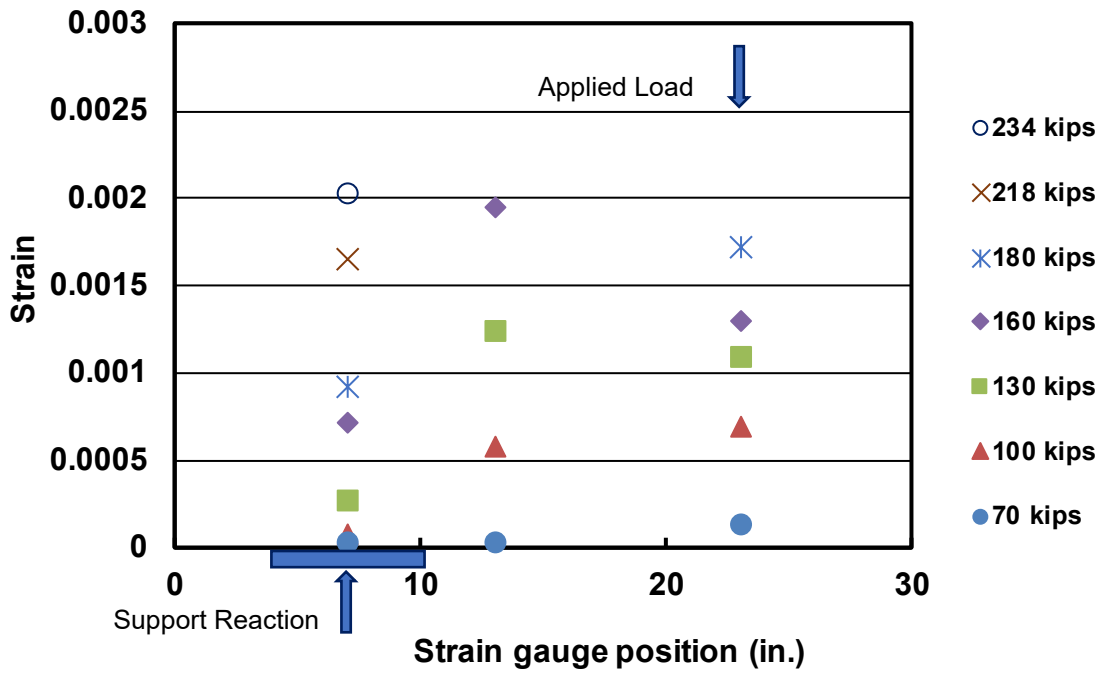


(b)

Figure 3.19 Strain along the longitudinal bars (a) Specimen H-2-8-5-9-F4.1-2, (b) Specimen NH-2-8-5-9-F4.1-2. Arrows correspond to location of the centroids of the support reaction and applied load

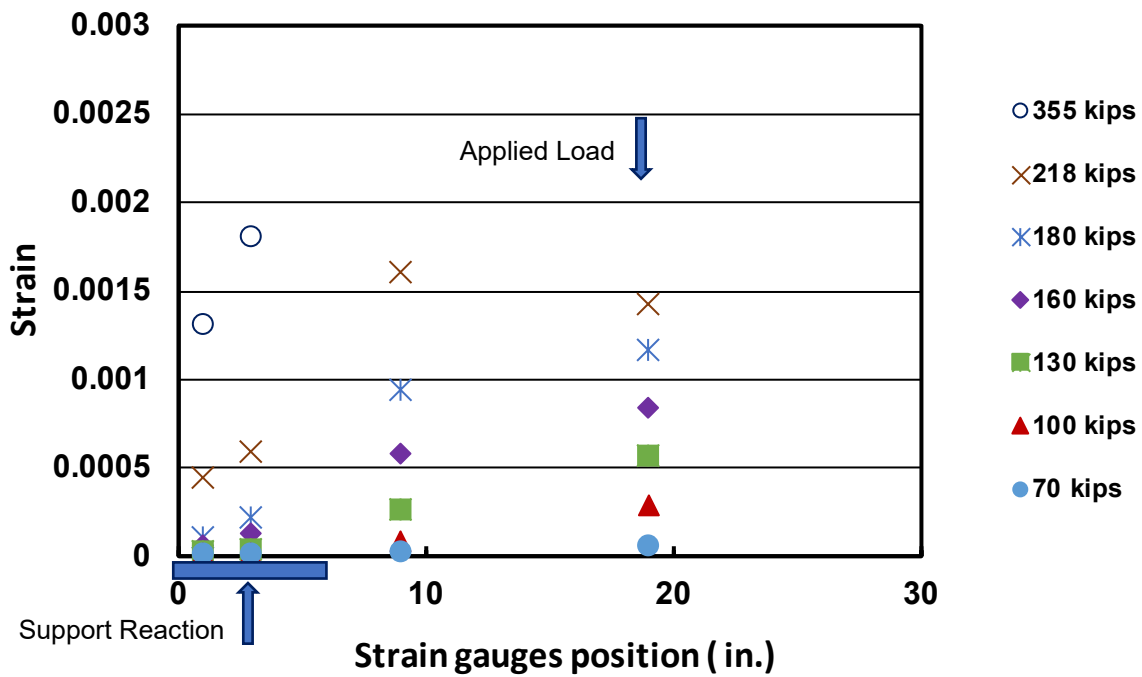


(a)

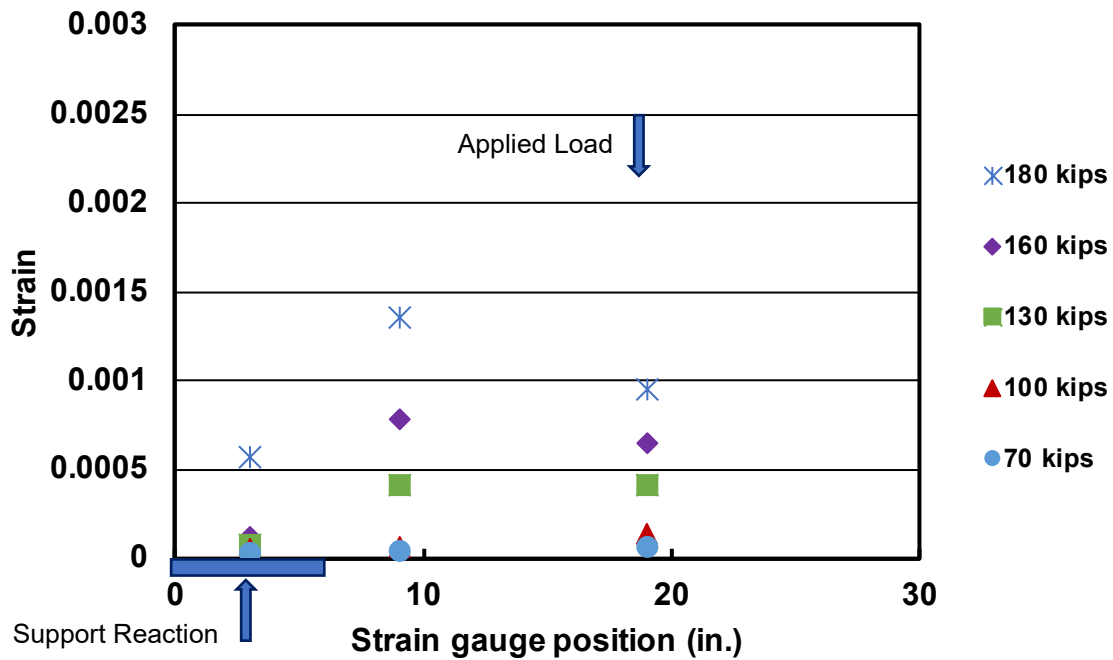


(b)

Figure 3.20 Strain along the longitudinal bars (a) Specimen H-2-8-5-13-F4.1-2, (b) Specimen NH-2-8-5-13-F4.1-2. Arrows correspond to location of the centroids of the support reaction and applied load

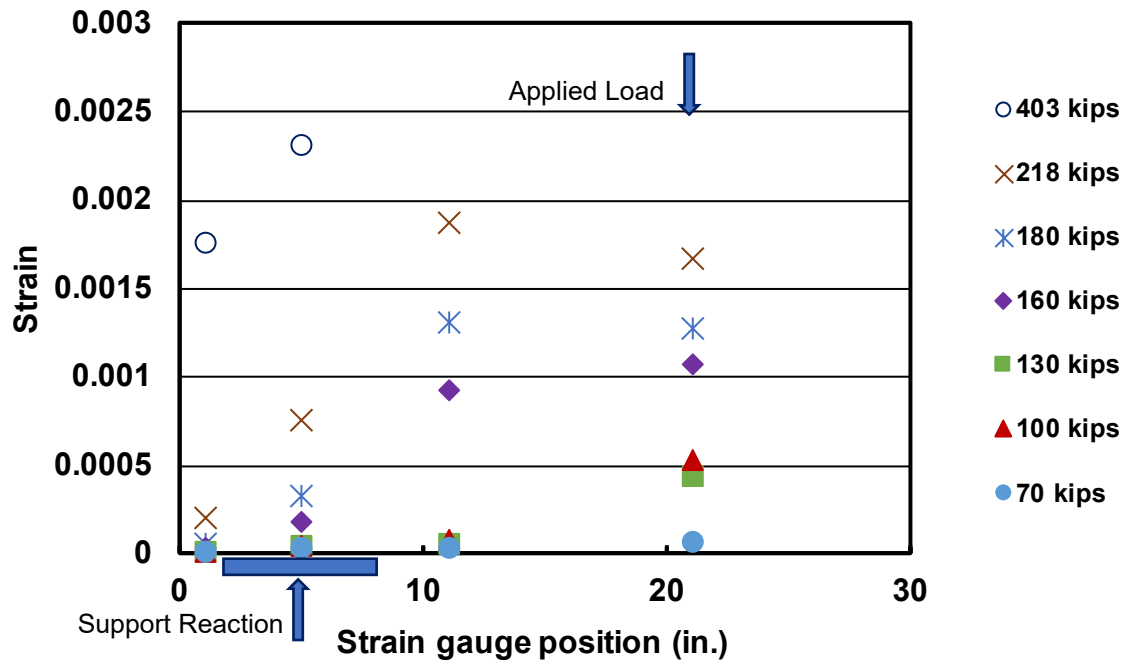


(a)

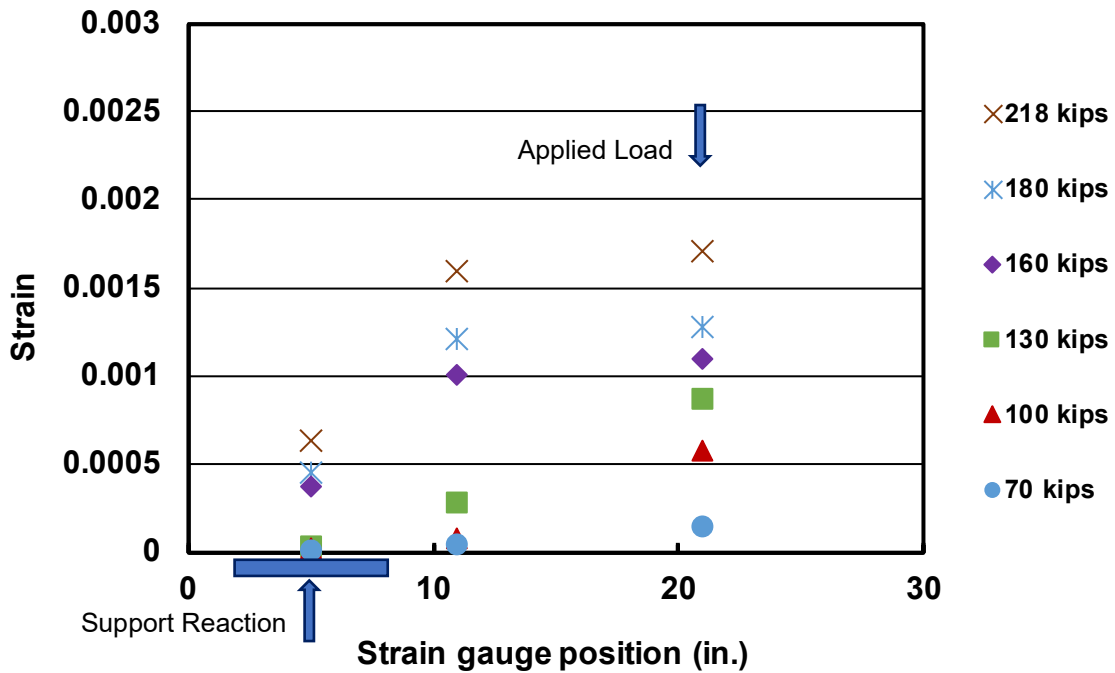


(b)

Figure 3.21 Strain along the longitudinal bars (a) Specimen H-3-8-5-9-F4.1-2, (b) Specimen NH-3-8-5-9-F4.1-2. Arrows correspond to location of the centroids of the support reaction and applied load

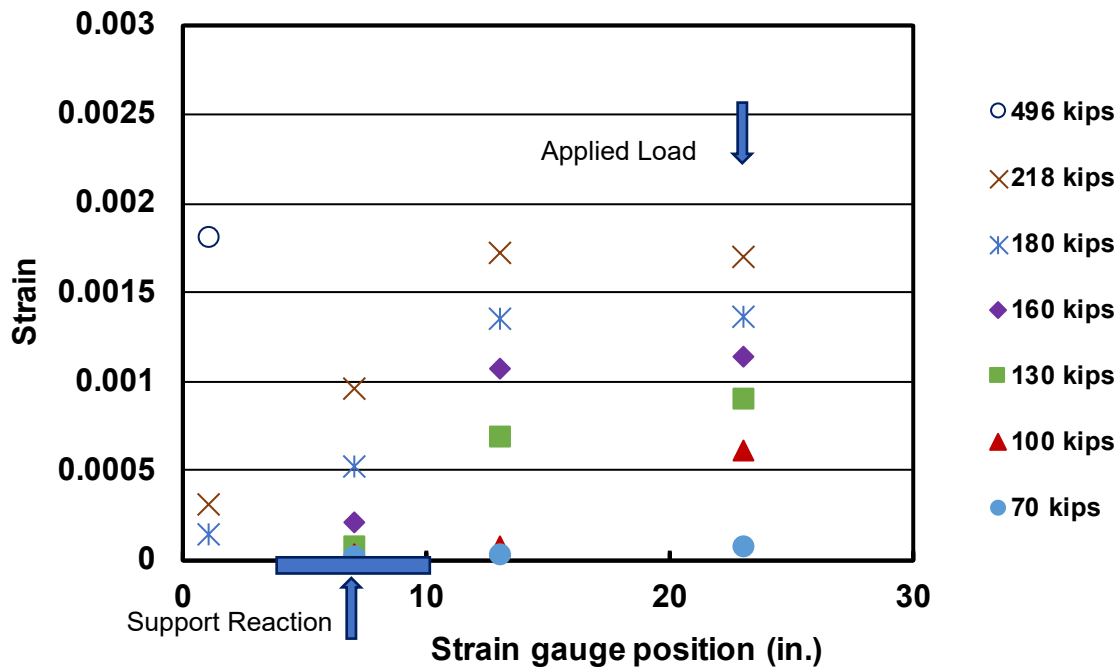


(a)

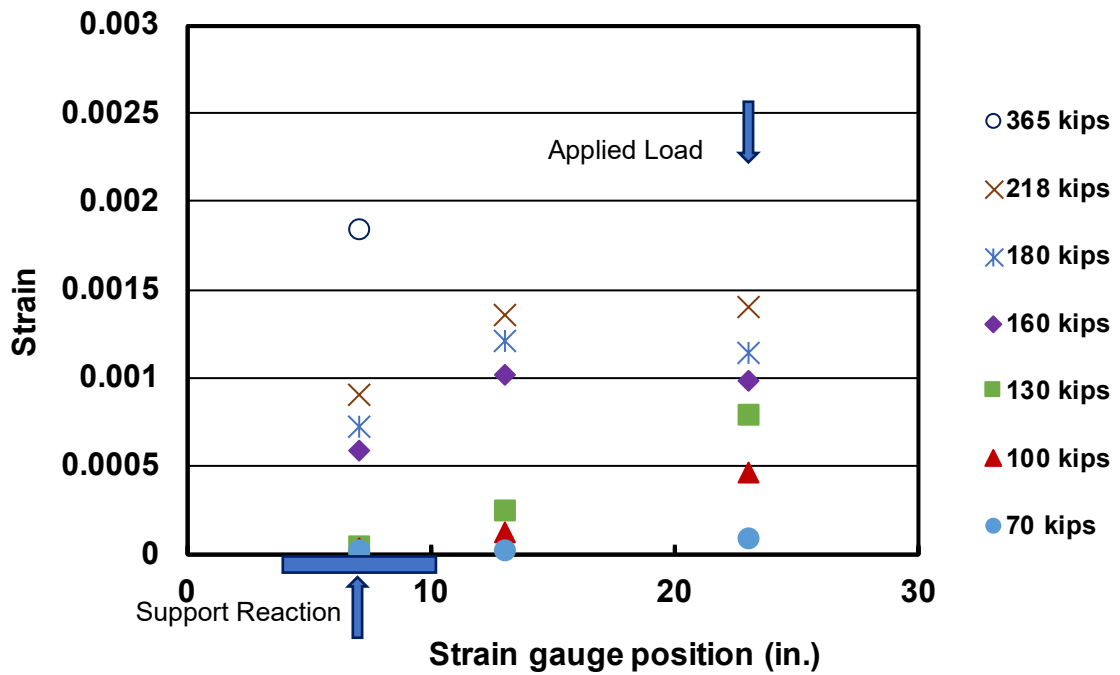


(b)

Figure 3.22 Strain along the longitudinal bars (a) Specimen H-3-8-5-11-F4.1-2, (b) Specimen NH-3-8-5-11-F4.1-2. Arrows correspond to location of the centroids of the support reaction and applied load



(a)

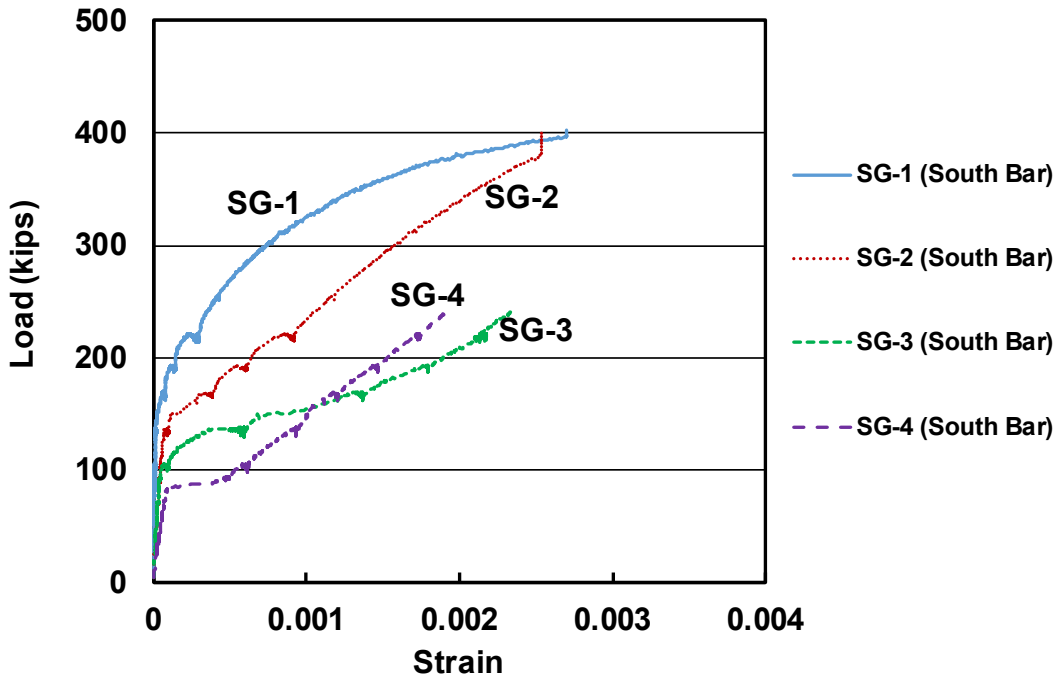


(b)

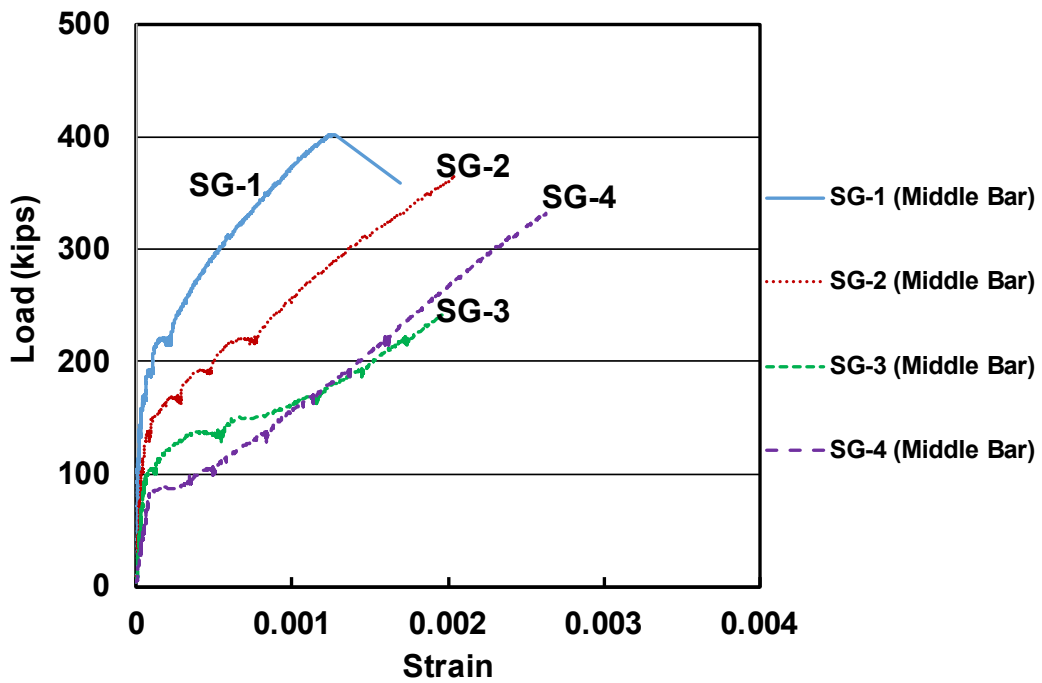
Figure 3.23 Strain along the longitudinal bars (a) Specimen H-3-8-5-13-F4.1-2, (b) Specimen NH-3-8-5-13-F4.1-2. Arrows correspond to location of the centroids of the support reaction and applied load

Figures 3.24 and 3.25 show load-strain curves for the three bars (South, Middle, and North bars, as shown in Figure 2.7) separately for the headed and non-headed ends of specimen H-3-8-5-11-F4.1-2 and NH-3-8-5-11-F4.1-2, respectively. The load-strain curves for all specimens are provided in Figures B.9 to B.26 in Appendix B. Generally, the strains in the headed bar at the boundary of the extended nodal zone and under the applied load started to develop when the load reached between 80 and 100 kips. Then, the strain increased approximately linearly with the applied load. The strain on the bar near the head started to develop when the load reached about 160 kips. Then, the strain increased non-linearly with the applied load. The non-linear behavior near the head means that the development of the strain was slow at the beginning and then increased more rapidly as the applied load increased. Similar behavior was observed at the non-headed end (Figure 3.25).

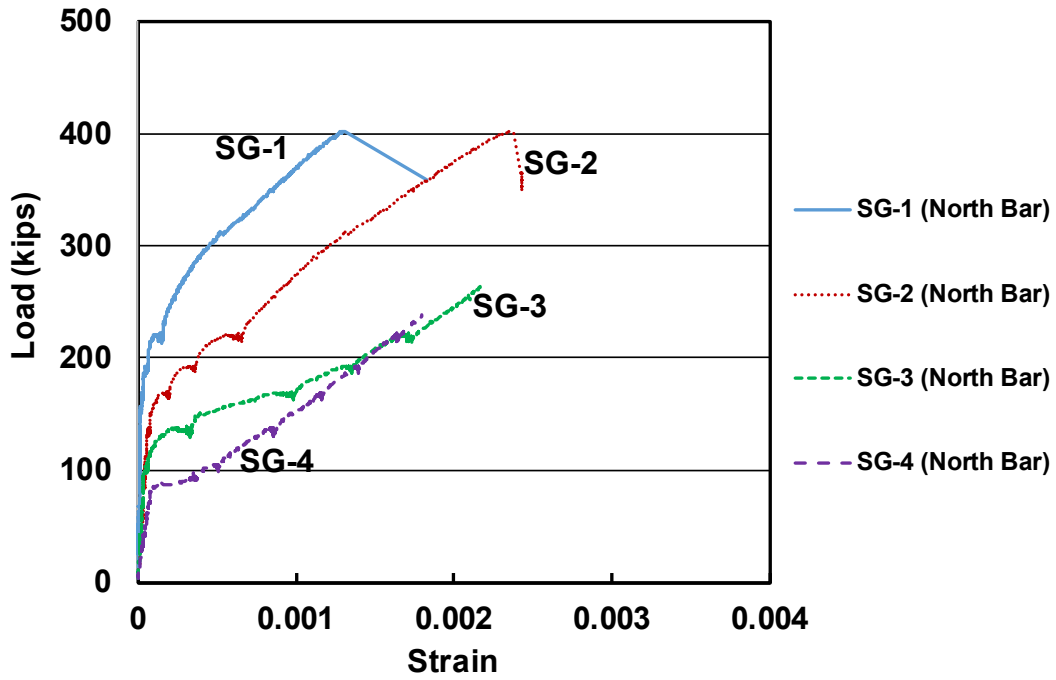
Figures 3.24 and 3.25 show that the strain gauges close to the applied load tended to fail prior to reaching the peak load. A comparison of the strain data shown in Figures 3.24 a, b, and c indicates that for a given load, strain was consistently higher in the south bar and lower in the north bar (headed end), while Figures 3.25 a, b, and c show that for a given load, strain was consistently higher in the north bar and lower in the south bar (Non-headed end). The reason is likely due to the hydraulic jacks at the left side providing a somewhat higher load than those on the right.



(a)

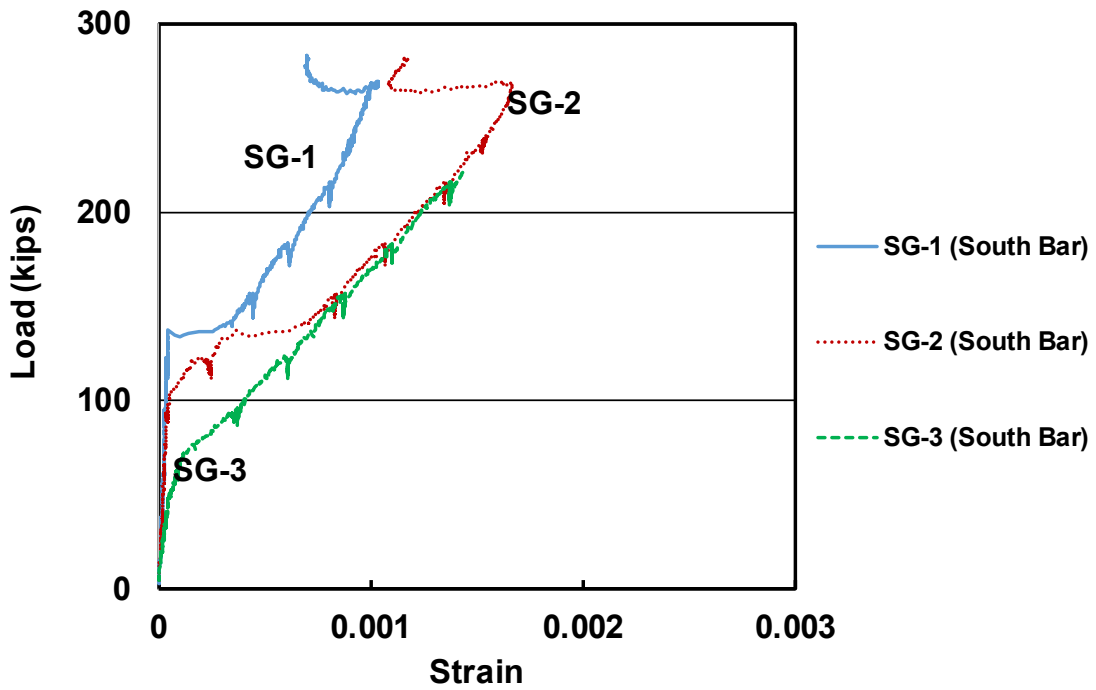


(b)

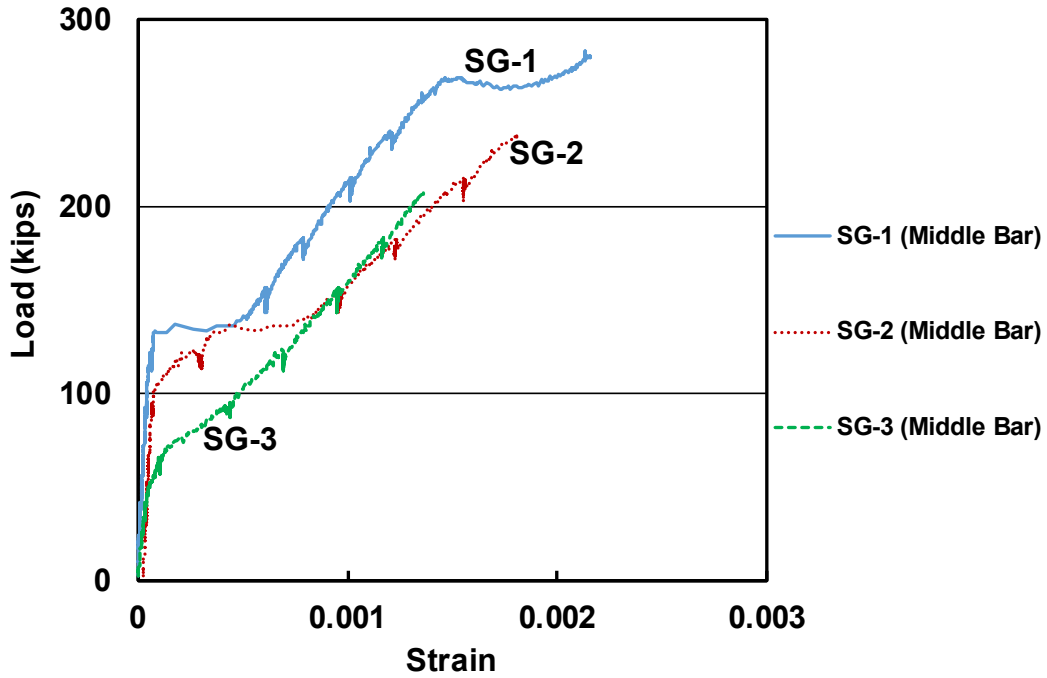


(c)

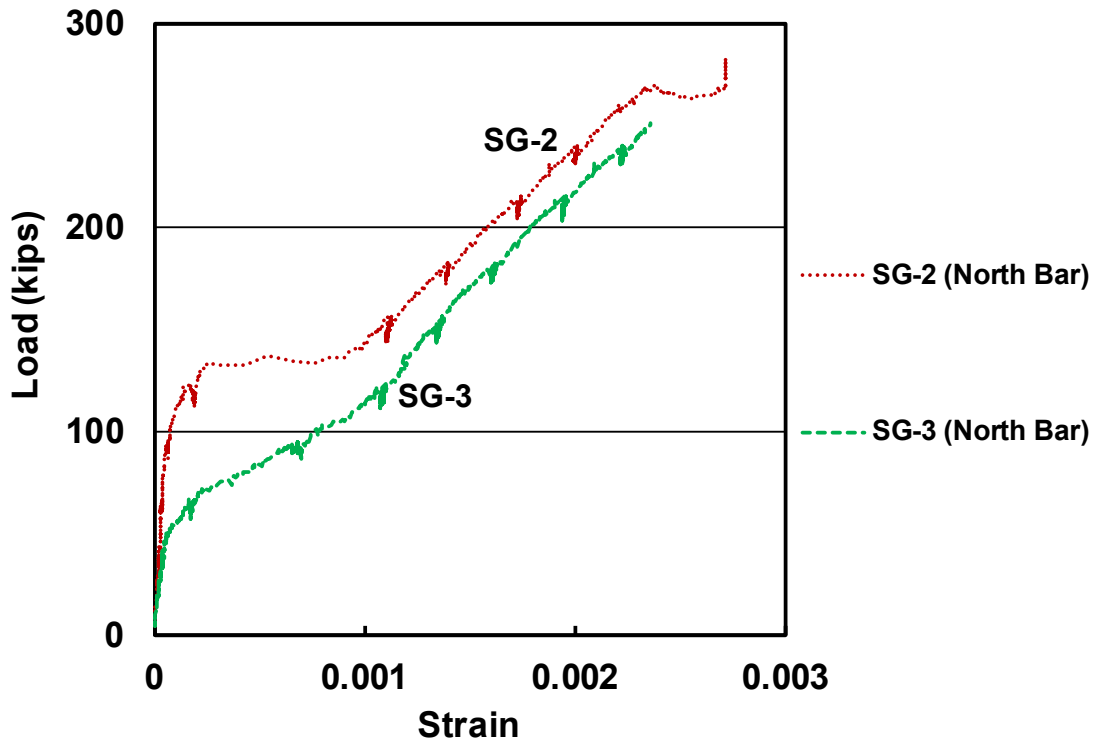
Figure 3.24 Load-strain curve for specimen H-3-8-5-11-F4.1-2, (a) south bar, (b) middle bar, (c) north bar. Some data is missing because some strain gauges failed prior to failure of the specimen



(a)



(b)



(c)

Figure 3.25 Load-strain curve for specimen NH-3-8-5-11-F4.1-2, (a) south bar, (b) middle bar, (c) north bar. Some data is missing because some strain gauges failed prior to failure of the specimen

3.5 HEAD SLIP

As described in Chapter 2, slip was taken as the displacement of the reinforcing bar ends with respect to that of the surrounding concrete. A separate potentiometer was used to record slip of each of the longitudinal bars (Figure 2.7).

Figure 3.26 shows the slip at the headed end for the three longitudinal bars in Specimen H-3-8-5-13-F4.1-2. For most of the test, slip of the middle bar was greater than the outer bars (approximately 50% greater at a load of 250 kips). These differences diminished as the specimen neared failure where, near the peak load, the recorded values were within 10%. This pattern, with the middle bar exhibiting greater slip throughout much of the test, was observed for all of the specimens with three longitudinal bars for which slip was recorded.

For comparison between specimens, recorded bar slip was averaged for the bars within a specimen. Figure 3.27 shows load versus average slip at the headed ends for Specimens H-2-8-5-9-F4.1-2, H-2-8-5-13-F4.1-2, H-3-8-5-9-F4.1-2, and H-3-8-5-13-F4.1-2. The bars did not slip until the applied load reached about 80 kips, coinciding with the initiation of the first crack. The average bar slip at the peak load was 0.020 in. for Specimen H-2-8-5-9-F4.1-2, 0.03 in. for Specimen H-2-8-5-13-F4.1-2, 0.025 in. for Specimen H-3-8-5-9-F4.1-2, and 0.037 in. for Specimen H-3-8-5-13-F4.1-2. As explained in Chapter 2, technical problems prevented recording slip of the non-headed bars.

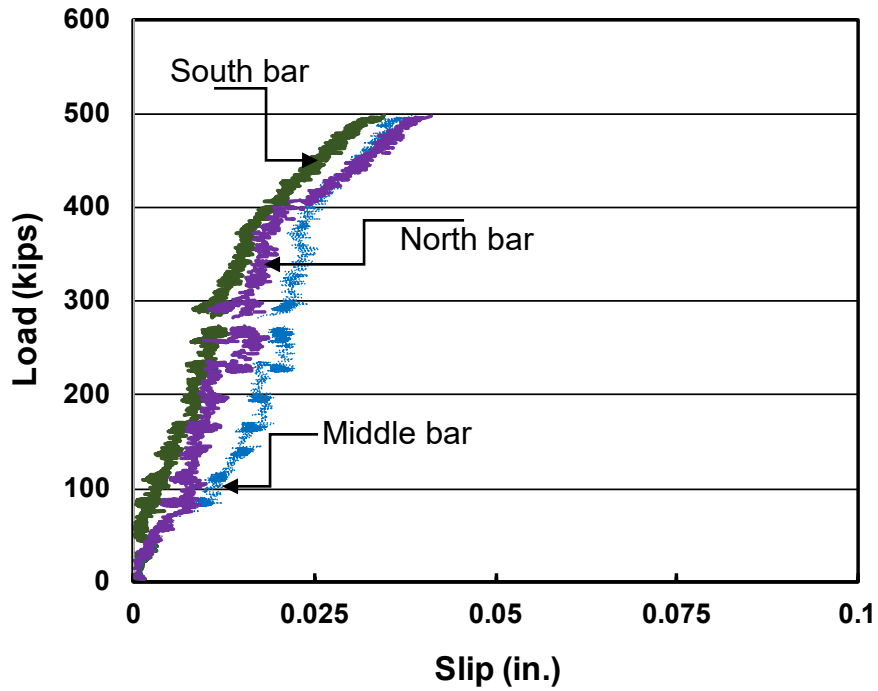


Figure 3.26 Load versus slip of the three headed bar ends in Specimen H-3-8-5-13-F4.1-2

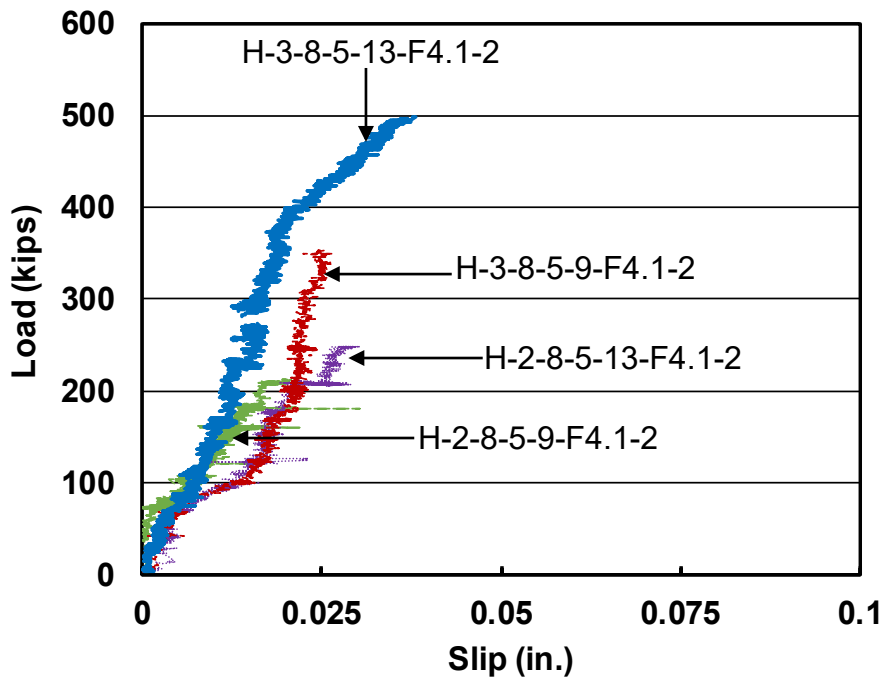


Figure 3.27 Load versus average slip of headed bars for Specimens H-2-8-5-9-F4.1-2, H-2-8-5-13-F4.1-2, H-3-8-5-9-F4.1-2, and H-3-8-5-13-F4.1-2

3.6 ANALYSIS OF INTERNAL ACTIONS

3.6.1 Strut Force, Tie Force, and Bar Stress

The forces in the strut and tie model (shown in Figure 3.28) were calculated and compared to limits prescribed in the ACI Building Code to corroborate observations that the strength of the specimens was limited by anchorage failure (as described in Section 3.1.2). Internal forces were estimated using equilibrium and assuming that the strut was oriented at an angle of 45° with the horizontal. Bar stress was determined based on the force in the tie obtained using the STM method. Values calculated based on the peak load in each specimen are listed in Table 3.6. Table 3.6 shows the concrete compressive strength, peak load, strut force, tie force, tie force/bar, and bar stress.

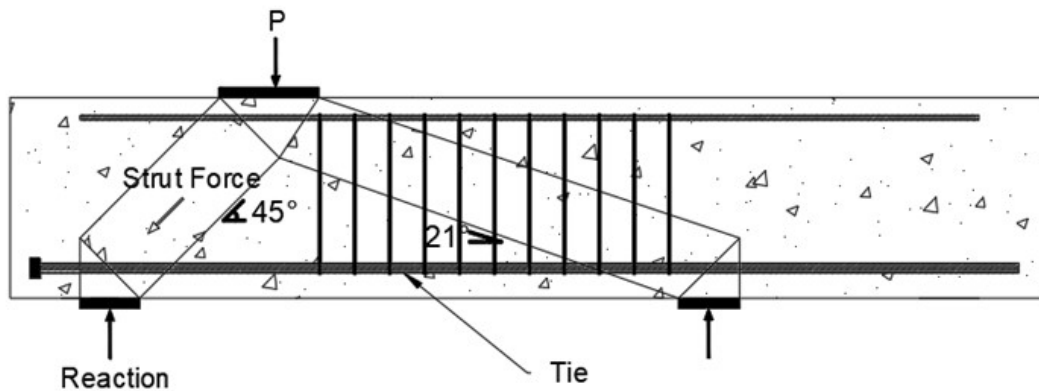


Figure 3.28 Strut-and-tie model

Table 3.6 Estimated strut and tie forces

Beam Type	Concrete Compressive Strength (psi)	Peak Load (kips)	Strut Force (kips)	Tie Force (kips)	Tie Force/Bar (kips)	Bar Stress (ksi)
Series 1/ Headed end						
H-2-8-5-9-F4.1-1	5740	278	288	204	102	128
H-2-8-5-10.4-F4.1-1	4490	346	359	254	127	160
H-3-8-5-9-F4.1-1	5800	446	463	327	109	137
H-3-8-5-11.4-F4.1-1	5750	386	400	283	94	119
H-3-8-5-14-F4.1-1	5750	495	513	363	121	152
Series 1/ Non-headed end						
NH-2-8-5-9-F4.1-1	5740	158	164	116	58	73
NH-2-8-5-10.4-F4.1-1	5330	236	245	173	87	109
NH-3-8-5-9-F4.1-1	5800	255	264	187	62	78
NH-3-8-5-11.4-F4.1-1	5750	245	254	180	60	75
NH-3-8-5-14-F4.1-1	5750	356	369	261	87	109
Series 2/ Headed end						
H-2-8-5-9-F4.1-2	4630	218	226	160	80	101
H-2-8-5-13-F4.1-2	4760	250	259	183	92	115
H-3-8-5-9-F4.1-2	4770	355	368	260	87	109
H-3-8-5-11-F4.1-2	4820	403	418	296	99	124
H-3-8-5-13-F4.1-2	4900	499	518	366	122	153
Series 2/ Non-headed end						
NH-2-8-5-9-F4.1-2	4630	218	226	160	80	101
NH-2-8-5-13-F4.1-2	4760	234	243	172	86	108
NH-3-8-5-9-F4.1-2	4770	205	213	150	50	63
NH-3-8-5-11-F4.1-2	4820	316	328	232	77	97
NH-3-8-5-13-F4.1-2	4900	365	379	268	89	112

3.6.2 Comparison of Capacity and Demand for Struts and Nodes

The nominal strut capacity (in kips) was calculated following the provisions of ACI Building Code (318-19) [Eq. (3.1)].

$$\text{Strut Capacity} = 0.85\beta_s f_{cm} A_{cs} \quad (3.1)$$

where $\beta_s = 0.6$, as required by ACI 318-19 for struts with no transverse reinforcement; f_{cm} = the measured concrete compressive strength; and A_{cs} = area of the strut. The area of the strut was assumed to be the product of the beam thickness (18 in.) and the width of the strut, which was limited by the width of the node over the support (Figure 3.29). As illustrated in Figure 3.29, the

horizontal and vertical dimensions of the node were taken as 6 in., resulting in a length of the hypotenuse, and thus strut width, of 8.5 in. The strength of the node was estimated using Eq. (3.1) with β_s replaced by $\beta_n = 0.8$ in accordance with ACI Building Code (where β_n is the factor used to account for the effect of the anchorage of ties on the effective compressive strength of a nodal zone). The calculated nodal capacity was, therefore, greater than the strut capacity by one-third ($\beta_n / \beta_s = 4/3$). Calculated strut and node capacities are compared to demand (based in the strut-and-tie model and maximum load on the specimen) in Table 3.7.

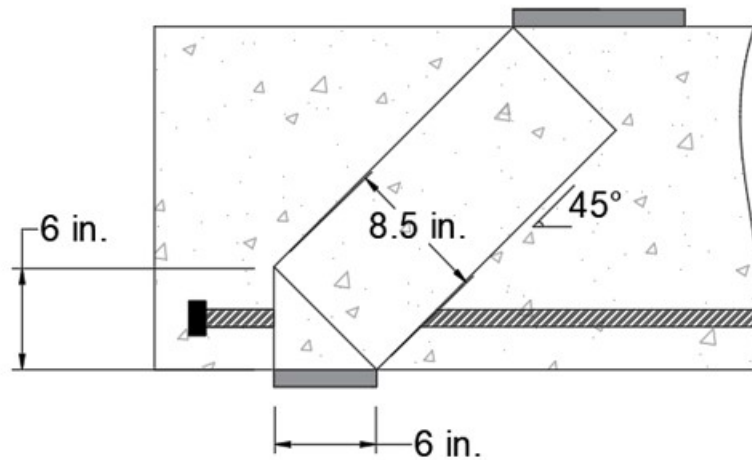


Figure 3.29 Assumed dimensions of the strut and node

Table 3.7 Estimated strut and node capacity and demand

Beam Type	Strut Demand (kips)	Strut Capacity (kips)	Strut Capacity/Demand	Node Capacity/Demand ¹
Series 1/ Headed end				
H-2-8-5-9-F4.1-1	288	448	1.6	2.1
H-2-8-5-10.4-F4.1-1	359	350	1.0	1.3
H-3-8-5-9-F4.1-1	463	453	1.0	1.3
H-3-8-5-11.4-F4.1-1	400	449	1.1	1.5
H-3-8-5-14-F4.1-1	513	449	0.9	1.2
Series 1/ Non-headed end				
NH-2-8-5-9-F4.1-1	164	448	2.7	3.6
NH-2-8-5-10.4-F4.1-1	245	416	1.7	2.3
NH-3-8-5-9-F4.1-1	264	453	1.7	2.3
NH-3-8-5-11.4-F4.1-1	254	449	1.8	2.4
NH-3-8-5-14-F4.1-1	369	449	1.2	1.6
Series 2/ Headed end				
H-2-8-5-9-F4.1-2	226	361	1.6	2.1
H-2-8-5-13-F4.1-2	259	371	1.4	1.9
H-3-8-5-9-F4.1-2	368	372	1.0	1.3
H-3-8-5-11-F4.1-2	418	376	0.9	1.2
H-3-8-5-13-F4.1-2	518	382	0.7	1.0
Series 2/ Non-headed end				
NH-2-8-5-9-F4.1-2	226	361	1.6	2.1
NH-2-8-5-13-F4.1-2	243	371	1.5	2.0
NH-3-8-5-9-F4.1-2	213	372	1.8	2.3
NH-3-8-5-11-F4.1-2	328	376	1.1	1.5
NH-3-8-5-13-F4.1-2	379	382	1.0	1.3

¹ For these specimens, node capacity/demand ratios are always 4/3 of the ratios calculated for the struts because the demand is equivalent and the calculated capacity of the node is 4/3 that of the strut.

As shown in Table 3.7, the strut capacity-to-demand ratio is greater than or equal to 1.0 for the majority of specimens, indicating that strut failure likely did not govern the strength of these specimens. For the three specimens with a strut capacity-to-demand ratio less than 1.0 (H-3-8-5-14-F4.1-1, H-3-8-5-11-F4.1-2, and H-3-8-5-13-F4.1-2), observations during testing strongly indicated that specimen strength was limited by side-face blowout (anchorage) and not strut failure.

Table 3.7 shows that node capacity-to-demand ratios are no less than 1.0 for all specimens. Observations made after testing, however, indicate that H-3-8-5-9-F4.1-2 may have failed due to crushing of concrete within the node despite having a node capacity-to-demand ratio of 1.4. It is, therefore, not clear whether anchorage controlled the capacity of this specimen. However, results from H-3-8-5-9-F4.1-2 does not omit from comparisons of measured to calculated anchorage strengths.

3.6.3 Stresses, Forces, and Embedment Length

Observations and calculations indicate that anchorage failures limited the strength of the CCT-node specimens, with the possible exception of Specimen H-3-8-5-9-F4.1-2 in Series 2, which exhibited crushing of concrete within the node. Estimated forces in the longitudinal bars at peak load can, therefore, be used to evaluate the adequacy of equations proposed for calculation of required embedment length. For this purpose, bar forces were estimated using two means, the strain measurements described in Section 3.4 and the strut-and-tie model described in Section 3.6.2.

Bar force estimated from measured strain: Results from tensile tests of the bar were used to develop relations between measured strain and bar force. The forces in the longitudinal bars at peak load were then estimated from bar strains recorded at the extended nodal zone just prior to failure. For the headed end tests, the bar forces based on the strain gauge readings for the two specimens that had strain gauge data recorded until the end of the test are listed in Table 3.8. For the non-headed end tests, the bar forces based on the strain gauge readings for the three specimens that had strain gauge data recorded until the end of the test are listed in Table 3.8 (See Tables 3.3 and 3.4 in Section 3.5).

Table 3.8 Estimated forces per bar using strain gauge results and strut-and-tie model

Beam Type	Force per Bar (kips)		Ratio
	From strain gauges	From strut-and-tie	Strut-and-tie/strain gauge
Series 1/ Headed end			
H-2-8-5-9-F4.1-1	*	102	
H-2-8-5-10.4-F4.1-1	105	127	1.21
H-3-8-5-9-F4.1-1	*	109	
H-3-8-5-11.4-F4.1-1	84	95	1.13
H-3-8-5-14-F4.1-1	*	121	
Series 1/ Non-headed end			
NH-2-8-5-9-F4.1-1	46	58	1.26
NH-2-8-5-10.4-F4.1-1	77	87	1.12
NH-3-8-5-9-F4.1-1	*	62	
NH-3-8-5-11.4-F4.1-1	*	60	
NH-3-8-5-14-F4.1-1	78	87	1.15
Series 2/ Headed end			
H-2-8-5-9-F4.1-2	*	80	
H-2-8-5-13-F4.1-2	*	92	
H-3-8-5-9-F4.1-2	*	87	
H-3-8-5-11-F4.1-2	*	99	
H-3-8-5-13-F4.1-2	*	122	
Series 2/ Non-headed end			
NH-2-8-5-9-F4.1-2	*	80	
NH-2-8-5-13-F4.1-2	*	86	
NH-3-8-5-9-F4.1-2	*	50	
NH-3-8-5-11-F4.1-2	*	77	
NH-3-8-5-13-F4.1-2	*	89	

*Strain gauge failed prior to failure of specimen

Bar force estimated using strut-and-tie model: Because the longitudinal bars serve as the tie in the strut-and-tie model, the average force per bar at failure can be calculated by dividing the tie force (Table 3.8) by the number of longitudinal bars. The calculated average force per bar is listed in Table 3.8. For specimens that had bar force estimated based on both strain gauge data and the strut-and-tie model, the strut-and-tie model tended to show 10 to 20% greater bar force than was estimated based on strain gauge.

Figure 3.30 compares the force per bar estimated from the strut-and-tie model with the embedment length measured from the boundary of the extended nodal zone to the face of the head for all headed end tests. Dummy variable analysis was conducted by treating the specimen with

three bars and those with two bars as separate populations (dummy variables analysis is a least squares regression analysis method that allows differences in populations to be considered when formulating relationships between principal variables). Figure 3.30 shows that there is no significant difference between specimens with two and three longitudinal bars in the relationship between the force per bar at failure and the embedment length.

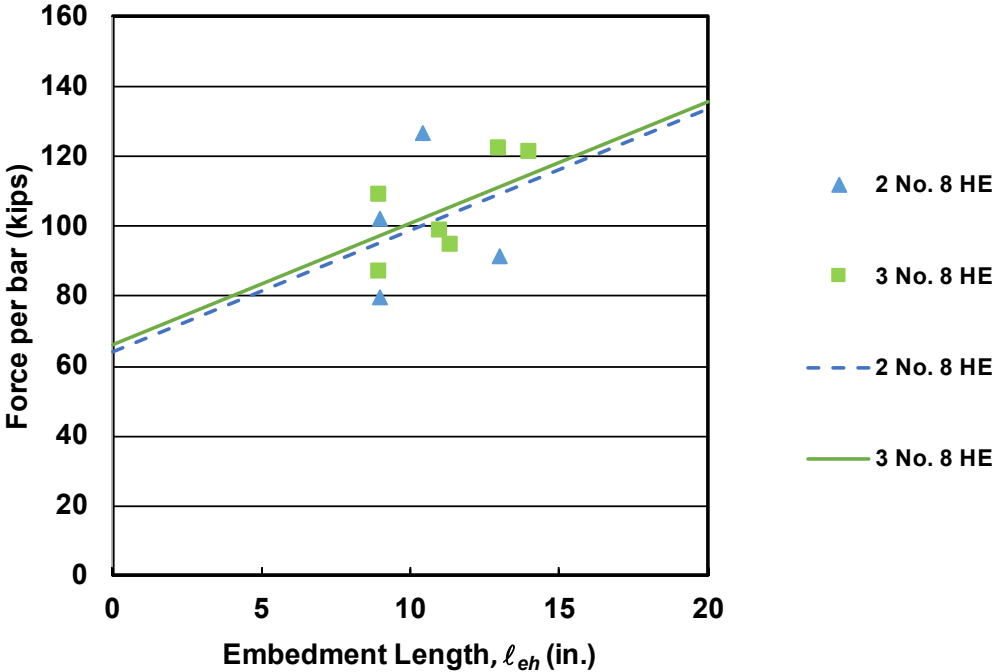


Figure 3.30 Force per bar estimated using a strut-and-tie model versus embedment length for the headed end

Figure 3.31 shows the force per bar calculated using the strut-and-tie model versus the embedment length measured from the boundary of the extended nodal zone to the end of the bar for the non-headed end tests. The trend line (based on dummy variable analysis) for specimens with two longitudinal bars is above the trend line for specimens with three longitudinal bars. However, Student’s t-test indicates that the difference between specimens with two and three longitudinal bars is not statistically significant ($p = 0.22$).

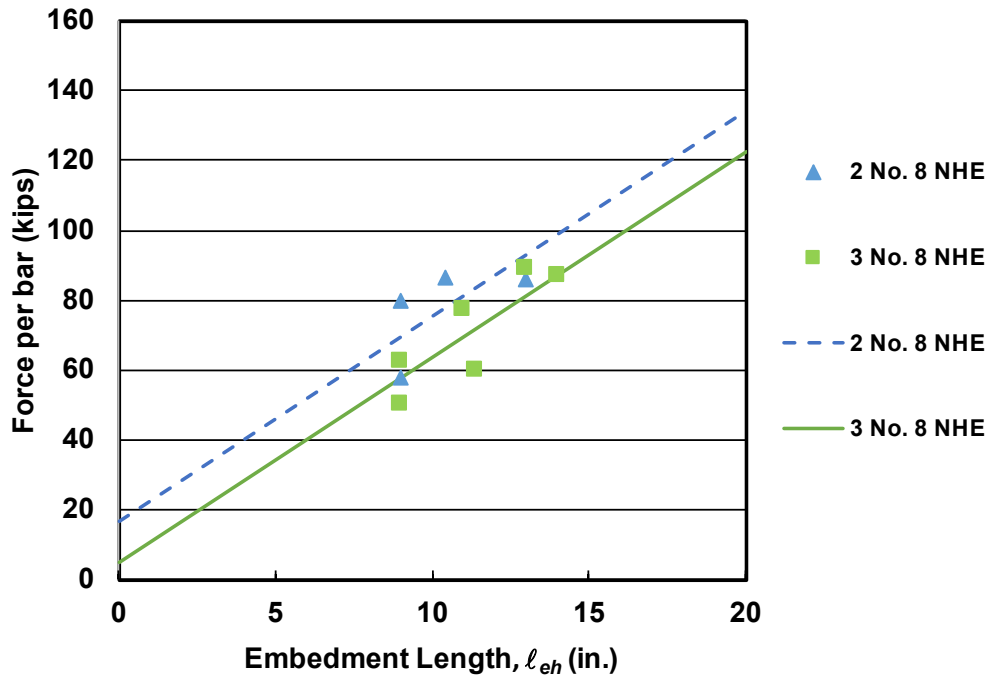


Figure 3.31 Force per bar estimated using a strut-and-tie model versus embedment length for the non-headed end

3.7 ANALYSIS OF TEST RESULTS USING DESCRIPTIVE EQUATION DEVELOPED BY SHAO ET AL. (2016)

In this section, the results of the CCT node specimens tested in the current study and by Thompson et al. (2006a) are compared with values calculated using the descriptive equation for the anchorage strength of headed bars developed by Shao et al. (2016). The purpose of these comparisons is to evaluate the ability of the descriptive equation to represent the anchorage strength of headed bars embedded at the end of beams within compression-compression-tension (CCT) nodes.

3.7.1 Descriptive Equation (Shao et al. 2016)

Shao et al. (2016) tested 64 beam-column joint specimens without confining reinforcement 30 specimens with widely-spaced bars (center-to-center spacing $\geq 8d_b$) and 34 specimens with closely spaced (center-to-center spacing $< 8d_b$) and 74 beam-column joint specimens with confining reinforcement within the joint region 43 specimens with widely-spaced bars (center-to-center spacing $\geq 8d_b$) and 31 specimens with closely spaced (center-to-center spacing $< 8d_b$). The

results of these tests were used to develop descriptive equations characterizing the behavior of headed bars in beam-column joints.

The descriptive equations [Eqs. (3.2) and (3.3)] developed by Shao et al. (2016) at the University of Kansas to calculate the anchorage strength of headed bars are:

For headed bars without confining reinforcement

$$T_h = \left(781 f_{cm}^{0.24} \ell_{eh}^{1.03} d_b^{0.35} \right) \left(0.0836 \frac{s}{d_b} + 0.3444 \right) \quad (3.2)$$

with $0.0836 \frac{s}{d_b} + 0.3444 \leq 1.0$

For headed bars with confining reinforcement:

$$T_h = \left(781 f_{cm}^{0.24} \ell_{eh}^{1.03} d_b^{0.35} + 48,800 \frac{A_u}{n} d_b^{0.88} \right) \left(0.0622 \frac{s}{d_b} + 0.5428 \right) \quad (3.3)$$

with $0.0622 \frac{s}{d_b} + 0.5428 \leq 1.0$ and $\frac{A_u}{n} \leq 0.3 A_b$

where T_h is the anchorage strength of a headed bar (lb), f_{cm} is the measured concrete compressive strength (psi), ℓ_{eh} is the embedment length (in.), d_b is the diameter of the headed bar (in.), s is the center-to-center spacing between the bars (in.), A_u is the total cross-sectional area of all confining reinforcement parallel to the headed bars being developed in beam-column joints and located within $8d_b$ of the headed bars in direction of the interior of the joint for No. 3 through No. 8 bars and within $10d_b$ of the bar in direction of the interior of the joint for No. 9 through No. 11 bars (in.²), and n is the number of developed headed bars.

A factor of 0.8 is applied to the calculated strength T_h [Eqs. (3.2), and (3.3)] when the headed bars are placed outside a column core with clear cover to the bar < 2.5 in. or placed in a member other than a beam-column joint with clear cover to the bar $< 8d_b$.

3.7.2 Comparison of Descriptive Equation for the CCT Node Specimens

3.7.2.1 CCT Node Tests (Current Study)

Table 3.9 shows the embedment length ℓ_{eh} , measured concrete compressive strength f_{cm} , center-to-center spacing between the bars in terms of bar diameter s/d_b , anchorage forces from the CCT node tests T (as described in Section 3.2) per bar, calculated force T_h using the descriptive equation, Eq. (3.2), and the ratio of the test to calculated force T/T_h . Of the two expressions, only Eq. (3.2) is applicable because the headed bars contained no confining reinforcement parallel to the bars. The bars had less than $8d_b$ clear cover, so the 0.8 modification factor described in Section 3.7.1 was applied.

Table 3.9 Test results for headed bars in CCT node specimens in the current study and comparisons with descriptive equation [Eq. (3.2)]

Specimen	ℓ_{eh} (in.)	f_{cm} (psi)	s/d_b	T (kips) ¹	T_h (kips) ²	T/T_h
H-2-8-5-10.4-F4.1-1	10.4	4490	12	126.9	52.5	2.42
H-2-8-5-9-F4.1-1	9	5740	12	101.9	47.9	2.13
H-3-8-5-11.4-F4.1-1	11.4	5750	6	94.6	51.8	1.83
H-3-8-5-9-F4.1-1	9	5800	6	109.0	40.7	2.68
H-3-8-5-14-F4.1-1	14	5750	6	121.0	64.0	1.89
H-2-8-5-9-F4.1-2	9	4630	12	79.9	45.5	1.76
H-2-8-5-13-F4.1-2	13	4760	12	91.7	66.9	1.37
H-3-8-5-9-F4.1-2	9	4770	6	86.8	38.8	2.24
H-3-8-5-11-F4.1-2	11	4820	6	98.5	47.8	2.06
H-3-8-5-13-F4.1-2	13	4900	6	122.0	57.0	2.14

¹ T anchorage strength based on strut-and-tie model

² T_h anchorage strength based on Eq. (3.2) including the 0.8 modification factor

Table 3.9 shows that with T/T_h ranges between 1.37 to 2.68, with an average of 2.05. The anchorage strength of all headed bars in the CCT node specimens were much higher than the anchorage strengths calculated using Eq. (3.2). The direct compressive force from the support reaction perpendicular to the bar may be the reason for the high anchorage strength of the headed bars at CCT nodes.

3.7.2.2 CCT Node Specimens Tested by Thompson et al. (2006a)

Thompson et al. (2006a) tested 64 CCT node specimens with headed bars. Of that total, 15 specimens had a net bearing area of at least $4A_b$. The other specimens are excluded from this comparison. The specimens contained a single bar with $2.5d_b$ side cover to the bar. In the

calculations, the bar spacing s is considered to be equal to the width of the specimen ($6d_b$). Two specimens (CCT-08-45-04.70(V)-1-C0.006 and CCT-08-45-04.70(V)-1-C0.012) were confined with No. 3 stirrups installed perpendicular to the bar within the nodal zone. To contribute to A_u in Eq. (3.8), the confining reinforcement must be placed parallel to the bar. For this reason, the stirrups in these two specimens are not considered in the calculations. As a result, Eq. (3.2) is used to calculate the anchorage force T_h for all specimens.

The anchorage forces T of the CCT node specimens tested by Thompson et al. (2006a) were measured with strain gauges mounted $7d_b$ from the bearing face of the head, which represented the approximate location of the boundary of the extended nodal zone for most of the specimens. For this reason, the embedment length is taken as $7d_b$ for the calculation of anchorage force T_h . The 0.8 modification factor is applied to the calculation of T_h . Table 3.10 shows embedment length ℓ_{eh} , and measured concrete compressive strength f_{cm} , measured anchorage forces T (based on strain gauges located at $7d_b$ from the face of the head), calculated anchorage forces T_h , and the ratio of test/calculated T/T_h .

Table 3.10 Test results for CCT node specimens tested by Thompson et al. (2006a) and comparisons with descriptive equation [Eq. (3.2)]

Specimen	Bar Size	ℓ_{eh} (in.)	f_{cm} (psi)	T (kips) ¹	T_h (kips)	T/T_h
CCT-08-55-04.70(H)-1 ^{2 4}	No. 8	7	4000	54.0 ²	28.7	1.88
CCT-08-55-04.70(V)-1 ⁴		7	3900	54.0	28.5	1.89
CCT-08-55-10.39-1 ²		7	4000	54.0 ²	28.7	1.88
CCT-08-45-04.04-1 ²		7	4000	48.2 ²	28.7	1.68
CCT-08-45-04.70(V)-1 ⁴		7	3900	54.0	28.5	1.89
CCT-08-30-04.04-1 ²		7	4100	48.2 ²	28.9	1.67
CCT-08-30-04.06-1 ²		7	4100	54.0 ²	28.9	1.87
CCT-08-30-10.39-1 ²		7	4100	54.0 ²	28.9	1.87
CCT-08-45-04.70(H)-1-S3 ⁴		7	3800	52.1	28.4	1.84
CCT-08-45-04.70(V)-1-C0.006 ^{3 4}		7	3800	50.6	28.4	1.79
CCT-08-45-04.70(V)-1-C0.012 ^{3 4}		7	3800	51.8	28.5	1.83
CCT-11-45-04.13(V)-1 ⁴		No. 11	9.87	4000	88.9	46.1
CCT-11-45-06.69(H)-1 ^{2 4}	9.87		4000	98.0 ²	46.1	2.12
CCT-11-45-06.69(V)-1 ^{2 4}	9.87		4000	98.0 ²	46.1	2.12
CCT-11-45-09.26-1 ²	9.87		4000	98.0 ²	46.1	2.12

¹ T is based on strain gauges located at $7d_b$ from the face of the head

² Specimen exhibited bar yielding before failure of the node

³ Specimen had transverse stirrups perpendicular to the headed bars within the nodal zone

⁴ "H" represents a rectangular head with the long side orientated horizontally; "V" represents a rectangular head with the long side orientated vertically

As shown in Table 3.10, the anchorage strengths of headed bars in the CCT node specimens are consistently higher than the anchorage strengths calculated using the descriptive equation. The values of T/T_h range from 1.67 to 2.21 with an average of 1.89. This matches the results from the current study (T/T_h from 1.37 to 2.68 with an average of 2.05; as described in Section 3.7.2.1). The anchorage forces for the CCT node tests from the current study and by Thompson et al. (2006a) exhibited higher values than values expected based on results for headed bars anchored in beam-column joints (Shao et al. (2016)).

The T/T_h values for the two specimens tested by Thompson et al. (2006a) with confining reinforcement perpendicular to the bar, CCT-08-45-04.70(V)-1-C0.006 and CCT-08-45-04.70(V)-1-C0.012, are equal to 1.79 and 1.83, respectively. These ratios are slightly less than the average T/T_h value of 1.89 for all specimens in Table 3.7. It is clear that providing transverse reinforcement perpendicular to the bar within a nodal zone does not increase the anchorage strength of headed bars in the CCT nodes.

From both the current study, and the study by Thompson, the strength predicted by the descriptive equation is conservative for the CCT node specimens. This suggests the 0.8 modification factor may not be required for headed bars placed at a beam end, even with clear cover to the bar $< 8d_b$.

3.8 ANALYSIS OF TEST RESULTS USING ACI 408R-03 EQUATION

In this section, the results of the non-headed end CCT node specimens tested in the current study are compared with values based on the ACI 408R-03 equation for the development strength of straight bars.

3.8.1 ACI 408R-03 Equation

The force developed by a straight bar based on the expression presented in ACI 408R-03 is given in Eq. (3.4) for specimens without confining reinforcement. ACI 408R-03 also includes an equation that accounts for the effect of confining reinforcement that is not presented here because the CCT node specimens do not have confining reinforcement in which the bars are developed.

$$T_{408} = f_c^{1/4} \left[59.9 \ell_d (c_{\min} + 0.5d_b) + 2400 A_b \right] \left(0.1 \frac{c_{\max}}{c_{\min}} + 0.9 \right) \quad (3.4)$$

where ℓ_d is the embedment length (in.), d_b is the diameter of the straight bar (in.), f_c is the concrete compressive strength (psi), A_b is the nominal area of the bar, c_{\min} is the minimum cover used in expressions for the bond strength of bars not confined by transverse reinforcement, and c_{\max} is maximum (c_b, c_s); c_b is the bottom concrete cover for reinforcing bar being developed or spliced and c_s is the minimum of [$c_{so}, c_{si} + 0.25$ in. (6.35 mm)]; $c_{si} = 1/2$ of the bar clear spacing and c_{so} is the side concrete cover for reinforcing bar.

3.8.1.2 CCT Node Tests (Non-Headed End) (Current Study)

Table 3.11 shows the embedment length ℓ_d , measured concrete compressive strength f_{cm} , bar diameter d_b , anchorage forces per bar from the CCT node tests, calculated force T_{408} using ACI 408R-03, Eq. (3.4), and the ratio of the test to calculated force T/T_{408} .

Table 3.11 Test results for straight bars in CCT node specimens in the current study and comparisons with ACI 408R-03 [Eq. (3.4)]

Specimens	ℓ_d (in.)	f_{cm} (psi)	d_b (in.)	T (kips) ¹	T_{408} (kips) ²	T/T_{408}
NH-2-8-5-9-F4.1-1	9	5740	1	57.9	30.58	1.89
NH-2-8-5-10.4-F4.1-1	10.4	5330	1	86.9	32.17	2.70
NH-3-8-5-9-F4.1-1	9	5800	1	63.3	30.66	2.06
NH-3-8-5-11.4-F4.1-1	11.4	5750	1	60.4	34.35	1.76
NH-3-8-5-14-F4.1-1	14	5750	1	87.3	38.42	2.27
NH-2-8-5-9-F4.1-2	9	4630	1	79.9	28.98	2.76
NH-2-8-5-13-F4.1-2	13	4760	1	85.8	35.15	2.44
NH-3-8-5-9-F4.1-2	9	4770	1	50.1	29.20	1.72
NH-3-8-5-11-F4.1-2	11	4820	1	77.2	32.27	2.39
NH-3-8-5-13-F4.1-2	13	4900	1	89.2	35.41	2.52

¹ T anchorage strength based on strut-and-tie model

² T_i anchorage strength based on Eq. (3.4)

Table 3.11 shows that T/T_{408} ranges between 1.72 and 2.76, with an average of 2.25. Like the headed bar tests, the anchorage strengths of all non-headed bars in the CCT node specimens were much higher than the anchorage strengths calculated using Eq. (3.4), again likely due to the direct compressive force from the support reaction perpendicular to the bar.

3.9 SUMMARY

Two groups of five beams were tested to investigate the behavior and strength of high strength headed bars terminating in CCT nodes. Each specimen contained either two or three No. 8 bars with $4.1A_b$ head size. One end of the specimen had bars terminated with heads and the other end had straight bars with no head. The nominal concrete compressive strength was 5,000 psi. The peak stresses in the bars ranged from 101 to 160 ksi for the headed end tests and from 63 to 112 ksi for the non-headed end tests. The ends of the specimens were tested separately: the end with the longitudinal reinforcement anchored with a head was tested first, followed by the end with the longitudinal bars anchored by a straight bar. Based on the member and test geometry, a diagonal strut was assumed to develop between the load point and the support plate with an inclination of 45 degrees with the horizontal axis of the beam. The beams contained no confining reinforcement within the strut or node. The nominal embedment lengths, defined as the distance between the bearing face of the head and the boundary of the extended nodal zone (the point where the bar intersects with the assumed strut) ranged from 9 to 14 in.

The results of the CCT node specimens tested in the current study and by Thompson et al. (2006a) (some specimens were confined with stirrups installed perpendicular to the bar within the nodal zone) were compared with values calculated using the descriptive equation for the anchorage strength of headed bars developed by Shao et al. (2016). The purpose of these comparisons was to evaluate the ability of the descriptive equation to represent the anchorage strength of headed bars embedded at the end of beams within compression-compression-tension (CCT) nodes. Further, the results of the non-headed end CCT node specimens tested in the current study were compared with values based on the ACI 408R-03 equation for the development strength of straight bars.

The following summarizes the primary findings:

- 1) Specimen strength was limited by anchorage failures, either side-face blowout for headed bars or pullout for straight bars, except for one test specimen that appeared to fail due to crushing of concrete within the assumed node region. This observation is based on damage to the specimens at failure and estimates of specimen capacity, which showed that most specimens failed at loads lower than the calculated strut and node capacities.

- 2) Comparisons of beam force-deflection responses showed that anchorage type (headed bars and straight bars) had minimal effect on initial beam stiffness.
- 3) Based on comparisons with the work by Thompson et al. (2006a), the anchorage strength of headed bars at the CCT nodes does not increase by providing transverse reinforcement perpendicular to the bar within a nodal zone.
- 4) The comparisons of test results for the CCT node specimens from the current study and those tested by Thompson (2006a) show that the descriptive equation developed by Shao et al. (2016) is very conservative for the headed bars in CCT nodes that have a compressive force placed perpendicular to the bar.
- 5) The comparisons for the CCT node specimens from the current study show that the descriptive equation developed by ACI Committee 408 (ACI 408R-03) very conservative for the straight bars in CCT nodes that have a compressive force placed perpendicular to the bar.

CHAPTER 4: COMPARISONS OF ANCHORAGE STRENGTH OF HEADED BARS WITH VALUES BASED ON DEVELOPMENT LENGTH AND ANCHORAGE DESIGN PROVISIONS

4.1 INTRODUCTION

In this chapter, anchorage strengths of headed bars in tension are compared with values based on the development length design provisions for headed bars from ACI 318-14, Shao et al. (2016), ACI 318-19, and Darwin and Dolan (2021)², as well as the anchorage provisions in Chapter 17 of ACI 318-19. In addition, the strut-and-tie method, which is recommended in Commentary Section R25.4.4.2 of ACI 318-19 for the design of beam-column joints with effective depth to development length ratios of 1.5 and greater, is used for comparisons with the strength of test specimens with confining reinforcement within the joint region that have ratios of effective depth to embedment length of 1.5 and greater. The analysis includes 178 beam-column joint specimens with headed bars with net head bearing areas ranging from 3.8 to 9.5 times the nominal area of the bar (A_b) tested at the University of Kansas by Shao et al. (2016): 82 without confining reinforcement and 96 with confining reinforcement. Of these, 40 specimens (18 specimens without confining reinforcement and 22 specimens with confining reinforcement) had $d_{eff}/\ell_{eh} \geq 1.5$.

4.2 TEST SPECIMENS

4.2.1 Beam-Column Joint Specimen (Shao et al. 2016)

Figure 4.1 shows a beam-column joint specimen designed to represent an exterior beam-column joint. No. 5, No. 8 and No. 11 headed bars placed in one layer, representing the longitudinal reinforcement of the beam, were loaded in tension. The shaded area represents the joint region. The longitudinal and transverse reinforcement outside of the joint region was designed to resist the flexural and shear stresses on the column. Concrete compressive strengths ranged from 3,960 to 16,030 psi, specimens contained two, three, or four headed bars with center-to-center spacing ranging from 3 to $11.8d_b$, embedment lengths ranged from 3.8 to 19.6 in., and net head bearing areas ranged from 3.8 to $14.9A_b$ (those with bearing areas ranging from 3.8 to $9.5A_b$ are used in the analysis), where A_b is the nominal cross-sectional area of the headed bar. Stresses in the headed bars at anchorage failure ranged from 26,100 to 153,200 psi.

² This reference is a textbook that is under preparation. It will be published in 2020 with a copyright date of 2021.

Most specimens had one of three levels of confining reinforcement in the joint region placed parallel to the headed bars: no confining reinforcement, two No. 3 stirrups, or No. 3 stirrups at a $3d_b$ center-to-center spacing, as shown in Figure 4.2. A few specimens were tested with different quantities of confining reinforcement (four No. 3 stirrups, five No. 3 stirrups, or four No. 4 stirrups within the joint region). Full specimen details are given in Appendix C.

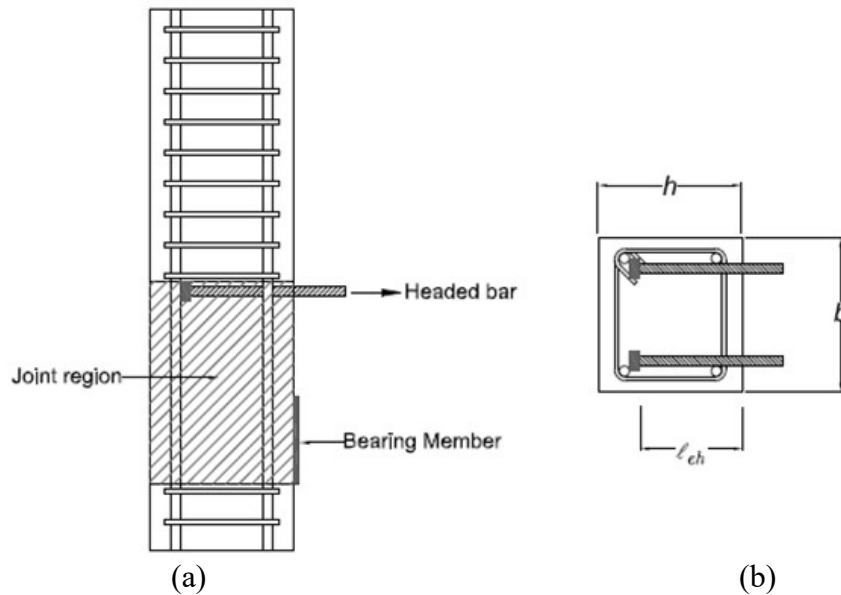


Figure 4.1 Typical beam-column joint specimen (a) side view (b) top view (Figure after Shao et al. 2016)

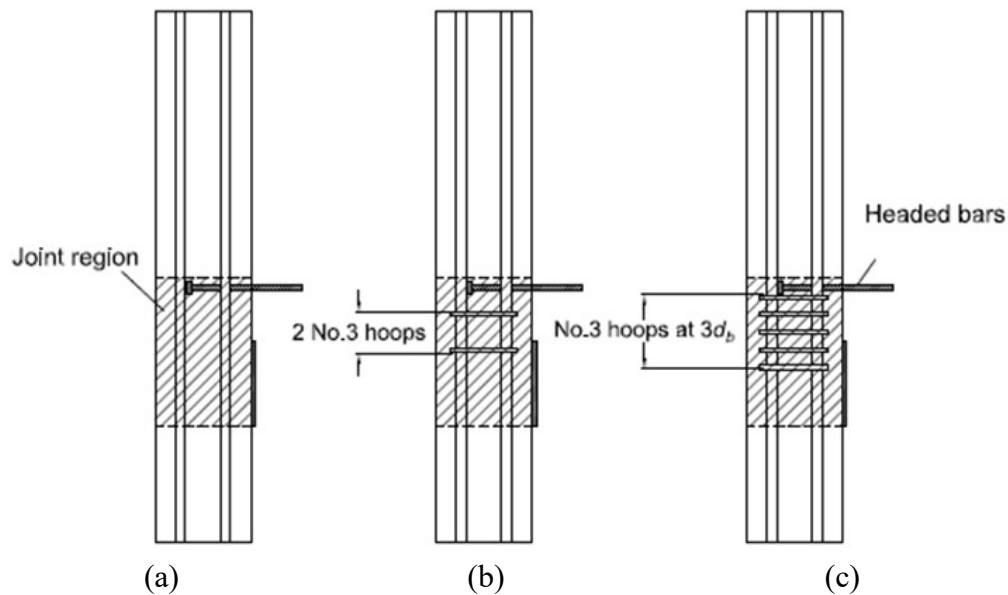


Figure 4.2 Confining reinforcement for beam-column joint specimens (a) no confining reinforcement, (b) two No. 3 hoops, (c) No. 3 hoops at $3d_b$ (Figure after Shao et al. 2016)

4.2.2 Beam-Column Joint Specimens with $d_{eff}/\ell_{eh} \geq 1.5$

Shao et al. (2016) found that headed bars with $h_{cl}/\ell_{eh} < 1.33$ showed higher anchorage strengths than headed bars with $h_{cl}/\ell_{eh} \geq 1.33$. h_{cl} was defined by Shao et al. (2016) as the distance from the center of the headed bar to the top of the bearing member (Figure 4.1). For comparison with design provisions, Shao et al. (2016) found that it would be more suitable to define this ratio in terms of the effective depth of the beam d rather than h_{cl} . To find the effective depth of the assumed beam, Shao et al. (2016) treated the upper edge of the bearing member as the location of the neutral axis of the beam. The effective depth of neutral axis c is calculated using Eq. (4.1), which was, in turn, based on the depth of the stress block a calculated using Eq. (4.2). The effective value of d , d_{eff} , is taken as the sum of h_{cl} and c , as shown in Figure 4.3. Shao et al. (2016) found that headed bars exhibited low anchorage strengths as the ratio d_{eff}/ℓ_{eh} increased above 1.5.

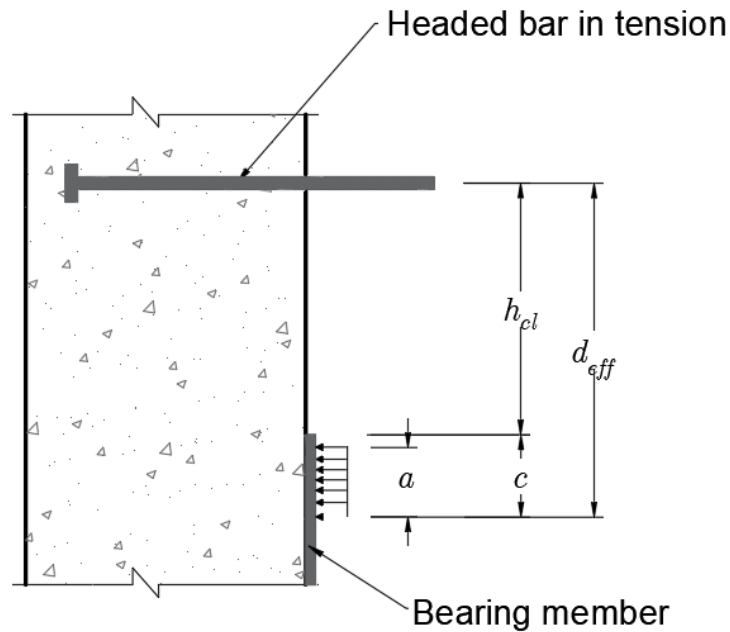


Figure 4.3 Effective depth d_{eff} (after Shao et al. 2016)

$$c = a/\beta_1 \quad (4.1)$$

where a is the depth of the equivalent rectangular compressive stress concrete block (in.) as shown in Figure 4.3, and found from Eq. (4.2) and given by

$$a = T_{\text{total}} / (0.85 f_{cm} b) \quad (4.2)$$

where T_{total} is the total force on the headed bars at failure (lb), b is the width of the column in a beam-column joint specimen (in.), and f_{cm} is the measured concrete compressive strength (psi). β_1 is the factor relating depth of equivalent rectangular compressive stress block to neutral axis depth and can be calculated using Eq. (4.3), as described in Section 22.2.2.4.3 of ACI 318-19.

$$\beta_1 = 0.85 - \frac{0.05(f_{cm} - 4000)}{1000} \quad (4.3)$$

with $0.65 \leq \beta_1 \leq 0.85$.

4.3 DESIGN APPROACHES

4.3.1 Development of Headed Bars in Tension (ACI 318-14)

According to Section 25.4.4.2 of ACI 318-14, the development length ℓ_{dt} required for anchoring headed bars in tension is given by Eq. (4.4)

$$\ell_{dt} = \left(\frac{0.016 f_y \psi_e}{\sqrt{f'_c}} \right) d_b \quad (4.4)$$

where ℓ_{dt} is not taken less than $8d_b$ or 6 in.; f_y is the yield stress of the reinforcement limited to 60,000 psi; f'_c is the concrete compressive strength limited to 6000 psi; ψ_e is taken as 1.2 for epoxy-coated reinforcement and 1.0 elsewhere; and d_b is the nominal bar diameter. Additional limits are applied on bar size (not exceeding No. 11), concrete (normalweight), clear cover and clear spacing between bars (not less than $2d_b$ and $4d_b$, respectively).

Equation (4.4) is converted to anchorage strength T_{318-14} by solving for the stress f_y , which is replaced by f_{318-14} , and multiplied by the area of the bar A_b , and by replacing the ℓ_{dt} with ℓ_{eh} and f'_c with f_{cm} , as shown in Eq. (4.5).

$$T_{318-14} = A_b f_{318-14} = A_b \left(\frac{\sqrt{f_{cm}} \ell_{eh}}{0.016 \psi_e d_b} \right) \quad (4.5)$$

For comparisons with test results, no limits are applied to either the concrete compressive strength

or the steel stress.

4.3.2 Shao et al. (2016)

The descriptive equations for anchorage strength T_h [Eqs. (4.6) and (4.7)] and the development length equation [Eq. (4.8)] proposed by Shao et al. (2016) for headed bars are as follows:

For headed bars without confining reinforcement:

$$T_h = \left(781 f_{cm}^{0.24} \ell_{eh}^{1.03} d_b^{0.35} \right) \left(0.0836 \frac{s}{d_b} + 0.3444 \right) \quad (4.6)$$

with $0.0386 \frac{s}{d_b} + 0.3444 \leq 1.0$

For headed bars with confining reinforcement:

$$T_h = \left(781 f_{cm}^{0.24} \ell_{eh}^{1.03} d_b^{0.35} + 48,800 \frac{A_{ti}}{n} d_b^{0.88} \right) \left(0.0622 \frac{s}{d_b} + 0.5428 \right) \quad (4.7)$$

with $0.0622 \frac{s}{d_b} + 0.5428 \leq 1.0$

where s is the center-to-center spacing between the bars (in.), A_{ti} is the total cross-sectional area of all confining reinforcement parallel to the headed bars being developed in beam-column joints and located within $8d_b$ of the headed bars in direction of the interior of the joint for No. 3 through No. 8 bars and within $10d_b$ of the bar in direction of the interior of the joint for No. 9 through No. 11 bars (in.²), and n is the number of the developed headed bars.

Applying a strength reduction (ϕ) factor to ensure an adequate probability against failure, solving for $\ell_{eh} = \ell_{dt}$, converting T_h to $A_b f_{su} = A_b f_y$, converting f_{cm} to f'_c , and simplifying the resulting equation, Shao et al. (2016) proposed the following expression for development length for use in design:

$$\ell_{dt} = \left(0.0024 \frac{f_y \psi_e \psi_{cs} \psi_o}{f_c'^{0.25}} \right) d_b^{1.5} \quad (4.8)$$

where f_y can have values up to 120,000 psi; f'_c can have values up to 16,000 psi. ψ_e is the modification factor for epoxy-coated or zinc and epoxy dual-coated bars used in ACI 318; ψ_{cs} is a modification factor for confining reinforcement and bar spacing (given below); and ψ_o is a

modification factor for bar location. ψ_o is taken as 1.0 for headed bars terminating inside a column core with clear side cover to the bar ≥ 2.5 in., or terminating in a supporting member with side cover to the bar $\geq 8d_b$; in other cases, ψ_o is taken as 1.25.

Solving Eq. (4.8) for anchorage strength T_{Shao} and replacing ℓ_{dt} with ℓ_{eh} and f'_c with f_{cm} gives

$$T_{\text{Shao}} = A_b \left(\frac{f_{cm}^{0.25} \ell_{eh}}{0.0024 d_b^{1.5} \psi_e \psi_{cs} \psi_o} \right) \quad (4.9)$$

ψ_{cs} for use in Eq. (4.8) and (4.9) is calculated using Eq. (4.10) for bars without confining reinforcement and Eq. (4.11) for bars with confining reinforcement.

$$\psi_{cs} = \frac{1}{12} \left(14 - \frac{s}{d_b} \right) \quad (4.10)$$

$$\psi_{cs} = \frac{1}{20} \left(18 - \frac{s}{d_b} \right) \left(1 - \frac{48,000}{f_y} \frac{A_{tt}}{A_{hs}} d_b^{0.75} \right) \quad (4.11)$$

Table 4.1 shows the values proposed for use with Eq. (4.8).

Table 4.1: Modification factor ψ_{cs} for confining reinforcement and spacing*

Confinement level	f_y	s	
		$2d_b$	$\geq 8d_b$
$\frac{A_{tt}}{A_{hs}} \geq 0.3$	$\leq 60,000$	0.6	0.4
	120,000	0.7	0.45
No confining reinforcement	all	1.0	0.5

* ψ_{cs} is permitted to be linearly interpolated for values of A_{tt}/A_{hs} between 0 and 0.3 and for spacing s or yield strength of headed bar f_y intermediate to those in the Table

4.3.3 Development of Headed Bars in Tension ACI 318-19

The development length criteria in ACI 318-19 are based on the work by Shao et al. (2016), but with a number of modifications. According to Section 25.4.4.2 of ACI 318-19, the development length ℓ_{dt} required for anchoring headed bars in tension is given by Eq. (4.12).

$$\ell_{dt} = \left(\frac{f_y \psi_e \psi_p \psi_o \psi_c}{75 \sqrt{f'_c}} \right) d_b^{1.5} \quad (4.12)$$

where ℓ_{dt} is not to be taken less than $8d_b$ or 6 in; f'_c is limited to 16,000 psi; ψ_e , ψ_p , ψ_o , and ψ_c , are calculated in accordance with Table 25.4.4.3 in ACI 318-19 and shown in Table 4.2. Additional limits are applied on bar size (not exceeding No. 11), concrete (normalweight), clear cover for bar not less than $2d_b$ and center-to-center spacing between bars not less than $3d_b$.

Equation (4.12) is solved for anchorage strength T_{318-19} and replacing ℓ_{dt} with ℓ_{eh} and f'_c with f_{cm} as shown in Eq. (4.13).

$$T_{318-19} = A_b \left(\frac{75 \sqrt{f_{cm}} \ell_{eh}}{\psi_e \psi_p \psi_o \psi_c d_b^{1.5}} \right) \quad (4.13)$$

For comparisons with test results, no limits are applied to either the concrete compressive strength or the steel stress.

Table 4.2: Modification factors for development of headed bars in tension

Modification factor	Condition	value of factor
Epoxy ψ_e	Epoxy coated or zinc and epoxy dual-coated reinforcement	1.2
	Uncoated or zinc coated (galvanized) reinforcement	1.0
Parallel tie reinforcement ψ_p	For No. 11 and smaller bars and $A_t \geq 0.3A_{hs}$ or $s^{[1]} \geq 6d_b$ [2,3]	1.0
	Other	1.6
Location ψ_o	1. for headed bars terminated inside column core with side cover to the bar ≥ 2.5 in.; or 2. with side cover to the bar $\geq 6d_b$	1.0
	Other	1.25
Concrete strength ψ_c	for $f'_c < 6000$ psi	$f'_c / 15000 + 0.6$
	for $f'_c \geq 6000$ psi	1.0

[1] s is the minimum center-to-center spacing of headed bars

[2] d_b is the nominal diameter of headed bar

[3] Refer to 25.4.4.5

4.3.4 Darwin and Dolan (2021)

The development length of headed deformed bars ℓ_{dt} proposed by Darwin and Dolan (2021) is shown in Eq. (4.14). If used in design, ψ_e would be added.

$$\ell_{dt} = \left(\frac{f_y \Psi_{cs} \Psi_o}{800 f_c^{0.25}} \right) d_b^{1.5} \quad (4.14)$$

where ψ_{cs} is a factor that account for the level of the confinement provided by parallel ties and spacing of headed deformed bars, as shown in Table 4.3; $\psi_o = 1.0$ for headed deformed bars terminating inside a column core with side cover to the bar ≥ 2.5 in., or in any member with a side cover to the bar $\geq 8d_b$; = 1.25 otherwise. No recommendations were made for headed deformed bars larger than No. 11.

Equation (4.14) can solved for anchorage strength T_D , and replacing the ℓ_{dt} with ℓ_{eh} and f_c with f_{cm} , as shown in Eq. (4.15)

$$T_D = A_b \left(\frac{800 f_{cm}^{0.25} \ell_{eh}}{\Psi_{cs} \Psi_o d_b^{1.5}} \right) \quad (4.15)$$

Table 4.3: Confinement and spacing factor ψ_{cs} ^[1]

Bar size and confinement level	Ψ_{cs}	
	$s/d_b^{[2,3]} = 2$	$s/d_b \geq 8$
$\frac{A_{th}}{A_{hs}} \geq 0.3$	1.2	0.8
$\frac{A_{th}}{A_{hs}} = 0$ (no confining reinforcement)	2.0	1.0

^[1] Interpolation permitted.

^[2] s is the center-to-center spacing of headed bars

^[3] d_b is the nominal diameter of headed bar

4.3.5 Anchorage Provisions ACI 318-19

Anchorage to concrete can be defined as the ability to transfer the axial, shear, and moment forces between the anchored bars and surrounding concrete. In this study, three modes of failure described in the anchorage provisions of ACI 318-19 for cast-in-place anchors were used to calculate the anchorage strength of headed bars in tension for the beam-column joint specimens. The three modes of failure are concrete breakout, concrete side-face blowout, and the strength of the anchor reinforcement, as described next.

4.3.5.1 Concrete Breakout Strength (N_{cb} and N_{cbg}) of Anchors in Tension

The concrete breakout strength for anchors in tension is calculated according to ACI 318-19 (Section 17.6.2.1). Figure 4.4 shows an idealized mode of failure for concrete breakout, which is assumed to occur as a 35° degree failure concrete cone. h_{ef} is the embedded depth of the anchored bar in concrete, measured from the critical section (where the stress is maximum) to the bearing face of the head, and is equal to the embedment length ℓ_{eh} for headed bars in this study.

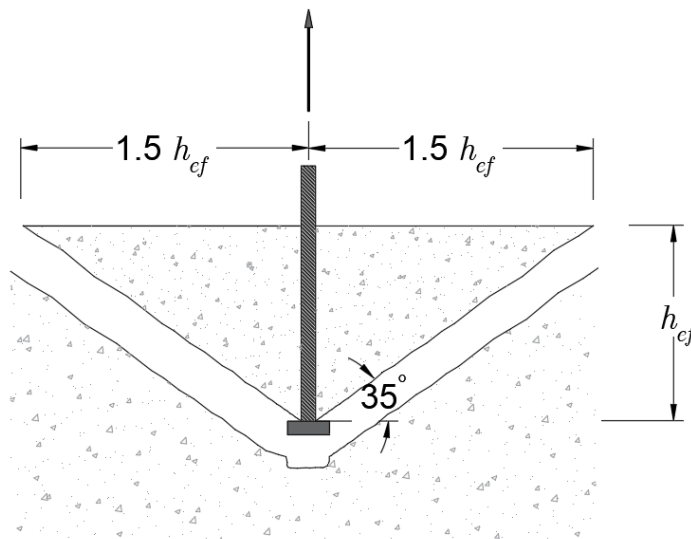


Figure 4.4 Concrete breakout failure (after ACI 318-19)

The nominal concrete breakout strength in tension, N_{cb} of a single anchor or N_{cbg} of a group of anchors is influenced by a number of factors, as shown in Eqs. (4.16) and (4.17).

(a) For a single anchor

$$N_{cb} = \frac{A_{Nc}}{A_{Nco}} \psi_{ed,N} \psi_{c,N} \psi_{cp,N} N_b \quad (4.16)$$

(b) For a group of anchors

$$N_{cbg} = \frac{A_{Nc}}{A_{Nco}} \psi_{ec,N} \psi_{ed,N} \psi_{c,N} \psi_{cp,N} N_b \quad (4.17)$$

where A_{Nc} is the total projected area for a single or group of anchors, and A_{Nco} is the maximum theoretical projected area for a single anchor. The limitations and equations for A_{Nc} and A_{Nco} can be found in ACI 318-19 (Section 17.6.2.1). $\psi_{ec,N}$ is the modification factor for a group of anchors loaded eccentrically in tension and defined in ACI 318-19 (Section 17.6.2.4); $\psi_{ed,N}$ is the modification factor for edge effects for a single anchor or group of anchors loaded in tension and is defined in ACI 318-19 (Section 17.6.2.5); $\psi_{c,N}$ is the modification factor where analysis indicates no cracking occurs at service load levels and is defined in ACI 318-19 (Section 17.6.2.6); and $\psi_{cp,N}$ is the modification factor for post-installed anchors designed for uncracked concrete and is defined in ACI 318-19 (Section 17.6.2.7). N_b is the basic concrete breakout strength of a single anchor in tension.

$$N_b = k_c \lambda_a \sqrt{f'_c} h_{ef}^{1.5} \quad (4.18)$$

where $k_c = 24$, $\lambda_a = 1.0$. For the comparisons, f'_c is replaced by f_{cm} . The limitations and equations can be found in ACI 318-19 (Section 17.6.2.2). For the comparisons in this study, no limits are applied to either concrete compressive strength or steel stress.

4.3.5.2 Concrete Side-Face Blowout Strength (N_{sb} and N_{sbg}) of Anchors in Tension

The concrete side-face blowout strength of anchors in tension is calculated according to ACI 318-19 (Section 17.6.4). It is influenced by the embedment depth h_{ef} and the minimum edge distance c_{al} (Figure 4.5). Figure 4.5 shows the mode of failure for the concrete side-face blowout. This mode of failure is applicable only when the anchored bar has an embedment depth $h_{ef} > 2.5c_{al}$.

The nominal concrete side-face blowout strength in tension, N_{sb} of a single anchor or N_{sbg} of a group of anchors is given by Eq. (4.19) and (4.20), respectively.

For a single anchor

$$N_{sb} = 160c_{a1}\sqrt{A_{brg}}\lambda_a\sqrt{f'_c} \quad (4.19)$$

For a group of anchors

$$N_{sbg} = \left(1 + \frac{s}{6c_{a1}}\right) N_{sb} \quad (4.20)$$

where A_{brg} is the net bearing area of the head of headed deformed bar (in.²), λ_a is a modification factor to reflect the reduced mechanical properties of lightweight concrete in certain concrete anchorage applications, and s is the distance between the outer anchors along the edge (in.). For the comparisons, f'_c is replaced by f_{cm} .

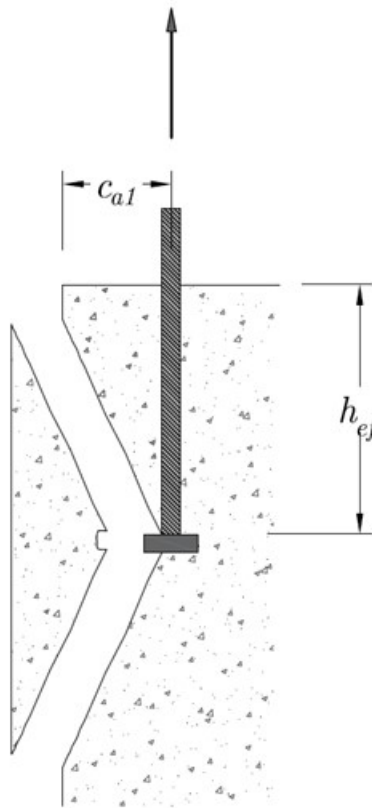


Figure 4.5 Concrete side-face blowout failure

4.5.3.3 Strength of Anchor Reinforcement (N_s)

According to ACI 318-19 (17.5.2.1 and R12.5.2.1), anchor reinforcement, provided by stirrups, ties, or hairpins, must be located within a radial distance not greater than $0.5h_{ef}$ from the anchor centerline, as shown in Figure 4.6. The nominal anchor reinforcement strength N_s may not exceed:

$$N_s = A_v f_y \quad (4.21)$$

where N_s is the strength of anchor reinforcement (lb), A_v is the area of anchor reinforcement (stirrups, ties, or hairpins spaced less than $0.5h_{ef}$ from the anchor centerline) (in.^2), and f_y is the steel yield strength (psi).

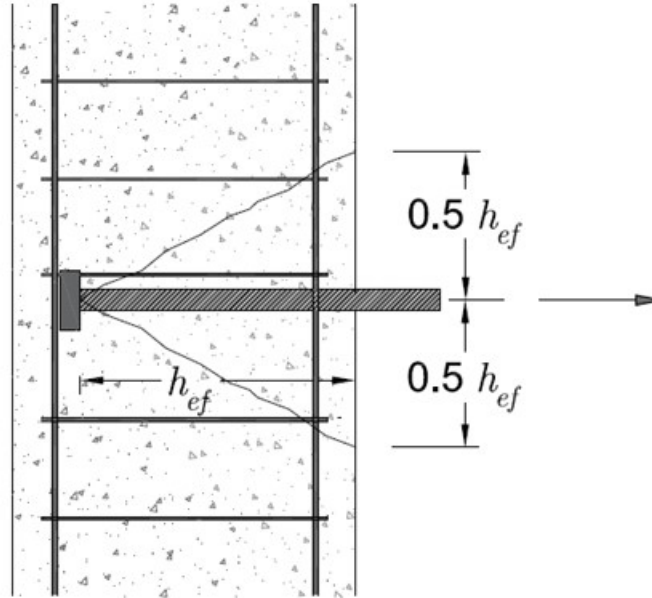


Figure 4.6 Effective anchor reinforcement

The nominal anchorage strength of each headed bar in tension in beam-column joints, N_{str} governed by concrete breakout, side-face blowout, or anchor reinforcement is calculated using Eq. (4.21). N_{cbg} , N_{sb} , and N_s are anchorage strengths calculated using Eq. (4.16), (4.18), and (4.20), respectively.

$$N_{str} = \max \left\{ \begin{array}{l} \min \left(\frac{N_{cbg}}{n}, \frac{N_{sb}}{n} \right) \\ \frac{N_s}{n} \end{array} \right\} \quad (4.22)$$

where n is the number of headed bars loaded simultaneously in tension.

4.3.6 Strut-and-Tie Method

Commentary Section R25.4.4.2 of ACI 318-19 suggests “providing reinforcement in the form of hoops and ties to establish a load path in accordance with strut-and-tie modeling principles” when the ratio of d/ℓ_{dt} exceeds 1.5; this matches the ratio d_{eff}/ℓ_{eh} used in this study; as a result, the anchorage strengths of beam-column joints with $d_{eff}/\ell_{eh} \geq 1.5$ with confining reinforcement in the joint region are calculated using the strut-and-tie modeling approach.

Figure 4.7 shows the load transfer path in the beam-column joint specimens using the strut-and-tie method. All of the confining reinforcement between the center of the headed bar and the top of the bearing member is considered to act as a single equivalent tie at the joint center. In this case, the total load T_{total} applied to the headed bars is transferred to the single tie at the joint center through a diagonal strut oriented at an angle θ with the horizontal. Finally, the load is transferred to the bearing member through a second strut, also oriented at an angle θ with the horizontal.

In design of a joint, although the force in the compression zone will normally equal the tensile force in the headed bar, using R_1 (compressive force in the compression zone calculated considering the column as a simply supported beam, as shown in Figure 4.7) provides a more accurate value to evaluate the specimens with $d_{eff}/\ell_{eh} \geq 1.5$ because of the test boundary conditions.

Applying the strut-and-tie method found that the anchorage strength of headed bars is controlled by the tie strength and is calculated as shown in Eq. 4.22.

$$T_{STM} = A_{vt}f_{yt} \quad (4.23)$$

where f_{yt} is the yield strength of the confining reinforcement (stirrups placed parallel to head) (psi), and A_{vt} is the total cross-sectional area of the stirrups between the centerline of the headed bars and the top of the bearing member (in.²).

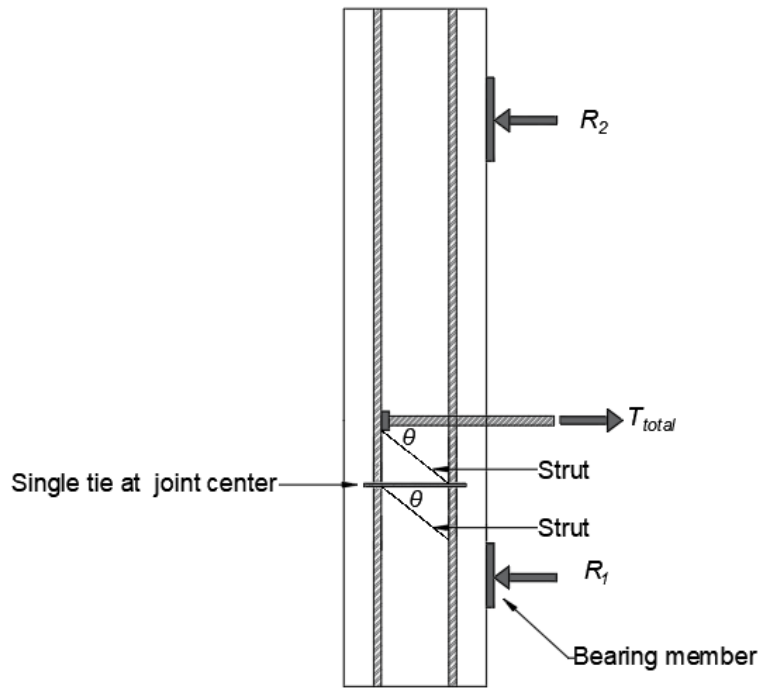


Figure 4.7 Mechanism of load transfer through the strut-and-tie (after Shao et al. 2016)

4.4 ANALYSIS AND RESULTS

4.4.1 Specimens with $d_{eff}/\ell_{eh} < 1.5$

4.4.1.1 Without Confining Reinforcement

The equations presented in Sections 4.3.1 through 4.3.5 are used to calculate the anchorage strength of headed bars for 64 beam-column joint specimens without confining reinforcement [30 specimens with widely-spaced bars (center-to-center spacing $\geq 8d_b$) and 34 specimens with closely-spaced bars (center-to-center spacing $< 8d_b$)] and $d_{eff}/\ell_{eh} < 1.5$. Tables 4.4 and 4.5 show the results for the widely and closely-spaced bars, respectively. Details of the specimens are listed in Appendix C.

Table 4.4: Comparisons for widely-spaced bars without confining reinforcement

Specimens	T	T_{318-14}	T_{Shao}	T_{318-19}	T_D	$N_{cbg/n}$	$N_{sb/n}$	N_s/n	N_{str}	ϕN_{str}
	kips	kips	kips	kips	kips	kips	kips	kips	kips	kips
8-5g-T4.0-0-i-2.5-3-12.5a	97.7	47.7	72.5	57.6	69.6	13.9	65.6	15.0	15.0	11.2
8-5g-T4.0-0-i-3.5-3-12.5a	93.4	49.1	73.4	58.9	70.4	16.3	86.2	15.0	16.3	12.2
8-5-T4.0-0-i-2.5-3-12.5a	83.3	49.0	73.6	47.0	70.7	14.2	65.8	15.0	15.0	11.2
8-5-T4.0-0-i-3.5-3-12.5a	91.9	50.1	74.6	60.2	71.7	16.6	92.7	15.0	16.6	12.4
8-8-F4.1-0-i-2.5-3-10.5	77.1	47.7	66.3	45.8	63.6	15.3	77.8	7.5	15.3	11.5
8-12-F4.1-0-i-2.5-3-10	71.8	51.9	66.4	62.2	63.8	17.5	93.7	7.5	17.5	13.1
8-5-S6.5-0-i-2.5-3-11.25	75.6	40.5	62.7	50.3	60.2	12.7	80.7	27.2	27.2	20.4
8-5-S6.5-0-i-2.5-3-14.25	87.7	52.2	80.8	51.8	77.6	14.1	75.6	27.2	27.2	20.4
8-5-O4.5-0-i-2.5-3-11.25	67.4	41.2	63.8	51.1	61.2	12.7	67.1	27.2	27.2	20.4
8-5-O4.5-0-i-2.5-3-14.25	85.0	51.7	80.1	64.2	76.9	14.1	67.1	27.2	27.2	20.4
8-5-T9.5-0-i-2.5-3-14.5	91.7	50.0	79.5	64.5	76.3	13.5	94.6	15.0	15.0	11.2
8-5-O9.1-0-i-2.5-3-14.5	94.8	50.0	79.5	64.5	76.3	13.5	94.5	15.0	15.0	11.2
8-15-T4.0-0-i-2.5-4.5-9.5	83.3	59.4	70.4	71.3	67.6	20.3	108.0	13.6	20.3	15.2
8-15-S9.5-0-i-2.5-3-9.5	81.7	59.4	70.4	71.3	67.6	20.3	173.4	13.6	20.3	15.2
8-8-T9.5-0-i-2.5-3-9.5	65.2	44.0	60.2	52.8	57.8	15.1	125.0	15.0	15.1	11.3
(2@9)8-12-F4.1-0-i-2.5-3-12	79.1	65.5	83.3	78.6	79.9	17.2	94.9	27.2	27.2	20.4
(2@9)8-12-F9.1-0-i-2.5-3-12	76.5	64.4	82.0	77.3	78.7	17.1	141.5	27.2	27.2	20.4
8-8-O4.5-0-i-2.5-3-9.5	58.4	37.2	54.7	44.6	52.6	12.9	75.7	7.5	12.9	9.7
(2@9)8-8-O4.5-0-i-2.5-3-9.5	58.8	36.4	53.6	43.7	51.5	11.3	75.7	7.5	11.3	8.5
(2@9)8-8-T4.0-0-i-2.5-3-9.5	61.8	38.1	56.0	45.8	53.8	11.6	70.3	13.6	13.6	10.2
5-5-F4.0-0-i-2.5-5-4	24.5	8.7	17.7	14.4	17.0	6.1	34.8	7.5	7.5	5.6
5-5-F4.0-0-i-2.5-3-6	32.7	12.7	26.0	21.2	24.9	6.9	35.1	7.5	7.5	5.6
5-12-F4.0-0-i-2.5-5-4	28.3	13.2	21.8	20.1	20.9	9.3	55.0	7.5	9.3	7.0
5-12-F4.0-0-i-2.5-3-6	41.7	19.5	32.1	29.7	30.9	10.6	53.8	7.5	10.6	8.0
11-5a-F3.8-0-i-2.5-3-17	97.5	72.9	102.6	84.7	98.5	16.5	79.5	27.2	27.2	20.4
11-5-F3.8-0-i-2.5-3-17	132.7	90.5	116.7	93.0	112.0	20.1	102.1	13.6	20.1	15.0
11-12-O4.5-0-i-2.5-3-16.75	169.6	123.4	135.7	124.7	130.3	27.5	152.6	27.2	27.5	20.6
11-12-S5.5-0-i-2.5-3-16.75	175.9	117.8	131.9	119.1	126.6	26.4	165.8	27.2	27.2	20.4
11-5-O4.5-0-i-2.5-3-19.25	157.9	99.0	129.6	104.0	124.4	20.5	106.0	27.2	27.2	20.4
11-5-S5.5-0-i-2.5-3-19.25	176.8	106.5	134.1	107.6	128.8	22.1	128.7	27.2	27.2	20.4

T = anchorage strength of headed bar from test, T_{318-14} = anchorage strength of headed bar from development of headed bars in tension ACI 318-14, T_{Shao} = anchorage strength of headed bar from Shao et al. (2016), T_{318-19} = anchorage strength of headed bar from development of headed bars in tension ACI 318-19, T_D = anchorage strength of headed bar from Darwin and Dolan equation, $N_{cbg/n}$ = anchorage strength of headed bar from breakout failure, $N_{sb/n}$ = anchorage strength of headed bar from side-face blowout failure, N_s/n = anchorage strength of headed bar from anchor reinforcement, N_{str} = unfactored governed anchorage strength of headed bar from anchorage provision, and ϕN_{str} = factored governed anchorage strength of headed bar from anchorage provisions.

Table 4.5: Comparisons for closely-spaced bars without confining reinforcement

Specimens	T	T_{318-14}	T_{Shao}	T_{318-19}	T_D	$N_{cbg/n}$	$N_{sb/n}$	N_s/n	N_{str}	ϕN_{str}
	kips	kips	kips	kips	kips	kips	kips	kips	kips	kips
(3@3)8-8-F4.1-0-i-2.5-3-10.5	54.8	48.0	36.4	36.0	35.0	7.2	77.8	10.0	10.0	7.5
(3@3)8-8-F4.1-0-i-2.5-3-10.5-HP	50.5	46.9	35.2	35.2	34.2	7.2	79.4	5.0	7.2	5.4
(3@4)8-8-F4.1-0-i-2.5-3-10.5	58.7	49.2	40.8	36.9	38.9	8.5	79.4	5.0	8.5	6.4
(3@5)8-8-F4.1-0-i-2.5-3-10.5	64.0	45.9	43.0	34.4	40.8	9.3	76.7	5.0	9.3	7.0
(3@5)8-8-F4.1-0-i-2.5-3-10.5-HP	59.9	46.0	43.2	34.5	41.8	9.4	76.9	5.0	9.4	7.1
(3@3)8-12-F4.1-0-i-2.5-3-10	42.2	51.3	36.6	38.5	35.4	8.0	88.9	10.0	10.0	7.5
(3@4)8-12-F4.1-0-i-2.5-3-10	48.9	52.4	40.5	39.3	38.9	9.6	92.4	10.0	10.0	7.5
(3@5)8-12-F4.1-0-i-2.5-3-10	55.1	52.4	45.3	39.3	43.2	10.9	92.5	10.0	10.9	8.2
(3@5.5)8-5-T9.5-0-i-2.5-3-14.5	73.4	49.6	55.6	39.9	53.4	8.9	90.7	10.0	10.0	7.5
(3@5.5)8-5-O9.1-0-i-2.5-3-14.5	75.7	49.9	56.0	40.2	53.7	9.0	88.8	10.0	10.0	7.5
(4@3.7)8-5-T9.5-0-i-2.5-3-14.5	60.8	52.7	47.6	40.7	45.7	7.1	98.1	7.5	7.5	5.6
(4@3.7)8-5-O9.1-0-i-2.5-3-14.5	61.2	51.8	46.3	40.0	44.4	7.1	94.1	7.5	7.5	5.6
(3@4)8-8-T9.5-0-i-2.5-3-9.5	40.3	43.4	35.6	32.6	34.2	8.3	125.0	10.0	10.0	7.5
(3@5)8-8-T9.5-0-i-2.5-3-9.5	44.5	46.8	41.6	35.1	40.0	10.0	131.1	10.0	10.0	7.5
(3@7)8-8-T9.5-0-i-2.5-3-9.5	68.7	47.3	53.4	56.8	51.7	12.7	132.7	9.1	12.7	9.5
(3@4)8-8-T9.5-0-i-2.5-3-14.5	76.6	68.5	56.2	51.3	53.9	10.0	125.0	10.0	10.0	7.5
(3@5)8-8-T9.5-0-i-2.5-3-14.5	93.2	71.8	63.0	53.8	59.7	12.0	131.1	10.0	12.0	9.0
(3@7)8-8-T9.5-0-i-2.5-3-14.5	104.0	72.4	82.4	86.9	79.1	15.2	132.7	18.1	18.1	13.6
(3@4.5)8-12-F4.1-0-i-2.5-3-12	75.2	66.1	52.7	49.6	51.0	11.5	94.8	18.1	18.1	13.6
(3@4.5)8-12-F9.1-0-i-2.5-3-12	75.4	65.2	52.4	48.9	50.3	11.4	136.8	18.1	18.1	13.6
(4@3)8-12-F4.1-0-i-2.5-3-12	49.3	65.0	45.1	48.8	43.3	8.5	92.8	13.6	13.6	10.2
(4@3)8-12-F9.1-0-i-2.5-3-12	50.3	66.8	46.1	50.1	44.2	8.7	143.1	13.6	13.6	10.2
(2@7)8-8-O4.5-0-i-2.5-3-9.5	54.5	37.4	47.2	44.9	45.4	9.9	75.7	7.5	9.9	7.4
(2@5)8-8-O4.5-0-i-2.5-3-9.5	51.2	36.4	36.8	27.3	35.3	8.3	74.1	7.5	8.3	6.2
(2@3)8-8-O4.5-0-i-2.5-3-9.5	47.7	36.4	29.6	27.3	28.4	6.8	74.1	7.5	7.5	5.6
(3@4.5)8-8-T4.0-0-i-2.5-3-9.5	40.7	38.0	35.2	28.5	33.8	7.7	71.8	9.1	9.1	6.8
(4@3)8-8-T4.0-0-i-2.5-3-9.5	26.2	38.1	30.6	28.6	29.5	5.7	68.1	6.8	6.8	5.1
(3@3)8-8-T4.0-0-i-2.5-3-9.5	39.4	38.5	31.2	28.9	29.9	6.2	70.3	10.0	10.0	7.5
(3@5.9)5-12-F4.0-0-i-2.5-4-5	28.0	16.4	20.3	24.9	19.4	6.6	52.6	5.0	6.6	5.0
(4@3.9)5-12-F4.0-0-i-2.5-4-5	25.6	16.9	16.3	16.0	15.4	5.0	52.6	3.7	5.0	3.8
(3@5.35)11-12-O4.5-0-i-2.5-3-16.75	106.8	121.9	92.2	77.0	89.0	18.2	152.6	18.1	18.2	13.7
(3@5.35)11-12-S5.5-0-i-2.5-3-16.75	109.0	117.7	91.1	74.3	87.4	17.6	162.9	18.1	18.1	13.6
(3@5.35)11-5-O4.5-0-i-2.5-3-19.25	128.7	99.4	90.3	65.2	87.1	13.7	107.9	18.1	18.1	13.6
(3@5.35)11-5-S5.5-0-i-2.5-3-19.25	137.40	106.1	92.3	67.0	88.6	14.7	128.7	18.1	18.1	13.6

T = anchorage strength of headed bar from test, T_{318-14} = anchorage strength of headed bar from development of headed bars in tension ACI 318-14, T_{Shao} = anchorage strength of headed bar from Shao et al. (2016), T_{318-19} = anchorage strength of headed bar from development of headed bars in tension ACI 318-19, T_D = anchorage strength of headed bar from Darwin and Dolan equation, $N_{cbg/n}$ = anchorage strength of headed bar from breakout failure, $N_{sb/n}$ = anchorage strength of headed bar from side-face blowout failure, N_s/n = anchorage strength of headed bar from anchor reinforcement, N_{str} = unfactored governed anchorage strength of headed bar from anchorage provision, and ϕN_{str} = factored governed anchorage strength of headed bar from anchorage provisions.

4.4.1.2 With Confining Reinforcement

The equations presented in Sections 4.3.1 through 4.3.5 were used to calculate the anchorage strength of headed bars for a total of 74 beam-column joint specimens with confining reinforcement [43 specimens with widely-spaced bars (center-to-center spacing $\geq 8d_b$) and 31 specimens with closely-spaced bars (center-to-center spacing $< 8d_b$)]. Tables 4.6 and 4.7 show the results for the specimens with widely and closely-spaced headed bars and confining reinforcement, respectively. Details of the specimens are listed in Appendix C.

Table 4.6: Comparisons for widely-spaced bars with confining reinforcement

Specimens	T	T_{318-14}	T_{Shao}	T_{318-19}	T_D	$N_{cbg/n}$	$N_{sb/n}$	N_s/n	N_{str}	ϕN_{str}
	kips	kips	kips	kips	kips	kips	kips	kips	kips	kips
8-5-T4.0-4#3-i-3-3-12.5a	87.5	43.5	76.4	55.7	82.5	13.6	68.4	44.9	44.9	33.7
8-5-T4.0-4#3-i-4-3-12.5a	96.2	43.7	74.6	54.7	81.6	15.8	93.9	44.9	44.9	33.7
8-5-T4.0-4#4-i-3-3-12.5a	109.0	43.7	74.6	55.9	82.9	13.7	69.6	81.6	81.6	61.2
8-5-T4.0-4#4-i-4-3-12.5a	101.5	41.9	72.9	54.5	80.3	15.0	88.5	81.6	81.6	61.2
8-5g-T4.0-5#3-i-2.5-3-9.5a	78.7	33.7	60.1	43.0	63.8	11.5	65.9	37.4	37.4	28.1
8-5g-T4.0-5#3-i-3.5-3-9.5a	79.5	36.3	62.3	43.8	66.2	14.1	83.4	37.4	37.4	28.1
8-5g-T4.0-4#4-i-2.5-3-9.5a	90.7	32.6	56.7	41.4	61.6	11.4	61.4	40.8	40.8	30.6
8-5g-T4.0-4#4-i-3.5-3-9.5a	96.7	36.1	60.1	43.5	65.8	14.3	95.7	40.8	40.8	30.6
8-5-T4.0-5#3-i-2.5-3-9.5a	74.2	35.5	61.5	42.7	64.6	12.2	65.9	37.4	37.4	28.1
8-5-T4.0-5#3-i-3.5-3-9.5a	80.6	35.9	60.1	43.1	64.1	14.4	89.9	37.4	37.4	28.1
8-5-T4.0-4#4-i-2.5-3-9.5a	90.5	36.7	60.3	44.0	65.5	12.7	69.9	40.8	40.8	30.6
8-5-T4.0-4#4-i-3.5-3-9.5a	85.6	36.0	60.3	43.2	64.9	14.3	88.3	40.8	40.8	30.6
8-8-F4.1-2#3-i-2.5-3-10	73.4	44.8	65.0	33.6	66.0	14.9	77.8	7.5	14.9	11.2
8-12-F4.1-5#3-i-2.5-3-10	87.2	53.5	76.2	64.3	82.3	17.7	86.4	22.4	22.4	16.8
8-5-S6.5-2#3-i-2.5-3-9.25	63.4	34.2	55.2	26.1	55.4	12.0	85.9	27.2	27.2	20.4
8-5-S6.5-2#3-i-2.5-3-12.25	86.0	46.1	72.8	35.2	74.7	13.5	81.6	34.7	34.7	26.0
8-5-O4.5-2#3-i-2.5-3-9.25	67.9	35.1	56.4	26.8	56.9	12.1	68.6	27.2	27.2	20.4
8-5-O4.5-2#3-i-2.5-3-12.25	78.5	44.9	71.4	34.3	72.8	13.4	67.2	34.7	34.7	26.0
8-5-S6.5-5#3-i-2.5-3-8.25	62.0	31.5	56.7	38.1	57.6	11.6	81.8	34.7	34.7	26.0
8-5-S6.5-5#3-i-2.5-3-11.25	84.5	41.5	70.5	50.1	75.7	13.0	81.8	42.2	42.2	31.6
8-5-O4.5-5#3-i-2.5-3-8.25	68.4	30.3	53.5	36.7	55.4	11.5	72.4	34.7	34.7	26.0
8-5-O4.5-5#3-i-2.5-3-11.25	82.2	42.2	72.0	51.0	77.0	13.1	68.1	42.2	42.2	31.6
8-5-T9.5-5#3-i-2.5-3-14.5	121.0	52.3	86.7	65.2	97.4	14.1	98.8	29.9	29.9	22.4
8-15-T4.0-2#3-i-2.5-4-5-7	59.0	44.2	55.6	33.1	55.4	18.0	85.3	13.6	18.0	13.5
8-15-S9.5-2#3-i-2.5-3-7	67.1	44.2	55.0	33.1	55.4	18.0	131.5	13.6	18.0	13.5
8-15-T4.0-5#3-i-2.5-4-5-5.5	63.3	34.4	48.0	41.3	48.9	16.3	83.5	21.1	21.1	15.8
8-15-S9.5-5#3-i-2.5-3-5.5	75.8	35.2	47.4	42.2	50.0	16.4	126.0	21.1	21.1	15.8
8-8-T9.5-2#3-i-2.5-3-9.5	68.7	43.1	61.8	32.3	62.4	15.1	130.2	22.4	22.4	16.8
(2@9)8-12-F4.1-5#3-i-2.5-3-12	111.9	65.0	89.0	77.9	99.1	17.1	85.5	42.2	42.2	31.6
(2@9)8-8-T4.0-5#3-i-2.5-3-9.5	76.7	38.7	64.4	46.4	68.1	11.6	70.3	28.6	28.6	21.4
5-5-F4.0-2#3-i-2.5-5-4	19.7	8.2	20.7	13.5	19.9	6.0	34.8	7.5	7.5	5.6
5-5-F4.0-5#3-i-2.5-5-4	26.5	8.9	21.0	14.7	21.7	6.2	35.5	15.0	15.0	11.2
5-5-F4.0-2#3-i-2.5-3-6	37.9	12.7	28.5	21.2	31.2	6.9	35.1	15.0	15.0	11.2
5-5-F4.0-5#3-i-2.5-3-6	43.5	12.9	28.3	21.4	31.5	7.0	35.1	22.4	22.4	16.8
5-12-F4.0-2#3-i-2.5-5-4	32.7	13.4	24.7	20.4	26.5	9.3	52.3	7.5	9.3	7.0
5-12-F4.0-5#3-i-2.5-5-4	38.9	13.7	24.7	20.8	27.1	9.4	51.2	15.0	15.0	11.2
11-5a-F3.8-2#3-i-2.5-3-17	118.2	76.7	109.5	55.7	108.8	16.9	81.8	34.7	34.7	26.0
11-5a-F3.8-6#3-i-2.5-3-17	116.2	73.6	115.9	53.4	115.7	16.5	79.5	42.2	42.2	31.6
11-5-F3.8-6#3-i-2.5-3-17	151.9	90.5	124.9	57.3	129.2	20.2	98.4	28.6	28.6	21.4
11-12-O4.5-6#3-i-2.5-3-16.75	201.5	121.2	140.0	76.5	148.9	27.2	141.2	42.2	42.2	31.6
11-12-S5.5-6#3-i-2.5-3-16.75	197.4	117.0	137.8	73.9	146.3	26.3	164.9	42.2	42.2	31.6
11-5-O4.5-6#3-i-2.5-3-19.25	181.4	100.0	138.7	65.7	146.2	20.6	104.0	42.2	42.2	31.6
11-5-S5.5-6#3-i-2.5-3-19.25	189.6	105.1	139.8	66.4	148.0	22.0	128.7	42.2	42.2	31.6

T = anchorage strength of headed bar from test, T_{318-14} = anchorage strength of headed bar from development of headed bars in tension ACI 318-14, T_{Shao} = anchorage strength of headed bar from Shao et al. (2016), T_{318-19} = anchorage strength of headed bar from development of headed bars in tension ACI 318-19, T_D = anchorage strength of headed bar from Darwin and Dolan equation, $N_{cbg/n}$ = anchorage strength of headed bar from breakout failure, $N_{sb/n}$ = anchorage strength of headed bar from side-face blowout failure, N_s/n = anchorage strength of headed bar from anchor reinforcement, N_{str} = unfactored governed anchorage strength of headed bar from anchorage provision, and ϕN_{str} = factored governed anchorage strength of headed bar from anchorage provisions.

Table 4.7: Comparisons for closely-spaced bars with confining reinforcement

Specimens	T	T_{318-14}	T_{Shao}	T_{318-19}	T_D	N_{cbg}/n	N_{sb}/n	N_s/n	N_{str}	ϕN_{str}
	kips	kips	kips	kips	kips	kips	kips	kips	kips	kips
(3@3)8-8-F4.1-2#3-i-2.5-3-10	61.9	45.2	44.9	33.9	37.2	7.0	76.9	10.0	10.0	7.5
(3@3)8-8-F4.1-2#3-i-2.5-3-10-HP	56.7	46.2	46.2	34.6	38.4	7.1	80.1	10.0	10.0	7.5
(3@4)8-8-F4.1-2#3-i-2.5-3-10	55.5	43.7	47.0	32.8	39.9	8.0	74.3	8.0	8.0	6.0
(3@4)8-8-F4.1-2#3-i-2.5-3-10-HP	69.8	45.8	48.9	34.3	41.8	8.2	77.5	8.2	8.2	6.1
(3@5)8-8-F4.1-2#3-i-2.5-3-10.5	56.1	43.9	49.3	33.0	42.8	9.2	76.1	9.2	9.2	6.9
(3@5)8-8-F4.1-2#3-i-2.5-3-10.5-HP	65.5	44.9	51.0	33.7	44.8	9.3	76.9	9.3	9.3	7.0
(3@3)8-12-F4.1-5#3-i-2.5-3-10	61.6	51.9	54.7	38.9	54.7	8.1	84.6	19.9	19.9	15.0
(3@4)8-12-F4.1-5#3-i-2.5-3-10	65.7	51.6	56.4	38.7	57.3	9.5	84.6	19.9	19.9	15.0
(3@5)8-12-F4.1-5#3-i-2.5-3-10	69.7	50.8	59.5	38.1	61.2	10.8	86.4	19.9	19.9	15.0
(3@5.5)8-5-T9.5-5#3-i-2.5-3-14.5	94.6	52.2	72.8	40.8	78.8	9.4	100.4	19.9	19.9	15.0
(4@3.7)8-5-T9.5-5#3-i-2.5-3-14.5	76.9	53.4	64.6	41.3	62.2	7.2	96.1	15.0	15.0	11.2
(3@4)8-8-T9.5-2#3-i-2.5-3-9.5	51.8	45.0	47.2	33.7	39.9	8.4	125.0	15.0	15.0	11.2
(3@5)8-8-T9.5-2#3-i-2.5-3-9.5	55.9	46.4	50.5	34.8	44.2	10.0	131.1	15.0	15.0	11.2
(3@7)8-8-T9.5-2#3-i-2.5-3-9.5	67.6	47.7	59.8	35.8	56.7	12.7	131.5	14.1	14.1	10.5
(3@4)8-8-T9.5-2#3-i-2.5-3-14.5	85.4	67.7	69.0	50.8	60.0	10.0	125.0	15.0	15.0	11.2
(3@5)8-8-T9.5-2#3-i-2.5-3-14.5	105.2	69.3	73.3	52.0	66.1	11.8	120.2	15.0	15.0	11.2
(3@7)8-8-T9.5-2#3-i-2.5-3-14.5	113.4	72.4	88.3	54.3	86.0	15.2	131.5	23.1	23.1	17.3
(3@4.5)8-12-F4.1-5#3-i-2.5-3-12	87.7	65.9	70.3	49.4	74.8	11.5	90.0	28.1	28.1	21.1
(3@4.5)8-12-F9.1-5#3-i-2.5-3-12	108.6	64.4	67.1	48.3	73.4	11.4	128.7	28.1	28.1	21.1
(4@3)8-12-F4.1-5#3-i-2.5-3-12	64.2	66.0	64.0	49.5	60.1	8.7	85.5	21.1	21.1	15.8
(4@3)8-12-F9.1-5#3-i-2.5-3-12	87.8	65.6	61.2	49.2	59.2	8.6	127.4	21.1	21.1	15.8
(3@4.5)8-8-T4.0-5#3-i-2.5-3-9.5	62.5	36.9	49.0	27.7	49.6	7.5	68.1	19.0	19.0	14.3
(4@3)8-8-T4.0-5#3-i-2.5-3-9.5	48.6	38.9	46.0	29.2	40.9	5.8	71.0	14.3	14.3	10.7
(3@3)8-8-T4.0-5#3-i-2.5-3-9.5	56.5	37.6	45.8	28.2	45.0	6.1	69.6	19.9	19.9	15.0
(3@5.9)5-12-F4.0-2#3-i-2.5-4-5	35.1	16.8	25.2	15.9	26.0	6.7	50.1	10.0	10.0	7.5
(3@5.9)5-12-F4.0-5#3-i-2.5-4-5	38.6	16.3	24.8	24.8	27.7	6.6	49.6	10.0	10.0	7.5
(4@3.9)5-12-F4.0-2#3-i-2.5-4-5	30.9	16.4	21.0	15.5	19.7	5.0	50.1	5.0	5.0	3.7
(3@5.35)11-12-O4.5-6#3-i-2.5-3-16.75	135.8	122.5	114.7	77.4	105.4	18.2	141.2	28.1	28.1	21.1
(3@5.35)11-12-S5.5-6#3-i-2.5-3-16.75	153.8	116.5	109.2	73.6	101.2	17.5	164.9	28.1	28.1	21.1
(3@5.35)11-5-O4.5-6#3-i-2.5-3-19.25	141.7	98.7	109.9	64.8	101.9	13.6	102.1	28.1	28.1	21.1
(3@5.35)11-5-S5.5-6#3-i-2.5-3-19.25	152.9	105.8	112	66.8	102.5	14.7	126.4	28.1	28.1	21.1

T = anchorage strength of headed bar from test, T_{318-14} = anchorage strength of headed bar from development of headed bars in tension ACI 318-14, T_{Shao} = anchorage strength of headed bar from Shao et al. (2016), T_{318-19} = anchorage strength of headed bar from development of headed bars in tension ACI 318-19, T_D = anchorage strength of headed bar from Darwin and Dolan equation, N_{cbg}/n = anchorage strength of headed bar from breakout failure, N_{sb}/n = anchorage strength of headed bar from side-face blowout failure, N_s/n = anchorage strength of headed bar from anchor reinforcement, N_{str} = unfactored governed anchorage strength of headed bar from anchorage provision, and ϕN_{str} = factored governed anchorage strength of headed bar from anchorage provisions.

4.4.1.3 Comparison with ACI 318-14

Figure 4.8 compares the ratio of the force obtained in the tests to the force based on the ACI 318-14 provisions with the measured concrete compressive strength for 30 beam-column joint specimens with widely-spaced headed bars *without* confining reinforcement. Figure 4.9 does the same for 43 beam-column joint specimens widely-spaced headed bars *with* confining reinforcement.

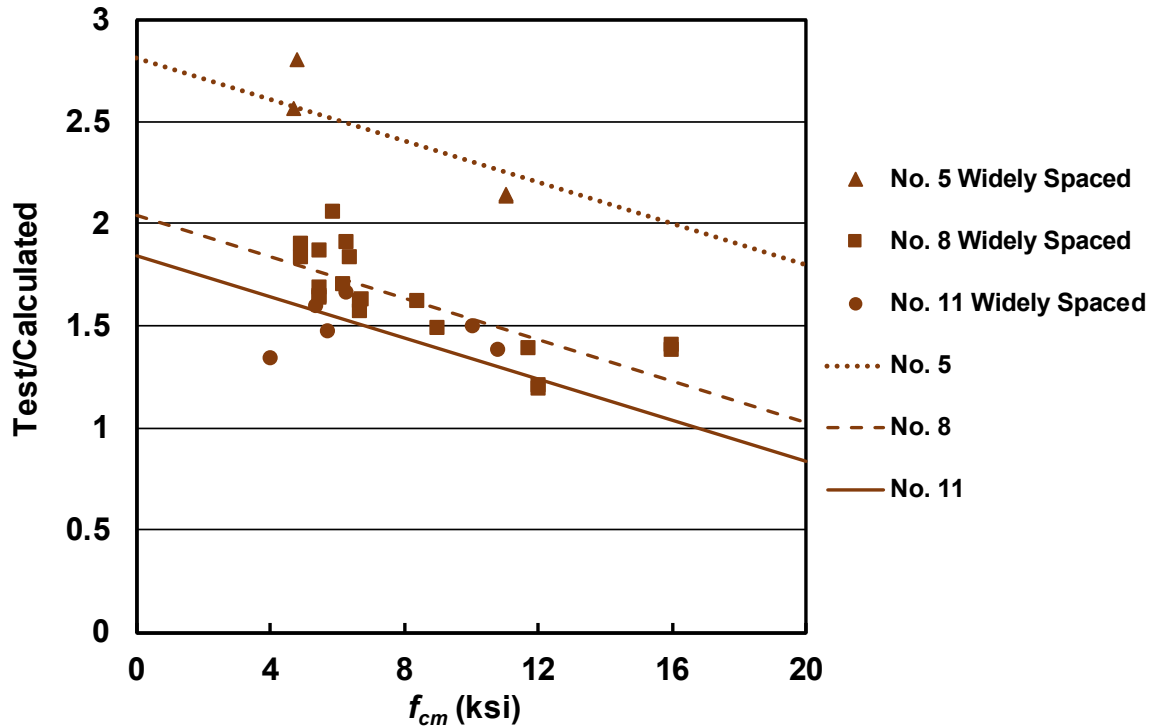


Figure 4.8 Ratio of test-to-calculated failure load (T/T_{318-14}) versus measured concrete compressive strength f_{cm} for specimens with widely-spaced headed bars without confining reinforcement (ACI 318-14)

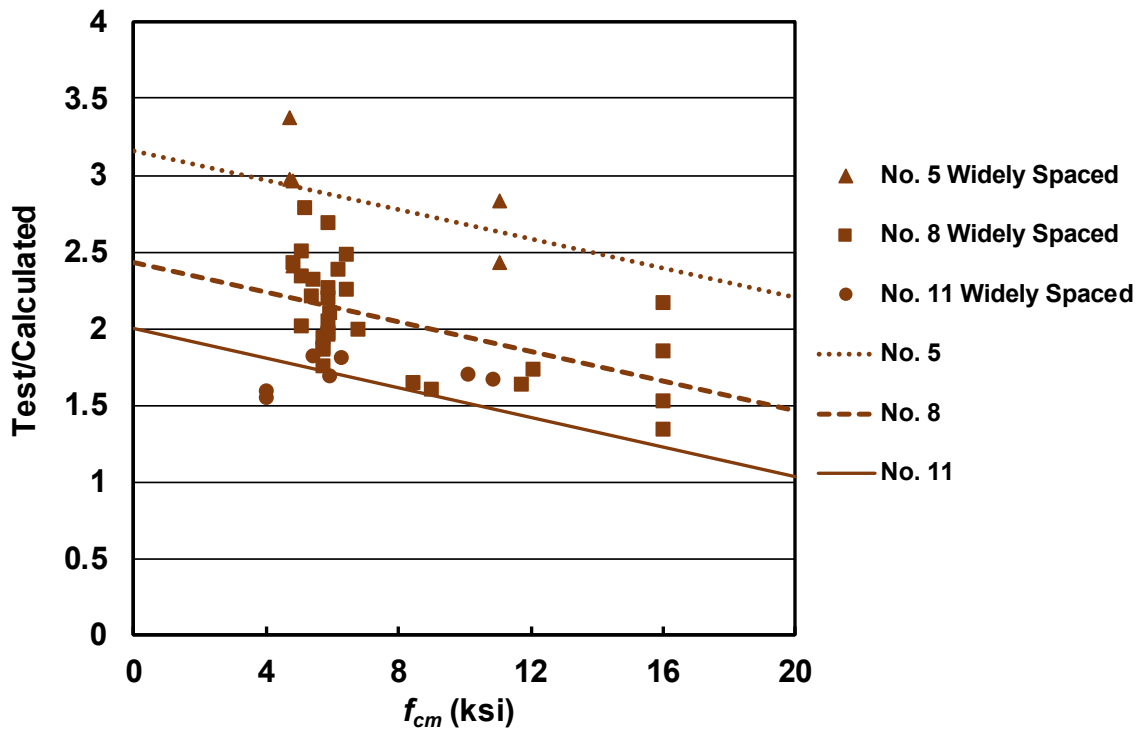


Figure 4.9 Ratio of test-to-calculated failure load (T/T_{318-14}) versus measured concrete compressive strength f_{cm} for specimens with widely-spaced headed bars with confining reinforcement (ACI 318-14)

The trend lines shown in Figures 4.8 and 4.9 are based on dummy variable analysis, a least squares regression analysis method that allows differences in populations to be taken into account when formulating relationships between principal variables. These trend lines have negative slopes. The negative slope indicates that the effect of concrete compressive strength is overestimated by the 0.5 power in the ACI 318-14 provisions. All the specimens have T/T_{318-14} values greater than 1 indicating that the ACI 318-14 provisions are conservative for headed bars with a center-to-center spacing of at least $8d_b$. The ACI 318-14 provisions are most conservative for No. 5 bars, becoming less so as the bar size increases.

Figures 4.8 and 4.9 also show that the T/T_{318-14} values increase with confining reinforcement. This should be expected since the ACI 318-14 provisions do not account for the presence of confining reinforcement

Figure 4.10 compares the ratio of force obtained from test results to the force obtained based on the ACI 318-14 provisions versus the center-to-center spacing for 64 beam-column joint specimens (widely and closely-spaced) without confining reinforcement; the statistical parameters (maximum, minimum, mean, standard deviation (STD), and coefficient of variation (COV)) are given in Table 4.8. Figure 4.11 compares the ratio of force obtained from test results to the force obtained from ACI 318-14 provisions versus center-to-center spacing for 74 beam-column joint specimens (widely and closely-spaced) with confining reinforcement; the statistical parameters (maximum, minimum, mean, standard deviation, and coefficient of variation) given in Table 4.9.

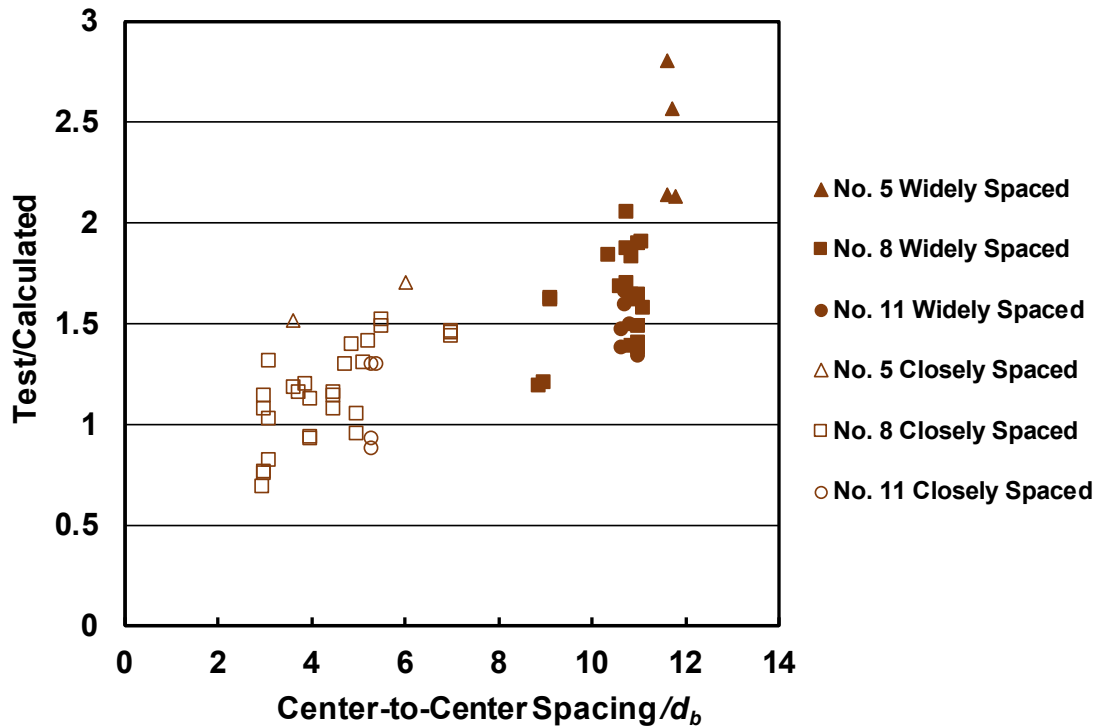


Figure 4.10 Ratio of test-to-calculated failure load (T/T_{318-14}) versus center-to-center spacing for specimens with widely and closely-spaced headed bars without confining reinforcement (ACI 318-14)

Table 4.8: Max, Min, Mean, STD, and COV of T/T_{318-14} for headed bars without confining reinforcement

(Number of specimens)	All (64)	Widely spaced $C/C^* \text{ spacing} \geq 8d_b$			Closely spaced $C/C^* \text{ spacing} < 8d_b$		
		No. 5 (4)	No. 8 (20)	No. 11 (6)	No. 5 (2)	No. 8 (28)	No. 11 (4)
Max	2.81	2.81	2.05	1.66	1.71	1.52	1.30
Min	0.69	2.13	1.19	1.34	1.52	0.69	0.88
Mean	1.42	2.41	1.62	1.49	1.61	1.15	1.10
STD	0.408	0.331	0.417	0.124	0.134	0.237	0.229
COV	0.287	0.513	0.257	0.083	0.083	0.206	0.208
$T/T_{318-14} < 1.0$	10	0	0	0	0	8	2

*C/C =Center-to-Center

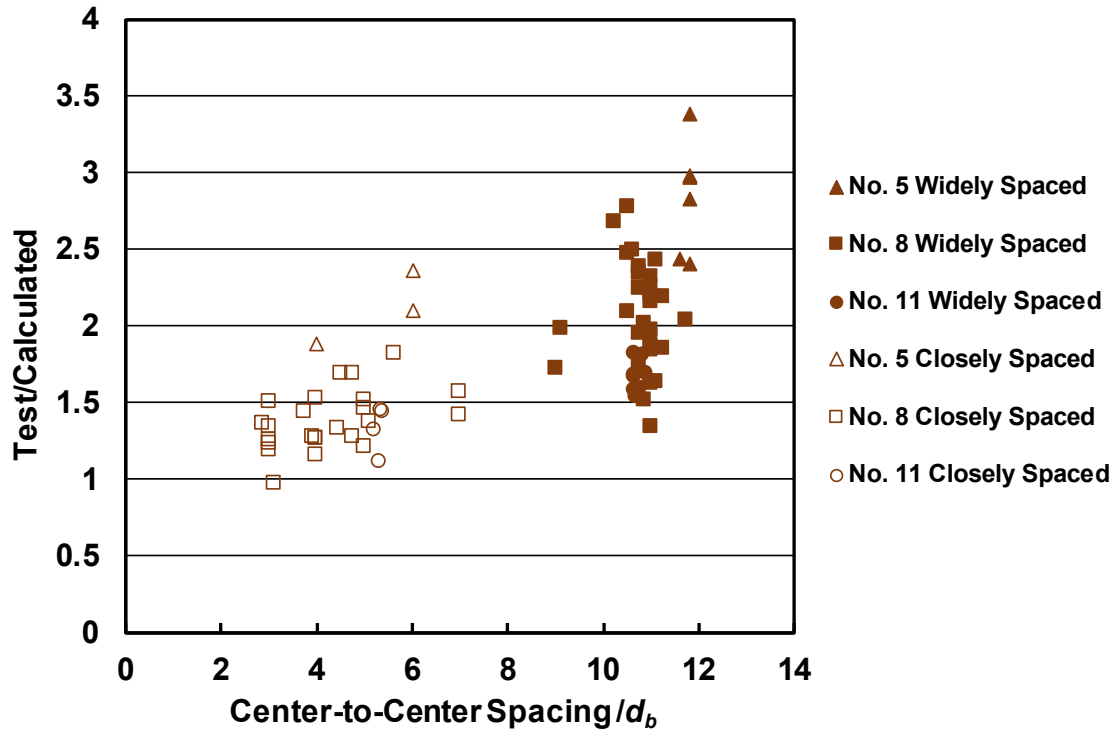


Figure 4.11 Ratio of test-to-calculated failure load (T/T_{318-14}) versus center-to-center spacing for specimens with widely and closely-spaced headed bars with confining reinforcement (ACI 318-14)

Table 4.9: Max, Min, Mean, STD, and COV of T/T_{318-14} for headed bars with confining reinforcement

(Number of specimens)	All (64)	Widely spaced $C/C^* \text{ spacing} \geq 8d_b$			Closely spaced $C/C^* \text{ spacing} < 8d_b$		
		No. 5 (4)	No. 8 (20)	No. 11 (6)	No. 5 (2)	No. 8 (28)	No. 11 (4)
Max	2.81	2.81	2.05	1.66	1.71	1.52	1.30
Min	0.69	2.13	1.19	1.34	1.52	0.69	0.88
Mean	1.42	2.41	1.62	1.49	1.61	1.15	1.10
STD	0.408	0.331	0.417	0.124	0.134	0.237	0.229
COV	0.287	0.513	0.257	0.083	0.083	0.206	0.208
$T/T_{318-14} < 1.0$	10	0	0	0	0	8	2

*C/C= Center-to-Center

Figures 4.10 and 4.11 show that the specimens with closely-spaced bars have lower anchorage strengths compared to T_{318-14} than the specimens with widely-spaced bars, becoming progressively lower as the bar spacing decreases, an effect that the provisions in ACI 318-14 do not capture. Eleven specimens (eight No. 8 bar specimens and two No. 11 bar specimens without

confining reinforcement and one No. 8 bar specimen with confining reinforcement) with a center-to-center spacing of $8d_b$ (the limit in ACI 318-14 is $5d_b$) have values of T/T_{318-14} less than 1.0.

The values of T/T_{318-14} for the 64 beam-column joint specimens without confining reinforcement range from 0.69 to 2.81, with an average of 1.42 and a coefficient of variation (COV) of 0.287. For the 74 beam-column joint specimens (with confining reinforcement), T/T_{318-14} ranges from 0.97 to 3.38, with an average of 1.83 and a coefficient of variation of 0.280. For both widely and closely-spaced bars, the ACI 318-14 provisions are conservative for No. 5 bars, becoming less conservative as bar size increases.

4.4.1.4 Comparison with Shao et al. (2016)

Shao et al. (2016) developed design equations that account for the effect of confining reinforcement and spacing between the headed bars and can be used for steel stresses up to 120 ksi and concrete compressive strengths up to 15,000 psi.

Figure 4.12 compares the ratio of the force obtained in the tests to the force based on the work of Shao et al. (2016) with the measured concrete compressive strength for the 30 beam-column joint specimens with widely-spaced headed bars *without* confining reinforcement. Figure 4.13 does the same for the 43 beam-column joint specimens widely-spaced headed bars *with* confining reinforcement.

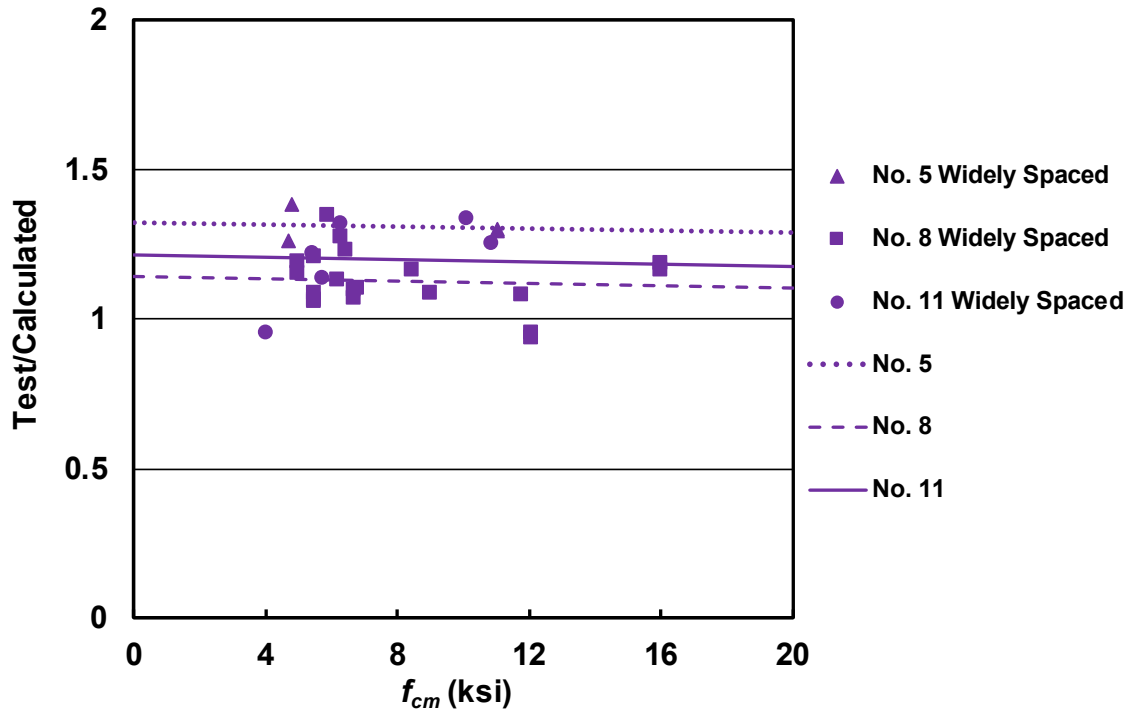


Figure 4.12 Ratio of test-to-calculated failure load (T/T_{Shao}) versus measured concrete compressive strength f_{cm} for specimens with widely spaced headed bars without confining reinforcement (Shao et al. 2016)

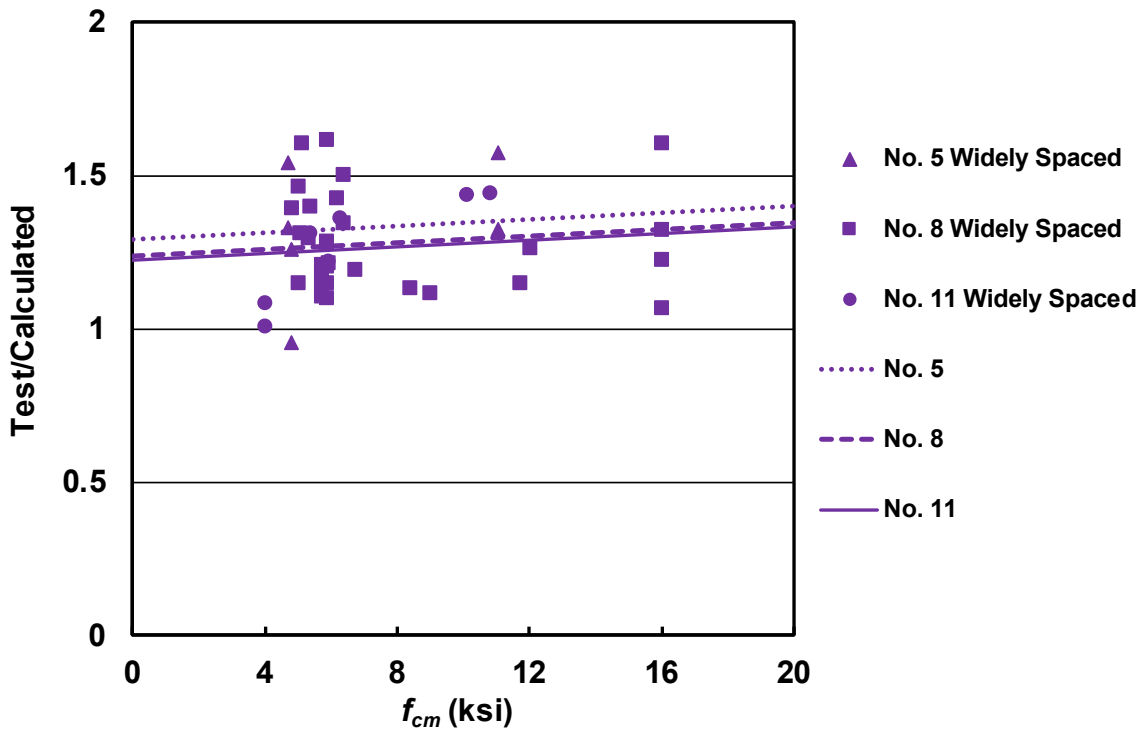


Figure 4.13 Ratio of test-to-calculated failure load (T/T_{Shao}) versus measured concrete compressive strength f_{cm} for specimens with widely-spaced headed bars with confining reinforcement (Shao et al. 2016)

The trend lines (based on dummy variable analysis) in Figures 4.12 and 4.13 are almost flat. The slight downward slope in Figure 4.12 indicates that the effect of concrete compressive strength is overestimated somewhat by the 0.25 power for the 30 specimens without confining reinforcement, and the slight upward slope in Figure 4.13 indicates that the effect of concrete compressive strength is underestimated by the 0.25 power for the 43 specimens with confining reinforcement. The order of the trend line in the two figures show that Shao et al. (2016) is more conservative for No. 5 bars than for the larger bar sizes, but that the difference is relatively small.

Figures 4.14 and 4.15 compare the ratio of force obtained from test results to the force obtained from Shao et al. (2016) versus center-to-center spacing for the beam-column joint specimens with both widely and closely-spaced bars for specimens without and with confining reinforcement, respectively. The respective statistical parameters are given in Tables 4.10 and 4.11. The figures show that the ratios T/T_{Shao} are independent of bar spacing indicating that ψ_{cs} captures the effect of spacing.

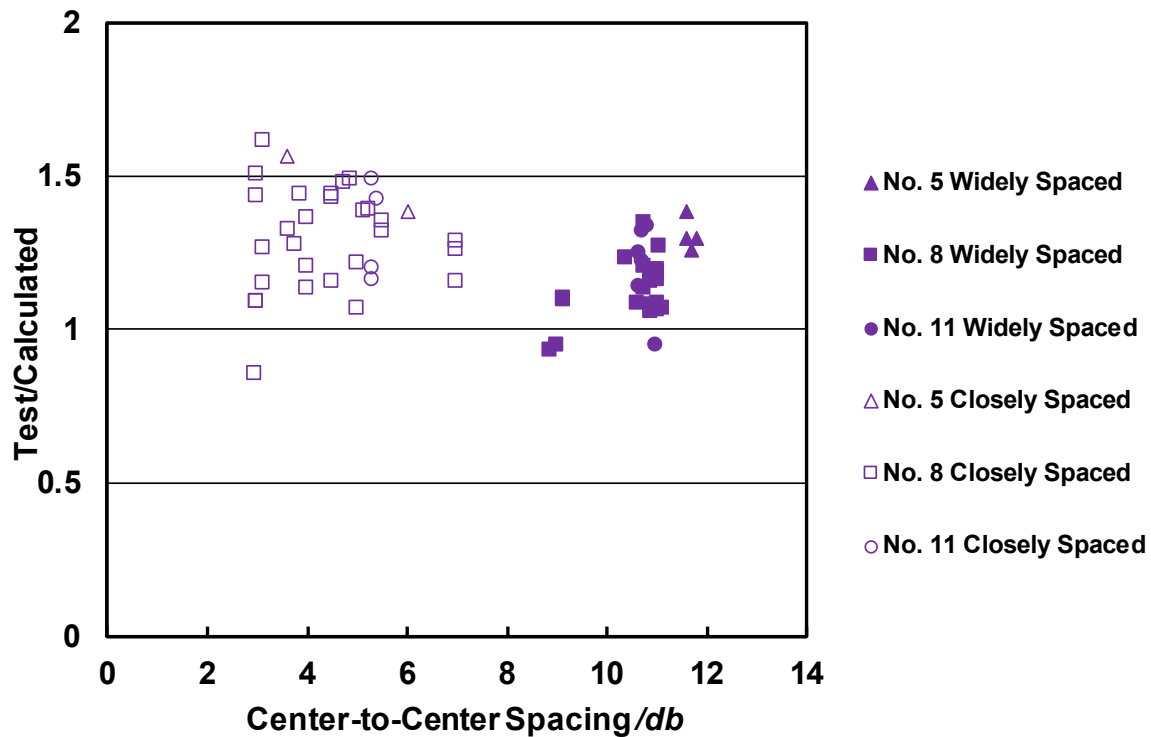


Figure 4.14 Ratio of test-to-calculated failure load (T/T_{Shao}) versus center-to-center spacing for specimens with widely and closely-spaced headed bars without confining reinforcement (Shao et al. 2016)

Table 4.10: Max, Min, Mean, STD, and COV of T/T_{Shao} for headed bars without confining reinforcement

(Number of specimens)	All (64)	Widely spaced $C/C^* \text{ spacing} \geq 8d_b$			Closely spaced $C/C^* \text{ spacing} < 8d_b$		
		No. 5 (4)	No. 8 (20)	No. 11 (6)	No. 5 (2)	No. 8 (28)	No. 11 (4)
Max	1.61	1.39	1.35	1.33	1.57	1.61	1.49
Min	0.85	1.26	0.93	0.95	1.38	0.85	1.16
Mean	1.24	1.31	1.13	1.20	1.48	1.29	1.32
STD	0.161	0.053	0.099	0.142	0.130	0.167	0.164
COV	0.130	0.040	0.088	0.118	0.088	0.129	0.125
$T/T_{Shao} < 1.0$	4	0	2	1	0	1	0

*C/C =Center-to-Center

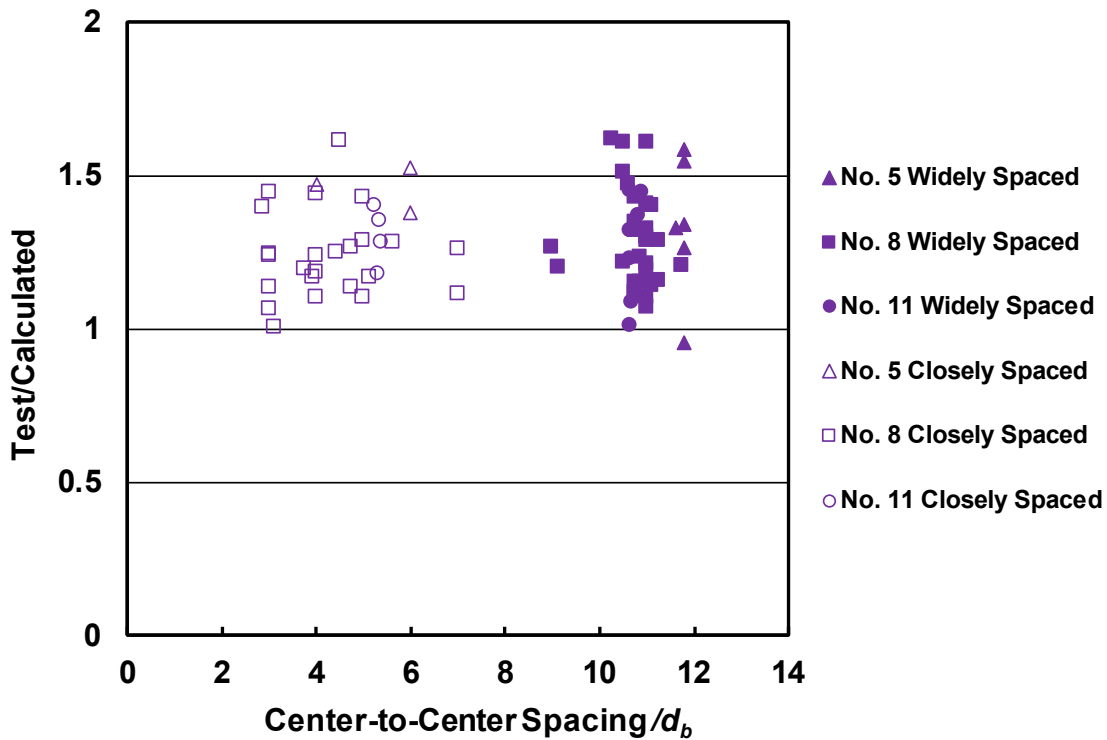


Figure 4.15 Ratio of test-to-calculated failure load (T/T_{Shao}) versus center-to-center spacing for specimens with widely and closely-spaced headed bars with confining reinforcement (Shao et al. 2016)

Table 4.11: Max, Min, Mean, STD, and COV of T/T_{Shao} for headed bars with confining reinforcement

(Number of specimens)	All (74)	Widely spaced C/C spacing $\geq 8d_b$			Closely spaced C/C spacing $< 8d_b$		
		No. 5 (6)	No. 8 (30)	No. 11 (7)	No. 5 (3)	No. 8 (24)	No. 11 (4)
Max	1.62	1.58	1.61	1.44	1.56	1.62	1.41
Min	0.95	0.95	1.06	1.00	1.39	1.00	1.18
Mean	1.28	1.33	1.28	1.26	1.48	1.24	1.31
STD	0.158	0.224	0.158	0.170	0.081	0.142	0.098
COV	0.124	0.169	0.124	0.135	0.055	0.114	0.075
$T/T_{Shao} < 1.0$	1	1	0	0	0	0	0

*C/C =Center-to-Center

As shown in Tables 4.10 and 4.11, values of T/T_{Shao} range from 0.85 to 1.61, with an average of 1.24 and a coefficient of variation of 0.130 for the specimens without confining reinforcement and from 0.95 to 1.62, with an average of 1.28 and a coefficient of variation of 0.124 for the specimens with confining reinforcement. T/T_{Shao} is less than 1.0 for five tests, two for No. 8 bar specimens without confining reinforcement and widely spaced bars, one for a No. 8 specimen without confining reinforcement and closely spaced bars, one for a No. 11 bar specimen without confining reinforcement and widely spaced bars, and one for a No. 5 specimen with confining reinforcement and widely spaced bars.

Compared the trend lines for T/T_{318-14} shown in Figures 4.8 and 4.9, the trend lines for T/T_{Shao} shown in Figures 4.12 and 4.13 are much more closely spaced indicating that the 1.5 power for d_b captures the effect of bar size on the anchorage strength of headed bars while d_b to the 1.0 power does not.

4.4.1.5 Comparison with ACI 318-19

As described in Section 4.3.2 and demonstrated in Section 4.4.1.4, the equation by Shao et al. (2016) can be safely used for the design of the anchorage strength of headed bars for steel stresses up to 120 ksi and concrete compressive strengths up to 16,000 psi. The equation accounts for the effect of confining reinforcement and spacing between the headed bars. However, the approach, along with some modifications that were considered by ACI Committee 318, was somewhat more complicated than desired. ACI Committee 318 modified the approach by using a 0.5 rather than 0.25 power of f'_c and using a modification factor, ψ_c , to approximate $f'_c{}^{0.25}$ for f'_c less than or equal to 6,000 psi. In addition, a modification factor ψ_p is used to account for the effect of confining

reinforcement and spacing between headed bars.

Figure 4.16 compares the ratio of the force obtained in the tests to the force based on the ACI 318-19 provisions with the measured concrete compressive strength for the 30 beam-column joint specimens with widely-spaced headed bars *without* confining reinforcement. Figure 4.17 does the same for the 43 beam-column joint specimens widely-spaced headed bars *with* confining reinforcement.

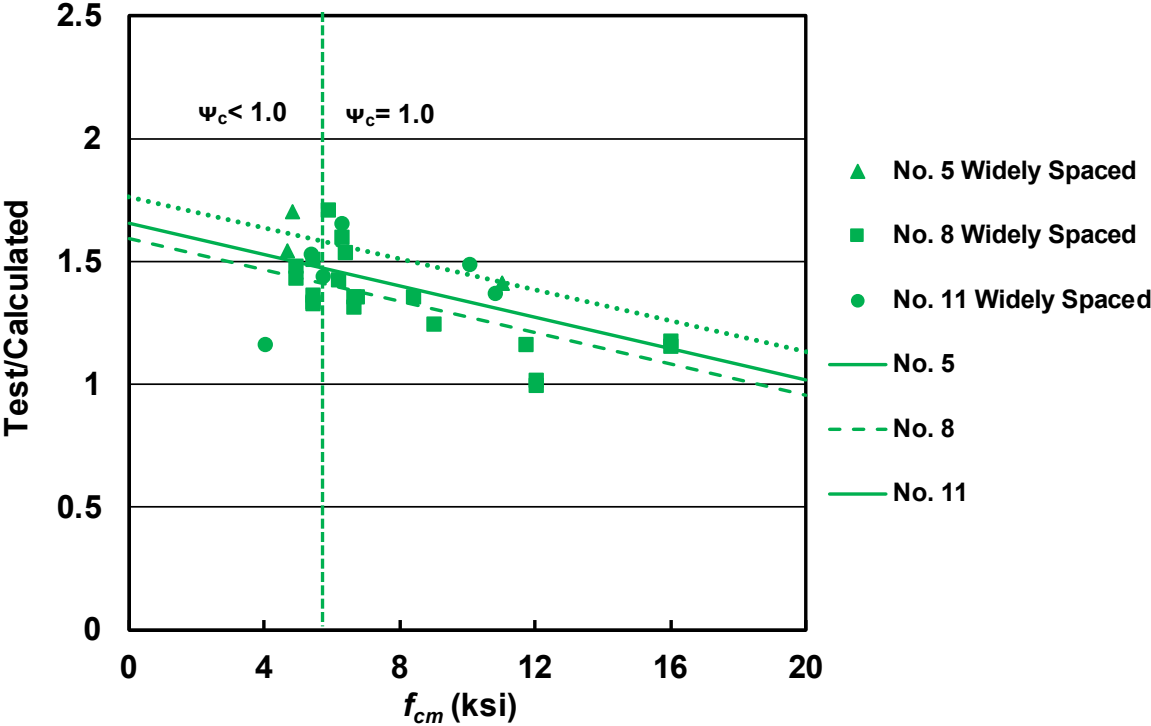


Figure 4.16 Ratio of test-to-calculated failure load (T/T_{318-19}) versus measured concrete compressive strength f_{cm} for specimens with widely-spaced headed bars without confining reinforcement (ACI 318-19)

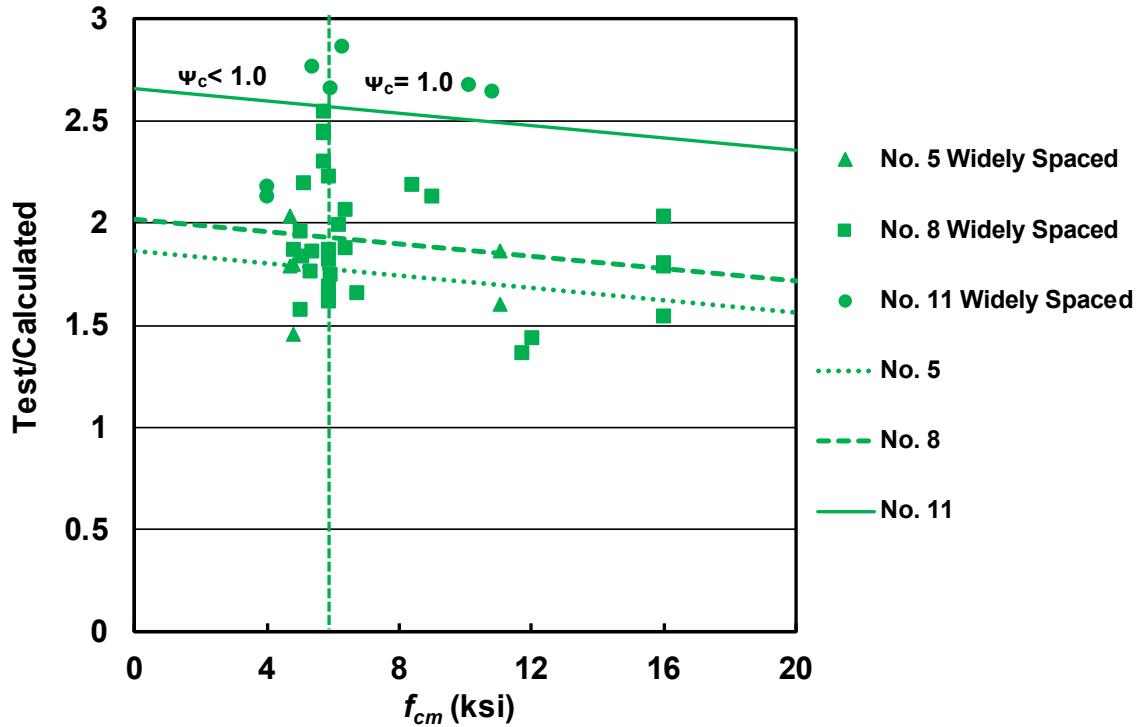


Figure 4.17 Ratio of test-to-calculated failure load (T/T_{318-19}) versus measured concrete compressive strength f_{cm} for specimens with widely-spaced headed bars with confining reinforcement (ACI 318-19)

The trend lines in Figures 4.16 and 4.17 have negative slopes, indicating that the effect of concrete compressive strength is overestimated by the 0.5 power in the ACI 318-19 provisions for compressive strengths above 6000 psi where the modification factor $\psi_c = 1.0$.

Figures 4.18 and 4.19 compare the ratio of force obtained from test results to the force obtained from the ACI 318-19 provisions versus center-to-center spacing for the beam-column joint specimens with both widely and closely-spaced bars for specimens without and with confining reinforcement, respectively. The respective statistical parameters are given in Tables 4.12 and 4.13. Like the comparisons for T/T_{Shao} , Figures 4.18 and 4.19 show that the ratio T/T_{318-19} is mostly independent of bar spacing indicating that ψ_{cs} captures the effect of spacing but that the $\psi_p = 1.0$ and 1.6 for widely and closely spaced headed bars without confining reinforcement, respectively, do not capture the effects of confining reinforcement and bar spacing as well as the provisions proposed by Shao et al. (2016), especially for the specimens with confining reinforcement.

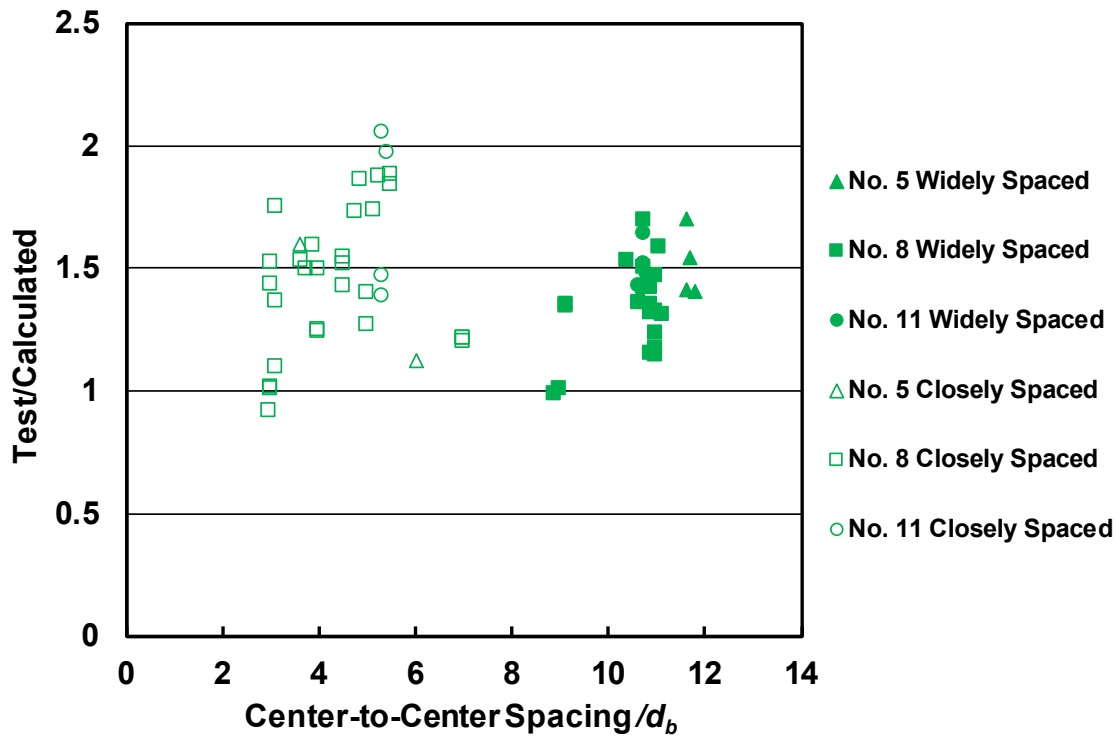


Figure 4.18 Ratio of test-to-calculated failure load (T/T_{318-19}) versus center-to-center spacing for specimens with widely and closely-spaced headed bars without confining reinforcement (ACI 318-19)

Table 4.12: Max, Min, Mean, STD, and COV of T/T_{318-19} for headed bars without confining reinforcement

(Number of specimens)	All (64)	Widely spaced C/C^* spacing $\geq 8d_b$			Closely spaced C/C^* spacing $< 8d_b$		
		No. 5 (4)	No. 8 (20)	No. 11 (6)	No. 5 (2)	No. 8 (28)	No. 11 (4)
Max	2.05	1.70	1.70	1.64	1.60	1.88	2.05
Min	0.91	1.41	0.99	1.15	1.13	0.91	1.39
Mean	1.43	1.52	1.33	1.43	1.36	1.44	1.72
STD	0.250	0.140	0.182	0.166	0.336	0.278	0.341
COV	0.175	0.092	0.136	0.116	0.246	0.193	0.198
$T/T_{318-19} < 1.0$	2	0	1	0	0	1	0

*C/C = Center-to-Center

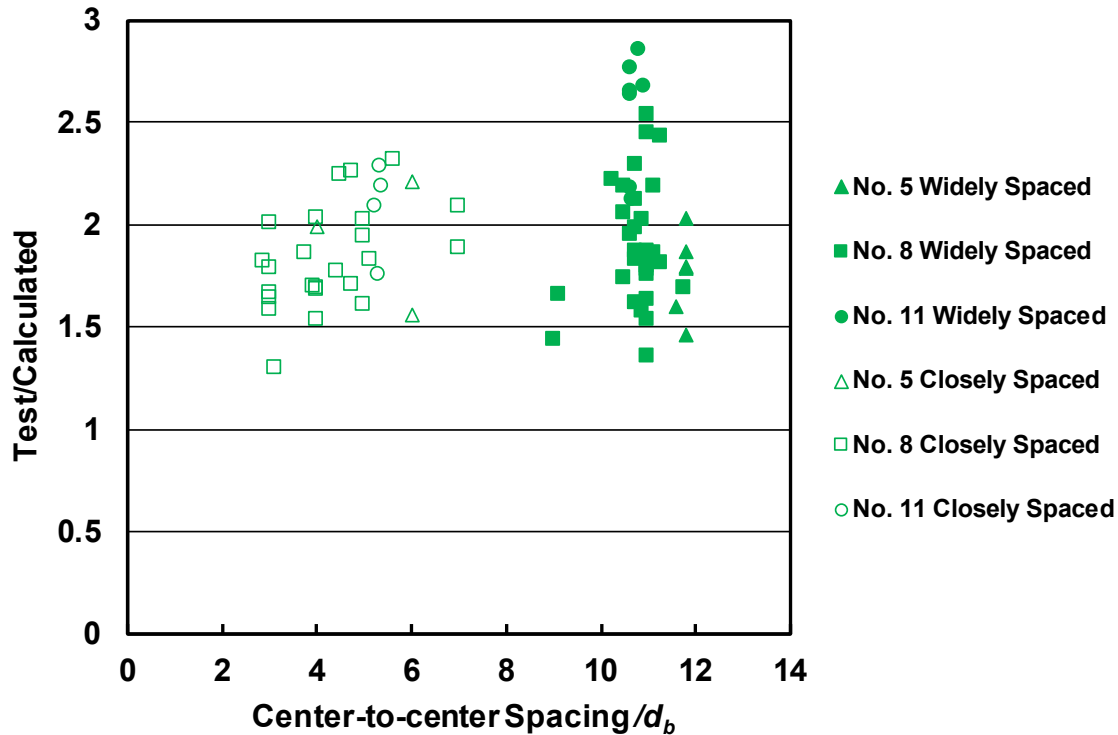


Figure 4.19 Ratio of test-to-calculated failure load (T/T_{318-19}) versus center-to-center spacing for specimens with widely and closely-spaced headed bars with confining reinforcement (ACI 318-19)

Table 4.13: Max, Min, Mean, STD, and COV of T/T_{318-19} for headed bars with confining reinforcement

(Number of specimens)	All (74)	Widely spaced C/C* spacing $\geq 8d_b$			Closely spaced C/C* spacing $< 8d_b$		
		No. 5 (6)	No. 8 (30)	No. 11 (7)	No. 5 (3)	No. 8 (24)	No. 11 (4)
		Max	2.86	2.03	2.54	2.86	2.21
Min	1.30	1.46	1.36	2.12	1.56	1.30	1.76
Mean	1.94	1.76	1.90	2.55	1.92	1.83	2.08
STD	0.338	0.202	0.300	0.287	0.332	0.248	0.231
COV	0.174	0.115	0.158	0.113	0.173	0.135	0.111
$T/T_{318-19} < 1.0$	0	0	0	0	0	0	0

*C/C =Center-to-Center

The values of T/T_{318-19} for the specimens without confining reinforcement range from 0.91 to 2.05, with an average of 1.43 and a coefficient of variation of 0.175, and from 1.30 to 2.86, with an average of 1.94 and a coefficient of variation of 0.174 for the specimens with confining reinforcement. The values of T/T_{318-19} are less than 1.0 for just two tests, both for No. 8 bar

specimens without confining reinforcement, one with widely spaced bars and one with closely spaced bars.

Compared the trend lines for T/T_{318-14} shown in Figures 4.8 and 4.9, the trend lines for T/T_{318-19} shown in Figures 4.18 and 4.19 are more closely spaced and not in the order of bar size. Compared to the trend lines for T/T_{Shao} shown in Figures 4.12 and 4.13, the trend lines for T/T_{318-19} shown in Figures 4.18 and 4.19, the trend lines for T/T_{318-19} are more widely spaced. The downward trend with increasing concrete compressive strength suggests that the provisions would be improved if compressive strength to the 0.25 power was used for the full range of compressive strengths, not just for values below 6000 psi.

4.4.1.6 Comparison with Darwin and Dolan (2021)

As demonstrated in Section 4.4.1.5, although the ACI 318-19 provisions are conservative, they do not fully reflect the anchorage strength of headed bars. Darwin and Dolan (2021) suggested other modifications to the approach proposed by Shao et al. (2016) that are easier to use by designers while maintaining accuracy.

Figure 4.20 compares the ratio of the force obtained in the tests to the force based on the provisions proposed by Darwin and Dolan (2021) with the measured concrete compressive strength for the 30 beam-column joint specimens with widely-spaced headed bars *without* confining reinforcement. Figure 4.21 does the same for the 43 beam-column joint specimens widely-spaced headed bars *with* confining reinforcement.

The trend lines in Figures 4.20 and 4.21 are almost flat. The slight downward slope in Figure 4.20 and slight upward slope in Figure 4.21 are similar to that observed in Figures 4.12 and 4.13 for the comparison with the provisions proposed by Shao et al. (2016).

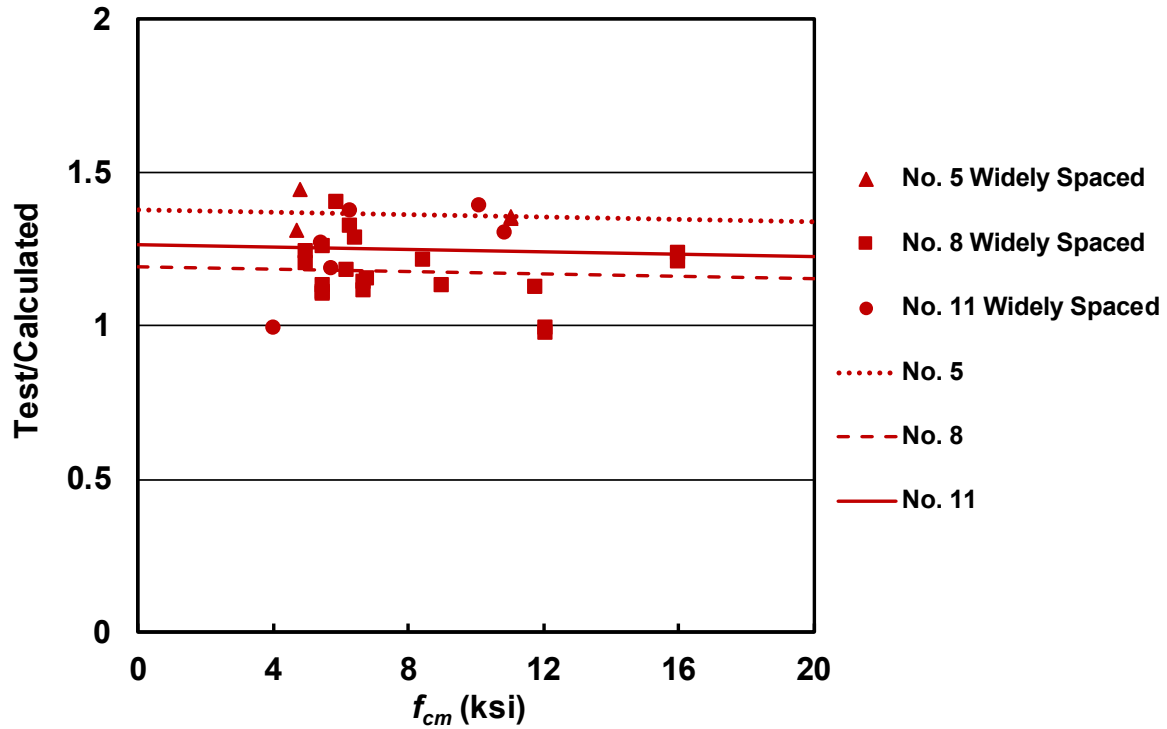


Figure 4.20 Ratio of test-to-calculated failure load (T/T_D) versus measured concrete compressive strength f_{cm} for specimens with widely-spaced headed bars without confining reinforcement (Darwin and Dolan 2021)

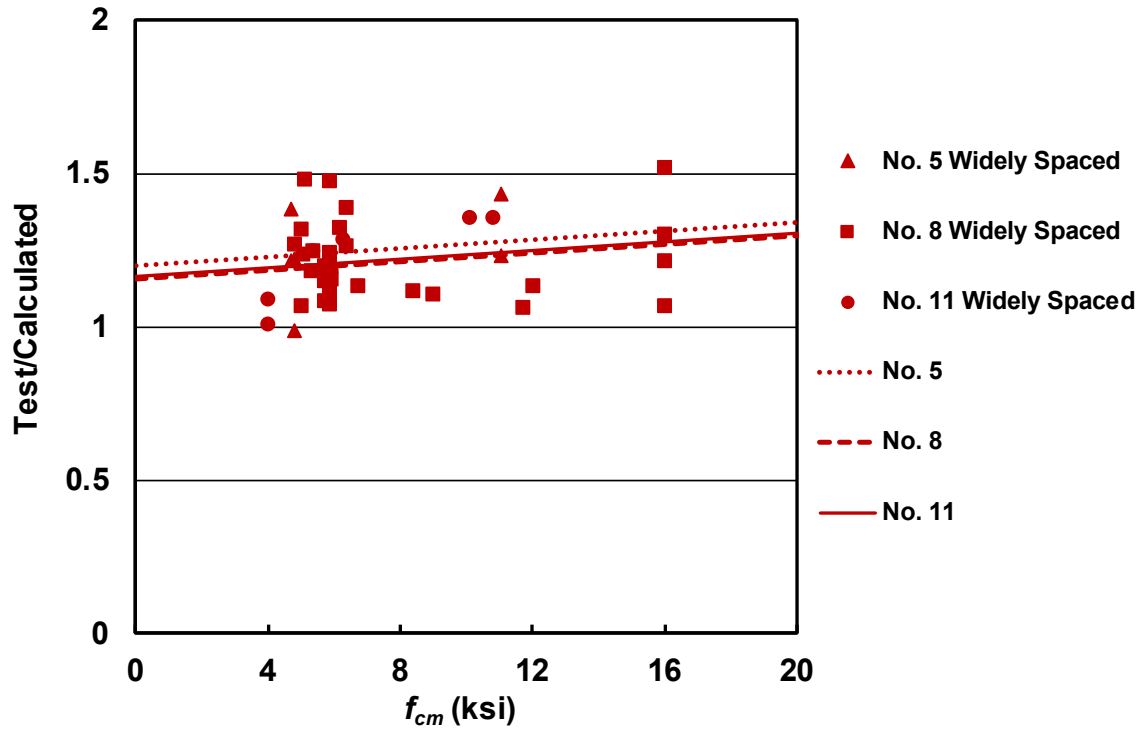


Figure 4.21 Ratio of test-to-calculated failure load (T/T_D) versus measured concrete compressive strength f_{cm} for specimens with widely-spaced headed bars with confining reinforcement (Darwin and Dolan 2021)

Figures 4.22 and 4.23 compare the ratio of force obtained from test results to the force obtained from Darwin and Dolan (2021) versus center-to-center spacing for beam-column joint specimens with both widely and closely-spaced bars without and with confining reinforcement, respectively. The respective statistical parameters are given in Tables 4.14 and 4.15. The two figures show that the ratio T/T_D as largely independent of bar spacing.

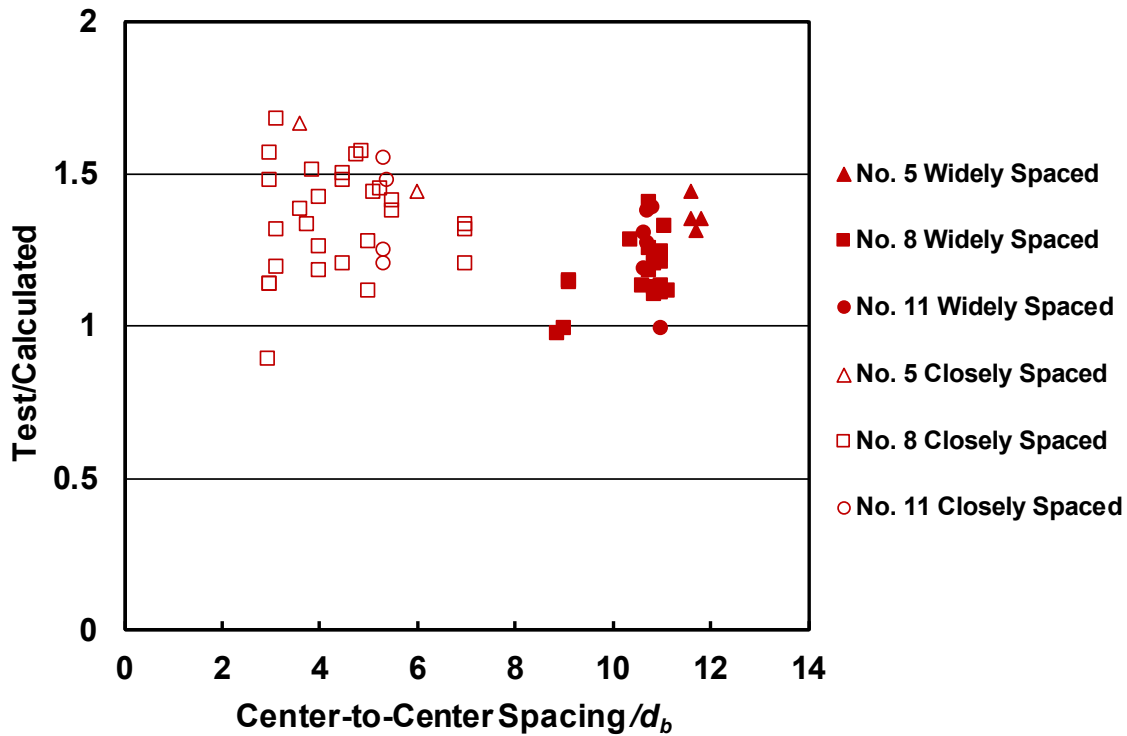


Figure 4.22 Ratio of test-to-calculated failure load (T/T_D) versus center-to-center spacing for specimens with widely and closely-spaced headed bars without confining reinforcement (Darwin and Dolan 2021)

Table 4.14: Max, Min, Mean, STD, and COV of T/T_D for headed bars without confining Reinforcement

(Number of specimens)	All (64)	Widely spaced C/C^* spacing $\geq 8d_b$			Closely spaced C/C^* spacing $< 8d_b$		
		No. 5 (4)	No. 8 (20)	No. 11 (6)	No. 5 (2)	No. 8 (28)	No. 11 (4)
Max	1.68	1.44	1.40	1.39	1.67	1.68	1.55
Min	0.89	1.31	0.97	0.99	1.44	0.89	1.20
Mean	1.29	1.37	1.17	1.25	1.55	1.35	1.37
STD	0.169	0.055	0.103	0.148	0.158	0.175	0.171
COV	0.131	0.040	0.088	0.118	0.102	0.130	0.125
$T/T_D < 1.0$	4	0	2	1	0	1	0

*C/C =Center-to-Center

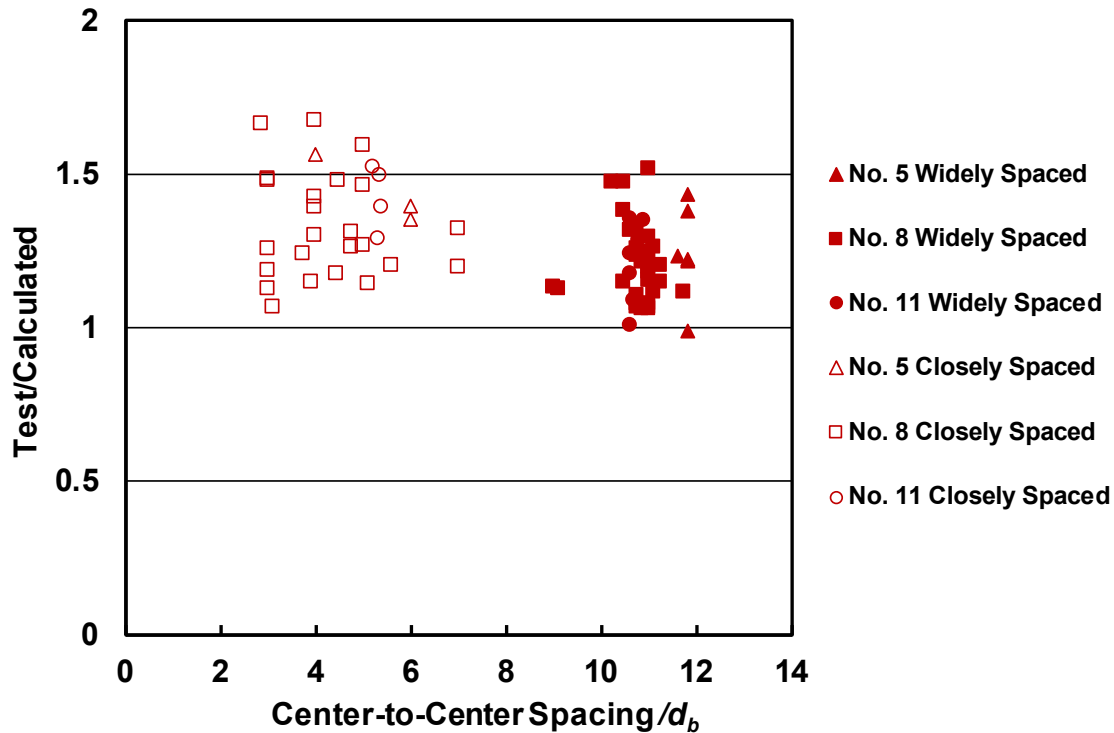


Figure 4.23 Ratio of test-to-calculated failure load (T/T_D) versus center-to-center spacing for specimens with widely and closely-spaced headed bars with confining reinforcement (Darwin and Dolan 2021)

Table 4.15: Max, Min, Mean, STD, and COV of T/T_D for headed bars with confining reinforcement

(Number of specimens)	All (74)	Widely spaced C/C^* spacing $\geq 8d_b$			Closely spaced C/C^* spacing $< 8d_b$		
		No. 5 (6)	No. 8 (30)	No. 11 (7)	No. 5 (3)	No. 8 (24)	No. 11 (4)
		Max	1.67	1.43	1.52	1.35	1.57
Min	0.99	0.99	1.06	1.00	1.35	1.07	1.29
Mean	1.27	1.25	1.21	1.21	1.44	1.33	1.42
STD	0.159	0.156	0.128	0.132	0.113	0.172	0.105
COV	0.125	0.125	0.106	0.109	0.079	0.130	0.074
$T/T_D < 1.0$	1	1	0	0	0	0	0

*C/C = Center-to-Center

The values of T/T_D for specimens without confining reinforcement range from 0.89 to 1.68, with an average of 1.29 and a coefficient of variation of 0.13, and from 0.99 to 1.67, with an average of 1.27 and a coefficient of variation of 0.125, for specimens with confining reinforcement. The values of T/T_D are less than 1.0 for five tests, two No. 8 bar specimens and one No. 11 bar specimen with widely spaced bars and no confining reinforcement, one No. 8 bar specimen with

closely spaced bars and no confining reinforcement, and one No. 5 bar specimen with widely spaced bars and confining reinforcement.

Unlike the trend lines for T/T_{318-14} shown in Figures 4.8 and 4.9 and for T/T_{318-19} in Figures 4.18 and 4.19 the trend lines for T/T_D in Figures 4.20 and 4.21 are independent of bar size and have little slope as a function of concrete compressive strength. They also exhibit less scatter. The comparisons indicate that the 1.5 power of d_b and the 0.25 power of f_{cm} accurately capture the effect of these parameters on the anchorage strength of headed bars.

The comparisons closely match those shown in Figures 4.12 and 4.13 for T/T_{Shao} . This close agreement is expected. The design approach proposed by Darwin and Dolan is easier to apply than that proposed by Shao et al.

4.4.1.7 Comparison with Anchorage Provisions (ACI 318-19)

ACI 318-19 Chapter 17 provides an alternative method for anchoring headed bars (described in Section 4.3.5). In this study, these anchorage provisions are used to calculate the anchorage strength of headed bars for the beam-column joint specimens.

As shown in Eq. (4.22), the anchorage strengths based on concrete breakout and side-face blowout are first compared, with the lower value governing. Tables 4.4 through 4.7 show that in all cases, concrete breakout strength was the weaker. The concrete breakout strength is then compared with strength of anchor reinforcement with the stronger value governing. As described below, for the specimens without confining reinforcement within the joint region, anchor reinforcement (ties in column above the joint) provided the higher strength in somewhat more than half the cases, while for the specimens with confining reinforcement within the joint region, anchor reinforcement (both ties in the joint and in column above the joint) provided the higher strength in the vast majority of the cases.

Figure 4.24 compares the ratio of the force obtained in the tests to the force based on the anchorage provisions in ACI 318-19 with the measured concrete compressive strength for the 30 beam-column joint specimens with widely-spaced headed bars *without* confining reinforcement. Figure 4.25 does the same for the 43 beam-column joint specimens widely-spaced headed bars *with* confining reinforcement.

The test/calculated ($T/\phi N_{str}$) values in Figures 4.24 and 4.25 ranged from 3.30 to 8.8 and

from 1.65 to 7.09, respectively. This indicates that the anchorage provisions are highly conservative and do not accurately represent the anchorage strength of headed bars in the beam-column joint specimens.

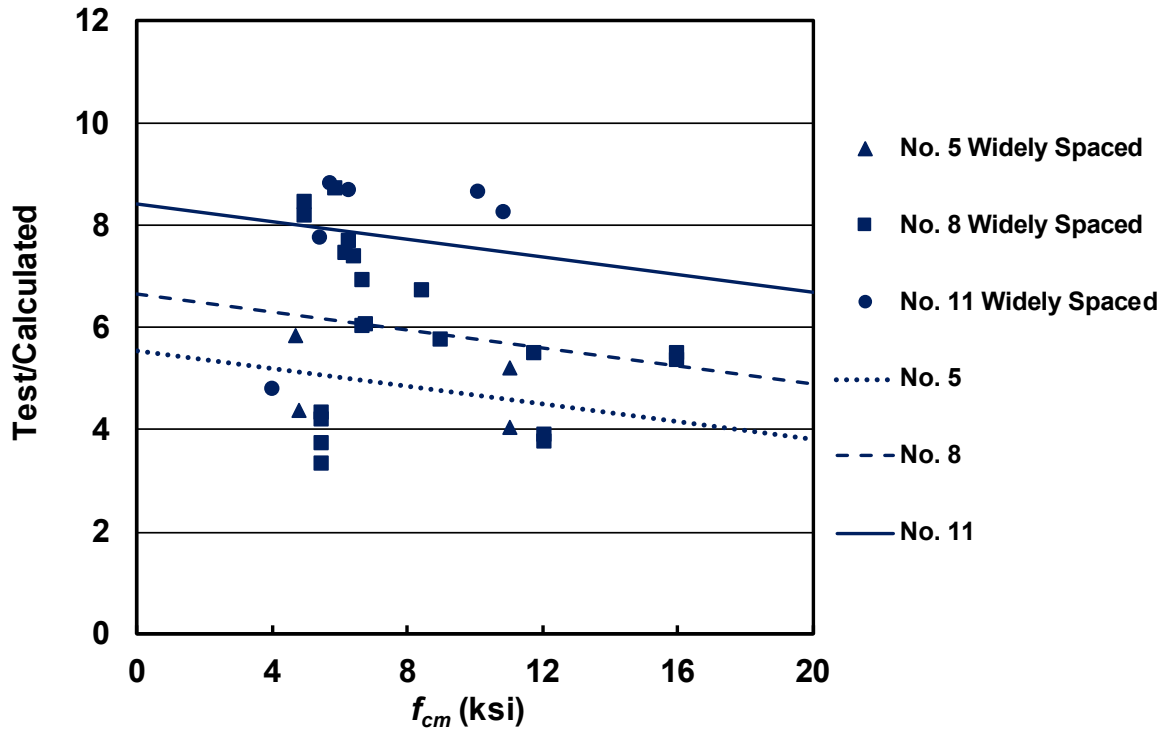


Figure 4.24 Ratio of test-to-calculated failure load ($T/\phi N_{str}$) versus measured concrete compressive strength f_{cm} for specimens with widely-spaced headed bars without confining reinforcement (Anchorage provisions)

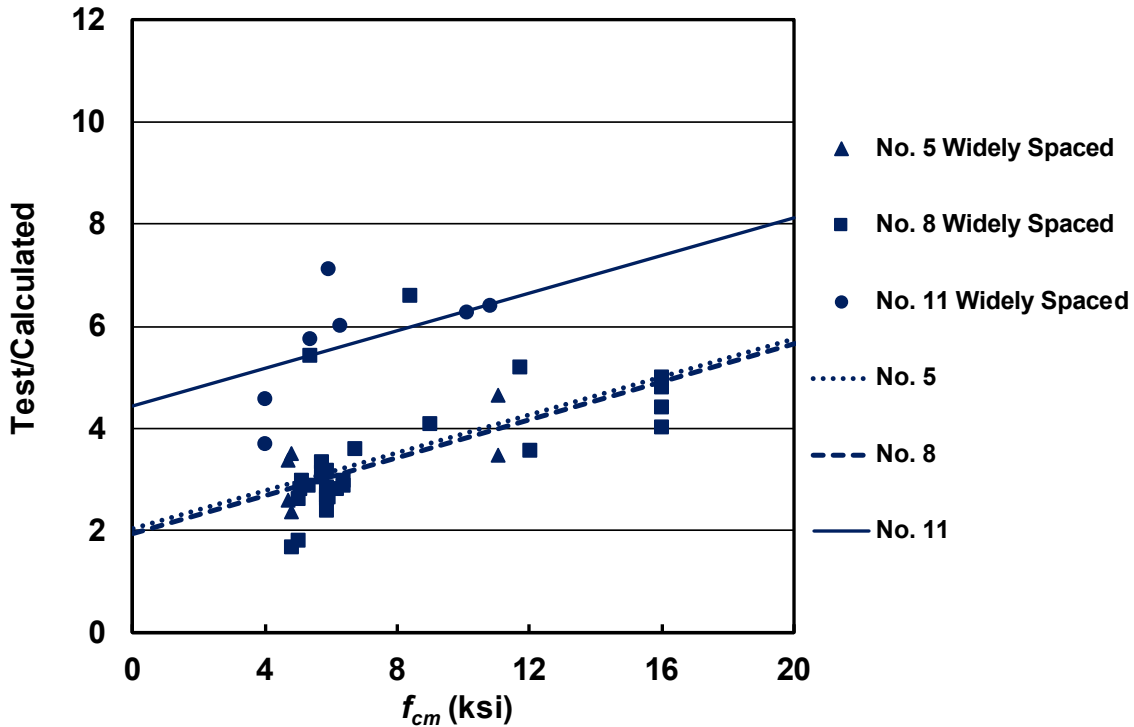


Figure 4.25 Ratio of test-to-calculated failure load ($T/\phi N_{str}$) versus measured concrete compressive strength f_{cm} for specimens with widely-spaced headed bars with confining reinforcement (Anchorage provisions)

For the 30 specimens with widely spaced headed bars without confining reinforcement, the strength of 17 specimens was governed by the anchor reinforcement (the difference between the calculated values from the anchor reinforcement and those from breakout strength ranged from 0.54 to 14.5 kips), and the strength of 13 specimens was governed by breakout failure. This suggests that the negative slope of the trend lines in Figure 4.24 could be due in part to overestimating the effect of concrete compressive strength, which is based on the 0.5 power [Eq. (4.18)].

For the 43 specimens with widely spaced headed bars with confining reinforcement, the strength of 39 specimens was governed by the anchor reinforcement (the difference between the calculated values from the anchor reinforcement and breakout strength ranged from 4 to 68 kips), and the strength of just 4 specimens was governed by breakout failure. As a result, the strength of the vast majority of the specimens was governed by anchor reinforcement, which does not account for the contribution of the concrete. This indicates that the positive slope of the trend lines in Figure 4.25 is due to factors independent of concrete compressive strength that may have, nonetheless,

been unintentionally correlated with concrete compressive strength in the design of the test specimens.

Figures 4.26 and 4.27 compare the ratio of force obtained from test results to the force based on the anchorage provisions in ACI 318-19 versus center-to-center spacing for beam-column joint specimens with both widely and closely-spaced bars without and with confining reinforcement, respectively. The respective statistical parameters are given in Tables 4.16 and 4.17. The two figures also show that values of $T/\phi N_{str}$ decrease as bar spacing increases.

Overall, for the 64 specimens without confining reinforcement, 37 specimens were governed by the anchor reinforcement and 27 specimens were governed by breakout failure. For the 74 specimens with confining reinforcement, 65 specimens were governed by the anchor reinforcement and 9 specimens were governed by breakout failure.

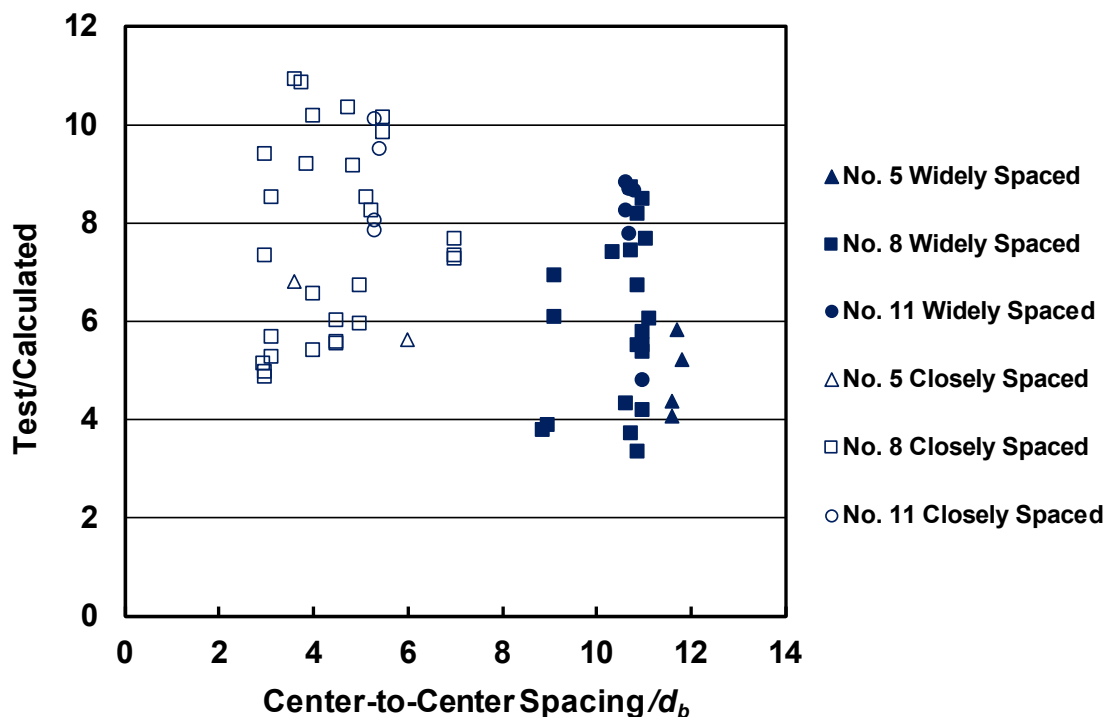


Figure 4.26 Ratio of test-to-calculated failure load ($T/\phi N_{str}$) versus center-to-center spacing for specimens with widely and closely-spaced headed bars without confining reinforcement (Anchorage provisions)

Table 4.16: Max, Min, Mean, STD, and COV of $T/\phi N_{str}$ for headed bars without confining reinforcement

(Number of specimens)	All (64)	Widely spaced C/C* spacing $\geq 8d_b$			Closely spaced C/C* spacing $< 8d_b$		
		No. 5 (4)	No. 8 (20)	No. 11 (6)	No. 5 (2)	No. 8 (28)	No. 11 (4)
Max	10.91	5.83	8.71	8.82	6.80	10.91	10.10
Min	3.30	4.06	3.30	4.78	5.63	4.83	7.82
Mean	6.95	4.87	5.93	7.81	6.22	7.57	8.85
STD	1.993	0.807	1.708	1.535	0.823	2.000	1.111
COV	0.287	0.166	0.288	0.197	0.132	0.264	0.125
$T/\phi N_{str} < 1.0$	0	0	0	0	0	0	0

*C/C = Center-to-Center

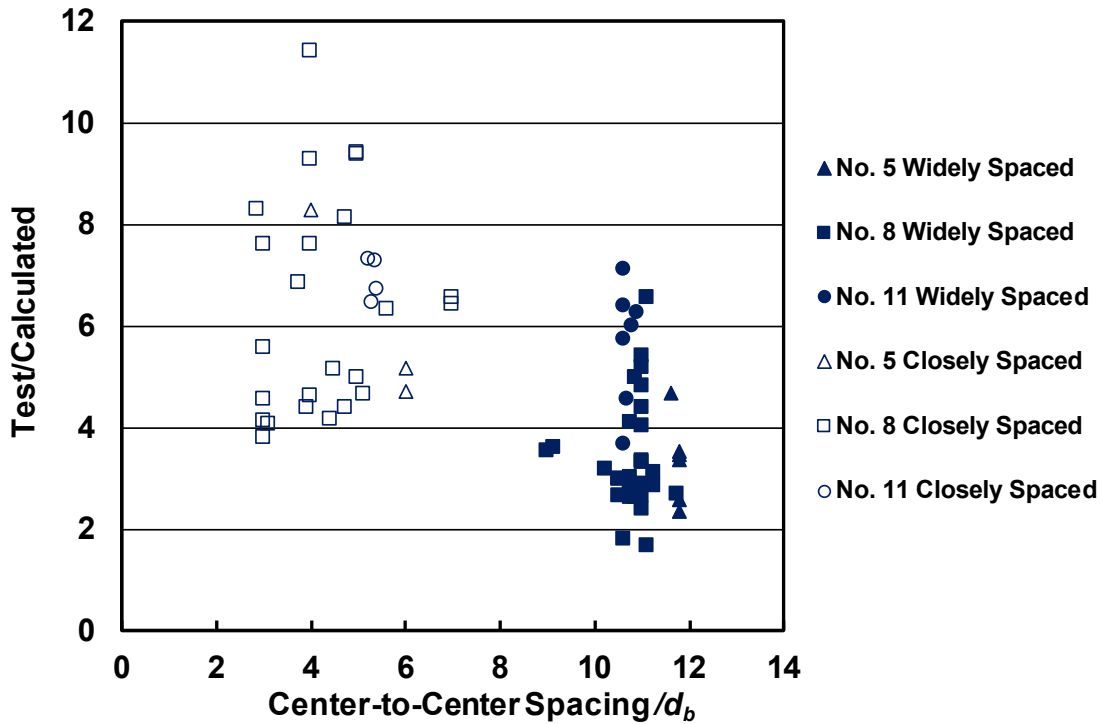


Figure 4.27 Ratio of test-to-calculated failure load ($T/\phi N_{str}$) versus center-to-center spacing for specimens with widely and closely-spaced headed bars with confining reinforcement (Anchorage provisions)

Table 4.17: Max, Min, Mean, STD, and COV of $T/\phi N_{str}$ for headed bars with confining reinforcement

(Number of specimens)	All (74)	Widely spaced C/C* spacing $\geq 8d_b$			Closely spaced C/C* spacing $< 8d_b$		
		No. 5	No. 8	No. 11	No. 5	No. 8	No. 11
		(6)	(30)	(7)	(3)	(24)	(4)
Max	11.40	4.67	6.56	7.09	8.29	11.40	7.30
Min	1.66	2.36	1.66	3.67	4.70	3.78	6.44
Mean	4.84	3.33	3.38	5.67	6.05	6.31	6.93
STD	2.082	0.816	1.104	1.169	1.951	2.138	0.416
COV	0.430	0.245	0.326	0.206	0.323	0.339	0.060
$T/\phi N_{str} < 1.0$	0	0	0	0	0	0	0

*C/C =Center-to-Center

The maximum, minimum, mean, standard deviation (STD), and coefficient of variation (COV) of the $T/\phi N_{str}$ for the 64 beam-column joint specimens (without confining reinforcement, ranges from 3.30 to 10.91, with an average of 6.95 and a coefficient of variation of 0.287. For the 74 beam-column joint specimens (with confining reinforcement), $T/\phi N_{str}$ ranges from 1.66 to 11.40, with an average of 4.84 and a coefficient of variation of 0.430.

Comparing the results from anchorage provisions with the results from ACI 318-14, Shao et al. (2016), ACI 318-19, and Darwin and Dolan (2021), the anchorage provisions are, in all cases, very conservative and exhibit much greater variation in the values of $T/\phi N_{str}$ than for T/T_{318-14} , T/T_{Shao} , T/T_{318-19} , or T/T_D , with the exception of T/T_{318-14} for specimens without confining reinforcement for which $T/\phi N_{str}$ and T/T_{318-14} have the same COV (0.287). A key difference between the anchorage provisions in ACI 318-19 and development length provisions of Shao (2016), ACI 318-19, and Darwin and Dolan (2021) is that the anchorage provisions do not permit the contribution of concrete strength and anchor reinforcement to be combined, while those of Shao (2016), ACI 318-19, and Darwin and Dolan (2021) account for the contributions of both concrete strength and confining reinforcement. Combining the contributions provides a more accurate representation of the anchorage strength of headed bars.

4.5 SPECIMENS WITH $d_{eff}/\ell_{eh} \geq 1.5$

4.5.1 Anchorage Strengths

The provisions presented in Sections 4.3.2 (Shao et al 2016) and 4.3.5 (Anchorage provisions of ACI 318-19) are used to calculate the anchorage strength of 40 beam-column joint specimens with $d_{eff}/\ell_{eh} \geq 1.5$. Eighteen specimens had no confining reinforcement [11 specimens with widely-spaced bars (center-to-center spacing $\geq 8d_b$) and 7 specimens with closely-spaced bars (center-to-center spacing $< 8d_b$)] and 22 specimens had confining reinforcement [14 specimens with widely-spaced bars (center-to-center spacing $\geq 8d_b$) and 8 specimens with closely-spaced bars (center-to-center spacing $< 8d_b$)]. Tables 4.18 and 4.19 show the results for the specimens without confining reinforcement, respectively, and Tables 4.20 and 4.21 show the results for the specimens with confining reinforcement, respectively. The strut-and-tie method (described in Section 4.3.6) is also used to calculate the anchorage strength T_{STM} of the 22 specimens with $d_{eff}/\ell_{eh} \geq 1.5$ and confining reinforcement. As explained in Section 4.3.6, comparisons are made between R_l (compressive force in the compression zone, as shown in Figure 4.7) and T_{STM} (the calculated anchorage strength of the headed bar using the strut-and-tie method) to find R_l/T_{STM} . Tables 4.22 and 4.23 show the results of the widely and closely spaced bars with confining reinforcement, respectively. Details of the specimens are listed in Appendix C.

Table 4.18: Comparisons for widely-spaced bars without confining reinforcement ($d_{eff}/\ell_{eh} \geq 1.5$)

Specimens	T	T_{Shao}	N_{cbg}/n	N_{sb}/n	N_s/n	N_{str}	ϕN_{str}
	kips	kips	kips	kips	kips	kips	kips
8-5-F4.1-0-i-2.5-7-6	28.7	33.6	9.5	63.2	7.5	9.5	7.1
8-5-F9.1-0-i-2.5-7-6	33.4	33.8	9.5	98.0	7.5	9.5	7.2
8-8-F4.1-0-i-2.5-3-10-DB	50.2	60.3	14.0	75.9	13.6	14.0	10.5
8-8-F9.1-0-i-2.5-3-10-DB	51.8	59.9	14.0	115.4	13.6	14.0	10.5
8-5-F4.1-0-i-2.5-3-10-DB	40.6	54.3	11.4	61.6	13.6	13.6	10.2
8-5-F9.1-0-i-2.5-3-10-DB	44.4	53.6	11.3	93.7	13.6	13.6	10.2
11-5a-F3.8-0-i-2.5-3-12	56.8	73.9	14.2	83.2	13.6	14.2	10.6
11-5a-F8.6-0-i-2.5-3-12	63.8	74.7	14.2	122.8	13.6	14.2	10.7
11-8-F3.8-0-i-2.5-3-14.5	79.1	108.6	22.7	120.7	13.6	22.7	17.0
11-5-F3.8-0-i-2.5-3-12	66.5	82.0	17.2	98.5	13.6	17.2	12.9
11-5-F8.6-0-i-2.5-3-14.5	82.8	99.0	18.9	148.0	13.6	18.9	14.1

T = anchorage strength of headed bar from test, T_{Shao} = anchorage strength of headed bar from Shao et al. (2016), N_{str} = unfactored governed anchorage strength of headed bar from anchorage provision, N_{cbg}/n = anchorage strength of headed bar from breakout failure, N_{sb}/n = anchorage strength of headed bar from side-face blowout failure, N_s/n = anchorage strength of headed bar from anchor reinforcement, ϕN_{str} = factored governed anchorage strength of headed bar from anchorage provision.

Table 4.19: Comparisons for closely-spaced bars without confining reinforcement ($d_{eff}/\ell_{eh} \geq 1.5$)

Specimens	T	T_{Shao}	N_{cbg}/n	N_{sb}/n	N_s/n	N_{str}	ϕN_{str}
	kips	kips	kips	kips	kips	kips	kips
(3@3)8-5-F4.1-0-i-2.5-7-6	20.6	18.9	4.5	63.2	5.0	5.0	3.7
(3@5)8-5-F4.1-0-i-2.5-7-6	23.9	23.8	6.1	65.7	5.0	6.1	4.5
(3@7)8-5-F4.1-0-i-2.5-7-6	27.1	29.8	7.5	64.5	5.0	7.5	5.6
(3@5.5)8-5-F9.1-0-i-2.5-7-6	23.0	24.5	6.5	96.3	5.0	6.5	4.9
(4@3.7)8-5-T9.5-0-i-2.5-6.5-6	21.7	19.7	4.8	98.4	3.7	4.8	3.6
(3@5.35)11-8-F3.8-0-i-2.5-3-14.5	52.9	76.2	15.3	125.7	9.1	15.3	11.5
(3@5.35)11-5-F8.6-0-i-2.5-3-14.5	65.1	69.4	12.9	151.3	9.1	12.9	9.7

T = anchorage strength of headed bar from test, T_{Shao} = anchorage strength of headed bar from Shao et al. (2016), N_{str} = unfactored governed anchorage strength of headed bar from anchorage provision, N_{cbg}/n = anchorage strength of headed bar from breakout failure, N_{sb}/n = anchorage strength of headed bar from side-face blowout failure, N_s/n = anchorage strength of headed bar from anchor reinforcement, ϕN_{str} = factored governed anchorage strength of headed bar from anchorage provisions

Table 4.20: Comparisons for widely-spaced bars with confining reinforcement ($d_{eff}/\ell_{eh} \geq 1.5$)

Specimens	T	T_{Shao}	N_{cbg}/n	N_{sb}/n	N_s/n	N_{str}	ϕN_{str}
	kips	kips	kips	kips	kips	kips	kips
8-5-F4.1-5#3-i-2.5-7-6	50.7	42.9	9.5	61.9	15.0	15.0	11.2
8-5-F9.1-5#3-i-2.5-7-6	53.8	41.6	9.5	90.5	15.0	15.0	11.2
8-8-F9.1-5#3-i-2.5-3-10-DB	68.2	67.2	13.9	115.4	21.1	21.1	15.8
8-5-F4.1-3#4-i-2.5-3-10-DB	64.6	63.2	11.5	60.3	13.6	13.6	10.2
8-5-F9.1-3#4-i-2.5-3-10-DB	65.8	60.7	11.3	93.7	13.6	13.6	10.2
8-5-F4.1-5#3-i-2.5-3-10-DB	70.2	63.8	11.6	64.1	21.1	21.1	15.8
8-5-F9.1-5#3-i-2.5-3-10-DB	70.5	62.1	11.4	93.7	21.1	21.1	15.8
11-8-F3.8-2#3-i-2.5-3-14.5	88.4	112.9	22.8	118.5	21.1	22.8	17.1
11-8-F3.8-6#3-i-2.5-3-14.5	112.7	123.7	22.8	113.9	28.6	28.6	21.4
11-5-F3.8-6#3-i-2.5-3-12	88.3	98.3	17.4	100.3	28.6	28.6	21.4
11-5-F8.6-6#3-i-2.5-3-14.5	112.3	112.3	18.9	150.8	28.6	28.6	21.4
11-5a-F3.8-2#3-i-2.5-3-12	67.3	75.9	14.1	75.5	21.1	21.1	15.8
11-5a-F3.8-6#3-i-2.5-3-12	78.0	86.6	14.2	82.4	28.6	28.6	21.4
11-5a-F8.6-6#3-i-2.5-3-12	79.2	90.5	14.6	127.7	28.6	28.6	21.4

T = anchorage strength of headed bar from test, T_{Shao} = anchorage strength of headed bar Shao et al. (2016), N_{str} = unfactored governed anchorage strength of headed bar from anchorage provision, N_{cbg}/n = anchorage strength of headed bar from breakout failure, N_{sb}/n = anchorage strength of headed bar from side-face blowout failure, N_s/n = anchorage strength of headed bar from anchor reinforcement, ϕN_{str} = factored governed anchorage strength of headed bar from anchorage provisions.

Table 4.21: Comparisons for closely-spaced bars with confining reinforcement ($d_{eff}/\ell_{eh} \geq 1.5$)

Specimens	T	T_{Shao}	N_{cbg}/n	N_{sb}/n	N_s/n	N_{str}	ϕN_{str}
	kips	kips	kips	kips	kips	kips	kips
(3@3)8-5-F4.1-5#3-i-2.5-7-6	32.1	28.8	4.4	61.9	10.0	10.0	7.5
(3@5)8-5-F4.1-5#3-i-2.5-7-6	37.5	34.3	6.0	65.7	10.0	10.0	7.5
(3@7)8-5-F4.1-5#3-i-2.5-7-6	42.3	38.6	7.5	64.5	14.1	14.1	10.5
(3@5.5)8-5-F9.1-5#3-i-2.5-7-6	43.1	35.4	6.5	96.3	14.1	14.1	10.5
(4@3.7)8-5-F9.1-5#3-i-2.5-7-6	31.6	28.4	4.8	94.4	10.5	10.5	7.9
(3@5.35)11-8-F3.8-2#3-i-2.5-3-14.5	72.6	89.3	15.2	118.9	15.2	15.2	11.4
(3@5.35)11-8-F3.8-6#3-i-2.5-3-14.5	83.7	99.2	15.4	125.7	28.1	28.1	21.1
(3@5.35)11-5-F8.6-6#3-i-2.5-3-14.5	75.6	87.9	12.9	154.2	28.1	28.1	21.1

T = anchorage strength of headed bar from test, T_{Shao} = anchorage strength of headed bar from Shao et al. (2016), N_{str} = unfactored governed anchorage strength of headed bar from anchorage provision, N_{cbg}/n = anchorage strength of headed bar from breakout failure, N_{sb}/n = anchorage strength of headed bar from side-face blowout failure, N_s/n = anchorage strength of headed bar from anchor reinforcement, ϕN_{str} = factored governed anchorage strength of headed bar from anchorage provisions

Table 4.22: Comparisons for widely-spaced bars with confining reinforcement (strut-and-tie)

Specimens	R_l	A_{vt}	T_{STM}	R_l/T_{STM}
	kips	in. ²	kips	
8-5-F4.1-5#3-i-2.5-7-6	60.5	0.66	45.0	1.34
8-5-F9.1-5#3-i-2.5-7-6	64.3	0.66	45.0	1.42
8-8-F9.1-5#3-i-2.5-3-10-DB	90.4	0.88	60.0	1.50
8-5-F4.1-3#4-i-2.5-3-10-DB	85.5	0.8	54.4	1.56
8-5-F9.1-3#4-i-2.5-3-10-DB	87.1	0.8	54.4	1.59
8-5-F4.1-5#3-i-2.5-3-10-DB	92.9	0.88	60.0	1.54
8-5-F9.1-5#3-i-2.5-3-10-DB	93.3	0.88	60.0	1.55
11-8-F3.8-2#3-i-2.5-3-14.5	117.1	0.44	30.0	3.89
11-8-F3.8-6#3-i-2.5-3-14.5	149.2	1.1	75.0	1.98
11-5-F3.8-6#3-i-2.5-3-12	116.8	1.1	75.0	1.55
11-5-F8.6-6#3-i-2.5-3-14.5	148.7	1.1	75.0	1.98
11-5a-F3.8-2#3-i-2.5-3-12	89.1	0.44	30.0	2.96
11-5a-F3.8-6#3-i-2.5-3-12	103.3	1.1	75.0	1.37
11-5a-F8.6-6#3-i-2.5-3-12	104.9	1.1	75.0	1.39

R_l = compressive force in the compression zone calculated depending on simply supported beam, A_{vt} = total cross-sectional area of the single tie, T_{STM} = anchorage strength of headed bar from strut -and -tie approach.

Table 4.23: Comparisons for closely-spaced bars with confining reinforcement (strut-and-tie)

Specimens	R_l	A_{vt}	T_{STM}	R_l/T_{STM}
	kips	in. ²	kips	
(3@3)8-5-F4.1-5#3-i-2.5-7-6	57.5	0.66	45.0	1.27
(3@5)8-5-F4.1-5#3-i-2.5-7-6	67.2	0.66	45.0	1.49
(3@7)8-5-F4.1-5#3-i-2.5-7-6	75.7	0.66	45.0	1.68
(3@5.5)8-5-F9.1-5#3-i-2.5-7-6	77.3	0.66	45.0	1.71
(4@3.7)8-5-F9.1-5#3-i-2.5-7-6	75.5	0.66	45.0	1.67
(3@5.35)11-8-F3.8-2#3-i-2.5-3-14.5	144.1	0.44	30.0	4.79
(3@5.35)11-8-F3.8-6#3-i-2.5-3-14.5	166.2	1.1	75.0	2.21
(3@5.35)11-5-F8.6-6#3-i-2.5-3-14.5	150.2	1.1	75.0	2.00

R_l is the compressive force in the compression zone calculated depending on simply supported beam, A_{vt} is the total cross-sectional area of the single tie, T_{STM} is the anchorage strength of headed bar from strut -and -tie approach

4.5.2 Comparisons

Figures 4.28 and 4.29 compare the ratio the force obtained from the tests to the force obtained, respectively, from the provisions proposed by Shao et al. (2016) T/T_{Shao} and the force obtained from the anchorage provisions $T/\phi N_{str}$ for the 18 specimens with $d_{eff}/\ell_{eh} \geq 1.5$ and the 64

beam-column specimens with $d_{eff}/l_{eh} < 1.5$ versus d_{eff}/l_{eh} for specimens with widely and closely-spaced bars and without confining reinforcement. The respective statistical parameters (maximum, minimum, mean, standard deviation (STD), and coefficient of variation (COV)) for the 18 specimens with $d_{eff}/l_{eh} \geq 1.5$ are given in Tables 4.24 and 4.25. T/T_{Shao} ranges from 0.69 to 1.10, with an average of 0.88 and a coefficient of variation of 0.132, and $T/\phi N_{str}$ ranges from 3.98 to 6.71, with an average of 5.07 and a coefficient of variation of 0.143.

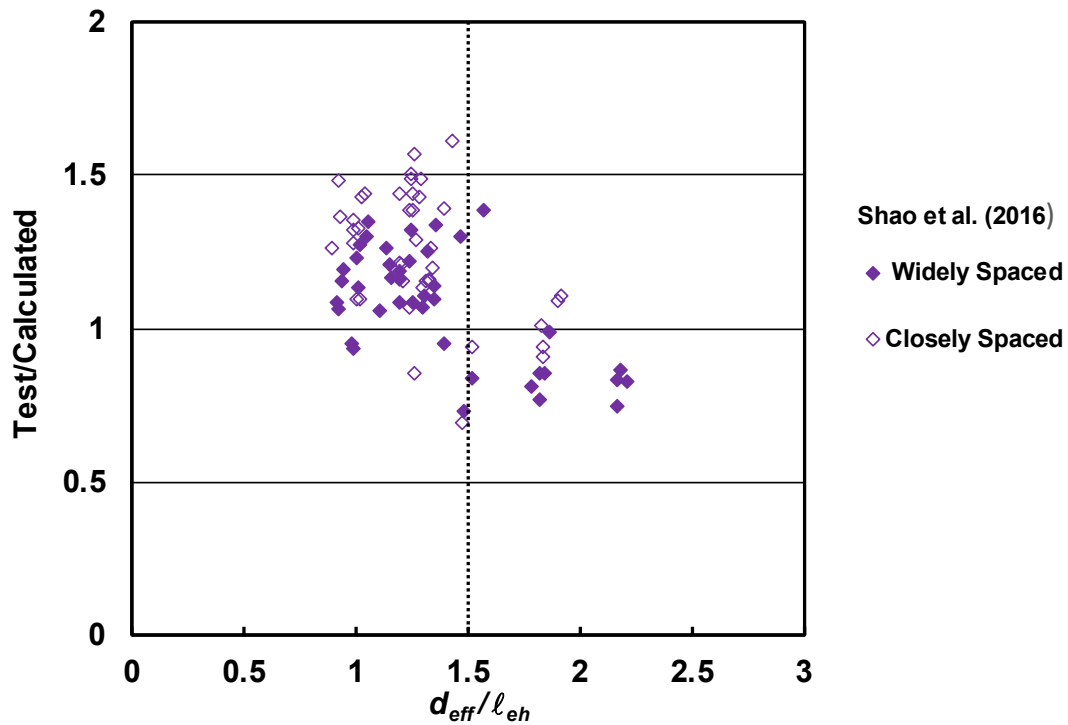


Figure 4.28 Ratio of test-to-calculated failure load (T/T_{Shao}) versus d_{eff}/l_{eh} for specimens with widely and closely-spaced headed bars without confining reinforcement (Shao et al. 2016)

Table 4.24: Max, Min, Mean, STD, and COV of T/T_{Shao} for headed bar specimens with

$d_{eff}/\ell_{eh} \geq 1.5$ without confining reinforcement

(Number of specimens)	All (18)	Widely spaced C/C* spacing $\geq 8d_b$			Closely spaced C/C* spacing $< 8d_b$		
		No. 5 (-)	No. 8 (6)	No. 11 (5)	No. 5 (-)	No. 8 (5)	No. 11 (2)
Max	1.10		0.99	0.85		1.10	0.94
Min	0.69		0.75	0.73		0.91	0.69
Mean	0.88		0.85	0.80		1.01	0.82
STD	0.116		0.078	0.051		0.087	0.172
COV	0.132		0.092	0.064		0.086	0.211
$T/T_{Shao} < 1.0$	15		6	5		2	2

*C/C Center-to-Center

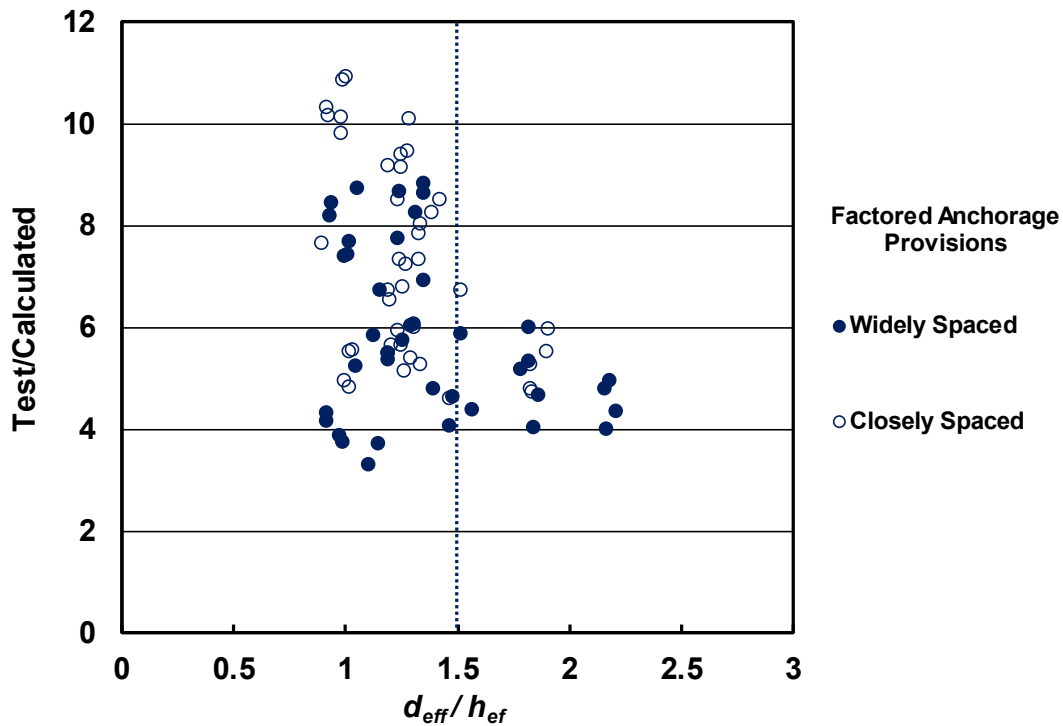


Figure 4.29 Ratio of test-to-calculated failure load ($T/\phi N_{str}$) versus d_{eff}/h_{ef} for specimens with widely and closely-spaced headed bars without confining reinforcement (Anchorage Provisions)

Table 4.25: Max, Min, Mean, STD, and COV of $T/\phi N_{str}$ for headed bar specimens with

$d_{eff}/\ell_{eh} \geq 1.5$ without confining reinforcement

(Number of specimens)	All (18)	Widely spaced C/C* spacing $\geq 8d_b$			Closely spaced C/C* spacing $< 8d_b$		
		No. 5 (-)	No. 8 (6)	No. 11 (5)	No. 5 (-)	No. 8 (5)	No. 11 (2)
Max	6.71		4.93	4.48		5.98	6.71
Min	3.98		3.98	3.48		4.71	4.61
Mean	5.07		4.46	4.05		5.25	5.66
STD	0.724		0.396	0.407		0.520	1.487
COV	0.143		0.089	0.101		0.099	0.263
$T/\phi N_{str} < 1.0$	0		0	0		0	0

*C/C =Center-to-Center

Figure 4.30 compares the ratio of the force obtained from test results to the force obtained from Shao et al. (2016) for the 22 specimens with $d_{eff}/\ell_{eh} \geq 1.5$ and for 74 beam-column specimens with $d_{eff}/\ell_{eh} < 1.5$ versus d_{eff}/ℓ_{eh} for the headed bars with confining reinforcement, with statistical parameters (maximum, minimum, mean, standard deviation (STD), and coefficient of variation (COV)) given in Table 4.26. Figure 4.31 and Table 4.27 show similar results based on the force obtained from the anchorage provisions.

The values of T/T_{Shao} range from 0.78 to 1.29, with an average of 1.01 and a coefficient of variation of 0.141 and the values of $T/\phi N_{str}$ range from 3.59 to 6.45, with an average of 4.64 and a coefficient of variation of 0.186.

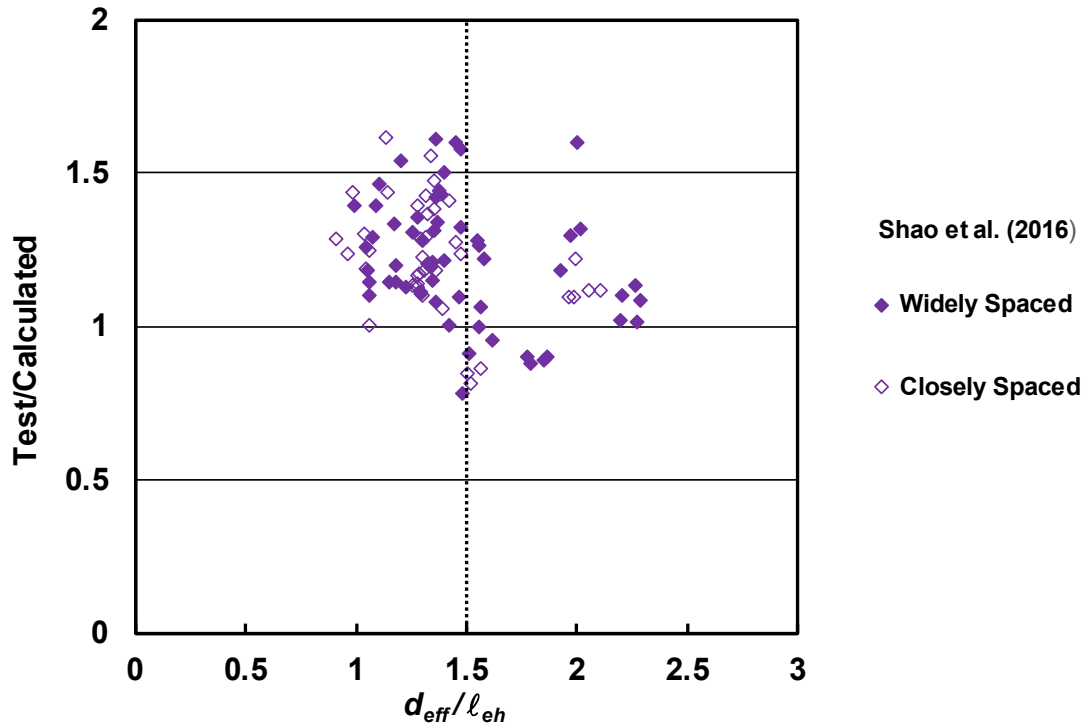


Figure 4.30 Ratio of test-to-calculated failure load (T/T_{Shao}) versus d_{eff}/l_{eh} for specimens with widely and closely-spaced headed bars with confining reinforcement (Shao et al. 2016)

Table 4.26: Max, Min, Mean, STD, and COV of T/T_{Shao} for headed bar specimens with $d_{eff}/l_{eh} \geq 1.5$ with confining reinforcement

(Number of specimens)	All (22)	Widely spaced C/C^* spacing $\geq 8d_b$			Closely spaced C/C^* spacing $< 8d_b$		
		No. 5 (-)	No. 8 (7)	No. 11 (7)	No. 5 (-)	No. 8 (5)	No. 11 (3)
Max	1.29		1.29	1.00		1.22	0.86
Min	0.78		1.01	0.78		1.09	0.81
Mean	1.01		1.12	0.89		1.13	0.84
STD	0.143		0.097	0.064		0.052	0.024
COV	0.141		0.087	0.071		0.046	0.029
$T/T_{Shao} < 1.0$	9		0	6		0	3

*C/C = Center-to-Center

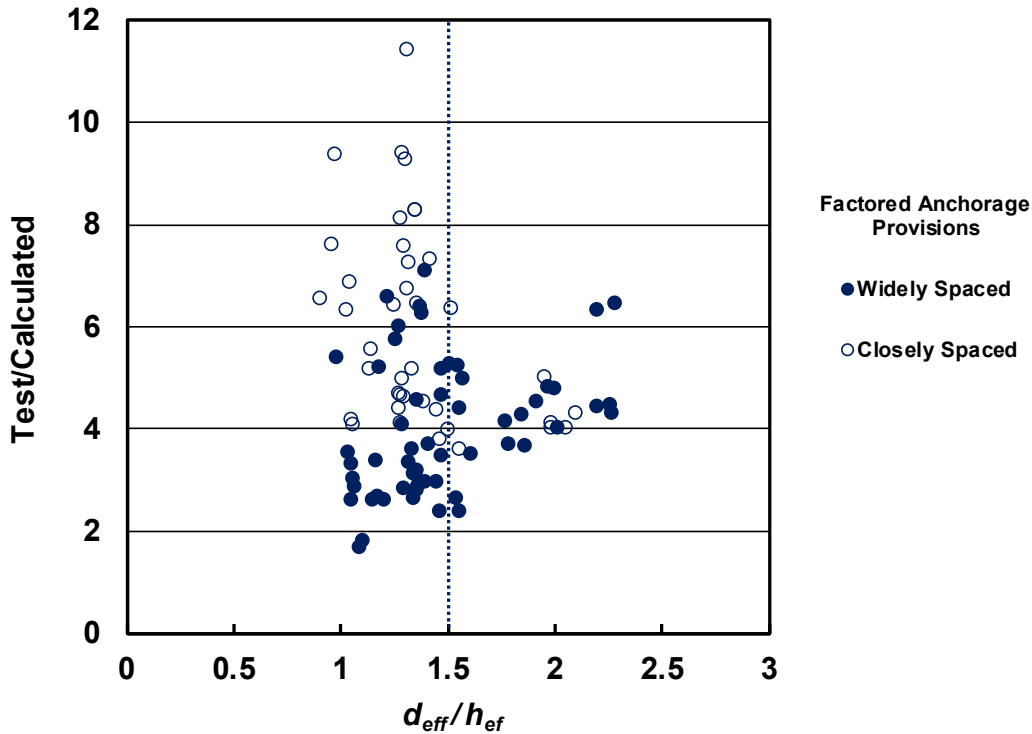


Figure 4.31 Ratio of test-to-calculated failure load ($T/\phi N_{str}$) versus d_{eff}/h_{ef} for specimens with widely and closely-spaced headed bars with confining reinforcement (Anchorage Provisions)

Table 4.27: Max, Min, Mean, STD, and COV of $T/\phi N_{str}$ for headed bar specimens with $d_{eff}/\ell_{eh} \geq 1.5$ with confining reinforcement

(Number of specimens)	All (22)	Widely spaced C/C* spacing $\geq 8d_b$			Closely spaced C/C* spacing $< 8d_b$		
		No. 5 (-)	No. 8 (7)	No. 11 (7)	No. 5 (-)	No. 8 (5)	No. 11 (3)
Max	6.45		6.45	3.95		5.02	6.36
Min	3.59		4.31	2.73		4.00	3.59
Mean	4.64		5.04	3.36		4.28	4.64
STD	0.862		0.93	0.543		0.427	1.506
COV	0.186		0.185	0.162		0.100	0.324
$T/\phi N_{str} < 1.0$	0		0	0		0	0

*C/C = Center-to-Center

Figure 4.28 shows that as the ratio of d_{eff}/ℓ_{eh} increased above 1.5, the ratio T/T_{Shao} dropped, with the majority of the specimens exhibiting a value below 1.0. Figure 4.29 shows that as the ratio of d_{eff}/h_{ef} increased above 1.5, $T/\phi N_{str}$ dropped, but remained high because of the very conservative nature of the anchorage provisions. As discussed in Section 4.3.6, these observations support Commentary Section R25.4.4.2 of ACI 318-19, which states that “providing reinforcement in the

form of hoops and ties to establish a load path in accordance with strut-and-tie modeling principles” is needed when the ratio of d/ℓ_{dt} exceeds 1.5. For this reason, the anchorage strengths of beam-column joints with $d_{eff}/\ell_{eh} \geq 1.5$ with confining reinforcement in the joint region are calculated using the strut-and-tie method to its accuracy for this application.

Like the comparisons for headed bars without confining reinforcement, Figure 4.30 shows that as the ratio of d_{eff}/ℓ_{eh} increased above 1.5, the ratio of strengths for headed bars with confining reinforcement based on Shao et al. 2016 started to exhibit lower relative anchorage strength, but the decrease is not as great as for headed bars without confining reinforcement. Figure 4.31 shows that as the ratio of d_{eff}/h_{ef} increased above 1.5, the ratio of strengths based on the anchorage provisions also exhibited lower values than for the specimens with d_{eff}/ℓ_{eh} below 1.5. This drop in the anchorage strength of beam-column joints with $d_{eff}/\ell_{eh} \geq 1.5$ justifies using the strut-and-tie modeling approach for joints containing confining reinforcement.

The results using strut-and-tie method for specimens with $d_{eff}/\ell_{eh} \geq 1.5$ are shown in Figure 4.32 and Table 4.28.

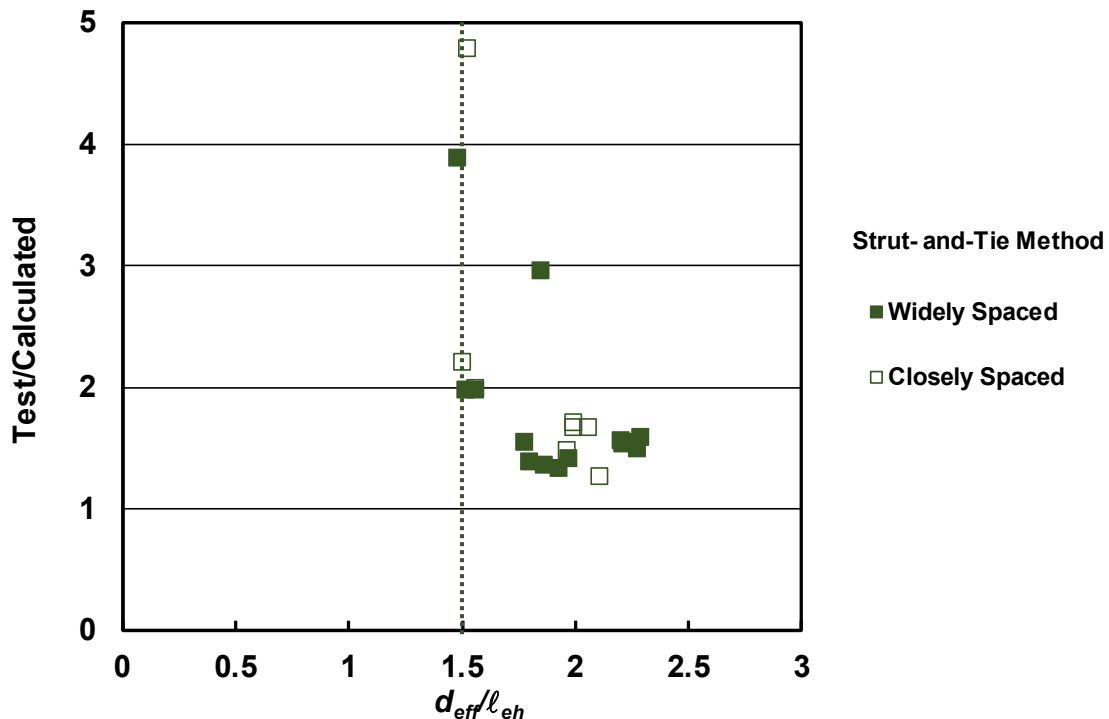


Figure 4.32 Ratio of test-to-calculated failure load (R_1/T_{STM}) versus d_{eff}/ℓ_{eh} for specimens with widely and closely-spaced headed bars with confining reinforcement (Strut-and-tie method)

Table 4.28: Max, Min, Mean, STD, and COV of R_1/T_{STM} for headed bar specimens with $d_{eff}/\ell_{eh} \geq 1.5$ with confining reinforcement

(Number of specimens)	All (22)	Widely spaced C/C* spacing $\geq 8d_b$			Closely spaced C/C* spacing $< 8d_b$		
		No. 5 (-)	No. 8 (7)	No. 11 (7)	No. 5 (-)	No. 8 (5)	No. 11 (3)
Max	4.79		1.71	2.96		4.79	2.00
Min	1.27		1.27	1.37		1.55	1.55
Mean	1.93		1.51	1.70		2.88	1.84
STD	0.875		0.178	0.561		1.387	0.254
COV	0.453		0.118	0.330		0.481	0.138
$R_1/T_{STM} < 1.0$	0		0	0		0	0

*C/C =Center-to-Center

The Maximum, Minimum, Mean, STD, and COV for the R_1/T_{STM} for the 22 beam-column joint specimens with $d_{eff}/\ell_{eh} \geq 1.5$ ranges from 1.27 to 4.79, with an average of 1.93 and a coefficient of variation of 0.453, indicating that although the scatter is high, the strut-and-tie method does give a conservative representation of the anchorage strength of headed bars in deep joints.

These results also show that the anchorage provisions are very conservative when compared to any of the other methods evaluated in this study and, if used, would lead to nearly unbuildable designs. Even though neither the anchorage provisions nor the strut-and-tie method account for the contribution of the concrete, the strut-and-tie method is clearly more accurate. Thus, the strut-and-tie method is recommended for the design of beam-column with effective depth to development ratios greater than 1.5.

4.6 SUMMARY AND CONCLUSIONS

In this chapter, the strength of headed bars in tension for beam-column joint specimens is compared to values based on the development length provisions in ACI 318-14 and ACI 318-19, and proposed by Shao et al. (2016) and Darwin and Dolan (2021), as well as the anchorage provisions in Chapter 17 of ACI 318-19. In addition, strut-and-tie method is used for beam-column joint specimens with confining reinforcement that have ratios of effective depth to embedment length of 1.5 and greater. For the ACI 318-19 anchorage provisions, three modes of failure were checked—breakout, side-face blowout, and strength of the anchor reinforcement. The analysis covers 178 beam-column joint specimens with head sizes between $3.8A_b$ and $9.5A_b$ tested by Shao

et al. (2016); 82 specimens without confining reinforcement and 96 specimens with confining reinforcement. Of these, 40 specimens (18 specimens without confining reinforcement and 22 specimens with confining reinforcement) had ratios of effective depth to embedment length of 1.5 or greater.

The following summarizes the primary findings of this chapter:

1. The provisions in ACI 318-14 for the development length of headed bars do not accurately estimate the anchorage strength of headed bars with high steel strength or concrete compressive strength. The equation, however, is generally conservative.
2. The development length design provisions proposed by Shao et al. (2016) can be safely used for the design of the anchorage strength of headed bars for steel strengths at least up to 120 ksi and concrete compressive strengths at least up to 16,000 psi.
3. The development length design provisions in ACI 318-19 for headed bars do not fully capture the effects of confining reinforcement and bar spacing and do not accurately represent the contribution of concrete compressive strength for compressive strengths above 6000 psi.
4. The development length design provisions proposed by Darwin and Dolan (2021) accurately reflect the anchorage strength of headed bars and provide a similar level of accuracy to that provided by the provisions proposed by Shao et al. (2016).
5. Specimens with ratios of effective depth to embedment length of 1.5 or greater exhibited lower anchorage strengths than the specimens with ratios below 1.5 for specimens both without and with confining reinforcement.
6. The strut-and-tie method should be used to design joints with ratios of effective depth to embedment length of 1.5.
7. The anchorage provisions in ACI 318-19 are very conservative when compared to any of the other methods evaluated in this study and, if used, would lead to nearly unbuildable designs.

CHAPTER 5: MODELING THE ANCHORAGE FAILURE FOR HEADED BARS AND STRAIGHT BARS USING 3D GRANULAR MICROMECHANICS BASED FINITE ELEMENT ANALYSIS

5.1 INTRODUCTION

Granular micromechanics is a method used for modeling materials where the microstructure and micromechanical properties have an important effect on the macroscopic behavior of this material. In the granular micromechanics method, the material is defined in terms of a representative volume element (RVE), which consists of a collection of grains connected with each other through different intergranular mechanisms. The microscopic behavior of the granular micromechanics materials is derived as an average response of grain-pair interaction at different orientations.

A granular micromechanics model to represent damage and plasticity of cementitious material developed by Misra and Yang (2010), Misra and Singh (2014), Misra and Poorsolhjouy (2015), and Poorsolhjouy and Misra (2017) has been highly successful for a number of applications representing nonlinear material behavior, but has not been used to represent reinforced concrete members. In this chapter, the finite element (FE) method is used to study the ability of that model to represent concrete fracture and the interaction between the concrete and steel reinforcing bars. For this purpose, two types of specimens are simulated. The first is a slab specimen with shallow embedment of headed bars installed at different locations with member strength governed by anchorage failure. The second is a beam-end specimen to measure the bond performance of a straight bar embedded in a concrete block. Concrete behavior in tension and compression is described using the nonlinear granular micromechanics model. The model is implemented via a user material (UMAT) subroutine into commercial FE software (ABAQUS). Reinforcement behavior is described using an elastic model. The interaction between concrete and reinforcement is modeled as cohesive behavior with damage (defined as part of the surface interaction properties of two contact surfaces). Three-dimensional FE discretized models of shallow embedment and beam-end test specimens are constructed and analyzed. The FE results are compared with those

from laboratory experiments performed by Ghimire et al. (2018) for the headed bars embedded in slabs and by Darwin and Graham (1993) for straight bars embedded in beam-end specimens.

5.7 FINITE ELEMENT ANALYSIS OF ANCHORAGE BEHAVIOR

Three-dimensional FE models were constructed consisting of a headed bar embedded in a concrete slab (shallow embedment specimen) and a straight bar embedded in a concrete block (beam-end specimen). The details of the concrete and steel material models are described next.

5.2.1 Material Properties

5.2.1.1 Concrete Model

A granular micromechanics model suitable for cementitious materials has been derived by Misra and Yang (2010), Misra and Singh (2014), Misra and Poolsolhjouy (2015), and Poolsolhjouy and Misra (2017) based on a thermomechanics framework. The model was derived by defining energy density and a dissipation potential function in both the macroscopic and microscopic (grain-scale) level. The expression for the Cauchy stress tensor (a second-order tensor named after Augustin-Louis Cauchy) is obtained in terms of the free energy of grain-pair interactions. Further, the free energy and dissipation potential of grain-pair interactions are used to find a grain-scale Clausius–Duhem type inequality (a way of expressing the second law of thermodynamics that is used in continuum mechanics). In the work of Misra et al., force laws that ensure asymmetric behavior in tension and compression have been defined. The model is used to simulate the nonlinear behavior of cementitious materials, such as concrete, in tension and compression. The model is implemented in ABAQUS using a user-defined material subroutine (UMAT).

Figure 5.1a shows the normal force-displacement curve assumed for a grain-pair in this model. For tension, the grain-pair normal force-displacement curve exhibits a peak followed by softening. For compression, the grain-pair normal force-displacement curve is nonlinear. The force and displacement in compression are considerably higher than in tension. For shear, the grain-pair force-displacement curve takes the same shape as that for tension, as shown in Figure 5.1b.

Figure 5.1c shows the shear direction damage parameters as a function of normal displacement. The effect of compression on the tangential behavior is modeled by defining B_w (the

damage parameter in shear) as a bi-linear function of the normal displacement governed by model parameters α_1 , α_2 , and α_3 (See Figure 5.1 c).

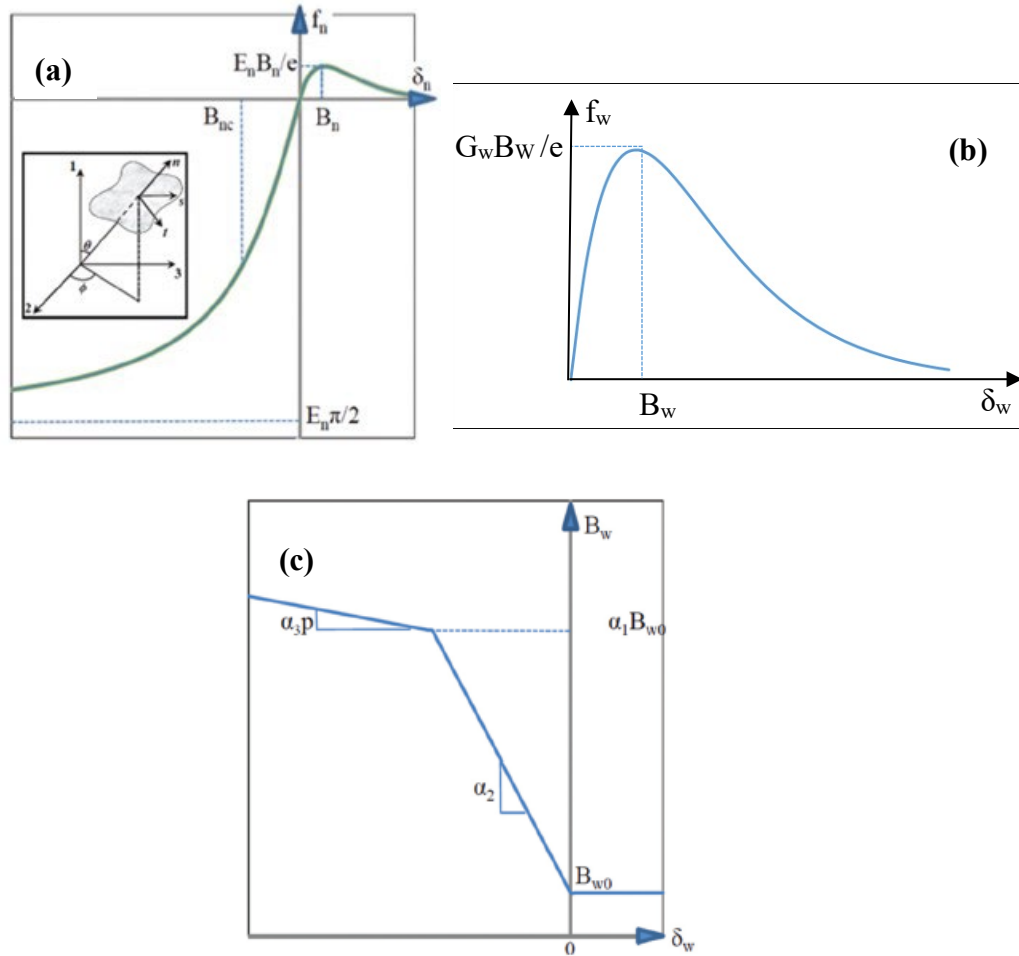


Figure 5.1 (a) Normal force-displacement relationship in compression and tension, The local cartesian coordinate system is shown in the inset, (b) Shear force-displacement relationship in tension, (c) Shear direction damage parameter as a function of normal displacement. (Misra and Poorsolhjuy 2015)

The physical meaning of the model parameters is shown in Figure 5.1. E_{no}^T is the grain-scale normal stiffness in tension; G_w , is the grain-scale elastic stiffness in shear; B_n , is the intergranular displacement where normal intergranular force reaches its peak in tensile intergranular force-displacement curve (see Fig. 5.1a). B_{wo} , is the intergranular shear yield parameter in tension, and R , the ratio of the maximum normal force in compression to the maximum normal force in tension. Additional parameters α_1 , α_2 , and α_3 are model parameters of creating shear damage parameter with respect to normal displacement in microscale. α_4 is a

constant that defines the growth of stiffness with increasing confinements. These parameters can be established based on results of confined axisymmetric triaxial tests by reducing the error between the experimentally measured and FE predicted stress-strain curve, following a procedure discussed in Misra and Poorsolhjouy (2015).

5.2.1.2 Stress-Strain Behavior of a Concrete Block under Uniaxial Tension and Compression

Prior to using the model in simulations, a concrete block is modeled to check the concrete model under tension and compression. Applied displacement and boundary conditions are as shown in Figure 5.2. The nodes are prevented from movement in the x-direction at surface 1, in the y-direction at surface 2, and in z-direction at surface 3. Displacement is applied at surface 4 in tension and compression.

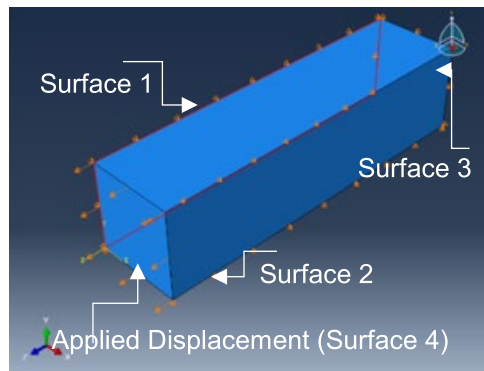


Figure 5.2 Boundary condition for concrete block.

ABAQUS linked with FORTRAN is used in the analysis. The UMAT subroutine governs the material behavior. Figure 5.3 shows the stress-strain behavior for the simulated concrete block under tension and compression for two models, representing concrete with compressive strengths of 5 and 8 ksi the values used in the simulations. For simplicity, the 5 ksi (5000 psi) model is used to represent concrete in test specimens with compressive strengths of 4200, 4630 and 5180 psi, and the 8 ksi (8000 psi) model is used to represent concrete in test specimens with a compressive strength of 7390 psi. Model parameters are listed in Table 5.1.

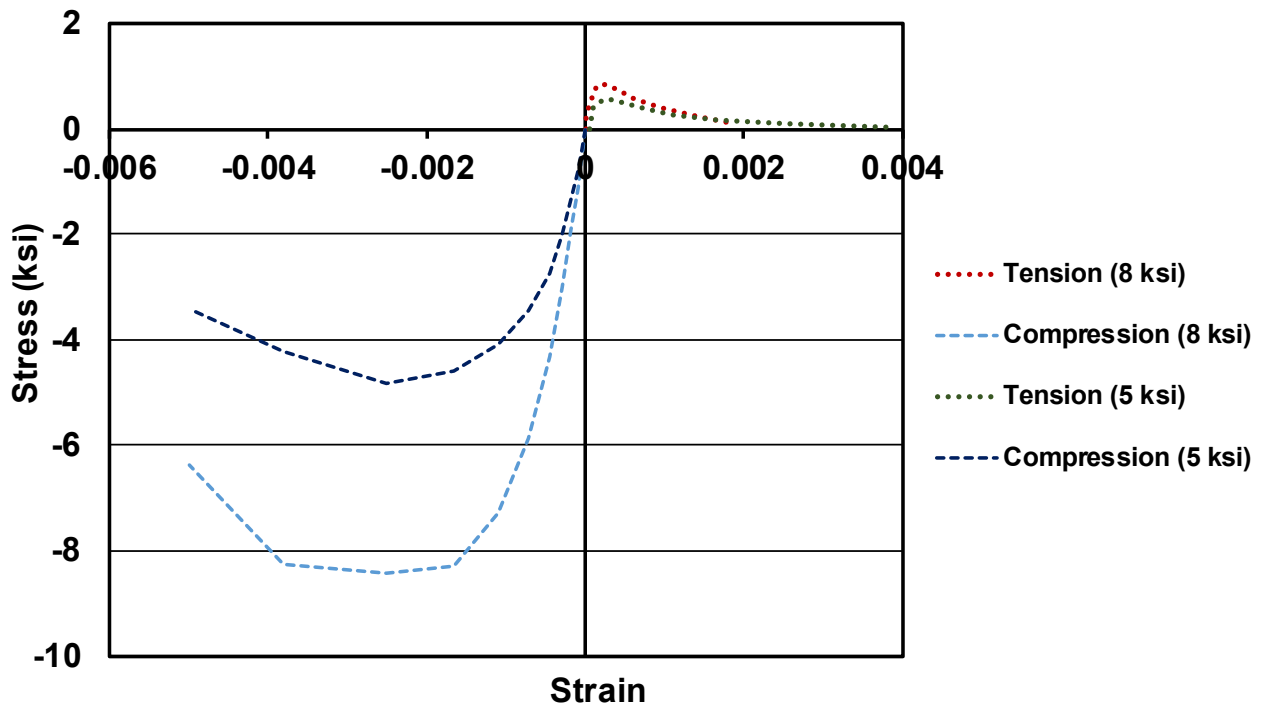


Figure 5.3 Stress-Strain curve for the concrete block under uniaxial tension and compression for concrete compressive strength of 5 ksi and 8 ksi

Table 5.1 Grain-scale model parameters for concrete with compressive strengths of 5 ksi and 8 ksi (model parameters are from Misra et al.)

Model Parameters	Concrete Compressive Strength (5 ksi)	Concrete Compressive Strength (8 ksi)
E_{no}^T	0.0315 kips/in.	0.04 kips/in.
G_w	0.0057 kips/in.	0.011 kips/in.
B_n	23.6 E-6 in.	27.5 E-6 in.
B_{wo}	47.2 E-6 in.	51.9 E-6 in.
R	12	12
α_1	9.5	10.5
α_2	6	7
α_3	0.0022	0.0012
α_4	0.113 ksi ⁻¹	0.182 ksi ⁻¹

5.2.1.3 Stress-Strain Behavior of a Concrete Block with Different Confinement Levels

Stress-strain curves for the concrete block with a compressive strength of 8 ksi are also modeled to investigate material behavior with different levels of confinement based on the properties of the material model. Figures 5.4a and b show the boundary conditions and two levels of confinement.

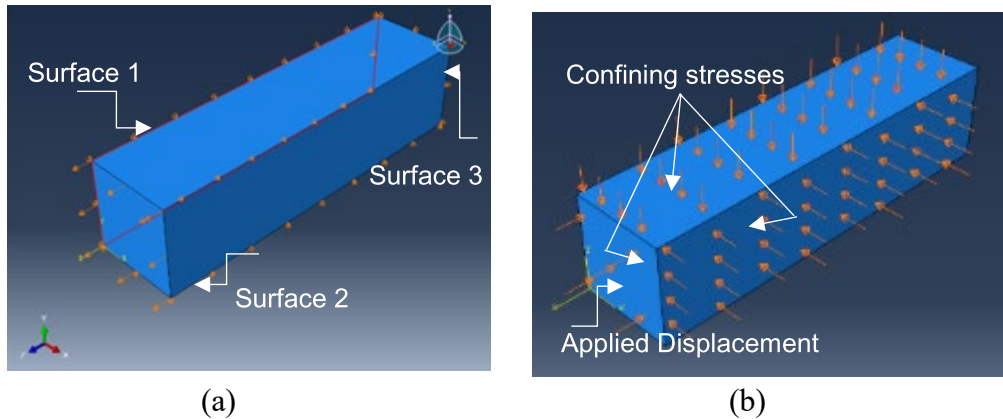


Figure 5.4 Loading and boundary conditions for concrete block. (a) Without confinement, (b) With confining stresses

The concrete block was subjected to a constant hydrostatic stress. An additional compressive and tensile displacement about a single axis was applied to the block; this displacement was increased until failure. Under compressive displacement, hydrostatic stresses of 0, 0.145, 0.29, 0.43, and 0.58 ksi were investigated; results are shown in Figure 5.5. Under tensile displacement, hydrostatic stress of 0 and 0.145 ksi were investigated; results are shown in Figure 5.6. Figures 5.5 and 5.6 show that increasing the confinement increases the stress attainable in both the axial and lateral directions. From Figure 5.5, it can also be observed that by increasing the confining stresses, the lateral strains (ϵ_{11} and ϵ_{22}) decrease, which affects the volumetric strain, $\epsilon_{11} + \epsilon_{22} + \epsilon_{33}$, as shown in Figure 5.7. As shown in Figure 5.7, increasing the confining stresses changes the volumetric strain behavior from compression-dilation to compression. This change occurs due to the grain-scale mechanism, as discussed by Misra and Poorsolhjouy (2015).

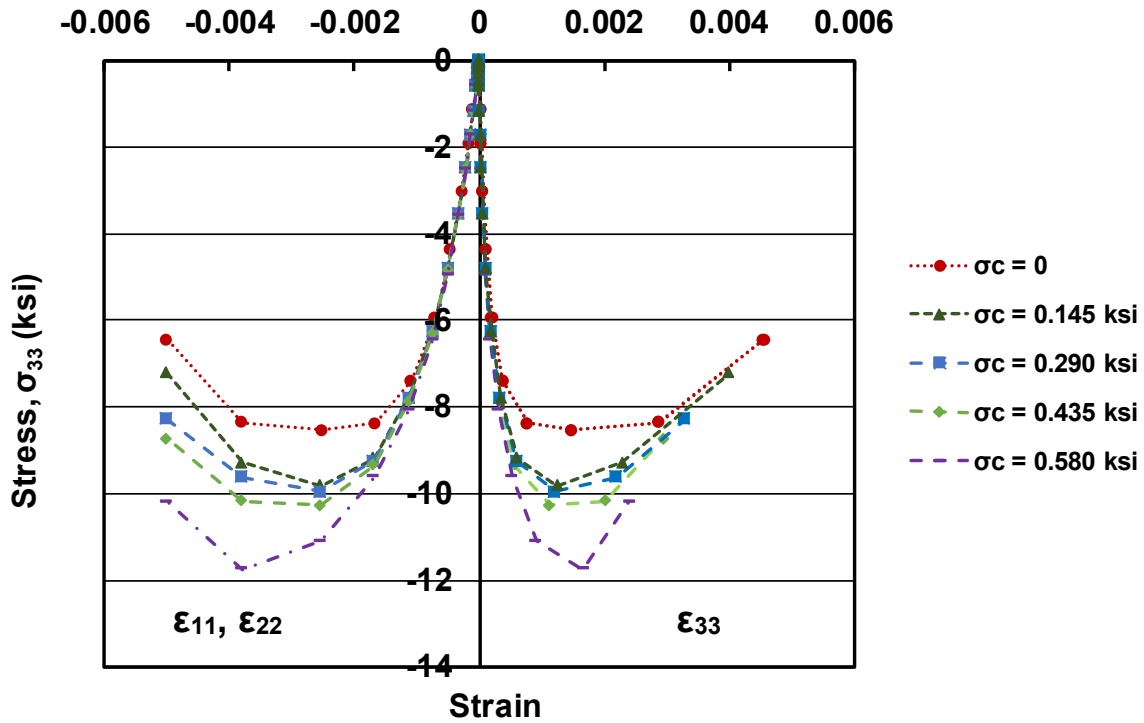


Figure 5.5 Stress-strain curves for concrete block with different levels of confinement in compression for concrete compressive strength of 8 ksi

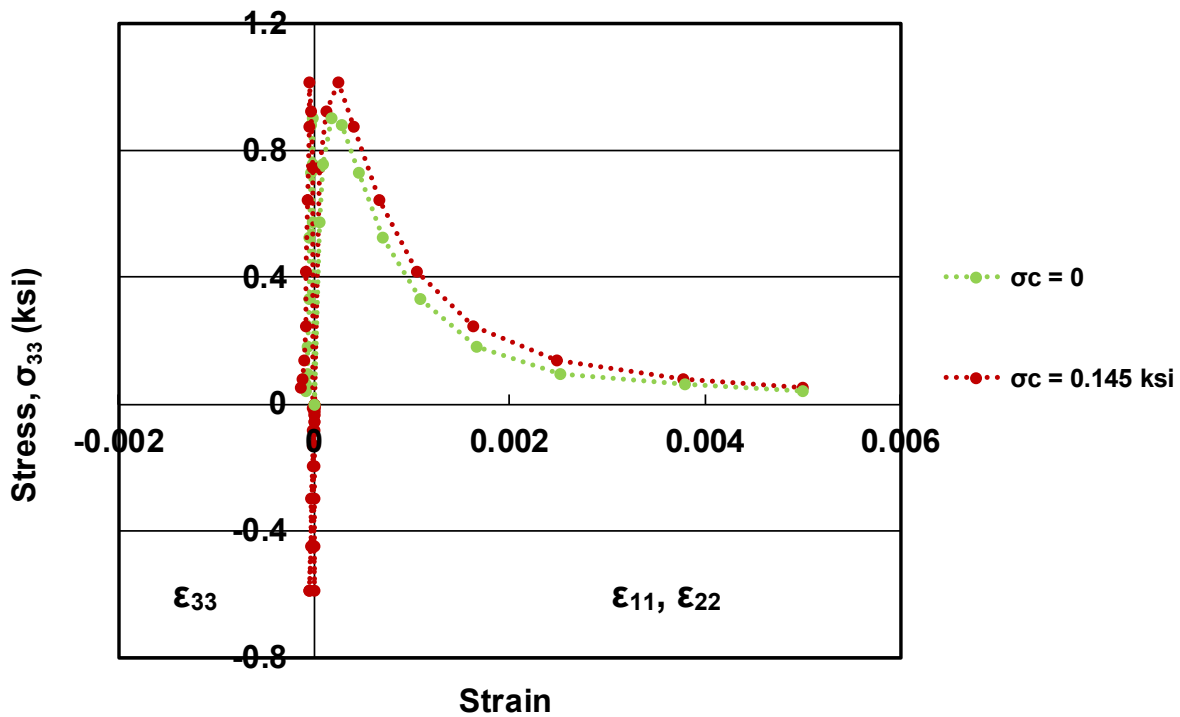


Figure 5.6 Stress-Strain curve for concrete block with confinement in tension for concrete compressive strength of 8 ksi

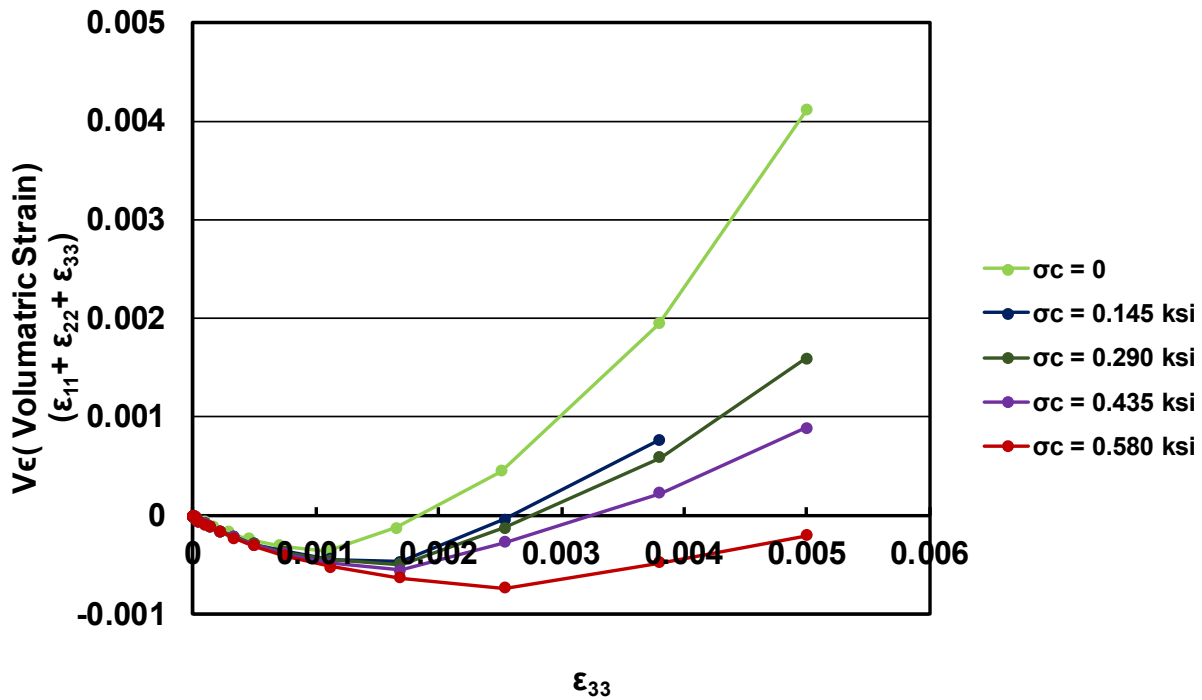


Figure 5.7 Volumetric strain-axial strain curve for a concrete block with confinement in compression for concrete compressive strength of 8 ksi

Figure 5.8 shows deviatoric stress ($q = \sigma_{33} - \sigma_{11}$) plotted versus mean stress ($p = 1/3\sigma_{ii}$, $\sigma_{ii} = \sigma_{11} + \sigma_{22} + \sigma_{33}$) (where σ_{11} represents the stress in x-direction, σ_{22} represents the stress in y-direction, and σ_{33} represents the stress in z-direction). The deviatoric stress-mean stress curve represents the stress path that begins from the initial confinement and ends at failure. The failure envelope is shaped by linking the end points of stress paths (see red curve in Figure 5.8). Under compression and with the increasing confining stresses, the failure envelope is found to be nonlinear, and this matches the experimental observations from previous studies.

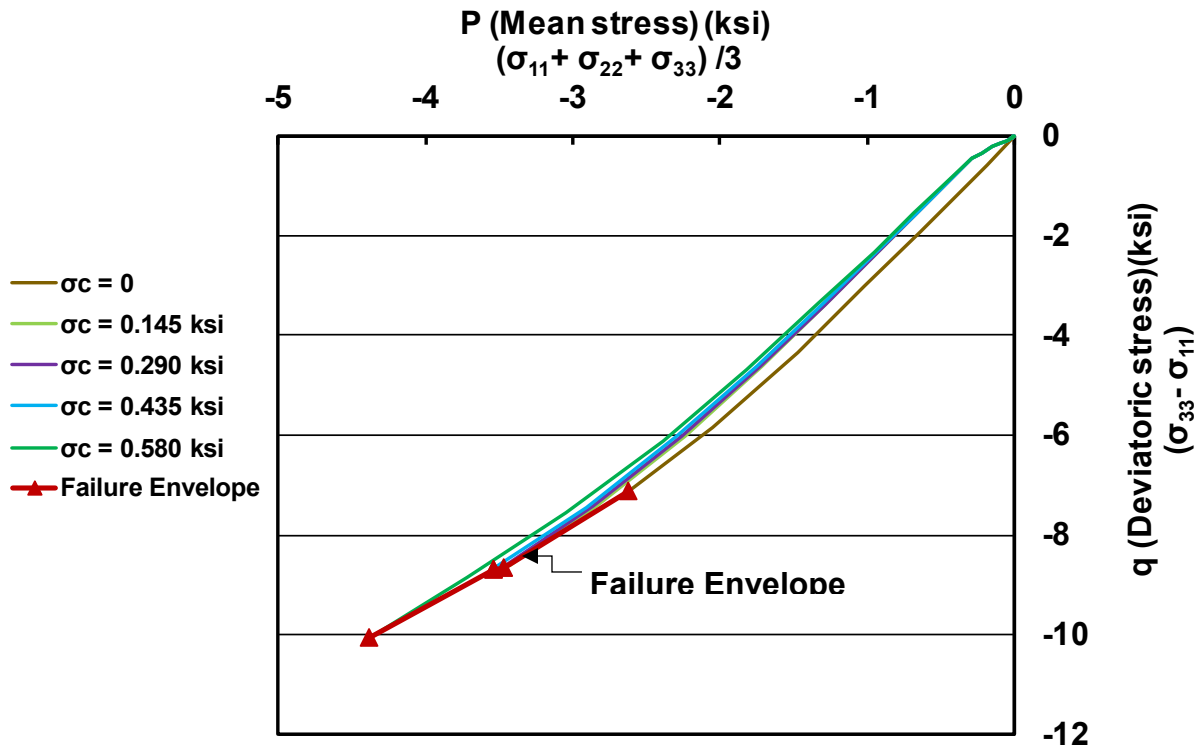


Figure 5.8 Stress paths plotted in the deviatoric stress–mean stress (q-p) space with confinement in compression. The failure envelope is shaped by linking the stress path end points

5.2.2 Steel Model

A linear-elastic model, with an elastic modulus of 29,000 ksi and Poisson’s ratio of 0.3, is used to model the steel reinforcement.

5.2.3 Concrete-Steel Interface Model

Cohesive behavior is used to model the interface between concrete and steel according to Simulia/ABAQUS V 6.11; Dassault Systèmes, RI, USA, Section 35.1.10. The cohesive behavior can be defined as part of the surface interaction properties of two contact surfaces and includes:

1. Linear-elastic traction-separation behavior.
2. Damage initiation criteria,
3. Damage evolution laws.

Figure 5.9 shows the traction-separation model, which assumes initially linear-elastic behavior followed by the initiation and evolution of damage.

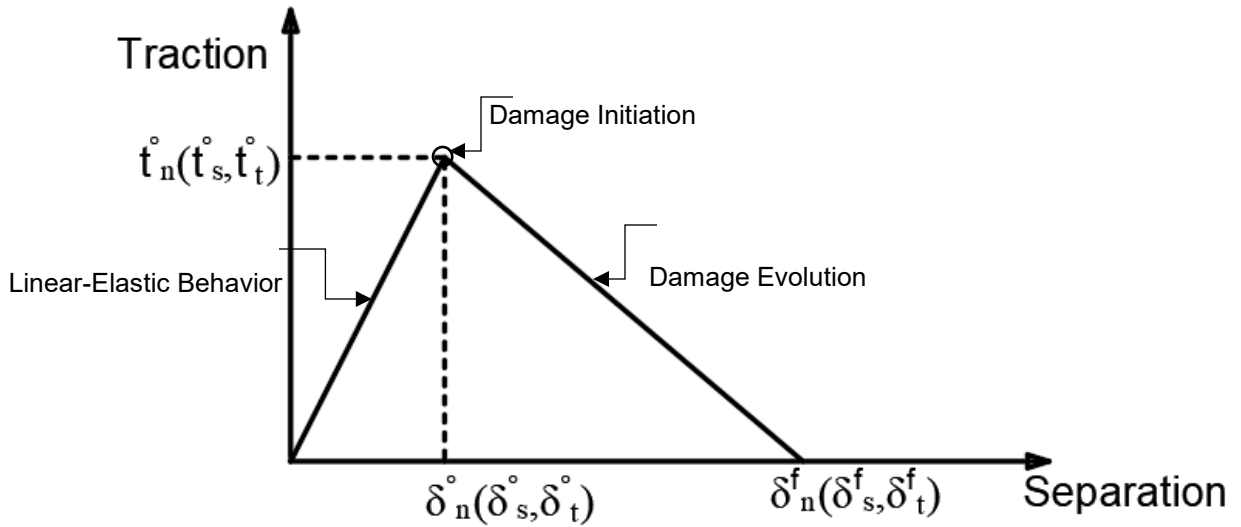


Figure 5.9 Typical traction-separation response (Simulia/ABAQUS V 6.11; Dassault Systèmes, RI, USA)

5.2.3.1 Linear Elastic Traction-Separation Behavior

The elastic behavior can be described by an elastic constitutive matrix that links the normal and shear stresses with normal and shear separations through the interface.

$$t = \begin{Bmatrix} t_n \\ t_s \\ t_t \end{Bmatrix} = \begin{bmatrix} K_{nn} & K_{ns} & K_{nt} \\ K_{ns} & K_{ss} & K_{st} \\ K_{nt} & K_{st} & K_{tt} \end{bmatrix} \begin{Bmatrix} \delta_n \\ \delta_s \\ \delta_t \end{Bmatrix} = K \delta \quad (5.1)$$

where t_n , t_s , and t_t represent the contact traction in the normal, first, and second shear directions, respectively; and δ_n , δ_s , δ_t , represent the contact separation in the normal, first, and second shear directions, respectively. ss and tt represent arbitrary directions that are perpendicular to the normal direction (or tangential with the interface).

In ABAQUS, for uncoupled traction-separation behavior, the terms (K_{nn}, K_{ss}, K_{tt}) must be defined. The off-diagonal terms $K_{ns} = K_{sn} = K_{nt} = K_{tn} = K_{st} = K_{ts} = 0$.

5.2.3.2 Damage Modeling:

Damage modeling is used to simulate the reduction and final failure of the bond between two cohesive surfaces. Failure involves both damage initiation and damage evolution.

5.2.3.2.1 Damage Initiation

Damage initiation is represented by the point on the traction-separation response which represent the beginning of the degradation of the cohesive response. In the current study, damage initiation is modeled according to Simulia/ABAQUS V 6.11; Dassault Systèmes, RI, USA, Section 35.1.10 as a maximum separation criteria. Modeling based on maximum separation criteria requires the displacement parameters (Normal only, shear-1 only, and shear-2 only. Normal only (δ_n°), shear-1 only (δ_s°), and shear-2 only (δ_t°) represent the maximum values of the contact separation, when the separation is either purely along the contact normal or purely in the first or the second shear directions, respectively (See Figure 5.9).

Damage is assumed to initiate when the maximum separation ratio (as defined in Eq. (5.2)) reaches a value of one.

$$\max \left\{ \frac{\langle \delta_n \rangle}{\delta_n^\circ}, \frac{\delta_s}{\delta_s^\circ}, \frac{\delta_t}{\delta_t^\circ} \right\} = 1.0 \quad (5.2)$$

where δ_n , δ_s , δ_t , represent the contact separation in the normal, first, and second shear directions, respectively. δ_n° , δ_s° , δ_t° , represent the maximum values of the contact separation in the normal, first, and second shear directions, respectively. The symbol $\langle \rangle$ is the Macaulay bracket, which is used to signify that a purely compressive displacement does not initiate damage.

Further details about damage initiation using this method could be found in Simulia/ABAQUS V 6.11; Dassault Systèmes, RI, USA, Section 35.1.10.

5.2.3.2.2 Damage Evolution

The damage evolution law represents the rate at which the linear-elastic part of the traction-separation response (cohesive stiffness) is reduced once the damage initiation criteria has been satisfied. The details of modeling damage evolution can be found in Simulia/ABAQUS V 6.11; Dassault Systèmes, RI, USA, Section 35.1.10.

There are two components that define damage evolution. In this study, the first component is dependent on the effective separation (effective separation is defined in Eq. (5.3)) at complete failure, δ_m^f , relative to effective separation at the initiation of damage, δ_m° .

$$\delta_m = \sqrt{\langle \delta_n \rangle^2 + \delta_s^2 + \delta_t^2} \quad (5.3)$$

The second component is the specification of the nature of the evolution of the damage variable between initiation of damage and final failure. This can be done by either defining linear or exponential softening. In the current study, damage evolution is specified as linear (see Figure 5.10a).

The parameters of mixed-mode ratio, the relative proportions between normal and shear separation at a contact point as shown in Figure 5.10b, were defined in a tabular form based on energy definition as explained in (Simulia/ABAQUS V 6.11; Dassault Systèmes, RI, USA, Section 35.1.10, Figure 35.1.10-4). Figure 5.10b shows traction on the vertical axis versus the magnitudes of the normal and the shear separations along the two horizontal axes. The unshaded triangles in the two vertical coordinate planes represent the response under pure normal and pure shear separation, respectively. All intermediate vertical planes (that contain the vertical axis) represent the damage response under mixed-mode conditions with different mode mixes. The mixed-mode definition based on energies are:

$$m_1 = G_n / G_T$$

$$m_2 = G_s / G_T$$

$$m_3 = G_t / G_T$$

where G_n , G_s , and G_t , represent the work done by the separation in the normal, first, and second shear direction under their conjugate tractions, respectively, and can be defined as

$$G_T = G_n + G_s + G_t$$

G_{ST} represents the portion of total work done by separation components under shear traction and defined as follow

$$G_{ST} = G_s + G_t$$

ABAQUS requires specifying material properties related to damage evolution as a function of $M_{m1} = m_2 + m_3 (= G_{ST} / G_T)$ and

$$M_{m2} = m_3 / (m_2 + m_3) (= G_t / G_{ST}).$$

In the current study, the values of the interfacial coefficients were calibrated based on test results (as described in Sections 5.6.2.1 and 5.6.6.1)

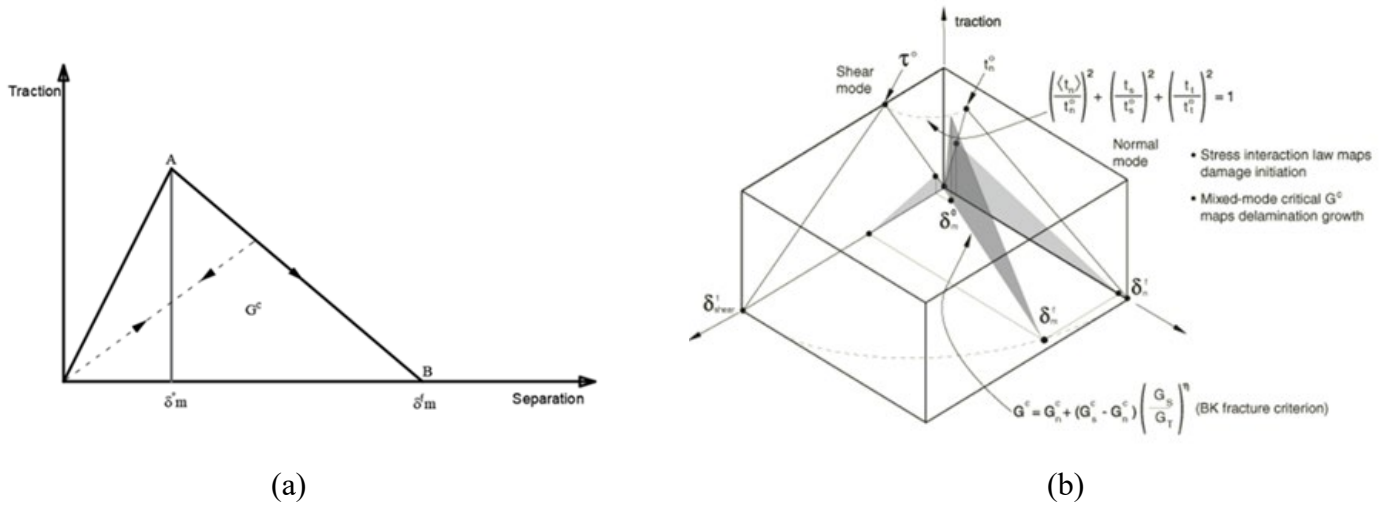


Figure 5.10 (a) Linear damage evolution (Simulia/ABAQUS V 6.11; Dassault Systèmes, RI, USA Section 35.1.10), (b) Mixed mode response in cohesive behavior (Simulia/ABAQUS V 6.11; Dassault Systèmes, RI, USA, Section 35.1.10)

5.8 ELEMENT TYPE

A 10-node quadratic tetrahedral element (C3D10), as shown in Figure 5.11, is used to model both concrete and steel in this study. This general-purpose element has four integration points, where the element response is monitored and controlled by the material model. These points are chosen in such a way that the results for a particular numerical integration scheme are the most accurate. The location of these points will vary based on the integration scheme used.

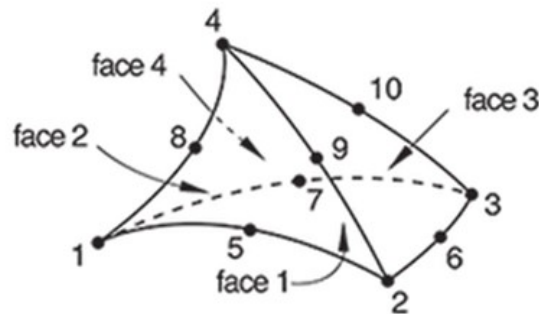


Figure 5.11 10-node tetrahedral element

5.4 SHALLOW EMBEDMENT SPECIMENS

Simulated slab specimens tested at the University of Kansas by Ghimire et al. (2018) were analyzed. The specimens consisted of a concrete slab in which headed bars representing column longitudinal reinforcement were embedded. The slab was designed as a simply supported beam to resist bending and shear. The specimens contained one, two, or three headed bars subjected to different loading conditions, with just one bar loaded at a time. In slabs with more than one headed bar, the bars were installed far enough apart so that the anchorage failure of one bar did not affect the anchorage capacity of the others. The specimen width was selected to be greater than the diameter of the anticipated concrete breakout failure surface. According to ACI 318-19 (Section 17.5.1.3.1 and Figure R17.5.1.3a), the anticipated concrete breakout failure surface can be defined as an area with a radius of $1.5\ell_{eh}$ measured from the center of the headed bar, where ℓ_{eh} is the embedment length of the headed bar.

In this section, specimens with a headed bar embedded at the center of the slab, a headed bar embedded close to the edge with unsymmetrical supports, and specimen with a headed bar embedded close to the edge and symmetrical supports are modeled. The specimen dimensions, the testing conditions, and finite element meshing, and boundary conditions are described in the following sections.

5.4.1 Specimen with One Headed Bar Embedded at the Center

The test specimen, specimen 8-5-F4.1-6#5-6 (Ghimeri et al. 2018), contained a single headed bar embedded at the center of the slab. The dimensions and details for this specimen are shown in Figure 5.12a. The specimen was tested using a self-reacting frame as shown in Figure 5.12b. The self-reacting frame consisted of two steel spreader beams placed along the longest dimension of the specimen (See Figure 5.12b). An upward force (tension force) was applied on the anchored bar using a hydraulic jack placed on top of the spreader beams (See Figure 5.12b). To prevent the beam from touching the slab, plates that served as support plates ($1 \times 6 \times 12$ in.) were used. The clear distance between the supports and the headed bar was 47.3 in., as shown in Figure 5.12b (for the FE analysis this distance was taken to the center of plate).

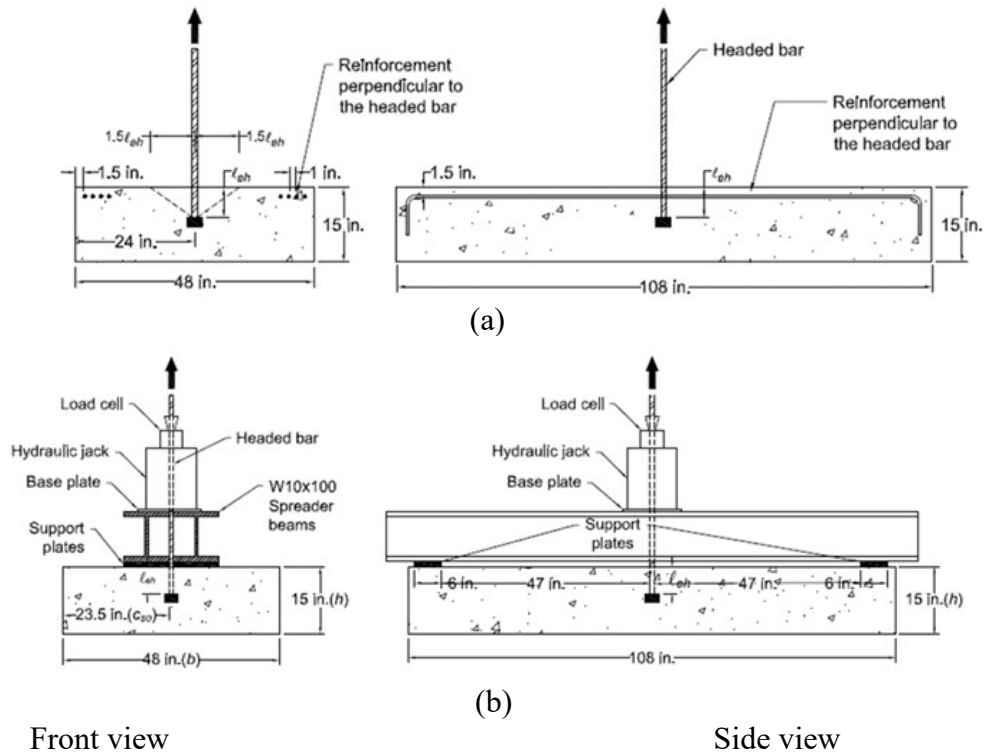


Figure 5.12 (a) Details of the specimen with one headed bar embedded at center of slab
 (b) Configuration of test for specimen with one headed bar embedded at center of slab (Ghimire et al. 2018)

The specimen had an embedment length ℓ_{eh} of 8.4 in., a concrete compressive strength f_{cm} of 4200 psi, a bar diameter d_b of 1 in., and a head with a net bearing area of $4.1A_b$, where A_b is the area of the bar. The peak load in the test was 39.1 kips. Deflections were not measured.

The FE simulation components for this specimen consist of the concrete slab and the headed bar (for simplicity, the bar is modeled with a square cross-sectional area). The specimen was inverted for modeling. Due to symmetry along the X and Y axes, only one quarter of the specimen need be modeled. Figure 5.13 shows the specimen components and meshing. Generally, the interaction between the concrete and steel at the noncontact surface of the head is negligible, and for this reason a gap is left to simplify the calculation and limit errors (see Figure 5.13a). In addition, the headed bar contact surface is modeled as a “master” and the concrete contact surface is modeled as a “slave.” When both surfaces in contact are deformable, ABAQUS allows the harder, the master, to penetrate into the softer, the slave.

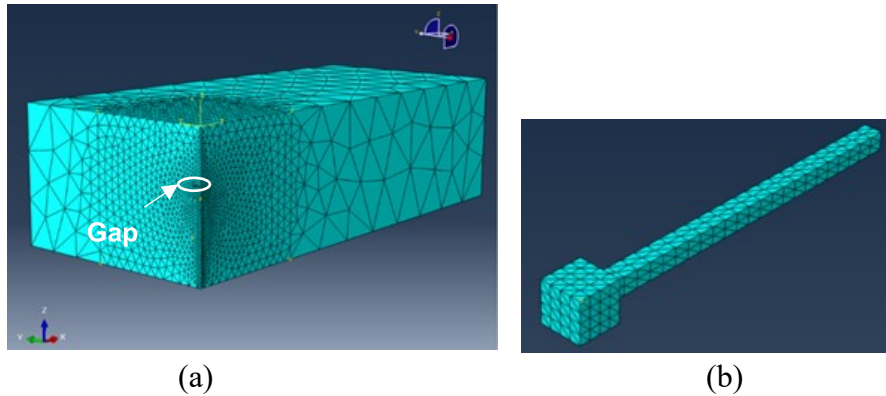


Figure 5.13 Simulation components and meshing. (a) Concrete and (b) Headed bar

Suitable boundary conditions (BC1) are applied to the simulation, as shown in Figure 5.14. The model is restrained to prevent the nodes from translating in x-direction at surface 1 and in z-direction at surface 2. The load is applied as a displacement at the non-headed end of the bar.

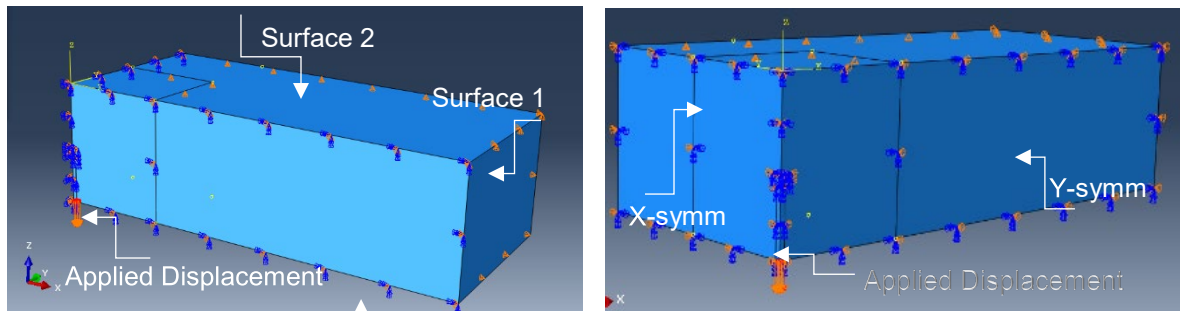


Figure 5.14 Boundary conditions 1 (BC1)

5.4.2 Specimen with One Bar Embedded Close to the Edge with Unsymmetrical Supports

The test specimen, specimen 8-5-F4.1-2#8-6 (Ghimeri et al. 2018), contained two headed bars embedded close to the edges at opposite ends of the slab. The dimensions and details for the specimen are shown in Figure 5.15a. The specimen was tested so that the clear distance between the proximal support and the headed bar was 10 in., while the clear distance between the distant support and the headed bar was 44.5 in., as shown in Figure 5.16b (for FE analysis this distance was taken to the center of the support). This arrangement was used to represent a column that is supported by a foundation and subjected to bending. The headed bar represents longitudinal reinforcement in the column, and the reaction support close to the headed bar represents the

compression zone of the column. The other reaction support was placed far away from the anchored bar to avoid interaction with the concrete breakout failure surface. During the test, only one bar was loaded at a time and, thus just one headed bar is modeled.

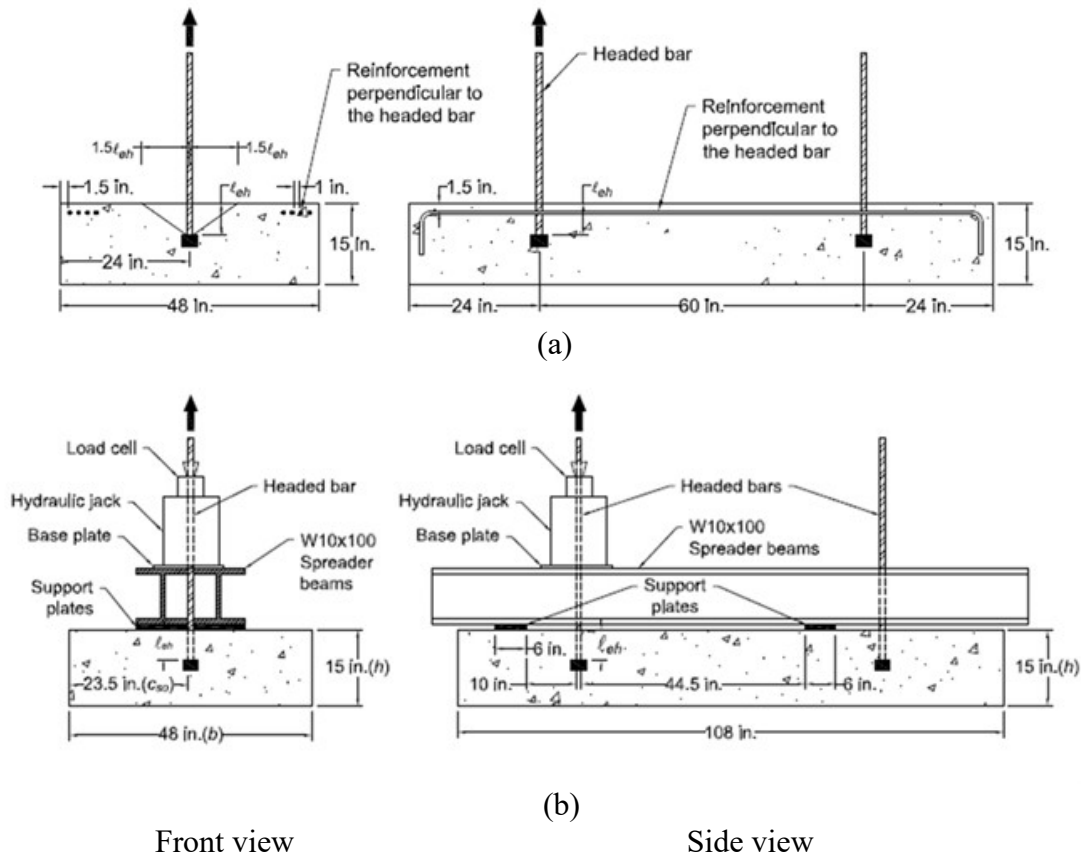


Figure 5.15 (a) Details of the specimen with two headed bars embedded close to the edges, Configuration of test for specimen with two headed bars embedded close to the edges (Ghimire et al. 2018)

The specimen had an embedment length ℓ_{eh} of 6.0 in., a concrete compressive strength f_{cm} of 7390 psi, a bar diameter d_b of 1 in., and a head with a net bearing area of $4.1A_b$, where A_b is the area of the bar. The peak load in the test was 66.0 kips. Deflections were not measured.

The FE simulation components consist of a headed bar and a concrete slab. Only half of the specimen is modeled because of the symmetry along the y-axis. Figure 5.16 shows the specimen meshing.

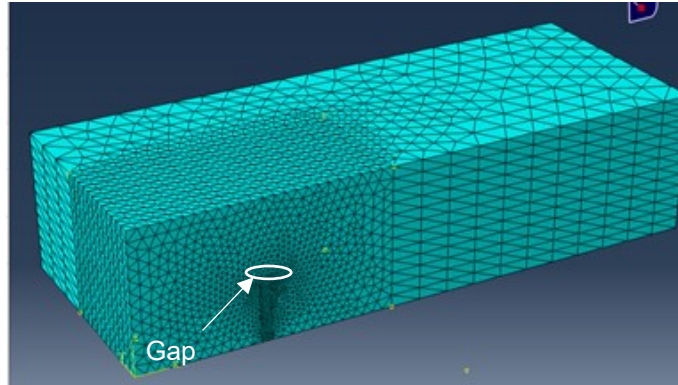
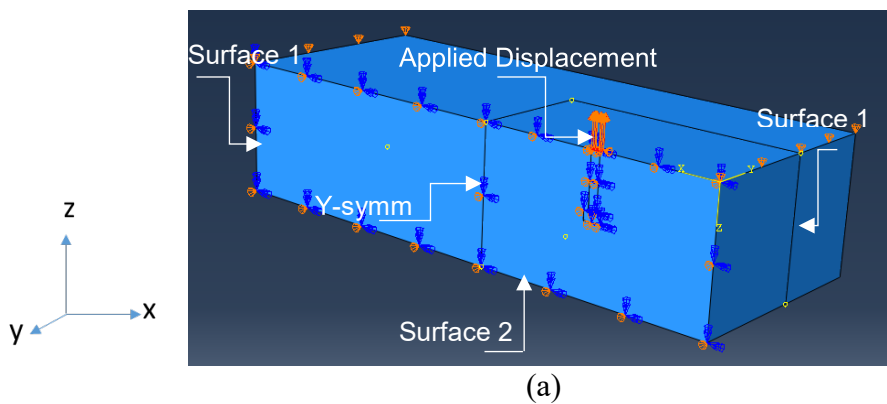


Figure 5.16 Specimen meshing

Suitable boundary conditions were applied to the simulation after assembling its components together as shown in Figure 5.17. As in the first simulation, the headed bar contact surface is modeled as a master and the concrete contact surface is modeled as a slave. Three different sets of boundary condition (BC1, BC2, and BC3), as shown in Figure 5.17a, b, and c, were used. The purpose of using different boundary conditions is to examine effect of the boundary condition on accurately simulating the actual boundary condition since it is not easy to identify the actual boundary condition from the test. Figure 5.17a shows boundary condition 1 (BC1), which is similar to the boundary condition shown in Figure 5.14. Figure 5.17b shows boundary condition 2 (BC2) in which the movement of the nodes in z-axis at edge 1 and 2 is restrained. Figure 5.17c shows the simulation with boundary condition 3 (BC3) where the nodes along the z-direction at strip 1 and 2 are restrained.



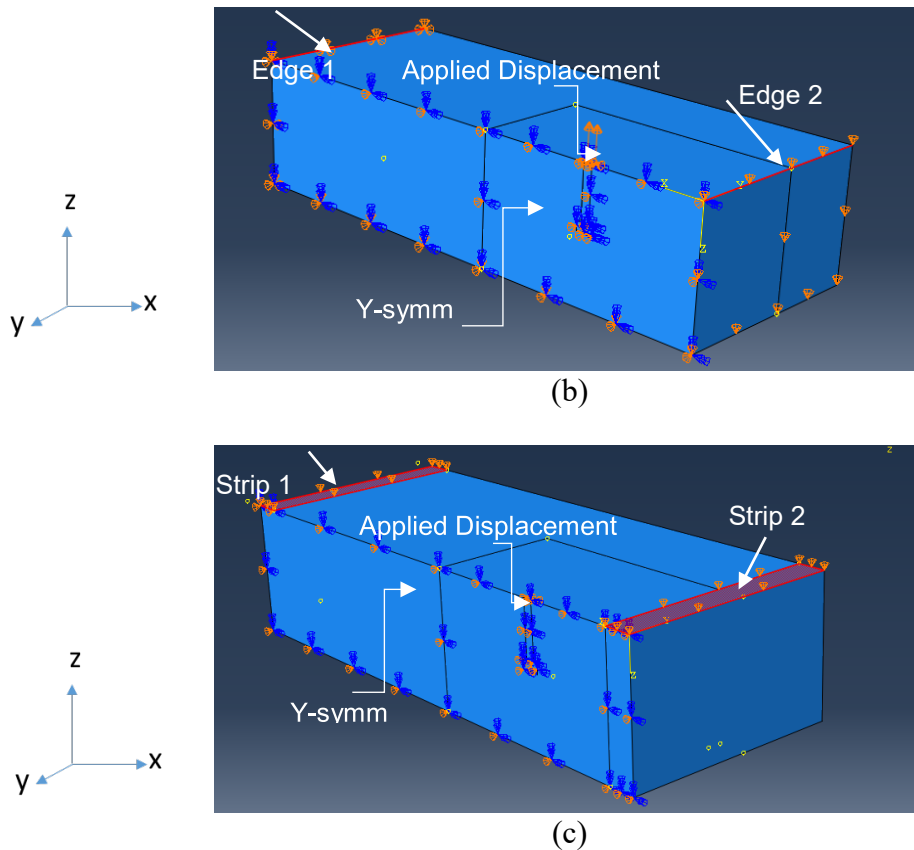


Figure 5.17 Boundary conditions (a) BC1, (b) BC2, and (c) BC3

5.4.3 Specimen with One Bar Embedded Close to the Edge with Symmetrical Supports

The test specimen, specimen 8-5-F4.1-4#5-6 (Ghimeri et al. 2018), contained three headed bars embedded in the slab. The dimensions and details for this specimen are shown in Figure 5.18a. The specimen was tested so that both supports were placed out of the anticipated failure area as shown in Figure 5.18b. The clear distance between the supports and the headed bar was 16.5 in (for the FE analysis, this distance was taken to the center of the support). During the test, only one bar was loaded at a time and, thus just one headed bar is modeled representing the bar which is installed close to the edge.

The specimen had an embedment length ℓ_{eh} of 6.0 in., a concrete compressive strength f_{cm} of 5180 psi, a bar diameter d_b of 1 in., and a head with a net bearing area of $4.1A_b$, where A_b is the area of the bar. The peak load in the test was 53.4 kips. Deflections were not measured.

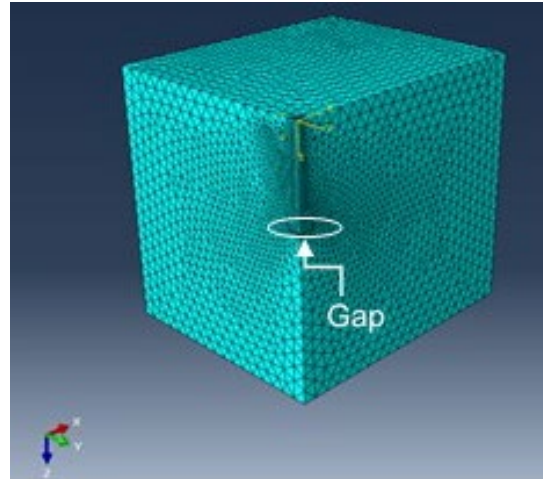


Figure 5.19 Simulation components and meshing

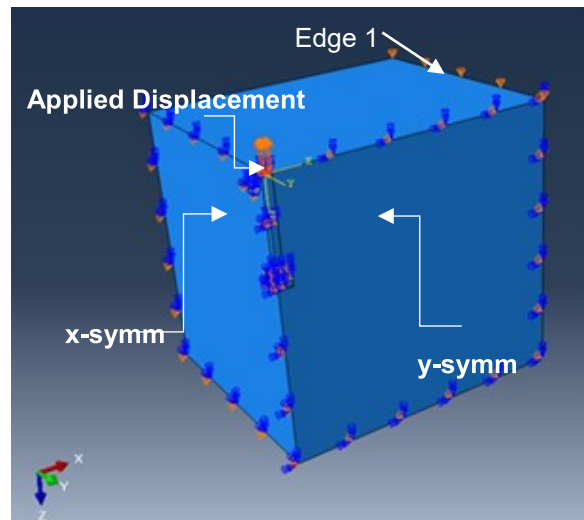


Figure 5.20 Boundary conditions (BC2)

Reinforcement was added perpendicular to the headed bar in the FE model based on the design of the test specimen. Figure 5.21a shows the cross section of the modeled specimen and the position of the reinforcement perpendicular to the headed bar, which consists of No. 5 (No. 16) reinforcing bars. In the model, the reinforcement perpendicular to the headed bar was perfectly bonded with the surrounding concrete. Figure 5.21b shows the FE model.

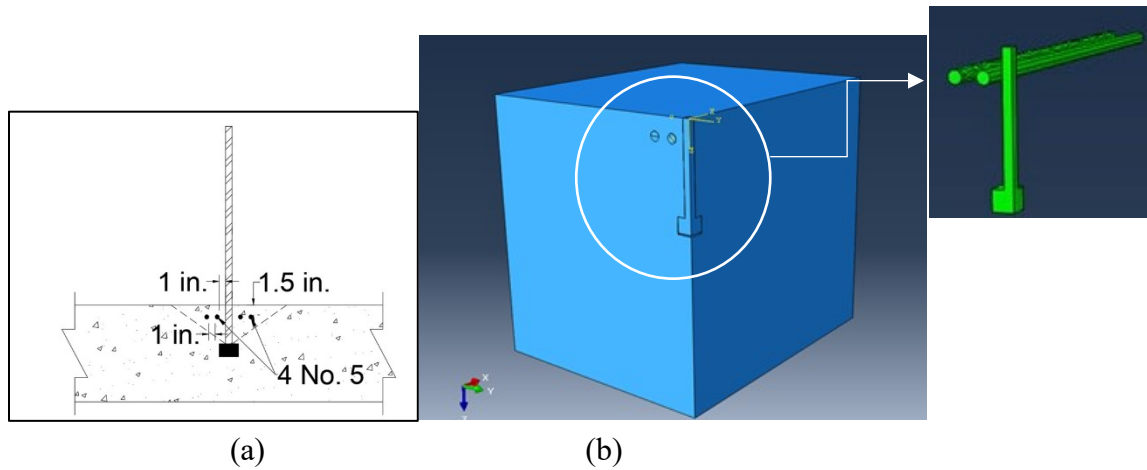


Figure 5.21 (a) Cross section area of the modeled specimen, (b) Simulation with perpendicular reinforcement

5.5 BEAM-END TEST SPECIMENS

In a beam-end specimen, the reinforcing bars are embedded in a concrete block and a tensile force is applied to the reinforcing bar. The compressive force (reaction) is located away from the reinforcing bars to minimize confinement of the concrete around the test bar.

In this section, a beam-end specimen tested by Darwin and Graham (1993) is simulated. Darwin and Graham tested beam-end specimens to study the effect of deformation height and relative rib area on the bond strength of straight bars with and without confining reinforcement. The height of the deformations ranged from 0.05 in. to 0.1 in. and the relative rib area ranged from 0.05 to 0.2. For this study, only the specimen without confining reinforcement was modeled. The specimen details are shown in Figure 5.22.

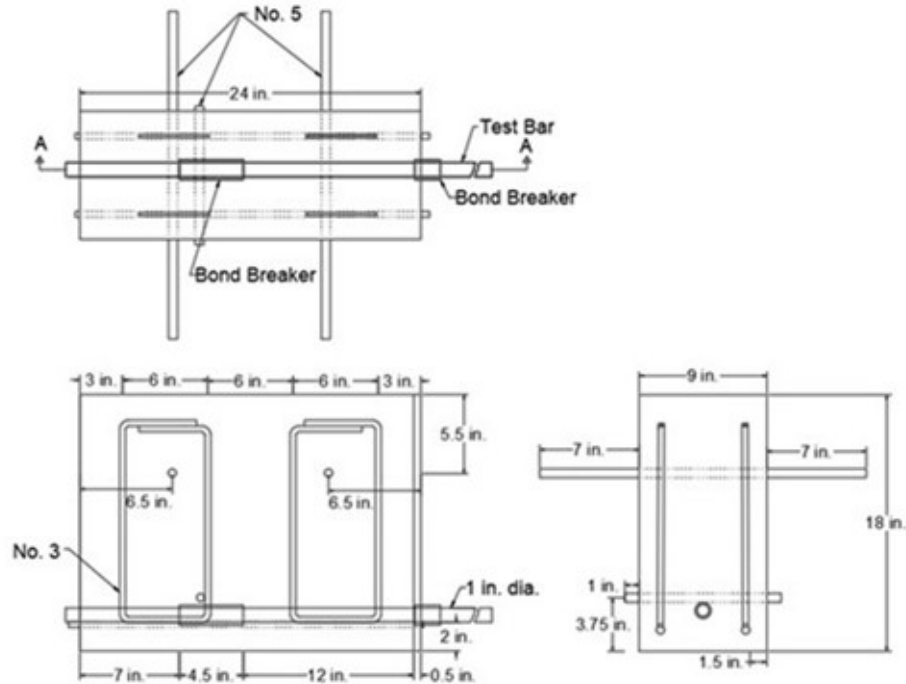


Figure 5.22 Details of the beam-end specimen without confining reinforcement (figure after Darwin and Graham 1993)

Tholen and Darwin (1996) performed a finite element study to model a beam-end specimen. Their finite element simulation was a portion of the full specimen, as shown in Figure 5.23a and b. Figure 5.23a shows the portion of the specimen with a 6 in. embedment length and 1 in. concrete cover. Figure 5.23b shows the portion of the specimen with a 12 in. embedment length and 2 in. concrete cover. Tholen and Darwin (1996) modeled the steel and the concrete as linear elastic, but modeled cracking in the concrete using a fracture mechanics model. The individual deformations on the reinforcing bar were modeled, and the interaction between the steel and the concrete at the bearing surfaces of the deformations was based on the coefficient of friction, as measured by Idun and Darwin (1995, 1999).

Generally, failure of beam-end specimens includes the formation of a dominant crack that extends along the length of the bar and through the top cover, in addition to other planar cracks that radiate from the bar. These cracks result from tensile stresses in the concrete that are produced by bearing of the ribs (deformations on the bar) on the concrete as the bar moves through the concrete.

The results of Tholen and Darwin (1996) show that, as in practice, increasing the concrete cover increased the bond force at peak load. There was a nearly linear, but not proportional, relationship between bond strength and the product of bonded length and concrete cover measured to the center of the bar, also as observed in practice. Increasing either the bonded length or the cover increased the bond force at the peak load. As also observed by Brown, Darwin, and McCabe (1993), the relationship between the area of cracked concrete and the bonded length was not proportional. The results of these studies led to a more nuanced understanding of the mechanism of bond behavior and helped in developing a theoretical model to predict the bond strength.

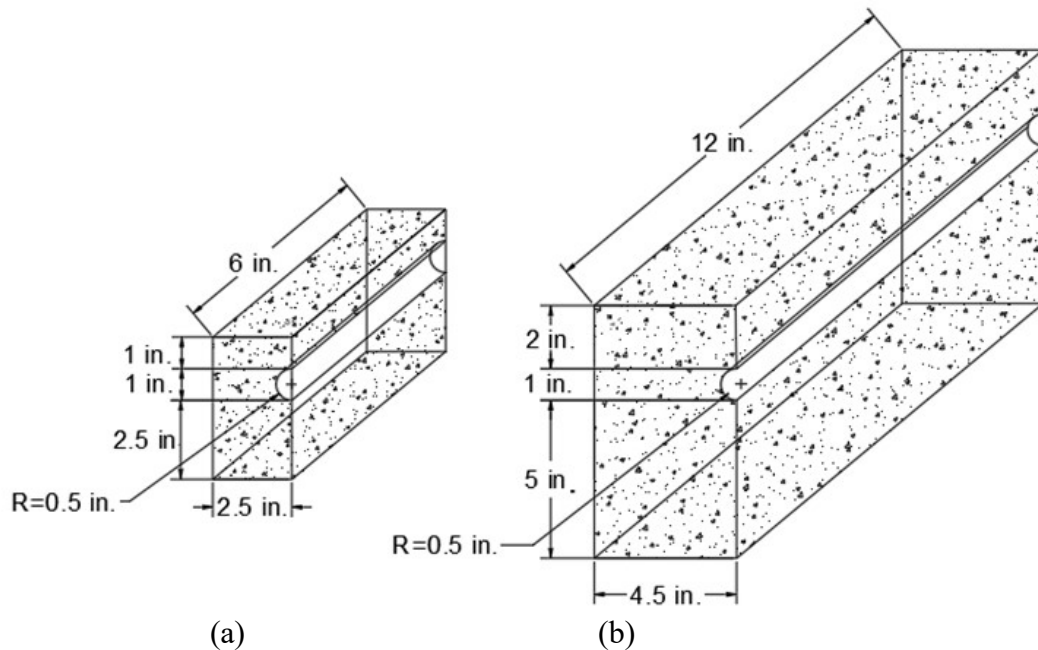


Figure 5.23 Beam-end specimen, (a) Portion of the specimen with 1 in. concrete cover and 6 in. bonded length, (b) Portion of the specimen with 2 in. concrete cover and 12 in. bonded length (figure after Tholen and Darwin 1996)

In this study, the FE simulation components consist of a concrete block and a steel bar (without ribs). Due to symmetry, only one-half of the specimen is modeled. Figure 5.24 shows the specimen components and meshing.

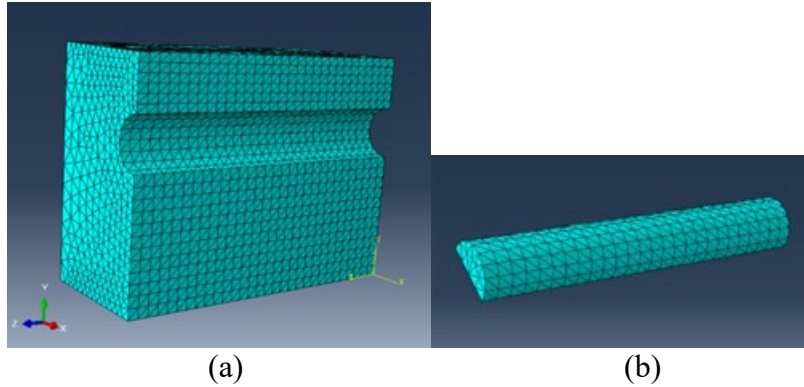


Figure 5.24 Specimen components and meshing, (a) concrete block, and (b) Steel bar

As in the slab models, the steel bar contact surface is modeled as a master and the concrete contact surface is modeled as a slave. The boundary conditions are applied, as shown in Figure 5.25, with nodes restrained in the z-direction at surface 1 and in the y-direction at surface 2. The load is applied as a displacement at the bar end.

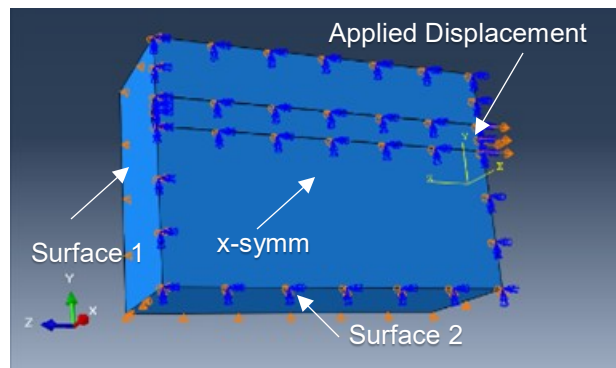


Figure 5.25 Boundary conditions

In this section, to calibrate the interfacial coefficients between the concrete and steel, the simulation is run first with the properties of the test specimen: bonded length of 12 in., concrete compressive strength f_{cm} of 4630 psi, bar diameter d_b of 1 in., and clear concrete cover of 2 in. The interfacial coefficients are adjusted so that the FE model results match that of the experimental data. Then, the calibrated interfacial coefficients are used to study the ability of the model to capture the effect of different concrete covers and bonded lengths. For this purpose, three simulations are conducted with 1, 2, and 3 in. concrete cover to the bar with 6 in. and 12 in. bonded lengths.

5.6 RESULTS AND DISCUSSION

In this section, the peak loads from the FE analyses are compared with those from tests performed by Ghimire et al. (2018) for the headed bars embedded in slab specimens, and the load-displacement curves and peak loads from the FE analyses are compared with those from the tests performed by Darwin and Graham (1993) for straight bars embedded in the beam-end specimens

5.6.1 Simulation Designation

The designation used for the simulations in this study is shown in Figure 5.26. The first two letters in a designation represent the simulation type: SC, represents a slab specimen with headed bar embedded at the center, SE represents a slab specimen with headed bar embedded close to edge with unsymmetrical supports, TE represents a slab specimen with headed bar embedded close to edge with symmetrical supports, and BE represent a beam-end test. (K) represents the linear-elastic traction-separation, the numbers (0.46, 0.23, and 0.23) represent the values of the stiffness coefficients K_{mn} , K_{ss} , and K_{tt} (defined in Section 5.3.3.1). The letter D represents the damage traction-separation coefficient (defined in Section 5.3.3.3), the number 0.0197 represents the value of δ_s° and δ_t° , the number 8 represents the concrete compressive strength in ksi, and BC1 represents the boundary condition.

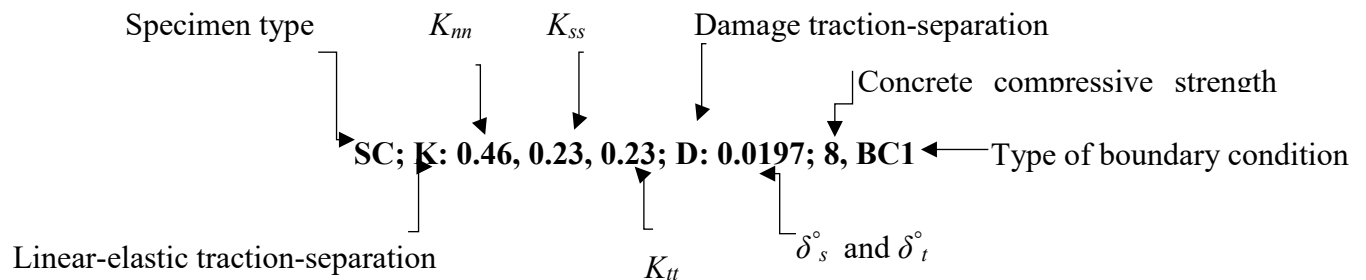


Figure 5.26 Specimens designation

5.6.2 Load-Displacement Behavior for Simulation with Headed Bar Embedded at the Center and Concrete Compressive Strength of 8 ksi

In this section, the effect of interfacial coefficients between concrete and steel on the load-displacement behavior and peak load is studied. The specimen described in Section 5.4.1 is modeled using a concrete compressive strength of 8 ksi (model parameters listed in Table 5.1) and

boundary condition 1 (BC1) (see Figure 5.14). Different linear-elastic traction separation and damage coefficients are used to model the interaction between concrete and the headed bar.

Figure 5.27 shows the load versus displacement at the non-headed end of the bar (loaded end) obtained using the FE model. Figure 5.27 shows that for the same concrete compressive strength (8 ksi), increasing the linear-elastic traction-separation coefficients (K_{nn} , K_{ss} , and K_{tt}) (defined in Section 5.2.3.1) from 0.23, 0.11, and 0.11 to 0.46, 0.23, and 0.23 kip/in. and keeping the damage (initiation and evolution) coefficient constant at 0.1969 in. (defined in Section 5.2.3.2) resulted in a stiffer load-displacement curve with a larger failure load.

Similarly, Figure 5.28 shows load versus displacement at the loaded end of the bar for the same concrete compressive strength and linear-elastic traction-separation coefficients K_{nn} , K_{ss} , and K_{tt} of 0.11, 0.061, and 0.06 kip/in., respectively. Increasing the values of the interfacial damage parameters (initiation and evolution) from (0.00004 in. to 0.0118 in.) results in stiffer, stronger behavior. The values of the linear-elastic coefficients and damage (initiation and evolution) coefficients are listed in Table 5.2.

In summary, Figures 5.28 and 5.29 show that for the same concrete compressive strength, increasing the linear-elastic traction-separation coefficients and damage (initiation and evolution) coefficient results in stiffer a load-displacement curve and a larger peak load. Figure 5.29 also shows that all the load-displacement curves have similar peak loads (about 41 kips), except for the simulation SC; k: 0.11, 0.06, 0.06; D: 0.0118; 8, BC1, which has a peak load of 50.0 kips.

To determine which set of parameters best represents actual concrete behavior, two of the models with peak loads close to 40 kips (simulations SC; k: 0.11, 0.06, 0.06; D: 0.0059; 5, BC1, and SC; k: 0.11, 0.06, 0.06; D: 0.0039; 5, BC1) were run with a concrete compressive strength of 5 ksi, matching one of the specimens tested by Ghimire et al. (2018) . As will be shown in Section 5.6.2.1, the simulation SC; k: 0.11, 0.06, 0.06; D: 0.0039; 5, BC1 provided a good agreement with the test result, while the simulation with SC; k: 0.11, 0.06, 0.06; D: 0.0059; 5, BC1 did not converge.

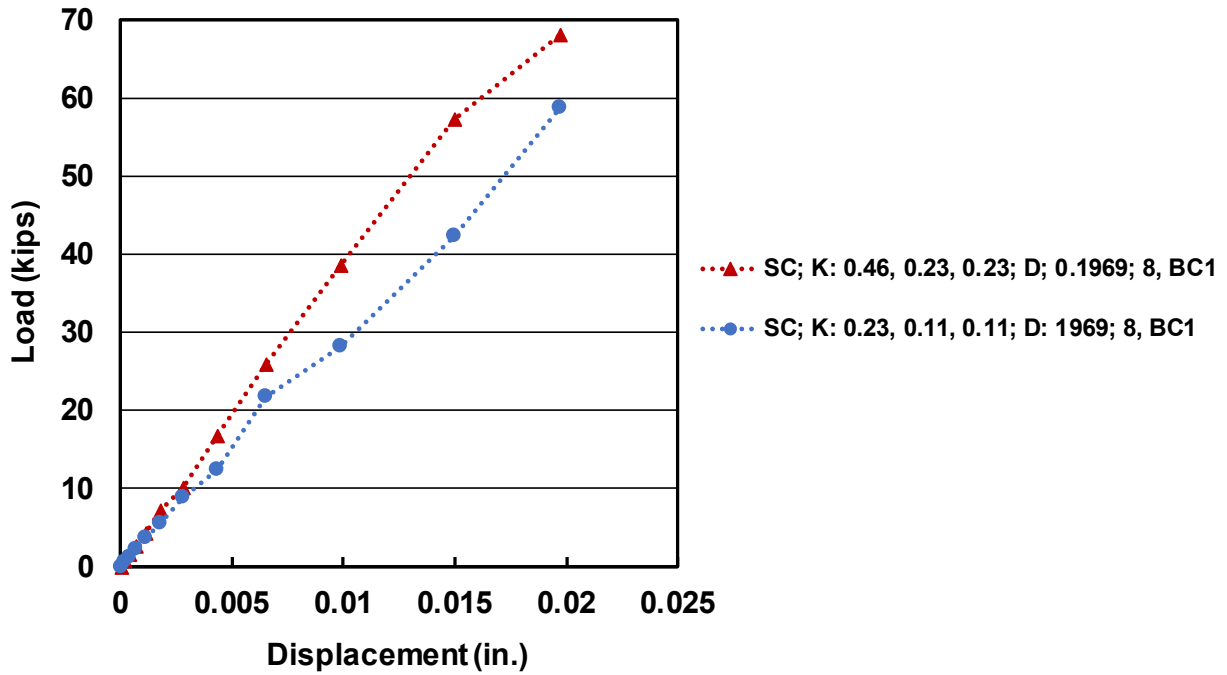


Figure 5.27 Load-displacement curve for the specimen with headed bar embedded at the center with different linear-elastic coefficients

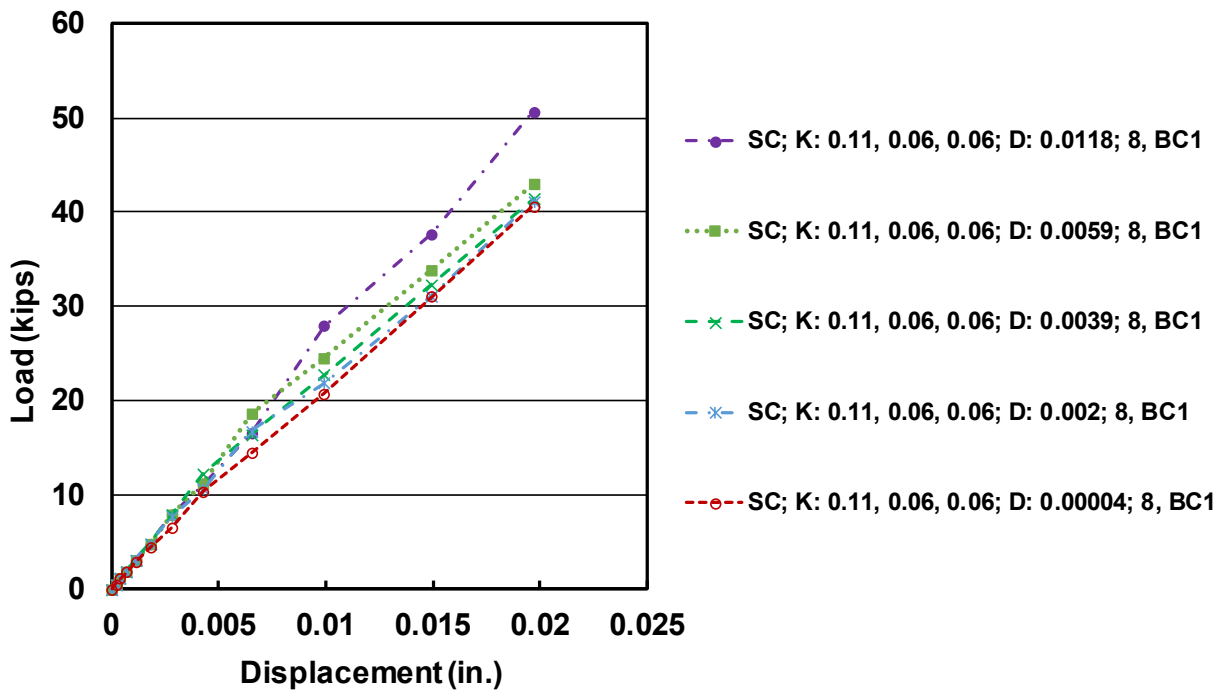


Figure 5.28 Load-displacement curve for the specimen with headed bar embedded the center with different damage (initiation and evolution) coefficients

Table 5.2 Values of linear-elastic and damage (initiation and evolution) coefficients

Slab specimen	Linear -elastic			Damage-initiation			Damage-evolution		
	K_{nm} (kip/in)	K_{ss} (kip/in)	K_{tt} (kip/in)	δ_n° (in.)	δ_s° (in.)	δ_t° (in.)	δ_m^f (in.)	M_{m1}	M_{m2}
SC; k: 0.46, 0.23, 0.23; D: 0.1969; 8, BC1	0.46	0.23	0.23	0.591	0.1969	0.1969	1.772	0	0.5
							0.709	0.01	0.5
							0.591	1	0.5
SC; k: 0.23, 0.11, 0.11; D: 0.1969; 8, BC1	0.23	0.11	0.11	0.591	0.1969	0.1969	1.772	0	0.5
							0.709	0.01	0.5
							0.591	1	0.5
SC; k: 0.11, 0.06, 0.06; D: 0.0118; 8, BC1	0.11	0.06	0.06	0.591	0.0118	0.0118	1.772	0	0.5
							0.047	0.01	0.5
							0.035	1	0.5
SC; k: 0.11, 0.06, 0.06; D: 0.0059; 8, BC1	0.11	0.06	0.06	0.591	0.0059	0.0059	1.772	0	0.5
							0.018	0.01	0.5
							0.017	1	0.5
SC; k: 0.11, 0.06, 0.06; D: 0.0039; 8, BC1	0.11	0.06	0.06	0.591	0.0039	0.0039	1.772	0	0.5
							0.024	0.01	0.5
							0.012	1	0.5
SC; k: 0.11, 0.06, 0.06; D: 0.002; 8, BC1	0.11	0.06	0.06	0.591	0.002	0.002	1.772	0	0.5
							0.007	0.01	0.5
							0.006	1	0.5
SC; k: 0.11, 0.06, 0.06; D: 0.00004; 8, BC1	0.11	0.06	0.06	0.591	0.00004	0.00004	1.772	0	0.5
							0.002	0.01	0.5
							0.001	1	0.5
SC; k: 0.11, 0.06, 0.06; D: 0.0039; 5, BC1**	0.11	0.06	0.06	0.591	0.0039	0.0039	1.772	0	0.5
							0.024	0.01	0.5
							0.012	1	0.5

**Simulation with 5 ksi concrete compressive strength

5.6.2.1 Load-Displacement Behavior for Simulation with Headed Bar Embedded at the Center and Concrete Compressive Strength of 5 ksi

The simulation with a headed bar embedded at the center of the slab was run using a concrete compressive strength of 5 ksi ($f_{cm} = 4200$ psi; concrete model parameters are listed in Table 5.1). Using a concrete compressive strength of 5 ksi provides a reasonable match with the test specimen properties. The simulation is designated as a SC; k: 0.11, 0.06, 0.06; D: 0.0039; 5, BC1. The values of linear-elastic coefficients and damage (initiation and evolution) coefficients for the specimen SC; k: 0.11, 0.06, 0.06; D: 0.0039; 5, BC1 are listed in Table 5.2. Figure 5.29 shows load versus displacement curve for the FE model. The peak load obtained from the FE analysis is 37.6 kips, which compares well with the peak load from the laboratory test of 39.1 kips (Ghimire et al. 2018). Based on this result, these parameters were used to evaluate other specimens tested by Ghimire et al. (2018) as described in the next section.

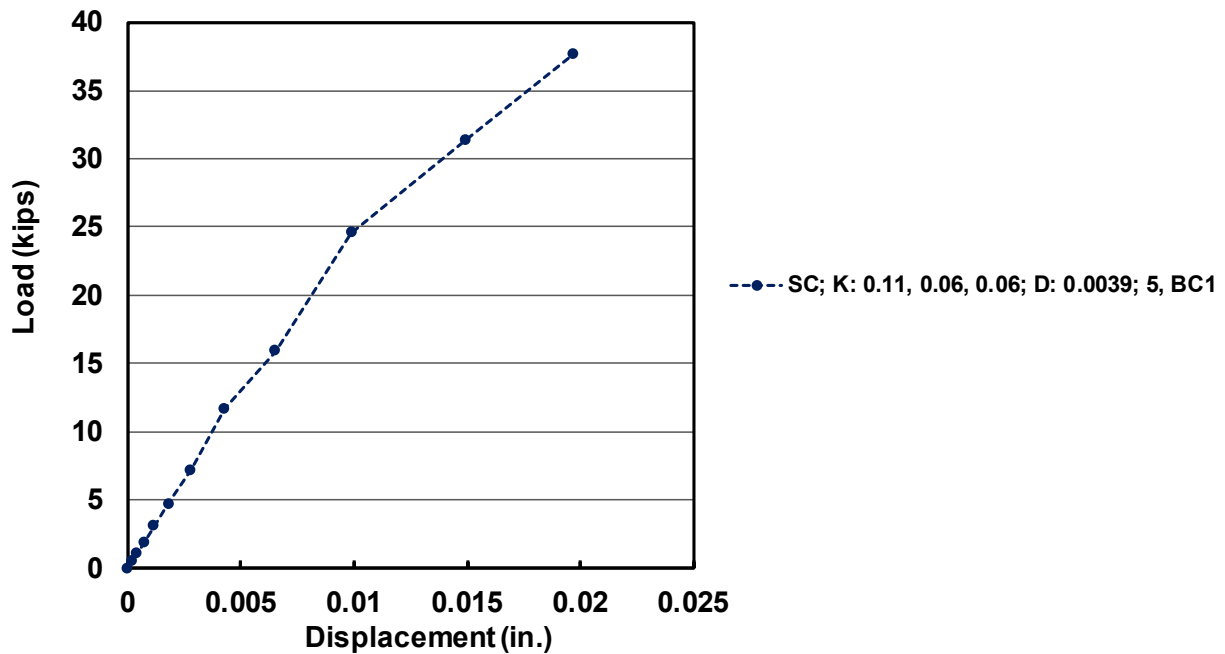


Figure 5.29 Load-displacement curve for simulation SC; k: 0.11, 0.06, 0.06; D: 0.0039; 5, BC1

5.6.2.2 Load-Displacement Behavior for Simulation with Headed Bar Embedded Close to Edge with Unsymmetrical Supports and Concrete Compressive Strength of 8 ksi

The simulation is designated as a (SE; K: 0.11, 0.06, 0.06; D: 0.0039; 8, BC1) with details in Section 5.4.2 (representing the specimen with a headed bar embedded close to edge with unsymmetrical supports) is modeled using concrete compressive strength of 8 ksi ($f_{cm} = 7390$ psi; model parameter listed in Table 5.1) and boundary condition 1 (BC1) (see Figure 5.17a). The linear-elastic traction separation and damage coefficients calibrated for the simulation (SC; K: 0.11, 0.06, 0.06; D: 0.0039; 5, BC1) with one headed bar embedded at the center are applied on this simulation. Figure 5.30 shows the load versus displacement at the end of the headed bar (loaded end). The peak load for the simulation SE; K: 0.11, 0.06, 0.06; D: 0.0039; 8, BC1, 66.0 kips compares well with the peak loads of the two headed bars in the test specimen, 64.4 and 65.0 kips.

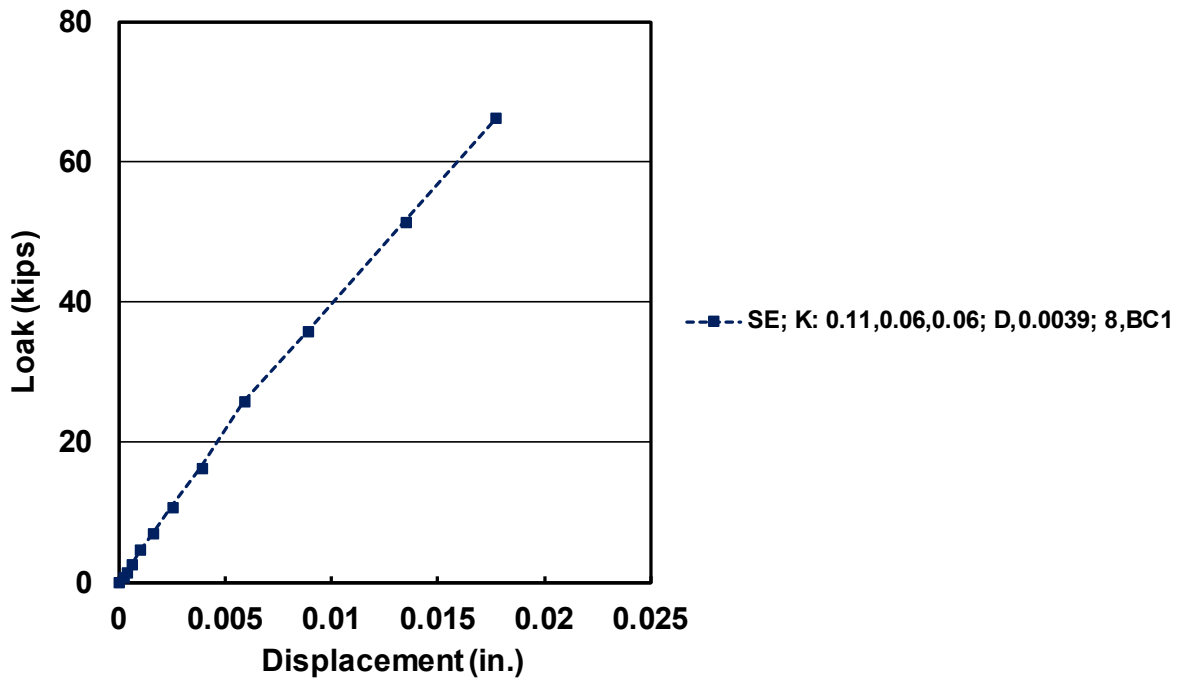


Figure 5.30 Load-displacement curve for simulation SE; K: 0.11, 0.06, 0.06; D: 0.0039; 8, BC1

As described in Section 5.4.2, boundary conditions BC1, BC2, and BC3, shown in Figure 5.17a, b, and c, were used to examine the response of the FE model as a function of the boundary conditions. Figure 5.31 shows the load versus displacement at the non-headed end of the bar (loaded end) for boundary conditions BC1, BC2, and BC3. The values of linear-elastic and damage (initiation and evolution) coefficients used in this comparison are the same as those used for the simulation shown in Figure 5.29. The values of linear-elastic and damage (initiation and evolution) coefficients are listed in Table 5.3. The peak load for the simulations SE; K: 0.11, 0.06, 0.06; D: 0.0039; 8, BC1, SE; K: 0.11, 0.06, 0.06; D: 0.0039; 8, BC2, and SE; K: 0.11, 0.06, 0.06; D: 0.0039; 8, BC3 are 66.0 kips, 64.0 kips, and 61.0 kips, respectively, all of which compare favorably with the peak loads in the test of 64.4 and 65.0 kips, showing a relatively small sensitivity ($\approx 8\%$) to the boundary conditions. This low sensitivity is likely due to the dominance of the local stresses near the bar governing deformation and failure and the relatively remote nature of the boundaries with respect to the bar.

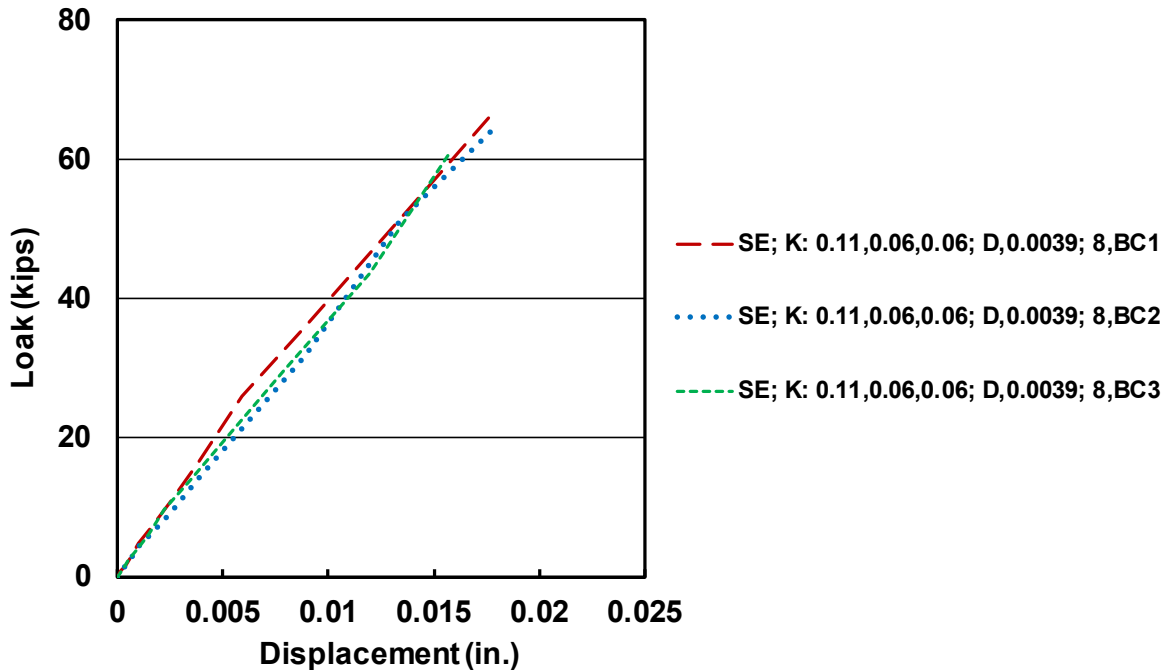


Figure 5.31 Load-displacement relationship for the simulation with headed bar imbedded close to edge with unsymmetrical supports using three different boundary conditions; the three simulations are; SE; K: 0.11, 0.06, 0.06; D: 0.0039; 8, BC1, SE; K: 0.11, 0.06, 0.06; D: 0.0039; 8, BC2, and SE; K: 0.11, 0.06, 0.06; D: 0.0039; 8, BC3

Table 5.3 Values of linear-elastic and damage (initiation and evolution) coefficients

specimen	Linear -elastic			Damage-initiation			Damage-evolution		
	K_{nn} (kip/in)	K_{ss} (kip/in)	K_{tt} (kip/in)	δ_n° (in.)	δ_s° (in.)	δ_t° (in.)	\mathcal{F}_m (in.)	M_{m1}	M_{m2}
SE K: 0.11, 0.06, 0.06; D: 0.0039; 8, BC1	0.11	0.06	0.06	0.591	0.0039	0.0039	1.772	0	0.5
							0.024	0.01	0.5
							0.012	1	0.5
SE; K: 0.11, 0.06, 0.06; D: 0.0039; 8, BC2	0.11	0.06	0.06	0.591	0.0039	0.0039	1.772	0	0.5
							0.024	0.01	0.5
							0.012	1	0.5
SE K: 0.11, 0.06, 0.06; D: 0.0039; 8, BC3	0.11	0.06	0.06	0.591	0.0039	0.0039	1.772	0	0.5
							0.024	0.01	0.5
							0.012	1	0.5

5.6.2.3 Load-Displacement Behavior for Simulation with Headed Bar Embedded Close to Edge with Symmetrical Supports and Concrete Compressive Strength of 5 ksi

The simulation designated as a (TE; K: 0.11, 0.06, 0.06; D: 0.0039; 5, BC2) with details in Section 5.4.3 (representing the specimen with headed bar embedded close to edge with

symmetrical supports) is modeled using concrete compressive strength of 5 ksi ($f_{cm} = 5180$ psi; model parameter listed in Table 5.1) and boundary condition 2 (BC2) (see Figure 5.20). The values of linear-elastic coefficients and damage (initiation and evolution) coefficients are listed in Table 5.4. The linear-elastic traction separation and damage coefficients calibrated for the simulation designated as a (SC; K: 0.11, 0.06, 0.06; D: 0.0039; 5, BC1) with one headed bar embedded at the center are applied to model the interaction between the concrete and headed bar in this simulation.

Figure 5.32 shows the load versus displacement at the non-headed end of the bar (loaded end). The peak load for slab specimen TE; K: 0.11, 0.06, 0.06; D: 0.0039; 5, BC2, 48.0 kips, compares well with the peak loads from the test, 53.4 and 53.5 kips.

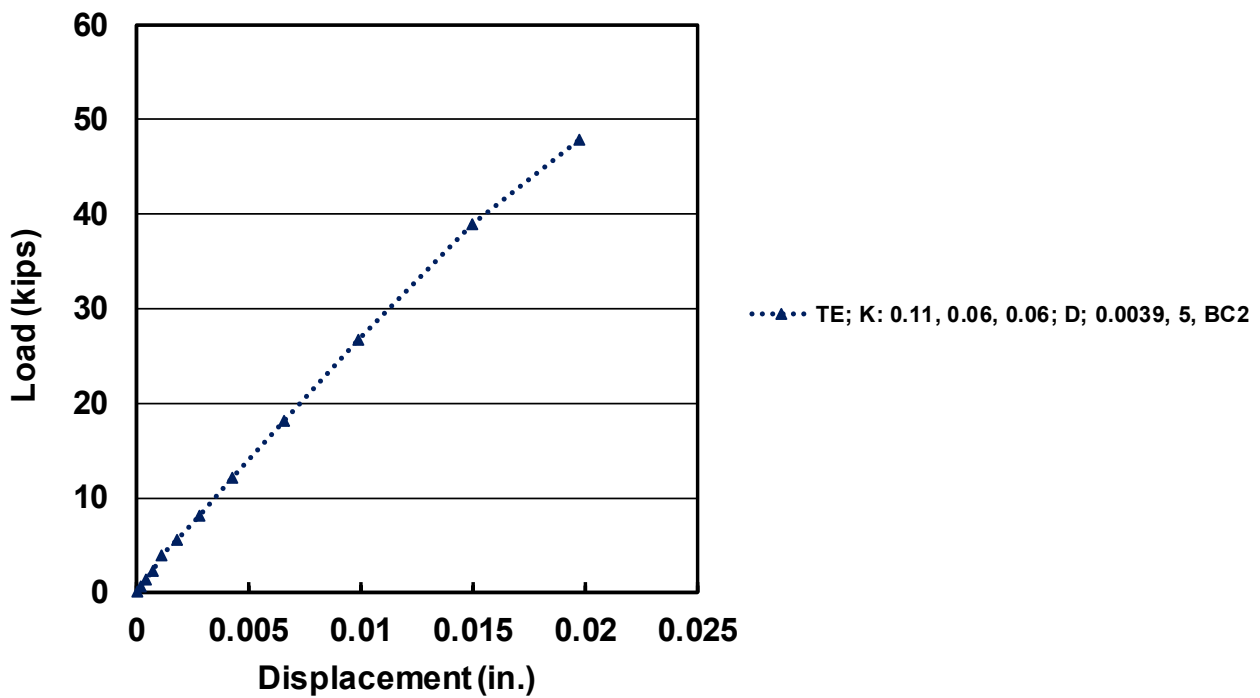


Figure 5.32 Load-displacement curve for the simulation TE; K: 0.11, 0.06, 0.06; D: 0.0039; 5, BC2

Table 5.4 Values of linear-elastic and damage (initiation and evolution) coefficients

specimen	Linear-elastic			Damage-initiation			Damage-evolution		
	K_{nn} (kip/in)	K_{ss} (kip/in)	K_{tt} (kip/in)	δ_n° (in.)	δ_s° (in.)	δ_t° (in.)	δ_m° (in.)	M_{m1}	M_{m2}
TE; k: 0.11, 0.06, 0.06; D;0.0039; 5, BC2	0.11	0.06	0.06	0.591	0.0039	0.0039	1.772	0	0.5
							0.024	0.01	0.5
							0.012	1	0.5

5.6.2.4 Comparison of Peak Loads

Figure 5.33 compares the peak loads from the test specimens with those obtained from the FE analyses for the simulations described in Sections 5.6.2.1 through 5.6.2.3. These results confirm the observation that as the anchor bar distance from the support increases beyond the anticipated failure area, the anchor peak load decreases. The reason for this behavior is the anchorage strength of a headed bar depends on the strut angle between the head and the compressive reaction. The flatter the angle, the lower the strength (Ghimire et al 2018). The comparisons also show that the granular micromechanics model accurately represents the behavior of reinforced concrete when the behavior of a member is dominated by the compressive and tensile properties of concrete, as it is in the slab specimens.

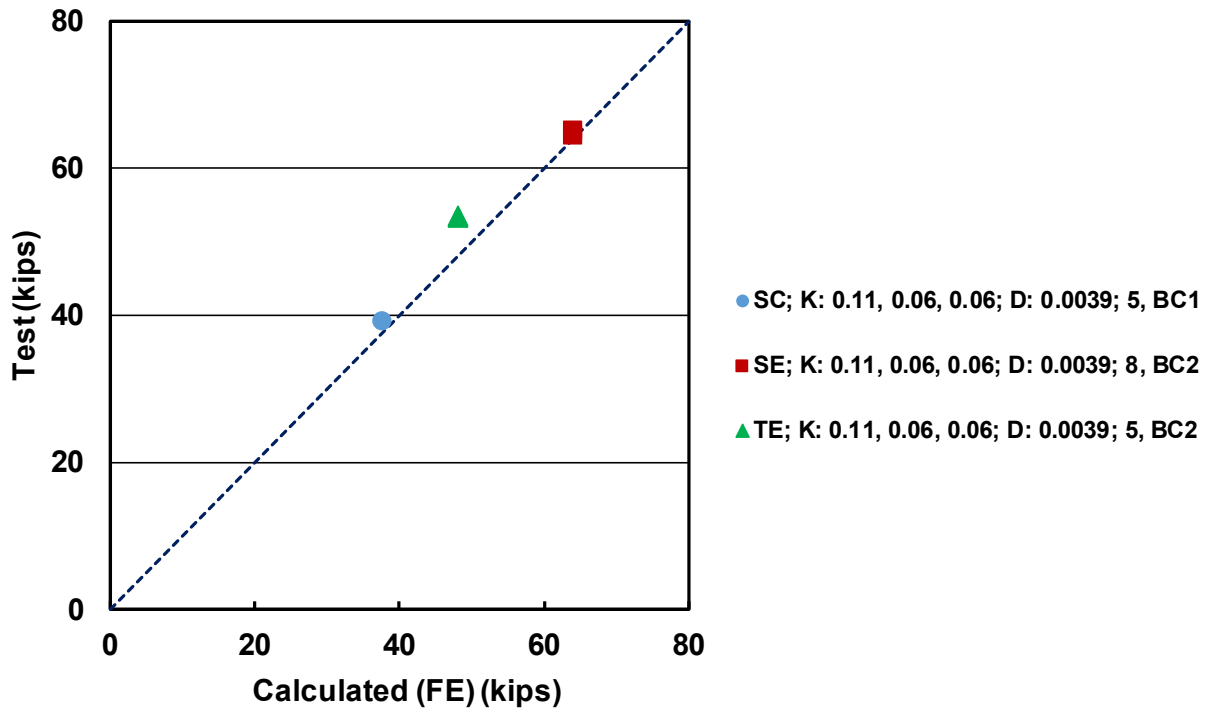


Figure 5.33 Test versus calculated for the simulations; Sc; K: 0.11, 0.06, 0.06; D: 0.0039; 5, BC1, SE; K: 0.11, 0.06, 0.06; D: 0.0039; 8, BC2, and TE; K: 0.11, 0.06, 0.06; D: 0.0039; 5, BC2

5.6.3 Reinforcement Strain

Figure 5.34 shows the calculated strain versus location along the headed bar for various levels of imposed force at the non-headed end of the bar for simulation SC; K: 0.11, 0.06, 0.06; D: 0.0039; 5, BC1, which represents the specimen with the headed bar embedded at the center (similar

behavior is expected for the other models). Figure 5.34 shows that the strain decreases along the bar towards the head. This change in strain along the bar is consistent with the assumption that a portion of the force in the bar is transferred from the bar to the concrete through bond along its length. This behavior is also consistent with the behavior of headed bars embedded within the CCT node of the test beams in both the current study (Chapter 3) and those tested by Thompson et al. (2005). Thompson et al. (2005) found that the anchorage of headed bars undergoes a transition as load is applied. Initially, load is carried by the bond force along the straight portion of the bar. As load increases, however, bond along the straight portion of the bar decreases (due to slippage), and some of the force is transferred to the head, which bears against the concrete. For simulation SC; K: 0.11, 0.06, 0.06; D: 0.0039; 5, BC1, the strain reading on the bar near the head remained less than 0.0001 until the applied force reached about 7.20 kips, at which point the strain began in increasing.

Figure 5.35a shows load versus strain near the head and near the concrete surface (inset Figure 5.23b shows the locations where the strain is calculated). Figure 5.35a shows that the calculated strain on the headed bar near the front face of the slab varies almost linearly with the load, while the calculated strain in the bar near the head has a nonlinear relationship with the applied load, reaching a value of approximately 0.0013 at the peak load. The nonlinear load-strain behavior near the head means that the development of the strain was slow in the beginning and then increased more rapidly with the increasing of the applied load. This behavior is consistent with the test results of the headed bars embedded in beam-column joint specimens and tested by Shao et al. 2016).

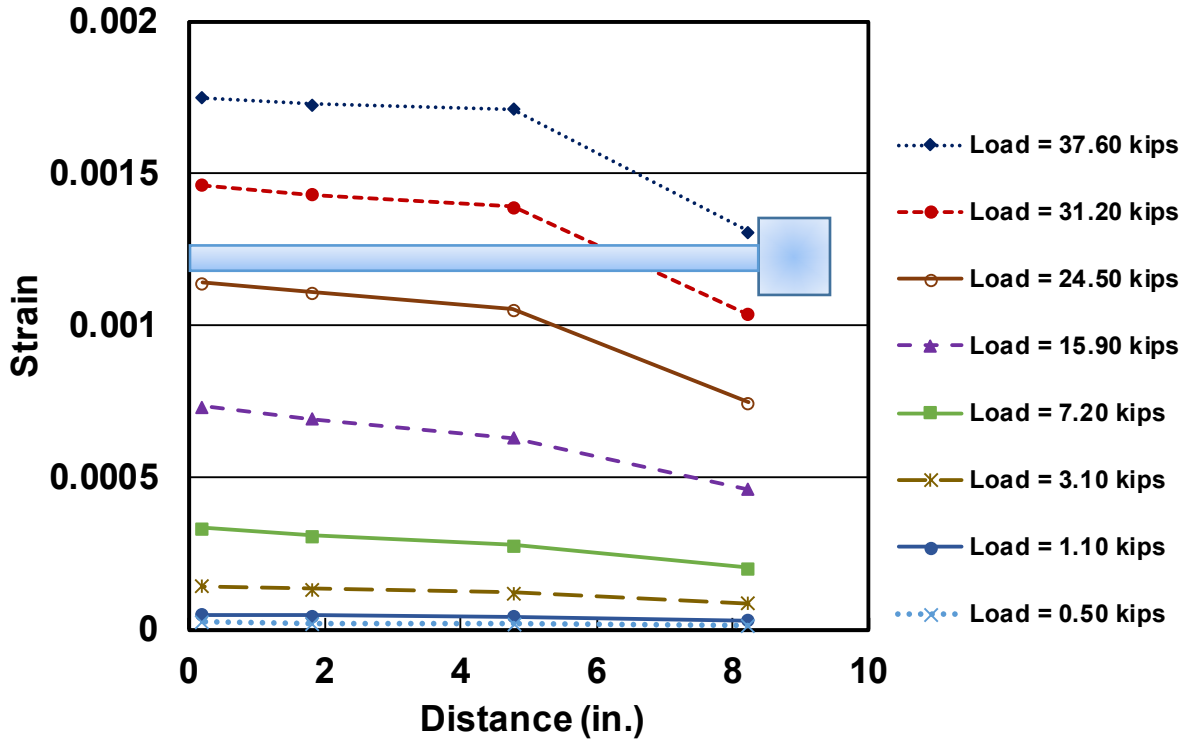


Figure 5.34 Strain along the headed bar for the specimen (SC; K: 0.11, 0.06, 0.06; D: 0.0039; 5, BC1)

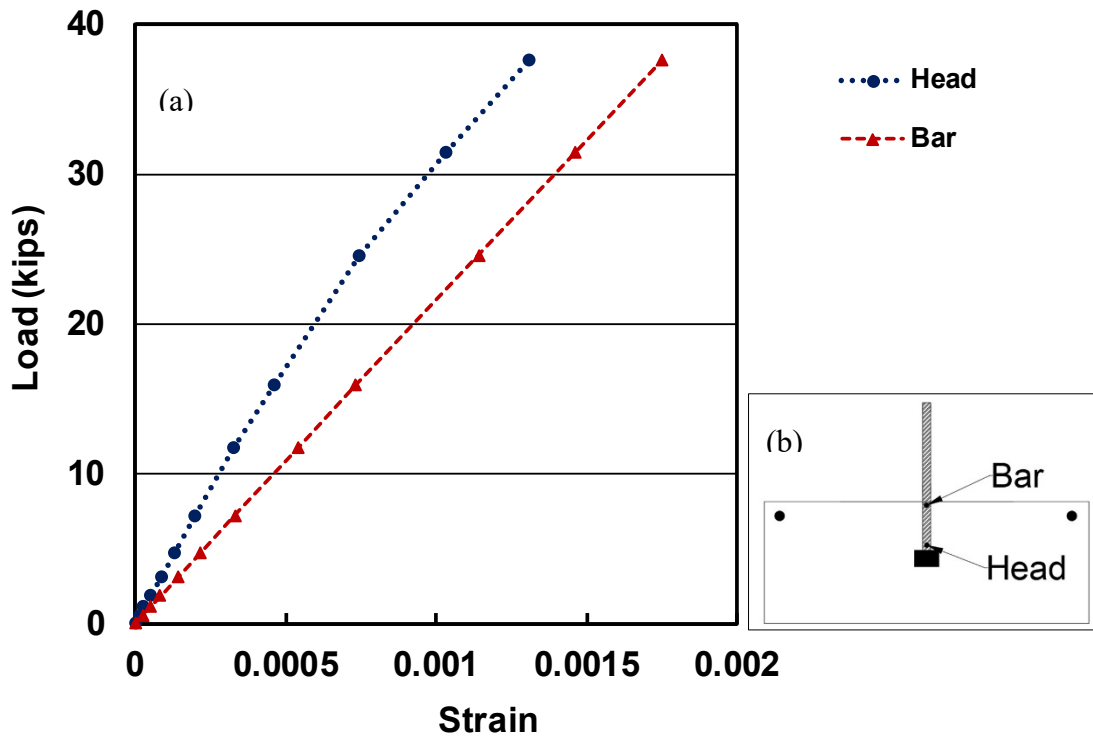


Figure 5.35 (a) Load versus strain in headed bar for slab specimen SC; K: 0.11, 0.06, 0.06; D: 0.0039; 5, BC1 (b) Calculated strain location

5.6.4 Summary

As described in Section 5.6.2.1, the interfacial coefficients between concrete and steel were calibrated based on the test results for the specimen with one headed bar embedded at the center. These coefficients were applied to models for the three slab specimen types with one headed bar embedded at the center, close to the edge with unsymmetrical supports, and close to edge with symmetrical supports. In addition, the effect of three sets of boundary conditions was studied. The results showed a good agreement between the value of the peak load from the test and the FE analysis. Further, the results showed that the granular micromechanics model accurately represents the behavior of reinforced concrete when the behavior of a member is dominated by the compressive and tensile properties of concrete, as it is in the slab specimens.

5.6.6 Beam-End Tests

5.6.6.1 Load-displacement Behavior

Figure 5.36 shows the load versus displacement measured at the loaded end of the bar for the set of calculations with different damage values compared with the test result for the beam-end test with details shown in Section 5.5. It is clear that the calculated results with a damage value of 0.0098 in. gave the best agreement with the test results. The values of linear-elastic and damage (initiation and evolution) coefficients are listed in Table 5.5.

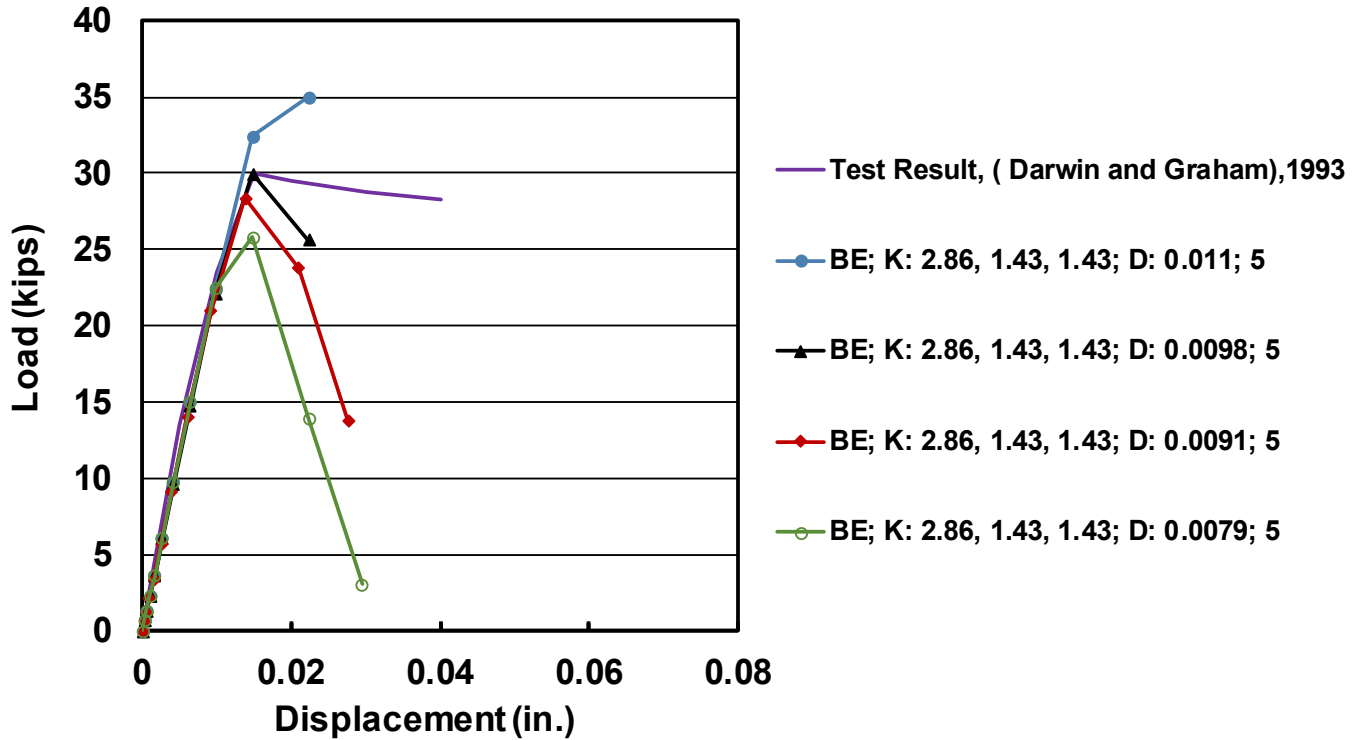


Figure 5.36 Load-displacement curve for the beam-end specimen (Darwin-Graham 1993) (12 in. embedment length and 2 in. concrete cover)

Table 5.5 Values of linear-elastic and damage (initiation and evolution)

specimen	Linear -elastic			Damage-initiation			Damage-evolution		
	K_{mn} (kip/in)	K_{ss} (kip/in)	K_{tt} (kip/in)	δ_n° (in.)	δ_s° (in.)	δ_t° (in.)	δ_m^f (in.)	M_{m1}	M_{m2}
BE; K: 2.86, 1.43, 1.43; D: 0.011; 5	2.86	1.43	1.43	0.591	0.011	0.011	1.7717	0	0.5
							0.0343	0.01	0.5
							0.0331	1	0.5
BE; K: 2.86, 1.43, 1.43; D: 0.0098; 5	2.86	1.43	1.43	0.591	0.0098	0.0098	1.7717	0	0.5
							0.0307	0.01	0.5
							0.0295	1	0.5
BE; K: 2.86, 1.43, 1.43; D: 0.0091; 5	2.86	1.43	1.43	0.591	0.0091	0.0091	1.7717	0	0.5
							0.0283	0.01	0.5
							0.0272	1	0.5
BE; K: 2.86, 1.43, 1.43; D: 0.0079; 5	2.86	1.43	1.43	0.591	0.0079	0.0079	1.7717	0	0.5
							0.0354	0.01	0.5
							0.0236	1	0.5

5.6.6.2 Effect of Different Embedment Lengths and Concrete Covers

Simulations were conducted with concrete clear covers to the bar of 1, 2, and 3 in. Each simulation considered bonded lengths of 6 and 12 in. The concrete compressive strength for these simulations was taken as 5 ksi. These simulations are similar to the simulation conducted by Tholen and Darwin (1996), described in Section 5.5 and shown in Figure 5.23b. Figures 5.37 and 5.38 show the load versus displacement calculated at the loaded end for the simulations with 1, 2, and 3 in. concrete cover for, respectively, 6 and 12 in. bonded lengths. The interfacial coefficients of the simulation are calibrated based on Darwin and Graham (1993) test specimen M31-12-5, which had a 2 in. concrete cover and a 12 in. bonded length. The linear-elastic traction-separation coefficients (K_{nn} , K_{ss} , and K_{tt}) of (2.86, 1.43, 1.43) kip/in. and damage (initiation and evolution) coefficient of (0.0098 in.) are used. These interfacial coefficients are also used for the simulations with 3 in. and 1 in. concrete cover. The values of linear-elastic and damage (initiation and evolution) coefficients are listed in Table 5.6.

Figures 5.37 and 5.38 show that the strength increases as the bonded length increases, but the strength does not increase with increasing of concrete cover, matching the observation of both the tests and in the FE model of Tholen and Darwin (1996). This observation indicates that this model can successfully represent the effect of bonded length but fails to simulate the effect of the bar deformations, which cause concrete to split and cause bond strength to be sensitive to cover – with increased cover requiring a greater force to cause splitting. These results demonstrate that, short of calibrating bond properties as a function of cover (and presumably bar spacing), or physically modeling deformation, a concrete-steel interface model of the type evaluated in this study will not produce a good match with member behavior in cases where member behavior is dominated by bar slip. To be generally applicable, a bond model must represent such behavior.

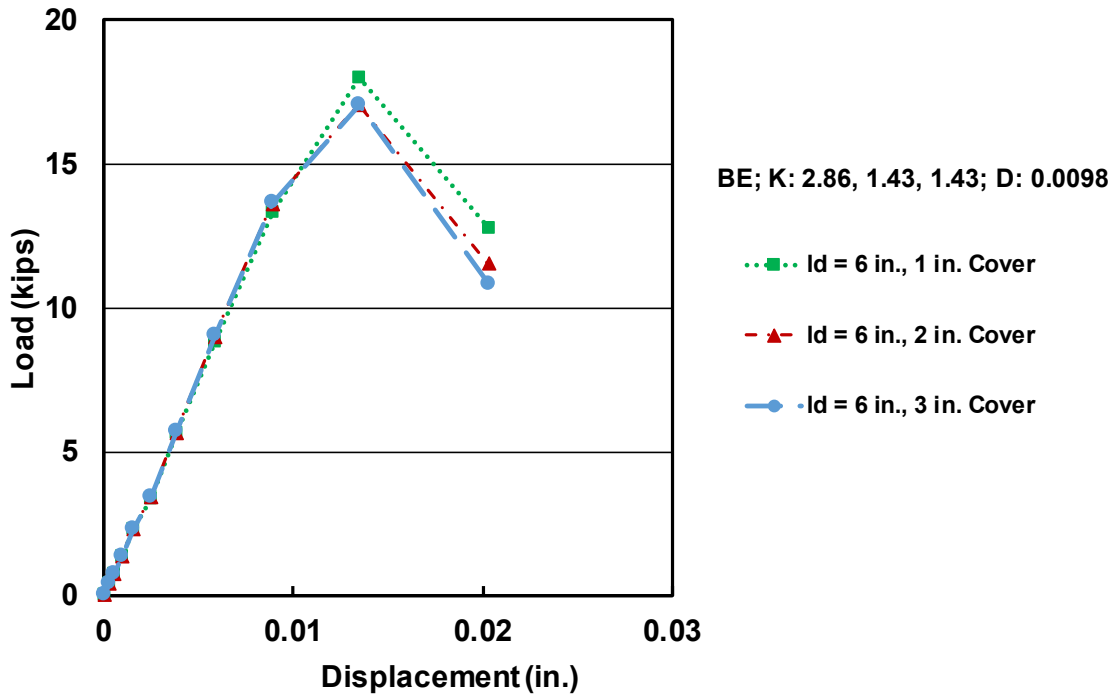


Figure 5.37 (a) Load-versus displacement for 1, 2, and 3 in. concrete covers with 6 in. bonded length

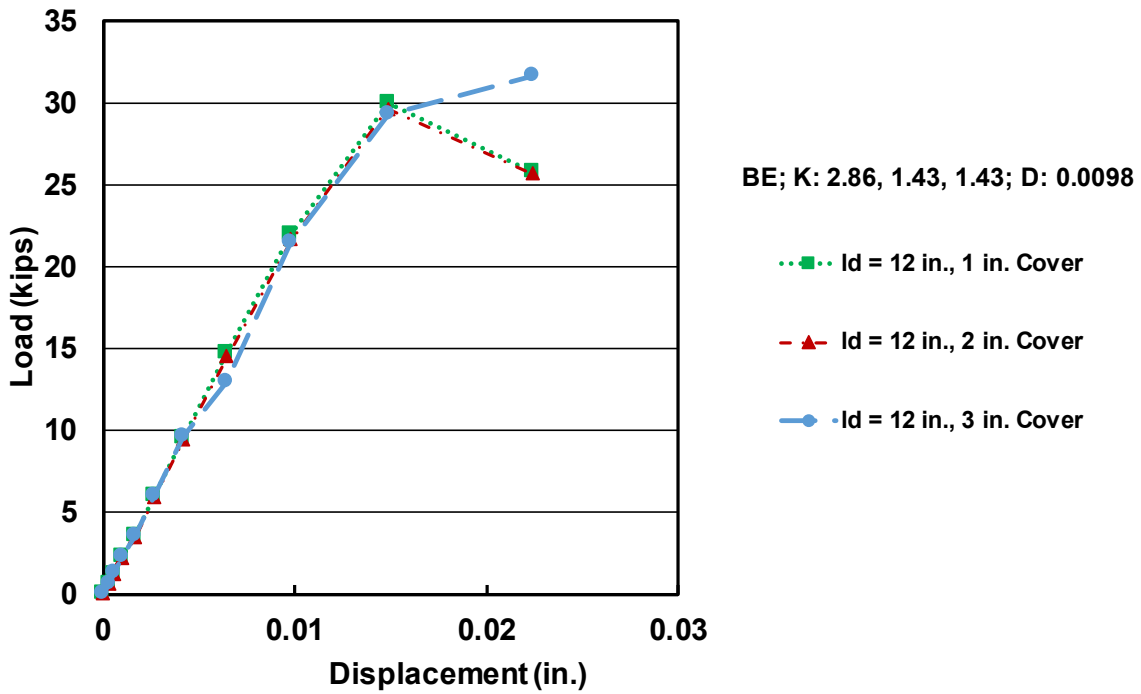


Figure 5.38 (a) Load-versus displacement for 1, 2, and 3 in. concrete covers with 12 in. embedment length

Table 5.6 Values of linear-elastic and damage (initiation and evolution)

specimen	Linear -elastic			Damage-initiation			Damage-evolution		
	K_{nn} (kip/in)	K_{ss} (kip/in)	K_{tt} (kip/in)	δ_n° (in.)	δ_s° (in.)	δ_t° (in.)	δ_m (in.)	M_{m1}	M_{m2}
BE; K: 2.86, 1.43, 1.43; D: 0.0098; 5 1 in. Cover	2.86	1.43	1.43	0.591	0.0098	0.0098	1.7717	0	0.5
							0.0307	0.01	0.5
							0.0295	1	0.5
BE; K: 2.86, 1.43, 1.43; D: 0.0098; 5 2 in. Cover	2.86	1.43	1.43	0.591	0.0098	0.0098	1.7717	0	0.5
							0.0307	0.01	0.5
							0.0295	1	0.5
BE; K: 2.86, 1.43, 1.43; D: 0.0098; 5 3 in. Cover	2.86	1.43	1.43	0.591	0.0098	0.0098	1.7717	0	0.5
							0.0307	0.01	0.5
							0.0295	1	0.5

5.6.6.3 Summary

In the Sections 5.6.6.1 and 5.6.6.2, the beam-end specimen tested by Darwin and Graham 1993 is modeled. The interfacial coefficients between the concrete and steel bar were calibrated based on the test results. The effect of embedment length and concrete cover were studied. The results showed that the model successfully captured the effect of embedment length but failed to capture the effect of concrete cover, largely because the model failed to replicate splitting of the concrete.

5.7 SUMMARY AND CONCLUSIONS

A granular micromechanics model to represent damage and plasticity of cementitious material developed by Misra and Yang (2010), Misra and Singh (2014), Misra and Poorsolhjouy (2015), and Poorsolhjouy and Misra (2017) has been highly successful for a number of applications representing nonlinear material behavior, but has not been used to represent reinforced concrete members. In this chapter, the finite element (FE) method is used to study the ability of that model to represent concrete fracture and the interaction between the concrete and reinforcing steel. For this purpose, two types of specimens are simulated. The first is a slab specimen with shallow embedment with headed bars installed at the center of the slab or headed bars embedded close to the slab edges and their strengths are governed by anchorage failure. The second is a beam-end

specimen used to measure the bond performance of a straight deformed bar embedded in a concrete block. Concrete behavior in tension and compression is described using the nonlinear granular micromechanics model. The model is implemented via a user material (UMAT) subroutine into commercial FE program (ABAQUS). The reinforcement (anchored bar) behavior is described using an elastic model. The interaction between concrete and reinforcement is modeled using a concrete-steel interface model with cohesive behavior. Three-dimensional FE models of the shallow embedment and beam-end test specimens are constructed and analyzed. The FE results are compared with results from tests performed by Ghimire et al. (2018) on headed bars embedded in slabs and by Darwin and Graham (1993) on beam-end specimens.

Based on the results and discussion presented in this chapter, it is observed that:

1. The combined concrete model provides a good representation of the anchorage strength of the headed bars embedded in slab specimens. Behavior of these specimens is dominated by the compressive and tensile properties of concrete, which are well represented by the granular micromechanics model.
2. The combined model does not provide a good representation of the behavior of beam-end specimens, which depends on splitting of concrete caused by to slip of the bar. Lack of representation of the local interaction between deformed bars and the surrounding concrete prevents the model from being generally applicable for use in representing reinforced concrete members, especially in cases where strength is governed by bond between reinforcing steel and concrete.

CHAPTER 6: SUMMARY AND CONCLUSIONS

6.1 SUMMARY

This study assesses the anchorage behavior of headed bars at the end of beams within compression-compression-tension (CCT) nodes subjected to monotonic loading. The test parameters include the embedment length, number, and spacing of the anchored bars, and the presence or absence of a head at the anchored end of the bar. The test results, along with that of members other than beam-column joints available in the literature, are compared to the descriptive equation developed by Shao et al. (2016) for headed bars anchored in beam-column joints. The test results from specimens with bars without heads are compared with anchorage strength predicted for straight bars based on work by ACI Committee 408. More broadly, test results for headed bars anchored in beam-column joints are compared with design provisions for the development length of headed bars in ACI 318-14 and ACI 318-19 and proposed by Shao et al. (2016) and Darwin and Dolan (2021), along with the anchorage provisions in Chapter 17 of ACI 318-19. Finally, a granular micromechanics model and associated model from reinforcing steel-concrete interaction are evaluated for their general applicability for use in finite element modeling of anchorage of headed and straight reinforcing bars to concrete.

Ten CCT node specimens were tested in which the tensile tie reinforcement consisted of 2 or 3 longitudinal bars. Embedment lengths were the same for both ends of a specimen, with each end of the specimens tested separately. At one end, the bars were terminated with a head, while at the other end, the bars were straight. The specimens were designed using the strut-and-tie method (STM) with a strut angle of 45° . The specimens were 20 in. deep and 18 in. wide, with a clear span of 60 in. and a total length of 104 in. Embedment lengths ranged from 10 to 14 in. Concrete with a nominal compressive strength of 5,000 psi was used for all specimens. No. 4 stirrups were used away from the strut and nodal zone to ensure that the specimens did not fail in shear.

Comparisons of the anchorage strength of headed bars in beam column joints are based on tests results from 178 beam-column joint specimens containing headed bars with a bearing area between 3.8 to 9.4 times the area of the bar: 82 specimens without confining reinforcement and 96 specimens with confining reinforcement. In comparisons with the anchorage provisions in Chapter 17 of ACI 318-19, three modes of failure were checked—breakout, side-face blowout, and strength

of the anchor reinforcement. Forty of the specimens (18 without confining reinforcement and 22 with confining reinforcement), had a ratio of effective depth of the beam to embedment length of 1.5 or more. In addition to the design provisions for development and anchorage, test results for these specimens are compared with strengths based on the strut-and-tie method in ACI 318-19.

A granular micromechanics model for damage and plasticity of cementitious materials developed by Misra and Yang (2010), Misra and Singh (2014), Misra and Poorsolhjoui (2015), and Poorsolhjoui and Misra (2017) is evaluated for its ability to model the anchorage failure of headed bars embedded in reinforced concrete slabs (shallow embedment specimens) and the bond performance of straight bars embedded in concrete blocks (beam-end specimens). A key point in the evaluation is to determine the importance of representing the local interaction between deformed bars and the surrounding concrete, which is not represented in this case, to obtain a fully objective model. Finite element results are compared with those from tests by Shao et al. (2016) and Ghimire et al. (2018) for the headed bars embedded in slabs and Darwin and Graham (1993) for the straight bars embedded in the concrete blocks.

6.2 CONCLUSIONS

The following conclusions are based on the results and analyses presented in this study.

6.2.1 CCT Node Tests

1. Specimen strength was limited by anchorage failure, either side-face blowout for headed bars or pullout for straight bars, except for one test specimen that appeared to fail due to crushing of concrete within the assumed node region.
2. Anchorage type (headed bars and straight bars) had a minimal effect on initial load-deflection behavior.
3. Based on comparisons with the work by Thompson et al. (2006a), the anchorage strength of headed bars at the CCT nodes does not increase by providing transverse reinforcement perpendicular to the bar within a nodal zone.
4. Comparisons of anchorage strengths based on test results for the CCT node specimens from the current study (test-to-calculate ratios ranging from 1.37 to 2.68 with an average of 2.05) and those tested by Thompson (2006a) (test-to-calculated ratios ranging from 1.67 to 2.21 with

an average of 1.89) show that the descriptive equation developed by Shao et al. (2016) is very conservative for headed bars in CCT nodes that have a compressive force placed perpendicular to the bar.

5. Comparisons of anchorage strengths based on tests results for the CCT node specimens from the current study show that the descriptive equation developed by ACI Committee 408 (ACI 408R-03) very conservative (test-to-calculated ratios ranging from 1.72 to 2.76 with an average of 2.25) for straight bars in CCT nodes that have a compressive force placed perpendicular to the bar.

6.2.2 Anchorage Strength of Headed Bars in Tension

1. The provisions in ACI 318-14 for the development length of headed bars do not accurately estimate the anchorage strength of headed bars with high steel strength or concrete compressive strength. The equation, however, is generally conservative.
2. The development length design provisions proposed by Shao et al. (2016) can be safely used for the design of the anchorage strength of headed bars for steel strengths at least up to 120 ksi and concrete compressive strengths at least up to 16,000 psi.
3. The development length design provisions in ACI 318-19 for headed bars do not fully capture the effects of confining reinforcement and bar spacing and do not accurately represent the contribution of concrete compressive strength for compressive strengths above 6000 psi.
4. The development length design provisions proposed by Darwin and Dolan (2021) accurately reflect the anchorage strength of headed bars and provide a similar level of accuracy to that provided by those proposed by Shao et al. (2016).
5. Specimens with ratios of effective depth to embedment length of 1.5 or greater exhibited lower anchorage strengths than the specimens with ratios below 1.5 for specimens both without and with confining reinforcement.
6. The strut-and-tie method should be used to design joints with ratios of effective depth to embedment length of 1.5.
7. The anchorage provisions in ACI 318-19 are very conservative when compared to any of the other methods evaluated in this study and, if used, would lead to nearly unbuildable designs.

6.2.3 Finite Element Analysis

1. The combined concrete model provides a good representation of the anchorage strength of the headed bars embedded in slab specimens. Behavior of these specimens is dominated by the compressive and tensile properties of concrete, which are well represented by the granular micromechanics model.
2. The combined model does not provide a good representation of the behavior of beam-end specimens, which depends on splitting of concrete caused by to slip of the bar. Lack of representation of the local interaction between deformed bars and the surrounding concrete prevents the model from being generally applicable for use in representing reinforced concrete members, especially in cases where strength is governed by bond between reinforcing steel and concrete.

REFERENCES

- AASHTO, 1998, *AASHTO LRFD Bridge Design Specifications*, 2nd edition, American Association of State Highway and Transportation Officials, Washington, 461 pp.
- ABAQUS (2012), *User Manual*, Version 6.12, Rhode Island, USA.
- ACI Committee 446, 1991, *Fracture Mechanics of Concrete: Concepts, Models and Determination of Material Properties*, ACI 446.1R-91, American Concrete Institute, Detroit, MI, 145 pp.
- ACI Committee 318, 1995, *Building Code Requirements for Structural Concrete (ACI 318-95) and Commentary*, ACI 318R-95, American Concrete Institute, Farmington Hills, Michigan, 369 pp.
- ACI Committee 318, 2002, *Building Code Requirements for Structural Concrete (ACI 318-02) and Commentary*, ACI 318R-02, American Concrete Institute, Farmington Hills, Michigan, 443 pp.
- ACI Committee 318, 2011, *Building Code Requirements for Structural Concrete (ACI 318-11) and Commentary*, ACI 318R-11, American Concrete Institute, Farmington Hills, MI, 505 pp.
- ACI Committee 318, 2014, *Building Code Requirements for Structural Concrete*, ACI 318-14, American Concrete Institute, Farmington Hills, MI, 518 pp.
- ACI Committee 318, 2019, “Building Code Requirements for Structural Concrete (ACI 318-19),” American Concrete Institute, Farmington Hills, MI, 625 pp.
- ACI Committee 408, 2003, *Bond and Development of Straight Reinforcing Bars in Tension*, ACI 408R-03, American Concrete Institute, Farmington Hills, Michigan, 518 pp.
- Allwood, R. J. and Bajarwan, A. A., 1996, “Modeling Nonlinear Bond-Slip Behavior for Finite Element Analysis of Reinforced Concrete Structures,” *ACI Structural Journal*, Vol. 93, No. 5, Sep.-Oct., pp. 538-544.
- ASTM A615, 2014, “Standard Specification for Deformed and Plain Carbon-Steel Bars for Concrete Reinforcement,” (ASTM A615/A615M-14), ASTM International, West Conshohocken, Pennsylvania, 7 pp.
- ASTM A970, 2018, *Standard Specification for Headed Steel Bars for Concrete Reinforcement*, (ASTM A970/A970M-18), ASTM International, West Conshohocken PA. 10 pp.
- ASTM A1035, 2015, “Standard Specification for Deformed and Plain, Low-Carbon, Chromium, Steel Bars for Concrete Reinforcement,” (ASTM A1035/A1035M-14), ASTM International, West Conshohocken, PA, 7 pp.

Bashandy, T. R., 1996, "Application of Headed Bars in Concrete Members," *Ph.D. dissertation*, University of Texas at Austin, Dec., 303 pp.

Berner, D.E., Gerwick, B.C., and Hoff, G.C., 1991, "T-Headed Stirrup Bars," *Concrete International*, Vol. 13, No. 5, May, pp. 49-53.

Berner, D. E. and Hoff, G. C., 1994, "Headed Reinforcement in Disturbed Strain Regions of Concrete Members," *Concrete International*, Vol. 16, No. 1, Jan., pp. 48-52.

Brown, C. J., Darwin, D., and McCabe, S. L., 1993, "Finite Element Fracture Analysis of Steel-Concrete Bond," *SM Report* No. 36, The University of Kansas Center for Research, Inc., Lawrence, Kansas, Nov., 98 pp.

Chun, S.-C., Oh, B., Lee, S.-H., and Naito, C. J., 2009, "Anchorage Strength and Behavior of Headed Bars in Exterior Beam-Column Joints," *ACI Structural Journal*, Vol. 106, No. 5, Sep.-Oct., pp. 579-590.

Cook, W. and Mitchell, D., 1988, "Studies of Disturbed Regions near Discontinuities in Reinforced Concrete Members," *ACI Structural Journal*, Vol. 85, No. 2, Mar.-Apr., pp. 206-216.

CSA Canadian Concrete Code, 1984, *Design of Concrete Structures for Buildings*, (CAN3-A23.3-M84), *Canadian Standards Association*, Rexdale, 281 pp.

Darwin, D., Dolan, W. C., and Nilson, H. A., 2016, *Design of Concrete Structures*, 15th ed., New York: McGraw-Hill, 776 pp.

Darwin, D., and Graham, E. K., 1993, "Effect of Deformation Height and Spacing on Bond Strength of Reinforcing Bars," Project 56, *SL Report* 93-1, The University of Kansas Center for Research, Inc., Lawrence, KS, Jan., 71 pp.

Degroot, A. K., Kusters, G. M., and Monnier, T., 1981, "Numerical modelling of bond-slip behavior," *Heron, concrete mechanic*, Vol. 26, pp. 6-38.

Ghimire, K., Darwin, D., and O'Reilly, M., 2018 "Anchorage of Headed Reinforcing Bars in Concrete," *SM Report* No. 127, University of Kansas Center for Research, Inc., Lawrence, KS, Jan., 278 pp.

Griffith, A.A., 1921, "The Phenomenon of Rupture and Flow in Solids," *Phil. Transactions of the Royal Society, London*, Vol. A221, pp. 163-197

Hillerborg, A., Modeer, M., and Peters son, P. E., 1976, "Analysis of Crack Formation and Crack Growth in Concrete by Means of Fracture Mechanics and Finite Elements," *Cement and Concrete Research*, Vol. 6, No. 6, Nov., pp. 773-782.

Idun, E. K. and Darwin, D., “Improving the Development Characteristics of Steel Reinforcing Bars,” *SM Report* No. 41, University of Kansas Center for Research, Inc., Lawrence, Kansas, August 1995, 267 pp.

Idun, E. K. and Darwin, D., “Epoxy-Coated Reinforcement: Coefficient of Friction and Rib Face Angle,” *ACI Structural Journal*, Vol. 96, No. 4, July-Aug., 1999, pp. 609-615.

Keuser, M. and Mehlhorn, G., 1987, “Finite element models for bond problems,” *Journal of Structural Engineering*, Vol. 113, pp. 2160-2173.

Lampert, P. and Thürlimann, B., 1971, “Ultimate Strength and Design of Reinforced Concrete Beams in Torsion and Bending,” IASBE Publications, Zurich, Switzerland, No. 31-1, pp. 107-131.

Lüchinger, P., 1977, “Bruchwiderstand von Kastenträgern aus Stahlbeton unter Torsion, Biegung, und Querkraft (Ultimate Strength of Box-Griders in Reinforced Concrete under Torsion, Bending, and Shear),” *Institut für Baustatik und Konstruktion-ETH, Zurich*, Switzerland, Bericht Nr. 69 pp.

McMackin, P.J., Slutter, R.G., and Fisher, J.W., 1973 “Headed Steel Anchor under Combined Loading,” *AISC Engineering Journal*, Vol. 10, No. 2, pp. 43-52.

Minor, J., 1971, “A Study of Bent Bar Anchorages in Concrete,” *Ph.D. Dissertation*, Rice University, Houston, TX, 135 pp.

Misra, A. and Poorsolhjouy, P., 2015, “Granular micromechanics model for damage and plasticity of cementitious material based upon thermomechanic,” *Mathematics and Mechanics of Solids*. Feb., pp. 1-26.

Misra, A. and Singh, V., 2014, “Thermomechanics-based nonlinear rate-dependent coupled damage-plasticity granular micromechanics model,” *Continuum Mechanics and Thermodynamics*, Vol. 27, No. 4-5, Sep., pp. 787-817.

Misra, A. and Singh, V., 2014, “Nonlinear granular micromechanics model for multi-axial rate-dependent behavior,” *International Journal of Solids and Structures*, Vol. 51, No. 13, Jun., pp. 2272-2282.

Misra, A. and Yang, Y., 2010, “Micromechanical model for cohesive materials based upon pseudo-granular structure,” *International Journal of Solids and Structures*, Vol. 47, No. 21, Oct., pp. 2970–2981.

Mitchell, D. and Collins, M., 1974, “Diagonal Compression Field Theory – A Rational Model for Structural Concrete in Pure Torsion,” *Journal of the American Concrete Institute*, Vol. 71, No. 8, Aug., pp. 396-408.

Mörsch, E., 1902, “Der Eisenbetonbau, seine Theorie und Anwendung (Reinforced Concrete, Theory and Application),” Stuttgart, Germany.

Mokhtar, A., Ghali, A., and Dilger, W., 1985, “Stud Shear Reinforcement for Flat Concrete Plates,” *ACI Structural Journal*, Vol. 82, No. 5, Sep.-Oct., pp. 676-683.

Ngo, D. and Scordelis, A. C., 1967, "Finite Element Analysis of Reinforced Concrete Beams," *ACI Journal*, Vol. 64, No. 3, Mar., pp. 152- 163.

Poorsolhjoui, P. and Misra, A., 2017, "Effect of intermediate principal stress and loading-path on failure of cementitious materials using granular micromechanics," *International Journal of Solids and Structures*, Vol. 108, Mar., pp 139-152.

Ramirez, J., and Breen, J.E., 1983, "Proposed Design Procedures for Shear and Torsion in Reinforced and Prestressed Concrete," *Center for Transportation Research Report No. 248-4F*, Austin, Texas.

Ramirez, J., and Breen, J.E., 1983, "Experimental Verification of Design Procedures for Shear and Torsion in Reinforced and Prestressed Concrete," *Center for Transportation Research Report No. 248-3F*, Austin, Texas.

Ramirez, J., and Breen, J.E., 1983, "Review of Design Procedures for Shear and Torsion in Reinforced and Prestressed Concrete," *Center for Transportation Research Report No. 248-2F*, Austin, Texas.

Richart, F., 1927, "An Investigation of Web Stresses in Reinforced Concrete Beams," University of Illinois Engineering Experiment Station, Bulletin No. 166, Urbana, Illinois.

Ritter, W., 1899, "Die Bauweise Hennebique (The Hennebique System)," *Schweizerische Bauzeitung*, Bd. XXXIII, No. 7, Zurich, Switzerland.

Runesson, K., 2006, "Constitutive Modeling of Engineering Materials– Theory and Computation," *Lecture Notes*, Dept. of Applied Mechanics, Chalmers University of Technology, Göteborg, Vol. 6, Mar., 213 pp.

Schlaich, J., Schäfer, K., and Jennewein, M., 1987, "Towards a Consistent Design of Structural Concrete," *PCI Journal*, Vol. 32, No. 3, May-Jun., pp. 74-150.

Schlaich, J., and Schäfer, K., 1991, "Design and detailing of structural concrete using strut-and-tie models," *The Structural Engineer Journal*, Vol. 69, No. 6, Mar., pp. 113-125.

Smith, B. J., 1972, "Exterior Reinforced Concrete Joints with Low Axial Load under Seismic Loading," *Master of Engineering Report*, University of Canterbury, 172 pp.

Talbot, A., 1909, "Tests of Reinforced Concrete Beams: Resistance to Web Stresses, Series of 1907 and 1908," University of Illinois Engineering Experiment Station, Bulletin No. 29, Urbana, Illinois.

Tholen, M.L., and Darwin, D., 1996, "Effects of Deformation Properties on the Bond of Reinforcing Bars," *SM Report No. 42*, University of Kansas Center for Research, Inc., Lawrence, Kansas, Sep. 1, 395 pp.

Thompson, M. K., 2002, "The Anchorage Behavior of Headed Reinforcement in CCT Nodes and Lap Splices," *PhD dissertation*, University of Texas at Austin, May, 502 pp.

Thompson, M. K., Ziehl, M. J., Jirsa, J. O., and Breen, J. E., 2005, "CCT Nodes Anchored by Headed Bars-Part 1: Behavior of Nodes," *ACI Structural Journal*, Vol. 102, No. 6, Nov.-Dec., pp. 808-815.

Thompson, M. K., Jirsa, J. O., and Breen, J. E., 2006, "CCT Nodes Anchored by Headed Bars-Part 2: Capacity of Nodes," *ACI Structural Journal*, Vol. 103, No. 1, Jan.-Feb., pp. 65-73.

Wallace, J. W., McConnell, S. W., Gupta, P., and Cote, P. A., 1998, "Use of Headed Reinforcement in Beam-Column Joints Subjected to Earthquake Loads," *ACI Structural Journal*, Vol. 95, No. 5, Sep.-Oct., pp. 590-606.

Shao, Y., Darwin, D., O'Reilly, M., Lequesne, R. D., Ghimire, K., and Hano, M., 2016, "Anchorage of Conventional and High-Strength Headed Reinforcing Bars," *SM Report No. 117*, University of Kansas Center for Research, Inc., Lawrence, KS, Aug., 234 pp.

APPENDIX A: NOTATION

a	depth of equivalent rectangular compressive stress block (Figure 4.3)
A_{ab}	Total cross-sectional area of all confining reinforcement parallel to ℓ_{dt} for headed bars being developed in beam-column joints and located within $8d_b$ of the bottom (top) of the headed bars in direction of the outside of the joint for No. 3 through No. 8 headed bars or within $10d_b$ of the bottom (top) of the bar in direction of the outside of the joint for No. 9 through No. 11 headed bars
A_b	Area of an individual headed bar
A_{brg}	Net bearing area of the head of headed deformed bar
A_{cs}	Cross-sectional area at one end of a strut in a strut-and-tie model, taken perpendicular to the axis of the strut
A_{hs}	Total cross-sectional area of headed bars being developed
$A_{tr,l}$	Area of single leg of confining reinforcement within joint region
A_{tt}	Total cross-sectional area of all confining reinforcement parallel to ℓ_{dt} for headed bars being developed in beam-column joints and located within $8d_b$ of the top (bottom) of the headed bars in direction of the interior of the joint for No. 3 through No. 8 headed bars or within $10d_b$ of the top (bottom) of the bar in direction of the interior of the joint for No. 9 through No. 11 headed bars; or minimum total cross-sectional area of all confining reinforcement parallel to headed bars being developed in members other than beam-column joints within $7\frac{1}{2}d_b$ on one side of the bar centerline for No. 3 through No. 8 headed bars or within $9\frac{1}{2}d_b$ on one side of the bar centerline for No. 9 through No. 11 headed bars
A_v	Area of confining reinforcement located between the headed bar and the top of the bearing member
A_{vt}	Total cross-sectional area of the single tie
b	Width of column (Figure 4.1)
c	Effective depth of neutral axis from the assumed extreme compression fiber for beam-column joint and shallow embedment pullout specimens (Figure 4.3)
c_{bc}	Clear cover measured from the back of the head to the back of the member
c_c	Clear concrete cover measured from the bar to the top edge of the concrete block at beam end test
c_h	Clear spacing between adjacent headed bars
c_o	Clear cover measured from the head to the side of the column
c_{sb}	Clear cover measured from the bottom of the beam to the headed bar
c_{so}	Clear cover measured from the side of the headed bar to the side of the member
$c_{so,avg}$	Average clear side cover of the headed bars
d	Distance from the centroid of the tension bar to the extreme compression fiber of the beam
d_b	Nominal diameter of bar
d_{eff}	Effective value of d for beam-column joint and shallow embedment pullout specimens (Figure 4.3)
d_{tr}	Nominal bar diameter of confining reinforcement within joint region
d_{tro}	Nominal bar diameter of confining reinforcement outside joint region
f'_c	Specified compressive strength of concrete
f_{cm}	Measured concrete compressive strength
$f_{su,max}$	Maximum stress in individual headed bar
f_y	Specified yield strength of headed bar

f_{yt}	Yield strength of transverse reinforcement
h	Depth of column (Figure 4.1), Depth of the CCT node beams
h_{cl}	Height measured from the center of the headed bar to the top of the bearing member
K_{tr}	Transverse reinforcement index
ℓ_d	Development length in tension of deformed bar, measured from end of bar toward critical section
ℓ_{dh}	Development length in tension of deformed bar or deformed wire with a standard hook, measured from outside end of hook, point of tangency, toward critical section
ℓ_{dt}	Development length in tension of headed deformed bar, measured from the critical section to the bearing face of the head
ℓ_{eh}	Embedment length measured from the bearing face of the head to the face of the member (or the end of the extended nodal zone, for CCT node specimens) (Figure 2.5)
$\ell_{eh,avg}$	Average embedment length of headed bars
n	Number of headed bars loaded simultaneously
N	Number of legs of confining reinforcement in joint region
N_{cb}	Anchorage strength of headed bar from anchorage provision (breakout failure) for single anchor
N_{cbg}	Anchorage strength of headed bar from anchorage provision (breakout failure) for a group of anchors
N_s	Anchorage strength of headed bar from anchorage provisions (Strength of Anchor Reinforcement)
N_{sb}	Anchorage strength of headed bar from anchorage provision (side-face blowout failure)
N_{str}	Governed anchorage strength of headed bar from anchorage provision
P	Mean stress
q	Deviatoric stress
R_1	Reaction from the bearing member for beam-column joint specimens
R_r	Relative rib area of the reinforcement
s	Center-to-center spacing between adjacent headed bars
s_{tr}	Center-to-center spacing of confining reinforcement (hoops) within joint region
s_{tro}	Center-to-center spacing of hoops outside joint region
T	Test failure load on a headed and straight bars; average load on headed and straight bars at failure
T_{calc}	Calculated failure load on a headed bar
T_D	Anchorage strength of a headed bar based on Darwin and Dolan 2021 equation
T_h	Anchorage strength of a headed bar
T_{ind}	Peak load on individual headed bar at failure
T_{max}	Maximum load on individual headed bar
T_{STM}	Calculated load on headed bars at anchorage failure based on strut-and-tie model
T_{total}	Sum of loads on headed bars at failure
T_{318-14}	Anchorage strength of a headed bar based on ACI 318-14
T_{318-19}	Anchorage strength of a headed bar based on ACI 318-19
T_{408}	Anchorage strength of a straight bar based on ACI 408R-03
t_d	A term representing the effect of bar size

t_r	A term representing the effect of relative rib area
V_ε	Volumetric strain
β_s	Factor used to account for the effect of cracking and confining reinforcement on the effective compressive strength of the concrete in a strut (see Section 4.6.2)
β_1	Factor relating depth of equivalent rectangular compressive stress block to neutral axis depth
ϕ	Strength reduction factor (see Section 4.4.1.1)
ψ_{cs}	Factor used to modify development length based on confining reinforcement and bar spacing
ψ_c	Factor used to modify development length based on concrete compressive strength (ACI-318-19)
ψ_e	Factor used to modify development length based on reinforcement coating
ψ_m	Factor used to modify development length based on bar spacing
ψ_o	Factor used to modify development length based on bar location within member
ψ_p	Factor used to modify development length based on confining reinforcement and spacing between the bars (ACI 318-19)
ψ_r	Factor used to modify development length based on confining reinforcement
λ	Modification factor to reflect the reduced mechanical properties of lightweight concrete relative to normal weight concrete of the same compressive strength

Acronym list

AASHTO	American Association of State Highway Transportation Officials
ACI	American Concrete Institute
ASTM	American Society of the International Association for Testing and Materials
BSG	Bulk Specific Gravity
CCT	Compression-compression-tension
FEM	Finite element method
HA	Class HA head dimensions shall satisfy (1) $A_{brg} \geq 4A_b$ and (2) Obstructions or interruptions of the bar deformations and non-planar features on the bearing face of the head shall not extend more than 5.25 times the nominal bar diameters from the bearing face and shall not have a diameter greater than 2.2 times the nominal bar diameters; Class HA also requires the development of the minimum specified tensile strength of the reinforcing bar
SG	Specific Gravity
SSD	Saturated Surface Dry
STM	Strut-and-tie model

Failure types

CB	Concrete breakout
SB	Side blowout
FP	Local front pullout (secondary failure)
BS	Back cover spalling (secondary failure)

APPENDIX B: DETAILED CCT NODE SPECIMEN RESULTS

B. 1: DETAILED CCT NODE SPECIMEN RESULTS

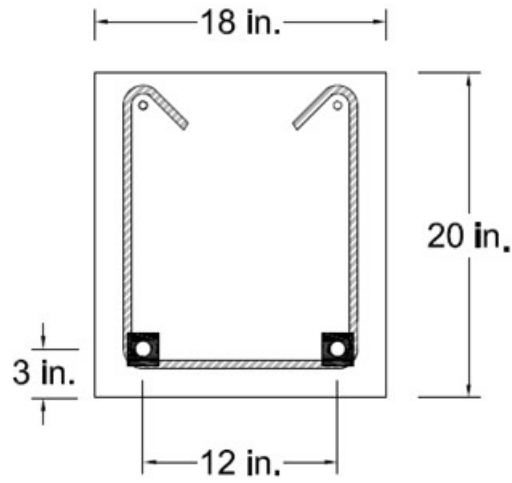


Figure B.1 Cross-section of the specimens with two headed bars

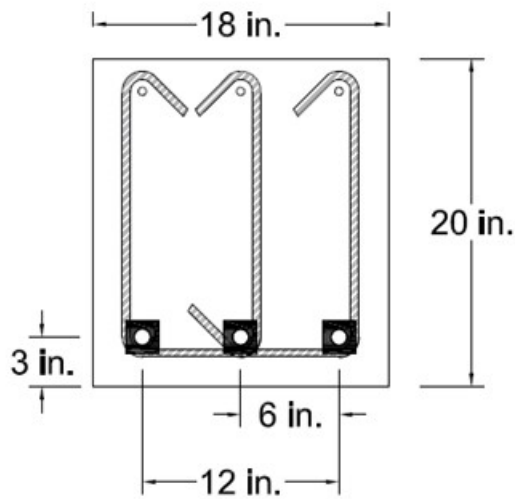


Figure B.2 Cross-section of the specimens with three headed bars

Table B.1 CCT node specimen detail

	Beam Type	l_{eh} in.	f_{cm} psi	d_b in.	b in.	h in.	n	c_{so} in.	c_{sb} in.	c_{bc} in.
Series 1 / Headed end										
1	H-2-8-5-9-F4.1-1	9	5740	1	18.0	20.0	2	2.5	2.5	2
2	H-2-8-5-10.4-F4.1-1	10.4	4490	1	18.1	20.3	2	2.5	2.5	2
3	H-3-8-5-9-F4.1-1	9	5800	1	18.3	20.1	3	2.5	2.5	2
4	H-3-8-5-11.4-F4.1-1	11.4	5750	1	18.0	20.1	3	2.5	2.5	2
5	H-3-8-5-14-F4.1-1	14	5750	1	18.1	20.0	3	2.5	2.5	2
Series 1/ Non-headed end										
6	NH-2-8-5-9-F4.1-1	9	5740	1	18.0	20.0	2	2.5	2.5	2
7	NH-2-8-5-10.4-F4.1-1	10.4	5330	1	18.3	20.0	2	2.5	2.5	2
8	NH-3-8-5-9-F4.1-1	9	5800	1	18.0	20.1	3	2.5	2.5	2
9	NH-3-8-5-11.4-F4.1-1	11.4	5750	1	18.0	20.1	3	2.5	2.5	2
10	NH-3-8-5-14-F4.1-1	14	5750	1	18.0	20.0	3	2.5	2.5	2
Series 2/ Headed end										
2	H-2-8-5-9-F4.1-2	9	4630	1	18.3	20.3	2	2.5	2.5	2
2	H-2-8-5-13-F4.1-2	13	4760	1	18.4	20.1	2	2.5	2.5	2
2	H-3-8-5-9-F4.1-2	9	4770	1	18.3	20.0	3	2.5	2.5	2
2	H-3-8-5-11-F4.1-2	11	4820	1	18.3	20.3	3	2.5	2.5	2
15	H-3-8-5-13-F4.1-2	13	4900	1	18.4	20.0	3	2.5	2.5	2
Series 2/ Non-headed end										
16	NH-2-8-5-9-F4.1-2	9	4630	1	18.4	20.3	2	2.5	2.5	2
17	NH-2-8-5-13-F4.1-2	13	4760	1	18.4	20.1	2	2.5	2.5	2
18	NH-3-8-5-9-F4.1-2	9	4770	1	18.3	20.0	3	2.5	2.5	2
19	NH-3-8-5-11-F4.1-2	11	4820	1	18.3	20.3	3	2.5	2.5	2
20	NH-3-8-5-13-F4.1-2	13	4900	1	18.4	20.0	3	2.5	2.5	2

Table B.1 Cont. Details of the CCT node specimens

	Beam Type	A_h in²	s in.	Bearing Plate Width in.	Peak Load kips	Deflection at Peak Load in.	Failure Type
Series 1 / Headed end							
1	H-2-8-5-9-F4.1-1	$4A_b$	12	6	278	0.2	Side blowout
2	H-2-8-5-10.4-F4.1-1	$4A_b$	12	6	346	0.3	Side blowout
3	H-3-8-5-9-F4.1-1	$4A_b$	6	6	446	*	Side blowout
4	H-3-8-5-11.4-F4.1-1	$4A_b$	6	6	386	0.33	Side blowout
5	H-3-8-5-14-F4.1-1	$4A_b$	6	6	495	*	Side blowout
Series 1/ Non-headed end							
6	NH-2-8-5-9-F4.1-1	$4A_b$	12	6	158	0.05	Pullout
7	NH-2-8-5-10.4-F4.1-1	$4A_b$	12	6	236	0.13	Pullout
8	NH-3-8-5-9-F4.1-1	$4A_b$	6	6	255	*	Pullout
9	NH-3-8-5-11.4-F4.1-1	$4A_b$	6	6	245	*	Pullout
10	NH-3-8-5-14-F4.1-1	$4A_b$	6	6	356	0.18	Pullout
Series 2/ Headed end							
11	H-2-8-5-9-F4.1-2	$4A_b$	12	6	218	0.1	Side blowout
12	H-2-8-5-13-F4.1-2	$4A_b$	12	6	250	0.11	Side blowout
13	H-3-8-5-9-F4.1-2	$4A_b$	6	6	355	0.14	Concrete crushing
14	H-3-8-5-11-F4.1-2	$4A_b$	6	6	403	0.19	Side blowout
15	H-3-8-5-13-F4.1-2	$4A_b$	6	6	499	0.37	Side blowout
Series 2/ Non-headed end							
16	NH-2-8-5-9-F4.1-2	$4A_b$	12	6	218	*	Pullout
17	NH-2-8-5-13-F4.1-2	$4A_b$	12	6	234	0.08	Pullout
18	NH-3-8-5-9-F4.1-2	$4A_b$	6	6	205	0.08	Pullout
19	NH-3-8-5-11-F4.1-2	$4A_b$	6	6	316	0.13	Pullout
20	NH-3-8-5-13-F4.1-2	$4A_b$	6	6	365	0.14	Pullout

*Data not available due to technical problems

B. 2: LOAD-DEFLECTION CURVES

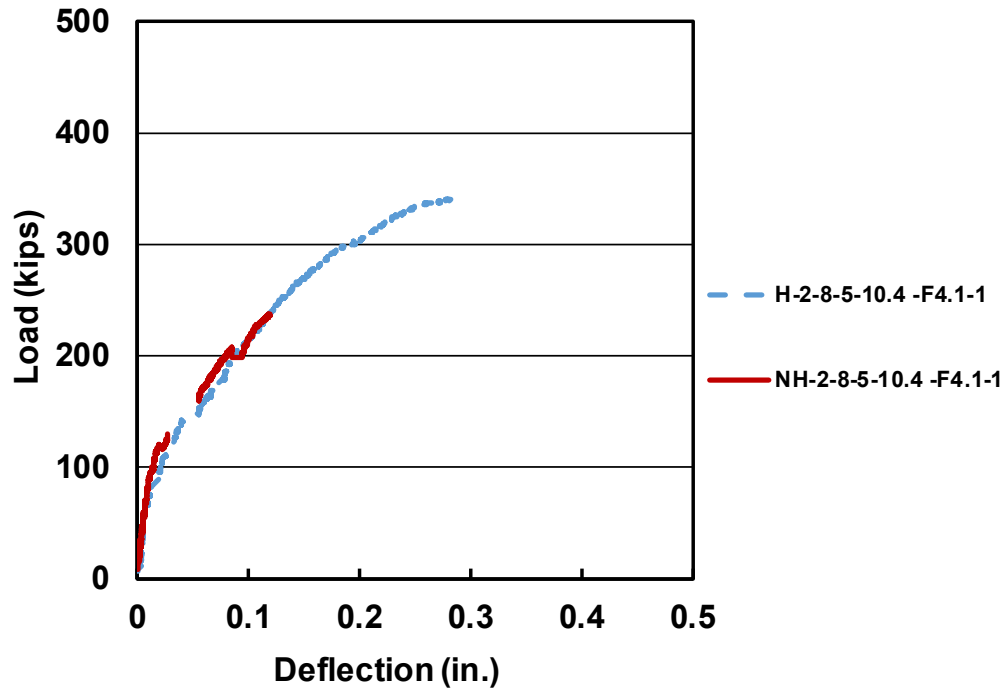


Figure B.3 Load versus deflection results for Specimens H-2-8-5-10.4-F4.1-1 and NH-2-8-5-10.4-F4.1-1

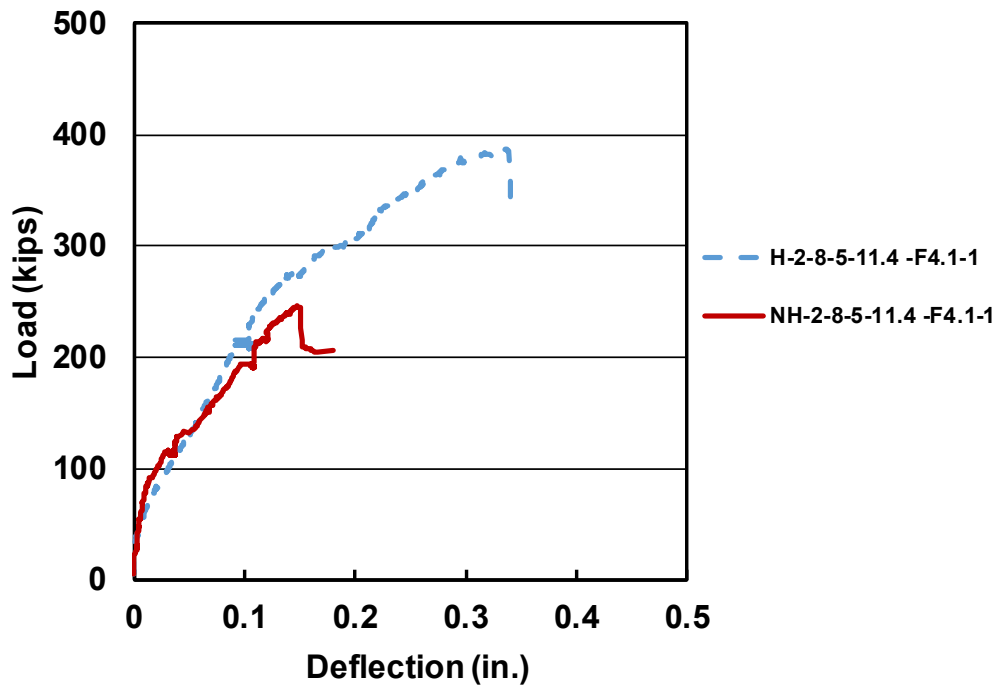


Figure B.4 Load versus deflection results for Specimens H-2-8-5-11.4-F4.1-1 and NH-2-8-5-11.4-F4.1-1

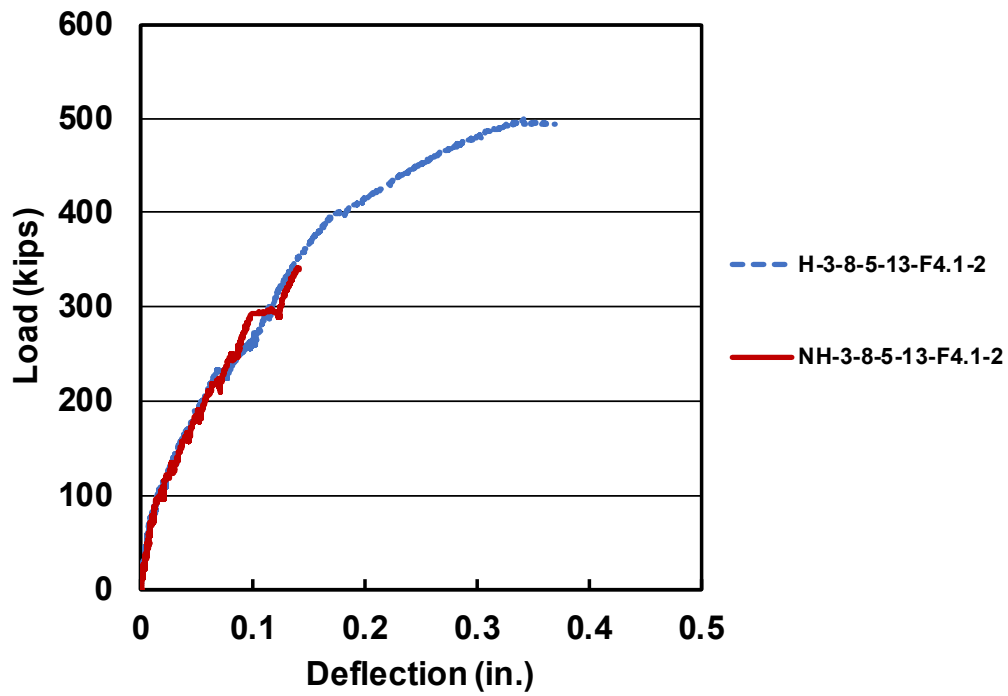


Figure B.5 Load versus deflection results for Specimens H-3-8-5-13-F4.1-2 and NH-3-8-5-13-F4.1-2

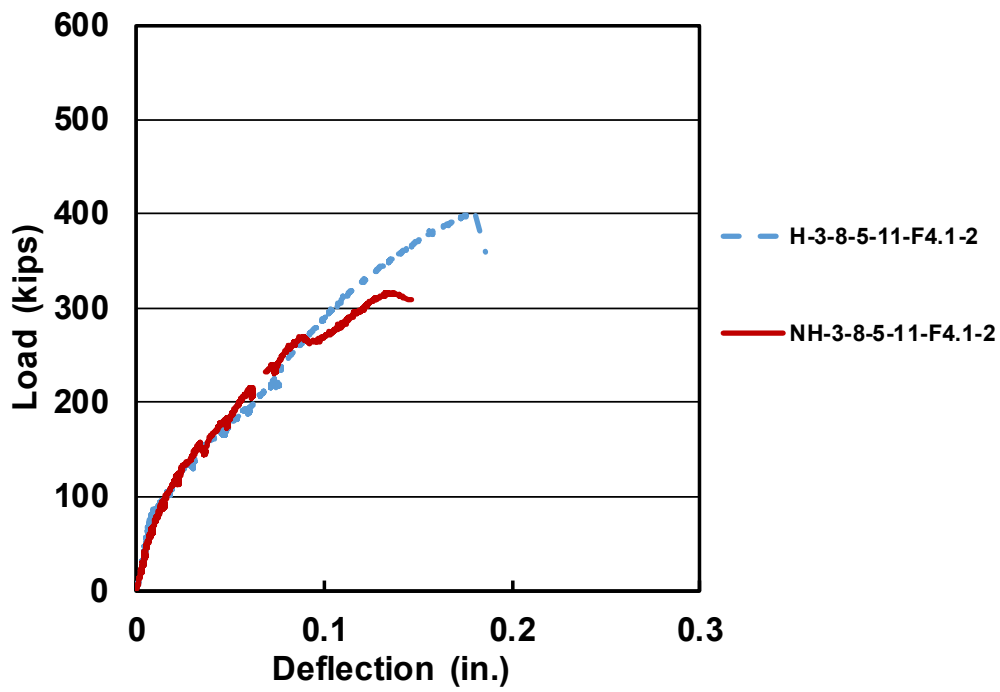


Figure B.6 Load versus deflection results for Specimens H-3-8-5-11-F4.2 and NH-3-8-5-11-F4.1-2

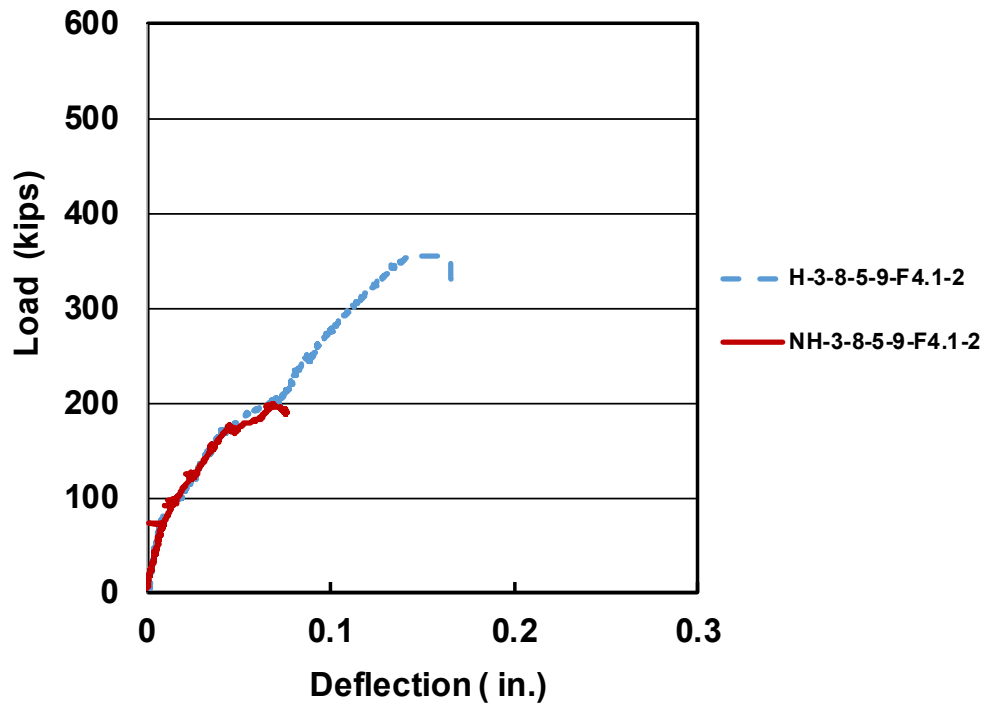


Figure B.7 Load versus deflection results for Specimens H-3-8-5-9-F4.1-2 and NH-3-8-5-9-F4.1-2

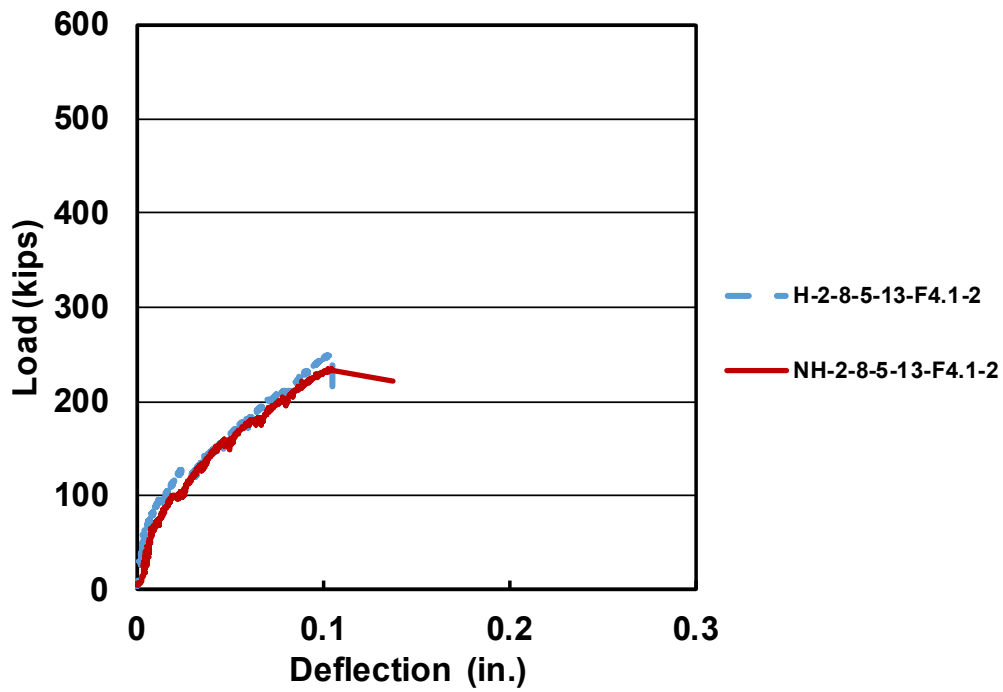


Figure B.8 Load versus deflection results for Specimens H-2-8-5-13-F4.1-2 and NH-2-8-5-13-F4.1-2

B. 3: LOAD-STRAIN CURVES

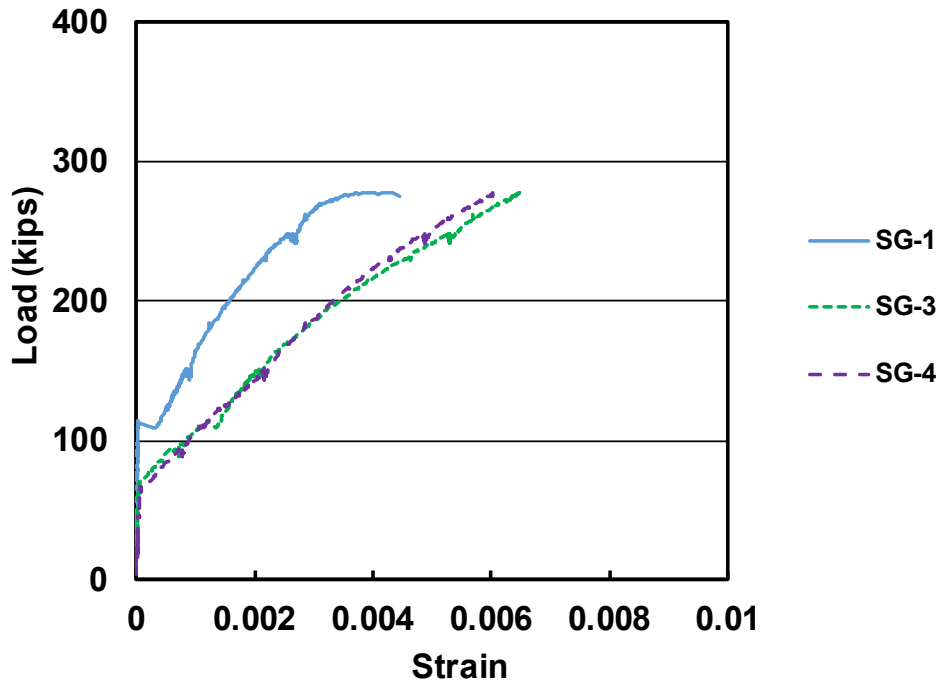


Figure B.9 Load-strain curve for specimen H-2-8-5-9-F4.1-1

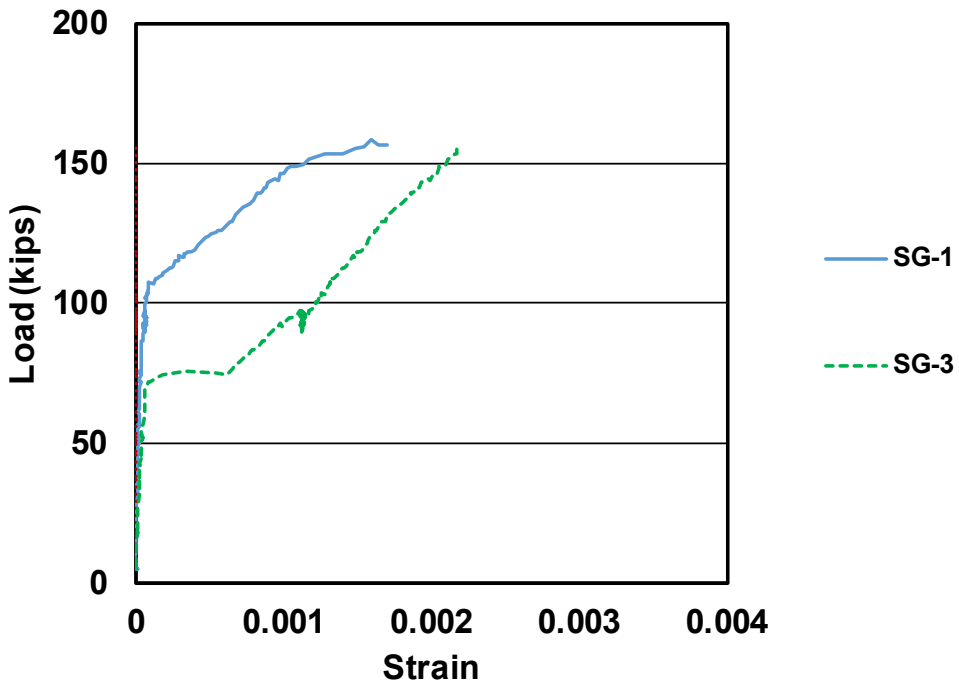


Figure B.10 Load-strain curve for specimen NH-2-8-5-9-F4.1-1

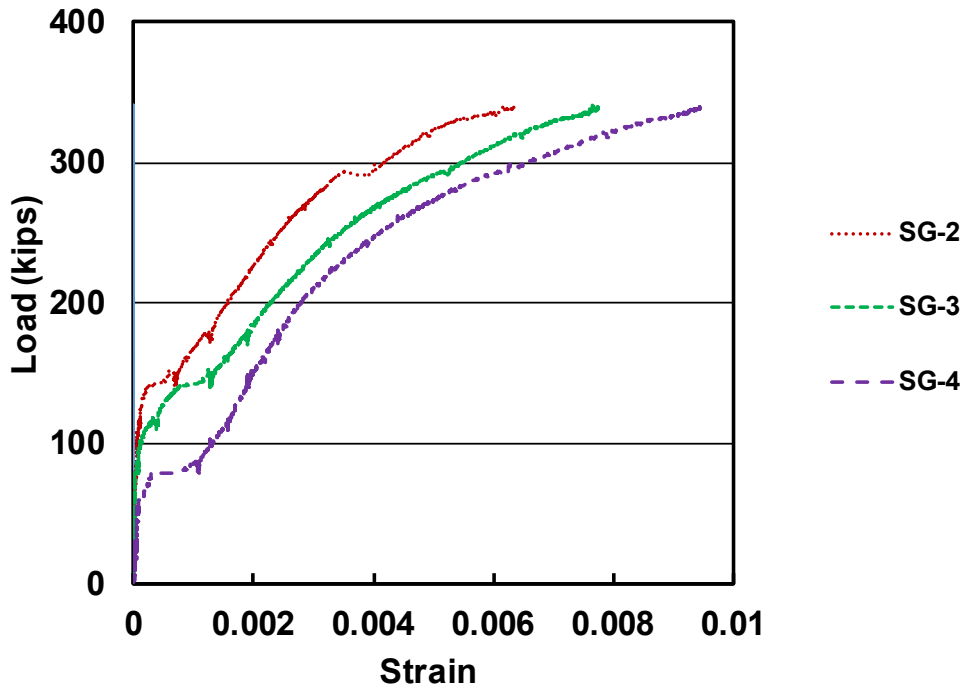


Figure B.11 Load-strain curve for specimen H-2-8-5-10.4-F4.1-1

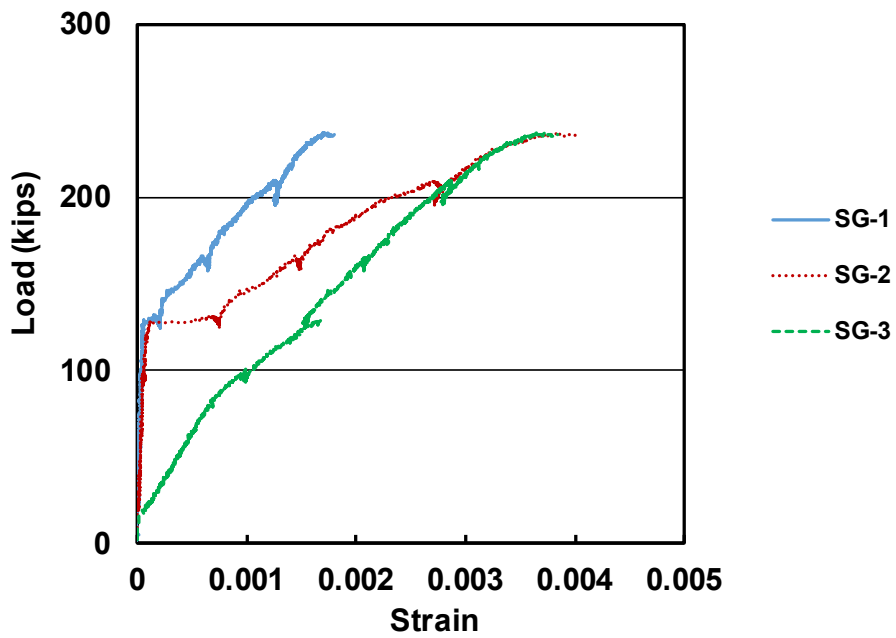


Figure B.12 Load-strain curve for specimen NH-2-8-5-10.4-F4.1-1

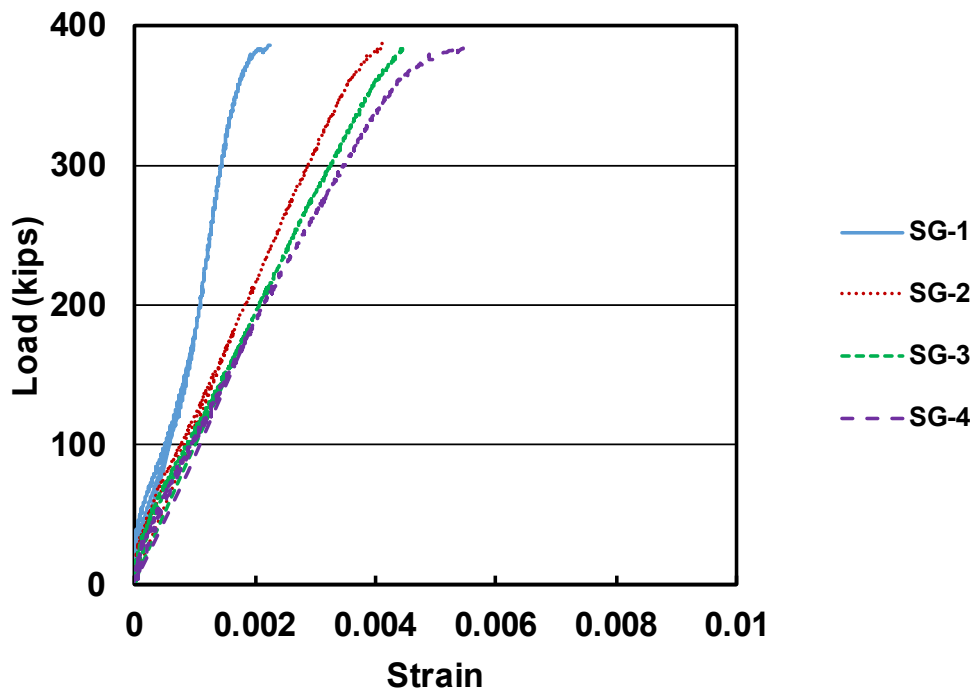


Figure B.13 Load-strain curve for specimen H-3-8-5-11.4-F4.1-1

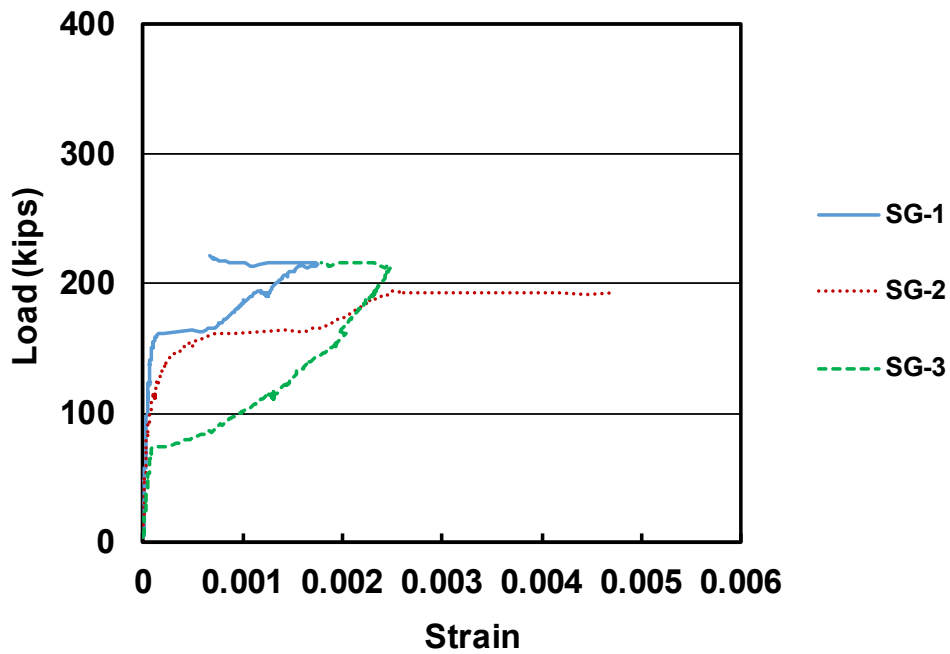


Figure B.14 Load-strain curve for specimen NH-3-8-5-11.4-F4.1-1

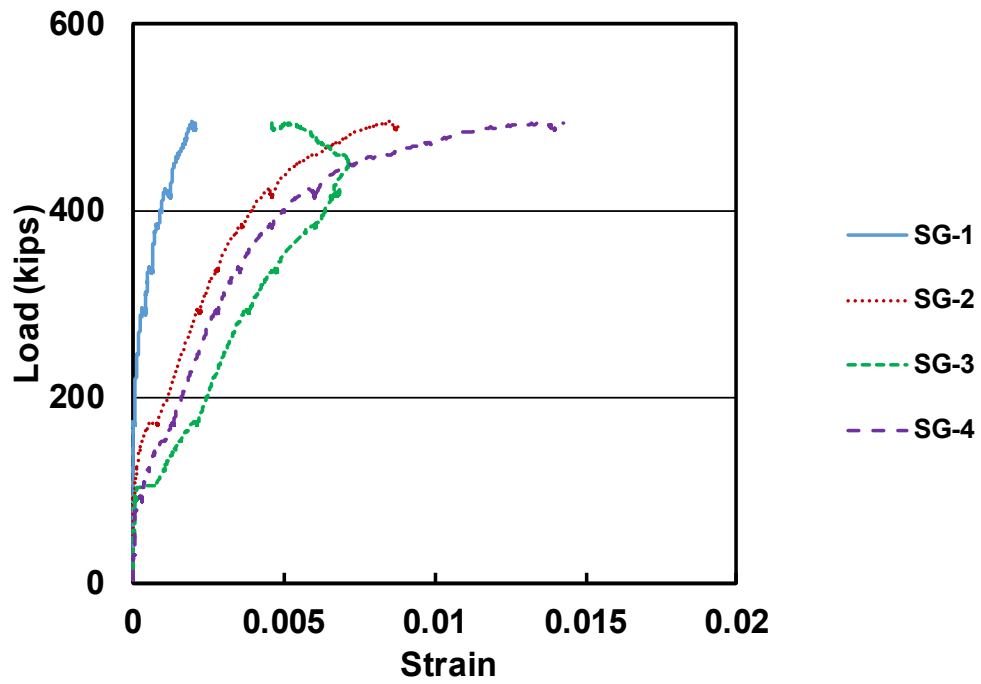


Figure B.15 Load-strain curve for specimen H-3-8-5-14-F4.1-1

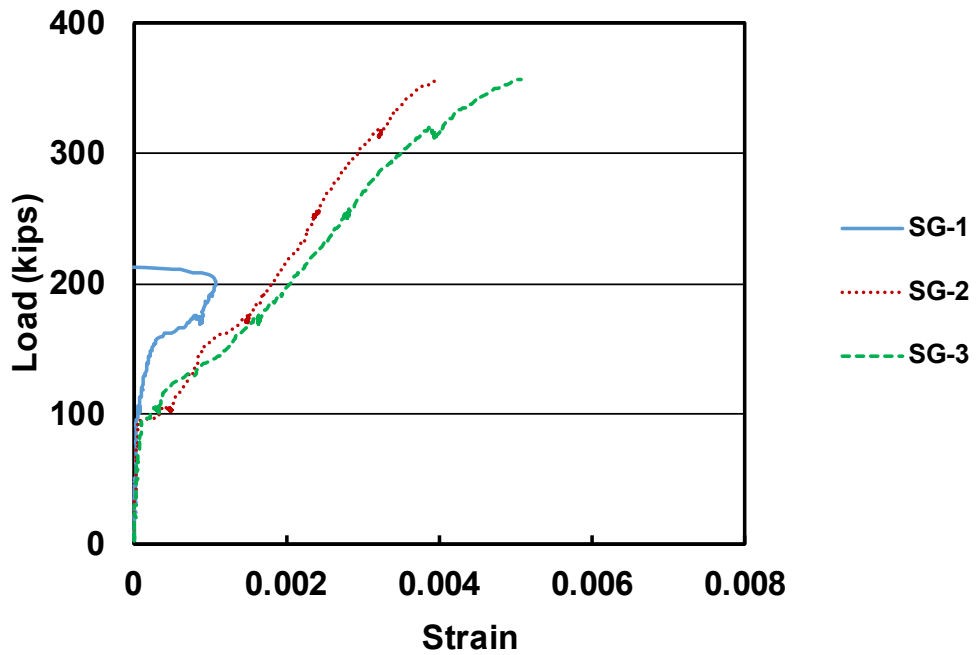
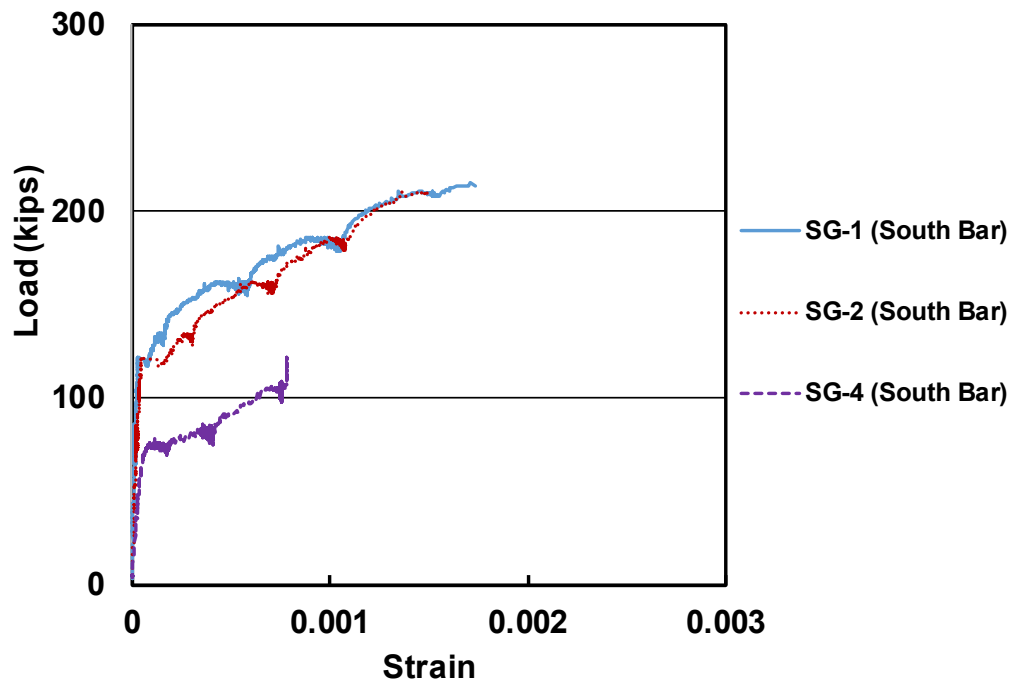
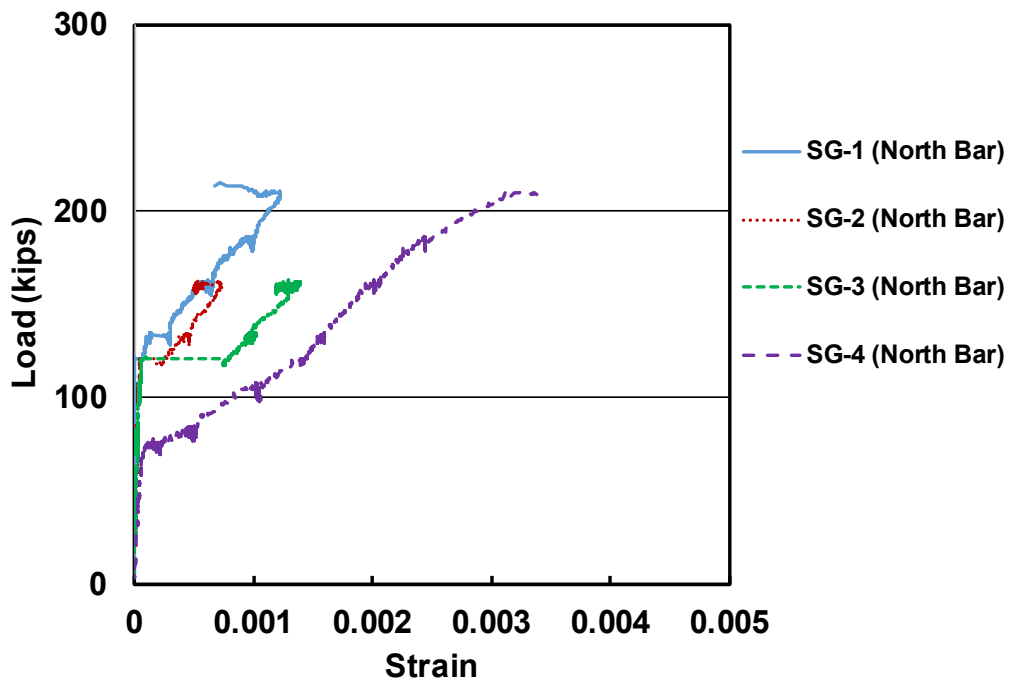


Figure B.16 Load-strain curve for specimen NH-3-8-5-14-F4.1-1

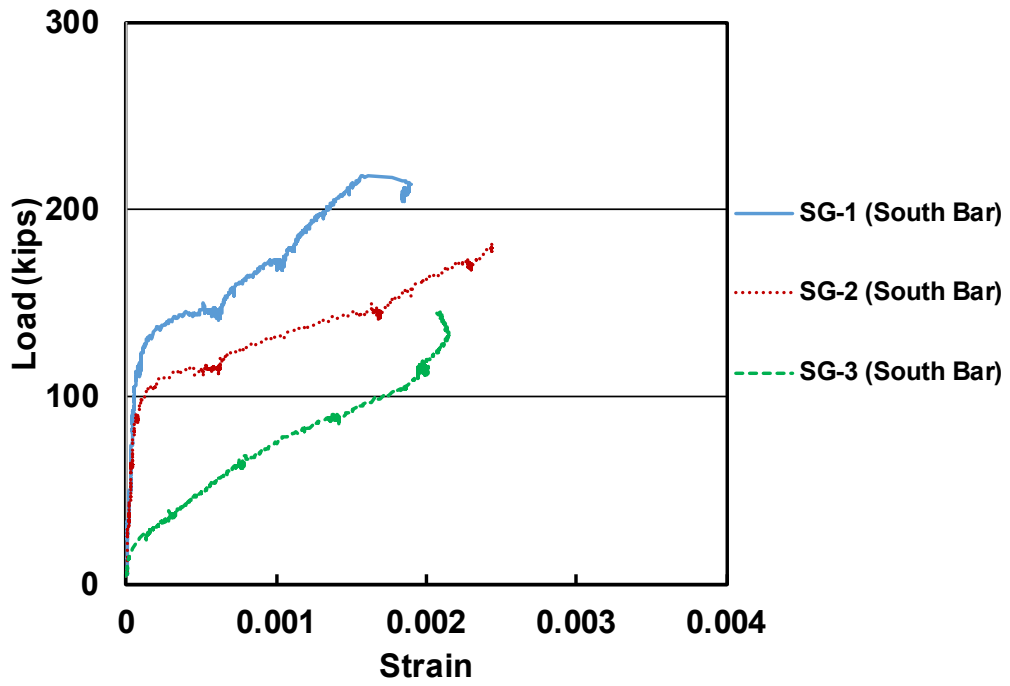


(a)

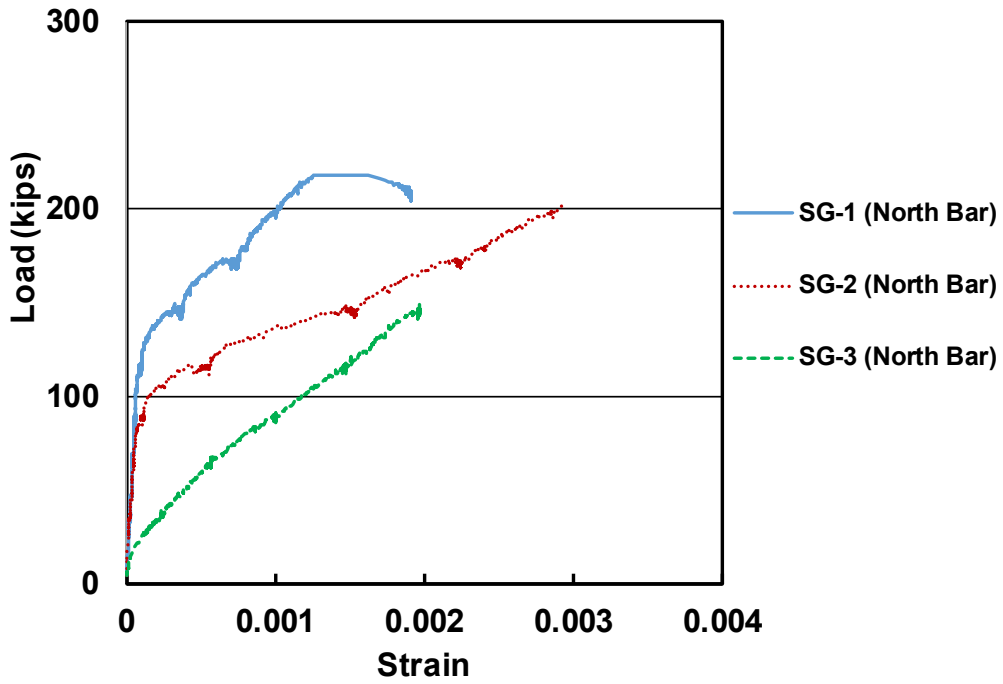


(b)

Figure B.17 Load-strain curve for specimen H-2-8-5-9-F4.1-2, (a) south bar, (b) north bar

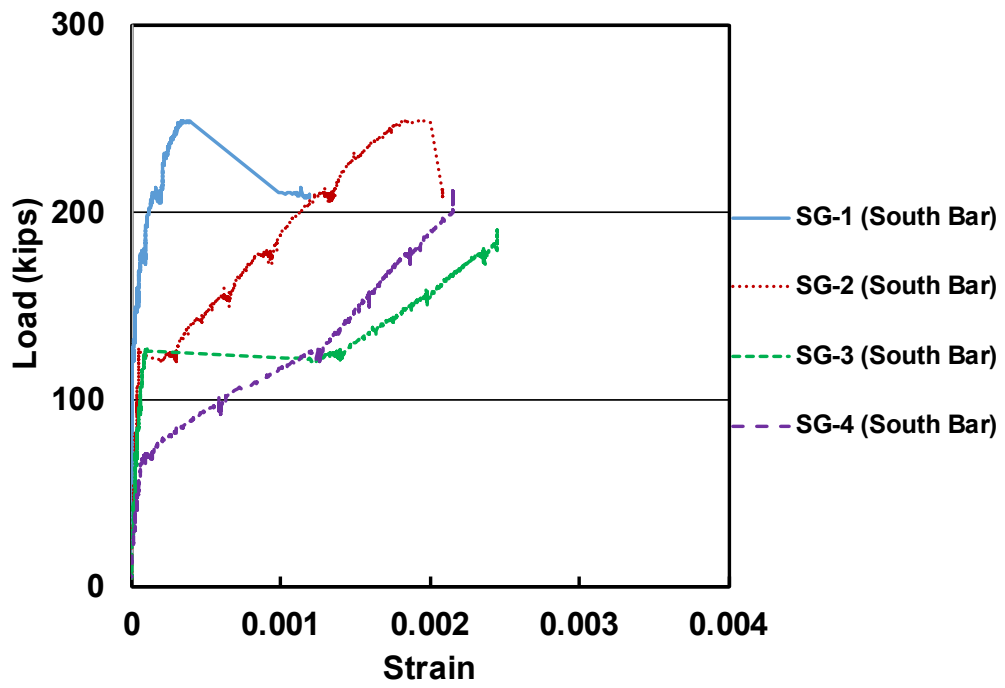


(a)

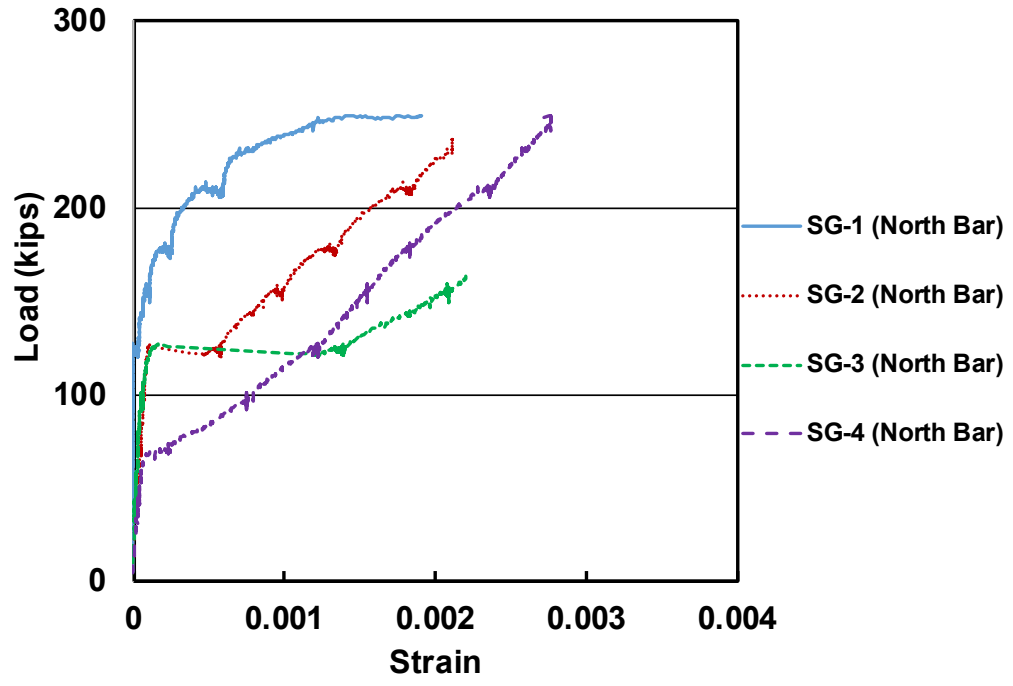


(b)

Figure B.18 Load-strain curve for specimen NH-2-8-5-9-F4.1-2, (a) south bar, (b) north bar

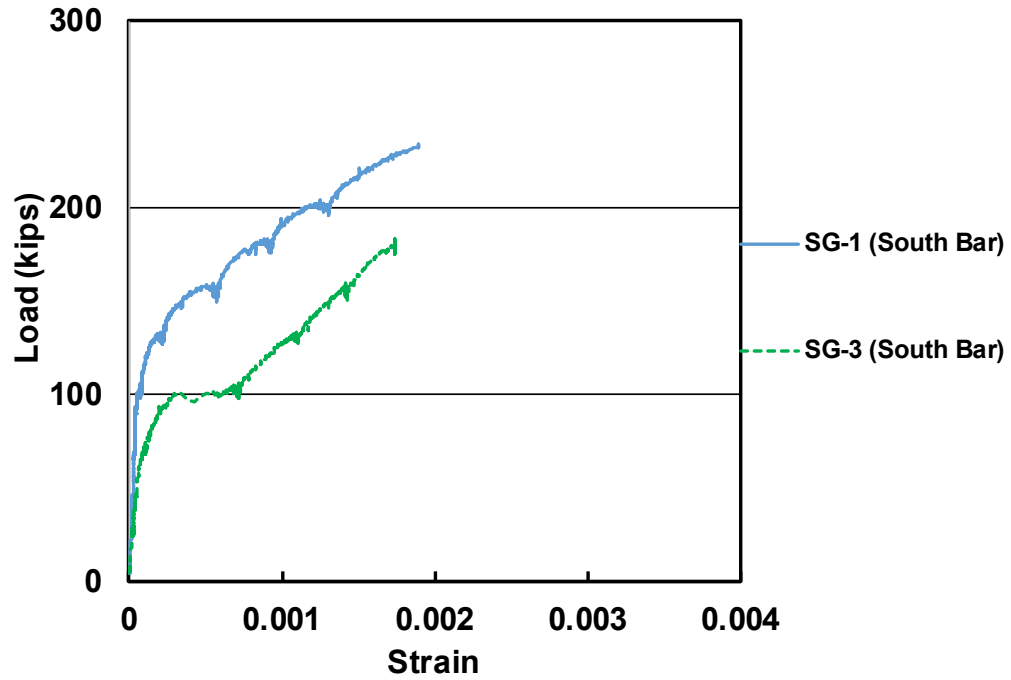


(a)

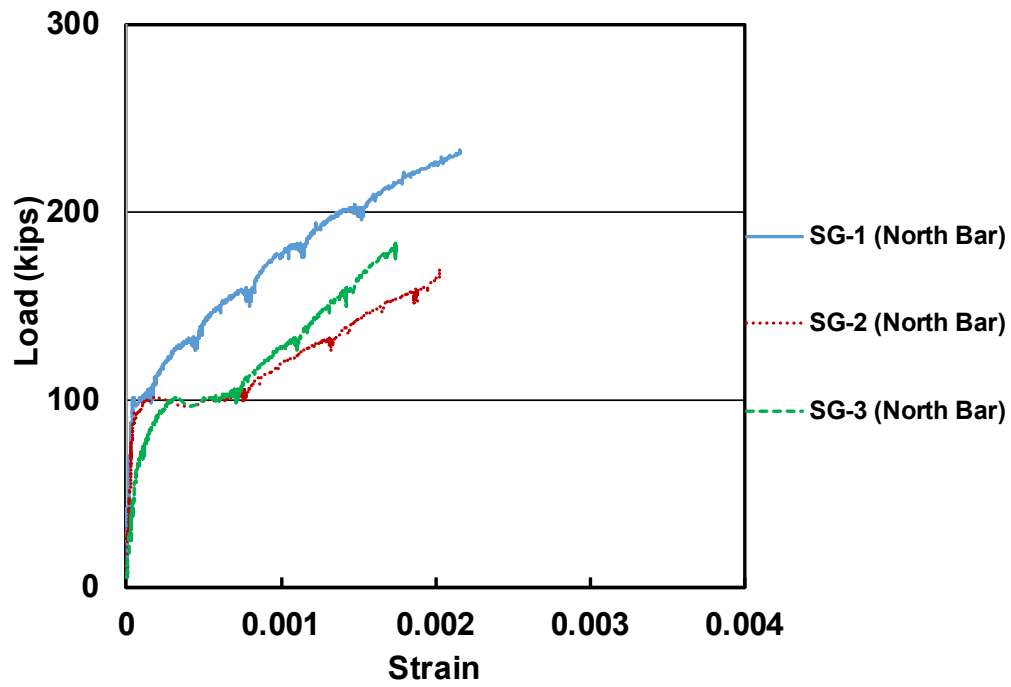


(b)

Figure B.19 Load-strain curve for specimen H-2-8-5-13-F4.1-2, (a) south bar, (b) north bar

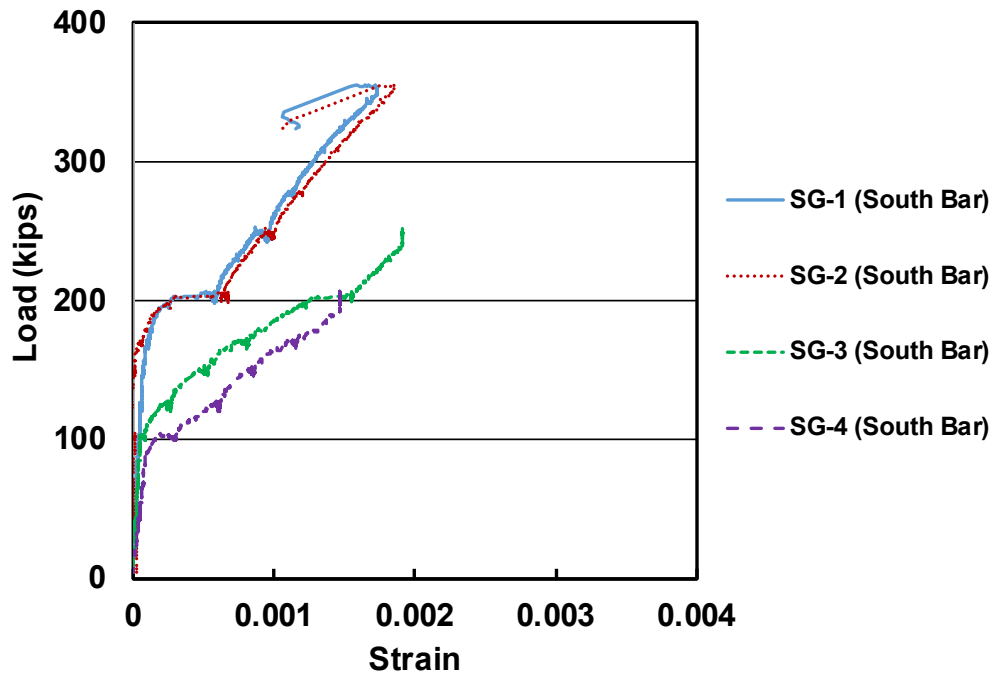


(a)

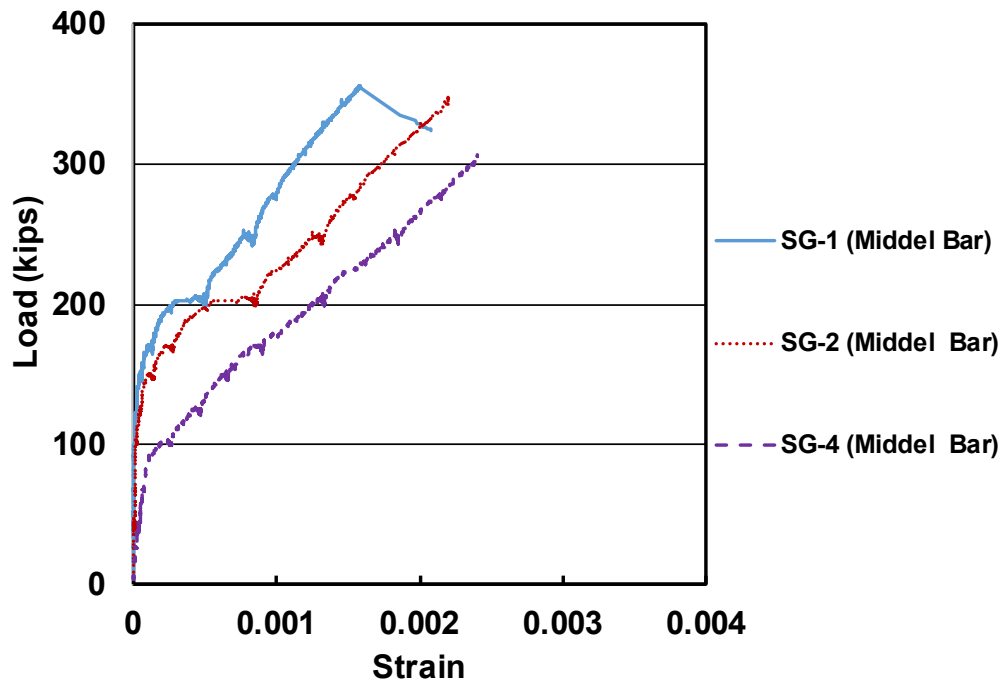


(b)

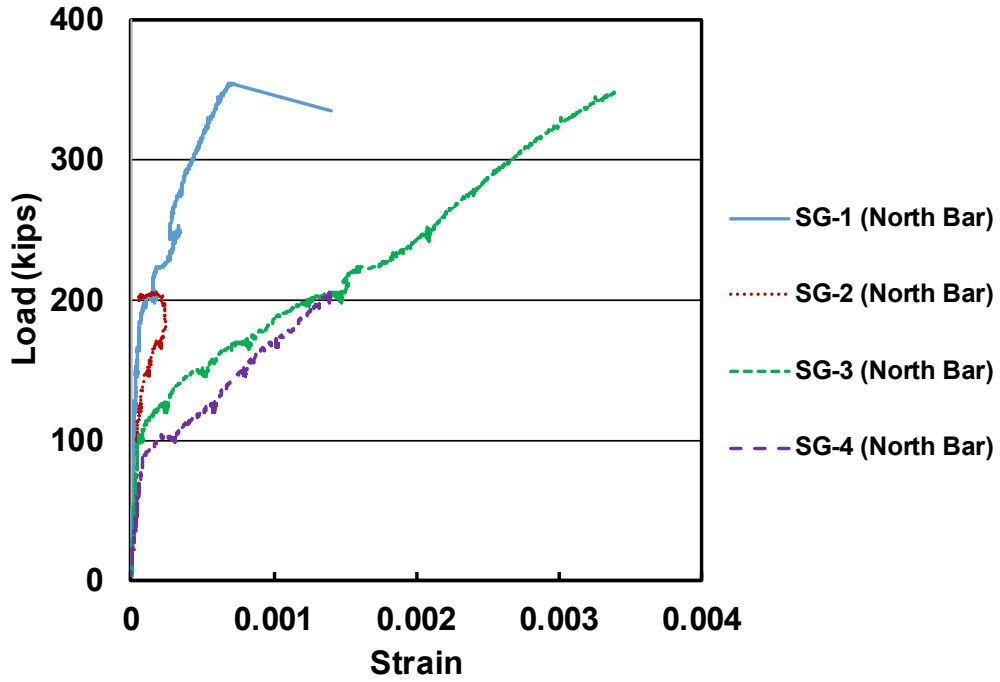
Figure B.20 Load-strain curve for specimen NH-2-8-5-13-F4.1-2, (a) south bar, (b) north bar



(a)

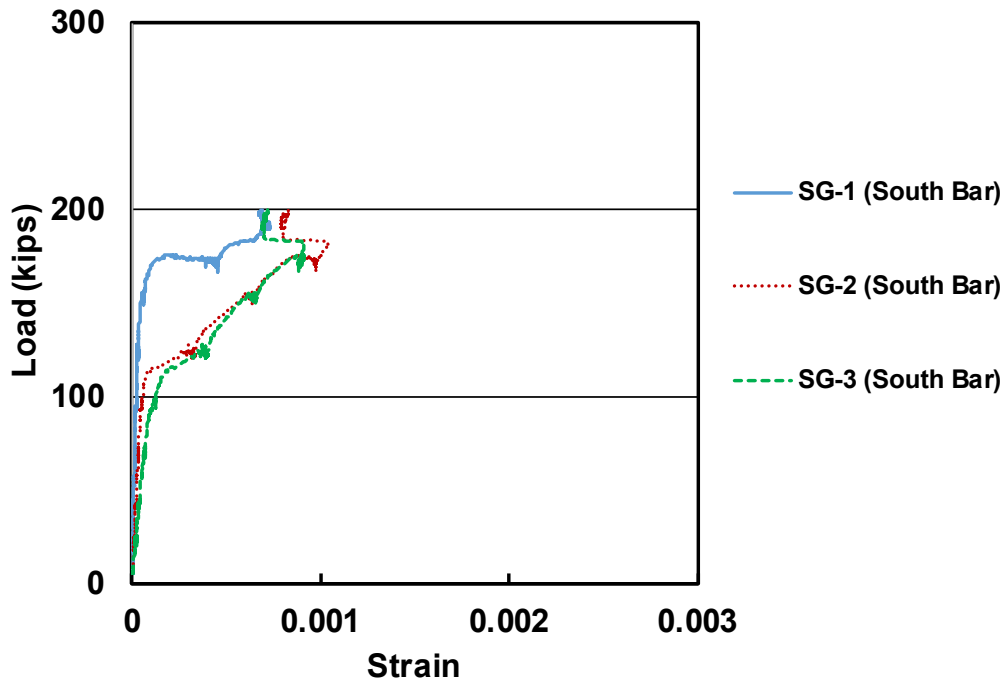


(b)

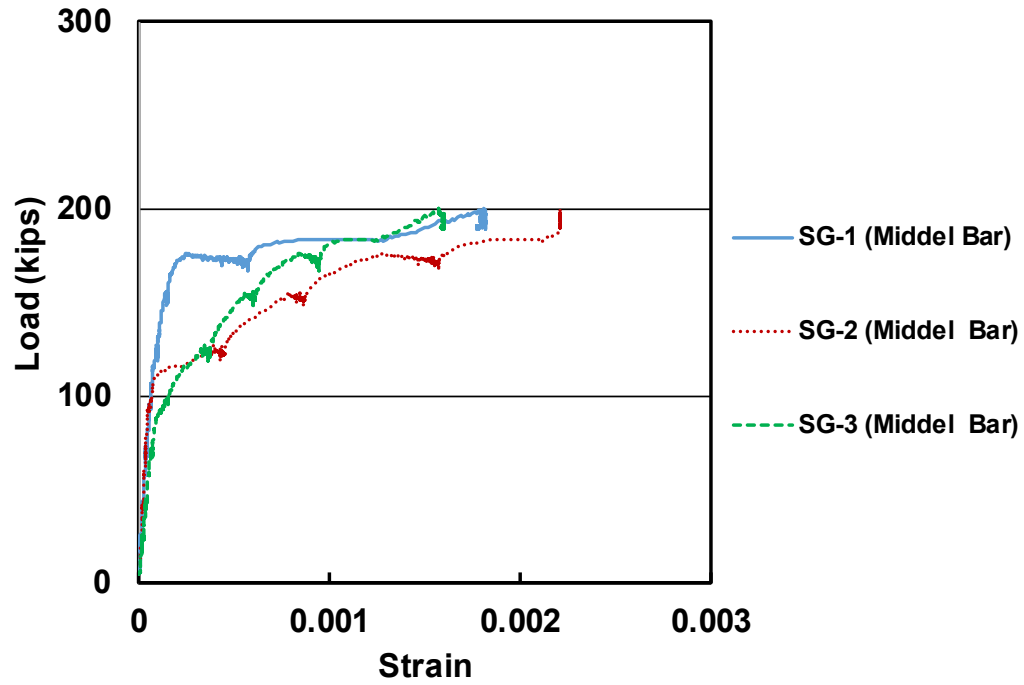


(c)

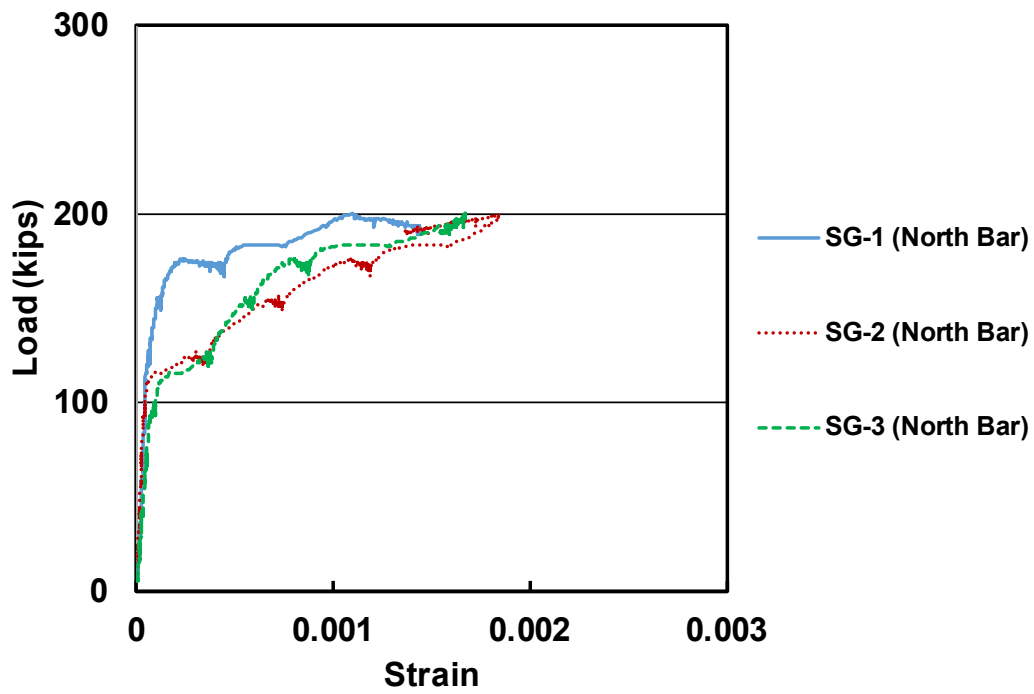
Figure B.21 Load-strain curve for specimen H-3-8-5-9-F4.1-2, (a) south bar, (b) middle bar, and (c) north bar



(a)

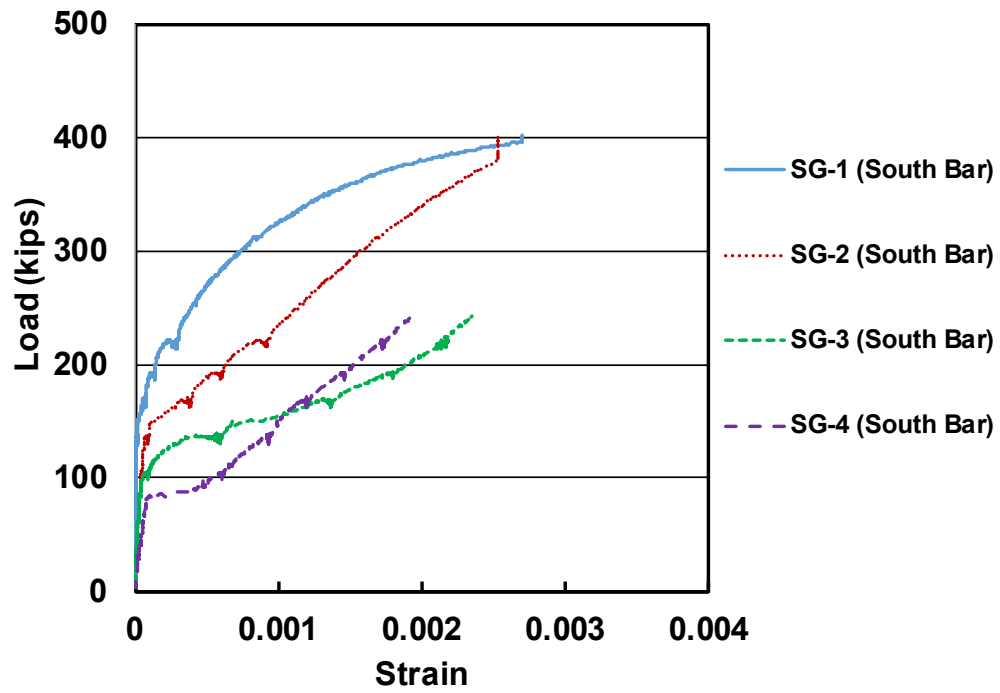


(b)

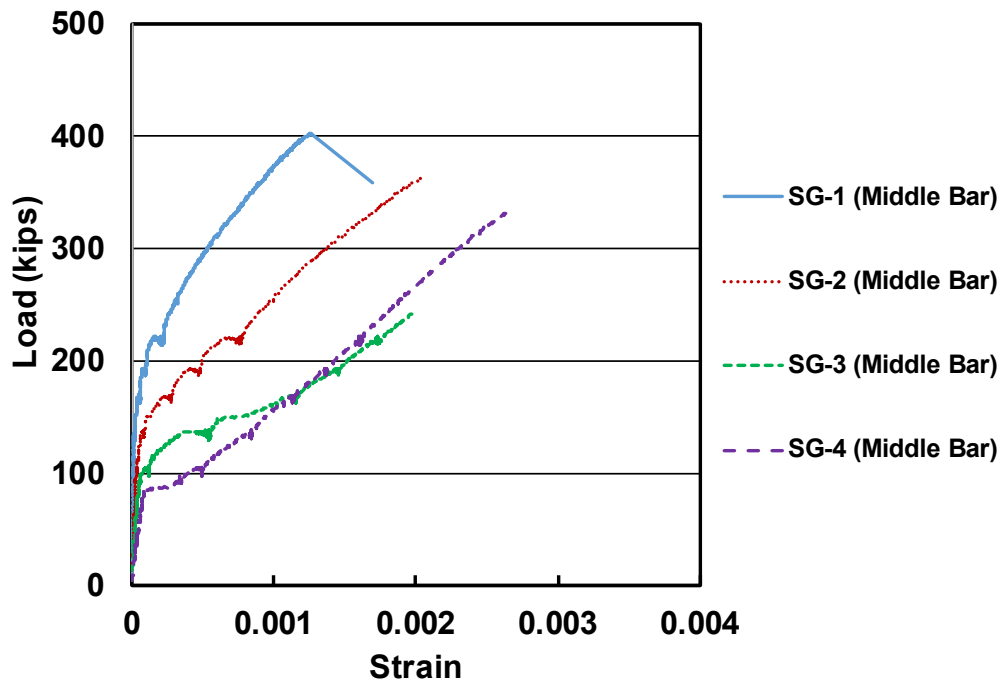


(c)

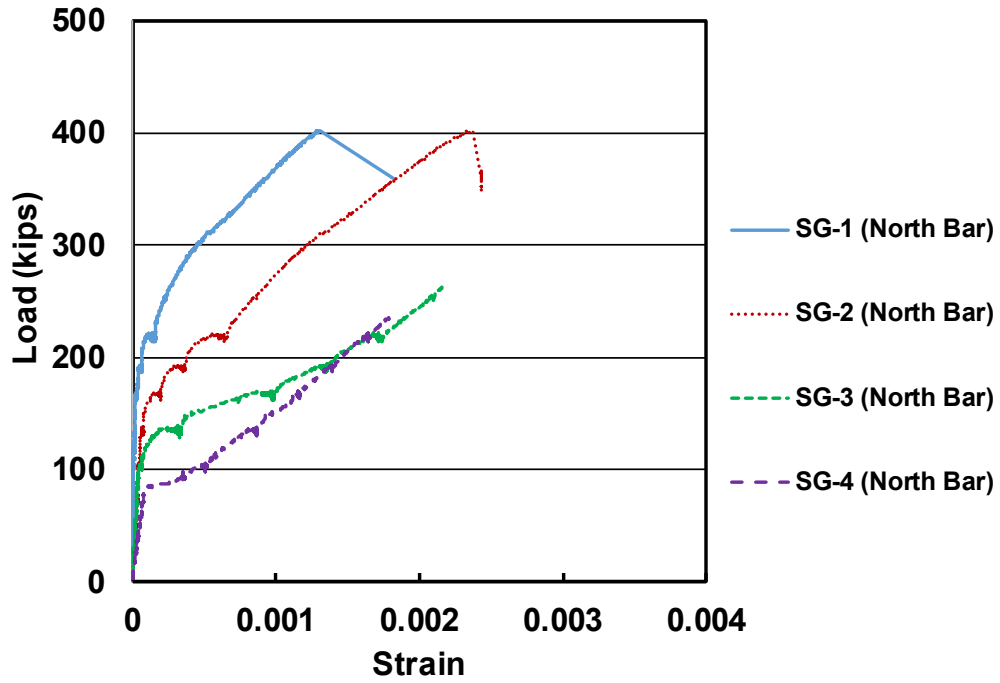
Figure B.22 Load-strain curve for specimen NH-3-8-5-9-F4.1-2, (a) south bar, (b) middle bar, and (c) north bar



(a)

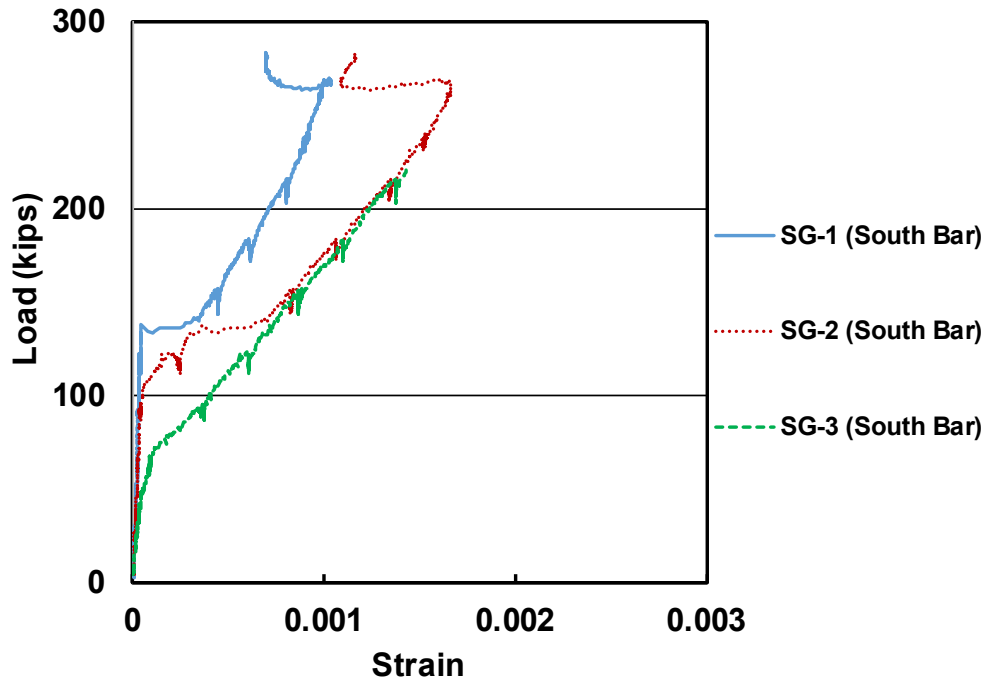


(b)

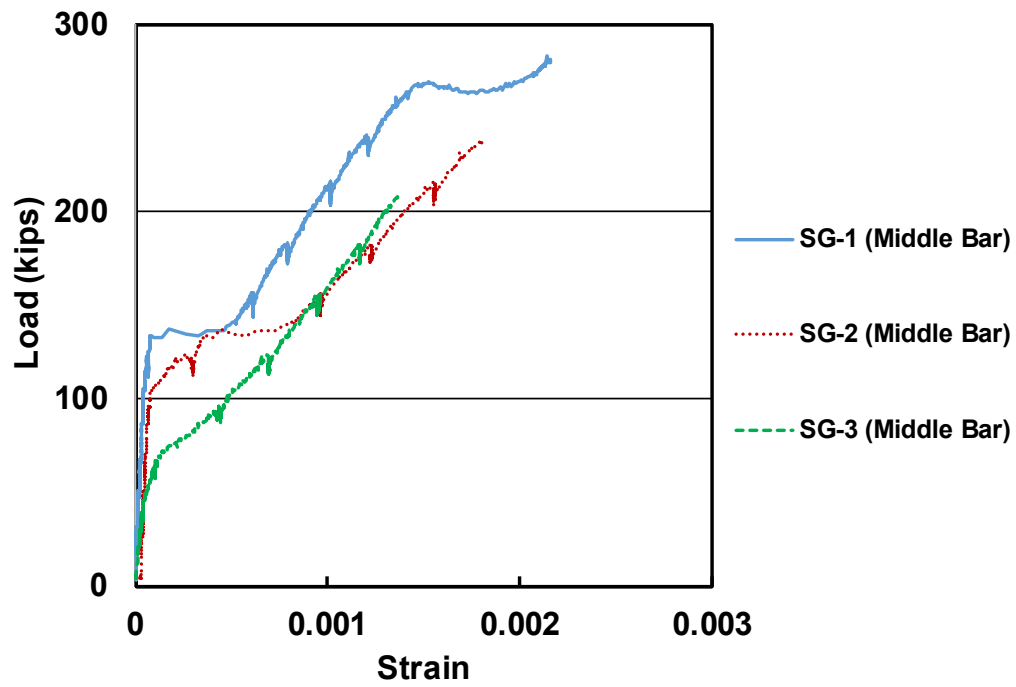


(c)

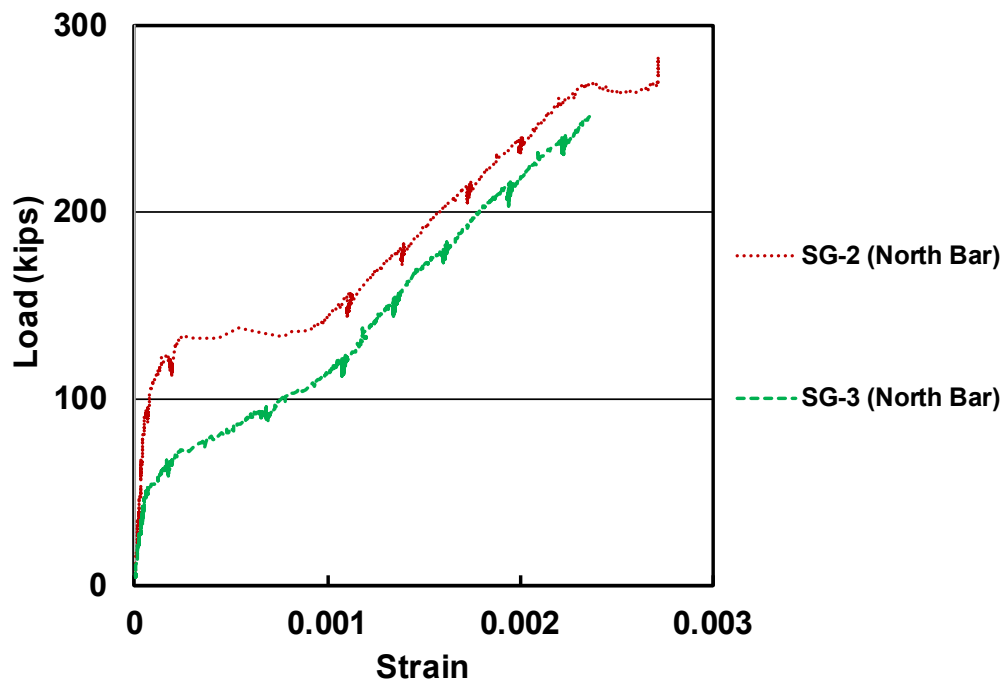
Figure B.23 Load-strain curve for specimen H-3-8-5-11-F4.1-2, (a) south bar, (b) middle bar, and (c) north bar



(a)

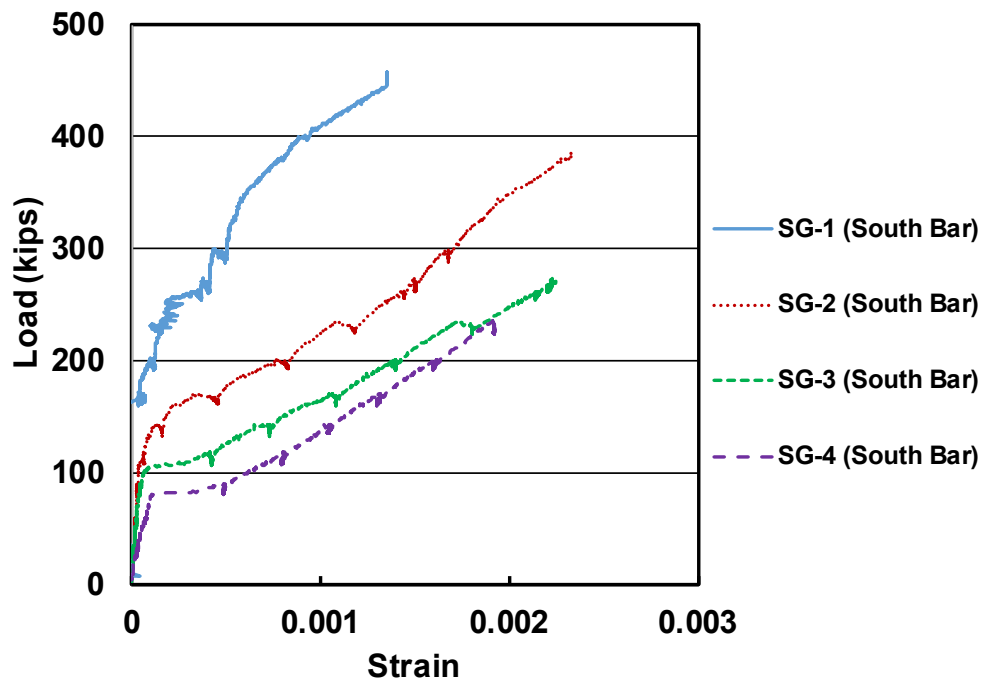


(b)

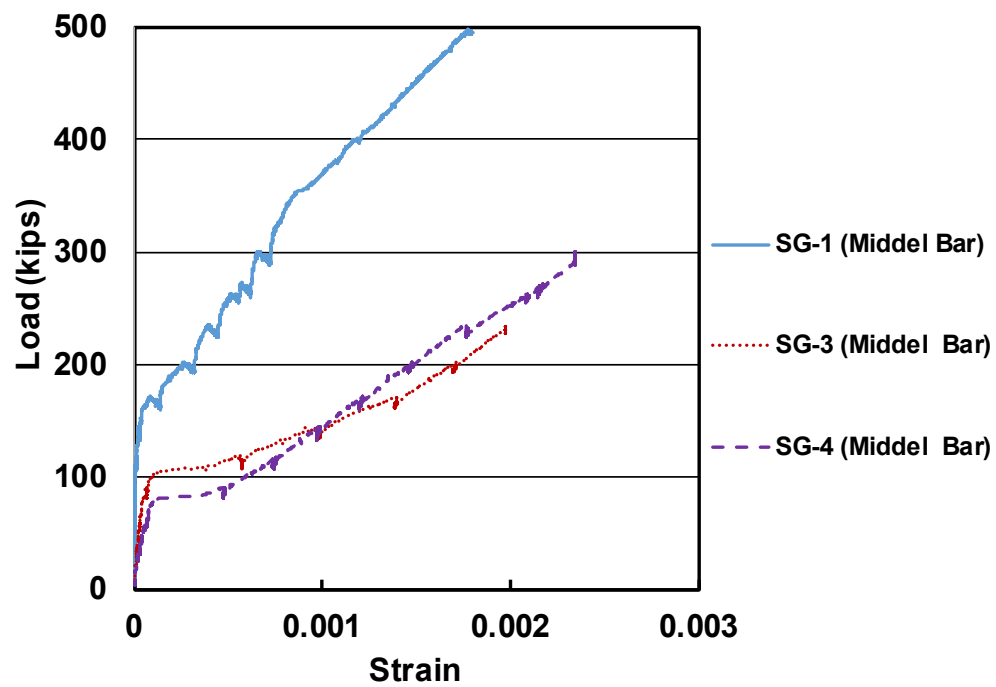


(c)

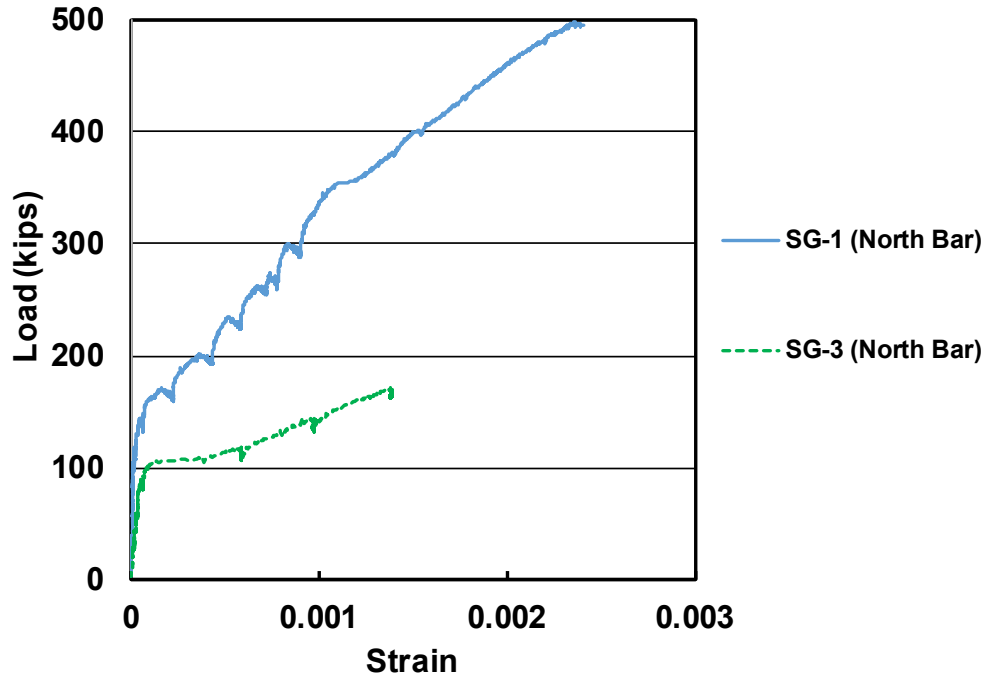
Figure B.24 Load-strain curve for specimen NH-3-8-5-11-F4.1-2, (a) south bar, (b) middle bar, and (c) north bar



(a)

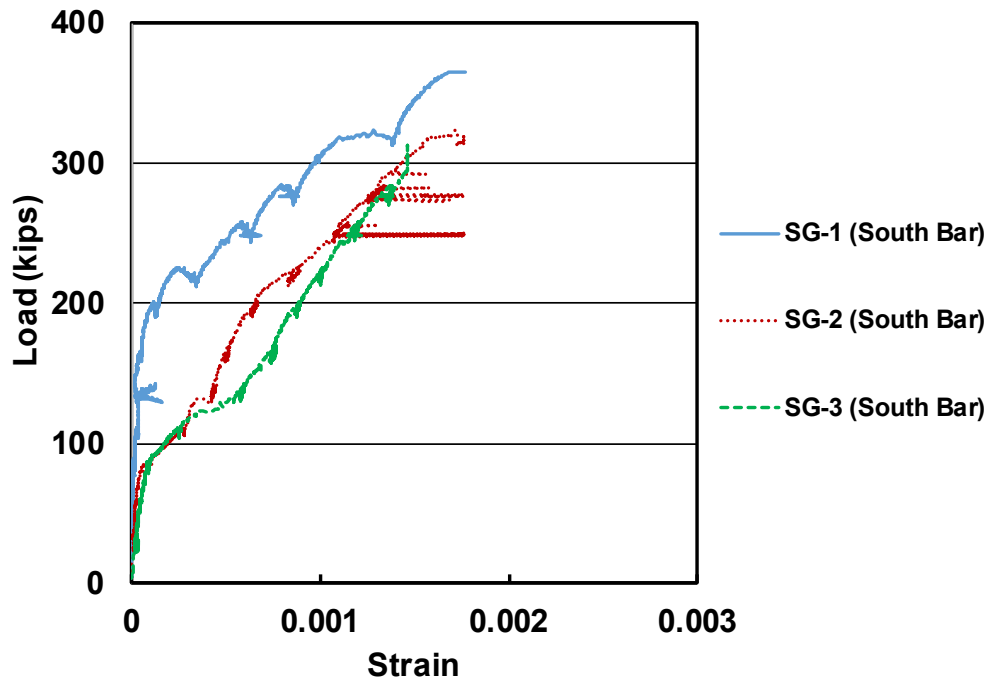


(b)

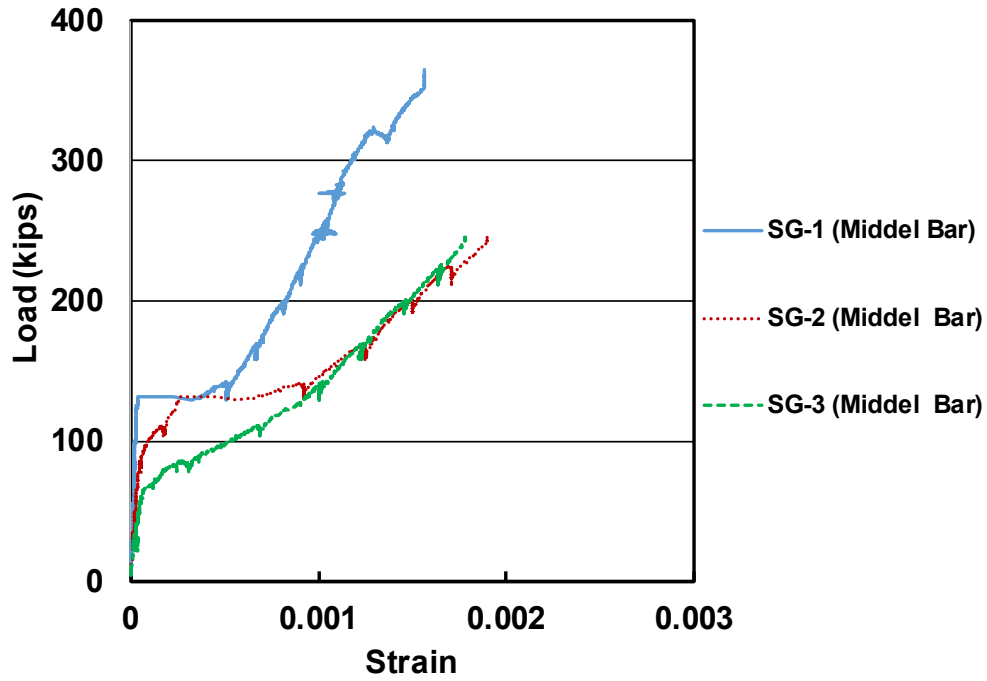


(c)

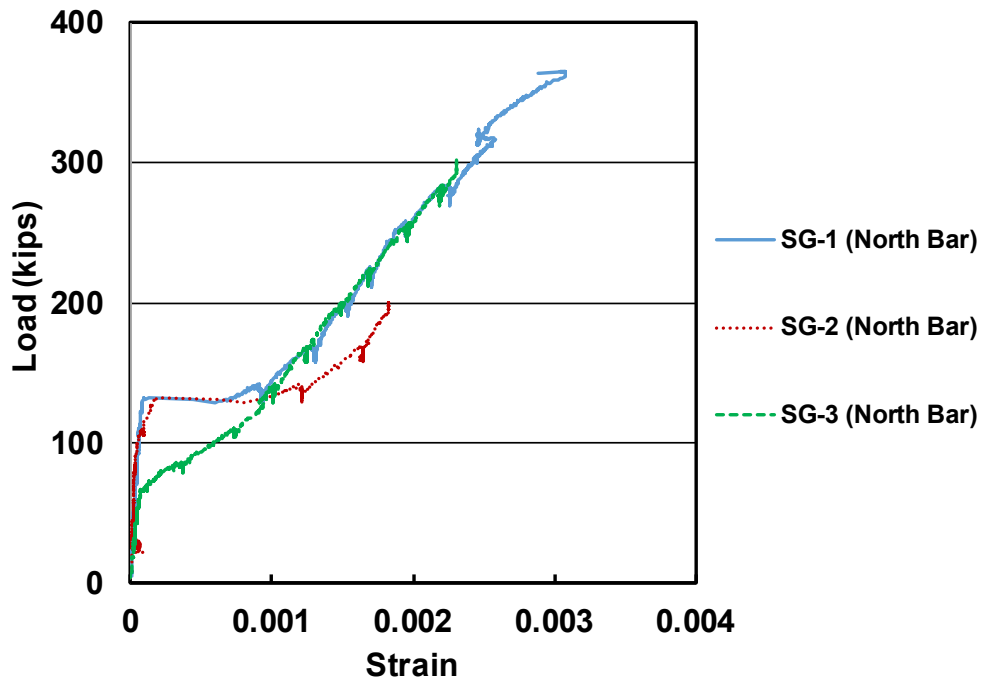
Figure B.25 Load-strain curve for specimen H-3-8-5-13-F4.1-2, (a) south bar, (b) middle bar, and (c) north bar



(a)



(b)



(c)

Figure B.26 Load-strain curve for specimen NH-3-8-5-13-F4.1-2, (a) south bar, (b) middle bar, and (c) north bar

APPENDIX C: TEST RESULTS AND SPECIMENS DETAILS

C.1: BEAM-COLUMN JOINT WITH $d_{eff}/\ell_{eh} < 1.5$

Table C.1 Details of the widely-spaced bars without confining reinforcement

No.	Specimen	Head	c_o in.	A_{brg}	ℓ_{eh} in.	$\ell_{eh,avg}$ in.	f_{cm} psi	Age days	d_b in.	A_b in. ²
1	8-5g-T4.0-0-i-2.5-3-12.5 ^a	A B	1.9	$4.0A_b$	12.69 12.44	12.56	5910	14	1	0.79
2	8-5g-T4.0-0-i-3.5-3-12.5 ^a	A B	2.9	$4.0A_b$	12.44 12.56	12.5	6320	15	1	0.79
3	8-5-T4.0-0-i-2.5-3-12.5 ^a	A B	1.9	$4.0A_b$	12.69 12.5	12.59	6210	8	1	0.79
4	8-5-T4.0-0-i-3.5-3-12.5 ^a	A B	2.9	$4.0A_b$	12.81 12.5	12.66	6440	9	1	0.79
5	8-8-F4.1-0-i-2.5-3-10.5	A B	2	$4.1A_b$	10.25 10.75	10.5	8450	9	1	0.79
6	8-12-F4.1-0-i-2.5-3-10	A B	2	$4.1A_b$	9.63 9.75	9.69	11760	34	1	0.79
7	8-5-S6.5-0-i-2.5-3-11.25	A B	1.8	$6.5A_b$	11 11.13	11.06	5500	6	1	0.79
8	8-5-S6.5-0-i-2.5-3-14.25	A B	1.8	$6.5A_b$	14.38 14.13	14.25	5500	6	1	0.79
9	8-5-O4.5-0-i-2.5-3-11.25	A B	1.6	$4.5A_b$	11 11.5	11.25	5500	6	1	0.79
10	8-5-O4.5-0-i-2.5-3-14.25	A B	1.6	$4.5A_b$	14.38 13.88	14.13	5500	6	1	0.79
11	8-5-T9.5-0-i-2.5-3-14.5	A B	1.4	$9.5A_b$	14.25 14.5	14.38	4970	8	1	0.79
12	8-5-O9.1-0-i-2.5-3-14.5	A B	1.3	$9.1A_b$	14.38 14.38	14.38	4970	8	1	0.79
13	8-15-T4.0-0-i-2.5-4.5-9.5	A B	1.9	$4.0A_b$	9.5 9.5	9.5	16030	88	1	0.79
14	8-15-S9.5-0-i-2.5-3-9.5	A B	1.4	$9.5A_b$	9.5 9.5	9.5	16030	88	1	0.79
15	8-8-T9.5-0-i-2.5-3-9.5	A B	1.4	$9.5A_b$	9.5 9.25	9.38	9040	12	1	0.79
16	(2@9)8-12-F4.1-0-i-2.5-3-12	A B	2	$4.1A_b$	12.13 12	12.06	12080	57	1	0.79
17	(2@9)8-12-F9.1-0-i-2.5-3-12	A B	2	$9.1A_b$	11.75 12	11.88	12080	57	1	0.79

^a Specimen contained crossies within joint region

Table C.1 Cont'd Details of the widely-spaced bars without confining reinforcement

No.	Specimen	Head	c_o in.	A_{brg}	ℓ_{eh} in.	$\ell_{eh,avg}$ in.	f_{cm} psi	Age days	d_b in.	A_b in. ²
18	8-8-O4.5-0-i-2.5-3-9.5	A B	1.6	$4.5A_b$	9.13 9.25	9.19	6710	16	1	0.79
19	(2@9)8-8-O4.5-0-i-2.5-3-9.5	A B	1.6	$4.5A_b$	9.13 8.88	9	6710	16	1	0.79
20	(2@9)8-8-T4.0-0-i-2.5-3-9.5	A B	1.9	$4.0A_b$	9.25 9.5	9.38	6790	17	1	0.79
21	5-5-F4.0-0-i-2.5-5-4	A B	2.2	$4.0A_b$	4 4.13	4.06	4810	8	0.625	0.31
22	5-5-F4.0-0-i-2.5-3-6	A B	2.2	$4.0A_b$	6 6	6	4690	7	0.625	0.31
23	5-12-F4.0-0-i-2.5-5-4	A B	2.2	$4.0A_b$	4.13 4	4.06	11030	35	0.625	0.31
24	5-12-F4.0-0-i-2.5-3-6	A B	2.2	$4.0A_b$	6 6	6	11030	36	0.625	0.31
25	11-5a-F3.8-0-i-2.5-3-17	A B	2	$3.8A_b$	16.38 16.75	16.56	4050	36	1.41	1.56
26	11-5-F3.8-0-i-2.5-3-17	A B	2	$3.8A_b$	17.5 17	17.25	5760	6	1.41	1.56
27	11-12-O4.5-0-i-2.5-3-16.75	A B	1.3	$4.5A_b$	17.13 17.13	17.13	10860	36	1.41	1.56
28	11-12-S5.5-0-i-2.5-3-16.75	A B	1.5	$5.5A_b$	16.75 17.13	16.94	10120	37	1.41	1.56
29	11-5-O4.5-0-i-2.5-3-19.25	A B	1.3	$4.5A_b$	19.63 19.25	19.44	5430	12	1.41	1.56
30	11-5-S5.5-0-i-2.5-3-19.25	A B	1.5	$5.5A_b$	19.38 19.38	19.38	6320	11	1.41	1.56

Table C.1 Cont'd Details of the widely-spaced bars without confining reinforcement

No.	Specimen	Head	<i>b</i> in.	<i>h</i> in.	<i>h_{cl}</i> in.	<i>d_{eff}</i> in.	<i>c_{so}</i> in.	<i>c_{so,avg}</i> in.	<i>c_{bc}</i> in.	<i>s</i> in.	<i>d_{tr}</i> in.	<i>A_{tr,t}</i> in. ²
1	8-5g-T4.0-0-i-2.5-3-12.5 ^a	A	16.8	17.2	10.25	13.28	2.5	2.5	3	10.8	-	-
		B					2.5		3.3			
2	8-5g-T4.0-0-i-3.5-3-12.5 ^a	A	18.7	17.1	10.25	12.74	3.3	3.3	3.2	11.1	-	-
		B					3.4		3.1			
3	8-5-T4.0-0-i-2.5-3-12.5 ^a	A	16.6	17.2	10.25	12.76	2.4	2.4	3	10.8	-	-
		B					2.5		3.2			
4	8-5-T4.0-0-i-3.5-3-12.5 ^a	A	18.5	17.2	10.25	12.68	3.5	3.6	2.9	10.4	-	-
		B					3.6		3.2			
5	8-8-F4.1-0-i-2.5-3-10.5	A	16.8	14.8	10.25	12.19	2.4	2.4	3.5	10.9	-	-
		B					2.5		3			
6	8-12-F4.1-0-i-2.5-3-10	A	16.9	14.2	10.25	11.55	2.4	2.5	3.5	10.9	0.375	-
		B					2.6		3.4			
7	8-5-S6.5-0-i-2.5-3-11.25	A	16.8	16.1	10.25	12.7	2.5	2.5	3.4	10.8	0.375	-
		B					2.5		3.3			
8	8-5-S6.5-0-i-2.5-3-14.25	A	16.3	19.1	10.25	13.1	2.3	2.3	3	10.6	0.375	-
		B					2.4		3.3			
9	8-5-O4.5-0-i-2.5-3-11.25	A	16.9	16.1	10.25	12.44	2.5	2.5	3.5	10.9	0.375	-
		B					2.5		3			
10	8-5-O4.5-0-i-2.5-3-14.25	A	17	19.1	10.25	13.01	2.5	2.5	3.1	11	0.375	-
		B					2.5		3.6			
11	8-5-T9.5-0-i-2.5-3-14.5	A	17	19.1	10.25	13.43	2.6	2.6	3.4	10.9	0.375	-
		B					2.5		3.1			
12	8-5-O9.1-0-i-2.5-3-14.5	A	17.3	19.2	10.25	13.54	2.5	2.6	3.2	11	0.375	-
		B					2.8		3.2			
13	8-15-T4.0-0-i-2.5-4.5-9.5	A	17	15.5	10.25	11.36	2.5	2.5	4.5	11	0.375	-
		B					2.5		4.5			
14	8-15-S9.5-0-i-2.5-3-9.5	A	17.3	15.2	10.25	11.33	2.8	2.6	2.9	11	0.375	-
		B					2.5		2.9			
15	8-8-T9.5-0-i-2.5-3-9.5	A	17	14.3	10.25	11.79	2.5	2.5	3.3	11	0.375	-
		B					2.5		3.5			
16	(2@9)8-12-F4.1-0-i-2.5-3-12	A	15	16.1	10.25	11.83	2.5	2.5	2.9	9	0.375	-
		B					2.5		3.1			
17	(2@9)8-12-F9.1-0-i-2.5-3-12	A	14.9	16	10.25	11.78	2.5	2.5	3.3	8.9	0.375	-
		B					2.5		3			

Table C.1 Cont'd Details of the widely-spaced bars without confining reinforcement

No.	Specimen	Head	<i>b</i> in.	<i>h</i> in.	<i>h_{cl}</i> in.	<i>d_{eff}</i> in.	<i>c_{so}</i> in.	<i>c_{so,avg}</i> in.	<i>c_{bc}</i> in.	<i>s</i> in.	<i>d_{tr}</i> in.	<i>A_{tr,l}</i> in. ²
18	8-8-O4.5-0-i-2.5-3-9.5	A B	17.3	14.1	10.25	11.93	2.8 2.4	2.6	3.3 3.2	11.1	0.375	-
19	(2@9)8-8-O4.5-0-i-2.5-3-9.5	A B	15.3	14.1	10.25	12.17	2.6 2.5	2.6	3.3 3.6	9.1	0.375	-
20	(2@9)8-8-T4.0-0-i-2.5-3-9.5	A B	15.1	14.1	10.25	12.26	2.5 2.5	2.5	3.4 3.1	9.1	0.375	-
21	5-5-F4.0-0-i-2.5-5-4	A B	12.9	9.8	5.25	6.39	2.5 2.5	2.5	5.3 5.1	7.3	-	-
22	5-5-F4.0-0-i-2.5-3-6	A B	13.1	9.8	5.25	6.8	2.5 2.6	2.6	3.3 3.3	7.3	-	-
23	5-12-F4.0-0-i-2.5-5-4	A B	13.1	9.8	5.25	5.96	2.6 2.6	2.6	5.1 5.3	7.3	-	-
24	5-12-F4.0-0-i-2.5-3-6	A B	13.1	9.6	5.25	6.3	2.6 2.5	2.6	3.1 3.1	7.4	-	-
25	11-5a-F3.8-0-i-2.5-3-17	A B	21.9	22	20	23.11	2.6 2.4	2.5	4.2 3.8	15.5	-	-
26	11-5-F3.8-0-i-2.5-3-17	A B	21.9	21.9	20	23.31	2.5 3	2.8	3 3.5	15	-	-
27	11-12-O4.5-0-i-2.5-3-16.75	A B	21.9	23.1	20	22.63	2.8 2.8	2.8	3.9 3.9	15	-	-
28	11-12-S5.5-0-i-2.5-3-16.75	A B	22.3	23.1	20	22.93	2.8 2.9	2.8	3.6 3.2	15.3	-	-
29	11-5-O4.5-0-i-2.5-3-19.25	A B	21.9	25.6	20	24.09	2.6 2.8	2.7	3.9 4.3	15.1	-	-
30	11-5-S5.5-0-i-2.5-3-19.25	A B	22	25.4	20	24.17	2.5 3	2.8	3.3 3.3	15.1	-	-

Table C.1 Cont'd Details of the widely-spaced bars without confining reinforcement

No.	Specimen	Head	<i>N</i>	<i>s_{tr}^c</i> in.	<i>A_{tr}</i> in.2	<i>d_{tro}</i> in.	<i>s_{tro}^c</i> in.	<i>A_{ab}</i> in.2	<i>n</i>	<i>A_{hs}</i> in.2	Long. Reinf. Layout
1	8-5g-T4.0-0-i-2.5-3-12.5 ^a	A B	-	-	-	0.375	3.5 (1.75)	0.44	2	1.58	B2
2	8-5g-T4.0-0-i-3.5-3-12.5 ^a	A B	-	-	-	0.375	3.5 (1.75)	0.44	2	1.58	B2
3	8-5-T4.0-0-i-2.5-3-12.5 ^a	A B	-	-	-	0.375	3.5 (1.75)	0.44	2	1.58	B2
4	8-5-T4.0-0-i-3.5-3-12.5 ^a	A B	-	-	-	0.375	3.5 (1.75)	0.44	2	1.58	B2
5	8-8-F4.1-0-i-2.5-3-10.5	A C	-	-	-	0.375	4 (2)	0.44	2	1.58	B1
6	8-12-F4.1-0-i-2.5-3-10	A C	-	-	-	0.375	4 (2)	0.44	2	1.58	B4
7	8-5-S6.5-0-i-2.5-3-11.25	A B	-	-	-	0.5	3.5 (1.75)	0.8	2	1.58	B4
8	8-5-S6.5-0-i-2.5-3-14.25	A B	-	-	-	0.5	3.5 (1.75)	0.8	2	1.58	B4
9	8-5-O4.5-0-i-2.5-3-11.25	A B	-	-	-	0.5	3.5 (1.75)	0.8	2	1.58	B4
10	8-5-O4.5-0-i-2.5-3-14.25	A B	-	-	-	0.5	3.5 (1.5)	0.8	2	1.58	B4
11	8-5-T9.5-0-i-2.5-3-14.5	A B	-	-	-	0.375	4 (2)	0.44	2	1.58	B4
12	8-5-O9.1-0-i-2.5-3-14.5	A C	-	-	-	0.375	4 (2)	0.44	2	1.58	B4
13	8-15-T4.0-0-i-2.5-4.5-9.5	A B	-	-	-	0.5	4 (2)	0.8	2	1.58	B6
14	8-15-S9.5-0-i-2.5-3-9.5	A B	-	-	-	0.5	4 (2)	0.8	2	1.58	B6
15	8-8-T9.5-0-i-2.5-3-9.5	A B	-	-	-	0.375	3 (1.5)	0.66	2	1.58	B6
16	(2@9)8-12-F4.1-0-i-2.5-3-12	A B	-	-	-	0.5	3 (1.5)	1.2	2	1.58	B5
17	(2@9)8-12-F9.1-0-i-2.5-3-12	A B	-	-	-	0.5	3 (1.5)	1.2	2	1.58	B5

^c Value in parenthesis is the spacing between the first hoop and the center of the headed bar

Table C.1 Cont'd Details of the widely-spaced bars without confining reinforcement

No.	Specimen	Head	N	s_{tr}^c in.	A_{tt} in.2	d_{tro} in.	s_{tro}^c in.	A_{ab} in.2	n	A_{hs} in.2	Long. Reinf. Layout
18	8-8-O4.5-0-i-2.5-3-9.5	A B	-	-	-	0.375	4 (2)	0.44	2	1.58	B4
19	(2@9)8-8-O4.5-0-i-2.5-3-9.5	A B	-	-	-	0.375	4 (2)	0.44	2	1.58	B4
20	(2@9)8-8-T4.0-0-i-2.5-3-9.5	A B	-	-	-	0.5	4 (2)	0.8	2	1.58	B9
21	5-5-F4.0-0-i-2.5-5-4	A B	-	-	-	0.375	3.5 (1.75)	0.22	2	0.62	B4
22	5-5-F4.0-0-i-2.5-3-6	A B	-	-	-	0.375	3.5 (1.75)	0.22	2	0.62	B4
23	5-12-F4.0-0-i-2.5-5-4	A B	-	-	-	0.375	3.5 (1.75)	0.22	2	0.62	B4
24	5-12-F4.0-0-i-2.5-3-6	A B	-	-	-	0.375	3.5 (1.75)	0.22	2	0.62	B4
25	11-5a-F3.8-0-i-2.5-3-17	A B	-	-	-	0.5	4 (2)	1.2	2	3.12	B10
26	11-5-F3.8-0-i-2.5-3-17	A B	-	-	-	0.5	6 (3)	0.8	2	3.12	B7
27	11-12-O4.5-0-i-2.5-3-16.75	A B	-	-	-	0.5	4 (2)	1.2	2	3.12	B16
28	11-12-S5.5-0-i-2.5-3-16.75	A B	-	-	-	0.5	4 (2)	1.2	2	3.12	B16
29	11-5-O4.5-0-i-2.5-3-19.25	A B	-	-	-	0.5	4 (2)	1.2	2	3.12	B16
30	11-5-S5.5-0-i-2.5-3-19.25	A B	-	-	-	0.5	4 (2)	1.2	2	3.12	B16

^c Value in parenthesis is the spacing between the first hoop and the center of the headed bar

Table C.1 Cont'd Details of the widely-spaced bars without confining reinforcement

No.	Specimen	Head	Failure Type	Lead (Head) in.	T_{max} kips	$f_{su,max}$ ksi	T_{ind} kips	T_{total} kips	T kips	f_{su} ksi
1	8-5g-T4.0-0-i-2.5-3-12.5 ^a	B	SB/FP	0.35	103.4	130.9	100.5	195.4	97.7	123.7
		A		-	117.6	148.9	99.3			
		B		0.022 (0.008)	96.1	121.6	96.1			
2	8-5g-T4.0-0-i-3.5-3-12.5 ^a	A	SB/FP	0.427	104.6	132.4	93.2	186.8	93.4	118.2
		B		0.056	95.8	121.3	95.8			
3	8-5-T4.0-0-i-2.5-3-12.5 ^a	A	SB/FP	-	84	106.3	84	166.6	83.3	105.4
		B		-	95	120.3	82.6			
4	8-5-T4.0-0-i-3.5-3-12.5 ^a	A	SB/FP	0.013	92.1	116.6	92.1	183.7	91.9	116.3
		B		-	89	112.7	84.6			
5	8-8-F4.1-0-i-2.5-3-10.5	A	CB	-	77.8	98.5	77.8	154.1	77.1	97.6
		C		0.168	63.6	80.5	63.6			
6	8-12-F4.1-0-i-2.5-3-10	A	CB	0.11	72.5	91.8	72.5	143.6	71.8	90.9
		C		0.122	66.7	84.4	66.6			
7	8-5-S6.5-0-i-2.5-3-11.25	A	SB/FP	0.161	74.9	94.8	74.9	151.1	75.6	95.6
		B		-	76.2	96.5	76.2			
8	8-5-S6.5-0-i-2.5-3-14.25	A	SB/FP	0.054	87.5	110.8	87.5	175.4	87.7	111
		B		-	103.4	130.9	88			
9	8-5-O4.5-0-i-2.5-3-11.25	A	SB/FP	0.037	67.6	85.6	67.6	134.8	67.4	85.3
		B		0.198	67.2	85	67.2			
10	8-5-O4.5-0-i-2.5-3-14.25	A	SB/FP	0.214 (0.023)	103.5	131	84.2	170	85	107.6
		B		-	82.4	104.3	82.4			
11	8-5-T9.5-0-i-2.5-3-14.5	A	SB/FP	0.13	91.5	115.8	91.5	183.3	91.7	116
		B		0.312	115.9	146.7	91.8			
12	8-5-O9.1-0-i-2.5-3-14.5	A	SB/FP	0.06	94.6	119.7	94.6	189.6	94.8	120
		C		0.217	72.6	91.9	72.6			
13	8-15-T4.0-0-i-2.5-4.5-9.5	A	CB	-	83.2	105.3	83.2	166.6	83.3	105.4
		B		0.237	83.4	105.6	83.4			
14	8-15-S9.5-0-i-2.5-3-9.5	A	CB	-	83.5	105.7	83.5	163.3	81.7	103.4
		B		-	79.9	101.1	79.9			
15	8-8-T9.5-0-i-2.5-3-9.5	A	CB	0.168	65	82.3	65	130.5	65.2	82.5
		B		0.127	65.5	82.9	65.5			
16	(2@9)8-12-F4.1-0-i-2.5-3-12	A	CB/FP	-	79.8	101	79.8	158.1	79.1	100.1
		B		-	78.3	99.1	78.3			
17	(2@9)8-12-F9.1-0-i-2.5-3-12	A	CB/BS	0.048	76.1	96.3	76.1	153	76.5	96.8
		B		-	76.9	97.3	76.9			

^a Specimen contained cross-ties within joint region

Table C.1 Cont'd Details of the widely-spaced bars without confining reinforcement

No.	Specimen	Head	Failure Type	Lead in.	T_{max} kips	$f_{su,max}$ ksi	T_{ind} kips	T_{total} kips	T kips	f_{su} ksi
18	8-8-O4.5-0-i-2.5-3-9.5	A	CB/FP	0.002	61.9	78.4	61.8	116.7	58.4	73.9
		B		0.002	54.9	69.5	54.9			
19	(2@9)8-8-O4.5-0-i-2.5-3-9.5	A	CB	0.014	57.5	72.8	57.5	117.6	58.8	74.4
		B		0.019	60.1	76.1	60.1			
20	(2@9)8-8-T4.0-0-i-2.5-3-9.5	A	CB	0.015	65	82.3	65	123.7	61.8	78.2
		B		0.016	58.7	74.3	58.7			
21	5-5-F4.0-0-i-2.5-5-4	A	CB	-	25.9	83.5	25.9	49.1	24.5	79
		B		-	23.1	74.5	23.1			
22	5-5-F4.0-0-i-2.5-3-6	A	SB	-	34.6 [†]	111.6 [†]	32.9	65.5	32.7	105.5
		B		-	33	106.5	32.6			
23	5-12-F4.0-0-i-2.5-5-4	A	CB	0.123	28.9	93.2	28.9	56.6	28.3	91.3
		B		0.055	27.7	89.4	27.7			
24	5-12-F4.0-0-i-2.5-3-6	A	SB	0.136	43.9	141.6	41.8	83.5	41.7	134.5
		B		0.226	41.6	134.2	41.6			
25	11-5a-F3.8-0-i-2.5-3-17	A	CB/FP	0.106	97.1	62.2	97.1	195.1	97.5	62.5
		B		0.043	98	62.8	98			
26	11-5-F3.8-0-i-2.5-3-17	A	CB/FP	0.115	132.6	85	132.6	265.5	132.7	85.1
		B		0.015	132.9	85.2	132.9			
27	11-12-O4.5-0-i-2.5-3-16.75	A	CB	0.032	168.4	107.9	168.3	339.3	169.6	108.7
		B		0.029	171	109.6	171			
28	11-12-S5.5-0-i-2.5-3-16.75	A	CB	0.091	179.1	114.8	179.1	351.9	175.9	112.8
		B		0.215	172.7	110.7	172.7			
29	11-5-O4.5-0-i-2.5-3-19.25	A	SB/FP	0.021	161.4	103.5	161.4	315.7	157.9	101.2
		B		0.128	154.4	99	154.3			
30	11-5-S5.5-0-i-2.5-3-19.25	A	SB/FP	0.117	176.9	113.4	176.9	353.6	176.8	113.3
		B		0.095	176.8 [†]	113.3 [†]	176.7			

[†] No anchorage failure on the bar

Table C.2 Details of the closely-spaced bars without confining reinforcement

No.	Specimen	Head	c_o in.	A_{brg}	ℓ_{eh} in.	$\ell_{eh,avg}$ in.	f_{cm} psi	Age days	d_b in.	A_b in. ²
1	(3@3)8-8-F4.1-0-i-2.5-3-10.5	A B C	2	$4.1A_b$	10.63 10.75 10.38	10.58	8450	9	1	0.79
2	(3@3)8-8-F4.1-0-i-2.5-3-10.5-HP	A B C	2	$4.1A_b$	10.13 10.13 10.75	10.33	8450	9	1	0.79
3	(3@4)8-8-F4.1-0-i-2.5-3-10.5	A B C	2	$4.1A_b$	10.88 10.75 10.88	10.83	8450	9	1	0.79
4	(3@5)8-8-F4.1-0-i-2.5-3-10.5	A B C	2	$4.1A_b$	10.5 10.38 10.19	10.35	8050	7	1	0.79
5	(3@5)8-8-F4.1-0-i-2.5-3-10.5-HP	A B C	2	$4.1A_b$	9.75 10.5 10.5	10.25	8260	8	1	0.79
6	(3@3)8-12-F4.1-0-i-2.5-3-10	A B C	2	$4.1A_b$	9.81 10 9.88	9.9	11040	31	1	0.79
7	(3@4)8-12-F4.1-0-i-2.5-3-10	A B C	2	$4.1A_b$	10 9.75 10	9.92	11440	32	1	0.79
8	(3@5)8-12-F4.1-0-i-2.5-3-10	A B C	2	$4.1A_b$	9.88 10.13 9.75	9.92	11460	33	1	0.79
9	(3@5.5)8-5-T9.5-0-i-2.5-3-14.5	A B C	1.4	$9.5A_b$	14.25 14.25 14.25	14.25	4960	9	1	0.79
10	(3@5.5)8-5-O9.1-0-i-2.5-3-14.5	A B C	1.3	$9.1A_b$	14.31 14.5 14.25	14.35	4960	9	1	0.79
11	(4@3.7)8-5-T9.5-0-i-2.5-3-14.5	A B C D	1.4	$9.5A_b$	14.25 14.38 14.25 14.19	14.3	5570	14	1	0.79
12	(4@3.7)8-5-O9.1-0-i-2.5-3-14.5	A B C D	1.3	$9.1A_b$	14.06 14.06 14.06 14.06	14.06	5570	14	1	0.79
13	(3@4)8-8-T9.5-0-i-2.5-3-9.5	A B C	1.4	$9.5A_b$	9 9.5 9.25	9.25	9040	12	1	0.79
14	(3@5)8-8-T9.5-0-i-2.5-3-9.5	A B C	1.4	$9.5A_b$	9.5 9.75 9.25	9.5	9940	11	1	0.79
15	(3@7)8-8-T9.5-0-i-2.5-3-9.5	A B C	1.4	$9.5A_b$	9.5 9.63 9.38	9.5	10180	10	1	0.79
16	(3@4)8-8-T9.5-0-i-2.5-3-14.5	A B C	1.4	$9.5A_b$	14.25 14.75 14.75	14.58	9040	12	1	0.79
17	(3@5)8-8-T9.5-0-i-2.5-3-14.5	A B C	1.4	$9.5A_b$	14.75 14.5 14.5	14.58	9940	11	1	0.79

Table C.2 Cont'd Details of the closely-spaced bars without confining reinforcement

No.	Specimen	Head	c_o in.	A_{brg}	ℓ_{eh} in.	$\ell_{eh,avg}$ in.	f_{cm} psi	Age days	d_b in.	A_b in. ²
18	(3@7)8-8-T9.5-0-i-2.5-3-14.5	A B C	1.4	9.5 A_b	14.44 14.56 14.63	14.54	10180	10	1	0.79
19	(3@4.5)8-12-F4.1-0-i-2.5-3-12	A B C	2	4.1 A_b	12.13 12.25 12.25	12.21	12040	58	1	0.79
20	(3@4.5)8-12-F9.1-0-i-2.5-3-12	A B C	2	9.1 A_b	12 12.13 12	12.04	12040	58	1	0.79
21	(4@3)8-12-F4.1-0-i-2.5-3-12	A B C D	2	4.1 A_b	12 12 12 12	12	12040	58	1	0.79
22	(4@3)8-12-F9.1-0-i-2.5-3-12	A B C D	2	9.1 A_b	12.06 12.13 12.25 12.25	12.17	12360	61	1	0.79
23	(2@7)8-8-O4.5-0-i-2.5-3-9.5	A B	1.6	4.5 A_b	9.38 9.13	9.25	6710	16	1	0.79
24	(2@5)8-8-O4.5-0-i-2.5-3-9.5	A B	1.6	4.5 A_b	9.13 8.88	9	6710	16	1	0.79
25	(2@3)8-8-O4.5-0-i-2.5-3-9.5	A B	1.6	4.5 A_b	9.13 8.88	9	6710	16	1	0.79
26	(3@4.5)8-8-T4.0-0-i-2.5-3-9.5	A B C	1.9	4.0 A_b	9.25 9.5 9.25	9.33	6790	17	1	0.79
27	(4@3)8-8-T4.0-0-i-2.5-3-9.5	A B C D	1.9	4.0 A_b	9.63 9.63 9.25 9.38	9.47	6650	20	1	0.79
28	(3@3)8-8-T4.0-0-i-2.5-3-9.5	A B C	1.9	4.0 A_b	9.25 9.63 9.5	9.46	6790	17	1	0.79
29	(3@5.9)5-12-F4.0-0-i-2.5-4-5	A B C	2.2	4.0 A_b	5.06 5.06 5	5.04	11030	36	0.625	0.31
30	(4@3.9)5-12-F4.0-0-i-2.5-4-5	A B C D	2.2	4.0 A_b	5.19 5.13 5.25 5.19	5.19	11030	39	0.625	0.31
31	(3@5.35)11-12-O4.5-0-i-2.5-3-16.75	A B C	1.3	4.5 A_b	16.88 17.13 16.75	16.92	10860	36	1.41	1.56
32	(3@5.35)11-12-S5.5-0-i-2.5-3-16.75	A B C	1.5	5.5 A_b	16.88 17 16.88	16.92	10120	38	1.41	1.56
33	(3@5.35)11-5-O4.5-0-i-2.5-3-19.25	A B C	1.3	4.5 A_b	19.5 19.63 19.38	19.5	5430	12	1.41	1.56
34	(3@5.35)11-5-S5.5-0-i-2.5-3-19.25	A B C	1.5	5.5 A_b	19.25 19.38 19.25	19.29	6320	11	1.41	1.56

Table C.2 Cont'd Details of the closely-spaced bars without confining reinforcement

No.	Specimen	Head	<i>b</i> in.	<i>h</i> in.	<i>h_{cl}</i> in.	<i>d_{eff}</i> in.	<i>c_{so}</i> in.	<i>c_{so,avg}</i> in.	<i>c_{bc}</i> in.	<i>s</i> in.	<i>d_{tr}</i> in.	<i>A_{tr,l}</i> in. ²
1	(3@3)8-8-F4.1-0-i-2.5-3-10.5	A	11.9	14.6	10.25	13.18	2.5	2.4	3	3	-	-
		B					-		2.8			
		C					2.4		3.2			
2	(3@3)8-8-F4.1-0-i-2.5-3-10.5-HP	A	11.8	14.6	10.25	12.95	2.5	2.5	3.4	3	-	-
		B					-		3.4			
		C					2.5		2.8			
3	(3@4)8-8-F4.1-0-i-2.5-3-10.5	A	13.9	14.7	10.25	12.94	2.5	2.5	2.8	3.9	-	-
		B					-		3			
		C					2.5		2.8			
4	(3@5)8-8-F4.1-0-i-2.5-3-10.5	A	15.9	14.7	10.25	12.95	2.5	2.5	3.2	4.9	-	-
		B					-		3.3			
		C					2.4		3.5			
5	(3@5)8-8-F4.1-0-i-2.5-3-10.5-HP	A	16	14.8	10.25	12.71	2.4	2.4	4	5.1	-	-
		B					-		3.3			
		C					2.5		3.3			
6	(3@3)8-12-F4.1-0-i-2.5-3-10	A	12	14.2	10.25	11.98	2.5	2.4	3.3	3.1	0.375	-
		B					-		3.2			
		C					2.4		3.3			
7	(3@4)8-12-F4.1-0-i-2.5-3-10	A	14	14	10.25	11.91	2.5	2.5	3	4	0.375	-
		B					-		3.3			
		C					2.5		3			
8	(3@5)8-12-F4.1-0-i-2.5-3-10	A	16.1	14.1	10.25	11.88	2.5	2.5	3.2	5	0.375	-
		B					-		3			
		C					2.5		3.3			
9	(3@5.5)8-5-T9.5-0-i-2.5-3-14.5	A	16.9	19.2	10.25	14.08	2.4	2.4	3.4	5.5	0.375	-
		B					-		3.4			
		C					2.5		3.4			
10	(3@5.5)8-5-O9.1-0-i-2.5-3-14.5	A	16.9	19.2	10.25	14.2	2.4	2.4	3.3	5.5	0.375	-
		B					-		3.1			
		C					2.5		3.3			
11	(4@3.7)8-5-T9.5-0-i-2.5-3-14.5	A	17.3	19.2	10.25	14.17	2.5	2.5	3.5	3.8	0.375	-
		B					-		3.3			
		C					-		3.5			
		D					2.5		3.5			
12	(4@3.7)8-5-O9.1-0-i-2.5-3-14.5	A	16.8	19.1	10.25	14.19	2.5	2.4	3.4	3.6	0.375	-
		B					-		3.4			
		C					-		3.4			
		D					2.4		3.4			
13	(3@4)8-8-T9.5-0-i-2.5-3-9.5	A	14	14	10.25	11.98	2.5	2.5	3.5	4	0.375	-
		B					-		3			
		C					2.5		3.3			
14	(3@5)8-8-T9.5-0-i-2.5-3-9.5	A	16	14.3	10.25	11.77	2.5	2.5	3.3	5	0.375	-
		B					-		3			
		C					2.5		3.5			
15	(3@7)8-8-T9.5-0-i-2.5-3-9.5	A	19.9	14.1	10.25	12.08	2.5	2.5	3.1	7	0.375	-
		B					-		2.9			
		C					2.5		3.2			
16	(3@4)8-8-T9.5-0-i-2.5-3-14.5	A	14	19	10.25	13.54	2.5	2.5	3.3	4	0.375	-
		B					-		2.8			
		C					2.5		2.8			
17	(3@5)8-8-T9.5-0-i-2.5-3-14.5	A	15.8	19.1	10.25	13.43	2.5	2.5	2.9	4.8	0.375	-
		B					-		3.1			
		C					2.5		3.1			

Table C.2 Cont'd Details of the closely-spaced bars without confining reinforcement

No.	Specimen	Head	<i>b</i> in.	<i>h</i> in.	<i>h_{cl}</i> in.	<i>d_{eff}</i> in.	<i>c_{so}</i> in.	<i>c_{so,avg}</i> in.	<i>c_{bc}</i> in.	<i>s</i> in.	<i>d_{tr}</i> in.	<i>A_{tr,t}</i> in. ²
18	(3@7)8-8-T9.5-0-i-2.5-3-14.5	A B C	20	19.1	10.25	13.02	2.5 - 2.5	2.5	3.1 3 2.9	7 7	0.375	-
19	(3@4.5)8-12-F4.1-0-i-2.5-3-12	A B C	14.8	16.1	10.25	12.51	2.5 - 2.5	2.5	2.9 2.8 2.8	4.5 4.3	0.375	-
20	(3@4.5)8-12-F9.1-0-i-2.5-3-12	A B C	14.8	16.1	10.25	12.52	2.4 - 2.4	2.4	3.1 2.9 3.1	4.5 4.5	0.375	-
21	(4@3)8-12-F4.1-0-i-2.5-3-12	A B C D	14.9	16	10.25	12.23	2.4 - - 2.5	2.4	3 3 3 3	3 3 3	0.375	-
22	(4@3)8-12-F9.1-0-i-2.5-3-12	A B C D	15	16.2	10.25	12.22	2.5 - - 2.5	2.5	3.1 3 2.9 2.9	3 3 3	0.375	-
23	(2@7)8-8-O4.5-0-i-2.5-3-9.5	A B	13.1	14.1	10.25	12.31	2.5 2.6	2.6	3.1 3.3	7	0.375	-
24	(2@5)8-8-O4.5-0-i-2.5-3-9.5	A B	11.3	14.2	10.25	12.53	2.5 2.5	2.5	3.4 3.7	5.3	0.375	-
25	(2@3)8-8-O4.5-0-i-2.5-3-9.5	A B	9.1	14.1	10.25	12.85	2.4 2.6	2.5	3.4 3.6	3.1	0.375	-
26	(3@4.5)8-8-T4.0-0-i-2.5-3-9.5	A B C	15.1	14.1	10.25	12.23	2.6 - 2.5	2.6	3.4 3.1 3.4	4.5 4.5	0.375	-
27	(4@3)8-8-T4.0-0-i-2.5-3-9.5	A B C D	14.8	14.2	10.25	11.97	2.4 - - 2.5	2.4	3.1 3.1 3.4 3.3	3 2.9 3	0.375	-
28	(3@3)8-8-T4.0-0-i-2.5-3-9.5	A B C	12.3	14	10.25	12.65	2.5 - 2.5	2.5	3.3 2.9 3	3.1 3.1	0.375	-
29	(3@5.9)5-12-F4.0-0-i-2.5-4-5	A B C	13.1	9.8	5.25	6.31	2.5 - 2.5	2.5	4.2 4.2 4.3	3.8 3.8	-	-
30	(4@3.9)5-12-F4.0-0-i-2.5-4-5	A B C D	12.8	9.6	5.25	6.54	2.5 - - 2.5	2.5	3.9 4 3.8 3.9	2.3 2.5 2.4	-	-
31	(3@5.35)11-12-O4.5-0-i-2.5-3-16.75	A B C	21.8	22.9	20	22.48	3 - 2.5	2.8	3.9 3.6 4	7.5 7.4	-	-
32	(3@5.35)11-12-S5.5-0-i-2.5-3-16.75	A B C	21.9	23.1	20	22.72	2.8 - 2.8	2.8	3.5 3.4 3.5	7.5 7.5	-	-
33	(3@5.35)11-5-O4.5-0-i-2.5-3-19.25	A B C	22	25.4	20	25	2.8 - 2.8	2.8	3.8 3.6 3.9	7.6 7.5	-	-
34	(3@5.35)11-5-S5.5-0-i-2.5-3-19.25	A B C	21.9	25.5	20	24.86	2.8 - 2.8	2.8	3.5 3.4 3.5	7.5 7.5	-	-

Table C.2 Cont'd Details of the closely-spaced bars without confining reinforcement

No.	Specimen	Head	<i>N</i>	<i>S_{tr}^c</i> in.	<i>A_{tr}</i> in. ²	<i>d_{tr}</i> in.	<i>S_{tr}^c</i> in.	<i>A_{ab}</i> in. ²	<i>n</i>	<i>A_{bs}</i> in. ²	Long. Reinf. Layout
1	(3@3)8-8-F4.1-0-i-2.5-3-10.5	A B C	-	-	-	0.375	3.5 (1.75)	0.44	3	2.37	B3
2	(3@3)8-8-F4.1-0-i-2.5-3-10.5-HP	A B C	-	-	-	0.375	3.5 (1.75)	0.44	3	2.37	B3
3	(3@4)8-8-F4.1-0-i-2.5-3-10.5	A B C	-	-	-	0.375	4 (2)	0.44	3	2.37	B3
4	(3@5)8-8-F4.1-0-i-2.5-3-10.5	A B C	-	-	-	0.375	4 (2)	0.44	3	2.37	B3
5	(3@5)8-8-F4.1-0-i-2.5-3-10.5-HP	A B C	-	-	-	0.375	4 (2)	0.44	3	2.37	B3
6	(3@3)8-12-F4.1-0-i-2.5-3-10	A B C	-	-	-	0.375	3 (1.5)	0.66	3	2.37	B5
7	(3@4)8-12-F4.1-0-i-2.5-3-10	A B C	-	-	-	0.375	3 (1.5)	0.66	3	2.37	B5
8	(3@5)8-12-F4.1-0-i-2.5-3-10	A B C	-	-	-	0.375	3 (1.5)	0.66	3	2.37	B5
9	(3@5.5)8-5-T9.5-0-i-2.5-3-14.5	A B C	-	-	-	0.375	4 (2)	0.44	3	2.37	B5
10	(3@5.5)8-5-O9.1-0-i-2.5-3-14.5	A B C	-	-	-	0.375	4 (2)	0.44	3	2.37	B5
11	(4@3.7)8-5-T9.5-0-i-2.5-3-14.5	A B C D	-	-	-	0.375	4 (2)	0.44	4	3.16	B5
12	(4@3.7)8-5-O9.1-0-i-2.5-3-14.5	A B C D	-	-	-	0.375	4 (2)	0.44	4	3.16	B5
13	(3@4)8-8-T9.5-0-i-2.5-3-9.5	A B C	-	-	-	0.375	3 (1.5)	0.66	3	2.37	B5
14	(3@5)8-8-T9.5-0-i-2.5-3-9.5	A B C	-	-	-	0.375	3 (1.5)	0.66	3	2.37	B5
15	(3@7)8-8-T9.5-0-i-2.5-3-9.5	A B C	-	-	-	0.5	4.5 (2.25)	0.8	3	2.37	B7
16	(3@4)8-8-T9.5-0-i-2.5-3-14.5	A B C	-	-	-	0.375	4 (2)	0.44	3	2.37	B5
17	(3@5)8-8-T9.5-0-i-2.5-3-14.5	A B C	-	-	-	0.375	3.5 (1.75)	0.44	3	2.37	B8

Table C.2 Cont'd Details of the closely-spaced bars without confining reinforcement

No.	Specimen	Head	<i>N</i>	<i>s_{tr}^c</i> in.	<i>A_{tr}</i> in. ²	<i>d_{tro}</i> in.	<i>s_{tro}^c</i> in.	<i>A_{ab}</i> in. ²	<i>n</i>	<i>A_{hs}</i> in. ²	Long. Reinf. Layout
18	(3@7)8-8-T9.5-0-i-2.5-3-14.5	A B C	-	-	-	0.5	4.5 (2.25)	0.8	3	2.37	B8
19	(3@4.5)8-12-F4.1-0-i-2.5-3-12	A B C	-	-	-	0.5	3 (1.5)	1.2	3	2.37	B5
20	(3@4.5)8-12-F9.1-0-i-2.5-3-12	A B C	-	-	-	0.5	3 (1.5)	1.2	3	2.37	B5
21	(4@3)8-12-F4.1-0-i-2.5-3-12	A B C D	-	-	-	0.5	3 (1.5)	1.2	4	3.16	B5
22	(4@3)8-12-F9.1-0-i-2.5-3-12	A B C D	-	-	-	0.5	3 (1.5)	1.2	4	3.16	B5
23	(2@7)8-8-O4.5-0-i-2.5-3-9.5	A B	-	-	-	0.375	4 (2)	0.44	2	1.58	B4
24	(2@5)8-8-O4.5-0-i-2.5-3-9.5	A B	-	-	-	0.375	4 (2)	0.44	2	1.58	B4
25	(2@3)8-8-O4.5-0-i-2.5-3-9.5	A B	-	-	-	0.375	4 (2)	0.44	2	1.58	B4
26	(3@4.5)8-8-T4.0-0-i-2.5-3-9.5	A B C	-	-	-	0.5	4 (2)	0.8	3	2.37	B9
27	(4@3)8-8-T4.0-0-i-2.5-3-9.5	A B C D	-	-	-	0.5	4 (2)	0.8	4	3.16	B9
28	(3@3)8-8-T4.0-0-i-2.5-3-9.5	A B C	-	-	-	0.375	3 (1.5)	0.66	3	2.37	B5
29	(3@5.9)5-12-F4.0-0-i-2.5-4-5	A B C	-	-	-	0.375	3.5 (1.75)	0.22	3	0.93	B5
30	(4@3.9)5-12-F4.0-0-i-2.5-4-5	A B C D	-	-	-	0.375	3.5 (1.75)	0.22	4	1.24	B5
31	(3@5.35)11-12-O4.5-0-i-2.5-3-16.75	A B C	-	-	-	0.5	4 (2)	1.2	3	4.68	B16
32	(3@5.35)11-12-S5.5-0-i-2.5-3-16.75	A B C	-	-	-	0.5	4 (2)	1.2	3	4.68	B16
33	(3@5.35)11-5-O4.5-0-i-2.5-3-19.25	A B C	-	-	-	0.5	4 (2)	1.2	3	4.68	B16
34	(3@5.35)11-5-S5.5-0-i-2.5-3-19.25	A B C	-	-	-	0.5	4 (2)	1.2	3	4.68	B16

^c Value in parenthesis is the spacing between the first hoop and the center of the headed bar

Table C.2 Cont'd Details of the closely-spaced bars without confining reinforcement

No.	Specimen	Head	Failure Type	Lead (Head) Slip in.	T_{max} kips	$f_{su,max}$ ksi	T_{ind} kips	T_{total} kips	T kips	f_{su} ksi
1	(3@3)8-8-F4.1-0-i-2.5-3-10.5	A	CB	0.17	49	62	49	164.3	54.8	69.4
		B		0.212	56.2	71.1	56.2			
		C		0.162	59.1	74.8	59.1			
2	(3@3)8-8-F4.1-0-i-2.5-3-10.5-HP	A	CB/FP	0.399	55.3	70	55.3	151.4	50.5	63.9
		B		0.448	50.2	63.5	50.2			
		C		0.075	46	58.2	46			
3	(3@4)8-8-F4.1-0-i-2.5-3-10.5	A	CB	0.117	62.8	79.5	62.8	176.1	58.7	74.3
		B		0.339	62.3	78.9	62.3			
		C		0.146	51.4	65.1	51			
4	(3@5)8-8-F4.1-0-i-2.5-3-10.5	A	CB	0.255	67.9	85.9	67.9	192	64	81
		B		0.172	65.7	83.2	65.7			
		C		0.237	58.4	73.9	58.4			
5	(3@5)8-8-F4.1-0-i-2.5-3-10.5-HP	A	CB	0.113	62.9	79.6	62.9	179.6	59.9	75.8
		B		-	60.8	77	60.8			
		C		-	55.9	70.8	55.9			
6	(3@3)8-12-F4.1-0-i-2.5-3-10	A	CB	-	38.5	48.7	38.5	126.5	42.2	53.4
		B		-	42.3	53.5	40.3			
		C		-	47.7	60.4	47.7			
7	(3@4)8-12-F4.1-0-i-2.5-3-10	A	CB	0.12	49.1	62.2	49.1	146.6	48.9	61.9
		B		0.069	55.1	69.7	55			
		C		0.118 (0.043)	42.5	53.8	42.5			
8	(3@5)8-12-F4.1-0-i-2.5-3-10	A	CB	0.079	57.1	72.3	57.1	165.4	55.1	69.7
		B		0.177	55.3	70	55.3			
		C		0.249 (0.081)	53	67.1	53			
9	(3@5.5)8-5-T9.5-0-i-2.5-3-14.5	A	CB	0.156	68.7	87	68.7	220.2	73.4	92.9
		B		0.138	78.8	99.7	78.8			
		C		0.217	72.6	91.9	72.6			
10	(3@5.5)8-5-O9.1-0-i-2.5-3-14.5	A	CB	0.081 (0.043)	91	115.2	91	227.1	75.7	95.8
		B		0.085	76.2	96.5	76.2			
		C		0.055	59.9	75.8	59.9			
11	(4@3.7)8-5-T9.5-0-i-2.5-3-14.5	A	CB	0.159	89.7	113.5	89.7	243.3	60.8	77
		B		0.236	46.9	59.4	46.9			
		C		-	57.6	72.9	57.6			
		D		0.168	49.1	62.2	49.1			
12	(4@3.7)8-5-O9.1-0-i-2.5-3-14.5	A	CB	0.088	67.9	85.9	67.9	244.9	61.2	77.5
		B		-	69.7	88.2	69.7			
		C		-	56.6	71.6	56.6			
		D		0.114 (0.085)	50.8	64.3	50.8			
13	(3@4)8-8-T9.5-0-i-2.5-3-9.5	A	CB	0.421	33.5	42.4	33.5	120.8	40.3	51
		B		0.232	43.2	54.7	43.2			
		C		0.356 (0.098)	44.2	55.9	44.1			
14	(3@5)8-8-T9.5-0-i-2.5-3-9.5	A	CB	-	54.5	69	54.5	133.5	44.5	56.3
		B		-	27.9	35.3	27.9			
		C		0.015 (0.055)	51	64.6	51			
15	(3@7)8-8-T9.5-0-i-2.5-3-9.5	A	CB	-	54.2	68.6	54.2	206.1	68.7	87
		B		0.18	66.3	83.9	66.3			
		C		0.094 (0.008)	85.6	108.4	85.6			
16	(3@4)8-8-T9.5-0-i-2.5-3-14.5	A	CB	-	80.9	102.4	80.9	229.7	76.6	97
		B		-	79.2	100.3	79.2			
		C		0.073	75	94.9	69.7			
17	(3@5)8-8-T9.5-0-i-2.5-3-14.5	A	CB	0.086	87.3	110.5	87	279.6	93.2	118
		B		-	104	131.6	104			
		C		0.090 (0.031)	88.5	112	88.5			

Table C.2 Cont'd Details of the closely-spaced bars without confining reinforcement

No.	Specimen	Head	Failure Type	Lead (Head) Slip in.	T_{max} kips	$f_{su,max}$ ksi	T_{ind} kips	T_{total} kips	T kips	f_{su} ksi
18	(3@7)8-8-T9.5-0-i-2.5-3-14.5	A	CB/BS	0.138	104.4	132.2	104.4	311.9	104	131.6
		B		0.166	99.2	125.6	99.2			
		C		0.13	108.3	137.1	108.3			
19	(3@4.5)8-12-F4.1-0-i-2.5-3-12	A	CB	0.133	79.1	100.1	79.1	225.7	75.2	95.2
		B		0.037	75.8	95.9	75.8			
		C		0.089	70.7	89.5	70.7			
20	(3@4.5)8-12-F9.1-0-i-2.5-3-12	A	CB	0.046	77.8	98.5	77.8	226.2	75.4	95.4
		B		-	63.3	80.1	63.3			
		C		0.117	85.1	107.7	85.1			
21	(4@3)8-12-F4.1-0-i-2.5-3-12	A	CB	-	41.7	52.8	41.7	197.2	49.3	62.4
		B		-	49.5	62.7	49.5			
		C		0.135	66.8	84.6	66.8			
		D		0.032	39.4	49.9	39.4			
22	(4@3)8-12-F9.1-0-i-2.5-3-12	A	CB	-	49.2	62.3	49.2	201.3	50.3	63.7
		B		-	45.7	57.8	45.7			
		C		-	53.2	67.3	53.2			
		D		-	53.1	67.2	53.1			
23	(2@7)8-8-O4.5-0-i-2.5-3-9.5	A	CB	0.01	57.2	72.4	57.2	109	54.5	69
		B		0.03	51.8	65.6	51.8			
24	(2@5)8-8-O4.5-0-i-2.5-3-9.5	A	CB	0.035	45.7	57.8	45.7	102.4	51.2	64.8
		B		0.041	56.7	71.8	56.7			
25	(2@3)8-8-O4.5-0-i-2.5-3-9.5	A	CB	0.037	51.9	65.7	51.9	95.5	47.7	60.4
		B		0.021	43.6	55.2	43.6			
26	(3@4.5)8-8-T4.0-0-i-2.5-3-9.5	A	CB	0.013	43.9	55.6	43.9	122.1	40.7	51.5
		B		0.013	27.9	35.3	27.9			
		C		0.013	50.3	63.7	50.3			
27	(4@3)8-8-T4.0-0-i-2.5-3-9.5	A	CB	-	25.2	31.9	25.2	104.6	26.2	33.1
		B		-	31.2	39.5	31.2			
		C		-	31.7	40.1	31.7			
		D		0.005	16.6	21	16.5			
28	(3@3)8-8-T4.0-0-i-2.5-3-9.5	A	CB	0.014	39.9	50.5	39.9	118.1	39.4	49.8
		B		0.016	44.3	56.1	44.3			
		C		0.014	33.9	42.9	33.9			
29	(3@5.9)5-12-F4.0-0-i-2.5-4-5	A	CB	-	27.1	87.4	27	84.1	28	90.4
		B		0.1	28.9	93.2	28.8			
		C		-	28.2	91	28.2			
30	(4@3.9)5-12-F4.0-0-i-2.5-4-5	A	CB	0.099	28.3	91.3	28.3	- [†]	25.6 [†]	82.7
		B		-	- [†]	- [†]	-			
		C		0.109	24.5	79	24.5			
		D		-	24.1	77.7	24.1			
31	(3@5.35)11-12-O4.5-0-i-2.5-3-16.75	A	CB	-	109.3	70.1	107.6	320.4	106.8	68.5
		B		0.003	114.1	73.1	114.1			
		C		0.003	98.7	63.3	98.7			
32	(3@5.35)11-12-S5.5-0-i-2.5-3-16.75	A	CB	-	117.1	75.1	117.1	327	109	69.9
		B		-	93.8	60.1	93.8			
		C		-	116.1	74.4	116.1			
33	(3@5.35)11-5-O4.5-0-i-2.5-3-19.25	A	CB	0.001	132.5	84.9	132.5	386	128.7	82.5
		B		-	127.5	81.7	127.5			
		C		-	126	80.8	126			
34	(3@5.35)11-5-S5.5-0-i-2.5-3-19.25	A	CB/BS	-	137.3	88	137.3	412.2	137.4	88.1
		B		0.321	140.5	90.1	140.4			
		C		0.105	134.9	86.5	134.5			

Table C.3 Details of the widely-spaced bars with confining reinforcement

No.	Specimen	Head	c_o	A_{brg}	l_{eh}	$l_{eh,avg}$	f_{cm}	Age days	d_b in.	A_b in. ²
			in.		in.	in.	psi			
1	8-5-T4.0-4#3-i-3-3-12.5 ^a	A B	2.4	4.0 A_b	12.06 12.69	12.38	5070	8	1	0.79
2	8-5-T4.0-4#3-i-4-3-12.5 ^a	A B	3.4	4.0 A_b	11.94 12.19	12.06	5380	11	1	0.79
3	8-5-T4.0-4#4-i-3-3-12.5 ^a	A B	2.4	4.0 A_b	12.56 12.31	12.44	5070	8	1	0.79
4	8-5-T4.0-4#4-i-4-3-12.5 ^a	A B	3.4	4.0 A_b	12.06 12.31	12.19	4850	7	1	0.79
5	8-5g-T4.0-5#3-i-2.5-3-9.5 ^a	A B	1.9	4.0 A_b	9.44 9.69	9.56	5090	7	1	0.79
6	8-5g-T4.0-5#3-i-3.5-3-9.5 ^a	A B	2.9	4.0 A_b	9.69 9.44	9.56	5910	14	1	0.79
7	8-5g-T4.0-4#4-i-2.5-3-9.5 ^a	A B	1.9	4.0 A_b	9.44 8.94	9.19	5180	8	1	0.79
8	8-5g-T4.0-4#4-i-3.5-3-9.5 ^a	A B	2.9	4.0 A_b	9.31 9.69	9.5	5910	14	1	0.79
9	8-5-T4.0-5#3-i-2.5-3-9.5 ^a	A B	1.9	4.0 A_b	9.44 9.19	9.31	5960	7	1	0.79
10	8-5-T4.0-5#3-i-3.5-3-9.5 ^a	A B	2.9	4.0 A_b	9.06 9.06	9.06	6440	9	1	0.79
11	8-5-T4.0-4#4-i-2.5-3-9.5 ^a	A B	1.9	4.0 A_b	9.19 9.31	9.25	6440	9	1	0.79
12	8-5-T4.0-4#4-i-3.5-3-9.5 ^a	A B	2.9	4.0 A_b	9.56 8.94	9.25	6210	8	1	0.79
13	8-8-F4.1-2#3-i-2.5-3-10	A B	2	4.1 A_b	9.75 10	9.88	8450	9	1	0.79
14	8-12-F4.1-5#3-i-2.5-3-10	A B	2	4.1 A_b	10 10	10	11760	34	1	0.79
15	8-5-S6.5-2#3-i-2.5-3-9.25	A B	1.8	6.5 A_b	9.25 9	9.13	5750	7	1	0.79
16	8-5-S6.5-2#3-i-2.5-3-12.25	A B	1.8	6.5 A_b	12.5 12.13	12.31	5750	7	1	0.79
17	8-5-O4.5-2#3-i-2.5-3-9.25	A B	1.6	4.5 A_b	9.38 9.38	9.38	5750	7	1	0.79
18	8-5-O4.5-2#3-i-2.5-3-12.25	A B	1.6	4.5 A_b	12 12	12	5750	7	1	0.79
19	8-5-S6.5-5#3-i-2.5-3-8.25	A B	1.8	6.5 A_b	8.38 8.25	8.31	5900	8	1	0.79
20	8-5-S6.5-5#3-i-2.5-3-11.25	A B	1.8	6.5 A_b	10.88 11	10.94	5900	8	1	0.79
21	8-5-O4.5-5#3-i-2.5-3-8.25	A B	1.6	4.5 A_b	8.13 7.88	8	5900	8	1	0.79

^a Specimen contained crossies within joint region

Table C.3 Cont'd Details of the widely-spaced bars with confining reinforcement

No.	Specimen	Head	c_o	A_{brg}	ℓ_{eh}	$\ell_{eh,avg}$	f_{cm}	Age	d_b	A_b
			in.		in.	in.	psi	days	in.	in. ²
22	8-5-O4.5-5#3-i-2.5-3-11.25	A	1.6	4.5 A_b	11.38	11.13	5900	8	1	0.79
		B			10.88					
23	8-5-T9.5-5#3-i-2.5-3-14.5	A	1.4	9.5 A_b	14.5	14.38	5420	13	1	0.79
		B			14.25					
24	8-15-T4.0-2#3-i-2.5-4.5-7	A	1.9	4.0 A_b	7.13	7.06	16030	87	1	0.79
		B			7					
25	8-15-S9.5-2#3-i-2.5-3-7	A	1.4	9.5 A_b	7.13	7.06	16030	87	1	0.79
		B			7					
26	8-15-T4.0-5#3-i-2.5-4.5-5.5	A	1.9	4.0 A_b	5.5	5.5	16030	88	1	0.79
		B			5.5					
27	8-15-S9.5-5#3-i-2.5-3-5.5	A	1.4	9.5 A_b	5.75	5.63	16030	88	1	0.79
		B			5.5					
28	8-8-T9.5-2#3-i-2.5-3-9.5	A	1.4	9.5 A_b	9	9.19	9040	12	1	0.79
		B			9.38					
29	(2@9)8-12-F4.1-5#3-i-2.5-3-12	A	2	4.1 A_b	11.94	11.97	12080	57	1	0.79
		B			12					
30	(2@9)8-8-T4.0-5#3-i-2.5-3-9.5	A	1.9	4.0 A_b	9.5	9.5	6790	17	1	0.79
		B			9.5					
31	5-5-F4.0-2#3-i-2.5-5-4	A	2.2	4.0 A_b	3.88	3.81	4810	8	0.625	0.31
		B			3.75					
32	5-5-F4.0-5#3-i-2.5-5-4	A	2.2	4.0 A_b	3.94	4.16	4810	8	0.625	0.31
		B			4.38					
33	5-5-F4.0-2#3-i-2.5-3-6	A	2.2	4.0 A_b	6	6	4690	7	0.625	0.31
		B			6					
34	5-5-F4.0-5#3-i-2.5-3-6	A	2.2	4.0 A_b	6	6.06	4690	7	0.625	0.31
		B			6.13					
35	5-12-F4.0-2#3-i-2.5-5-4	A	2.2	4.0 A_b	4.13	4.13	11030	35	0.625	0.31
		B			4.13					
36	5-12-F4.0-5#3-i-2.5-5-4	A	2.2	4.0 A_b	4.19	4.22	11030	35	0.625	0.31
		B			4.25					
37	11-5a-F3.8-2#3-i-2.5-3-17	A	2	3.8 A_b	17.44	17.44	4050	36	1.41	1.56
		B			17.44					
38	11-5a-F3.8-6#3-i-2.5-3-17	A	2	3.8 A_b	16.75	16.72	4050	36	1.41	1.56
		B			16.69					
39	11-5-F3.8-6#3-i-2.5-3-17	A	2	3.8 A_b	16.88	16.94	5970	7	1.41	1.56
		B			17					
40	(3@5.35)11-12-O4.5-6#3-i-2.5-3-16.75	A	1.3	4.5 A_b	16.88	17	10860	37	1.41	1.56
		B			17.13					
		C			17					
41	(3@5.35)11-12-S5.5-6#3-i-2.5-3-16.75	A	1.5	5.5 A_b	16.75	16.75	10120	38	1.41	1.56
		B			17					
		C			16.5					
42	11-5-O4.5-6#3-i-2.5-3-19.25	A	1.3	4.5 A_b	19.5	19.63	5430	12	1.41	1.56
		B			19.75					
43	11-5-S5.5-6#3-i-2.5-3-19.25	A	1.5	5.5 A_b	19.13	19.13	6320	13	1.41	1.56
		B			19.13					

Table C.3 Cont'd Details of the widely-spaced bars with confining reinforcement

No.	Specimen	Head	<i>b</i> in.	<i>h</i> in.	<i>h_{cl}</i> in.	<i>d_{eff}</i> in.	<i>c_{so}</i> in.	<i>c_{so,avg}</i> in.	<i>c_{bc}</i> in.	<i>s</i> in.	<i>d_{tr}</i> in.	<i>A_{tr,l}</i> in. ²
1	8-5-T4.0-4#3-i-3-3-12.5 ^a	A B	17.6	17.4	10.25	13.08	2.9 2.9	2.9	3.8 3.2	10.9	0.375	0.11
2	8-5-T4.0-4#3-i-4-3-12.5 ^a	A B	20	17.3	10.25	12.94	3.9 4.1	4	3.9 3.6	11	0.375	0.11
3	8-5-T4.0-4#4-i-3-3-12.5 ^a	A B	17.5	17.3	10.25	13.78	2.9 3	2.9	3.2 3.4	10.6	0.5	0.2
4	8-5-T4.0-4#4-i-4-3-12.5 ^a	A B	20.1	17.3	10.25	13.3	3.9 4.1	4	3.7 3.4	11.1	0.5	0.2
5	8-5g-T4.0-5#3-i-2.5-3-9.5 ^a	A B	17.3	14.1	10.25	12.94	2.8 2.8	2.8	3.2 2.9	10.8	0.375	0.11
6	8-5g-T4.0-5#3-i-3.5-3-9.5 ^a	A B	18.9	14.2	10.25	12.46	3.3 3.4	3.3	3 3.3	11.3	0.375	0.11
7	8-5g-T4.0-4#4-i-2.5-3-9.5 ^a	A B	16.5	14.1	10.25	13.32	2.5 2.5	2.5	3.2 3.7	10.5	0.5	0.2
8	8-5g-T4.0-4#4-i-3.5-3-9.5 ^a	A B	19	14.3	10.25	12.94	4 3.8	3.9	3.4 3.1	10.3	0.5	0.2
9	8-5-T4.0-5#3-i-2.5-3-9.5 ^a	A B	16.5	14.3	10.25	12.54	2.5 2.5	2.5	3.3 3.6	10.5	0.375	0.11
10	8-5-T4.0-5#3-i-3.5-3-9.5 ^a	A B	18.6	14.3	10.25	12.38	3.1 3.8	3.4	3.7 3.7	10.8	0.375	0.11
11	8-5-T4.0-4#4-i-2.5-3-9.5 ^a	A B	16.6	14.1	10.25	12.92	2.6 2.5	2.6	3.4 3.3	10.5	0.5	0.2
12	8-5-T4.0-4#4-i-3.5-3-9.5 ^a	A B	18.6	14.2	10.25	12.56	3.5 3.4	3.4	3.1 3.8	10.8	0.5	0.2
13	8-8-F4.1-2#3-i-2.5-3-10	A B	17	14.1	10.25	12.1	2.5 2.4	2.4	3.3 3.1	11.1	0.375	0.11
14	8-12-F4.1-5#3-i-2.5-3-10	A B	17	14.2	10.25	11.83	2.5 2.5	2.5	3.2 3.2	11	0.375	0.11
15	8-5-S6.5-2#3-i-2.5-3-9.25	A B	17.5	14	10.25	12.25	2.8 2.5	2.6	3 3.3	11.3	0.375	0.11
16	8-5-S6.5-2#3-i-2.5-3-12.25	A B	16.9	17.1	10.25	12.96	2.4 2.5	2.5	2.8 3.2	11	0.375	0.11
17	8-5-O4.5-2#3-i-2.5-3-9.25	A B	17	14.1	10.25	12.39	2.5 2.5	2.5	3.1 3.1	11	0.375	0.11
18	8-5-O4.5-2#3-i-2.5-3-12.25	A B	16.6	16.9	10.25	12.73	2.4 2.5	2.4	3.3 3.3	10.8	0.375	0.11
19	8-5-S6.5-5#3-i-2.5-3-8.25	A B	16.9	13.1	10.25	12.18	2.5 2.4	2.4	3 3.1	11	0.375	0.11
20	8-5-S6.5-5#3-i-2.5-3-11.25	A B	17.6	16	10.25	12.87	2.5 2.4	2.4	3.4 3.3	11.8	0.375	0.11
21	8-5-O4.5-5#3-i-2.5-3-8.25	A B	17.3	13	10.25	12.37	2.5 2.8	2.6	3.3 3.5	11	0.375	0.11

^a Specimen contained crossies within joint region

Table C.3 Cont'd Details of the widely-spaced bars with confining reinforcement

No.	Specimen	Head	<i>b</i> in.	<i>h</i> in.	<i>h_{cl}</i> in.	<i>d_{eff}</i> in.	<i>c_{so}</i> in.	<i>c_{so,avg}</i> in.	<i>c_{bc}</i> in.	<i>s</i> in.	<i>d_{tr}</i> in.	<i>A_{tr,l}</i> in. ²
22	8-5-O4.5-5#3-i-2.5-3-11.25	A	16.6	15.9	10.25	12.81	2.5	2.4	2.9	10.8	0.375	0.11
		B					2.4		3.4			
23	8-5-T9.5-5#3-i-2.5-3-14.5	A	17.1	19.2	10.25	14.22	2.5	2.6	3.2	11	0.375	0.11
		B					2.6		3.5			
24	8-15-T4.0-2#3-i-2.5-4-5-7	A	17	13.1	10.25	11.03	2.5	2.5	4.5	11	0.375	0.11
		B					2.5		4.6			
25	8-15-S9.5-2#3-i-2.5-3-7	A	16.9	13.1	10.25	11.14	2.5	2.5	3.2	10.9	0.375	0.11
		B					2.5		3.3			
26	8-15-T4.0-5#3-i-2.5-4-5-5.5	A	16.9	11.7	10.25	11.09	2.4	2.4	4.7	11	0.375	0.11
		B					2.5		4.7			
27	8-15-S9.5-5#3-i-2.5-3-5.5	A	16.8	11.5	10.25	11.26	2.3	2.4	3	11	0.375	0.11
		B					2.5		3.3			
28	8-8-T9.5-2#3-i-2.5-3-9.5	A	17	14	10.25	11.87	2.8	2.6	3.5	10.8	0.375	0.11
		B					2.5		3.1			
29	(2@9)8-12-F4.1-5#3-i-2.5-3-12	A	14.9	16.1	10.25	12.49	2.5	2.5	3.2	9	0.375	0.11
		B					2.4		3.1			
30	(2@9)8-8-T4.0-5#3-i-2.5-3-9.5	A	15.1	14	10.25	12.74	2.5	2.5	3	9.1	0.375	0.11
		B					2.5		3			
31	5-5-F4.0-2#3-i-2.5-5-4	A	13	9.6	5.25	6.16	2.5	2.5	5.3	7.4	0.375	0.11
		B					2.5		5.4			
32	5-5-F4.0-5#3-i-2.5-5-4	A	13.1	9.8	5.25	6.48	2.6	2.6	5.3	7.4	0.375	0.11
		B					2.5		4.9			
33	5-5-F4.0-2#3-i-2.5-3-6	A	13.1	9.7	5.25	7.04	2.6	2.6	3.2	7.4	0.375	0.11
		B					2.5		3.2			
34	5-5-F4.0-5#3-i-2.5-3-6	A	13.1	9.7	5.25	7.31	2.5	2.6	3.2	7.4	0.375	0.11
		B					2.6		3.1			
35	5-12-F4.0-2#3-i-2.5-5-4	A	13.1	9.6	5.25	6.08	2.8	2.6	5	7.3	0.375	0.11
		B					2.5		5			
36	5-12-F4.0-5#3-i-2.5-5-4	A	13.1	9.5	5.25	6.23	2.5	2.6	4.8	7.4	0.375	0.11
		B					2.6		4.8			
37	11-5a-F3.8-2#3-i-2.5-3-17	A	21.7	21.8	20	23.77	2.6	2.6	3	15.1	0.375	0.11
		B					2.6		3			
38	11-5a-F3.8-6#3-i-2.5-3-17	A	21.4	21.9	20	23.7	2.4	2.5	3.8	15	0.375	0.11
		B					2.6		3.8			
39	11-5-F3.8-6#3-i-2.5-3-17	A	21.5	22	20	23.7	2.6	2.6	3.8	15	0.375	0.11
		B					2.5		3.6			
40	(3@5.35)11-12-O4.5-6#3-i-2.5-3-16.75	A	21.8	22.9	20	23.16	2.5	2.6	3.9	7.5	0.375	0.11
		B					-		3.7			
		C					2.8		3.8			
41	(3@5.35)11-12-S5.5-6#3-i-2.5-3-16.75	A	21.9	22.8	20	23.84	2.6	2.8	3.3	7.4	0.375	0.11
		B					-		3			
		C					3		3.5			
42	11-5-O4.5-6#3-i-2.5-3-19.25	A	21.7	25.6	20	24.7	2.5	2.6	3.9	15	0.375	0.11
		B					2.8		3.7			
43	11-5-S5.5-6#3-i-2.5-3-19.25	A	22.2	25.3	20	24.47	2.8	2.8	3.4	15.3	0.375	0.11
		B					2.8		3.4			

Table C.3 Cont'd Details of the widely-spaced bars with confining reinforcement

No.	Specimen	Head	N	s_{tr}^c in.	A_{tr} in. ²	d_{tro} in.	s_{tro}^c in.	A_{ab} in. ²	n	A_{hs} in. ²	Long. Reinf. Layout
1	8-5-T4.0-4#3-i-3-3-12.5 ^a	A B	8	3 (1.5)	0.66	0.375	3 (1.5)	0.66	2	1.58	B2
2	8-5-T4.0-4#3-i-4-3-12.5 ^a	A B	8	3 (1.5)	0.66	0.375	3 (1.5)	0.66	2	1.58	B2
3	8-5-T4.0-4#4-i-3-3-12.5 ^a	A B	8	4 (2)	0.8	0.5	4 (2)	0.8	2	1.58	B17
4	8-5-T4.0-4#4-i-4-3-12.5 ^a	A B	8	4 (2)	0.8	0.5	4 (2)	0.8	2	1.58	B17
5	8-5g-T4.0-5#3-i-2.5-3-9.5 ^a	A B	10	3 (1.5)	0.66	0.375	3.5 (1.75)	0.44	2	1.58	B2
6	8-5g-T4.0-5#3-i-3.5-3-9.5 ^a	A B	10	3 (1.5)	0.66	0.375	3.5 (1.75)	0.44	2	1.58	B2
7	8-5g-T4.0-4#4-i-2.5-3-9.5 ^a	A B	8	4 (2)	0.8	0.5	3.5 (1.75)	0.8	2	1.58	B17
8	8-5g-T4.0-4#4-i-3.5-3-9.5 ^a	A B	8	4 (2)	0.8	0.5	3.5 (1.75)	0.8	2	1.58	B17
9	8-5-T4.0-5#3-i-2.5-3-9.5 ^a	A B	10	3 (1.5)	0.66	0.375	3.5 (1.75)	0.44	2	1.58	B2
10	8-5-T4.0-5#3-i-3.5-3-9.5 ^a	A B	10	3 (1.5)	0.66	0.375	3.5 (1.75)	0.44	2	1.58	B2
11	8-5-T4.0-4#4-i-2.5-3-9.5 ^a	A B	8	4 (2)	0.8	0.5	3.5 (1.75)	0.8	2	1.58	B17
12	8-5-T4.0-4#4-i-3.5-3-9.5 ^a	A B	8	4 (2)	0.8	0.5	3.5 (1.75)	0.8	2	1.58	B17
13	8-8-F4.1-2#3-i-2.5-3-10	A B	4	5 (5.5)	0.22	0.375	4 (2)	0.44	2	1.58	B1
14	8-12-F4.1-5#3-i-2.5-3-10	A B	10	3 (1.5)	0.66	0.375	4 (2)	0.44	2	1.58	B5
15	8-5-S6.5-2#3-i-2.5-3-9.25	A B	4	5.5 (5)	0.22	0.5	3 (1.5)	1.2	2	1.58	B4
16	8-5-S6.5-2#3-i-2.5-3-12.25	A B	4	5.5 (5)	0.22	0.5	3 (1.5)	1.2	2	1.58	B4
17	8-5-O4.5-2#3-i-2.5-3-9.25	A B	4	5.5 (5)	0.22	0.5	3 (1.5)	1.2	2	1.58	B4
18	8-5-O4.5-2#3-i-2.5-3-12.25	A B	4	5.5 (5)	0.22	0.5	3 (1.5)	1.2	2	1.58	B4
19	8-5-S6.5-5#3-i-2.5-3-8.25	A B	10	3 (1.5)	0.66	0.5	2.5 (1.25)	1.2	2	1.58	B4
20	8-5-S6.5-5#3-i-2.5-3-11.25	A B	10	3 (1.5)	0.66	0.5	3 (1.5)	1.2	2	1.58	B4
21	8-5-O4.5-5#3-i-2.5-3-8.25	A B	10	3 (1.5)	0.66	0.5	2.5 (1.25)	1.2	2	1.58	B4

^a Specimen contained crossies within joint region

^c Value in parenthesis is the spacing between the first hoop and the center of the headed bar

Table C.3 Cont'd Details of the widely-spaced bars with confining reinforcement

No.	Specimen	Head	N	s_{tr}^c in.	A_{tr} in. ²	d_{tro} in.	s_{tro}^c in.	A_{ab} in. ²	n	A_{hs} in. ²	Long. Reinf. Layout
22	8-5-O4.5-5#3-i-2.5-3-11.25	A B	10	3 (1.5)	0.66	0.5	3 (1.5)	1.2	2	1.58	B4
23	8-5-T9.5-5#3-i-2.5-3-14.5	A B	10	3 (1.5)	0.66	0.375	4 (2)	0.44	2	1.58	B6
24	8-15-T4.0-2#3-i-2.5-4.5-7	A B	4	5.5 (5)	0.22	0.5	4 (2)	0.8	2	1.58	B6
25	8-15-S9.5-2#3-i-2.5-3-7	A B	4	5.5 (5)	0.22	0.5	4 (2)	0.8	2	1.58	B6
26	8-15-T4.0-5#3-i-2.5-4.5-5.5	A B	10	3 (1.5)	0.66	0.5	4 (2)	0.8	2	1.58	B7
27	8-15-S9.5-5#3-i-2.5-3-5.5	A B	10	3 (1.5)	0.66	0.5	4 (2)	0.8	2	1.58	B7
28	8-8-T9.5-2#3-i-2.5-3-9.5	A B	4	6 (4.5)	0.22	0.375	3 (1.5)	0.66	2	1.58	B6
29	(2@9)8-12-F4.1-5#3-i-2.5-3-12	A B	10	3 (1.5)	0.66	0.5	3 (1.5)	1.2	2	1.58	B5
30	(2@9)8-8-T4.0-5#3-i-2.5-3-9.5	A B	10	3 (1.5)	0.66	0.5	4 (2)	0.8	2	1.58	B5
31	5-5-F4.0-2#3-i-2.5-5-4	A B	4	3.5 (2.625)	0.22	0.375	3.5 (1.75)	0.22	2	0.62	B4
32	5-5-F4.0-5#3-i-2.5-5-4	A B	10	1.75 (0.875)	0.66	0.375	3.5 (1.75)	0.22	2	0.62	B4
33	5-5-F4.0-2#3-i-2.5-3-6	A B	4	3.5 (2.625)	0.22	0.375	3.5 (1.75)	0.22	2	0.62	B4
34	5-5-F4.0-5#3-i-2.5-3-6	A B	10	1.75 (0.875)	0.66	0.375	3.5 (1.75)	0.22	2	0.62	B4
35	5-12-F4.0-2#3-i-2.5-5-4	A B	4	3.5 (2.625)	0.22	0.375	3.5 (1.75)	0.22	2	0.62	B4
36	5-12-F4.0-5#3-i-2.5-5-4	A B	10	1.75 (0.875)	0.66	0.375	3.5 (1.75)	0.22	2	0.62	B4
37	11-5a-F3.8-2#3-i-2.5-3-17	A B	4	8 (6)	0.22	0.5	4 (2)	1.2	2	3.12	B10
38	11-5a-F3.8-6#3-i-2.5-3-17	A B	12	4 (2)	0.66	0.5	4 (2)	1.2	2	3.12	B10
39	11-5-F3.8-6#3-i-2.5-3-17	A B	12	4 (2)	0.66	0.5	6 (3)	0.8	2	3.12	B7
40	(3@5.35)11-12-O4.5-6#3-i-2.5-3-16.75	A B C	12	4 (2)	0.66	0.5	4 (2)	1.2	3	4.68	B16
41	(3@5.35)11-12-S5.5-6#3-i-2.5-3-16.75	A B C	12	4 (2)	0.66	0.5	4 (2)	1.2	3	4.68	B16
42	11-5-O4.5-6#3-i-2.5-3-19.25	A B	12	4 (2)	0.66	0.5	4 (2)	1.2	2	3.12	B16
43	11-5-S5.5-6#3-i-2.5-3-19.25	A B	12	4 (2)	0.66	0.5	4 (2)	1.2	2	3.12	B16

^c Value in parenthesis is the spacing between the first hoop and the center of the headed bar

Table C.3 Cont'd Details of the widely-spaced bars with confining reinforcement

No.	Specimen	Head	Failure	Lead (Head) Slip in.	T_{max} kips	$f_{su,max}$ ksi	T_{ind} kips	T_{total} kips	T kips	f_{su} ksi
1	8-5-T4.0-4#3-i-3-3-12.5 ^{a c}	A	SB/FP	0.227	87.9	111.3	87.9	175	87.5	110.8
		B		-	- [†]	- [†]	87.1			
2	8-5-T4.0-4#3-i-4-3-12.5 ^a	A	SB/FP	-	110.8	140.3	97.2	192.3	96.2	121.7
		B		0.239	95.2	120.5	95.1			
3	8-5-T4.0-4#4-i-3-3-12.5 ^a	A	SB/FP	0.049	109.5	138.6	109.4	218.1	109	138
		B		-	111	140.5	108.6			
4	8-5-T4.0-4#4-i-4-3-12.5 ^a	A	SB/FP	0.228	102.5	129.7	102.5	203	101.5	128.5
		B		0.35	103.4	130.9	100.5			
5	8-5g-T4.0-5#3-i-2.5-3-9.5 ^a	A	SB	0.19	78.9	99.9	78.9	157.4	78.7	99.6
		B		0.545	92.6	117.2	78.5			
6	8-5g-T4.0-5#3-i-3.5-3-9.5 ^a	A	SB	0.599	88.4	111.9	80.3	159	79.5	100.6
		B		0.193	78.7	99.6	78.7			
7	8-5g-T4.0-4#4-i-2.5-3-9.5 ^a	A	SB	0.187	92.2	116.7	92.2	181.5	90.7	114.8
		B		0.498 (0.032)	102.2	129.4	89.3			
8	8-5g-T4.0-4#4-i-3.5-3-9.5 ^a	A	SB	-	112	141.8	97.6	193.4	96.7	122.4
		B		0.056	95.8	121.3	95.8			
9	8-5-T4.0-5#3-i-2.5-3-9.5 ^a	A	SB	0.185	74.5	94.3	74.5	148.5	74.2	93.9
		B		0.163	74	93.7	74			
10	8-5-T4.0-5#3-i-3.5-3-9.5 ^a	A	SB/FP	-	80.7	102.2	80.7	161.1	80.6	102
		B		0.57	96.1	121.6	80.4			
11	8-5-T4.0-4#4-i-2.5-3-9.5 ^a	A	SB/FP	-	94.9	120.1	91.6	181.1	90.5	114.6
		B		0.005	89.5	113.3	89.5			
12	8-5-T4.0-4#4-i-3.5-3-9.5 ^a	A	SB/FP	0.186	86.6	109.6	86.6	171.1	85.6	108.4
		B		-	89	112.7	84.6			
13	8-8-F4.1-2#3-i-2.5-3-10	A	CB	0.107	73.5	93	73.5	146.8	73.4	92.9
		B		0.168	73.3	92.8	73.3			
14	8-12-F4.1-5#3-i-2.5-3-10	A	SB/FP	-	88.4	111.9	88.4	174.3	87.2	110.4
		B		0.006	86	108.9	86			
15	8-5-S6.5-2#3-i-2.5-3-9.25	A	CB	0.012	62.6	79.2	62.6	126.7	63.4	80.2
		B		-	64.1	81.2	64.1			
16	8-5-S6.5-2#3-i-2.5-3-12.25	A	SB/FP	0.34	84.6	107.1	84.6	171.9	86	108.8
		B		0.254	89.3	113	87.3			
17	8-5-O4.5-2#3-i-2.5-3-9.25	A	SB/FP	0.309	67.6	85.6	67.1	135.8	67.9	86
		B		0.205	68.7	86.9	68.7			
18	8-5-O4.5-2#3-i-2.5-3-12.25	A	SB/FP	0.305	82.8	104.8	77.4	157	78.5	99.4
		B		0.22	79.6	100.8	79.6			
19	8-5-S6.5-5#3-i-2.5-3-8.25	A	CB/FP	0.363	61.9	78.4	61.9	124.1	62	78.5
		B		0.5	62.2	78.7	62.2			
20	8-5-S6.5-5#3-i-2.5-3-11.25	A	SB/FP	-	100.8	127.6	84.2	169	84.5	106.9
		B		0.046	84.7	107.2	84.7			
21	8-5-O4.5-5#3-i-2.5-3-8.25	A	SB/FP	0.457	68.3	86.5	68.3	136.8	68.4	86.6
		B		0.383	68.5	86.7	68.5			

^a Specimen contained crossties within joint region

[†] No anchorage failure on the bar

Table C.3 Cont'd Details of the widely-spaced bars with confining reinforcement

No.	Specimen	Head	Failure	Lead (Head) Slip in.	T_{max} kips	$f_{su,max}$ ksi	T_{ind} kips	T_{total} kips	T kips	f_{su} ksi
22	8-5-O4.5-5#3-i-2.5-3-11.25	A	SB/FP	0.171	85	107.6	82.1	164.5	82.2	104.1
		B		-	82.4	104.3	82.4			
23	8-5-T9.5-5#3-i-2.5-3-14.5	A	SB/FP	-	120.7 [†]	152.8 [†]	120.6	242	121	153.2
		B		-	121.4	153.7	121.4			
24	8-15-T4.0-2#3-i-2.5-4.5-7	A	CB	-	59.1	74.8	59.1	118	59	74.7
		B		-	58.9	74.6	58.9			
25	8-15-S9.5-2#3-i-2.5-3-7	A	CB	-	66.4	84.1	66.4	134.3	67.1	84.9
		B		-	67.9	85.9	67.9			
26	8-15-T4.0-5#3-i-2.5-4.5-5.5	A	CB	-	64	81	64	126.6	63.3	80.1
		B		-	62.6	79.2	62.6			
27	8-15-S9.5-5#3-i-2.5-3-5.5	A	CB	-	76.6	97	76.6	151.6	75.8	95.9
		B		-	75	94.9	75			
28	8-8-T9.5-2#3-i-2.5-3-9.5	A	CB	-	69	87.3	69	137.5	68.7	87
		B		0.103 (0.003)	68.5	86.7	68.5			
29	(2@9)8-12-F4.1-5#3-i-2.5-3-12	A	SB/FP	0.126	112.5 [†]	142.4 [†]	112.5	223.8	111.9	141.6
		B		0.126	111.3	140.9	111.3			
30	(2@9)8-8-T4.0-5#3-i-2.5-3-9.5	A	SB/FP	0.078	70.7	89.5	70.7	153.3	76.7	97.1
		B		0.035	87.5	110.8	82.6			
31	5-5-F4.0-2#3-i-2.5-5-4	A	CB	-	20.1	64.8	20.1	39.3	19.7	63.5
		B		-	19.2	61.9	19.2			
32	5-5-F4.0-5#3-i-2.5-5-4	A	CB	-	27	87.1	27	53	26.5	85.5
		B		-	26.1 [†]	84.2 [†]	26			
33	5-5-F4.0-2#3-i-2.5-3-6	A	SB/FP	-	40	129	35.5	75.7	37.9	122.3
		B		-	40.3	130	40.3			
34	5-5-F4.0-5#3-i-2.5-3-6	A	SB/FP	-	42.4	136.8	42.4	86.9	43.5	140.3
		B		-	44.6	143.9	44.6			
35	5-12-F4.0-2#3-i-2.5-5-4	A	CB	0.072	33.7	108.7	33.7	65.4	32.7	105.5
		B		0.015	31.7	102.3	31.7			
36	5-12-F4.0-5#3-i-2.5-5-4	A	CB	0.196	40.2	129.7	40.2	77.7	38.9	125.5
		B		0.308	37.5	121	37.5			
37	11-5a-F3.8-2#3-i-2.5-3-17	A	SB/FP	0.337	117.7	75.4	117.7	236.5	118.2	75.8
		B		0.235	133.4	85.5	118.8			
38	11-5a-F3.8-6#3-i-2.5-3-17	A	SB/FP	0.13	119.9	76.9	114.5	232.4	116.2	74.5
		B		0.041	118	75.6	118			
39	11-5-F3.8-6#3-i-2.5-3-17	A	CB	0.157	154.9	99.3	154.9	303.7	151.9	97.4
		B		0.051	148.9	95.4	148.9			
40	(3@5.35)11-12-O4.5-6#3-i-2.5-3-16.75	A	CB	-	131.7	84.4	131.7	407.4	135.8	87.1
		B		0.213	131.8	84.5	131.8			
		C		0.145	143.9	92.2	143.9			
41	(3@5.35)11-12-S5.5-6#3-i-2.5-3-16.75	A	CB	-	155.9	99.9	155.9	461.3	153.8	98.6
		B		0.095	154.9	99.3	154.9			
		C		-	150.6	96.5	150.6			
42	11-5-O4.5-6#3-i-2.5-3-19.25	A	SB/FP	0.012	180.4 [†]	115.6 [†]	180.3	362.9	181.4	116.3
		B		0.036	182.6	117.1	182.6			
43	11-5-S5.5-6#3-i-2.5-3-19.25	A	SB/FP	0.316	191.5 [†]	122.8 [†]	191.5	379.2	189.6	121.5
		B		0.147	187.7	120.3	187.7			

[†] No anchorage failure on the bar

Table C.4 Details of the closely-spaced bars with confining reinforcement

No.	Specimen	Head	c_o in.	A_{brg}	l_{eh} in.	$l_{eh,avg}$ in.	f_{cm} psi	Age days	d_b in.	A_b in. ²
1	(3@3)8-8-F4.1-2#3-i-2.5-3-10	A B C	2	4.1A _b	10.13 10 10.13	10.08	8260	8	1	0.79
2	(3@3)8-8-F4.1-2#3-i-2.5-3-10-HP	A B C	2	4.1A _b	10.25 10.13 10.5	10.29	8260	8	1	0.79
3	(3@4)8-8-F4.1-2#3-i-2.5-3-10	A B C	2	4.1A _b	9.75 9.63 10.25	9.88	8050	7	1	0.79
4	(3@4)8-8-F4.1-2#3-i-2.5-3-10-HP	A B C	2	4.1A _b	10 10.75 10.25	10.33	8050	7	1	0.79
5	(3@5)8-8-F4.1-2#3-i-2.5-3-10.5	A B C	2	4.1A _b	9.63 9.75 10	9.79	8260	8	1	0.79
6	(3@5)8-8-F4.1-2#3-i-2.5-3-10.5-HP	A B C	2	4.1A _b	9.88 10 10.13	10	8260	8	1	0.79
7	(3@3)8-12-F4.1-5#3-i-2.5-3-10	A B C	2	4.1A _b	10 10.13 9.88	10	11040	31	1	0.79
8	(3@4)8-12-F4.1-5#3-i-2.5-3-10	A B C	2	4.1A _b	9.81 9.88 9.63	9.77	11440	32	1	0.79
9	(3@5)8-12-F4.1-5#3-i-2.5-3-10	A B C	2	4.1A _b	9.75 9.38 9.69	9.6	11460	33	1	0.79
10	(3@5.5)8-5-T9.5-5#3-i-2.5-3-14.5	A B C	1.4	9.5A _b	14.5 14.38 14.38	14.42	5370	10	1	0.79
11	(4@3.7)8-5-T9.5-5#3-i-2.5-3-14.5	A B C D	1.4	9.5A _b	14.44 14.38 14.63 14.5	14.5	5570	14	1	0.79
12	(3@4)8-8-T9.5-2#3-i-2.5-3-9.5	A B C	1.4	9.5A _b	9.75 9.5 9.5	9.58	9040	12	1	0.79
13	(3@5)8-8-T9.5-2#3-i-2.5-3-9.5	A B C	1.4	9.5A _b	9.5 9.5 9.25	9.42	9940	11	1	0.79
14	(3@7)8-8-T9.5-2#3-i-2.5-3-9.5	A B C	1.4	9.5A _b	9.5 9.75 9.5	9.58	10180	10	1	0.79
15	(3@4)8-8-T9.5-2#3-i-2.5-3-14.5	A B C	1.4	9.5A _b	14.5 14.5 14.25	14.42	9040	12	1	0.79

Table C.4 Cont'd Details of the closely-spaced bars with confining reinforcement

No.	Specimen	Head	c_o in.	A_{brg}	ℓ_{eh} in.	$\ell_{eh,avg}$ in.	f_{cm} psi	Age days	d_b in.	A_b in. ²
16	(3@5)8-8-T9.5-2#3-i-2.5-3-14.5	A B C	1.4	9.5A _b	14 14.25 14	14.08	9940	11	1	0.79
17	(3@7)8-8-T9.5-2#3-i-2.5-3-14.5	A B C	1.4	9.5A _b	14.5 14.63 14.5	14.54	10180	10	1	0.79
18	(3@4.5)8-12-F4.1-5#3-i-2.5-3-12	A B C	2	4.1A _b	12.13 12.19 12.19	12.17	12040	58	1	0.79
19	(3@4.5)8-12-F9.1-5#3-i-2.5-3-12	A B C	2	9.1A _b	11.94 11.88 11.88	11.9	12040	58	1	0.79
20	(4@3)8-12-F4.1-5#3-i-2.5-3-12	A B C D	2	4.1A _b	12 12 12.13 12	12.03	12360	61	1	0.79
21	(4@3)8-12-F9.1-5#3-i-2.5-3-12	A B C D	2	9.1A _b	12 12 12 11.81	11.95	12360	61	1	0.79
22	(3@4.5)8-8-T4.0-5#3-i-2.5-3-9.5	A B C	1.9	4.0A _b	9.13 9.25 9.13	9.17	6650	20	1	0.79
23	(4@3)8-8-T4.0-5#3-i-2.5-3-9.5	A B C D	1.9	4.0A _b	9.75 9.63 9.88 9.38	9.66	6650	20	1	0.79
24	(3@3)8-8-T4.0-5#3-i-2.5-3-9.5	A B C	1.9	4.0A _b	9.25 9.38 9.38	9.33	6650	20	1	0.79
25	(3@5.9)5-12-F4.0-2#3-i-2.5-4-5	A B C	2.2	4.0A _b	5.13 5.13 5.19	5.15	11030	36	0.625	0.31
26	(3@5.9)5-12-F4.0-5#3-i-2.5-4-5	A B C	2.2	4.0A _b	5.19 4.88 5	5.02	11030	36	0.625	0.31
27	(4@3.9)5-12-F4.0-2#3-i-2.5-4-5	A B C D	2.2	4.0A _b	5 5 5.13 5	5.03	11030	39	0.625	0.31
28	(3@5.35)11-12-O4.5-6#3-i-2.5-3-16.75	A B C	1.3	4.5A _b	16.88 17.13 17	17	10860	37	1.41	1.56
29	(3@5.35)11-12-S5.5-6#3-i-2.5-3-16.75	A B C	1.5	5.5A _b	16.75 17 16.5	16.75	10120	38	1.41	1.56
30	(3@5.35)11-5-O4.5-6#3-i-2.5-3-19.25	A B C	1.3	4.5A _b	19.38 19.63 19.13	19.38	5430	13	1.41	1.56
31	(3@5.35)11-5-S5.5-6#3-i-2.5-3-19.25	A B C	1.5	5.5A _b	19 19.38 19.38	19.25	6320	13	1.41	1.56

Table C.4 Cont'd Details of the closely-spaced bars with confining reinforcement

No.	Specimen	Head	<i>b</i> in.	<i>h</i> in.	<i>h_{cl}</i> in.	<i>d_{eff}</i> in.	<i>c_{so}</i> in.	<i>c_{so,avg}</i> in.	<i>c_{bc}</i> in.	<i>s</i> in.	<i>d_{tr}</i> in.	<i>A_{tr,t}</i> in. ²
1	(3@3)8-8-F4.1-2#3-i-2.5-3-10	A	11.8	14.2	10.25	13.64	2.5	2.4	3.1	2.9	0.375	0.11
		B					-		3.2			
		C					2.4		3.1			
2	(3@3)8-8-F4.1-2#3-i-2.5-3-10-HP	A	12.1	14	10.25	13.36	2.5	2.6	2.8	3	0.375	0.11
		B					-		2.9			
		C					2.6		2.5			
3	(3@4)8-8-F4.1-2#3-i-2.5-3-10	A	13.8	14.2	10.25	12.92	2.4	2.4	3.4	4	0.375	0.11
		B					-		3.5			
		C					2.4		2.9			
4	(3@4)8-8-F4.1-2#3-i-2.5-3-10-HP	A	14.3	14.8	10.25	13.61	2.5	2.5	3.8	4	0.375	0.11
		B					-		3			
		C					2.5		3.5			
5	(3@5)8-8-F4.1-2#3-i-2.5-3-10.5	A	15.3	14.2	10.25	12.55	2.4	2.4	3.6	4.8	0.375	0.11
		B					-		3.4			
		C					2.4		3.2			
6	(3@5)8-8-F4.1-2#3-i-2.5-3-10.5-HP	A	16	14.1	10.25	12.94	2.4	2.4	3.2	5	0.375	0.11
		B					-		3.1			
		C					2.5		2.9			
7	(3@3)8-12-F4.1-5#3-i-2.5-3-10	A	12	13.9	10.25	12.81	2.4	2.4	2.9	3	0.375	0.11
		B					-		2.8			
		C					2.4		3.1			
8	(3@4)8-12-F4.1-5#3-i-2.5-3-10	A	13.8	14	10.25	12.48	2.4	2.4	3.2	3.9	0.375	0.11
		B					-		3.1			
		C					2.5		3.3			
9	(3@5)8-12-F4.1-5#3-i-2.5-3-10	A	16.3	14.3	10.25	12.31	2.5	2.5	3.5	5.1	0.375	0.11
		B					-		3.9			
		C					2.5		3.6			
10	(3@5.5)8-5-T9.5-5#3-i-2.5-3-14.5	A	17.4	19.1	10.25	14.93	2.5	2.6	3.1	5.6	0.375	0.11
		B					-		3.2			
		C					2.8		3.2			
11	(4@3.7)8-5-T9.5-5#3-i-2.5-3-14.5	A	17.1	19.1	10.25	15.2	2.4	2.4	3.2	3.8	0.375	0.11
		B					-		3.2			
		C					-		3			
		D					2.5		3.1			
12	(3@4)8-8-T9.5-2#3-i-2.5-3-9.5	A	14	14.3	10.25	12.47	2.5	2.5	3	4	0.375	0.11
		B					-		3.3			
		C					2.5		3.3			
13	(3@5)8-8-T9.5-2#3-i-2.5-3-9.5	A	16	14.3	10.25	12.16	2.5	2.5	3.3	5	0.375	0.11
		B					-		3.3			
		C					2.5		3.5			
14	(3@7)8-8-T9.5-2#3-i-2.5-3-9.5	A	20.1	14.3	10.25	12.05	2.5	2.5	3.3	7	0.375	0.11
		B					-		3			
		C					2.5		3.3			
15	(3@4)8-8-T9.5-2#3-i-2.5-3-14.5	A	14	19	10.25	13.92	2.5	2.5	3	4	0.375	0.11
		B					-		3			
		C					2.5		3.3			

Table C.4 Cont'd Details of the closely-spaced bars with confining reinforcement

No.	Specimen	Head	<i>b</i> in.	<i>h</i> in.	<i>h_{cl}</i> in.	<i>d_{eff}</i> in.	<i>c_{so}</i> in.	<i>c_{so,avg}</i> in.	<i>c_{bc}</i> in.	<i>s</i> in.	<i>d_{tr}</i> in.	<i>A_{tr,t}</i> in. ²
16	(3@5)8-8-T9.5-2#3-i-2.5-3-14.5	A B C	15.5	19.3	10.25	13.84	2.3 - 2.3	2.3	3.8 3.5 3.8	5	0.375	0.11
17	(3@7)8-8-T9.5-2#3-i-2.5-3-14.5	A B C	20	19.1	10.25	13.28	2.5 - 2.5	2.5	3.1 2.9 3.1	7 7	0.375	0.11
18	(3@4.5)8-12-F4.1-5#3-i-2.5-3-12	A B C	15.2	16.1	10.25	12.89	2.6 - 2.6	2.6	2.9 2.9 2.9	4.4 4.5	0.375	0.11
19	(3@4.5)8-12-F9.1-5#3-i-2.5-3-12	A B C	15	16	10.25	13.51	2.5 - 2.5	2.5	3.1 3.1 3.1	4.5	0.375	0.11
20	(4@3)8-12-F4.1-5#3-i-2.5-3-12	A B C D	15.1	16.2	10.25	12.76	2.4 - - 2.5	2.5	3.2 3.2 3 3.2	3.1 3 3	0.375	0.11
21	(4@3)8-12-F9.1-5#3-i-2.5-3-12	A B C D	14.9	16	10.25	13.68	2.4 - - 2.5	2.5	3 3 3 3.2	3 3 3	0.375	0.11
22	(3@4.5)8-8-T4.0-5#3-i-2.5-3-9.5	A B C	15.3	14.2	10.25	13.33	2.4 - 2.5	2.4	3.6 3.4 3.6	4.8 4.6	0.375	0.11
23	(4@3)8-8-T4.0-5#3-i-2.5-3-9.5	A B C D	15.3	14.1	10.25	13.45	2.6 - - 2.5	2.6	2.9 3 2.8 3.3	3 3.1 3	0.375	0.11
24	(3@3)8-8-T4.0-5#3-i-2.5-3-9.5	A B C	12.1	14.1	10.25	13.73	2.6 - 2.4	2.5	3.3 3.2 3.2	3 3.1	0.375	0.11
25	(3@5.9)5-12-F4.0-2#3-i-2.5-4-5	A B C	13.1	9.7	5.25	6.58	2.5 - 2.5	2.5	4.1 4.1 4	3.8 3.8	0.375	0.11
26	(3@5.9)5-12-F4.0-5#3-i-2.5-4-5	A B C	12.9	9.6	5.25	6.71	2.4 - 2.6	2.5	3.9 4.3 4.1	3.8 3.6	0.375	0.11
27	(4@3.9)5-12-F4.0-2#3-i-2.5-4-5	A B C D	13	9.6	5.25	6.81	2.5 - - 2.5	2.5	4.1 4.1 3.9 4.1	2.5 2.4 2.5	0.375	0.11
28	(3@5.35)11-12-O4.5-6#3-i-2.5-3-16.75	A B C	21.8	22.9	20	23.16	2.5 - 2.8	2.6	3.9 3.7 3.8	7.5 7.6	0.375	0.11
29	(3@5.35)11-12-S5.5-6#3-i-2.5-3-16.75	A B C	21.9	22.8	20	23.84	2.6 - 3	2.8	3.3 3 3.5	7.4 7.5	0.375	0.11
30	(3@5.35)11-5-O4.5-6#3-i-2.5-3-19.25	A B C	21.8	25.4	20	25.5	2.5 - 2.6	2.6	3.9 3.6 4.1	7.6 7.6	0.375	0.11
31	(3@5.35)11-5-S5.5-6#3-i-2.5-3-19.25	A B C	21.8	25.4	20	25.41	2.6 - 2.8	2.7	3.6 3.3 3.3	7.3 7.8	0.375	0.11

Table C.4 Cont'd Details of the closely-spaced bars with confining reinforcement

No.	Specimen	Head	N	s_{tr}^c in.	A_{tr} in. ²	d_{tro} in.	s_{tro}^c in.	A_{ab} in. ²	n	A_{hs} in. ²	Long. Reinf. Layout
1	(3@3)8-8-F4.1-2#3-i-2.5-3-10	A B C	4	5 (5.5)	0.22	0.375	3 (1.5)	0.66	3	2.37	B3
2	(3@3)8-8-F4.1-2#3-i-2.5-3-10-HP	A B C	4	5 (5.5)	0.22	0.375	3 (1.5)	0.66	3	2.37	B3
3	(3@4)8-8-F4.1-2#3-i-2.5-3-10	A B C	4	5 (5.5)	0.22	0.375	3.5 (1.75)	0.44	3	2.37	B3
4	(3@4)8-8-F4.1-2#3-i-2.5-3-10-HP	A B C	4	5 (5.5)	0.22	0.375	3.5 (1.75)	0.44	3	2.37	B3
5	(3@5)8-8-F4.1-2#3-i-2.5-3-10.5	A B C	4	5 (5.5)	0.22	0.375	4 (2)	0.44	3	2.37	B3
6	(3@5)8-8-F4.1-2#3-i-2.5-3-10.5-HP	A B C	4	5 (5.5)	0.22	0.375	4 (2)	0.44	3	2.37	B3
7	(3@3)8-12-F4.1-5#3-i-2.5-3-10	A B C	10	3 (1.5)	0.66	0.375	3 (1.5)	0.66	3	2.37	B5
8	(3@4)8-12-F4.1-5#3-i-2.5-3-10	A B C	10	3 (1.5)	0.66	0.375	3 (1.5)	0.66	3	2.37	B5
9	(3@5)8-12-F4.1-5#3-i-2.5-3-10	A B C	10	3 (1.5)	0.66	0.375	3 (1.5)	0.66	3	2.37	B5
10	(3@5.5)8-5-T9.5-5#3-i-2.5-3-14.5	A B C	10	3 (1.5)	0.66	0.375	4 (2)	0.44	3	2.37	B5
11	(4@3.7)8-5-T9.5-5#3-i-2.5-3-14.5	A B C D	10	3 (1.5)	0.66	0.375	3 (1.5)	0.66	4	3.16	B5
12	(3@4)8-8-T9.5-2#3-i-2.5-3-9.5	A B C	4	6 (4.5)	0.22	0.375	3 (1.5)	0.66	3	2.37	B5
13	(3@5)8-8-T9.5-2#3-i-2.5-3-9.5	A B C	4	6 (4.5)	0.22	0.375	3 (1.5)	0.66	3	2.37	B5
14	(3@7)8-8-T9.5-2#3-i-2.5-3-9.5	A B C	4	6 (4.5)	0.22	0.5	4.5 (2.25)	0.8	3	2.37	B7
15	(3@4)8-8-T9.5-2#3-i-2.5-3-14.5	A B C	4	6 (4.5)	0.22	0.375	4 (2)	0.44	3	2.37	B5

Table C.4 Cont'd Details of the closely-spaced bars with confining reinforcement

No.	Specimen	Head	<i>N</i>	<i>S_{tr}</i> ^c in.	<i>A_{tr}</i> in. ²	<i>d_{tr}</i> in.	<i>S_{tr}</i> ^c in.	<i>A_{tr}</i> in. ²	<i>n</i>	<i>A_{tr}</i> in. ²	Long. Reinf. Layout
16	(3@5)8-8-T9.5-2#3-i-2.5-3-14.5	A B C	4	6 (4.5)	0.22	0.375	3.5 (1.75)	0.44	3	2.37	B8
17	(3@7)8-8-T9.5-2#3-i-2.5-3-14.5	A B C	4	6 (4.5)	0.22	0.5	4.5 (2.25)	0.8	3	2.37	B8
18	(3@4.5)8-12-F4.1-5#3-i-2.5-3-12	A B C	10	3 (1.5)	0.66	0.5	3 (1.5)	1.2	3	2.37	B5
19	(3@4.5)8-12-F9.1-5#3-i-2.5-3-12	A B C	10	3 (1.5)	0.66	0.5	3 (1.5)	1.2	3	2.37	B5
20	(4@3)8-12-F4.1-5#3-i-2.5-3-12	A B C D	10	3 (1.5)	0.66	0.5	3 (1.5)	1.2	4	3.16	B5
21	(4@3)8-12-F9.1-5#3-i-2.5-3-12	A B C D	10	3 (1.5)	0.66	0.5	3 (1.5)	1.2	4	3.16	B5
22	(3@4.5)8-8-T4.0-5#3-i-2.5-3-9.5	A B C	10	3 (1.5)	0.66	0.5	4 (2)	0.8	3	2.37	B5
23	(4@3)8-8-T4.0-5#3-i-2.5-3-9.5	A B C D	10	3 (1.5)	0.66	0.5	4 (2)	0.8	4	3.16	B5
24	(3@3)8-8-T4.0-5#3-i-2.5-3-9.5	A B C	10	3 (1.5)	0.66	0.375	3 (1.5)	0.66	3	2.37	B5
25	(3@5.9)5-12-F4.0-2#3-i-2.5-4-5	A B C	4	3.5 (2.625)	0.22	0.375	3.5 (1.75)	0.22	3	0.93	B5
26	(3@5.9)5-12-F4.0-5#3-i-2.5-4-5	A B C	10	1.75 (0.875)	0.66	0.375	3.5 (1.75)	0.22	3	0.93	B5
27	(4@3.9)5-12-F4.0-2#3-i-2.5-4-5	A B C D	4	3.5 (2.625)	0.22	0.375	3.5 (1.75)	0.22	4	1.24	B5
28	(3@5.35)11-12-O4.5-6#3-i-2.5-3-16.75	A B C	12	4 (2)	0.66	0.5	4 (2)	1.2	3	4.68	B16
29	(3@5.35)11-12-S5.5-6#3-i-2.5-3-16.75	A B C	12	4 (2)	0.66	0.5	4 (2)	1.2	3	4.68	B16
30	(3@5.35)11-5-O4.5-6#3-i-2.5-3-19.25	A B C	12	4 (2)	0.66	0.5	4 (2)	1.2	3	4.68	B16
31	(3@5.35)11-5-S5.5-6#3-i-2.5-3-19.25	A B C	12	4 (2)	0.66	0.5	4 (2)	1.2	3	4.68	B16

^c Value in parenthesis is the spacing between the first hoop and the center of the headed bar

Table C.4 Cont'd Details of the closely-spaced bars with confining reinforcement

No.	Specimen	Head	Failure	Lead (Head) Slip in.	T_{max}	$f_{su,max}$	T_{ind}	T_{total}	T	f_{su}
					kips	ksi	kips	kips	kips	ksi
1	(3@3)8-8-F4.1-2#3-i-2.5-3-10	A	CB	0.097	53.2	67.3	53.2	185.8	61.9	78.4
		B		0.202	65.3	82.7	65.3			
		C		0.127	67.3	85.2	67.3			
2	(3@3)8-8-F4.1-2#3-i-2.5-3-10-HP	A	CB	0.1	51.4	65.1	51.4	170.1	56.7	71.8
		B		0.15	58.7	74.3	58.7			
		C		0.151	60	75.9	60			
3	(3@4)8-8-F4.1-2#3-i-2.5-3-10	A	CB	0.113	61.7	78.1	61.7	166.4	55.5	70.3
		B		0.213	52.9	67	52.9			
		C		0.203	51.8	65.6	51.8			
4	(3@4)8-8-F4.1-2#3-i-2.5-3-10-HP	A	CB	0.143	70.6	89.4	70.5	209.5	69.8	88.4
		B		0.338	70.2	88.9	70.2			
		C		-	68.8	87.1	68.8			
5	(3@5)8-8-F4.1-2#3-i-2.5-3-10.5	A	CB	-	61.4	77.7	61.4	168.2	56.1	71
		B		0.388	56.1	71	50.1			
		C		0.217	56.7	71.8	56.7			
6	(3@5)8-8-F4.1-2#3-i-2.5-3-10.5-HP	A	CB	0.036	62	78.5	62	196.4	65.5	82.9
		B		0.171	70.8	89.6	70.8			
		C		0.168	63.6	80.5	63.6			
7	(3@3)8-12-F4.1-5#3-i-2.5-3-10	A	CB	0.23	65.7	83.2	65.7	187.4	61.6	78
		B		0.252	63.9	80.9	63.9			
		C		0.123	55.1	69.7	55.1			
8	(3@4)8-12-F4.1-5#3-i-2.5-3-10	A	CB/FP	0.138	64	81	64	197.1	65.7	83.2
		B		0.24	66.5	84.2	66.5			
		C		0.26	66.7	84.4	66.6			
9	(3@5)8-12-F4.1-5#3-i-2.5-3-10	A	CB/FP	0.164	77.2	97.7	77.2	209.1	69.7	88.2
		B		0.123	65.4	82.8	65.4			
		C		0.122	66.7	84.4	66.6			
10	(3@5.5)8-5-T9.5-5#3-i-2.5-3-14.5	A	CB	0.121	91.5	115.8	91.5	283.8	94.6	119.7
		B		0.086	91.5	115.8	91.5			
		C		0.223	100.8	127.6	100.8			
11	(4@3.7)8-5-T9.5-5#3-i-2.5-3-14.5	A	CB	0.32	- [†]	- [†]	-	- [†]	76.9 [†]	97.3
		B		-	82.2	104.1	82.2			
		C		-	74.6	94.4	74.6			
		D		0.161	73.8	93.4	73.8			
12	(3@4)8-8-T9.5-2#3-i-2.5-3-9.5	A	CB	0.44	51.5	65.2	51.5	155.3	51.8	65.6
		B		0.293	54.5	69	54.5			
		C		0.230 (0.051)	49.3	62.4	49.3			
13	(3@5)8-8-T9.5-2#3-i-2.5-3-9.5	A	CB	0.373	55.7	70.5	55.2	167.8	55.9	70.8
		B		0.43	60.6	76.7	60.6			
		C		0.342 (0.001)	52	65.8	52			
14	(3@7)8-8-T9.5-2#3-i-2.5-3-9.5	A	CB	0.469	65.7	83.2	65.2	202.9	67.6	85.6
		B		0.124	62.6	79.2	62.6			
		C		0.145 (0.011)	75.1	95.1	75.1			
15	(3@4)8-8-T9.5-2#3-i-2.5-3-14.5	A	CB	0.122	79.5	100.6	79.5	256.3	85.4	108.1
		B		-	89.3	113	89.3			
		C		0.165 (0.016)	87.5	110.8	87.5			

[†] Load on headed bar A was not recorded due to a malfunction of load cell; T taken as the average load of the other three bars

Table C.4 Cont'd Details of the closely-spaced bars with confining reinforcement

No.	Specimen	Head	Failure Type	Lead (Head) Slip in.	T_{max} kips	$f_{su,max}$ ksi	T_{ind} kips	T_{total} kips	T kips	f_{su} ksi
16	(3@5)8-8-T9.5-2#3-i-2.5-3-14.5	A	CB	0.144	93.8	118.7	93.7	315.5	105.2	133.2
		B		-	99.3	125.7	99.3			
		C		0.083	122.5	155.1	122.5			
17	(3@7)8-8-T9.5-2#3-i-2.5-3-14.5	A	CB	-	105.8	133.9	105.8	340.3	113.4	143.5
		B		-	98.7	124.9	97.9			
		C		0.027	136.6	172.9	136.6			
18	(3@4.5)8-12-F4.1-5#3-i-2.5-3-12	A	CB	0.17	83.8	106.1	83.8	263.1	87.7	111
		B		0.094	86	108.9	86			
		C		0.169	93.2	118	93.2			
19	(3@4.5)8-12-F9.1-5#3-i-2.5-3-12	A	CB	0.25	108.1	136.8	108.1	325.7	108.6	137.4
		B		0.096	110.7	140.1	110.7			
		C		0.234	106.9	135.3	106.9			
20	(4@3)8-12-F4.1-5#3-i-2.5-3-12	A	CB	0.03	73.8	93.4	73.8	256.7	64.2	81.2
		B		-	63.3	80.1	63.3			
		C		0.101	48.2	61	48.2			
		D		0.093	71.5	90.5	71.5			
21	(4@3)8-12-F9.1-5#3-i-2.5-3-12	A	CB	-	85.2	107.8	85.2	351.3	87.8	111.1
		B		-	72.8	92.2	72.8			
		C		-	111.1	140.6	111.1			
		D		-	82.1	103.9	82.1			
22	(3@4.5)8-8-T4.0-5#3-i-2.5-3-9.5	A	CB/FP	0.015	56.5	71.5	55.3	187.4	62.5	79.1
		B		0.558	68.6	86.8	65.8			
		C		0.003	66.4	84.1	66.3			
23	(4@3)8-8-T4.0-5#3-i-2.5-3-9.5	A	CB	0.005	57.7	73	57.7	194.6	48.6	61.5
		B		-	30.1	38.1	30.1			
		C		-	52.3	66.2	52.3			
		D		0.015	54.4	68.9	54.4			
24	(3@3)8-8-T4.0-5#3-i-2.5-3-9.5	A	CB	0.003	56.9	72	56.8	169.6	56.5	71.6
		B		-	63.6	80.5	63.6			
		C		0.007	49.3	62.4	49.2			
25	(3@5.9)5-12-F4.0-2#3-i-2.5-4-5	A	CB	0.169	34.5	111.3	34.5	105.4	35.1	113.3
		B		-	35.3	113.9	35.3			
		C		-	35.6	114.8	35.6			
26	(3@5.9)5-12-F4.0-5#3-i-2.5-4-5	A	CB	0.266	42.5	137.1	42.3	115.9	38.6	124.6
		B		0.216	33.3	107.4	32.7			
		C		-	41.3	133.2	40.9			
27	(4@3.9)5-12-F4.0-2#3-i-2.5-4-5	A	CB	0.123	33.5	108.1	33.3	-	30.9 [†]	99.7
		B		-	- [†]	- [†]	-			
		C		0.228	30.7	99	30.7			
		D		-	28.7	92.6	28.7			
28	(3@5.35)11-12-O4.5-6#3-i-2.5-3-16.75	A	CB	-	131.7	84.4	131.7	407.4	135.8	87.1
		B		0.213	131.8	84.5	131.8			
		C		0.145	143.9	92.2	143.9			
29	(3@5.35)11-12-S5.5-6#3-i-2.5-3-16.75	A	CB	-	155.9	99.9	155.9	461.3	153.8	98.6
		B		0.095	154.9	99.3	154.9			
		C		-	150.6	96.5	150.6			
30	(3@5.35)11-5-O4.5-6#3-i-2.5-3-19.25	A	CB	-	137.4	88.1	137.4	425.1	141.7	90.8
		B		-	137.1	87.9	137.1			
		C		0.042	150.7	96.6	150.7			
31	(3@5.35)11-5-S5.5-6#3-i-2.5-3-19.25	A	CB	-	151.6	97.2	151.6	458.6	152.9	98
		B		-	157.4	100.9	157.4			
		C		0.02	149.5	95.8	149.5			

[†] Load on headed bar A was not recorded due to a malfunction of load cell; T taken as the average load of the other three bar

C.2: BEAM-COLUMN WITH $d_{eff}/\ell_{eh} \geq 1.5$

Table C.5 Details of the widely-spaced bars without confining reinforcement

No.	Specimen	Head	c_o in.	A_{brg}	ℓ_{eh} in.	$\ell_{eh,avg}$ in.	f_{cm} psi	Age days	d_b in.	A_b in. ²
1	8-5-F4.1-0-i-2.5-7-6	A	2	$4.1A_b$	6.06	6.09	4930	14	1	0.79
		B			6.13					
2	8-5-F9.1-0-i-2.5-7-6	A	2	$9.1A_b$	6.13	6.13	4940	15	1	0.79
		B			6.13					
3	11-5a-F3.8-0-i-2.5-3-12	A	2	$3.8A_b$	12.19	12	3960	35	1.41	1.56
		B			11.81					
4	11-5a-F8.6-0-i-2.5-3-12	A	2	$8.6A_b$	12.13	12.13	3960	35	1.41	1.56
		B			12.13					
5	8-8-F4.1-0-i-2.5-3-10-DB	A	2	$4.1A_b$	9.88	9.88	7410	49	1	0.79
		B			9.88					
6	8-8-F9.1-0-i-2.5-3-10-DB	A	2	$9.1A_b$	9.88	9.81	7410	49	1	0.79
		B			9.75					
7	8-5-F4.1-0-i-2.5-3-10-DB	A	2	$4.1A_b$	9.88	9.88	4880	19	1	0.79
		B			9.88					
8	8-5-F9.1-0-i-2.5-3-10-DB	A	2	$9.1A_b$	9.63	9.75	4880	19	1	0.79
		B			9.88					
9	11-8-F3.8-0-i-2.5-3-14.5	A	2	$3.8A_b$	14.5	14.5	8660	19	1.41	1.56
		B			14.5					
10	11-5-F3.8-0-i-2.5-3-12	A	2	$3.8A_b$	12.13	12.13	5760	6	1.41	1.56
		B			12.13					
11	11-5-F8.6-0-i-2.5-3-14.5	A	2	$8.6A_b$	14.5	14.5	5970	7	1.41	1.56
		B			14.5					

Table C.5 Cont'd Details of the widely-spaced bars without confining reinforcement

No.	Specimen	Head	b in.	h in.	h_{cl} in.	d_{eff} in.	c_{so} in.	$c_{so,avg}$ in.	c_{bc} in.	s in.	d_r in.	$A_{r,l}$ in. ²
1	8-5-F4.1-0-i-2.5-7-6	A	17.3	14.2	10.25	11.25	2.5	2.6	7.2	11	0.375	-
		B					2.8		7.1			
2	8-5-F9.1-0-i-2.5-7-6	A	17.3	14.2	10.25	11.42	2.8	2.8	7	10.8	0.375	-
		B					2.8		7			
3	11-5a-F3.8-0-i-2.5-3-12	A	21.7	16.5	20	21.84	2.6	2.7	2.9	14.9	-	-
		B					2.8		3.3			
4	11-5a-F8.6-0-i-2.5-3-12	A	21.7	16.8	20	22.07	2.8	2.6	3.3	15	-	-
		B					2.5		3.3			
5	8-8-F4.1-0-i-2.5-3-10-DB	A	17.1	14.3	20	21.38	2.5	2.6	3.4	11	-	-
		B					2.6		3.4			
6	8-8-F9.1-0-i-2.5-3-10-DB	A	17.3	14.2	20	21.42	2.6	2.6	3.3	11	-	-
		B					2.6		3.4			
7	8-5-F4.1-0-i-2.5-3-10-DB	A	17.4	14.1	20	21.43	2.5	2.6	3.3	11.3	-	-
		B					2.6		3.3			
8	8-5-F9.1-0-i-2.5-3-10-DB	A	17.5	14.3	20	21.56	2.6	2.6	3.6	11.3	-	-
		B					2.6		3.4			
9	11-8-F3.8-0-i-2.5-3-14.5	A	21.8	19.3	20	21.54	2.8	2.6	3.4	15.1	-	-
		B					2.5		3.4			
10	11-5-F3.8-0-i-2.5-3-12	A	21.7	17	20	21.66	2.8	2.6	3.5	15	-	-
		B					2.5		3.5			
11	11-5-F8.6-0-i-2.5-3-14.5	A	21.7	19.1	20	22.02	2.5	2.6	3.3	15.1	-	-
		B					2.6		3.3			

Table C.5 Cont'd Details of the widely-spaced bars without confining reinforcement

No.	Specimen	Head	<i>N</i>	<i>s_{tr}</i> ^c in.	<i>A_{tr}</i> in.2	<i>d_{tro}</i> in.	<i>s_{tro}</i> ^c in.	<i>A_{ab}</i> in.2	<i>n</i>	<i>A_{hs}</i> in.2	Long.Reinf.
1	8-5-F4.1-0-i-2.5-7-6	A B	-	-	-	0.375	3 (1.5)	0.66	2	1.58	B4
2	8-5-F9.1-0-i-2.5-7-6	A B	-	-	-	0.375	3 (1.5)	0.66	2	1.58	B4
3	11-5a-F3.8-0-i-2.5-3-12	A B	-	-	-	0.5	5 (2.5)	1.2	2	3.12	B11
4	11-5a- F8.6-0-i-2.5-3-12	A B	-	-	-	0.5	5 (2.5)	1.2	2	3.12	B11
5	8-8-F4.1-0-i-2.5-3-10-DB	A B	-	-	-	0.5	5 (2.5)	0.8	2	1.58	B12
6	8-8-F9.1-0-i-2.5-3-10-DB	A B	-	-	-	0.5	5 (2.5)	0.8	2	1.58	B12
7	8-5-F4.1-0-i-2.5-3-10-DB	A B	-	-	-	0.5	5 (2.5)	0.8	2	1.58	B12
8	8-5-F9.1-0-i-2.5-3-10-DB	A B	-	-	-	0.5	5 (2.5)	0.8	2	1.58	B12
9	11-8-F3.8-0-i-2.5-3-14.5	A B	-	-	-	0.5	5 (2.5)	1.2	2	3.12	B12
10	11-5-F3.8-0-i-2.5-3-12	A B	-	-	-	0.5	5 (2.5)	1.2	2	3.12	B6
11	11-5- F8.6-0-i-2.5-3-14.5	A B	-	-	-	0.5	5 (2.5)	1.2	2	3.12	B12

^c Value in parenthesis is the spacing between the first hoop and the center of the headed bar

Table C.5 Cont'd Details of the widely-spaced bars without confining reinforcement

No.	Specimen	Head	Failure Type	Lead (Head) Slip in.	<i>T_{max}</i> kips	<i>f_{su,max}</i> ksi	<i>T_{ind}</i> kips	<i>T_{total}</i> kips	<i>T</i> kips	<i>f_{su}</i> ksi
1	8-5-F4.1-0-i-2.5-7-6	A B	CB	0.005 0.027	30.2 29.7	38.2 37.6	27.7 29.7	57.3	28.7	36.3
2	8-5-F9.1-0-i-2.5-7-6	A B	CB	0.001 -	32.4 34.8	41 44.1	32 34.8	66.8	33.4	42.3
3	11-5a-F3.8-0-i-2.5-3-12	A B	CB	0.025 0.006	54.2 59.5	34.7 38.1	54.2 59.5	113.7	56.8	36.4
4	11-5a- F8.6-0-i-2.5-3-12	A B	CB	0.202 0.145	63.7 75.4	40.8 48.3	63.7 64	127.7	63.8	40.9
5	8-8-F4.1-0-i-2.5-3-10-DB	A B	CB	0.129 0.065	49.9 50.5	63.2 63.9	49.9 50.5	100.3	50.2	63.5
6	8-8-F9.1-0-i-2.5-3-10-DB	A B	CB	0.01 0.036	47.4 56.2	60 71.1	47.4 56.2	103.6	51.8	65.6
7	8-5-F4.1-0-i-2.5-3-10-DB	A B	CB/FP	0.188 0.322	37.4 44.4	47.3 56.2	37.4 43.9	81.3	40.6	51.4
8	8-5-F9.1-0-i-2.5-3-10-DB	A B	CB	0.061 0.008	42.6 49.7	53.9 62.9	39 49.7	88.7	44.4	56.2
9	11-8-F3.8-0-i-2.5-3-14.5	A B	CB	0.123 0.008	79.4 78.7	50.9 50.4	79.4 78.7	158.1	79.1	50.7
10	11-5-F3.8-0-i-2.5-3-12	A B	CB	0.14 0.262	68.7 64.3	44 41.2	68.7 64.3	132.9	66.5	42.6
11	11-5- F8.6-0-i-2.5-3-14.5	A B	CB	0.005 0.783	83.6 82.1	53.6 52.6	83.6 82.1	165.7	82.8	53.1

Table C.6 Details of the closely-spaced bars without confining reinforcement

No.	Specimen	Head	c_o in.	A_{brg}	ℓ_{eh} in.	$\ell_{eh,avg}$ in.	f_{cm} psi	Age days	d_b in.	A_b in. ²
1	(3@3)8-5-F4.1-0-i-2.5-7-6	A B C	2	4.1 A_b	6.06 6.25 6.25	6.19	4930	14	1	0.79
2	(3@5)8-5-F4.1-0-i-2.5-7-6	A B C	2	4.1 A_b	6.5 6.25 6.25	6.33	4930	14	1	0.79
3	(3@7)8-5-F4.1-0-i-2.5-7-6	A B C	2	4.1 A_b	6.25 6.25 6.25	6.25	4940	15	1	0.79
4	(3@5.5)8-5-F9.1-0-i-2.5-7-6	A B C	2	9.1 A_b	6.25 6.13 6.25	6.21	5160	16	1	0.79
5	(4@3.7)8-5-T9.5-0-i-2.5-6.5-6	A B C D	1.4	9.5 A_b	6.19 6.13 6.19 6	6.13	5160	16	1	0.79
6	(3@5.35)11-8-F3.8-0-i-2.5-3-14.5	A B C	2	3.8 A_b	14.38 14.75 14.75	14.63	8720	20	1.41	1.56
7	(3@5.35)11-5- F8.6-0-i-2.5-3-14.5	A B C	2	8.6 A_b	14.38 15.25 14.5	14.71	6240	8	1.41	1.56

Table C.6 Cont'd Details of the closely-spaced bars without confining reinforcement

No.	Specimen	Head	b in.	h in.	h_{ct} in.	d_{eff} in.	c_{so} in.	$c_{so,avg}$ in.	c_{bc} in.	s in.	d_{tr} in.	$A_{tr,t}$ in. ²
1	(3@3)8-5-F4.1-0-i-2.5-7-6	A B C	12.6	13.7	10.25	11.78	2.8 - 2.5	2.6	6.6 6.4 6.4	3.3 3.1	0.375	-
2	(3@5)8-5-F4.1-0-i-2.5-7-6	A B C	16.9	14.2	10.25	11.58	2.8 - 2.8	2.8	6.7 6.9 6.9	5.1 5.3	0.375	-
3	(3@7)8-5-F4.1-0-i-2.5-7-6	A B C	20.5	14.3	10.25	11.45	2.8 - 2.6	2.7	7 7 7	7.1 7	0.375	-
4	(3@5.5)8-5-F9.1-0-i-2.5-7-6	A B C	17.3	14.4	10.25	11.42	2.5 - 2.8	2.6	7.1 7.3 7.1	5.5 5.5	0.375	-
5	(4@3.7)8-5-T9.5-0-i-2.5-6.5-6	A B C D	17	14.2	10.25	11.72	2.8 - - 2.5	2.6	6.5 6.6 6.5 6.7	3.5 3.6 3.6	0.375	-
6	(3@5.35)11-8-F3.8-0-i-2.5-3-14.5	A B C	22	19.3	20	21.53	2.8 - 2.8	2.8	3.6 3.2 3.2	7.5 7.6	-	-
7	(3@5.35)11-5- F8.6-0-i-2.5-3-14.5	A B C	21.3	19.2	20	22.32	2.6 - 2.5	2.6	3.4 2.6 3.3	7.3 7.5	-	-

Table C.6 Cont'd Details of the closely-spaced bars without confining reinforcement

No.	Specimen	Head	N	s_{tr}^c	A_{tr}	d_{tr}	s_{tr}^c	A_{ab}	n	A_{hs}	Long. Reinf. Layout
				in.	in.2	in.	in.	in.2		in.2	
1	(3@3)8-5-F4.1-0-i-2.5-7-6	A	-	-	-	0.375	3	0.66	3	2.37	B4
		B									
		C									
2	(3@5)8-5-F4.1-0-i-2.5-7-6	A	-	-	-	0.375	3	0.66	3	2.37	B5
		B									
		C									
3	(3@7)8-5-F4.1-0-i-2.5-7-6	A	-	-	-	0.375	3	0.66	3	2.37	B8
		B									
		C									
4	(3@5.5)8-5-F9.1-0-i-2.5-7-6	A	-	-	-	0.375	3	0.66	3	2.37	B5
		B									
		C									
5	(4@3.7)8-5-T9.5-0-i-2.5-6.5-6	A	-	-	-	0.375	3	0.66	4	3.16	B5
		B									
		C									
		D									
6	(3@5.35)11-8-F3.8-0-i-2.5-3-14.5	A	-	-	-	0.5	5	1.2	3	4.68	B13
		B									
		C									
7	(3@5.35)11-5- F8.6-0-i-2.5-3-14.5	A	-	-	-	0.5	5	1.2	3	4.68	B15
		B									
		C									

^c Value in parenthesis is the spacing between the first hoop and the center of the headed bar

Table C.6 Cont'd Details of the closely-spaced bars without confining reinforcement

No.	Specimen	Head	Failure Type	Lead (Head)	T_{max}	$f_{su,max}$	T_{ind}	T_{total}	T	f_{su}
				Slip in.	kips	ksi	kips	kips	kips	ksi
1	(3@3)8-5-F4.1-0-i-2.5-7-6	A	CB	-	15.5	19.6	14.9	61.8	20.6	26.1
		B		-	24.3	30.8	24.3			
		C		-	22.7	28.7	22.7			
2	(3@5)8-5-F4.1-0-i-2.5-7-6	A	CB	0.026	24.1	30.5	24	71.8	23.9	30.3
		B		-	23.8	30.1	23.3			
		C		0.002	24.5	31	24.5			
3	(3@7)8-5-F4.1-0-i-2.5-7-6	A	CB	0.001	31.1	39.4	31.1	81.2	27.1	34.3
		B		-	19.1	24.2	19			
		C		0.013	31.1	39.4	31.1			
4	(3@5.5)8-5-F9.1-0-i-2.5-7-6	A	CB	0.014	28.6	36.2	28.6	68.9	23	29.1
		B		-	13.9	17.6	13.9			
		C		0.015	26.4	33.4	26.4			
5	(4@3.7)8-5-T9.5-0-i-2.5-6.5-6	A	CB	0.001	25.9	32.8	25.9	86.9	21.7	27.5
		B		0.016	14.6	18.5	14.6			
		C		-	17.8	22.5	17.8			
		D		0.024	28.8	36.5	28.6			
6	(3@5.35)11-8-F3.8-0-i-2.5-3-14.5	A	CB	-	51.9	33.3	51.9	158.7	52.9	33.9
		B		0.04	54.9	35.2	54.9			
		C		-	51.9	33.3	51.9			
7	(3@5.35)11-5- F8.6-0-i-2.5-3-14.5	A	CB	-	66.5	42.6	66.5	195.4	65.1	41.7
		B		0.013	61.7	39.6	61.7			
		C		0.068	67.1	43	67.1			

Table C.7 Details of the widely-spaced bars with confining reinforcement

No.	Specimen	Head	c_o in.	A_{brg}	l_{eh} in.	$l_{eh,avg}$ in.	f_{cm} psi	Age days	d_b in.	A_b in. ²
1	8-5-F4.1-5#3-i-2.5-7-6	A B	2	4.1A _b	6.25 6.25	6.25	4930	14	1	0.79
2	8-5-F9.1-5#3-i-2.5-7-6	A B	2	9.1A _b	6.19 6.13	6.16	4940	15	1	0.79
3	11-5a-F3.8-2#3-i-2.5-3-12	A B	2	3.8A _b	11.81 12.19	12	3960	35	1.41	1.56
4	11-5a-F3.8-6#3-i-2.5-3-12	A B	2	3.8A _b	12.13 12.06	12.09	3960	35	1.41	1.56
5	11-5a- F8.6-6#3-i-2.5-3-12	A B	2	8.6A _b	12.69 12.44	12.56	4050	36	1.41	1.56
6	8-8-F9.1-5#3-i-2.5-3-10-DB	A B	2	9.1A _b	9.63 9.63	9.63	7410	49	1	0.79
7	8-5-F4.1-3#4-i-2.5-3-10-DB	A B	2	4.1A _b	10 10.25	10.13	4880	19	1	0.79
8	8-5-F9.1-3#4-i-2.5-3-10-DB	A B	2	9.1A _b	9.75 9.75	9.75	4880	20	1	0.79
9	8-5-F4.1-5#3-i-2.5-3-10-DB	A B	2	4.1A _b	10.25 10.13	10.19	4880	20	1	0.79
10	8-5-F9.1-5#3-i-2.5-3-10-DB	A B	2	9.1A _b	10 9.88	9.94	4880	20	1	0.79
11	11-8-F3.8-2#3-i-2.5-3-14.5	A B	2	3.8A _b	14.63 14.75	14.69	8660	19	1.41	1.56
12	11-8-F3.8-6#3-i-2.5-3-14.5	A B	2	3.8A _b	14.88 14.5	14.69	8660	19	1.41	1.56
13	11-5-F3.8-6#3-i-2.5-3-12	A B	2	3.8A _b	12.5 12.5	12.5	5760	6	1.41	1.56
14	11-5- F8.6-6#3-i-2.5-3-14.5	A B	2	8.6A _b	14.5 14.75	14.63	5970	7	1.41	1.56

Table C.7 Cont'd Details of the widely-spaced bars with confining reinforcement

No.	Specimen	Head	<i>b</i> in.	<i>h</i> in.	<i>h_{ct}</i> in.	<i>d_{eff}</i> in.	<i>c_{so}</i> in.	<i>c_{so,avg}</i> in.	<i>c_{bc}</i> in.	<i>s</i> in.	<i>d_{tr}</i> in.	<i>A_{tr,l}</i> in. ²
1	8-5-F4.1-5#3-i-2.5-7-6	A B	17.1	14	10.25	12.02	2.5 2.6	2.6	6.8 6.8	11	0.375	0.11
2	8-5-F9.1-5#3-i-2.5-7-6	A B	17	14.1	10.25	12.13	2.5 2.5	2.5	6.9 7	11	0.375	0.11
3	11-5a-F3.8-2#3-i-2.5-3-12	A B	21.4	17.1	20	22.18	2.4 2.4	2.4	3.9 3.5	15.3	0.375	0.11
4	11-5a-F3.8-6#3-i-2.5-3-12	A B	21.6	17	20	22.53	2.8 2.5	2.7	3.5 3.6	14.9	0.375	0.11
5	11-5a- F8.6-6#3-i-2.5-3-12	A B	22	17.3	20	22.53	2.8 2.7	2.7	3.3 3.5	15.2	0.375	0.11
6	8-8-F9.1-5#3-i-2.5-3-10-DB	A B	17.4	14.2	20	21.88	2.5 2.8	2.6	3.6 3.6	11.1	0.375	0.11
7	8-5-F4.1-3#4-i-2.5-3-10-DB	A B	17.3	14.1	20	22.27	2.5 2.5	2.5	3.1 2.9	11.3	0.5	0.2
8	8-5-F9.1-3#4-i-2.5-3-10-DB	A B	17.3	14.4	20	22.31	2.6 2.6	2.6	3.6 3.6	11	0.5	0.2
9	8-5-F4.1-5#3-i-2.5-3-10-DB	A B	17.5	14.3	20	22.47	2.6 2.8	2.7	3.1 3.2	11.1	0.375	0.11
10	8-5-F9.1-5#3-i-2.5-3-10-DB	A B	17.3	14.2	20	22.48	2.6 2.6	2.6	3.2 3.3	11	0.375	0.11
11	11-8-F3.8-2#3-i-2.5-3-14.5	A B	21.8	19.3	20	21.72	2.5 2.6	2.6	3.3 3.1	15.3	0.375	0.11
12	11-8-F3.8-6#3-i-2.5-3-14.5	A B	21.7	19.4	20	22.19	2.4 2.5	2.4	3.2 3.6	15.4	0.375	0.11
13	11-5-F3.8-6#3-i-2.5-3-12	A B	21.8	16.9	20	22.2	2.6 2.8	2.7	3.1 3.1	15	0.375	0.11
14	11-5- F8.6-6#3-i-2.5-3-14.5	A B	21.5	19.5	20	22.74	2.6 2.6	2.6	3.6 3.4	14.9	0.375	0.11

Table C.7 Cont'd Details of the widely-spaced bars with confining reinforcement

No.	Specimen	Head	<i>N</i>	<i>s_{tr}</i> ^c in.	<i>A_{tt}</i> in.2	<i>d_{tro}</i> in.	<i>s_{tro}</i> ^c in.	<i>A_{ab}</i> in.2	<i>n</i>	<i>A_{hs}</i> in.2	Long. Layout
1	8-5-F4.1-5#3-i-2.5-7-6	A B	10	3 (1.5)	0.66	0.375	3 (1.5)	0.66	2	1.58	B4
2	8-5-F9.1-5#3-i-2.5-7-6	A B	10	3 (1.5)	0.66	0.375	3 (1.5)	0.66	2	1.58	B9
3	11-5a-F3.8-2#3-i-2.5-3-12	A B	4	8 (6)	0.22	0.5	5 (2.5)	1.2	2	3.12	B11
4	11-5a-F3.8-6#3-i-2.5-3-12	A B	12	4 (2)	0.66	0.5	5 (2.5)	1.2	2	3.12	B11
5	11-5a-F8.6-6#3-i-2.5-3-12	A B	12	4 (2)	0.66	0.5	5 (2.5)	1.2	2	3.12	B11
6	8-8-F9.1-5#3-i-2.5-3-10-DB	A B	10	5 (2.5)	0.44	0.5	5 (2.5)	0.8	2	1.58	B12
7	8-5-F4.1-3#4-i-2.5-3-10-DB	A B	6	7.5 (6)	0.4	0.5	5 (2.5)	0.8	2	1.58	B12
8	8-5-F9.1-3#4-i-2.5-3-10-DB	A B	6	7.5 (6)	0.4	0.5	5 (2.5)	0.8	2	1.58	B12
9	8-5-F4.1-5#3-i-2.5-3-10-DB	A B	10	5 (2.5)	0.44	0.5	5 (2.5)	0.8	2	1.58	B12
10	8-5-F9.1-5#3-i-2.5-3-10-DB	A B	10	5 (2.5)	0.44	0.5	5 (2.5)	0.8	2	1.58	B12
11	11-8-F3.8-2#3-i-2.5-3-14.5	A B	4	8 (6)	0.22	0.5	5 (2.5)	1.2	2	3.12	B12
12	11-8-F3.8-6#3-i-2.5-3-14.5	A B	12	4 (2)	0.66	0.5	5 (2.5)	1.2	2	3.12	B12
13	11-5-F3.8-6#3-i-2.5-3-12	A B	12	4 (2)	0.66	0.5	5 (2.5)	1.2	2	3.12	B12
14	11-5-F8.6-6#3-i-2.5-3-14.5	A B	12	4 (2)	0.66	0.5	5 (2.5)	1.2	2	3.12	B12

^c Value in parenthesis is the spacing between the first hoop and the center of the headed bar

Table C.7 Cont'd Details of the widely-spaced bars with confining reinforcement

No.	Specimen	Head	Failure Type	Lead Slip Head in.	T_{max} kips	$f_{su,max}$ ksi	T_{ind} kips	T_{total} kips	T kips	f_{su} ksi
1	8-5-F4.1-5#3-i-2.5-7-6	A	CB	0.027	51.6	65.3	48.8	101.3	50.7	64.1
		B		0.023	52.7	66.7	52.5			
2	8-5-F9.1-5#3-i-2.5-7-6	A	CB	0.017	53.4	67.6	53.4	107.6	53.8	68.1
		B		0.033	54.3	68.7	54.2			
3	11-5a-F3.8-2#3-i-2.5-3-12	A	CB	0.231	67.2	43.1	67.2	134.6	67.3	43.1
		B		0.007	67.4	43.2	67.4			
4	11-5a-F3.8-6#3-i-2.5-3-12	A	CB/FP	0.007	77.4	49.6	77.4	156	78	50
		B		0.429	82.3	52.8	78.6			
5	11-5a-F8.6-6#3-i-2.5-3-12	A	CB	0.237	78.3	50.2	78.3	158.4	79.2	50.8
		B		0.25	80.2	51.4	80.2			
6	8-8-F9.1-5#3-i-2.5-3-10-DB	A	CB	0.012	65.5	82.9	65.5	136.5	68.2	86.3
		B		0.102	71	89.9	71			
7	8-5-F4.1-3#4-i-2.5-3-10-DB	A	CB	0.081	60.6	76.7	60.6	129.2	64.6	81.8
		B		0.18	68.7	87	68.7			
8	8-5-F9.1-3#4-i-2.5-3-10-DB	A	CB	0.017	62.4	79	62.4	131.5	65.8	83.3
		B		0.258	69.1	87.5	69.1			
9	8-5-F4.1-5#3-i-2.5-3-10-DB	A	CB	0.019	63.2	80	63.2	140.4	70.2	88.9
		B		0.12	77.2	97.7	77.2			
10	8-5-F9.1-5#3-i-2.5-3-10-DB	A	CB	0.12	66.8	84.6	66.8	141	70.5	89.2
		B		0.248	74.2	93.9	74.2			
11	11-8-F3.8-2#3-i-2.5-3-14.5	A	CB	0.591	87.8	56.3	87.8	176.9	88.4	56.7
		B		0.008	89.1	57.1	89.1			
12	11-8-F3.8-6#3-i-2.5-3-14.5	A	CB	0.14	112.4	72.1	112.4	225.3	112.7	72.2
		B		0.178	112.9	72.4	112.9			
13	11-5-F3.8-6#3-i-2.5-3-12	A	CB	0.041	88.2	56.5	88.2	176.5	88.3	56.6
		B		0.008	88.3	56.6	88.3			
14	11-5-F8.6-6#3-i-2.5-3-14.5	A	CB	0.144	113.9	73	113.9	224.6	112.3	72
		B		0.01	110.7	71	110.7			

Table C.8 Details of the closely-spaced bars with confining reinforcement

No.	Specimen	Head	c_o in.	A_{brg}	ℓ_{eh} in.	$\ell_{eh,avg}$ in.	f_{cm} psi	Age days	d_b in.	A_b in. ²
1	(3@3)8-5-F4.1-5#3-i-2.5-7-6	A B C	2	4.1A _b	6 6 6	6	4930	14	1	0.79
2	(3@5)8-5-F4.1-5#3-i-2.5-7-6	A B C	2	4.1A _b	6.25 6.13 6.5	6.29	4930	14	1	0.79
3	(3@7)8-5-F4.1-5#3-i-2.5-7-6	A B C	2	4.1A _b	6 6.19 6.13	6.1	4940	15	1	0.79
4	(3@5.5)8-5-F9.1-5#3-i-2.5-7-6	A B C	2	9.1A _b	6.13 6.25 6.38	6.25	5160	16	1	0.79
5	(4@3.7)8-5-F9.1-5#3-i-2.5-7-6	A B C D	2	9.1A _b	6 6 6 6.13	6.03	5160	16	1	0.79
6	(3@5.35)11-8-F3.8-2#3-i-2.5-3-14.5	A B C	2	3.8A _b	14.5 14.63 14.5	14.54	8720	20	1.41	1.56
7	(3@5.35)11-8-F3.8-6#3-i-2.5-3-14.5	A B C	2	3.8A _b	15.13 14.88 14.75	14.92	8720	20	1.41	1.56
8	(3@5.35)11-5-F8.6-6#3-i-2.5-3-14.5	A B C	2	8.6A _b	14.75 14.5 14.38	14.54	6240	8	1.41	1.56

Table C.8 Details of the closely-spaced bars with confining reinforcement

No.	Specimen	Head	<i>b</i> in.	<i>h</i> in.	<i>h_{cl}</i> in.	<i>d_{eff}</i> in.	<i>c_{so}</i> in.	<i>c_{so,avg}</i> in.	<i>c_{bc}</i> in.	<i>s</i> in.	<i>d_{tr}</i> in.	<i>A_{tr,l}</i> in. ²	
1	(3@3)8-5-F4.1-5#3-i-2.5-7-6	A	12.5	14	10.25	12.63	2.5	2.6	7	3.3	0.375	0.11	
		B					-		7				
		C					2.6		7				3.1
2	(3@5)8-5-F4.1-5#3-i-2.5-7-6	A	16.8	14.3	10.25	12.34	2.8	2.8	7	5.3	0.375	0.11	
		B					-		7.1				
		C					2.8		6.8				5
3	(3@7)8-5-F4.1-5#3-i-2.5-7-6	A	20.5	14.1	10.25	12.13	2.6	2.7	7.1	7.1	0.375	0.11	
		B					-		6.9				
		C					2.8		7				7
4	(3@5.5)8-5-F9.1-5#3-i-2.5-7-6	A	17.3	14.4	10.25	12.44	2.5	2.6	7.3	5.5	0.375	0.11	
		B					-		7.1				
		C					2.8		7				5.5
5	(4@3.7)8-5-F9.1-5#3-i-2.5-7-6	A	17.4	14.3	10.25	12.39	2.5	2.6	7.3	3.8	0.375	0.11	
		B					-		7.3				3.8
		C					-		7.3				
		D					2.6		7.1				3.8
6	(3@5.35)11-8-F3.8-2#3-i-2.5-3-14.5	A	21.8	19.2	20	22.1	2.5	2.6	3.3	7.5	0.375	0.11	
		B					-		3.2				
		C					2.6		3.3				7.8
7	(3@5.35)11-8-F3.8-6#3-i-2.5-3-14.5	A	22.2	19.6	20	22.42	2.8	2.8	3.1	7.6	0.375	0.11	
		B					-		3.4				
		C					2.8		3.5				7.6
8	(3@5.35)11-5-F8.6-6#3-i-2.5-3-14.5	A	21.4	19.1	20	22.7	2.5	2.6	3	7.4	0.375	0.11	
		B					-		3.3				
		C					2.8		3.4				7.4

Table C.8 Details of the closely-spaced bars with confining reinforcement

No.	Specimen	Head	N	s_{tr}^c in.	A_{tr} in.2	d_{tro} in.	s_{tro}^c in.	A_{ab} in.2	n	A_{hs} in.2	Long. Layout
1	(3@3)8-5-F4.1-5#3-i-2.5-7-6	A B C	10	3 (1.5)	0.66	0.375	3 (1.5)	0.66	3	2.37	B5
2	(3@5)8-5-F4.1-5#3-i-2.5-7-6	A B C	10	3 (1.5)	0.66	0.375	3 (1.5)	0.66	3	2.37	B5
3	(3@7)8-5-F4.1-5#3-i-2.5-7-6	A B C	10	3 (1.5)	0.66	0.5	4 (2)	0.8	3	2.37	B8
4	(3@5.5)8-5-F9.1-5#3-i-2.5-7-6	A B C	10	3 (1.5)	0.66	0.5	4 (2)	0.8	3	2.37	B5
5	(4@3.7)8-5-F9.1-5#3-i-2.5-7-6	A B C D	10	3 (1.5)	0.66	0.5	3 (1.5)	1.2	4	3.16	B5
6	(3@5.35)11-8-F3.8-2#3-i-2.5-3-14.5	A B C	4	8 (6)	0.22	0.5	5 (2.5)	1.2	3	4.68	B14
7	(3@5.35)11-8-F3.8-6#3-i-2.5-3-14.5	A B C	12	4 (2)	0.66	0.5	5 (2.5)	1.2	3	4.68	B14
8	(3@5.35)11-5- F8.6-6#3-i-2.5-3-14.5	A B C	12	4 (2)	0.66	0.5	4.5 (2.25)	1.2	3	4.68	B15

^c Value in parenthesis is the spacing between the first hoop and the center of the headed bar

Table C.8 Details of the closely-spaced bars with confining reinforcement

No.	Specimen	Head	Failure Type	Lead (Head) Slip in.	T_{max}	$f_{su,max}$	T_{ind}	T_{total}	T	f_{su}
					kips	ksi	kips	kips	kips	ksi
1	(3@3)8-5-F4.1-5#3-i-2.5-7-6	A	CB	-	32.2	40.8	32.2	96.3	32.1	40.6
		B		-	30.8	39	30.8			
		C		-	33.3	42.2	33.3			
2	(3@5)8-5-F4.1-5#3-i-2.5-7-6	A	CB	0.007	31.3	39.6	30.9	112.6	37.5	47.5
		B		0.014	38.3	48.5	38.3			
		C		0.014	43.8	55.5	43.4			
3	(3@7)8-5-F4.1-5#3-i-2.5-7-6	A	CB	-	44.1	55.8	44.1	126.8	42.3	53.5
		B		-	35.2	44.6	35.2			
		C		-	47.5	60.1	47.5			
4	(3@5.5)8-5-F9.1-5#3-i-2.5-7-6	A	CB	0.025	40.5	51.3	39.9	129.4	43.1	54.6
		B		-	46.5	58.9	46.5			
		C		0.022	43	54.4	43			
5	(4@3.7)8-5-F9.1-5#3-i-2.5-7-6	A	CB	-	39.5	50	39.5	126.5	31.6	40
		B		-	31.5	39.9	31.5			
		C		-	20.4	25.8	20.4			
		D		0.023	35.1	44.4	35.1			
6	(3@5.35)11-8-F3.8-2#3-i-2.5-3-14.5	A	CB	-	74	47.4	74	217.7	72.6	46.5
		B		0.26	72.1	46.2	72.1			
		C		-	71.6	45.9	71.6			
7	(3@5.35)11-8-F3.8-6#3-i-2.5-3-14.5	A	CB	-	93.2	59.7	93.2	251	83.7	53.7
		B		0.211	85.3	54.7	85.3			
		C		0.292	72.4	46.4	72.4			
8	(3@5.35)11-5-F8.6-6#3-i-2.5-3-14.5	A	CB	-	68.8	44.1	68.8	226.9	75.6	48.5
		B		0.287	83.3	53.4	83.2			
		C		0.016	74.9	48	74.9			

